Thèse de doctorat de
l'Université Bourgogne Franche-Comté,
en cotutelle avec
Universidad Técnica Federico Santa María,
preparée à

École doctorale n° 37
Sciences Pour l'Ingénieur et Microtechniques

Doctorat d'Automatique (UBFC)
Doctorado en Ingeniería Electrónica (UTFSM)

par

Cristóbal Matías PONCE SALAZAR

Modélisation Hamiltonienne à ports, discrétisation et commande en forme de systèmes mécaniques flexibles multidimensionnels

Thèse soutenue publiquement le 11 décembre 2024, à Besançon,
devant le jury composé de:

Laurent Lefèvre	Professeur des Universités, Université Grenoble Alpes	Président et Rapporteur
Bernhard Maschke	Professeur des Universités, Université Claude Bernhard Lyon 1	Rapporteur
Arjan van der Schaft	Professeur Émérite, Université de Groningen	Examinateur
Denis Matignon	Professeur des Universités, ISAE-SUPAERO ONERA	Examinateur
Francisco Vargas	Professeur Adjoint, Université Technique Federico Santa María	Examinateur
Yongxin Wu	Maître de Conférences, HDR, Université Bourgogne Franche-Comté	Examinateur
Yann Le Gorrec	Professeur des Universités, Université Bourgogne Franche-Comté	Directeur de thèse
Hector Ramirez	Professeur Associé, HDR, Université Technique Federico Santa María	Directeur de thèse

Ph.D. thesis of the
University Bourgogne Franche-Comté,
in double degree agreement with
Universidad Técnica Federico Santa María,
prepared at

Doctoral school n° 37
Engineering Sciences and Microtechnologies

PhD. in Automatic (UBFC)
PhD. in Electronic Engineering (UTFSM)

by

Cristóbal Matías PONCE SALAZAR

Port-Hamiltonian modeling, discretization and shape control of multidimensional flexible mechanical systems

Thesis defended publicly on December 11, 2024, in Besançon,
composition of jury:

Laurent Lefèvre	Professor of University, Grenoble Alpes University	President and Reviewer
Bernhard Maschke	Professor of University, Claude Bernard University Lyon 1	Reviewer
Arjan van der Schaft	Professor Emeritus, University of Groningen	Examiner
Denis Matignon	Professor of University, ISAE-SUPAERO ONERA	Examiner
Francisco Vargas	Assistant Professor, Federico Santa María Technical University	Examiner
Yongxin Wu	Associate Professor, University Bourgogne Franche-Comté	Examiner
Yann Le Gorrec	Professor of University, Supmicrotech-ENSMM	Supervisor
Hector Ramirez	Associate Professor, Federico Santa María Technical University	Supervisor

To my wife and cats.

Acknowledgment

First of all, I would like to express my deepest gratitude to my two supervisors, Dr. Hector Ramirez and Dr. Yann Le Gorrec, for giving me the opportunity to work alongside them, for their constant encouragement to strive for excellence, and for teaching me through their example how to be both efficient and meticulous. Along these lines, I would like to extend a special thanks to Dr. Yongxin Wu, who was a tremendous support from the moment I arrived in Besançon, always willing to assist, both technically and personally. I would also like to express my gratitude to the members of the thesis jury for their valuable comments and feedback, which helped improve the final version of this manuscript.

I also want to express my heartfelt gratitude to Dr. Juan Yuz, who, without knowing me, took the time to respond to my inquiries and meet with me when I was full of uncertainty about joining the PhD program at UTFSM. His guidance and encouragement were pivotal, and his words played a significant role in helping me take the leap that I now proudly complete. I will always be grateful for his support during that crucial moment. I also extend my appreciation to the entire Department of Electronic Engineering at UTFSM for their ongoing encouragement throughout my academic journey.

My sincere thanks also go to the members of the French-Dutch-German Doctoral College: Port-Hamiltonian Systems, Modeling, Numerics and Control and the Advanced Center for Electrical and Electronic Engineering (AC3E) for their support and for fostering an environment of intellectual exchange. I deeply appreciate the opportunity to engage with such inspiring individuals in both of these vibrant communities.

To the incredible individuals I had the privilege to meet during my time at FEMTO-ST, thank you: Ning Liu, Amal Hammoud, Javier Caballería, Ignacio Díaz, Mario Vargas, Liseth Pasaguayo, Rafael Orita, Lavinia Lanting, María Isabel Haro, Lorenzo Masucci, and especially Nelson Cisneros. Your companionship, support, and insights were invaluable to me.

To my high school friends, who have remained close and supportive throughout the years: Juan Pablo Díaz, Ignacio Fernandez, Pablo Leyton, Claudio Daza, Rodrigo Arro, Diego Castro, and Erick Saavedra. I am also grateful to my friends from mechanical engineering: Felipe Cuevas, Cristian Michell, Omar Castillo, Carlos Barrientos, José Carlos Turra, Tomás Herrera, Santiago Henríquez, and Roberto Quinteros, who stood by me through every step of this journey.

Lastly, and with the deepest sense of gratitude, I want to thank my family—my parents, sisters, uncles, aunts, cousins, and grandparents. Your love and belief in me have been a constant source of strength. To my parents in-laws, brothers-in-law, and sisters-in-law, thank you for your warmth and encouragement. Finally, my most profound thanks go to my beloved wife, Andrea Sanhueza. Your unwavering support, patience, advice, and love have been my guiding light through this entire journey. Without you, none of this would have been possible.

Cristobal Ponce Salazar
January 10, 2025

Preface

This thesis has been developed under a cotutelle agreement between the Universidad Técnica Federico Santa María (UTFSM) in Chile and the Université Bourgogne-Franche-Comté (UBFC) in France. The first two years of the doctoral program were conducted in Chile at the Advanced Center for Electrical and Electronic Engineering (AC3E), while the subsequent two years were carried out in France at the research institute Franche-Comté Électronique Mécanique Thermique et Optique - Sciences et Technologies (FEMTO-ST). The research was supported by the following projects: ANID/Becas/Doctorado Nacional/2021-21211290, ECOS-ANID 220040, and ANID/BASAL FB0008 from the Chilean side, and the ISITE-BFC project - CPHS2D - ANR-15-IDEX-0003 from the French side.

The primary focus of this work is on the modeling and discretization of mechanical systems using the continuum mechanics approach. Given the significance of a solid understanding of this field, a comprehensive introduction to continuum mechanics is provided in Appendix A. It is highly recommended that readers who are not familiar with this topic consult this appendix, particularly before engaging with Chapter II, where the discussion builds upon this foundational background. Although each chapter briefly revisits key concepts, detailed explanations are reserved for the appendix to maintain clarity and focus within the main chapters.

A substantial portion of the discussion in Chapter III, which addresses mixed Finite Element discretization of linear port-Hamiltonian systems, was influenced by discussions with Tobias Thoma and Paul Kotyczka from the Technical University of Munich (TUM) during my internship. I extend my deepest gratitude to them for their valuable insights and feedback, which were instrumental in shaping the content presented in that chapter.

Due to the extensive notation required to describe the introduced variables, the notation is frequently redefined and overwritten in each chapter. Each chapter is self-contained in this respect, but readers are advised to be aware of these potential changes in notation throughout the manuscript.

Finally, this work represents a four-year effort and an important milestone in my academic career. I sincerely hope that it will prove useful and contribute meaningfully to the fields of modeling, discretization, and control of flexible mechanical systems, particularly within the framework of port-Hamiltonian systems.

Cristobal Ponce Salazar
January 10, 2025

Contents

List of Figures

Summary in French

S.1 Introduction

Cette section présente la motivation, les objectifs et les principales contributions de la thèse. Elle se concentre sur la modélisation et la discrétisation spatiale préservant la structure des systèmes mécaniques flexibles dans le cadre formel des systèmes port-Hamiltoniens (PHS). La recherche vise à faire progresser la conception de commande en forme basée sur l'énergie, apportant des améliorations à la modélisation et au commande des systèmes.

S.1.1 Motivation

Modélisation: Les corps flexibles qui subissent de grands déplacements et déformations sont courants dans des disciplines d'ingénierie telles que la mécanique, la biomécanique, l'aéronautique, la robotique, entre autres. L'incorporation de non-linéarités dans les modèles, que ce soit à travers la description géométrique du mouvement ou à travers les relations constitutives du matériau, est essentielle pour prédire avec précision des comportements réalistes dans ces domaines.

Discrétisation: Les méthodes de discrétisation basées sur la méthode des éléments finis (FEM) se sont révélées efficaces pour trouver des modèles approximatifs destinés à la simulation et à la conception des correcteurs pour des systèmes décrits sur des géométries complexes, comme illustré dans la Fig. 1a montrant la réponse électromécanique d'un actionneur diélectrique élastomère (DEA), et dans la Fig. 1b illustrant le modèle d'un cœur biologique.

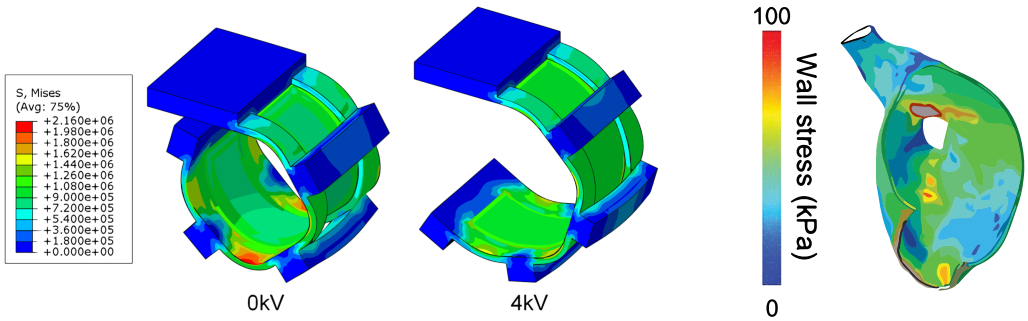

(a) Actionneur diélectrique à élastomère [Zhou 2019] (b) Cœur [Ozturk 2022]

Figure 1 – Exemples d'application de FEM.

Commande en forme: La commande des systèmes flexibles est un domaine important dans les sciences de l'ingénierie en raison de ses applications variées, y compris la réduction des niveaux de vibration et l'obtention de déformations précises, ce qui est connu sous le nom de commande en forme. Les applications du commande en forme comprennent la compensation des erreurs de surface résultant de la fabrication ou des déformations thermiques, ainsi que la commande des réponses acoustiques [Agrawal 1997]. De plus, ce domaine trouve des applications potentielles dans la robotique continue et souple, comme l'illustre la Fig. 2a montrant un robot parallèle continu [Childs 2021], et dans la Fig. 2a montrant une pince flexible souple basée sur des actionneurs électrostatiques auto-réparateurs amplifiés par hydraulique (HASEL) Yoder 2023.

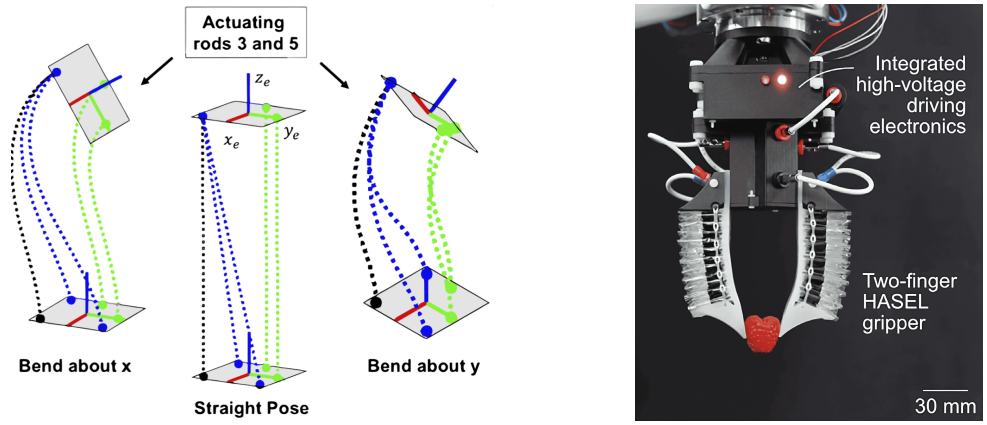

(a) Robot parallèle continu [Childs 2021] (b) Pince souple HASEL [Yoder 2023]

Figure 2 – Exemples d'applications de commande.

Systèmes port-Hamiltoniens: Le formalisme port-Hamiltonien (PH) offre un cadre géométrique pour la modélisation et la commande de systèmes multiphysiques complexes non linéaires, considérés comme l'interconnexion de sous-systèmes plus simples. Parmi ses caractéristiques notables figurent la passivité, le flux d'énergie entre les sous-systèmes, la séparation de la structure d'interconnexion des relations constitutives et des effets dissipatifs [Duindam 2009]. La conception de correcteurs utilisant les formulations de passivité et de PH implique de configurer des fonctions d'énergie en boucle fermée et/ou de modifier la structure d'interconnexion et les fonctions de dissipation afin que le système se comporte avec les propriétés souhaitées.

Objectif de la thèse: Cette thèse vise à unifier la modélisation, la discrétisation et la commande en forme d'une classe de systèmes mécaniques flexibles multidimensionnels, y compris ceux avec des contraintes algébriques, en utilisant le cadre PHS.

S.1.2 Organisation de la thèse et contributions

Chapitre I: Ce chapitre aborde la motivation derrière les approches de modélisation et de discrétisation destinées à la simulation et au commande en forme des systèmes mécaniques flexibles multidimensionnels. Il examine les caractéristiques clés du cadre port-Hamiltonien à la fois en dimensions finies et infinies, y compris les extensions aux systèmes dissipatifs et aux systèmes avec des contraintes algébriques imposées par des multiplicateurs de Lagrange. Enfin, le chapitre présente une revue de la littérature pour contextualiser l'état de l'art et comprendre les contributions de cette thèse.

Chapitre II: Le chapitre propose des méthodologies de modélisation systématiques basées sur le principe de Hamilton généralisé étendu pour la modélisation de systèmes mécaniques linéaires, non linéaires et non linéaires contraints flexibles en tant que PHS. Il propose quatre méthodologies de modélisation systématiques pour obtenir des représentations PH de systèmes multidimensionnels:

- Systèmes mécaniques linéaires en tant que PHS explicite.
- Systèmes mécaniques non linéaires en tant que PHS explicite.
- Systèmes mécaniques non linéaires contraints en tant que PH-DAE implicite.
- Systèmes mécaniques non linéaires contraints en tant que PHS explicite.

Chapitre III: Le chapitre propose des formulations faibles pour des systèmes mécaniques de dimension infinie basées sur la méthode mLLM et une extension naturelle du principe de puissance virtuelle, rappelant le principe de Hamilton généralisé étendu. En conséquence, il propose trois approches FEM mixtes pour la discrétisation préservant la structure des systèmes mécaniques flexibles multidimensionnels. Ces approches sont:

- Approche à deux champs pour la discrétisation des PHS linéaires.
- Approche à trois champs pour la discrétisation des PHS non linéaires.
- Approche à quatre champs pour la discrétisation des PH-DAE non linéaires.

Chapitre IV: Le chapitre propose une classe de correcteurs PH de dimension finie synthétisés à partir d'une représentation d'ordre faible d'un PHS linéaire discrétisé de haute dimension (grande échelle). Les principales contributions sont que la stratégie de commande:

- Est applicable à un large éventail de systèmes, qu'ils soient entièrement actionnés ou sous-actionnés, avec actionnement aux limites et/ou en domaine.
- Permet d'affecter indépendamment la réponse dynamique, atteignant la configuration d'équilibre optimale et les taux d'atténuation des oscillations souhaités.
- Fournit une marge de stabilité asymptotique qui garantit la stabilité dans le modèle discretisé de haute dimension.

Chapitre V: Ce chapitre fournit des conclusions sur les résultats des chapitres précédents et décrit les orientations de recherche futures. Il synthétise les résultats clés, met en lumière les avancées en matière de modélisation, de discrétisation et de commande des systèmes mécaniques flexibles dans le cadre PHS, et suggère de nouvelles lignes de recherche pour une investigation plus approfondie et des applications potentielles.

S.2 Modélisation des systèmes flexibles

En cette section, un résumé concis des résultats liés à la modélisation de systèmes flexibles basés sur l'élasticité linéaire, non linéaire et avec contraintes est présenté. Une discussion détaillée sur les méthodologies systématiques pour dériver de tels modèles et des exemples d'applications peut être trouvée au Chapitre II.

S.2.1 Systèmes linéaires

Soit $x(\mathtt{X},t) = [p(\mathtt{X},t)^\top \ \epsilon(\mathtt{X},t)^\top \ r(\mathtt{X},t)^\top]^\top \in \mathbb{R}^{2n+m}$ les variables d'énergie, et $\delta_x H(x) = [e_p(\mathtt{X},t)^\top \ e_\epsilon(\mathtt{X},t)^\top \ -b(\mathtt{X})^\top]^\top \in \mathbb{R}^{2n+m}$ les variables de co-énergie. La dynamique du système définit un PHS linéaire de dimension infinie de la forme:

$$\underbrace{\begin{bmatrix}\dot p(\mathtt{X},t)\\ \dot\epsilon(\mathtt{X},t)\\ \dot r(\mathtt{X},t)\end{bmatrix}}_{\dot x(\mathtt{X},t)} = \underbrace{\begin{bmatrix}0 & -\mathcal{F}_{\mathtt{x}}{}^* & -1\\ \mathcal{F}_{\mathtt{x}} & 0 & 0\\ 1 & 0 & 0\end{bmatrix}}_{\mathcal{J}=-\mathcal{J}^*}\underbrace{\begin{bmatrix}e_p(\mathtt{X},t)\\ e_\epsilon(\mathtt{X},t)\\ -b(\mathtt{X})\end{bmatrix}}_{\delta_x H} + \underbrace{\begin{bmatrix}B_d\\ 0\\ 0\end{bmatrix}}_{\mathcal{G}} u_d(\mathtt{X},t)$$

$$y_d(\mathtt{X},t) = \mathcal{G}^*\delta_x H = B_d^\top e_p(\mathtt{X},t)$$

$$u_\partial(\mathtt{S},t) = [\tau_N(\mathtt{S},t)^\top \ v_D(\mathtt{S},t)^\top]^\top, \quad y_\partial(\mathtt{S},t) = [v_N(\mathtt{S},t)^\top \ \tau_D(\mathtt{S},t)^\top]^\top$$

$$H(x) = \int_\Omega \left(\frac{1}{2}\, p(\mathtt{X},t)^\top \mathcal{M}(\mathtt{X})^{-1} p(\mathtt{X},t) + \frac{1}{2}\,\epsilon(\mathtt{X},t)^\top \mathcal{K}_\epsilon(\mathtt{X})\epsilon(\mathtt{X},t) - r(\mathtt{X},t)^\top b(\mathtt{X})\right) d\mathtt{X},$$

avec $p(\mathtt{X},t) = \mathcal{M}(\mathtt{X})\dot r(\mathtt{X},t)$ le vecteur de quantité de mouvement généralisée, et les tractions et vitesses généralisées données par:

$$\begin{aligned}\tau_N(\mathtt{S},t) &= F_\partial\, e_\epsilon(\mathtt{S},t), \quad v_N(\mathtt{S},t) = e_p(\mathtt{S},t) \quad (\text{sur } \partial\Omega_N),\\ \tau_D(\mathtt{S},t) &= F_\partial\, e_\epsilon(\mathtt{S},t), \quad v_D(\mathtt{S},t) = e_p(\mathtt{S},t) \quad (\text{sur } \partial\Omega_D),\end{aligned}$$

où F_∂ est une matrice de frontière induite par l'opérateur $\mathcal{F}_{\mathtt{x}}$.

Dans le PHS linéaire en dimension infinie ci-dessus, $\mathcal{J} = -\mathcal{J}^*$ est l'opérateur différentiel linéaire anti-symétrique (opérateur d'interconnexion), et $\delta_x H(x)$ désigne la dérivée variationnelle de $H(x)$ par rapport à $x(\mathtt{X},t)$. L'énergie totale est donnée par l'Hamiltonien $H(x)$, où $\mathcal{M}(\mathtt{X}) = \mathcal{M}(\mathtt{X})^\top > 0 \in \mathbb{R}^{n\times n}$ est la matrice de densité de masse, et $\mathcal{K}_\epsilon(\mathtt{X}) = \mathcal{K}_\epsilon(\mathtt{X})^\top > 0 \in \mathbb{R}^{m\times m}$ est la matrice de densité

de rigidité. À partir des variables d'énergie, $p(\mathtt{X},t) = \mathcal{M}(\mathtt{X})\dot{r}(\mathtt{X},t) \in \mathbb{R}^n$ est la quantité de mouvement généralisée avec $r(\mathtt{X},t) \in \mathbb{R}^n$ le déplacement généralisé, et $\epsilon(\mathtt{X},t) = \mathcal{F}_{\mathtt{x}}\, r(\mathtt{X},t) \in \mathbb{R}^m$ est la déformation généralisée (représentant la cinématique, relation déformation-déplacement). À partir des variables de co-énergie, $e_p(\mathtt{X},t) = \mathcal{M}(\mathtt{X})^{-1}\, p(\mathtt{X},t) = \dot{r}(\mathtt{X},t)$ est la vitesse généralisée, $e_\epsilon(\mathtt{X},t) = \mathcal{K}_\epsilon(\mathtt{X})\, \epsilon(\mathtt{X},t)$ est l'effort généralisée (représentant la loi de Hooke, relation effort-déformation), et $b(\mathtt{X})$ est la force généralisée, généralement considérée comme le poids du corps. À partir des entrées et sorties de frontière, $\tau_D(\mathtt{S},t)$, $\tau_N(\mathtt{S},t)$ et $v_D(\mathtt{S},t)$, $v_N(\mathtt{S},t) \in \mathbb{R}^n$ sont les tractions et vitesses généralisées aux frontières, respectivement. Enfin, $\partial\Omega_D$ et $\partial\Omega_N$ représentent respectivement les parties Dirichlet et Neumann de la frontière.

S.2.2 Systèmes non linéaires

Dans les représentations PHS de systèmes non linéaires, l'opérateur différentiel est désormais modulé par le déplacement généralisé, c'est-à-dire $\mathcal{F}_{\mathtt{x}}(r)$, représentant la non-linéarité géométrique due aux grandes déformations. L'énergie potentielle élastique n'est plus une fonction quadratique de la déformation généralisée $\epsilon(\mathtt{X},t)$ et de la matrice de densité de rigidité $\mathcal{K}_\epsilon(\mathtt{X})$, mais est maintenant donnée par une fonction non linéaire $\Psi(\epsilon) \in \mathbb{R}$ qui représente la fonction de densité d'énergie de déformation généralisée modélisant le comportement hyperélastique du matériau.

Alors, soit $x(\mathtt{X},t) = [p(\mathtt{X},t)^\top\ \epsilon(\mathtt{X},t)^\top\ r(\mathtt{X},t)^\top]^\top \in \mathbb{R}^{2n+m}$ les variables d'énergie, et $\delta_x H(x) = [e_p(\mathtt{X},t)^\top\ e_\epsilon(\mathtt{X},t)^\top\ -b(\mathtt{X})^\top]^\top \in \mathbb{R}^{2n+m}$ les variables de co-énergie. La dynamique du système définit un PHS non linéaire de dimension infinie de la forme:

$$\underbrace{\begin{bmatrix}\dot{p}(\mathtt{X},t)\\ \dot{\epsilon}(\mathtt{X},t)\\ \dot{r}(\mathtt{X},t)\end{bmatrix}}_{\dot{x}(\mathtt{X},t)} = \underbrace{\begin{bmatrix}0 & -\mathcal{F}_{\mathtt{x}}(r)^* & -1\\ \mathcal{F}_{\mathtt{x}}(r) & 0 & 0\\ 1 & 0 & 0\end{bmatrix}}_{\mathcal{J}(x)=-\mathcal{J}(x)^*} \underbrace{\begin{bmatrix}e_p(\mathtt{X},t)\\ e_\epsilon(\mathtt{X},t)\\ -b(\mathtt{X})\end{bmatrix}}_{\delta_x H} + \underbrace{\begin{bmatrix}B_d\\ 0\\ 0\end{bmatrix}}_{\mathcal{G}} u_d(\mathtt{X},t)$$

$$y_d(\mathtt{X},t) = \mathcal{G}^*\delta_x H = B_d^\top e_p(\mathtt{X},t)$$

$$u_\partial(\mathtt{S},t) = [\tau_N(\mathtt{S},t)^\top\ v_D(\mathtt{S},t)^\top]^\top, \quad y_\partial(\mathtt{S},t) = [v_N(\mathtt{S},t)^\top\ \tau_D(\mathtt{S},t)^\top]^\top$$

$$H(x) = \int_\Omega \left(\frac{1}{2}\, p(\mathtt{X},t)^\top \mathcal{M}(\mathtt{X})^{-1} p(\mathtt{X},t) + \Psi(\epsilon(\mathtt{X},t)) - r(\mathtt{X},t)^\top b(\mathtt{X})\right) d\mathtt{X},$$

avec $p(\mathtt{X},t) = \mathcal{M}(\mathtt{X})\dot{r}(\mathtt{X},t)$ le vecteur de quantité de mouvement généralisée, et les tractions et vitesses généralisées données par:

$$\begin{aligned}\tau_N(\mathtt{S},t) &= F_\partial(r)\, e_\epsilon(\mathtt{S},t), \quad v_N(\mathtt{S},t) = e_p(\mathtt{S},t) \quad (\text{sur } \partial\Omega_N),\\ \tau_D(\mathtt{S},t) &= F_\partial(r)\, e_\epsilon(\mathtt{S},t), \quad v_D(\mathtt{S},t) = e_p(\mathtt{S},t) \quad (\text{sur } \partial\Omega_D),\end{aligned}$$

où $F_\partial(r)$ est une matrice de frontière induite par l'opérateur $\mathcal{F}_{\mathtt{x}}(r)$.

S.2.3 Systèmes non linéaires avec contraintes

Les modèles précédents peuvent être étendus à la forme PH-DAE en incluant des contraintes algébriques du type $\gamma(\epsilon) = 0 \in \mathbb{R}$, qui sont imposées par un multiplicateur de Lagrange $\lambda(\mathtt{X}, t) \in \mathbb{R}$. En dérivant temporellement la contrainte, nous obtenons la relation $0 = \mathcal{L}_{\mathtt{x}}(\epsilon, r)\, e_p(\mathtt{X}, t)$, où $\mathcal{L}_{\mathtt{x}}(\epsilon, r)$ est un opérateur différentiel modulé par la déformation et le déplacement généralisés.

Alors, considérons $x(\mathtt{X}, t) = [p(\mathtt{X}, t)^\top\ \epsilon(\mathtt{X}, t)^\top\ r(\mathtt{X}, t)^\top\ \lambda(\mathtt{X}, t)]^\top \in \mathbb{R}^{2n+m+1}$ comme les variables d'énergie, et $\mathcal{Z}(\mathtt{X}, t) = [e_p(\mathtt{X}, t)^\top\ e_\epsilon(\mathtt{X}, t)^\top - b(\mathtt{X})^\top\ \lambda(\mathtt{X}, t)]^\top \in \mathbb{R}^{2n+m+1}$ comme la fonction d'effort. La dynamique du système avec contraintes définit un PH-DAE non linéaire de dimension infinie de la forme:

$$\underbrace{\begin{bmatrix} 1 & 0 & 0 & 0 \\ 0 & 1 & 0 & 0 \\ 0 & 0 & 1 & 0 \\ 0 & 0 & 0 & 0 \end{bmatrix}}_{\mathcal{E}} \underbrace{\begin{bmatrix} \dot{p}(\mathtt{X}, t) \\ \dot{\epsilon}(\mathtt{X}, t) \\ \dot{r}(\mathtt{X}, t) \\ \dot{\lambda}(\mathtt{X}, t) \end{bmatrix}}_{\dot{x}} = \underbrace{\begin{bmatrix} 0 & -\mathcal{F}_{\mathtt{x}}(r)^* & -1 & -\mathcal{L}_{\mathtt{x}}(\epsilon, r)^* \\ \mathcal{F}_{\mathtt{x}}(r) & 0 & 0 & 0 \\ 1 & 0 & 0 & 0 \\ \mathcal{L}_{\mathtt{x}}(\epsilon, r) & 0 & 0 & 0 \end{bmatrix}}_{\mathcal{J}(x) = -\mathcal{J}(x)^*} \underbrace{\begin{bmatrix} e_p(\mathtt{X}, t) \\ e_\epsilon(\mathtt{X}, t) \\ -b(\mathtt{X}) \\ \lambda(\mathtt{X}, t) \end{bmatrix}}_{\mathcal{Z}(\mathtt{X}, t)} + \underbrace{\begin{bmatrix} B_d \\ 0 \\ 0 \\ 0 \end{bmatrix}}_{\mathcal{G}} u_d(\mathtt{X}, t)$$

$$y_d(\mathtt{X}, t) = \mathcal{G}^* \mathcal{Z}(\mathtt{X}, t) = B_d^\top e_p(\mathtt{X}, t)$$

$$u_\partial(\mathtt{S}, t) = [\tau_N(\mathtt{S}, t)^\top\ v_D(\mathtt{S}, t)^\top]^\top, \quad y_\partial(\mathtt{S}, t) = [v_N(\mathtt{S}, t)^\top\ \tau_D(\mathtt{S}, t)^\top]^\top$$

$$H(x) = \int_\Omega \left(\frac{1}{2}\, p(\mathtt{X}, t)^\top \mathcal{M}(\mathtt{X})^{-1} p(\mathtt{X}, t) + \Psi(\epsilon(\mathtt{X}, t)) - r(\mathtt{X}, t)^\top b(\mathtt{X}) \right) d\mathtt{X},$$

avec $p(\mathtt{X}, t) = \mathcal{M}(\mathtt{X})\dot{r}(\mathtt{X}, t)$ le vecteur de quantité de mouvement généralisée, et les tractions et vitesses généralisées données par:

$$\tau_N(\mathtt{S}, t) = F_\partial(r)\, e_\epsilon(\mathtt{S}, t) + L_\partial(\epsilon, r)\lambda(\mathtt{S}, t), \quad v_N(\mathtt{S}, t) = e_p(\mathtt{S}, t) \quad (\text{sur } \partial\Omega_N),$$
$$\tau_D(\mathtt{S}, t) = F_\partial(r)\, e_\epsilon(\mathtt{S}, t) + L_\partial(\epsilon, r)\lambda(\mathtt{S}, t), \quad v_D(\mathtt{S}, t) = e_p(\mathtt{S}, t) \quad (\text{sur } \partial\Omega_D),$$

où $F_\partial(r)$ et $L_\partial(\epsilon, r)$ sont des matrices de frontière induites par les opérateurs $\mathcal{F}_{\mathtt{x}}(r)$ et $\mathcal{L}_{\mathtt{x}}(\epsilon, r)$, respectivement.

S.3 Discrétisation spatiale qui préserve la structure

Dans cette section, nous résumons les résultats relatifs au développement de stratégies de discrétisation basées sur des éléments finis mixtes. La première concerne les systèmes PHS linéaires et la méthode est basée sur la méthode modifiée des multiplicateurs de Lagrange liés. La deuxième approche repose sur un principe de puissance virtuelle dérivé du principe de Hamilton généralisé, ce qui permet de discrétiser des systèmes PHS non linéaires. Enfin, ce principe est étendu pour incorporer des contraintes algébriques afin de discrétiser les PH-DAE. Les détails peuvent être trouvés dans le Chapitre III.

S.3.1 Systèmes linéaires

Suivant la méthode modifiée des multiplicateurs de Lagrange liés, où $\Omega_D \subset \Omega$ est défini comme le domaine de Dirichlet (tous les éléments en contact avec $\partial\Omega_D$), la forme faible locale du PHS linéaire de dimension infinie est donnée par:

$$\begin{aligned}
\delta P_p^e(\dot{r}^e, e_\epsilon^e) = &\int_{\Omega^e} \delta\dot{r}^e(\mathtt{X},t)\cdot(\dot{p}^e(\mathtt{X},t) + \mathcal{F}_{\mathtt{x}}{}^* e_\epsilon^e(\mathtt{X},t) - b^e(\mathtt{X}) - B_d u_d^e(\mathtt{X},t))\, d\mathtt{X} ... \\
&... + \int_{\partial\Omega_N^e} \delta\dot{r}^e(\mathtt{S},t)\cdot(F_\partial(\mathtt{S}) e_\epsilon^e(\mathtt{S},t) - \tau_N^e(\mathtt{S},t))\, d\mathtt{S} ... \\
&... + \frac{1}{\beta}\int_{\Omega_D^e} \delta\dot{\epsilon}^e(\mathtt{X},t)\cdot(e_\epsilon^e(\mathtt{X},t) - \mathcal{K}_\epsilon(\mathtt{X})\,\epsilon^e(\mathtt{X},t))\, d\mathtt{X}, \\
\delta P_e^e(\dot{r}^e, e_\epsilon^e) = &\frac{1}{\beta}\int_{\Omega_D^e} \delta e_\epsilon^e(\mathtt{X},t)\cdot(\dot{\epsilon}^e(\mathtt{X},t) - \mathcal{F}_{\mathtt{x}}\dot{r}^e(\mathtt{X},t))\, d\mathtt{X} ... \\
&... + \int_{\partial\Omega_D^e} \delta e_\epsilon^e(\mathtt{S},t)\cdot F_\partial(\mathtt{S})^\top(\dot{r}^e(\mathtt{S},t) - v_D^e(\mathtt{S},t))\, d\mathtt{S},
\end{aligned}$$

où $\beta > 1$ est le facteur de liaison. De plus, l'Hamiltonien dans chaque élément est écrit comme: $H^e(\dot{r}^e, r^e, e_\epsilon^e) = T^e(\dot{r}^e) + U_T^e(r^e) + \Delta U_{\Omega_D^e}^e(r^e, e_\epsilon^e)$, où $T^e(\dot{r}^e)$ et $U_T^e(r^e)$ représentent respectivement l'énergie cinétique et l'énergie potentielle totale, et $\Delta U_{\Omega_D^e}^e(r^e, e_\epsilon^e)$ représente l'énergie potentielle élastique liée sur Ω_D, donnée par: $\Delta U_{\Omega_D^e}^e(r^e, e_\epsilon^e) = \frac{1}{\beta}\left[U^e(e_\epsilon^e) - U^e(r^e)\right]_{\Omega_D^e} = 0$, avec $U^e(r^e)$ l'énergie potentielle élastique exprimée en fonction de $r(\mathtt{X},t)$, et $U^e(e_\epsilon^e)$ l'énergie potentielle élastique exprimée en fonction de $e_\epsilon(\mathtt{X},t)$ et de la matrice de densité de conformité $\mathcal{C}_\epsilon(\mathtt{X}) = \mathcal{K}_\epsilon(\mathtt{X})^{-1}$.

La discrétisation qui préserve la structure du PHS linéaire de dimension infinie basée sur la formulation faible ci-dessus, utilisant des approximations locales:

$$\begin{aligned}
&\tilde{r}^e(\mathtt{X},t) = N_r^e(\mathtt{X})\,\hat{r}^e(t), \quad && \delta\tilde{r}^e(\mathtt{X},t) = N_r^e(\mathtt{X})\,\delta\hat{r}^e(t), \quad && v_D^e(\mathtt{S},t) = N_{r_D}^e(\mathtt{S})\,\hat{v}_D^e(t), \\
&\tilde{e}_\epsilon^e(\mathtt{X},t) = N_e^e(\mathtt{X})\,\hat{e}_{\epsilon_D}^e(t), && \delta\tilde{e}_\epsilon^e(\mathtt{X},t) = N_e^e(\mathtt{X})\,\delta\hat{e}_{\epsilon_D}^e(t), && \tau_N^e(\mathtt{S},t) = N_{\tau_N}^e(\mathtt{S})\,\hat{\tau}_N^e(t), \\
&u_d^e(\mathtt{X},t) = N_{u_d}^e(\mathtt{X})\,\hat{u}_d^e(t), &&&&
\end{aligned}$$

conduit au PHS linéaire de dimension finie de la forme:

$$\begin{aligned}
\underbrace{\begin{bmatrix}\dot{\hat{p}}(t)\\ \dot{\hat{\epsilon}}_D(t)\\ \dot{\hat{r}}(t)\end{bmatrix}}_{\dot{\hat{x}}(t)} &= \underbrace{\begin{bmatrix}0 & -\hat{F}_D^\top & -I_{N_\Omega}\\ \hat{F}_D & 0 & 0\\ I_{N_\Omega} & 0 & 0\end{bmatrix}}_{\hat{J}=-\hat{J}^\top}\underbrace{\begin{bmatrix}\hat{e}_p(t)\\ \hat{e}_{\epsilon_D}(t)\\ \hat{e}_r(t)\end{bmatrix}}_{\nabla_{\hat{x}}\hat{H}_{LLM}(\hat{x})} + \underbrace{\begin{bmatrix}\hat{B}_d & \hat{B}_{\tau_N} & 0\\ 0 & 0 & \hat{B}_D\\ 0 & 0 & 0\end{bmatrix}}_{\hat{G}}\underbrace{\begin{bmatrix}\hat{u}_d(t)\\ \hat{\tau}_N(t)\\ \hat{v}_D(t)\end{bmatrix}}_{\hat{u}(t)} \\
\hat{y}(t) &= \hat{G}^\top\nabla_{\hat{x}}\hat{H}_{LLM}(\hat{x})
\end{aligned}$$

$$\hat{H}_{LLM}(\hat{x}) = \frac{1}{2}\,\hat{p}(t)^\top\hat{M}^{-1}\hat{p}(t) + \frac{1}{2}\,\hat{r}(t)^\top\hat{K}_r\,\hat{r}(t) - \hat{r}(t)^\top\hat{b} + \Delta\hat{U}_{\Omega_D}(\hat{r},\hat{\epsilon}_D),$$

$$\Delta\hat{U}_{\Omega_D}(\hat{r},\hat{\epsilon}_D) = \frac{1}{2}\hat{\epsilon}_D(t)^\top\hat{C}_{\epsilon_D}^{-1}\,\hat{\epsilon}_D(t) - \frac{1}{2}\,\hat{r}(t)^\top\hat{K}_D\,\hat{r}(t),$$

où $\hat{p}(t) = \hat{M}\dot{\hat{r}}(t)$ et $\hat{\epsilon}_{_D}(t) = \hat{C}_{\epsilon_D}\,\hat{e}_{\epsilon_D}(t)$ sont les variables de quantité de mouvement généralisée et de déformation discrètes, et $\hat{e}_r(t) = (\hat{K}_r - \hat{K}_{_D})\,\hat{r}(t) - \hat{b}$ est le gradient de $\hat{H}_{LLM}(\hat{x})$ par rapport à $\hat{r}(t)$. La façon d'obtenir les matrices discrétisées est expliquée en détail dans le Chapitre III à la Section III.3.1.

S.3.2 Systèmes non linéaires

La forme faible locale du PHS non linéaire de dimension infinie, suivant le principe de la puissance virtuelle dérivé du principe de Hamilton généralisé, est donnée par:

$$\begin{aligned}
\delta P_p^e &= \int_{\Omega^e} \delta\dot{r}^e(\mathtt{X},t)\cdot(\dot{p}^e(\mathtt{X},t) + \mathcal{F}_{\mathtt{x}}(r^e)^* e_\epsilon^e(\mathtt{X},t) - b^e(\mathtt{X}) - B_d u_d^e(\mathtt{X},t))\,d\mathtt{X}... \\
&\qquad ... + \int_{\partial\Omega_N^e} \delta\dot{r}^e(\mathtt{S},t)\cdot(F_\partial(r^e)e_\epsilon^e(\mathtt{S},t) - \tau_N^e(\mathtt{S},t))\,d\mathtt{S}, \\
\delta P_e^e &= \int_{\Omega^e} \delta e_\epsilon^e(\mathtt{X},t)\cdot(\dot{\epsilon}^e(\mathtt{X},t) - \mathcal{F}_{\mathtt{x}}(r^e)\dot{r}^e(\mathtt{X},t))\,d\mathtt{X}... \\
&\qquad ... + \int_{\partial\Omega_D^e} \delta e_\epsilon^e(\mathtt{S},t)\cdot F_\partial(r^e)^\top(\dot{r}^e(\mathtt{S},t) - v_D^e(\mathtt{S},t))\,d\mathtt{S}, \\
\delta P_\epsilon^e &= \int_{\Omega^e} \delta\dot{\epsilon}^e(\mathtt{X},t)\cdot\left(e_\epsilon^e(\mathtt{X},t) - \frac{\partial\Psi}{\partial\epsilon}\Big|_{\epsilon=\tilde{\epsilon}^e(\mathtt{X},t)}\right)d\mathtt{X},
\end{aligned}$$

où $r(\mathtt{X},t)$, $\epsilon(\mathtt{X},t)$, et $e_\epsilon(\mathtt{X},t)$ sont traités comme des champs indépendants.

La discrétisation qui préserve la structure du PHS non linéaire de dimension infinie basée sur la formulation faible ci-dessus, en utilisant des approximations locales:

$$\begin{aligned}
&\tilde{r}^e(\mathtt{X},t) = N_r^e(\mathtt{X})\,\hat{r}^e(t), \quad && \delta\tilde{r}^e(\mathtt{X},t) = N_r^e(\mathtt{X})\,\delta\hat{r}^e(t), \quad && v_D^e(\mathtt{S},t) = N_{r_D}^e(\mathtt{S})\,\hat{v}_D^e(t), \\
&\tilde{e}_\epsilon^e(\mathtt{X},t) = N_e^e(\mathtt{X})\,\hat{e}^e(t), \quad && \delta\tilde{e}_\epsilon^e(\mathtt{X},t) = N_e^e(\mathtt{X})\,\delta\hat{e}^e(t), \quad && \tau_N^e(\mathtt{S},t) = N_{\tau_N}^e(\mathtt{S})\,\hat{\tau}_N^e(t), \\
&\tilde{\epsilon}^e(\mathtt{X},t) = N_\epsilon^e(\mathtt{X})\,\hat{\epsilon}^e(t), \quad && \delta\tilde{\epsilon}^e(\mathtt{X},t) = N_\epsilon^e(\mathtt{X})\,\delta\hat{\epsilon}^e(t), \quad && u_d^e(\mathtt{X},t) = N_{u_d}^e(\mathtt{X})\,\hat{u}_d^e(t),
\end{aligned}$$

conduit au PHS non linéaire de dimension finie sous la forme suivante:

$$\begin{aligned}
\underbrace{\begin{bmatrix}\dot{\hat{p}}(t)\\ \dot{\hat{\epsilon}}(t)\\ \dot{\hat{r}}(t)\end{bmatrix}}_{\dot{\hat{x}}(t)} &= \underbrace{\begin{bmatrix}0 & -\hat{F}_x(\hat{r})^\top & -I_{N_\Omega}\\ \hat{F}_x(\hat{r}) & 0 & 0\\ I_{N_\Omega} & 0 & 0\end{bmatrix}}_{\hat{J}(\hat{x})=-\hat{J}(\hat{x})^\top}\underbrace{\begin{bmatrix}\hat{e}_p(t)\\ \hat{e}_\epsilon(\hat{\epsilon})\\ -\hat{b}\end{bmatrix}}_{\nabla_{\hat{x}}\hat{H}_{GHP}(\hat{x})} + \underbrace{\begin{bmatrix}\hat{B}_d & \hat{B}_{\tau_N} & 0\\ 0 & 0 & \hat{B}_v(\hat{r})\\ 0 & 0 & 0\end{bmatrix}}_{\hat{G}(\hat{x})}\underbrace{\begin{bmatrix}\hat{u}_d(t)\\ \hat{\tau}_N(t)\\ \hat{v}_D(t)\end{bmatrix}}_{\hat{u}(t)} \\
\hat{y}(t) &= \hat{G}(\hat{x})^\top\nabla_{\hat{x}}\hat{H}_{GHP}(\hat{x}) \\
\hat{H}_{GHP}(\hat{x}) &= \frac{1}{2}\,\hat{p}(t)^\top\hat{M}^{-1}\hat{p}(t) + \hat{U}(\hat{\epsilon}) - \hat{r}(t)^\top\hat{b},
\end{aligned}$$

où $\hat{p}(t) = \hat{M}\dot{\hat{r}}(t)$ est la quantité de mouvement généralisée discrète, et $\hat{e}_\epsilon(\hat{\epsilon}) = \nabla_{\hat{\epsilon}}\hat{U}(\hat{\epsilon})$ est l'effort généralisée discrète. La façon d'obtenir les matrices discrétisées est expliquée en détail dans le Chapitre III à la Section III.3.2.

S.3.3 Systèmes non linéaires avec contraintes

La forme faible locale des systèmes PH-DAE non linéaires de dimension infinie, suivant le principe de puissance virtuelle dérivé du principe de Hamilton généralisé étendu, est donnée par:

$$
\begin{aligned}
\delta P_p^e &= \int_{\partial\Omega_N^e} \delta\dot{r}^e(\mathtt{S},t)\cdot(F_\partial(r^e)e_\epsilon^e(\mathtt{S},t)+L_\partial(\epsilon^e,r^e)\lambda^e(\mathtt{S},t)-\tau_N^e(\mathtt{S},t))\,d\mathtt{S}...\\
&...+\int_{\Omega^e}\delta\dot{r}^e(\mathtt{X},t)\cdot(\dot{p}^e(\mathtt{X},t)+\mathcal{F}_\mathtt{x}(r^e)^*e_\epsilon^e(\mathtt{X},t)-b^e(\mathtt{X})+\mathcal{L}_\mathtt{x}(\epsilon^e,r^e)^*\lambda^e(\mathtt{X},t)-B_du_d^e(\mathtt{X},t))\,d\mathtt{X},\\
\delta P_e^e &= \int_{\Omega^e}\delta e_\epsilon^e(\mathtt{X},t)\cdot(\dot{\epsilon}^e(\mathtt{X},t)-\mathcal{F}_\mathtt{x}(r^e)\dot{r}^e(\mathtt{X},t))\,d\mathtt{X}...\\
&\qquad ...+\int_{\partial\Omega_D^e}\delta e_\epsilon^e(\mathtt{S},t)\cdot F_\partial(r^e)^\top(\dot{r}^e(\mathtt{S},t)-v_D^e(\mathtt{S},t))\,d\mathtt{S},\\
\delta P_\epsilon^e &= \int_{\Omega^e}\delta\dot{\epsilon}^e(\mathtt{X},t)\cdot\left(e_\epsilon^e(\mathtt{X},t)-\frac{\partial\Psi}{\partial\epsilon}\Big|_{\epsilon=\tilde{\epsilon}^e(\mathtt{X},t)}\right)d\mathtt{X},\\
\delta P_\lambda^e &= -\int_{\Omega^e}\delta\lambda^e(\mathtt{X},t)\cdot\mathcal{L}_\mathtt{x}(\epsilon^e,r^e)\dot{r}^e(\mathtt{X},t))\,d\mathtt{X}...\\
&\qquad ...+\int_{\partial\Omega_D^e}\delta\lambda^e(\mathtt{S},t)\cdot L_\partial(\epsilon^e,r^e)^\top(\dot{r}^e(\mathtt{S},t)-v_D^e(\mathtt{S},t))\,d\mathtt{S},
\end{aligned}
$$

où $r(\mathtt{X},t)$, $\epsilon(\mathtt{X},t)$, $e_\epsilon(\mathtt{X},t)$ et $\lambda(\mathtt{X},t)$ sont traités comme des champs indépendants.

La discrétisation qui préserve la structure des systèmes PH-DAE non linéaires de dimension infinie, basée sur la formulation faible ci-dessus et utilisant des approximations locales:

$$
\begin{aligned}
&\tilde{r}^e(\mathtt{X},t)=N_r^e(\mathtt{X})\,\hat{r}^e(t), && \delta\tilde{r}^e(\mathtt{X},t)=N_r^e(\mathtt{X})\,\delta\hat{r}^e(t), && v_D^e(\mathtt{S},t)=N_{r_D}^e(\mathtt{S})\,\hat{v}_D^e(t),\\
&\tilde{e}_\epsilon^e(\mathtt{X},t)=N_e^e(\mathtt{X})\,\hat{e}^e(t), && \delta\tilde{e}_\epsilon^e(\mathtt{X},t)=N_e^e(\mathtt{X})\,\delta\hat{e}^e(t), && \tau_N^e(\mathtt{S},t)=N_{\tau_N}^e(\mathtt{S})\,\hat{\tau}_N^e(t),\\
&\tilde{\epsilon}^e(\mathtt{X},t)=N_\epsilon^e(\mathtt{X})\,\hat{\epsilon}^e(t), && \delta\tilde{\epsilon}^e(\mathtt{X},t)=N_\epsilon^e(\mathtt{X})\,\delta\hat{\epsilon}^e(t), && u_d^e(\mathtt{X},t)=N_{u_d}^e(\mathtt{X})\,\hat{u}_d^e(t),\\
&\tilde{\lambda}^e(\mathtt{X},t)=N_\lambda^e(\mathtt{X})\,\hat{\lambda}^e(t), && \delta\tilde{\lambda}^e(\mathtt{X},t)=N_\lambda^e(\mathtt{X})\,\delta\hat{\lambda}^e(t), &&
\end{aligned}
$$

conduit au systèmes PH-DAE non linéaires de dimension finie sous la forme:

$$
\begin{aligned}
\underbrace{\begin{bmatrix}\hat{E}\end{bmatrix}\begin{bmatrix}\dot{\hat{p}}(t)\\ \dot{\hat{\epsilon}}(t)\\ \dot{\hat{r}}(t)\\ \dot{\hat{\lambda}}(t)\end{bmatrix}}_{\dot{\hat{x}}(t)} &= \underbrace{\begin{bmatrix}0 & -\hat{F}_x(\hat{r})^\top & -I_{N_\Omega} & -\hat{L}_x(\hat{\epsilon},\hat{r})^\top\\ \hat{F}_x(\hat{r}) & 0 & 0 & 0\\ I_{N_\Omega} & 0 & 0 & 0\\ \hat{L}_x(\hat{\epsilon},\hat{r}) & 0 & 0 & 0\end{bmatrix}}_{\hat{J}(\hat{x})=-\hat{J}(\hat{x})^\top}\underbrace{\begin{bmatrix}\hat{e}_p(t)\\ \hat{e}_\epsilon(\hat{\epsilon})\\ -\hat{b}\\ \hat{\lambda}(t)\end{bmatrix}}_{\hat{Z}(\hat{x})}+\underbrace{\begin{bmatrix}\hat{B}_d & \hat{B}_{\tau_N} & 0\\ 0 & 0 & \hat{B}_v(\hat{r})\\ 0 & 0 & 0\\ 0 & 0 & \hat{B}_L(\hat{\epsilon},\hat{r})\end{bmatrix}}_{\hat{G}(\hat{x})}\underbrace{\begin{bmatrix}\hat{u}_d(t)\\ \hat{\tau}_N(t)\\ \hat{v}_D(t)\end{bmatrix}}_{\hat{u}(t)}\\
\hat{y}(t) &= \hat{G}(\hat{x})^\top\hat{Z}(\hat{x})
\end{aligned}
$$

$$
\hat{H}_{GHP}(\hat{x})=\frac{1}{2}\,\hat{p}(t)^\top\hat{M}^{-1}\hat{p}(t)+\hat{U}(\hat{\epsilon})-\hat{r}(t)^\top\hat{b},
$$

où $\hat{E} = \text{diag}\,(I_{N_\Omega}, I_{M_\Omega}, I_{N_\Omega}, 0_{NN_\Omega})$, $\hat{p}(t) = \hat{M}\dot{\hat{r}}(t)$ est la quantité de mouvement généralisée discrète, $\hat{e}_\epsilon(\hat{\epsilon}) = \nabla_{\hat{\epsilon}}\hat{U}(\hat{\epsilon})$ représente l'effort généralisée discrète, et $\nabla_{\hat{x}}\hat{H}_{GHP}(\hat{x}) = \hat{E}^\top\hat{Z}(\hat{x})$ définit les variables généralisée de co-énergie discrètes. La façon d'obtenir les matrices discrétisées est expliquée en détail dans le Chapitre III à la Section III.3.3.

S.4 Commande en forme basé sur l'énergie

Dans cette section, nous présentons de manière résumée les résultats concernant la commande en forme des systèmes linéaires. Nous montrons la classe de correcteurs dérivés à partir de modèles d'ordre réduit, qui stabilisent le système discrétisé d'ordre élevé autour d'une configuration optimale souhaitée. Les détails sont abordés dans le Chapitre IV.

En suivant la méthode de modelage d'énergie avec commande par interconnexion, la classe de correcteurs pour aborder la commande en forme est donnée par:

$$\begin{aligned} \dot{x}_c &= u_c \\ y_c &= \Sigma_c(\alpha)(x_c + C_0) - \Gamma_c(\alpha)\,\eta_c^\star + D_c\,u_c, \end{aligned}$$

où $\alpha > 0$ est un paramètre de réglage, avec $\alpha > 1$ pour des oscillations plus rapides et $\alpha < 1$ pour des oscillations plus lentes, toutes deux par rapport à la réponse en boucle ouverte. $\Sigma_c(\alpha)$ et $\Gamma_c(\alpha)$ sont des matrices conçues pour modifier les caractéristiques oscillatoires, D_c est une matrice conçue pour modifier le taux d'amortissement des oscillations, $\eta_c^\star$ est un vecteur conçu pour obtenir la meilleure approximation de la forme souhaitée, et C_0 est un invariant structurel du système.

Exemple: Commande en forme d'une plaque Mindlin

Dans cet exemple, nous considérons une plaque de Mindlin avec des entrées ponctuelles comme montré dans la Fig. 3. Nous notons $w_0(\mathtt{X}, t) \in \mathbb{R}$ comme le déplacement vertical, et $\psi(\mathtt{X}, t) = [\psi_1(\mathtt{X}, t)\ \psi_2(\mathtt{X}, t)]^\top \in \mathbb{R}^2$ les angles de rotation par la section transversale. La forme désirée pour $w_0(\mathtt{X}, t)$ est choisie comme:

$$f_w(\mathtt{X}) = (\cos(31.5X_1) - 1)(8(X_2 - 0.025)^2 - 4(X_1 - 0.06)^2),$$

la matrice D_c du correcteur est choisie comme $D_c = 0.5\,I_m$ avec I_m la matrice identité, et les matrices (Σ_c, Γ_c) sont calculées avec les paramètres $\alpha = 0.25$ et $\alpha = 4$. Les résultats peuvent être vus graphiquement dans la Fig. 4. On peut constater que le correcteur est capable de modifier la réponse oscillatoire, d'introduire un amortissement et de faire converger le système vers la forme optimale.

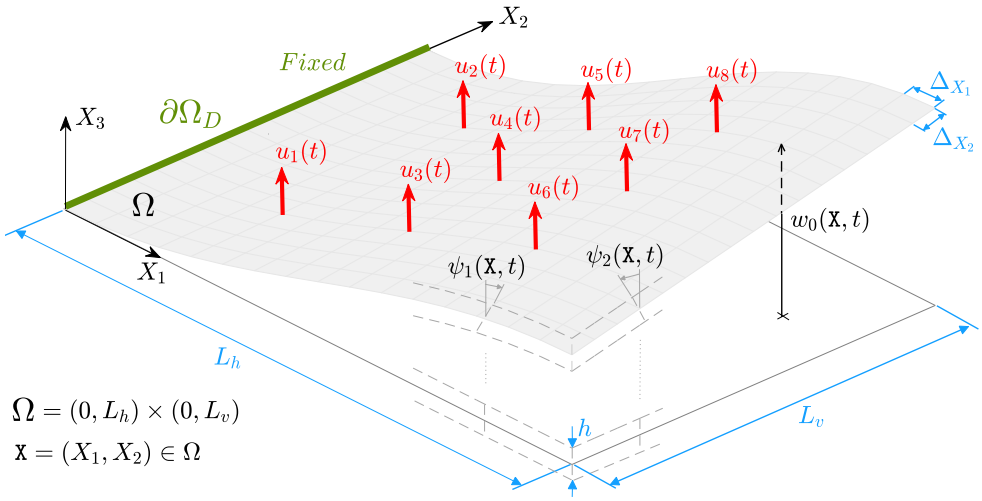

Figure 3 – Plaque Mindlin avec des entrées ponctuelles.

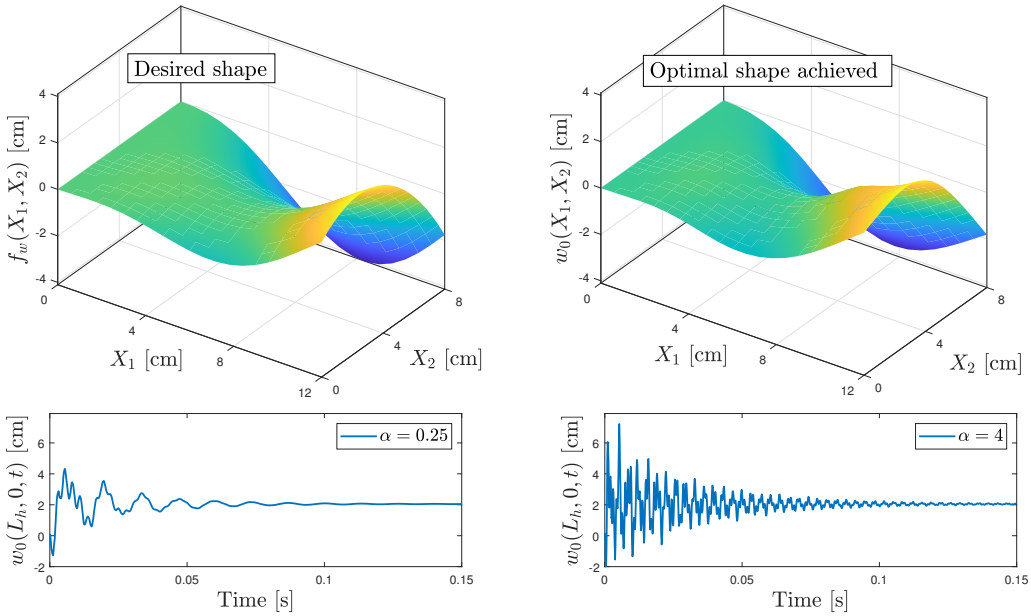

Figure 4 – Réponse en boucle fermée.

S.5 Conclusions et perspectives

S.5.1 Conclusions

Cette thèse traite de la modélisation, de la discrétisation et du commande des systèmes mécaniques flexibles en utilisant le cadre des systèmes port-Hamiltoniens, avec des contributions dans trois domaines clés.

Premièrement, elle développe des méthodologies généralisées pour la modélisation des systèmes mécaniques linéaires et non linéaires, fondées sur le principe de Hamilton généralisé étendu. Ces approches systématiques permettent de dériver des représentations PHS explicites et PH-DAE implicites, en intégrant de grandes déformations, des matériaux hyperélastiques et des contraintes, constituant ainsi un progrès par rapport à l'état de l'art. Deuxièmement, la thèse se concentre sur des techniques de discrétisation préservant la structure à l'aide de méthodes mixtes d'éléments finis. Ces méthodes préservent la structure PHS du système original et s'appliquent aussi bien aux systèmes linéaires que non linéaires. La validation numérique dans des exemples en 1D et 2D démontre leur précision pour capturer le comportement dynamique tout en maintenant la structure physique du système pendant la discrétisation. Troisièmement, la thèse conçoit des correcteurs pour des systèmes PHS linéaires basés sur des modèles d'ordre réduit ou de faible dimension, en utilisant la commande basé sur la passivité. Ces correcteurs garantissent une stabilité asymptotique et une convergence optimale vers les configurations souhaitées, appliquées à des systèmes tels que les poutres de Timoshenko et les plaques de Mindlin. Le cadre permet des ajustements efficaces tout en préservant les caractéristiques fondamentales du système. Dans l'ensemble, cette thèse propose un cadre polyvalent pour la modélisation, la discrétisation et la commande des systèmes flexibles dans le cadre des PHS, offrant une base pour des recherches et des applications futures.

S.5.2 Perspectives

Les travaux futurs sur le cadre de modélisation établi dans cette thèse peuvent être étendus pour intégrer des phénomènes plus complexes tels que la viscoélasticité, l'électroélasticité et les interactions fluide-structure. Ces avancées permettront de modéliser des systèmes sophistiqués comme les actionneurs diélectriques élastomères (DEA) et les actionneurs électrostatiques auto-réparants amplifiés hydrauliquement (HASEL).

En termes de discrétisation, les systèmes non linéaires présentent des défis, notamment en raison de la nécessité d'intégrer et d'assembler les matrices à chaque pas de temps, ce qui est très coûteux en calcul. De plus, la structure des matrices change à chaque étape, compliquant leur utilisation dans la conception des correcteurs. Le développement de méthodes permettant d'obtenir des matrices globales explicites, comme celles proposées par [Pedersen 2006; Gülümser 2014], pourrait améliorer l'efficacité des simulations et la conception des correcteurs.

Les méthodologies de commande développées dans cette thèse nécessitent une validation expérimentale. Un dispositif expérimental a été construit au FEMTO-ST, comprenant une poutre en fibre de carbone équipée d'actionneurs HASEL. Le montage expérimental et les résultats préliminaires en boucle ouverte sont présentés dans les Figs. 5 et 6. D'autres perspectives pour la conception de correcteurs incluent la démonstration de la stabilité des PHS de dimension infinie interconnectés avec des correcteurs de dimension finie, la détermination du placement optimal des entrées, l'assurance du suivi efficace de trajectoires pour des formes variables dans le temps, et l'extension des techniques de commande aux systèmes non linéaires.

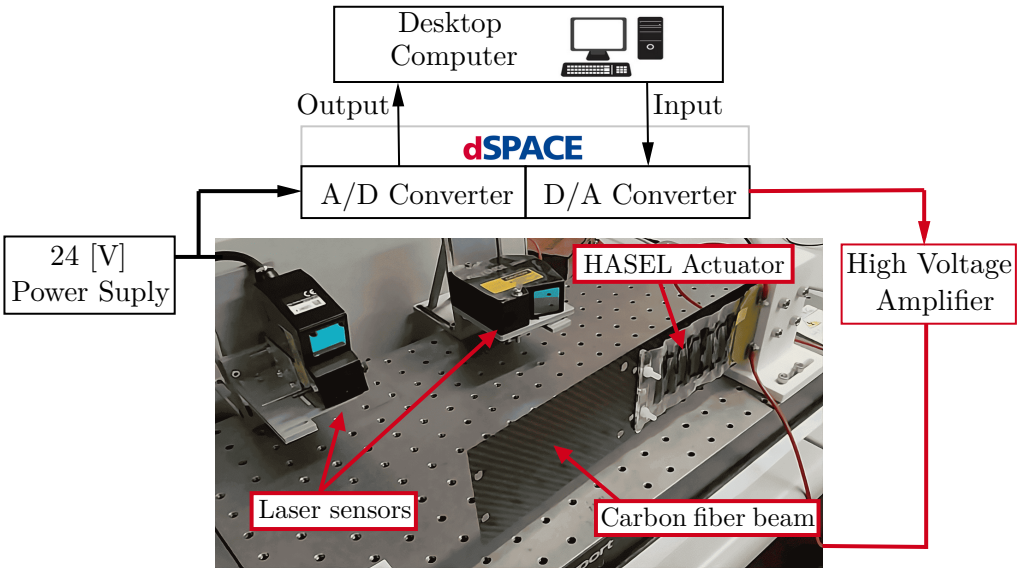

Figure 5 – Montage expérimental: Poutre actionnée par HASEL.

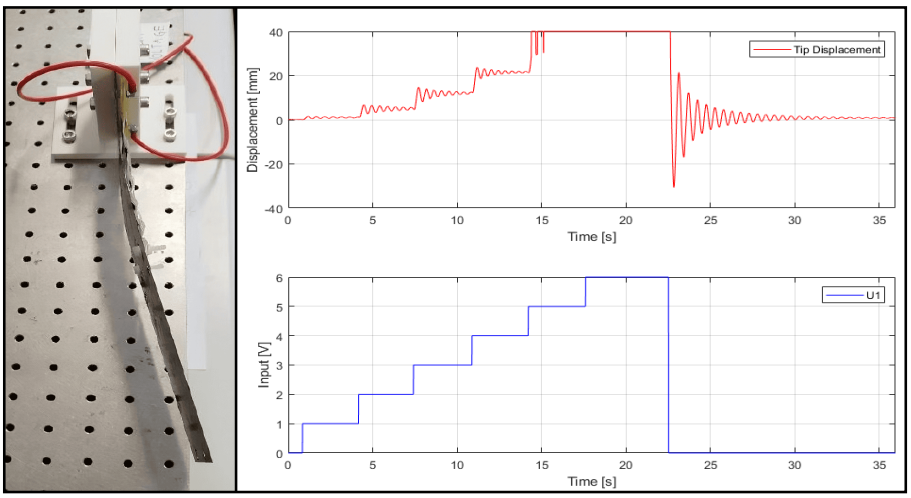

Figure 6 – Montage expérimental: Réponse en boucle ouverte.

Chapter I
Introduction

I.1 Motivation and context

Flexible bodies that experience large displacements and deformations are common in engineering areas such as mechanics, biomechanics, aeronautics, robo-tics, among some. The incorporation of nonlinearities into models, either through the geometric description of the motion or through the constitutive relationships of the material, are essential for accurately predicting realistic behaviors across these fields. This is the case of Dielectric Elastomeric Actuators (DEA), where large deformations and incompressibility of the material are crucial to predict phenomena of electromechanical instability and breakdown [Li 2013]. From a numerical point of view, discretization methods based on the Finite Element Method (FEM) have proven to be effective for simulating complex behaviors of such systems described over intricate geometries, as depicted in Fig. I.1a showing the electromechanical response of a DEA [Zhou 2019], and in Fig. I.1b illustrating the model of a biological heart [Ozturk 2022].

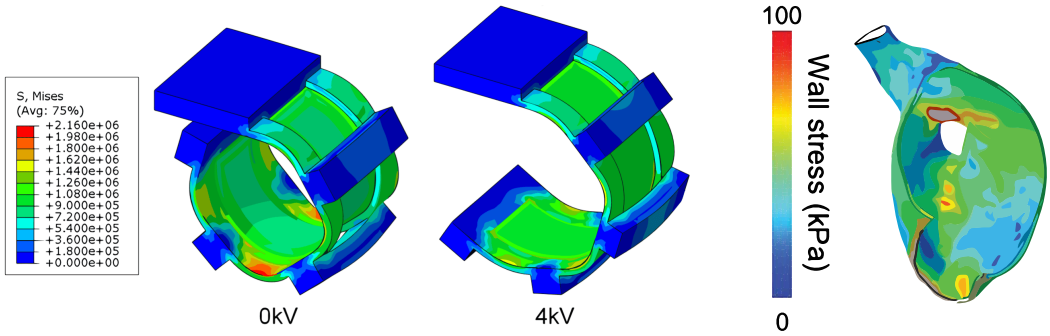

(a) Dielectric Elastomer Actuator [Zhou 2019] (b) Heart model [Ozturk 2022]

Figure I.1 – FEM application examples.

The control of flexible systems is an important area in engineering sciences due to its wide-ranging applications, including reducing vibration levels and achieving precise deformations, which is known as dynamic shape control. Dynamic shape control applications encompass compensating for surface errors arising from manufacturing or thermal distortions, as well as controlling acoustic responses [Agrawal 1997]. Moreover, the field finds potential applications in continuum and soft robotics, as illustrated in Fig. I.2a showing a continuous parallel robot [Childs 2021], and in Fig. I.2a showing a soft flexible gripper based on Hydraulically Amplified Self-Healing Electrostatic (HASEL) actuators [Yoder 2023].

The port-Hamiltonian (PH) formalism offers a geometric framework for the modeling of complex nonlinear multiphysical systems as the interconnection of simpler subsystems. Notable features include passivity, power flow between subsystems, separation of interconnection structure to constitutive relationships and dissipative effects, and the utilization of this structure for analysis and control [Duindam

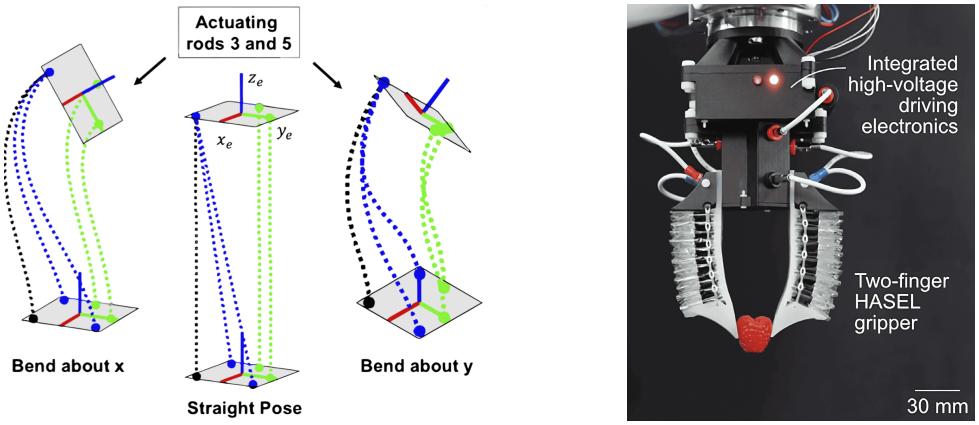

(a) Continuous parallel robot [Childs 2021] (b) Soft HASEL gripper [Yoder 2023]

Figure I.2 – Control application examples.

2009]. Initially proposed for finite-dimensional systems described by ordinary differential equations (ODE) [Maschke 1992], it has been extended to distributed parameter systems described by partial differential equations (PDE) [van der Schaft 2002], and more recently to implicit differential-algebraic equations (DAE) accommodating algebraic constraints [van der Schaft 2013] or systems with implicitly defined energy [van der Schaft 2018; Maschke 2023; Mehrmann 2023]. Designing controllers using passivity and PH formulations involves configuring closed-loop energy functions and/or modifying the interconnection structure and dissipation functions such that the system behaves with desired properties [Ortega 2002].

This thesis employs the port-Hamiltonian systems (PHS) framework to unify the modeling, spatial discretization, and shape control of flexible mechanical systems. The approach stems from the modeling of these systems, encompassing scenarios that involve nonlinear effects and algebraic constraints.

I.2 Port-Hamiltonian systems

Over the last twenty years, PHS have been an active field of research in areas such as modeling, structure-preserving discretization, structure-preserving order reduction, and passivity-based control (PBC), among others. A more in-depth review on PHS is provided in Section I.3, or the reader can refer to [Rashad 2020].

As previously mentioned, the aim of this thesis is to address the modeling, discretization and control of flexible systems whithin the PHS framework. This section provides introductory notions about finite-dimensional PHS described by ODEs, finite-dimensional PHS with algebraic constraints, known as PH-DAE sys-

tems, and infinite-dimensional PHS described by PDEs. Additionally, some examples are presented to illustrate the connections between PHS representations with variational principles and FEM.

I.2.1 Finite-dimensional PHS

A dynamic system is called explicit finite-dimensional PHS if it can be written as [van der Schaft 2017]:

$$\begin{aligned} \dot{x} &= [J(x) - R(x)]\nabla_x H(x) + g(x)u \\ y &= g(x)^\top \nabla_x H(x), \end{aligned} \tag{I.1}$$

where $x(t) \in \mathbb{R}^n$ is the state vector, $u(t) \in \mathbb{R}^m$ is the input vector, $H(x) : \mathbb{R}^n \to \mathbb{R}$ is the total stored energy called Hamiltonian, $J(x) = -J(x)^\top \in \mathbb{R}^{n\times n}$ is the skew-symmetric interconnection matrix, $R(x) = R(x)^\top \geq 0$ is the dissipation matrix, $g(x) \in \mathbb{R}^{n\times m}$ is the input map, and $y(t) \in \mathbb{R}^m$ is the output vector which is power-conjugated to $u(t)$. Finite-dimensional PHS are characterized by an underlying geometric structure called Dirac structure, linking the flow variables $\dot{x}$, the effort variables $\nabla_x H$, and the system's inputs and outputs.

I.2.1.a Dirac structure

Let $\mathscr{F}$, $\mathscr{E}$ and $\mathscr{B}$ be finite-dimensional spaces, where $\mathscr{F}$ is the flow space, its dual w.r.t. the usual inner product $\langle\cdot|\cdot\rangle_{in} : \mathscr{F} \times \mathscr{E} \to \mathbb{R}$ is the effort space $\mathscr{E}$, and $\mathscr{B} = \mathscr{F} \times \mathscr{E}$ is called the bond space of power variables. Consider the following symmetric bilinear form $\langle\langle\cdot,\cdot\rangle\rangle$ as:

$$\langle\langle(\mathtt{f}_1, \mathtt{e}_1), (\mathtt{f}_2, \mathtt{e}_2)\rangle\rangle = \langle \mathtt{e}_1 | \mathtt{f}_2 \rangle_{in} + \langle \mathtt{e}_2 | \mathtt{f}_1 \rangle_{in}. \tag{I.2}$$

A Dirac structure on $\mathscr{B} = \mathscr{F} \times \mathscr{E}$ is a subspace $\mathscr{D} \subset \mathscr{B}$ which is maximally isotropic under $\langle\langle\cdot,\cdot\rangle\rangle$. Equivalently, $\mathscr{D} = \mathscr{D}^\perp$ with respect to $\langle\langle\cdot,\cdot\rangle\rangle$ [van der Schaft 2002]. From the previous definition we have that for any $(\mathtt{f}, \mathtt{e}) \in \mathscr{D}$ it is satisfied that $\langle\langle(\mathtt{f}, \mathtt{e}), (\mathtt{f}, \mathtt{e})\rangle\rangle = 0$. Therefore, if $(\mathtt{f}, \mathtt{e})$ is a pair of power variables (for example forces and velocities in a mechanical context), then the condition $(\mathtt{f}, \mathtt{e}) \in \mathscr{D}$ implies energy-conservation.

Now, consider the finite-dimensional PHS in (I.1) but without dissipation ($R(x) = 0$). If we choose $\mathtt{f} = [\mathtt{f}_s, \mathtt{f}_e]^\top$ and $\mathtt{e} = [\mathtt{e}_s, \mathtt{e}_e]^\top$, where $\mathtt{f}_s = \dot{x}$, $\mathtt{f}_e = u$, $\mathtt{e}_s = \nabla_x H(x)$, $\mathtt{e}_e = -y$, then the set:

$$\mathscr{D} = \{(\mathtt{f}, \mathtt{e}) \in \mathscr{B} \mid \mathtt{f}_s = J(x)\mathtt{e}_s + g(x)\mathtt{f}_e\,,\ \mathtt{e}_e = -g(x)^\top \mathtt{e}_s\} \tag{I.3}$$

is a Dirac structure. With the above definitions for $\mathtt{f}$ and $\mathtt{e}$, it is easy to show that the system in (I.1) without dissipation conserves energy, that is, $\langle \mathtt{e} | \mathtt{f} \rangle_{in} = 0$, and the energy exchange with the environment is given by the product between inputs and outputs, that is:

$$\dot{H} = y^\top u = -\langle \mathtt{e}_e | \mathtt{f}_e \rangle_{in}. \tag{I.4}$$

To include dissipation ($R(x) \geq 0$), the ports of the system are divided into the open ports (u, y) and the resistive ports (u_r, y_r), so that the corresponding system defines an extended Dirac structure. So, consider the following system:

$$\begin{aligned} \dot{x} &= J(x)\nabla_x H(x) + g_r(x)u_r + g(x)u \\ y_r &= g_r(x)^\top \nabla_x H(x), \\ y &= g(x)^\top \nabla_x H(x), \end{aligned} \tag{I.5}$$

where $u_r = -R_r\, y_r$, with $R_r = R_r^\top \geq 0$ is a linear resistor. Note that the minus sign is due to the fact that $u_r^\top y_r$ is the power flowing from the port, and this cannot be positive for a realistic dissipation. So, taking into account the above, the system (I.5) can be rewritten as (I.1), where $R(x) = g_r(x) R_r\, g_r(x)^\top$. Now, choosing $\mathtt{f} = [\mathtt{f}_s, \mathtt{f}_e, \mathtt{f}_r]^\top$ and $\mathtt{e} = [\mathtt{e}_s, \mathtt{e}_e, \mathtt{e}_r]^\top$, where $\mathtt{f}_s = \dot{x}$, $\mathtt{f}_e = u$, $\mathtt{f}_r = u_r$, $\mathtt{e}_s = \nabla_x H(x)$, $\mathtt{e}_e = -y$, $\mathtt{e}_r = -y_r$, then the set:

$$\begin{aligned} \mathscr{D} = \{(\mathtt{f}, \mathtt{e}) \in \mathscr{B} \mid\ & \mathtt{f}_s = J(x)\mathtt{e}_s + g_r(x)\mathtt{f}_r + g(x)\mathtt{f}_e\,, \\ & \mathtt{e}_e = -g(x)^\top \mathtt{e}_s\,,\ \mathtt{e}_r = -g_r(x)^\top \mathtt{e}_s \Big\} \end{aligned} \tag{I.6}$$

is a Dirac structure. With the above definitions for $\mathtt{f}$ and $\mathtt{e}$, we can show that the system in (I.5) (equivalent to (I.1)) conserves energy, and the energy exchange with the environment is given by the product between open and resistive ports, that is:

$$\dot{H} = y^\top u + y_r^\top u_r = y^\top u - \nabla_x H(x)^\top R(x) \nabla_x H(x) = -\langle \mathtt{e}_e, \mathtt{e}_r | \mathtt{f}_e, \mathtt{f}_r \rangle_{in}. \tag{I.7}$$

I.2.1.b Example of finite-dimensional PHS

To illustrate the finite-dimensional PHS representation, we consider the mass-spring-damper system in Fig. I.3. The system consists of two lumped masses, m_1 and m_2, connected by the spring-damper chains characterized by the stiffness coefficients k_1, k_2, k_3, and damping coefficients d_1, d_2, d_3. External forces f_1 and f_2 act on each mass, and the system's dynamics is described by the time evolution of the displacements r_1 and r_2. To derive the equations of motion of the system many different approaches can be applied. In order to establish connections with the following chapters, we use here the variational method called Hamilton's principle.

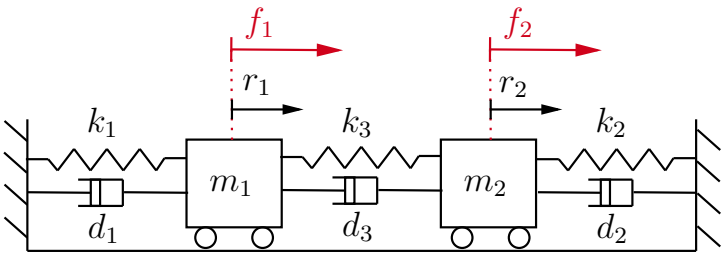

Figure I.3 – Mass-spring-damper system.

Hamilton's principle states that the true evolution of the displacement vector $r = [r_1 \; r_2]^\top \in \mathbb{R}^2$, between two specific times t_1 and t_2, is a stationary point of the action functional under admissible small variations (δr) in the configuration of the system. Mathematically, Hamilton's principle states that [Bedford 1985]:

$$\int_{t_1}^{t_2} [\delta(T - U) + \delta W_E] \, dt = 0, \tag{I.8}$$

$$\delta r(t_1) = \delta r(t_2) = 0, \tag{I.9}$$

where δ is the variational operator, $T \in \mathbb{R}$ is the kinetic energy, $U \in \mathbb{R}$ is the elastic potential energy, and $\delta W_E \in \mathbb{R}$ is the virtual work associated to the external forces and dissipative effects. For the system illustrated in Fig. I.3, these quantities are:

$$T = \frac{1}{2}\dot{r}^\top M \, \dot{r}, \quad U = \frac{1}{2} r^\top K \, r, \quad \delta W_E = \delta r^\top (u - D\dot{r}),$$

where $u = [f_1 \; f_2]^\top \in \mathbb{R}^2$ is the input vector corresponding to the applied forces, $M = M^\top > 0 \in \mathbb{R}^{2\times 2}$ is the mass matrix, $K = K^\top > 0 \in \mathbb{R}^{2\times 2}$ is the stiffness matrix, and $D = D^\top \geq 0 \in \mathbb{R}^{2\times 2}$ is the viscous damping matrix. These matrices are given by:

$$M = \begin{bmatrix} m_1 & 0 \\ 0 & m_2 \end{bmatrix}, \quad K = \begin{bmatrix} k_1 + k_3 & -k_3 \\ -k_3 & k_2 + k_3 \end{bmatrix}, \quad D = \begin{bmatrix} d_1 + d_3 & -d_3 \\ -d_3 & d_2 + d_3 \end{bmatrix}. \tag{I.10}$$

So, applying Hamilton's principle to the system we obtain:

$$\int_{t_1}^{t_2} [\delta(T - U) + \delta W_E] \, dt = \int_{t_1}^{t_2} \delta r^\top \left(-M\ddot{r} - D\dot{r} - Kr + u\right) dt = 0,$$

since δr is arbitrary, by the fundamental lemma of variational calculus we obtain:

$$-M\ddot{r} - D\dot{r} - Kr + u = 0, \tag{I.11}$$

which corresponds to the Lagrangian dynamic model. Defining the momentum vector as $p = M\dot{r}$, (I.11) can be written as a finite-dimensional PHS of the form:

$$\begin{aligned} \underbrace{\begin{bmatrix} \dot{p} \\ \dot{r} \end{bmatrix}}_{\dot{x}} &= \Bigg(\underbrace{\begin{bmatrix} 0 & -I \\ I & 0 \end{bmatrix}}_{J_I} - \underbrace{\begin{bmatrix} D & 0 \\ 0 & 0 \end{bmatrix}}_{R_D} \Bigg) \underbrace{\begin{bmatrix} M^{-1} & 0 \\ 0 & K \end{bmatrix}}_{Q} \underbrace{\begin{bmatrix} p \\ r \end{bmatrix}}_{x} + \underbrace{\begin{bmatrix} I \\ 0 \end{bmatrix}}_{G_I} u \\ y &= G_I^\top \nabla_x H(x) = M^{-1} p = \dot{r}, \end{aligned} \tag{I.12}$$

where $\nabla_x H(x) = Q \, x$, with Hamiltonian

$$H(x) = \frac{1}{2} x^\top Q \, x = \frac{1}{2} p^\top M^{-1} p + \frac{1}{2} r^\top K r, \tag{I.13}$$

and power exchange with the environment given by:

$$\dot{H} = \nabla_x H(x)^\top \dot{x} = y^\top u - \dot{r}^\top D \dot{r}. \tag{I.14}$$

From now on, the variables in the state vector x are called energy variables, and their time derivatives are flows. Efforts, also known as co-energy variables and denoted by e_x, are defined as $e_x = \nabla_x H(x)$.

Similar representations than PHS one can be used depending on the objective. Note that we can still refer to it as PHS even if we use co-energy variables. To illustrate this point in the upcoming Section I.2.2.d, consider the following reciprocal PHS representation [van der Schaft 2011], which commonly arises in discretized models of infinite-dimensional linear mechanical systems using mixed FEM, as presented in [Thoma 2022b].

By defining $v = \dot{r}$ as the velocity vector, the PHS in (I.12) can alternatively be expressed in the following finite-dimensional reciprocal PHS form:

$$\begin{aligned} \underbrace{\begin{bmatrix} M & 0 \\ 0 & K \end{bmatrix}}_{\bar{Q}} \underbrace{\begin{bmatrix} \dot{v} \\ \dot{r} \end{bmatrix}}_{\dot{\bar{x}}} &= \left(\underbrace{\begin{bmatrix} 0 & -K \\ K & 0 \end{bmatrix}}_{J_K} - \underbrace{\begin{bmatrix} D & 0 \\ 0 & 0 \end{bmatrix}}_{R_D} \right) \underbrace{\begin{bmatrix} v \\ r \end{bmatrix}}_{\bar{x}} + \underbrace{\begin{bmatrix} I \\ 0 \end{bmatrix}}_{G_I} u \\ y &= G_I^\top \bar{x} = v, \end{aligned} \tag{I.15}$$

$$\bar{H}(\bar{x}) = \frac{1}{2} \bar{x}^\top \bar{Q}\, \bar{x} = \frac{1}{2} v^\top M v + \frac{1}{2} r^\top K r, \tag{I.16}$$

and power exchange with the environment given by:

$$\dot{\bar{H}} = \nabla_{\bar{x}} \bar{H}(\bar{x})^\top \dot{\bar{x}} = y^\top u - v^\top D v, \tag{I.17}$$

where $\nabla_{\bar{x}} \bar{H}(\bar{x}) = \bar{Q}\, \bar{x}$.

Note that in both (I.12) and (I.15), the matrices on the left side of $\dot{x}$ or $\dot{\bar{x}}$ are I and $\bar{Q}$, respectively, and are full rank and invertible, implying that the systems are described solely by ODEs. However, when these matrices are singular, it implies that some equations are algebraically related, resulting in a model described by a combination of ODEs and algebraic equations, leading to a PH-DAE system.

I.2.2 Finite-dimensional PH-DAE

PHS theory is based on the idea that complex systems can be viewed as interconnected subsystems linked by energy flows. This interconnection often leads to algebraic constraints that must be satisfied as the system evolves, resulting in a system of differential-algebraic equations (DAE systems). These algebraic constraints can be formulated in terms of energy and co-energy variables, which represent the energy relations of the system. In [van der Schaft 2018; van der Schaft 2020], it has been shown that formulating algebraic constraints in terms of energy relations is equivalent to replacing the gradients of Hamiltonian functions with general Lagrangian subspaces, resulting in systems where the energy is implicitly defined. For more details on PH-DAE and Lagrangian subspaces, readers are referred to [van der Schaft 2013; van der Schaft 2018; Beattie 2018; van der Schaft 2020; Mehrmann 2023; Maschke 2023; van der Schaft 2023].

In this introductory presentation, the focus is on the PH-DAE representation of systems with algebraic constraints enforced by Lagrange multipliers, where the energy is explicitly defined (gradients are not replaced by Lagrangian subspaces).

A dynamic system is called finite-dimensional PH-DAE if it can be written as [van der Schaft 2017]:

$$\begin{aligned} \dot{x} &= [J(x) - R(x)]\nabla_x H(x) + g_\lambda(x)\lambda + g(x)u \\ y &= g(x)^\top \nabla_x H(x), \\ 0 &= g_\lambda(x)^\top \nabla_x H(x), \end{aligned} \tag{I.18}$$

where $x(t) \in \mathbb{R}^n$ is the state vector, $u(t) \in \mathbb{R}^m$ is the input vector, $H(x)$ is the Hamiltonian function, $J(x) = -J(x)^\top \in \mathbb{R}^{n\times n}$ is the skew-symmetric interconnection matrix, $R(x) = R(x)^\top \geq 0$ is the dissipation matrix, $g(x) \in \mathbb{R}^{n\times m}$ is the input map, and $y(t) \in \mathbb{R}^m$ is the output vector which is power-conjugated with $u(t)$. In addition, we have $\lambda(t) \in \mathbb{R}^k$, which is the Lagrange multiplier introduced to enforce the algebraic constraint: $0 = g_\lambda(x)^\top \nabla_x H(x)$, where $g_\lambda(x) \in \mathbb{R}^{n\times k}$ is the map of the Lagrange multiplier. Notice that (I.18) can equivalently be written as:

$$\begin{aligned} \underbrace{\begin{bmatrix} I & 0 \\ 0 & 0 \end{bmatrix}}_{E} \underbrace{\begin{bmatrix} \dot{x} \\ -\dot{\lambda} \end{bmatrix}}_{\dot{x}_E} &= \Bigg(\underbrace{\begin{bmatrix} J(x) & g_\lambda(x) \\ -g_\lambda(x)^\top & 0 \end{bmatrix}}_{J_E(x)} - \underbrace{\begin{bmatrix} R(x) & 0 \\ 0 & 0 \end{bmatrix}}_{R_E(x)} \Bigg) \underbrace{\begin{bmatrix} \nabla_x H(x) \\ \lambda \end{bmatrix}}_{z(x_E)} + \underbrace{\begin{bmatrix} g(x) \\ 0 \end{bmatrix}}_{g_E(x)} u \\ y &= g_E(x)^\top z(x_E) = g(x)^\top \nabla_x H(x), \end{aligned} \tag{I.19}$$

where $\nabla_x H(x) = E^\top z(x_E)$, and according to [Mehrmann 2019], $z(x_E) \in \mathbb{R}^{n+k}$ is defined as the effort function, and $E \in \mathbb{R}^{(n+k)\times(n+k)}$ is defined as the flow matrix (which is singular). The other variables, $x_E(t)$, $J_E(x)$, $R_E(x)$, and $g_E(x)$, maintain their meanings as the state vector, interconnection matrix, dissipation matrix, and input map matrix, respectively.

I.2.2.a Dirac structure of constrained systems

Consider the case with dissipation ($R(x) \geq 0$), where the ports of the system are divided into the open ports (u, y) and the resistive ports (u_r, y_r). So, the PH-DAE in (I.18) is rewritten as:

$$\begin{aligned} \dot{x} &= J(x)\nabla_x H(x) + g_r(x)u_r + g_\lambda(x)\lambda + g(x)u \\ y_r &= g_r(x)^\top \nabla_x H(x), \\ y &= g(x)^\top \nabla_x H(x), \\ 0 &= g_\lambda(x)^\top \nabla_x H(x), \end{aligned} \tag{I.20}$$

where $u_r = -R_r\, y_r$ with $R_r = R_r^\top \geq 0$ a linear resistor, such that $R(x) = g_r(x) R_r\, g_r(x)^\top$. Now, choosing $\mathtt{f} = [\mathtt{f}_s, \mathtt{f}_e, \mathtt{f}_r]^\top$ and $\mathtt{e} = [\mathtt{e}_s, \mathtt{e}_e, \mathtt{e}_r]^\top$, where $\mathtt{f}_s = \dot{x}$, $\mathtt{f}_e = u$, $\mathtt{f}_r = u_r$, $\mathtt{e}_s = \nabla_x H(x)$, $\mathtt{e}_e = -y$, $\mathtt{e}_r = -y_r$, then the set:

$$\begin{aligned} \mathscr{D} = \{(\mathtt{f}, \mathtt{e}) \in \mathscr{B} \mid\ & \mathtt{f}_s = J(x)\mathtt{e}_s + g_r(x)\mathtt{f}_r + g_\lambda(x)\lambda + g(x)\mathtt{f}_e\,, \\ & \mathtt{e}_e = -g(x)^\top \mathtt{e}_s\,,\ \mathtt{e}_r = -g_r(x)^\top \mathtt{e}_s\,,\ 0 = g_\lambda(x)^\top \mathtt{e}_s \Big\} \end{aligned} \tag{I.21}$$

is a Dirac structure [Duindam 2009, Chapter 2.4.1]. So, for $\mathtt{f}$, $\mathtt{e}$ and λ is easy to show that the PH-DAE in (I.20) (equivalent to (I.18) and (I.19)) conserves energy, and the energy exchange with the environment is given by the product between open and resistive ports, as in (I.7).

I.2.2.b Elimination of Lagrange multipliers in linear PH-DAE

For simulation or control purposes, it may be convenient to eliminate the Lagrange multiplier from the PH-DAE to obtain a PHS described solely by ODEs. The elimination process presented here was originally proposed in [Wu 2014] and considers that the PH-DAE is linear. So, consider a linear PH-DAE with the structure of (I.18), where $\nabla_x H(x) = Q\,x$, with $Q = Q^\top > 0 \in \mathbb{R}^{n\times n}$ a constant matrix, and J, R, g_λ and g being constant matrices. Define the transformation matrix $T_\lambda \in \mathbb{R}^{n\times n}$ as:

$$T_\lambda = \begin{bmatrix} g_\lambda^\perp \\ g_\lambda^+ \end{bmatrix}, \tag{I.22}$$

where $g_\lambda^\perp \in \mathbb{R}^{(n-k)\times n}$ is the left-annihilator of g_λ (such that $g_\lambda^\perp g_\lambda = 0$), and $g_\lambda^+ \in \mathbb{R}^{k\times n}$ is the left inverse of g_λ (given by $g_\lambda^+ = (g_\lambda^\top g_\lambda)^{-1} g_\lambda^\top$). Using the transformations $\tilde{x} = T_\lambda\,x$, and $x = T_\lambda^{-1}\tilde{x}$, the transformed linear PH-DAE is given by:

$$\underbrace{\begin{bmatrix} \dot{\tilde{x}}_1 \\ \dot{\tilde{x}}_2 \end{bmatrix}}_{\dot{\tilde{x}}} = \Bigg(\underbrace{\begin{bmatrix} \tilde{J}_{11} & \tilde{J}_{12} \\ \tilde{J}_{21} & \tilde{J}_{22} \end{bmatrix}}_{\tilde{J}} - \underbrace{\begin{bmatrix} \tilde{R}_{11} & \tilde{R}_{12} \\ \tilde{R}_{21} & \tilde{R}_{22} \end{bmatrix}}_{\tilde{R}} \Bigg) \underbrace{\begin{bmatrix} \tilde{Q}_{11} & \tilde{Q}_{12} \\ \tilde{Q}_{21} & \tilde{Q}_{22} \end{bmatrix}}_{\tilde{Q}} \underbrace{\begin{bmatrix} \tilde{x}_1 \\ \tilde{x}_2 \end{bmatrix}}_{\tilde{x}} + \underbrace{\begin{bmatrix} \tilde{g}_1 \\ \tilde{g}_2 \end{bmatrix}}_{\tilde{g}} u + \underbrace{\begin{bmatrix} 0 \\ I_k \end{bmatrix}}_{\tilde{g}_\lambda} \lambda, \tag{I.23}$$

$$y = \tilde{g}^\top \tilde{Q}\,\tilde{x}, \tag{I.24}$$

$$0 = \tilde{g}_\lambda^\top \tilde{Q}\,\tilde{x}, \tag{I.25}$$

where $\tilde{x}_1 \in \mathbb{R}^{n-k}$, $\tilde{x}_2 \in \mathbb{R}^k$, $\tilde{J} = T_\lambda J\,T_\lambda^\top \in \mathbb{R}^{n\times n}$ is skew-symmetric, $\tilde{R} = T_\lambda R\,T_\lambda^\top \in \mathbb{R}^{n\times n}$ is symmetric and positive semi-definite, $\tilde{Q} = T_\lambda^{-\top} Q\,T_\lambda^{-1} \in \mathbb{R}^{n\times n}$ is symmetric and positive definite, $\tilde{g} = T_\lambda g \in \mathbb{R}^{n\times m}$, $\tilde{g}_\lambda = T_\lambda g_\lambda \in \mathbb{R}^{n\times k}$, and $I_k \in \mathbb{R}^{k\times k}$ is an identity matrix. From (I.25) we get:

$$\tilde{x}_2 = -\tilde{Q}_{22}^{-1}\tilde{Q}_{21}\tilde{x}_1, \tag{I.26}$$

so, replacing the above in (I.23) we obtain:

$$\dot{\tilde{x}}_1 = (\tilde{J}_{11} - \tilde{R}_{11})(\tilde{Q}_{11} - \tilde{Q}_{12}\tilde{Q}_{22}^{-1}\tilde{Q}_{21})\,\tilde{x}_1 + \tilde{g}_1\,u, \tag{I.27}$$

$$\dot{\tilde{x}}_2 = (\tilde{J}_{21} - \tilde{R}_{21})(\tilde{Q}_{11} - \tilde{Q}_{12}\tilde{Q}_{22}^{-1}\tilde{Q}_{21})\,\tilde{x}_1 + \tilde{g}_2\,u + \lambda. \tag{I.28}$$

Solving for λ from (I.28), using (I.27) and the time derivative of (I.26) we obtain:

$$\lambda = \tilde{A}\,\tilde{x}_1 + \tilde{B}\,u, \tag{I.29}$$

where

$$\tilde{A} = -\left[\tilde{Q}_{22}^{-1}\tilde{Q}_{21}(\tilde{J}_{11} - \tilde{R}_{11}) + (\tilde{J}_{21} - \tilde{R}_{21})\right](\tilde{Q}_{11} - \tilde{Q}_{12}\tilde{Q}_{22}^{-1}\tilde{Q}_{21}), \tag{I.30}$$

$$\tilde{B} = -\left(\tilde{Q}_{22}^{-1}\tilde{Q}_{21}\tilde{g}_1 + \tilde{g}_2\right). \tag{I.31}$$

Notice that (I.27) is an unconstrained finite-dimensional PHS since it is described solely by ODEs, but it has encoded the dynamics of the constrained system. On the other hand, once $\tilde{x}_1$ and the input u are known, the value of λ can be computed using the expression in (I.29).

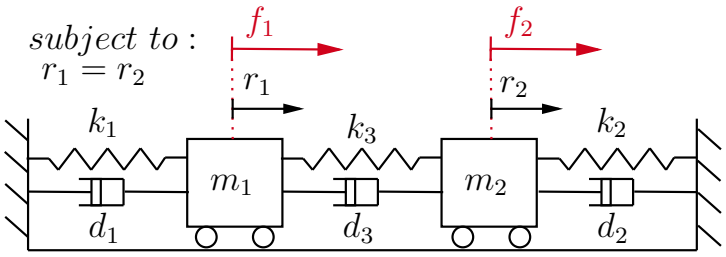

Figure I.4 – Constrained mass-spring-damper system.

I.2.2.c Example of finite-dimensional PH-DAE

To illustrate the finite-dimensional PH-DAE, let's continue with the mass-spring-damper system in Fig. I.3, but now enforcing that $r_1 = r_2$, as illustrated in Fig. I.4. To derive the equations of motion of the constrained system, here is used the variational method called extended Hamilton's principle. This principle states that the true evolution of the displacement vector $r = [r_1 \; r_2]^\top \in \mathbb{R}^2$, subject to algebraic constraints of the form $\gamma(r) = 0 \in \mathbb{R}^k$, between two specific times t_1 and t_2, is a stationary point of the extended action functional under admissible small variations δr and $\delta\lambda$. Mathematically, the extended Hamilton's principle states that [Bedford 1985]:

$$\int_{t_1}^{t_2} [\delta(T - U) + \delta W_E - \delta C_\lambda] \, dt = 0, \tag{I.32}$$

$$\delta r(t_1) = \delta r(t_2) = 0, \tag{I.33}$$

where δ is the variational operator, $T \in \mathbb{R}$ is the kinetic energy, $U \in \mathbb{R}$ is the elastic potential energy, $\delta W_E \in \mathbb{R}$ is the virtual work associated to the external forces and dissipative effects, and $C_\lambda = \lambda \cdot \gamma(r) \in \mathbb{R}$ is the constraint functional with $\lambda \in \mathbb{R}^k$ the Lagrange multiplier. For the system illustrated in Fig. I.4, T, U and δW_E are the same as in the unconstrained mass-spring-damper system used as example in Section I.2.1.b, that is, $T = \frac{1}{2}\dot{r}^\top M \, \dot{r}$, $U = \frac{1}{2} r^\top K \, r$, $\delta W_E = \delta r^\top (u - D\dot{r})$, where $u = [f_1 \; f_2]^\top \in \mathbb{R}^2$ is the input vector corresponding to the applied forces, and whose matrices M, K, $D \in \mathbb{R}^{2\times 2}$ are given in (I.10). The algebraic constraint is given by:

$$\gamma(r) = r_1 - r_2 = [1 \quad -1] \, r = B_\lambda \, r. \tag{I.34}$$

So, applying the extended Hamilton's principle to the constrained system we obtain:

$$\int_{t_1}^{t_2} [\delta(T - U) + \delta W_E - \delta C_\lambda] \, dt = \int_{t_1}^{t_2} [\delta r^\top \left(-M\ddot{r} - D\dot{r} - Kr + u - B_\lambda^\top \lambda \right) \ldots \\ \ldots - \delta\lambda \, B_\lambda \, r] \, dt = 0,$$

since δr and $\delta\lambda$ are arbitrary, from the above expression we obtain:

$$-M\ddot{r} - D\dot{r} - Kr + u - B_\lambda^\top \lambda = 0, \tag{I.35}$$

$$B_\lambda \, r = 0, \tag{I.36}$$

which corresponds to the constrained Lagrangian dynamic model. Defining the momentum vector as $p = M\dot{r}$, and taking the time derivative of (I.36), the constrained Lagrangian model can be written as a finite-dimensional PH-DAE of the form:

$$\begin{aligned} \underbrace{\begin{bmatrix}\dot{p}\\ \dot{r}\end{bmatrix}}_{\dot{x}} &= \Bigg(\underbrace{\begin{bmatrix}0 & -I\\ I & 0\end{bmatrix}}_{J_I} - \underbrace{\begin{bmatrix}D & 0\\ 0 & 0\end{bmatrix}}_{R_D}\Bigg)\underbrace{\begin{bmatrix}M^{-1}p\\ Kr\end{bmatrix}}_{\nabla_x H(x)} + \underbrace{\begin{bmatrix}I\\ 0\end{bmatrix}}_{G_I} u + \underbrace{\begin{bmatrix}-B_\lambda^\top\\ 0\end{bmatrix}}_{G_\lambda}\lambda \\ y &= G_I^\top \nabla_x H(x) = M^{-1}p = \dot{r}, \\ 0 &= G_\lambda^\top \nabla_x H(x) = -B_\lambda \dot{r}, \end{aligned} \tag{I.37}$$

with Hamiltonian

$$H(x) = \frac{1}{2}p^\top M^{-1}p + \frac{1}{2}r^\top K r, \tag{I.38}$$

and power exchange with the environment given by:

$$\dot{H} = \nabla_x H(x)^\top \dot{x} = y^\top u - \dot{r}^\top D\dot{r}. \tag{I.39}$$

Analogously as the finite-dimensional PHS in (I.15), using $v = \dot{r}$, the PH-DAE in (I.37) can alternatively be expressed in the following reciprocal PH-DAE form:

$$\begin{aligned} \underbrace{\begin{bmatrix}M & 0\\ 0 & K\end{bmatrix}}_{\bar{Q}}\underbrace{\begin{bmatrix}\dot{v}\\ \dot{r}\end{bmatrix}}_{\dot{\bar{x}}} &= \Bigg(\underbrace{\begin{bmatrix}0 & -K\\ K & 0\end{bmatrix}}_{J_K} - \underbrace{\begin{bmatrix}D & 0\\ 0 & 0\end{bmatrix}}_{R_D}\Bigg)\underbrace{\begin{bmatrix}v\\ r\end{bmatrix}}_{\bar{x}} + \underbrace{\begin{bmatrix}I\\ 0\end{bmatrix}}_{G_I} u + \underbrace{\begin{bmatrix}-B_\lambda^\top\\ 0\end{bmatrix}}_{G_\lambda}\lambda \\ y &= G_I^\top \bar{x} = v, \\ 0 &= G_\lambda^\top \bar{x} = -B_\lambda v, \end{aligned} \tag{I.40}$$

with Hamiltonian

$$\bar{H}(\bar{x}) = \frac{1}{2}v^\top M v + \frac{1}{2}r^\top K r, \tag{I.41}$$

and power exchange with the environment given by:

$$\dot{\bar{H}} = \nabla_{\bar{x}} \bar{H}(\bar{x})^\top \dot{\bar{x}} = y^\top u - v^\top D v. \tag{I.42}$$

I.2.2.d Equivalent unconstrained finite-dimensional PHS representation

Since the resulting PH-DAE in (I.37) is linear, we can apply the procedure presented in Section I.2.2.b to eliminate the Lagrange multiplier and obtain an unconstrained finite-dimensional PHS. Note that when applying this procedure, the resulting PHS takes the form of (I.27), where $\tilde{x}_1$ loses its physical meaning since it is a linear combination of x, defined by the transformation $\tilde{x} = T_\lambda\, x$.

In this brief section, our objective is to illustrate how another linear transformation, commonly used in FEM assembly process, can eliminate the Lagrange multiplier while preserving the physical meaning of the state variables when applied to the reciprocal PH-DAE of the form (I.40).

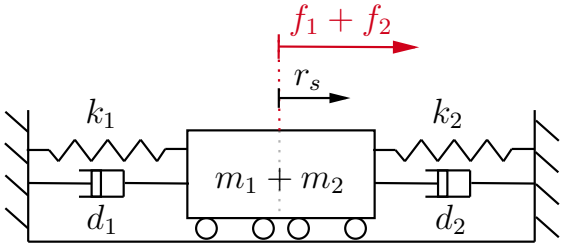

Figure I.5 – Equivalent representation of constrained mass-spring-damper system.

First of all, note that the constrained system is equivalent to the system illustrated in Fig. I.5, which represents a single mass, denoted as $m_s = m_1 + m_2$, where the external forces f_1 and f_2 act. The system's dynamics is then governed by the displacement of mass m_s, denoted as r_s. It is clear that the system in Fig. I.5 is a one degree-of-freedom (DOF) system with equivalent stiffness and damping $k_s = k_1 + k_2$ and $d_s = d_1 + d_2$, respectively. So, applying Hamilton's principle, we obtain the Lagrangian model given by:

$$-m_s\ddot{r}_s - d_s\dot{r}_s - k_s r_s + f_1 + f_2 = 0. \tag{I.43}$$

Defining $p_s = m_s\dot{r}_s$, (I.43) can be written as a finite-dimensional PHS of the form:

$$\begin{aligned} \underbrace{\begin{bmatrix}\dot{p}_s\\ \dot{r}_s\end{bmatrix}}_{\dot{x}_s} &= \left(\underbrace{\begin{bmatrix}0 & -1\\ 1 & 0\end{bmatrix}}_{J_s} - \underbrace{\begin{bmatrix}d_s & 0\\ 0 & 0\end{bmatrix}}_{R_s}\right) \underbrace{\begin{bmatrix}\frac{p_s}{m_s}\\ k_s r_s\end{bmatrix}}_{\nabla_{x_s} H(x_s)} + \underbrace{\begin{bmatrix}1 & 1\\ 0 & 0\end{bmatrix}}_{G_s} u \\ y &= G_s^\top \nabla_{x_s} H(x_s) = [\dot{r}_s \;\; \dot{r}_s]^\top. \end{aligned} \tag{I.44}$$

Additionally, with $v_s = \dot{r}_s$, it can be expressed in this alternative reciprocal form:

$$\begin{aligned} \underbrace{\begin{bmatrix}m_s & 0\\ 0 & k_s\end{bmatrix}}_{\bar{Q}_s} \underbrace{\begin{bmatrix}\dot{v}_s\\ \dot{r}_s\end{bmatrix}}_{\dot{\bar{x}}_s} &= \left(\underbrace{\begin{bmatrix}0 & -k_s\\ k_s & 0\end{bmatrix}}_{J_{k_s}} - \underbrace{\begin{bmatrix}d_s & 0\\ 0 & 0\end{bmatrix}}_{R_s}\right) \underbrace{\begin{bmatrix}v_s\\ r_s\end{bmatrix}}_{\bar{x}_s} + \underbrace{\begin{bmatrix}1 & 1\\ 0 & 0\end{bmatrix}}_{G_s} u \\ y &= G_s^\top \bar{x}_s = [v_s \;\; v_s]^\top. \end{aligned} \tag{I.45}$$

Note that the states $\bar{x} \in \mathbb{R}^4$ and $\bar{x}_s \in \mathbb{R}^2$ of the reciprocal PH-DAE (I.40) and the reciprocal PHS (I.45), respectively, are related by $\bar{x} = T_v\,\bar{x}_s$, where $T_v \in \mathbb{R}^{4\times 2}$ is given by:

$$\underbrace{\begin{bmatrix}v_1\\ v_2\\ r_1\\ r_2\end{bmatrix}}_{\bar{x}} = \underbrace{\begin{bmatrix}1 & 0\\ 1 & 0\\ 0 & 1\\ 0 & 1\end{bmatrix}}_{T_v} \underbrace{\begin{bmatrix}v_s\\ r_s\end{bmatrix}}_{\bar{x}_s}. \tag{I.46}$$

So, T_v contains the constraint's information: $v_1 = v_2 = v_s$ and $r_1 = r_2 = r_s$. With this, we obtain the following relations between the matrices of (I.40) and (I.45):

$$\bar{Q}_s = T_v^\top \bar{Q}\, T_v, \quad J_{k_s} = T_v^\top J_K T_v, \quad R_s = T_v^\top R_D T_v, \quad G_s = T_v^\top G_I T_v, \quad 0 = T_v^\top G_\lambda T_v,$$

where from the last expression we can see that T_v effectively eliminates the Lagrange multiplier λ, and allows us to obtain a PHS with state variables that have straightforward physical meaning. Lastly, it is important to note that a transformation of the form $x = T_p\, x_s$ cannot be established between the state $x \in \mathbb{R}^4$ of the PH-DAE in (I.37) and the state $x_s \in \mathbb{R}^2$ of the PHS in (I.44). Consequently, the PH-DAE in (I.37) cannot be reduced to an explicit PHS using this approach. This highlights the importance of selecting the appropriate representation based on the specific objectives of the analysis, particularly in this case, where the objective is to eliminate Lagrange multipliers while preserving the physical interpretation of the state variables.

I.2.3 Infinite-dimensional PHS

In the previous sections, we presented systems with lumped parameters, where the dynamic behavior is characterized by only functions of time. However, in the context of continuous systems, also known as infinite-dimensional or distributed-parameter systems, the dynamic behavior is described by functions of both space and time, which can be evaluated at an infinite number of spatial points. These models are governed by PDEs, involving spatial differential operators to capture the continuous nature of the system's dynamics.

As an introductory overview, the main differences between infinite-dimensional PHS and finite-dimensional PHS are:

- The state vector x becomes a function of space and time.
- $H(x)$ becomes an integral functional over the spatial domain, and the efforts are defined as the variational derivatives of $H(x)$ with respect to x.
- The skew-symmetric interconnection matrix in $\mathbb{R}^{n\times n}$ $J = -J^\top$ becomes a formal skew-adjoint differential interconnection operator in L^2 $\mathcal{J} = -\mathcal{J}^*$.
- The ports are divided into distributed ports over the spatial domain, and boundary ports corresponding to the PDE's boundary conditions. The latter are derived from the energy balance $\dot{H}$ and integration by parts.
- The Dirac structure is extended to the Stokes-Dirac structure to handle infinite-dimensional spaces and to include distributed and boundary ports.

I.2.3.a Reminder of mathematical tools

Let $\Omega \subset \mathbb{R}^\ell$ be an open set representing an ℓ-dimensional spatial domain and $\partial\Omega$ its boundary, such that $\mathtt{X} \in \Omega$ and $\mathtt{S} \in \partial\Omega$. An integral functional H of the dependent function $w(\mathtt{X}, t) \in \mathbb{R}^n$ is defined as:

$$H(w(\mathtt{X}, t)) = \int_\Omega \mathcal{H}(\mathtt{X}, w(\mathtt{X}, t))\, d\mathtt{X}, \tag{I.47}$$

where $\mathcal{H}(\mathtt{X}, w(\mathtt{X}, t)) \in \mathbb{R}$ is the functional density. The variational derivative of $H(w)$ with respect to $w(\mathtt{X}, t)$, denoted as $\frac{\delta H}{\delta w} = \delta_w H$, is defined from the following expression:

$$\delta H = \lim_{\alpha \to 0} \frac{d}{d\alpha} \left(\int_\Omega \mathcal{H}(\mathtt{X}, w + \alpha\eta)\, d\mathtt{X} \right) = \int_\Omega \left(\frac{\delta H}{\delta w} \cdot \delta w \right) d\mathtt{X}, \tag{I.48}$$

where δH is the first variation of $H(w)$, $\eta(\mathtt{X}, t) = \delta w(\mathtt{X}, t) \in \mathbb{R}^n$ is an arbitrary function that vanishes in $\partial\Omega$, and $\alpha \in \mathbb{R}$ is a scalar [Bedford 1985]. Note that when the functional density only depends explicitly on the dependent variable $w(\mathtt{X}, t)$, that is $\mathcal{H}(w)$, the variational derivative of $H(w)$ is equivalent to:

$$\delta_w H = \frac{\delta H}{\delta w} = \frac{\partial \mathcal{H}}{\partial w}. \tag{I.49}$$

On the other hand, a differential operator is a transformation that combines operations such as differentiation and multiplication by a function. In many physical systems, differential operators $\mathcal{F}_\mathtt{x}$ and their formal adjoints $\mathcal{F}_\mathtt{x}{}^*$ arise and can be generally defined as follows.

Definition I.1. *Let $\mathtt{X} = \{X_1, ..., X_\ell\}$ be a set of orthogonal coordinate axes, $\Omega \subset \mathbb{R}^\ell$ an open set, $w(\mathtt{X}) \in \mathbb{R}^n$ and $v(\mathtt{X}) \in \mathbb{R}^m$ two smooth vector functions with compact support on Ω. The first order nonlinear differential operator $\mathcal{F}_\mathtt{x}$ and its formal adjoint $\mathcal{F}_\mathtt{x}{}^*$ are defined as:*

$$\mathcal{F}_\mathtt{x} w(\mathtt{X}) = F_0(\mathtt{X}) w(\mathtt{X}) + \textstyle\sum_{k=1}^{\ell} F_k(\mathtt{X}) \partial_k w(\mathtt{X}), \tag{I.50}$$

$$\mathcal{F}_\mathtt{x}{}^* v(\mathtt{X}) = F_0(\mathtt{X})^\top v(\mathtt{X}) - \textstyle\sum_{k=1}^{\ell} \partial_k \left(F_k(\mathtt{X})^\top v(\mathtt{X}) \right), \tag{I.51}$$

with $\partial_k = \partial/\partial X_k$, $F_0(\mathtt{X}) \in \mathbb{R}^{m \times n}$ and $F_k(\mathtt{X}) \in \mathbb{R}^{m \times n}$ real matrices.

Notice that, similar to finite-dimensional spaces, where a linear operator (a matrix) $A \in \mathbb{R}^{m \times n}$ and its transpose $A^\top \in \mathbb{R}^{n \times m}$ satisfy:

$$\langle Aw \,|\, v \rangle_{in} = \langle w \,|\, A^\top v \rangle_{in},$$

with $\langle \cdot | \cdot \rangle_{in}$ denoting the inner product on finite-dimensional vector spaces, the differential operator $\mathcal{F}_\mathtt{x}$ with associated matrices $F_0(\mathtt{X}), F_k(\mathtt{X}) \in \mathbb{R}^{m \times n}$ and its formal adjoint $\mathcal{F}_\mathtt{x}{}^*$ satisfy:

$$\langle \mathcal{F}_\mathtt{x} w \,|\, v \rangle_{in}^{\Omega} = \langle w \,|\, \mathcal{F}_\mathtt{x}{}^* v \rangle_{in}^{\Omega}, \tag{I.52}$$

with $\langle \cdot | \cdot \rangle_{in}^{\Omega}$ denoting the inner product on infinite-dimensional Hilbert spaces.

I.2.3.b Infinite-dimensional PHS on Stokes-Dirac structures

A conservative dynamic system is called infinite-dimensional PHS if it can be written as:

$$\begin{aligned} \text{for all } \mathtt{X} \in \Omega: \quad \dot{x}(\mathtt{X}, t) &= \mathcal{J}(x)\, \delta_x H(x) + \mathcal{G}(x)\, u_d(\mathtt{X}, t) \\ y_d(\mathtt{X}, t) &= \mathcal{G}(x)^* \delta_x H(x), \\ \text{for all } \mathtt{S} \in \partial\Omega: \quad u_\partial(\mathtt{S}, t) &= \mathcal{B}_\partial\, \delta_x H(x), \\ y_\partial(\mathtt{S}, t) &= \mathcal{C}_\partial\, \delta_x H(x), \end{aligned} \tag{I.53}$$

where $x(\mathtt{X},t)$ is the state, $u_d(\mathtt{X},t)$, $y_d(\mathtt{X},t)$ are the distributed input and output ports, respectively. $\mathcal{J}(x) = -\mathcal{J}(x)^*$ is a formal skew-adjoint differential operator, $\mathcal{G}(x)$, $\mathcal{G}(x)^*$ are the input map operator and its formal adjoint, respectively. $\delta_x H(x)$ is the variational derivative of the Hamiltonian functional $H(x)$ with respect to $x(\mathtt{X},t)$ and defines the co-energy variables. $\mathcal{B}_\partial$, $\mathcal{C}_\partial$ are boundary operators that provide the boundary input $u_\partial(\mathtt{S},t)$ and boundary output $y_\partial(\mathtt{S},t)$ [Le Gorrec 2004; Le Gorrec 2005]. In order to define an infinite-dimensional PHS in the Stokes-Dirac structure, the operators $\mathcal{J}(x)$, $\mathcal{B}_\partial$ and $\mathcal{C}_\partial$ must satisfy an integration by parts formula. For more details see [Brugnoli 2020, Assumption 1].

Let $\mathscr{B}_d$, $\mathscr{F}_d$, and $\mathscr{E}_d$ be Hilbert spaces, where $\mathscr{F}_d$ is the flow space, its dual $\mathscr{E}_d$ is the effort space, and $\mathscr{B}_d = \mathscr{F}_d \times \mathscr{E}_d$ is called the bond space of power variables. A Stokes-Dirac structure on $\mathscr{B}_d$ is a subspace $\mathscr{D}_s \subset \mathscr{B}_d$ such that $\mathscr{D}_s = \mathscr{D}_s^\perp$ with respect to a bilinear form $\langle\langle \cdot, \cdot \rangle\rangle$ given by [Le Gorrec 2005]:

$$\begin{aligned}\langle\langle(\mathtt{f}_1, \mathtt{f}_{\partial_1}, \mathtt{e}_1, \mathtt{e}_{\partial_1}), (\mathtt{f}_2, \mathtt{f}_{\partial_2}, \mathtt{e}_2, \mathtt{e}_{\partial_2})\rangle\rangle = \\ \langle \mathtt{e}_1 | \mathtt{f}_2 \rangle_{in}^{\Omega} + \langle \mathtt{e}_2 | \mathtt{f}_1 \rangle_{in}^{\Omega} - \langle \mathtt{e}_{\partial_1} | \mathtt{f}_{\partial_2} \rangle_{in}^{\partial\Omega} - \langle \mathtt{e}_{\partial_2} | \mathtt{f}_{\partial_1} \rangle_{in}^{\partial\Omega},\end{aligned} \tag{I.54}$$

where $\langle \cdot | \cdot \rangle_{in}^{\Omega}$ and $\langle \cdot | \cdot \rangle_{in}^{\partial\Omega}$ are inner products defined over the spatial domain Ω, and its boundary $\partial\Omega$, respectively. Therefore, for any $(\mathtt{f}, \mathtt{f}_\partial, \mathtt{e}, \mathtt{e}_\partial) \in \mathscr{D}_s$ it is satisfied that $\langle\langle(\mathtt{f}, \mathtt{f}_\partial, \mathtt{e}, \mathtt{e}_\partial), (\mathtt{f}, \mathtt{f}_\partial, \mathtt{e}, \mathtt{e}_\partial)\rangle\rangle = 0$, which is verified in a general way using the Stokes' theorem [Le Gorrec 2005].

Now, consider the infinite-dimensional PHS in (I.53), if we choose $\mathtt{f} = [\mathtt{f}_s, \mathtt{f}_e, \mathtt{f}_\partial]^\top$ and $\mathtt{e} = [\mathtt{e}_s, \mathtt{e}_e, \mathtt{e}_\partial]^\top$, where $\mathtt{f}_s = \dot{x}$, $\mathtt{f}_e = u_d$, $\mathtt{f}_\partial = u_\partial$, $\mathtt{e}_s = \delta_x H$, $\mathtt{e}_e = -y_d$, $\mathtt{e}_\partial = -y_\partial$, then the set:

$$\mathscr{D}_s = \{(\mathtt{f}, \mathtt{e}) \in \mathscr{B}_d \mid \mathtt{f}_s = \mathcal{J}\mathtt{e}_s + \mathcal{G}\mathtt{f}_e\,,\ \mathtt{e}_e = -\mathcal{G}^*\mathtt{e}_s\,,\ \mathtt{f}_\partial = \mathcal{B}_\partial \mathtt{e}_s\,,\ \mathtt{e}_\partial = -\mathcal{C}_\partial \mathtt{e}_s\} \tag{I.55}$$

is a Stokes-Dirac structure. With the above definitions for $\mathtt{f}$ and $\mathtt{e}$, it is easy to show that the system (I.53) is conservative, and that the energy exchange with the environment is determined by the distributed and boundary ports by the expression:

$$\dot{H} = \langle y_d |\, u_d \rangle_{in}^{\Omega} + \langle y_\partial |\, u_\partial \rangle_{in}^{\partial\Omega}. \tag{I.56}$$

Similarly to the finite-dimensional case, infinite-dimensional PHS have been generalized to dissipative systems in Stokes-Dirac structures dividing the distributed ports into the open and resistive ports. For additional details refer to [van der Schaft 2002; Macchelli 2004b].

Remark I.1. *There also exist infinite-dimensional PHS defined in jet-bundle structures of variational complexes, often referred as port-Lagrangian systems (PLS) [Nishida 2005]. This approach uses the language of differential geometry and leverages the framework of jet-bundles to capture the relationships between fields and their higher-order spatial derivatives, providing a powerful tool for modeling and analyzing complex systems. For more details on PHS in jet-bundles, the reader is referred to [Nishida 2006; Schöberl 2014], and for a comparative perspective with PHS in Stokes-Dirac structures, see [Schöberl 2013].*

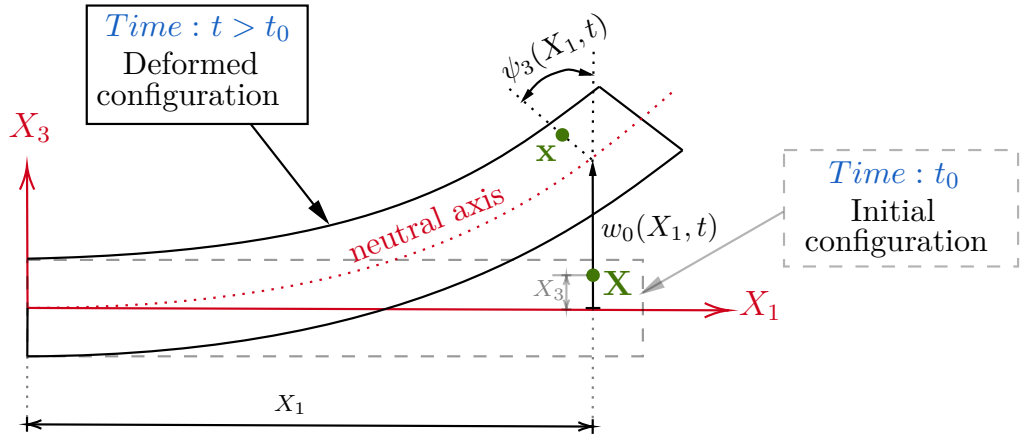

Figure I.6 – Kinematic assumption of Timoshenko beam.

I.2.3.c Example of infinite-dimensional PHS: Timoshenko beam

In general, dynamic models of flexible continuous bodies can also be derived by applying variational principles. Based on the theory of continuum mechanics and elasticity, the deformation of the body is hypothesized and mathematically expressed through a key variable in elasticity theory: the displacement field $\mathbf{u}(\mathbf{X}, t) = \mathbf{x}(\mathbf{X}, t) - \mathbf{X}$. This field provides the position of an arbitrary point $\mathbf{x}(\mathbf{X}, t) \in \mathbb{R}^3$ of the body in the deformed configuration relative to its position $\mathbf{X} \in \mathbb{R}^3$ in an initial or reference configuration. A comprehensive introduction to continuum mechanics and elasticity is provided in Appendix A, and the topic of modeling based on variational principles will be detailed in Chapter II.

In this section, the Timoshenko beam model is used to illustrate the infinite-dimensional PHS framework. This model is based on the kinematic assumption of first-order shear deformation theory [Reddy 2006, Chapter 10.1], which states that plane sections normal to the neutral axis before deformation remain plane but are not necessarily normal to the neutral axis after deformation. This is illustrated in the Fig. I.6, where $w_0(X_1, t) \in \mathbb{R}$ represents the vertical displacement of a point in the neutral axis, and $\psi_3(X_1, t) \in \mathbb{R}$ represents the angle of rotation of the cross-section. Then, the kinematic assumption of the Timoshenko beam is equivalent to the displacement field $\mathbf{u}(\mathbf{X}, t)$:

$$\mathbf{u}(\mathbf{X}, t) = \mathbf{x}(\mathbf{X}, t) - \mathbf{X} = \begin{bmatrix} -X_3\, \psi_3(X_1, t) \\ 0 \\ w_0(X_1, t) \end{bmatrix}, \tag{I.57}$$

where the hypothesis of small deformation was used. For this example we have that $X_1 \in \Omega = (0, L)$, with L the length of the beam in the initial configuration, $\mathtt{S} = \{0, L\}$ are the boundary points, where in $\mathtt{S} = 0$ are imposed the Dirichlet boundary conditions that specify the displacement $w_0(0, t) = \hat{w}_0(t)$ and angle

$\psi_3(0,t) = \hat{\psi}_0(t)$, and in $\mathtt{S} = L$ are imposed the Neumann boundary conditions that specify the shearing force $\hat{V}_L(t)$ and bending moment $\hat{M}_L(t)$. The Lagrangian model of the Timoshenko beam, obtained for instance by applying Hamilton's principle [Reddy 2006, Chapter 2.2.3], is given by:

$$\begin{aligned} \text{for all } X_1 \in \Omega: \quad & \rho\bar{I}\frac{\partial^2\psi_3}{\partial t^2} + \kappa GA\left(\psi_3 - \frac{\partial w_0}{\partial X_1}\right) - \frac{\partial}{\partial X_1}\left(E\bar{I}\frac{\partial\psi_3}{\partial X_1}\right) = 0, \\ & \rho A\frac{\partial^2 w_0}{\partial t^2} + \frac{\partial}{\partial X_1}\left[\kappa GA\left(\psi_3 - \frac{\partial w_0}{\partial X_1}\right)\right] = 0, \end{aligned} \tag{I.58}$$

$$\begin{aligned} \text{for } \mathtt{S} = L: \quad & \hat{M}_L(t) = E\bar{I}\frac{\partial\psi_3}{\partial X_1}\Big|_{\mathtt{S}=L}, \\ & \hat{V}_L(t) = \kappa GA\left(\frac{\partial w_0}{\partial X_1} - \psi_3\right)\Big|_{\mathtt{S}=L}, \end{aligned} \tag{I.59}$$

$$\begin{aligned} \text{for } \mathtt{S} = 0: \quad & \hat{\psi}_0(t) = \psi_3(0,t), \\ & \hat{w}_0(t) = w_0(0,t), \end{aligned} \tag{I.60}$$

where A is the cross section area, $\bar{I}$ is the second moment of inertia of the cross section, ρ, G, E are properties of the material, and κ is a correction factor. For the PH representation of the Timoshenko beam model, the energy variables of the system are chosen as [Macchelli 2004a]:

$$p_1 = \rho\bar{I}\frac{\partial\psi_3}{\partial t}, \qquad p_2 = \rho A\frac{\partial w_0}{\partial t}, \qquad \epsilon_1 = \frac{\partial\psi_3}{\partial X_1}, \qquad \epsilon_2 = \left(\frac{\partial w_0}{\partial X_1} - \psi_3\right), \tag{I.61}$$

where p_1 is the generalized angular momentum, p_2 the generalized linear momentum, ϵ_1 is the deformation due to bending (also called curvature), and ϵ_2 is the shear deformation. The Hamiltonian functional that represents the total stored energy in the system is given by:

$$H(p,\epsilon) = \frac{1}{2}\int_0^L \left(\frac{p_1^2}{\rho\bar{I}} + \frac{p_2^2}{\rho A} + E\bar{I}\epsilon_1^2 + \kappa GA\epsilon_2^2\right) dX_1, \tag{I.62}$$

where the first and second terms are the rotational and translational kinetic energies, respectively, and the third and fourth terms are the elastic potential energy due to the bending and shearing, respectively. So, the flow and effort variables are given by:

$$\begin{aligned} f_{p_1} &= \frac{\partial p_1}{\partial t} = \rho\bar{I}\frac{\partial^2\psi_3}{\partial t^2}, & e_{p_1} &= \frac{\delta H}{\delta p_1} = \frac{p_1}{\rho\bar{I}} = \frac{\partial\psi_3}{\partial t}, \\ f_{p_2} &= \frac{\partial p_2}{\partial t} = \rho A\frac{\partial^2 w_0}{\partial t^2}, & e_{p_2} &= \frac{\delta H}{\delta p_2} = \frac{p_2}{\rho A} = \frac{\partial w_0}{\partial t}, \\ f_{\epsilon_1} &= \frac{\partial\epsilon_1}{\partial t} = \frac{\partial}{\partial t}\left(\frac{\partial\psi_3}{\partial X_1}\right), & e_{\epsilon_1} &= \frac{\delta H}{\delta\epsilon_1} = E\bar{I}\epsilon_1 = E\bar{I}\frac{\partial\psi_3}{\partial X_1}, \\ f_{\epsilon_2} &= \frac{\partial\epsilon_2}{\partial t} = \frac{\partial}{\partial t}\left(\frac{\partial w_0}{\partial X_1} - \psi_3\right), & e_{\epsilon_2} &= \frac{\delta H}{\delta\epsilon_2} = \kappa GA\epsilon_2 = \kappa GA\left(\frac{\partial w_0}{\partial X_1} - \psi_3\right), \end{aligned} \tag{I.63}$$

where f_{p_1} is the inertial moment, f_{p_2} the inertial force, f_{ϵ_1} the bending strain velocity, f_{ϵ_2} shearing strain velocity, e_{p_1} the angular velocity, e_{p_2} the linear velocity, e_{ϵ_1} the internal bending moment and e_{ϵ_2} the internal shearing force. With all the

above and using the notation $\partial_1 = \partial/\partial X_1$, the PH representation of the Timoshenko beam is given by:

$$\text{for all } X_1 \in \Omega: \quad \underbrace{\begin{bmatrix} \dot{p}_1(X_1,t) \\ \dot{p}_2(X_1,t) \\ \dot{\epsilon}_1(X_1,t) \\ \dot{\epsilon}_2(X_1,t) \end{bmatrix}}_{\dot{x}(X_1,t)} = \underbrace{\begin{bmatrix} 0 & 0 & \partial_1 & 1 \\ 0 & 0 & 0 & \partial_1 \\ \partial_1 & 0 & 0 & 0 \\ -1 & \partial_1 & 0 & 0 \end{bmatrix}}_{\mathcal{J}=-\mathcal{J}^*} \underbrace{\begin{bmatrix} e_{p_1}(X_1,t) \\ e_{p_2}(X_1,t) \\ e_{\epsilon_1}(X_1,t) \\ e_{\epsilon_2}(X_1,t) \end{bmatrix}}_{\delta_x H(x)}, \tag{I.64}$$

$$\text{for all } \mathtt{S} \in \partial\Omega: \quad \begin{aligned} u_\partial(\mathtt{S},t) &= \begin{bmatrix} e_{p_1}(0,t) & e_{p_2}(0,t) & e_{\epsilon_1}(L,t) & e_{\epsilon_2}(L,t) \end{bmatrix}, \\ y_\partial(\mathtt{S},t) &= \begin{bmatrix} e_{p_1}(L,t) & e_{p_2}(L,t) & -e_{\epsilon_1}(0,t) & -e_{\epsilon_2}(0,t) \end{bmatrix}. \end{aligned}$$

Note that $x(X_1,t) \in \mathbb{R}^4$ consists of four variables, corresponding to four dynamic equations. The two first equations in (I.64) are equivalent to the Lagrangian model presented in (I.58), and the two last are compatibility equations. Additionally, the boundary input $u_\partial(\mathtt{S},t)$ encompasses both, the time derivatives of the Dirichlet boundary conditions in (I.60), and the Neumann boundary conditions in (I.59).

I.3 Literature review

This section provides a literature review of the key topics addressed in this thesis, namely the PH modeling of flexible mechanical systems, the structure-preserving discretization, and the shape control of flexible systems. Additionally, relevant literature is cited throughout the individual chapters to support and contextualize the discussion.

I.3.1 Modeling of flexible mechanical systems

The modeling of flexible mechanical systems traditionally employs two fundamental approaches: Newton's method and d'Alembert's principle. Newton's method derives equations of motion from the forces acting on the system, whereas d'Alembert's principle uses the concept of virtual work. Applying d'Alembert's principle yields the Euler-Lagrange (E-L) equations, where the Lagrangian functional that depends on the energy of the system is the key quantity used. This approach offers a more compact description of the system, which allows the use of variational techniques to obtain approximate and analytical solutions [Goldstein 2002; Lanczos 2012]. Therefore, the E-L equations can also be derived from fundamental physics principles, such as Hamilton's principle [Landau 2013]. The connection between the E-L equations and Hamiltonian mechanics is demonstrated through the Legendre transform and the Poisson structure [Arnol'd 2013; Hassani 2013]. In classical Hamiltonian mechanics, the equations describe the temporal evolution of the system through a skew-symmetric matrix called symplectic matrix, which is nothing more than a representation of the set of transformations that leaves the Poisson brackets invariant [Hassani 2013]. In addition, the Poisson structure

defines the algebra of the brackets and allows the study of the dynamic properties of the system [León 2011]. In this thesis we focus on PHS, which are a class of geometrically defined open physical systems with ports. PHS come from the network modeling of physical systems through bond-graphs, which are associated with a Dirac structure that generalizes the Poisson structure of the classical Hamiltonian approach [Maschke 1992; van der Schaft 2002]. In [Mattioni 2021], it is demonstrated that the E-L equations of flexible mechanisms can be derived by applying Hamilton's principle to a system with a properly defined Lagrangian functional. Then, through a suitable change of variables it can be rewritten as an infinite-dimensional PHS. In this line, [Nishida 2005] shows a one-to-one correspondence between E-L equations and field port-Lagrangian systems (PLS) on variational complexes of jet bundles. When the Lagrangian functional is known, a systematic procedure for the transformation to a port-Lagrangian model is presented. It should be noted that although these works typically begin with another model representation, such as the Lagrangian model from the E-L equations, they are grounded in specific kinematic assumptions and constitutive laws.

Port-Hamiltonian models of linear mechanical systems

From a kinematic perspective, linear models account for small displacements and strains using the infinitesimal strain tensor to measure deformation, resulting in what are known as geometrically linear systems. Additionally, linear models assume a linear relationship between infinitesimal strains and stresses based on the generalized Hooke's law, leading to what are referred to as materially linear systems. Since the introduction of finite-dimensional PHS in [Maschke 1992] and their subsequent extension to infinite dimensions in [van der Schaft 2002], the usual way to derive the PHS representation of existing infinite-dimensional linear models involves choosing energy variables appropriately. Despite the fact that this procedure may require intuition to select the correct set of state variables ensuring the emergence of the skew-adjoint differential operator, it has proven to be effective for reformulating classical linear elasticity-based models within the PH framework. Well known linear examples include vibrating string [Talasila 2002], Euler-Bernoulli beam [Nishida 2004], Timoshenko beam [Macchelli 2004a], and classical plate models [Macchelli 2005; Brugnoli 2019a; Brugnoli 2019b], among others. A more general treatment of linear elastodynamics is presented in [Brugnoli 2020], where it is shown that defining energy variables as vector or tensor fields leads to PH models associated with coordinate-free differential operators.

Port-Hamiltonian models of nonlinear mechanical systems

Based on the assumption of finite deformation, characterized by large displacements and strains, the Green-Lagrange strain tensor, is used to measure deformation, leading to what are known as geometrically nonlinear systems. Intermediate strain measures also fall into this category, such as the von Kármán strains, which account for moderate deformation by neglecting certain terms of the Green-Lagrange strain tensor. In addition, when the constitutive relation between strains

and stresses is nonlinear and defined by an arbitrary strain energy density function, this results in hyperelastic systems. It is important to note that in Hooke's law, the strain energy density function is a quadratic function of the strain, making it the simplest hyperelastic constitutive model. Several researchers have made notable contributions in the domain of geometrically nonlinear modeling employing formulations based on von Kármán strains. [Brugnoli 2021] presented an Euler-Bernoulli beam model, while [Voss 2008] explored a piezo-actuated Euler-Bernoulli beam. In a similar vein, [Voss 2014] introduced a piezo-actuated Timoshenko beam. [Trivedi 2015] proposed a cart-mounted Timoshenko beam model, incorporating the additional constraint of inextensibility. Notably, [Brugnoli 2022a] extended this idea by introducing a two-dimensional von Kármán plate model. In a broader context, [Thoma 2022a; Thoma 2024] formulated elasticity incorporating geometric nonlinearity through the Green-Lagrange strain tensor, while maintaining material linearity through the assumption of hyperelasticity via a Saint Venant-Kirchhoff material, which is the extension of Hooke's law for finite deformation. To the best of the author's knowledge, the only known work incorporating both sources of nonlinearities within an infinite-dimensional PHS model is the study by [Kinon 2023], where the focus is made on modeling a geometrically exact string, considering hyperelasticity with a neo-Hookean material.

I.3.2 Structure-preserving reduction methods

Reduction methods include spatial discretization, which transforms infinite-dimensional PDEs into finite-dimensional ODEs, and model reduction, which simplifies large-scale ODEs into smaller, more manageable systems.

Structure-preserving spatial discretization

Classical numerical methods like finite difference, finite volume, and finite element methods often fail to capture the intrinsic properties and structure of systems, such as energy conservation and symmetry, especially when they are applied to infinite-dimensional PHS [Seslija 2012]. Therefore, specialized structure-preserving discretization methods are needed to ensure that the resulting finite-dimensional models retain the inherent properties of the original system. The principles of mimetic discretizations is extensively discussed in [Bochev 2006].

The first structure-preserving discretization methods based on finite differences have been presented in [Clemente-Gallardo 2002; Lopezlena 2004], where the methods aim to discretize the domain in a mesh of nodes where finite differences are used to approximate the variables. A drawback of this methods is that only uniform meshes can be used. In [Trenchant 2018] that problem was avoided by using staggered-grids finite differences. In [Kotyczka 2016], a finite volume method based on the generalized leapfrog method was introduced for 1D systems and, in [Serhani 2018] was extended to 2D linear and nonlinear systems.

Standard FEM (sFEM) is a single field based method that only approximate the primary unknowns [Cook 2007; Reddy 2014]. It can also be applied to mechanical systems by means of the Hamilton's principle and the Galerkin method [Reddy 2017], such that the discretized model preserves the Lagrangian structure and therefore can be written as a finite-dimensional PHS. The partitioned FEM (pFEM) was introduced in [Cardoso-Ribeiro 2018], which consists in rewriting the system in weak form where only some of the equations are integrated by parts, so that the interconnection structure and the constitutive equations are discretized separately. This separation provides the possibility to tackle parabolic and nonlinear systems, at the cost of solving a system written as a finite-dimensional PH-DAE. In the particular case of linear hyperbolic PDEs, the constitutive laws can be taken into account in the first steps in order to put the finite-dimensional PHS in explicit form and recover an ODE system [Brugnoli 2020b]. The pFEM has been successfully applied for the discretization and simulation of Mindlin and Kirchhoff-Love plate models, respectively in [Brugnoli 2019a; Brugnoli 2019b]. In [Warsewa 2021], a connection between the sFEM and pFEM is done. In that work, the pFEM is applied to discretize one-dimensional structural elements and shown that complex structures can be assembled by interconnecting individual discretized system via coupling constraints, which leads to DAEs that can be reduced to ODEs by means of a transformation. Afterward, by eliminating linearly dependent effort variables the resulting system coordinates can be transformed to the usual space of global degrees of freedom used in sFEM. Recently, [Brugnoli 2024] examines the equivalences among Lagrangian, Hamiltonian and mixed FEM formulations for linear wave phenomena. Regarding other methods based on FEM, exterior calculus approaches have been presented in [Seslija 2011; Seslija 2012; Seslija 2014; Brugnoli 2022b], and a mixed FEM (mFEM) approach was presented in [Golo 2004]. In the latter, the interconnection structure of the PDE system is discretized in the first stage, and differential forms are used to approximate the constitutive equations of the energy variables in the second stage. It has been successfully applied to one-dimensional problems [Hamroun 2010; Golo 2002] and two-dimensional problems [Wu 2015; Eberard 2007]. In [Moulla 2012], a pseudospectral method is introduced that can be considered as a generalization of mFEM. This method uses different kinds of polynomials as approximation bases, resulting in higher accuracy for lower-order approximations. In addition, in [Thoma 2022b; Thoma 2022a] are presented two-fields-based mFEM approaches reminiscent to the Hellinger-Reissner (H-R) variational principle, applied to linear and geometrically nonlinear mechanical systems, respectively, where both, Dirichlet and Neumann boundary conditions are weakly imposed, leading to explicit finite-dimensional PHS representations without the need of algebraic constraints. Lastly, [Kinon 2023] introduces a three-fields-based mFEM approach reminiscent to the Hu-Washizu variational principle. This approach allows for the inclusion of material nonlinearities, but Dirichlet boundary conditions are imposed using Lagrange multipliers, similar to the method described in [Brugnoli 2020a]. As a result, the final system is a finite-dimensional PH-DAE.

Structure-preserving model order reduction

Finite-dimensional discretized approximations often yield very high-order (large scale) systems, making them impractical for simulation and control design. Consequently, model order reduction techniques that preserve the PHS structure and properties are necessary. For instance, in [Hartmann 2010], order reduction of linear second-order PHS is achieved by defining a balancing transformation that scales certain Hankel singular values. As this parameter approaches zero, the reduced model retains the PHS structure. Similarly, [Kawano 2018] generalizes this idea for nonlinear PHS using the controllability and observability functions introduced in [Scherpen 1993]. Additionally, a method based on proper orthogonal decompositions and optimization to find bases for nonlinear PHS is presented in [Chaturantabut 2016]. For linear PHS, the classic moment matching at infinity approach is extended in [Polyuga 2010b]. Using Krylov's methods, the Galerkin projection (Arnoldi method) and Galerkin-Petrov projection (Lanczos method) are applied for model reduction in a specific coordinate system to preserve a set of Markov parameters and the PHS structure. Moreover, [Ionescu 2013] obtains families of reduced-order models of linear PHS through time-domain moment matching. In [Mourllion 2013], a modal decomposition of linear Hamiltonian systems is presented, where the reduced model is obtained by truncating up to a certain number of eigenvalues. This approach is straightforwardly extendable to linear mechanical PHS with a canonical interconnection matrix. Additional structure-preserving order reduction methods can be found in [Polyuga 2010a; Wolf 2010; Gugercin 2012; Xu 2019; Schulze 2023]. These methods collectively contribute to the field by providing various approaches to maintaining the PHS structure during the model order reduction process.

I.3.3 Shape control of flexible systems

One of the first works where the term shape control was used is [Haftka 1985], where an analytic procedure is described to control quasi-stationary deformations in large flexible structures using thermal actuators. In that work, and generally in the related literature, static shape control is understood as achieving desired deformed configurations dealing with static models, while dynamic shape control deals with dynamic models. One of the most common topics in static shape control consists in determining the spatial arrangement of actuators and the magnitudes of the control inputs to achieve desired shapes. For instance, [Agrawal 1999] studies this problem by minimizing the error between the desired shape and the achieved shape. The optimization problem addresses the spatial layout of piezoelectric actuators along an Euler-Bernoulli beam and the optimal voltage magnitudes. Similarly, [Agrawal 1994] addresses this problem for a Kirchhoff-Love plate with piezoelectric actuators. [Agrawal 1997] focuses solely on optimizing the control input magnitudes for a layered composite plate model with higher-order shearing effects, and [Luo 2006] does the same for a Mindlin plate. The influence of layers ordering in composite beams is studied in [Donthireddy 1996] to determine its ef-

fect on performance and actuation capabilities. The effect of locating piezoelectric actuators to suppress static deflection on Mindlin plates under different boundary conditions is discussed in [Ghosh 1995]. [Plotnikova 2020] concludes that placing a piezoelectric actuator at the geometric center of a Kirchhoff-Love plate is optimal for counteracting uniformly distributed loads. [Yang 2000] presents analytical results showing that a piezoelectric-actuated beam can be deformed into quadratic or cubic shapes due to the equivalent action of applying a pair of opposite torques on the piezoelectric boundary. In [Chandrashekhara 1997], an optimal, quasi-static, closed-loop control strategy is proposed to achieve the desired shape of a composite beam under unknown perturbations. The scheme determines the optimal piezoelectric actuator voltages by minimizing the error between a desired output vector and the measured output, and it is extended to a composite Mindlin plate model in [Varadarajan 1998]. The problem of actuator location and optimal magnitude is also explored in [Liu 2018], which considers a Timoshenko beam model with dielectric elastomeric actuators (DEA) and uses stochastic techniques and genetic algorithms to solve the optimization problem. Regarding dynamic shape control, [Yang 2006] conducts experimental tests on beams and plates using shape memory alloy actuators. For the beam, a first-order dynamic model is experimentally identified, and a PID controller is designed to improve the transient response and reduce the steady-state error for given deformation references.

In the PHS framework, [Voß 2011] explores dynamic shape control of a Timoshenko beam model with piezoelectric patches as actuators. By applying passivity-based control techniques such as energy shaping and damping injection for each piezoelectric patch, a decentralized control scheme is achieved. The first result on control by interconnection for infinite-dimensional PHS with in-domain actuation is presented in [Trenchant 2017], which considers fully actuated systems, positive feedback, and the late lumping approach (designing the controller in the infinite-dimensional setting and later discretizing). [Malzer 2019] applies the late lumping approach with negative feedback and the jet bundle formalism to design a finite-dimensional port-Hamiltonian controller for a piezo-actuated Euler-Bernoulli beam, later extending it to a Kirchhoff-Love plate in [Malzer 2020]. [Zhou 2021] considers a Timoshenko beam actuated by ionic polymer metal composite (IPMC) actuators. The control strategy follows the early lumping approach (first discretize, then design the controller in the finite-dimensional setting) using the interconnection and damping assignment-passivity based control (IDA-PBC) technique, complemented with integral action. The resulting nonlinear control law is validated with experimental tests. Finally, [Liu 2024] presents control by interconnection of infinite-dimensional 1D linear PHS using positive feedback, the early lumping approach with the discretization scheme proposed in [Golo 2004], and both fully actuated and underactuated systems. The main control objectives are to stabilize the closed-loop system at the origin and to modify dynamic performance. A remarkable result is that they demonstrate asymptotic stability in the infinite-dimensional PHS controlled by the finite-dimensional PH controller.

I.4 Thesis organization and contributions

This thesis is organized in five main chapters:

Chapter I: This chapter addresses the motivation behind the modeling and discretization approaches aimed for simulation and shape control of multidimensional flexible mechanical systems. It reviews the key characteristics of the port-Hamiltonian framework in both finite and infinite dimensions, including extensions to dissipative systems and systems with algebraic constraints enforced via Lagrange multipliers. Finally, the chapter presents a literature review to contextualize the state of the art to understand the contributions of this thesis.

Chapter II: This chapter addresses the modeling of multidimensional flexible mechanical systems using the generalized extended Hamilton's principle. This principle generalizes both Hamilton's principle and the Hu-Washizu variational principle by incorporating an extended Lagrangian functional that accommodates both Dirichlet and Neumann boundary conditions, integrates constraints, and considers independent variations in displacement, strain, stress, and Lagrange multipliers fields. Using this principle, the chapter first presents general methodologies for modeling linear mechanical systems employing the infinitesimal strain tensor and Hooke's law. It then extends the methodology to geometrically nonlinear systems with the Green-Lagrange strain tensor and general hyperelastic materials. Finally, the chapter expands the approach to include algebraic constraints, presenting two equivalent representations: one as a PH-DAE, and another as an explicit PHS that internally resolves the algebraic constraints.

Contributions: The chapter proposes systematic modeling methodologies based on the generalized extended Hamilton's principle for the modeling of linear, nonlinear, and constrained nonlinear flexible mechanical systems as PHS. It proposes four systematic modeling methodologies to obtain PH representations of multidimensional:

- Linear mechanical systems as explicit PHS.
- Nonlinear mechanical systems as explicit PHS.
- Constrained nonlinear mechanical systems as implicit PH-DAE.
- Constrained nonlinear mechanical systems as explicit PHS.

Chapter III: In this chapter, we address the structure-preserving discretization of multidimensional flexible mechanical systems using mixed FEM approaches. First, we focus on the discretization of linear mechanical systems through the application of a mixed FEM strategy based on two fields, known as the modified Linked Lagrange Multiplier (mLLM) method, employed to weakly impose Dirichlet boundary conditions in mechanical systems. Subsequently, we move to the discretization of geometrically nonlinear and hyperelastic systems by applying a natural extension

of the virtual power principle, reminiscent to the generalized extended Hamilton's principle, resulting in a mixed FEM scheme based on three fields. Finally, we further extend this scheme to accommodate algebraic constraints, leading to a mixed FEM scheme based on four fields. Simulated examples of both linear and nonlinear systems are also presented in this chapter.

Contributions: The chapter proposes weak formulations for infinite-dimensional mechanical systems based on the mLLM method and a natural extension of the virtual power principle, reminiscent to the generalized extended Hamilton's principle. Consequently, it proposes three mixed FEM approaches for the structure-preserving discretization of multidimensional flexible mechanical systems. These approaches are:

- Two-fields based approach for discretization of linear PHS.
- Three-fields based approach for discretization of nonlinar PHS.
- Four-fields based approach for discretization of nonlinear PH-DAE.

Chapter IV: This chapter focuses on reduced-order energy shaping control for high-dimensional linear PHS arising from the discretization of infinite-dimensional PHS representations. It presents dynamic controllers based on low-dimensional and reduced-order models. Initially, it defines the controller structure and asymptotic stability criteria using the full-order model. It then compares two design methods: one using a low-dimensional discretized model and another one using a reduced-order model through modal truncation. For shape control applications, it parameterizes the system's equilibrium points with respect to the controller parameters to establish an optimal criterion for minimizing errors between intended and actual closed-loop equilibrium states. Additionally, it provides an asymptotic stability margin related to the stiffness matrices of the full-order and reduced-order models, connecting this to closed-loop transient performances. The chapter demonstrates the approach's effectiveness through applications to a Mindlin plate, illustrating successful dynamic shape control.

Contributions: The chapter proposes a class of finite-dimensional PH controllers synthesized from a low-order representation of a of high-dimensional (large scale) discretized linear PHS. The key contributions are that the control strategy:

- Is applicable to a wide range of systems, whether fully actuated or underactuated, with boundary and/or in-domain actuation.
- Allows for independently affecting the dynamic response, achieving the optimal equilibrium configuration, and desired oscillation decay rates.
- Provides an asymptotic stability margin that guarantee stability in the high-dimensional discretized model.

Chapter V: This chapter provides conclusions on the results from the previous chapters and outlines future research directions. It synthesizes key findings, highlights advancements in modeling, discretization, and control of flexible mechanical systems within the PHS framework, and suggests new research lines for further investigation and potential applications.

I.5 List of publications

As result of this research, the following journal papers were produced:

- Cristobal Ponce, Yongxin Wu, Yann Le Gorrec, Hector Ramirez. «A systematic methodology for port-Hamiltonian modeling of multidimensional flexible linear mechanical systems». *Applied Mathematical Modelling (2024)*. (Published)
- Cristobal Ponce, Hector Ramirez, Yann Le Gorrec. «Reduced-order energy shaping control of large-scale linear port-Hamiltonian systems». *Automatica (2025)*. (Published)

the following conference papers:

- Cristobal Ponce, Hector Ramirez, Yann Le Gorrec, Francisco Vargas. «A comparative study of reduced model based boundary control design for linear port-Hamiltonian systems». *IFAC-PapersOnLine, 55(26), 107-112, (2022)*. (Published)
- Cristobal Ponce, Hector Ramirez, Yann Le Gorrec. «Finite dimensional shape control design of linear port-Hamiltonian systems with in-domain pointwise inputs». *IFAC-PapersOnLine, 56(2), 6777-6782, (2023)*. (Published)
- Cristobal Ponce, Yongxin Wu, Yann Le Gorrec, Hector Ramirez. «Port-Hamiltonian modeling of a geometrically nonlinear hyperelastic beam». *IFAC-PapersOnLine, 56(6), 309-314, (2024)*. (Published)
- Cristobal Ponce, Nelson Cisneros, Yongxin Wu, Kanty Rabenorosoa, Yann Le Gorrec, Hector Ramirez. «Port-Hamiltonian modeling of large-scale curling HASEL actuators». *IFAC MICNON (2024)*. (Published)
- Cristobal Ponce, Yongxin Wu, Yann Le Gorrec, Hector Ramirez (2024). «Structure-preserving discretization of multidimensional linear port-Hamiltonian systems using FEM approaches». *IEEE CDC (2024)*. (Accepted)
- Cristobal Ponce, Hector Ramirez, Yann Le Gorrec, Yongxin Wu (2025). «Constrained port-Hamiltonian modeling and structure-preserving discretization of the Rayleigh beam». *IFAC CPDE (2025)*. (Submitted)
- Nelson Cisneros, Cristobal Ponce, Yongxin Wu, Alessandro Macchelli, Yann Le Gorrec, Hector Ramirez (2025). «Position and anti-drift control of large-scale curling HASEL actuators». *IFAC NOLCOS (2025)*. (Submitted)

and the following preprint paper:

- Cristobal Ponce, Yongxin Wu, Yann Le Gorrec, Hector Ramirez. «Port-Hamiltonian modeling of multidimensional flexible mechanical structures defined by linear elastic relations». *Preprint arXiv:2311.03796 (2023)*.

Chapter II
Modeling methodologies for flexible systems

II.1 Introduction

The modeling of flexible mechanical systems has traditionally centered on two foundational approaches: Newton's method and d'Alembert's principle. Newton's method derives the system's equations of motion from the forces acting upon it, while d'Alembert's principle introduces the concept of virtual work, leading to the derivation of the Euler-Lagrange (E-L) equations. These equations describe the system's dynamics in terms of a Lagrangian functional, which encapsulates the system's energy. This formulation, rooted in variational principles, allows for the use of powerful mathematical techniques to derive both approximate and analytical solutions [Goldstein 2002; Lanczos 2012]. The E-L equations themselves can be derived from Hamilton's principle [Landau 2013], and further transformed into Hamiltonian form through the Legendre transformation. Hamiltonian mechanics provides an alternative yet equivalent formulation, describing system dynamics via a skew-symmetric matrix, where the evolution is governed by gradients of the Hamiltonian function. The port-Hamiltonian systems (PHS) framework extends this classical Hamiltonian approach, offering a more generalized structure that is particularly suited for modeling open physical systems. Unlike the closed systems typically treated by classical Hamiltonian mechanics, PHS explicitly accounts for energy exchanges through system boundaries, making it ideal for a wide variety of practical applications where energy flow is a key consideration [Maschke 1992; van der Schaft 2002]. Recent research has demonstrated that flexible bodies, such as beams and plates, can be systematically modeled using Hamilton's principle. For example, [Mattioni 2021] derived E-L equations by applying Hamilton's principle to systems with a defined Lagrangian functional, and subsequently transformed these into infinite-dimensional PHS via a suitable change of variables. Similarly, [Nishida 2005] establishes a one-to-one correspondence between the E-L equations and field port-Lagrangian systems (PLS) within variational complexes of jet bundles, also called PHS on jet bundles. Given a known Lagrangian functional, the transformation to a PLS is achieved through a systematic procedure. It is important to note that these approaches typically start from an established model representation, such as the Lagrangian form, however, it is crucial to remember that these models are based on specific kinematic assumptions and constitutive laws, which form the foundations of the modeling process.

In this chapter, we focus on the modeling of a class of flexible mechanical systems using the continuum mechanics approach, emphasizing the concepts of displacement, strain, and stress fields. The modeling begins with kinematic assumptions represented as a specific factorization of the displacement field, from which are identified primary generalized coordinates termed generalized displacements. From this field, we derive real strains based on designated measures: infinitesimal strains for geometrically linear systems, and Green-Lagrange or von Kármán strains for geometrically nonlinear systems. This process leads to the definition of secondary generalized coordinates, referred to as generalized strains. Using hyperelasticity

theory for the constitutive laws, including Hooke's law for materially linear systems, we then define the generalized stresses. For systems subject to constraints, the constraint function is reformulated in a suitable manner, enforced through Lagrange multipliers. With all the above, in this chapter we propose systematic methodologies for deriving infinite-dimensional PHS and PH-DAE representations for a class of flexible mechanical systems defined over any spatial dimension, using the generalized extended Hamilton's principle to derive the dynamic equations. These methodologies avoid the laborious algebraic manipulations typically associated with application of variational principles, which have been pre-computed for the entire class of systems. This approach removes the need for intuitive guesswork by providing explicit definitions of energy variables, co-energy variables, and boundary inputs and outputs, thus facilitating the systematic construction of the skew-adjoint differential operator and the PHS or PH-DAE representations. The PH models derived using these methodologies align with the well-established categories of linear, geometrically nonlinear, and hyperelastic mechanical systems, and find application in areas such as structural dynamics, robotics, biomechanics, and aerospace engineering. The chapter begins with a summary of the necessary background in continuum mechanics and variational principles, where most of the details are omitted. However, interested readers can refer to Appendix A or the cited references for more information. Following this, we present the general methodology for modeling linear mechanical systems using the infinitesimal strain tensor and Hooke's law. This methodology is then extended to geometrically nonlinear systems using the Green-Lagrange strain tensor and general hyperelastic materials. Finally, the chapter expands the approach to include algebraic constraints, presenting two equivalent representations: a PH-DAE formulation enforcing the algebraic constraint via Lagrange multipliers, and an explicit PHS representation that internally resolves the algebraic constraint.

II.2 Preliminaries

II.2.1 Continuum mechanics

Continuum mechanics studies the behavior of materials modeled as continuous masses rather than discrete particles. It includes the study of kinematics, focusing on motion and deformation without considering the forces causing them, and conservation laws, which govern the conservation of mass, linear and angular momentum, and energy in material bodies. Hyperelasticity, a subset of continuum mechanics, addresses the nonlinear elastic behavior of materials under large deformations, making it essential for modeling materials like rubber and biological tissues. Additionally, variational principles use energy minimization to derive the governing equations of mechanical systems.

From [Reddy 2007], a continuous medium is a portion of matter composed of an infinite set of particles studied macroscopically, without considering possible microscopic discontinuities. Continuum mechanics proposes a unified model for the mechanics of deformable solids, rigid solids, and fluids, treating them as continuous media. In solid mechanics, key quantities are **strain**: a measure of the relative deformation between particles excluding rigid-body displacements; and **stress**: a measure of an internal force per unit area that expresses the interaction with the surrounding particles in some direction in the continuous medium. The equations governing the motion and deformation of a solid body can be classified into four basic categories: kinematics (strain-displacement relations), kinetics (conservation of momentum), thermodynamics (first and second laws), and constitutive equations (stress-strain relations).

Topic of study	Physical law	Equations
1. Kinematics	None (based on geometric changes)	strain-displacement relations
2. Kinetics	Conservation of momentum	equations of motion
3. Thermodynamics	First and second laws	energy equation
4. Constitutive equations	Constitutive axioms	stress-strain relations

Table II.1 – Relationship between physical principles and governing equations.

Fundamentals of motion

There exists two ways of describing the motion: in the spatial or in the reference configuration. In finite deformation analysis, different descriptions are used to characterize continuum quantities. When a quantity is expressed in terms of its position before deformation, it is referred to as a material or Lagrangian description (described in the reference configuration, also called the initial configuration). Conversely, when a quantity is expressed in terms of its position during deformation, it is known as a spatial or Eulerian description (described in the current configuration, also called the deformed configuration). From Fig. II.1, let $\{X_1, X_2, X_3\}$ and $\{x_1, x_2, x_3\}$ denote two Cartesian bases at times $t = t_0$ and

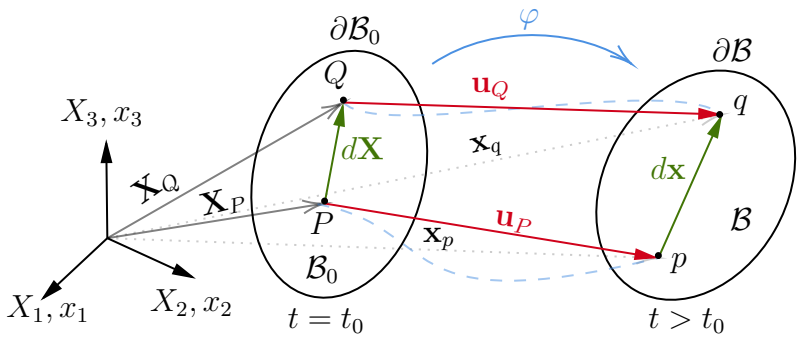

Figure II.1 – Material and spatial description of motion.

$t > t_0$, respectively. The body is considered as a collection of material particles labeled by coordinates $\mathbf{X}$, where the volume of the body and its boundary are denoted as $\mathcal{B}_0$ and $\partial\mathcal{B}_0$ in the reference configuration, and as $\mathcal{B}$ and $\partial\mathcal{B}$ in the current configuration, respectively. Therefore, $\mathbf{X} = [X_1\ X_2\ X_3]^\top \in \mathcal{B}_0$ represents the material position vector of an arbitrary point in the initial configuration at $t = t_0$. Similarly, $\mathbf{x} = [x_1\ x_2\ x_3]^\top \in \mathcal{B}$ represents the spatial position vector of an arbitrary point in the current configuration at $t > t_0$. The motion of a material point can be mathematically described as:

$$\mathbf{x} = \varphi(\mathbf{X}, t), \tag{II.1}$$

$$\mathbf{X} = \varphi^{-1}(\mathbf{x}, t), \tag{II.2}$$

where $\varphi : \mathcal{B}_0 \to \mathcal{B}$ is the motion mapping, $\mathbf{x}$ is the current (spatial) position of a material point that occupies the position $\mathbf{X}$ in the initial configuration. Additionally, from Fig. II.1 we can define the displacement field $\mathbf{u}(\mathbf{X}, t) \in \mathbb{R}^3$ as:

$$\mathbf{u}(\mathbf{X}, t) = \varphi(\mathbf{X}, t) - \mathbf{X}, \tag{II.3}$$

which assigns to each material point $\mathbf{X} \in \mathcal{B}_0$ of the body a displacement vector that specifies its current position at time $t > t_0$ in the deformed configuration regarding its position in the initial configuration at time $t = t_0$. The motion mapping φ allows us to relate positions between the initial and current configurations, but it does not provide information about changes in the immediate vicinity of a point after deformation. To fully describe deformation, we need to characterize how deformation affects the surrounding area of a point. The deformation gradient tensor $\underline{\mathbf{F}} \in \mathbb{R}^{3\times3}$ enables us to relate the spatial positions of neighboring points before and after deformation. From Fig. II.1,

$$d\mathbf{x} = \mathbf{x}_q - \mathbf{x}_p = \frac{\partial\varphi}{\partial\mathbf{X}}\, d\mathbf{X} = \underline{\mathbf{F}}\, d\mathbf{X}. \tag{II.4}$$

From the above, we define the deformation gradient tensor $\underline{\mathbf{F}} \in \mathbb{R}^{3\times3}$ as:

$$\underline{\mathbf{F}} = \frac{\partial\varphi}{\partial\mathbf{X}} = \nabla_0\varphi = \begin{bmatrix} \frac{\partial x_1}{\partial X_1} & \frac{\partial x_1}{\partial X_2} & \frac{\partial x_1}{\partial X_3} \\ \frac{\partial x_2}{\partial X_1} & \frac{\partial x_2}{\partial X_2} & \frac{\partial x_2}{\partial X_3} \\ \frac{\partial x_3}{\partial X_1} & \frac{\partial x_3}{\partial X_2} & \frac{\partial x_3}{\partial X_3} \end{bmatrix}, \tag{II.5}$$

where ∇_0 represents the gradient operator with respect to material coordinates.

Remark II.1. *$\underline{\boldsymbol{F}}$ is usually referred to as a two-point tensor, since it relates the reference and spatial configurations. Volume elements in the reference and spatial configurations, dV_0 and dV respectively, are related by $dV = J_\epsilon\, dV_0$, where $J_\epsilon = \det(\underline{\boldsymbol{F}})$. When $J_\varepsilon = 1$, the volume is preserved during deformation, which is known as isochoric or incompressible deformation. This condition is often included as constraint in polymer models to represent incompressibility, which is crucial to predict realistic behaviors.*

Kinamatics and kinetics

The analysis of deformation can be subdivided into three deformation theories depending on the amount of strain [Reddy 2007]:

- **Finite** strain theory, also called large strain theory or large deformation theory, deals with deformations in which displacements, rotations and strains are arbitrarily large. It leads to geometrically nonlinear models.
- **Infinitesimal** strain theory, also called small strain theory, small deformation theory or small displacement theory, assumes that displacements, rotations and strains are small, specifically: $\|\nabla_0 \mathbf{u}\| << 1$. Compared to Finite strain theory, infinitesimal theory neglects all nonlinear terms. It leads to geometrically linear models.
- **von Kármán** theory, also called moderate-deformation theory or moderate-rotation theory, assumes small strains but large displacements and rotations. Compared to Finite strain theory, von Kármán theory neglects only the nonlinear stretch terms. It leads to simplified geometrically nonlinear models.

Stress tensors measure internal forces (also called internal tractions) per unit area. The three most commonly used are:

- **Cauchy** stress tensor $\underline{\boldsymbol{\sigma}}_C \in \mathbb{R}^{3\times3}$, that measure force in the current configuration per unit of current area.
- **First Piola-Kirchhoff** stress tensor $\underline{\mathbf{P}} \in \mathbb{R}^{3\times3}$, that measure force in the current configuration per unit of initial area.
- **Second Piola-Kirchhoff** stress tensor $\underline{\mathbf{S}} \in \mathbb{R}^{3\times3}$, that measure force in the initial configuration per unit of initial area.

For all these theories, different velocity and acceleration vectors, strains and stresses tensors can be defined and related in both, the current and reference configurations. The main quantities are presented in Table II.2 below. The velocity and acceleration vectors, $\mathbf{v}$ and $\mathbf{a}$, respectively, are spatial vectors independently if they are expressed in terms of material coordinates $\mathbf{X}$ or spatial coordinates $\mathbf{x}$. The

	Reference configuration	Current configuration
Velocity	$\mathbf{v}(\mathbf{X},t) = \frac{\partial \varphi(\mathbf{X},t)}{\partial t} = \dot{\mathbf{u}}(\mathbf{X},t)$	$\mathbf{v}(\mathbf{x},t) = \mathbf{v}(\varphi^{-1}(\mathbf{x},t),t)$
Acceleration	$\mathbf{a}(\mathbf{X},t) = \frac{\partial^2 \varphi(\mathbf{X},t)}{\partial t^2} = \ddot{\mathbf{u}}(\mathbf{X},t)$	$\mathbf{a}(\mathbf{x},t) = \frac{D\mathbf{v}(\mathbf{x},t)}{Dt} = \frac{\partial \mathbf{v}}{\partial t} + (\nabla \mathbf{v}(\mathbf{x},t))\mathbf{v}(\mathbf{x},t)$
Strain	$\underline{\mathbf{C}} = \underline{\mathbf{F}}^\top \underline{\mathbf{F}}$ $\underline{\mathbf{E}} = \frac{1}{2}(\underline{\mathbf{C}} - \underline{\mathbf{I}})$	$\underline{\mathbf{b}} = \underline{\mathbf{F}}\,\underline{\mathbf{F}}^\top$ $\underline{\mathbf{e}} = \frac{1}{2}\left(\underline{\mathbf{I}} - \underline{\mathbf{b}}^{-1}\right)$
Stress	$\underline{\mathbf{P}} = \det(\underline{\mathbf{F}})\underline{\boldsymbol{\sigma}}_C \underline{\mathbf{F}}^{-\top}$ $\underline{\mathbf{S}} = \det(\underline{\mathbf{F}})\underline{\mathbf{F}}^{-1}\underline{\boldsymbol{\sigma}}_C \underline{\mathbf{F}}^{-\top}$	$\underline{\boldsymbol{\sigma}}_C = \det(\underline{\mathbf{F}})^{-1}\underline{\mathbf{P}}\,\underline{\mathbf{F}}^\top$ $= \det(\underline{\mathbf{F}})^{-1}\underline{\mathbf{F}}\,\underline{\mathbf{S}}\,\underline{\mathbf{F}}^\top$

Table II.2 – Summary of kinematic and kinetic quantities.

notation $D(\cdot)/Dt$ denotes the material time derivative, which for quantities expressed in terms of material coordinates is equivalent to: $D(\cdot)/Dt = \partial(\cdot)/\partial t$, and for quantities expressed in terms of spatial coordinates is equivalent to: $D(\cdot)/Dt = \partial(\cdot)/\partial t + (\nabla(\cdot))\mathbf{v}(\mathbf{x}, t)$, where $\nabla(\cdot)$ represents the gradient operator with respect to spatial coordinates. Regarding material strain tensors, $\underline{\mathbf{C}}$ and $\underline{\mathbf{E}}$ are the symmetric right Green-Cauchy tensor and the Green-Lagrange strain tensor, respectively. The tensors $\underline{\mathbf{F}}$ and $\underline{\mathbf{E}}$ are usually written in terms of the displacement field $\mathbf{u}(\mathbf{X}, t)$ as:

$$\underline{\mathbf{F}} = \nabla_0 \mathbf{u} + \underline{\mathbf{I}}, \tag{II.6}$$

$$\underline{\mathbf{E}} = \frac{1}{2}\left(\nabla_0 \mathbf{u} + (\nabla_0 \mathbf{u})^\top + (\nabla_0 \mathbf{u})^\top \nabla_0 \mathbf{u}\right), \tag{II.7}$$

with $\underline{\mathbf{I}} \in \mathbb{R}^{3\times 3}$ the second-order identity tensor. For a material Cartesian basis $\{X_1, X_2, X_3\}$, the components of the Green-Lagrange strain tensor $\underline{\mathbf{E}}$ are obtained from:

$$E_{ij} = \frac{1}{2}\left(\frac{\partial u_i}{\partial X_j} + \frac{\partial u_j}{\partial X_i} + \sum_{k=1}^{3} \frac{\partial u_k}{\partial X_i}\frac{\partial u_k}{\partial X_j}\right), \tag{II.8}$$

with $\mathbf{u} = [u_1 \ u_2 \ u_3]^\top$. Regarding spatial strain tensors, $\underline{\mathbf{b}}$ and $\underline{\mathbf{e}}$ in Table II.2 are the symmetric left Green-Cauchy tensor and the Euler-Almansi strain tensor, respectively. Regarding the stress tensors, the Cauchy stress tensor $\underline{\boldsymbol{\sigma}}_C$ is a symmetric spatial tensor, the second Piola-Kirchhoff tensor $\underline{\mathbf{S}}$ is a symmetric material tensor, and the first Piola-Kirchhoff tensor $\underline{\mathbf{P}}$ is a non-symmetric two-point tensor.

With all the previous quantities, the balance of linear and angular momentum, which constitute the equations of motion of the body, can be expressed equivalently as:

$$\begin{aligned} &\text{Current configuration :} \quad && \rho(\mathbf{x}, t)\mathbf{a}(\mathbf{x}, t) = \operatorname{div}(\underline{\boldsymbol{\sigma}}_C) + \mathbf{f}(\mathbf{x}, t) \\ & && \underline{\boldsymbol{\sigma}}_C = \underline{\boldsymbol{\sigma}}_C^\top \end{aligned} \tag{II.9}$$

$$\begin{aligned} &\text{Reference configuration :} \quad && \rho_0(\mathbf{X})\ddot{\mathbf{u}}(\mathbf{X}, t) = \operatorname{DIV}(\underline{\mathbf{P}}) + \mathbf{f}_0(\mathbf{X}, t) \\ & && \underline{\mathbf{P}}\underline{\mathbf{F}}^\top = \underline{\mathbf{F}}\underline{\mathbf{P}}^\top \end{aligned} \tag{II.10}$$

$$\begin{aligned} &\text{Reference configuration :} \quad && \rho_0(\mathbf{X})\ddot{\mathbf{u}}(\mathbf{X}, t) = \operatorname{DIV}(\underline{\mathbf{F}}\underline{\mathbf{S}}) + \mathbf{f}_0(\mathbf{X}, t) \\ & && \underline{\mathbf{S}} = \underline{\mathbf{S}}^\top \end{aligned} \tag{II.11}$$

where $\rho(\mathbf{x}, t)$ and $\rho_0(\mathbf{X})$ are the densities in the current and reference configurations, respectively, $\mathbf{f}(\mathbf{x}, t)$ and $\mathbf{f}_0(\mathbf{X}, t)$ are the external forces acting on the body referred to as the current and reference configurations, respectively, and $\operatorname{div}(\cdot)$ and $\operatorname{DIV}(\cdot)$ are the divergence operators with respect to spatial and material coordinates, respectively.

Remark II.2. *From kinematics we obtained the relationships between strain and displacement, from kinetics we obtained the equilibrium equations, and to complete them it is necessary to relate stress and strain, which is given by constitutive laws.*

Constitutive laws: Hyperelasticity

The fundamental concept in hyperelasticity is the strain energy density function $W : \mathbb{R}^{3\times3} \to \mathbb{R}$, which represents the stored elastic energy per unit volume of material. It is typically expressed as a function of $\underline{\mathbf{F}}$, $\underline{\mathbf{C}}$ or $\underline{\mathbf{E}}$, and represents energy per unit initial volume. This function must satisfy certain conditions to ensure physical realism, such as positive definiteness and objectivity, the latter meaning that quantities must not depend on the specific frame of reference chosen to describe them. In other words, the strain energy density function W must depend only on objective quantities that are invariant under rigid body motions, which implies that rigid body motion does not produce internal stresses.

Assuming that the strain energy density function is written as a function of $\underline{\mathbf{F}}$, that is $W(\underline{\mathbf{F}}) \in \mathbb{R}$, by definition, the first Piola-Kirchhoff stress tensor $\underline{\mathbf{P}}$ is obtained from:

$$\underline{\mathbf{P}} = \frac{\partial W(\underline{\mathbf{F}})}{\partial \underline{\mathbf{F}}}. \tag{II.12}$$

On the other hand and abusing of notation, when W is expressed as $W(\underline{\mathbf{C}})$ or $W(\underline{\mathbf{E}})$, the second Piola-Kirchhoff stress tensor $\underline{\mathbf{S}}$ is obtained from:

$$\underline{\mathbf{S}} = 2\frac{\partial W(\underline{\mathbf{C}})}{\partial \underline{\mathbf{C}}} = \frac{\partial W(\underline{\mathbf{E}})}{\partial \underline{\mathbf{E}}}. \tag{II.13}$$

The strain energy density function W usually is written as a function of the invariants of $\underline{\mathbf{F}}$, $\underline{\mathbf{C}}$ and/or $\underline{\mathbf{E}}$, where for an arbitrary second order tensor $\underline{\mathbf{A}}$, the first, second and third invariants are respectively given by:

$$I_A = \mathrm{tr}(\underline{\mathbf{A}}) = \underline{\mathbf{I}} : \underline{\mathbf{A}}, \tag{II.14}$$

$$II_A = \mathrm{cof}(\underline{\mathbf{A}}) = \frac{1}{2}\left[(\mathrm{tr}(\underline{\mathbf{A}}))^2 - \mathrm{tr}(\underline{\mathbf{A}}^2)\right], \tag{II.15}$$

$$III_A = \det(\underline{\mathbf{A}}). \tag{II.16}$$

Example: Saint-Venant-Kirchhoff material

Probably the simplest constitutive model is given by the Saint-Venant-Kirchhoff material [Reddy 2007, Chapter 6.3], which extends Hooke's law to finite deformation theory, where:

$$W(\underline{\mathbf{E}}) = \frac{\lambda_L}{2}[\mathrm{tr}(\underline{\mathbf{E}})]^2 + \mu_L\,\mathrm{tr}(\underline{\mathbf{E}}) = \frac{1}{2}(\underline{\underline{\mathbf{C}}_L} : \underline{\mathbf{E}}) : \underline{\mathbf{E}}, \tag{II.17}$$

where $\underline{\underline{\mathbf{C}}_L} : \mathbb{R}^{3\times3} \to \mathbb{R}^{3\times3}$ is a constant, symmetric, positive definite, isotropic fourth-order constitutive tensor, and $\lambda_L, \mu_L \in \mathbb{R}_+$ are the Lamé constants of the material. Then, the second Piola-Kirchhoff stress $\underline{\mathbf{S}}$ is given by:

$$\underline{\mathbf{S}} = \frac{\partial W(\underline{\mathbf{E}})}{\partial \underline{\mathbf{E}}} = \lambda_L \mathrm{tr}(\underline{\mathbf{E}})\underline{\mathbf{I}} + 2\mu_L\,\underline{\mathbf{E}} = \underline{\underline{\mathbf{C}}_L} : \underline{\mathbf{E}}, \tag{II.18}$$

where the relation between the Green-Lagrange strain tensor $\underline{\mathbf{E}}$ and the second Piola-Kirchhoff stress tensor $\underline{\mathbf{S}}$ is linear, which is called material linearity.

Remark II.3. *Hyperelasticity with non-quadratic strain energy density function leads to nonlinear stress-strain relations, which is called as material nonlinearity.*

Linear elasticity

Linear elasticity corresponds to a particular case of the general theory presented above. In this context, the assumptions lead to geometrically and materially linear models. Specifically, it is based on the infinitesimal strain theory and uses Hooke's law as its constitutive model. Given the assumptions of small strains and displacements, it can be approximated that $\mathbf{x} \approx \mathbf{X}$, $\underline{\mathbf{F}} \approx \underline{\mathbf{I}}$ and $\underline{\mathbf{E}} \approx \underline{\boldsymbol{\varepsilon}}$, where $\underline{\boldsymbol{\varepsilon}} \in \mathbb{R}^{3\times3}$ is the infinitesimal strain tensor given by:

$$\underline{\boldsymbol{\varepsilon}} = \frac{1}{2}\left(\nabla_0\mathbf{u} + (\nabla_0\mathbf{u})^\top\right) = \frac{1}{2}\left(\nabla\mathbf{u} + (\nabla\mathbf{u})^\top\right) = \mathrm{Grad}(\mathbf{u}), \tag{II.19}$$

where $\mathrm{Grad}(\cdot)$ is the symmetric part of the gradient operator. So, when Cartesian bases $\{X_1, X_2, X_3\}$ or $\{x_1, x_2, x_3\}$ are used, the components of the infinitesimal strain tensor $\underline{\boldsymbol{\varepsilon}}$ are obtained from:

$$\varepsilon_{ij} = \frac{1}{2}\left(\frac{\partial u_i}{\partial X_j} + \frac{\partial u_j}{\partial X_i}\right) = \frac{1}{2}\left(\frac{\partial u_i}{\partial x_j} + \frac{\partial u_j}{\partial x_i}\right). \tag{II.20}$$

On the other hand, Hooke's law is equivalent to the Saint-Venant-Kirchhoff material where the strain energy density function is now written as function of the infinitesimal strain tensor $\underline{\boldsymbol{\varepsilon}}$, that is:

$$W(\underline{\boldsymbol{\varepsilon}}) = \frac{\lambda_L}{2}[\mathrm{tr}(\underline{\boldsymbol{\varepsilon}})]^2 + \mu_L\,\mathrm{tr}(\underline{\boldsymbol{\varepsilon}}) = \frac{1}{2}(\underline{\underline{\mathbf{C}}}_L : \underline{\boldsymbol{\varepsilon}}) : \underline{\boldsymbol{\varepsilon}}. \tag{II.21}$$

So, for linear elasticity the three stress tensors approximately coincide [Reddy 2007] and are given by:

$$\underline{\boldsymbol{\sigma}}_C \approx \underline{\mathbf{P}} \approx \underline{\mathbf{S}} = \lambda_L \mathrm{tr}(\underline{\boldsymbol{\varepsilon}})\underline{\mathbf{I}} + 2\mu_L\,\underline{\boldsymbol{\varepsilon}} = \underline{\underline{\mathbf{C}}}_L : \underline{\boldsymbol{\varepsilon}}. \tag{II.22}$$

Remark II.4. *Due to the approximations in linear elasticity, the different configurations and the various strain and stress measures are typically not distinguished and are simply referred to as the strain and stress tensors. However, for describing the motion of fully nonlinear systems, it is crucial to differentiate between all these aspects.*

Voigt-Kelvin notation

The Voigt-Kelvin notation simplifies tensor operations by reducing second-order tensors to vectors, and fourth-order tensors to matrices, making calculations more compact and intuitive. For a symmetric stress tensor, here simply denoted as $\underline{\boldsymbol{\sigma}} \in \mathbb{R}^{3\times3}$, and a symmetric strain tensor, here simply denoted as $\underline{\boldsymbol{\varepsilon}} \in \mathbb{R}^{3\times3}$, the Voigt-Kelvin notation defines the Voigt-stress vector $\vec{\boldsymbol{\sigma}} \in \mathbb{R}^6$, and Voigt-strain vector $\vec{\boldsymbol{\varepsilon}} \in \mathbb{R}^6$, which are respectively given by:

$$\vec{\boldsymbol{\sigma}} = \begin{bmatrix}\sigma_{11} & \sigma_{22} & \sigma_{33} & \sigma_{12} & \sigma_{13} & \sigma_{23}\end{bmatrix}^\top, \tag{II.23}$$

$$\vec{\boldsymbol{\varepsilon}} = \begin{bmatrix}\varepsilon_{11} & \varepsilon_{22} & \varepsilon_{33} & 2\varepsilon_{12} & 2\varepsilon_{13} & 2\varepsilon_{23}\end{bmatrix}^\top. \tag{II.24}$$

In addition, using the Voigt-Kelvin notation it is possible to express the constitutive relation of materially linear systems as:

$$\underline{\boldsymbol{\sigma}} = \underline{\underline{\mathbf{C}_L}} : \underline{\boldsymbol{\varepsilon}} \quad \sim \quad \vec{\boldsymbol{\sigma}} = \underline{\mathbf{C}_L}\, \vec{\boldsymbol{\varepsilon}},$$

where $\underline{\mathbf{C}_L} = \underline{\mathbf{C}_L}^{\top} > 0 \in \mathbb{R}^{6\times 6}$ is a constitutive matrix. For example, for isotropic materials the fourth-order constitutive tensor $\underline{\underline{\mathbf{C}_L}}$ reduces to:

$$\underline{\mathbf{C}_L} = \begin{bmatrix} 2\mu_L+\lambda_L & \lambda_L & \lambda_L & 0 & 0 & 0 \\ \lambda_L & 2\mu_L+\lambda_L & \lambda_L & 0 & 0 & 0 \\ \lambda_L & \lambda_L & 2\mu_L+\lambda_L & 0 & 0 & 0 \\ 0 & 0 & 0 & \mu_L & 0 & 0 \\ 0 & 0 & 0 & 0 & \mu_L & 0 \\ 0 & 0 & 0 & 0 & 0 & \mu_L \end{bmatrix}, \tag{II.25}$$

with μ_L and λ_L the Lamé constants defined as:

$$\mu_L = \frac{E}{2(1+\nu)} = G, \quad \lambda_L = \frac{\nu E}{(1+\nu)(1-2\nu)}, \tag{II.26}$$

where E is Young's modulus, ν is Poisson's ratio (ratio between transverse elongation and axial shortening), and $\mu_L = G$ is also known as the shear modulus.

II.2.2 Variational principles in continuum media

Consider a three-dimensional continuum body as the one of Fig. II.2, whose volume in the reference configuration is denoted as $\mathcal{B}_0 \subset \mathbb{R}^3$, and its boundary surface is denoted as $\partial\mathcal{B}_0 = \partial\mathcal{B}_0^D \cup \partial\mathcal{B}_0^N$, where $\partial\mathcal{B}_0^D$ is the boundary portion where Dirichlet boundary conditions are applied, that is, where the displacement field $\mathbf{u}_D(S,t) \in \mathbb{R}^3$ is prescribed (with $S \in \partial\mathcal{B}_0$ a coordinate along $\partial\mathcal{B}_0$), and $\partial\mathcal{B}_0^N$ is the boundary portion where Neumann boundary conditions are applied, that is, where the surface traction $\mathbf{t}_N(S,t) \in \mathbb{R}^3$ is prescribed.

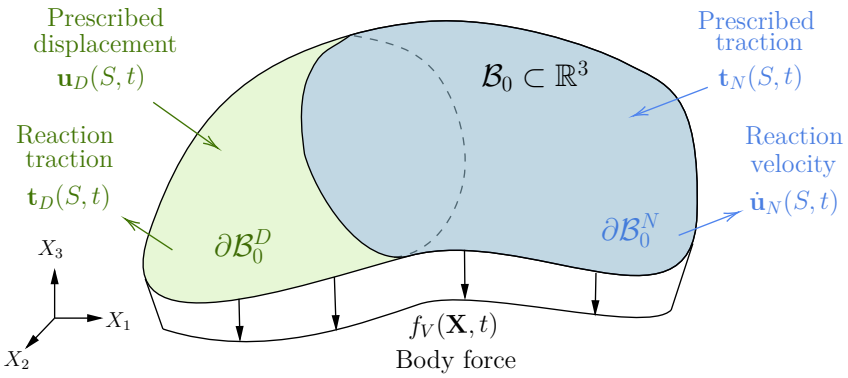

Figure II.2 – Three-dimensional continuum body.

Variational principles are often used to derive the Euler-Lagrange (E-L) equations for elastodynamics, or the equilibrium equations for elastostatics. They also serve to obtain finite element approximations, thus unifying the modeling and FEM discretization of mechanical systems [Reddy 2014; Reddy 2017]. Hamilton's principle is probably the most widely known and used in the modeling of elastodynamic systems, while its counterpart, the principle of minimum potential energy, is commonly applied in elastostatics. Other well known principles in elastostatics are the Hellinger-Reissner (H-R) and the Hu-Washizu principles [Zienkiewicz 2005].

Hamilton's principle

Hamilton's principle for continuum media states that the true evolution of $\mathbf{u}(\mathbf{X}, t)$, between two specific states $\mathbf{u}(\mathbf{X}, t_1)$ and $\mathbf{u}(\mathbf{X}, t_2)$ at two specific times t_1 and t_2, is a stationary point of the action functional. Define as generalized coordinates the variables that define the configuration of the system, and as configuration space the space generated by these coordinates. Hamilton's principle states that, as the system evolves, a path is traced through the configuration space, where the real path $\mathbf{u}(\mathbf{X}, t)$ taken by the system has a stationary action under admissible small variations ($\delta\mathbf{u}$) in the configuration of the system. Thus, an admissible variation $\delta\mathbf{u}$, also called virtual displacement, must be consistent with the Dirichlet boundary conditions.

Definition II.1. *Hamilton's principle states [Reddy 2017]:*

$$\int_{t_1}^{t_2} \left[\delta(\mathcal{T} - \mathcal{U}) + \delta\mathcal{W}_E\right] dt = 0, \tag{II.27}$$

$$\delta\boldsymbol{u}(S, t) = 0 \text{ on } \partial\mathcal{B}_0^D \text{ for all } t, \tag{II.28}$$

$$\delta\boldsymbol{u}(\boldsymbol{X}, t_1) = \delta\boldsymbol{u}(\boldsymbol{X}, t_2) = 0 \text{ for all } \boldsymbol{X}, \tag{II.29}$$

where δ is the variational operator, $\mathcal{T} \in \mathbb{R}$ is the kinetic energy, $\mathcal{U} \in \mathbb{R}$ is the elastic potential energy, and $\delta\mathcal{W}_E \in \mathbb{R}$ is the virtual work associated to the external forces.

These quantities are respectively defined as:

$$\mathcal{T} = \frac{1}{2}\int_{\mathcal{B}_0} \rho_0(\mathbf{X})\, \dot{\mathbf{u}}(\mathbf{X}, t) \cdot \dot{\mathbf{u}}(\mathbf{X}, t)\, d\mathbf{X}, \tag{II.30}$$

$$\mathcal{U} = \int_{\mathcal{B}_0} W(\underline{\mathbf{E}}(\mathbf{X}, t))\, d\mathbf{X}, \tag{II.31}$$

$$\delta\mathcal{W}_E = \int_{\mathcal{B}_0} f_V(\mathbf{X}, t) \cdot \delta\mathbf{u}(\mathbf{X}, t)\, d\mathbf{X} + \int_{\partial\mathcal{B}_0^N} \mathbf{t}_N(S, t) \cdot \delta\mathbf{u}(S, t)\, dS. \tag{II.32}$$

Note that Hamilton's principle (and the principle of minimum potential energy) only admits variations of the displacement field $\mathbf{u}(\mathbf{X}, t)$, leading to displacement-based equations, without directly imposing Dirichlet boundary conditions. The Hellinger-Reissner principle allows variations in stress and displacement fields leading to stress-displacement equilibrium equations, and uses the stress field as a Lagrange multiplier to weakly enforce Dirichlet boundary conditions [Lu 2019]. On

the other hand, the Hu-Washizu principle admits variations in strain, stress and displacement fields, leading to a stress-strain-displacement equilibrium equation, a stress-strain relation (constitutive law), and a strain-displacement relation (kinematics). For an in-depth review of these principles and their implications for finite element models, refer to [Zienkiewicz 2005]. The application of these concepts to the discretization of PHS will be discussed in Chapter III.

Extended Hamilton's principle

Hamilton's principle for continuum media has been extended to incorporate algebraic constraints and is often called extended Hamilton's principle. The algebraic constraint is given by $\Gamma(\mathbf{u}(\mathbf{X},t)) = 0 \in \mathbb{R}^{n_\lambda}$, with $\Gamma(\mathbf{u}(\mathbf{X},t))$ being some smooth function of $\mathbf{u}(\mathbf{X},t)$, and it is enforced via Lagrange multiplier $\Lambda(\mathbf{X},t) \in \mathbb{R}^{n_\lambda}$. This principle states that the true evolution of $\mathbf{u}(\mathbf{X},t)$, subject to algebraic constraints of the form $\Gamma(\mathbf{u}) = 0 \in \mathbb{R}^{n_\lambda}$, between two specific times t_1 and t_2, is a stationary point of the extended action functional under admissible small variations of $\delta\mathbf{u}$ and $\delta\Lambda$.

Definition II.2. *The extended Hamilton's principle states [Bedford 1985]:*

$$\int_{t_1}^{t_2} \left[\delta(\mathcal{T} - \mathcal{U}) + \delta\mathcal{W}_E - \delta\mathcal{C}_\lambda\right] dt = 0, \tag{II.33}$$

$$\delta\boldsymbol{u}(S,t) = 0 \text{ on } \partial\mathcal{B}_0^D \text{ for all } t, \tag{II.34}$$

$$\delta\boldsymbol{u}(\boldsymbol{X},t_1) = \delta\boldsymbol{u}(\boldsymbol{X},t_2) = 0 \text{ for all } \boldsymbol{X}, \tag{II.35}$$

where δ is the variational operator, $\mathcal{T} \in \mathbb{R}$ is the kinetic energy, $\mathcal{U} \in \mathbb{R}$ is the elastic potential energy, $\delta\mathcal{W}_E \in \mathbb{R}$ is the virtual work associated to the external forces, and $\mathcal{C}_\lambda \in \mathbb{R}$ is the constraint functional.

The constraint functional $\mathcal{C}_\lambda \in \mathbb{R}$ is defined as:

$$\mathcal{C}_\lambda = \int_{\mathcal{B}_0} \Lambda(\mathbf{X},t) \cdot \Gamma(\mathbf{u}(\mathbf{X},t))\, d\mathbf{X}. \tag{II.36}$$

This principle is often used to obtain finite element models where Dirichlet boundary conditions are enforced via Lagrange multipliers with $\Gamma(\mathbf{u}) = (\mathbf{u} - \mathbf{u}_D)$ on $\partial\Omega_D$ [Babuška 1973a], resulting in a set of differential-algebraic equations (DAEs).

Remark II.5. *To avoid the resulting DAEs of the previous approach, the Lagrange multiplier can be substituted by a penalty factor $\beta_\infty \to \infty$, and the algebraic constraint takes the quadratic form $\Gamma(\boldsymbol{u}) = \frac{1}{2}(\boldsymbol{u} - \boldsymbol{u}_D)\cdot(\boldsymbol{u} - \boldsymbol{u}_D)$ on $\partial\Omega_D$. This method to enforce Dirichlet boundary conditions is called the Penalty method [Babuška 1973b], and constitutes one of the most used methods in structural mechanics.*

Generalized extended Hamilton's principle

The dynamic version of the Hu-Washizu principle, called generalized Hamilton's principle, was originally presented in [Yi-Yuan 1964]. This principle accounts for independent and simultaneous variations of the Green-Lagrange strain tensor $\underline{\mathbf{E}}(\mathbf{X},t)$, the second Piola-Kirchhoff stress tensor $\underline{\mathbf{S}}(\mathbf{X},t)$, and the displacement field $\mathbf{u}(\mathbf{X},t)$. Additionally, it uses the reaction surface traction $\mathbf{t}_D(S,t) \in \mathbb{R}^3$ (see Fig. II.2) to weakly enforce Dirichlet boundary conditions. This principle can be easily extended to cases with constraints, where we call it as the generalized extended Hamilton's principle. For example, in this new context, the algebraic constraint can be a function of the strain field $\underline{\mathbf{E}}(\mathbf{X},t)$, which is convenient to enforce incompressible deformation on models.

Then, the generalized extended Hamilton's principle states that the true evolution of $\mathbf{u}(\mathbf{X},t)$, subject to algebraic constraints of the form $\Gamma(\underline{\mathbf{E}}(\mathbf{X},t)) = 0 \in \mathbb{R}^{n_\lambda}$, between two specific times t_1 and t_2, is a stationary point of the generalized extended action functional under admissible small variations $\delta\mathbf{u}$, $\delta\underline{\mathbf{E}}$, $\delta\underline{\mathbf{S}}$ and $\delta\Lambda$.

Definition II.3. *The generalized extended Hamilton's principle states:*

$$\int_{t_1}^{t_2} \left[\delta(\mathcal{T} - \mathcal{U}_\mathcal{E} + \mathcal{W}_\mathcal{E}) - \delta\mathcal{C}_\mathcal{E}\right] dt = 0, \tag{II.37}$$

$$\delta\boldsymbol{u}(S,t) = 0 \text{ on } \partial\mathcal{B}_0^D \text{ for all } t, \tag{II.38}$$

$$\delta\boldsymbol{u}(\boldsymbol{X},t_1) = \delta\boldsymbol{u}(\boldsymbol{X},t_2) = 0 \text{ for all } \boldsymbol{X}, \tag{II.39}$$

where δ is the variational operator, $\mathcal{T} \in \mathbb{R}$ is the kinetic energy, $\mathcal{U}_\mathcal{E} \in \mathbb{R}$ is the extended elastic potential energy, $\mathcal{W}_\mathcal{E} \in \mathbb{R}$ is the extended work associated to the external forces, and $\mathcal{C}_\mathcal{E} \in \mathbb{R}$ is the extended constraint functional.

The extended elastic potential energy $\mathcal{U}_\mathcal{E} \in \mathbb{R}$, the extended work $\mathcal{W}_\mathcal{E} \in \mathbb{R}$, and the extended constraint functional $\mathcal{C}_\mathcal{E} \in \mathbb{R}$ are respectively defined as:

$$\mathcal{U}_\mathcal{E} = \int_{\mathcal{B}_0} \left\{\underline{\mathbf{S}}(\mathbf{X},t) : [\underline{\mathbf{E}}(\mathbf{u}) - \underline{\mathbf{E}}(\mathbf{X},t)] + W(\underline{\mathbf{E}}(\mathbf{X},t))\right\} d\mathbf{X}, \tag{II.40}$$

$$\mathcal{W}_\mathcal{E} = \int_{\mathcal{B}_0} f_V(\mathbf{X},t)\cdot\mathbf{u}(\mathbf{X},t)\, d\mathbf{X} + \int_{\partial\mathcal{B}_0^N} \mathbf{t}_N(S,t)\cdot\mathbf{u}(S,t)\, dS + \ldots \tag{II.41}$$

$$\ldots \int_{\partial\mathcal{B}_0^D} \mathbf{t}_D(S,t)\cdot[\mathbf{u}(S,t) - \mathbf{u}_D(S,t)]\, dS,$$

$$\mathcal{C}_\mathcal{E} = \int_{\mathcal{B}_0} \Lambda(\mathbf{X},t)\cdot\Gamma(\underline{\mathbf{E}}(\mathbf{X},t))\, d\mathbf{X}, \tag{II.42}$$

where $\underline{\mathbf{E}}(\mathbf{u})$ denotes the Green-Lagrange strain tensor expressed in terms of the displacement field $\mathbf{u}(\mathbf{X},t)$. Therefore, $\underline{\mathbf{E}}(\mathbf{u})$ is not considered an independent field and its variation must be expressed in terms of $\delta\mathbf{u}$.

II.3 Systematic methodologies for PH modeling

In [Thoma 2022a], the authors have formulated a geometrically nonlinear 3D elasticity model using $\underline{\mathbf{E}}$ modulated by the deformation gradient tensor $\underline{\mathbf{F}}$, and both the first and second Piola-Kirchhoff tensors, $\underline{\mathbf{P}}$ and $\underline{\mathbf{S}}$, respectively. Later, in [Thoma 2024], they formulated the same problem with $\underline{\mathbf{E}}$ modulated by $\mathbf{u}(\mathbf{X}, t)$, using only $\underline{\mathbf{S}}$ as stress. On the other hand, [Kinon 2023] have formulated a 1D model of a geometrically and materially nonlinear string, using the right Green-Cauchy tensor $\underline{\mathbf{C}}$ and the stress tensor $\underline{\mathbf{S}}$. Modulating $\underline{\mathbf{E}}$ with $\underline{\mathbf{F}}$ directly connects the strain to the kinematics of the deformation, as the deformation gradient fully describes both rotation and stretch, making it a natural choice for large deformation theory. This approach maintains generality and is widely used when considering material nonlinear formulations. On the other hand, modulating $\underline{\mathbf{E}}$ by $\mathbf{u}(\mathbf{X}, t)$ links the strain to the displacement field, which can offer a more intuitive interpretation of the deformation in terms of observable quantities, especially when dealing with perturbations around a reference configuration. In terms of stress measures, the first Piola-Kirchhoff tensor, $\underline{\mathbf{P}}$, directly relates the forces in the current configuration to the reference configuration. Although $\underline{\mathbf{P}}$ can be used to implement traction boundary conditions, it is asymmetric and less intuitive to interpret in terms of physical stress. On the other hand, the second Piola-Kirchhoff tensor, $\underline{\mathbf{S}}$, is symmetric and operates entirely within the reference configuration, providing a more mathematically tractable option, particularly in variational formulations and Total Lagrangian approaches. $\underline{\mathbf{S}}$ is conjugate to the Green-Lagrange strain tensor, making it more convenient for material descriptions, but like $\underline{\mathbf{P}}$, it must be transformed when working in the current configuration. Thus, choosing between these formulations depends on the specific context of the problem, as each approach has distinct advantages in terms of mathematical convenience, physical interpretation, and computational complexity. The decision involves a compromise based on the needs of the model and the desired outcomes.

Since one of the intended applications of these models is for shape control design, in this section, we formulate systematic methodologies to derive multidimensional PHS models of flexible mechanical systems using the generalized extended Hamilton's principle, which uses the Green-Lagrange strain tensor $\underline{\mathbf{E}}$ modulated by the displacement field $\mathbf{u}(\mathbf{X}, t)$, the infinitesimal strain tensor $\underline{\boldsymbol{\varepsilon}}$ for the linear case, and the second Piola-Kirchhoff tensor $\underline{\mathbf{S}}$ as the stress measure.

Remark II.6. *Note that with all these choices, the dynamics of the systems will be described in material coordinates $\boldsymbol{X}$, and the strain energy density functions W will be defined per unit initial volume. From a numerical perspective, this implies that the matrices obtained by applying FEM will be integrated with respect to the initial configuration (which is known), rather than the current configuration, which is unknown.*

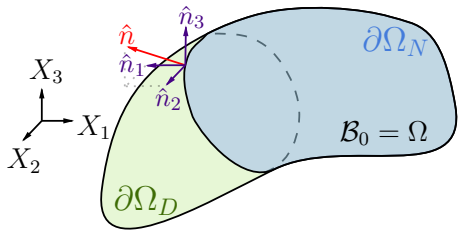

(a) 3D domain

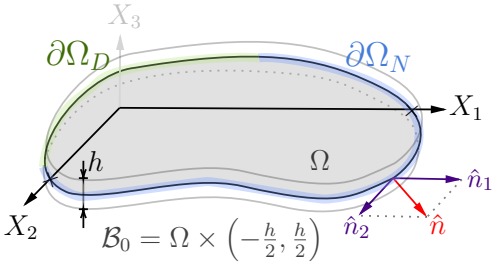

(b) 2D domain

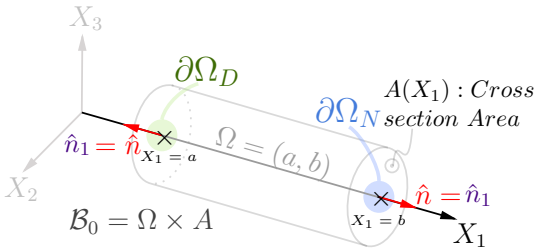

(c) 1D domain

Figure II.3 – Schemes to illustrate notation.

Notation

Since this section addresses the modeling of a whole class of multidimensional systems, it is necessary to establish a notation that effectively groups and distinguishes them, to ensure clarity and consistency as results are presented.

Let $\mathbf{X} = \{X_1, X_2, X_3\} \in \mathcal{B}_0$ be a set of material Cartesian coordinates for a 3D body, such as those illustrated in Fig. II.3. Consider that $\mathcal{B}_0 = \Omega \times \Omega^c \subset \mathbb{R}^3$ is the total initial volume of the elastic body, where $\Omega \subset \mathbb{R}^\ell$ is the ℓ-dimensional spatial domain where the parameters of the model are distributed, and Ω^c is a complementary domain. Similarly, the boundary surface $\partial\mathcal{B}_0$ of the 3D body is divided as $\partial\mathcal{B}_0 = \partial\Omega \times \Omega^c$, where $\partial\Omega = \partial\Omega_D \cup \partial\Omega_N$ is the boundary of the spatial domain $\Omega \subset \mathbb{R}^\ell$, and $\partial\Omega_D$ and $\partial\Omega_N$ are the Dirichlet and Neumann boundary portions, where Dirichlet and Neumann boundary conditions are applied, respectively. Let $\mathtt{X} \subset \mathbf{X}$ with $\mathtt{X} \in \Omega$ be the subset of material coordinates where the parameters are distributed, and $\mathtt{X}^c \subset \mathbf{X}$ with $\mathtt{X}^c \in \Omega^c$ the complement of $\mathtt{X}$ such that $\mathbf{X} = \mathtt{X} \cup \mathtt{X}^c$ and $\mathtt{X} \cap \mathtt{X}^c = \{\emptyset\}$, where $\{\emptyset\}$ denotes the empty set. Similarly, let $\mathtt{S} \in \partial\Omega$ be a coordinate along the boundary $\partial\Omega$. With the above, a differential of volume $d\mathcal{B}_0$ and the integral of an arbitrary separable function $g(\mathbf{X}) = g_1(\mathtt{X})g_2(\mathtt{X}^c)$ over $\mathcal{B}_0$ are:

$$d\mathcal{B}_0 = dX_3 dX_2 dX_1 = d\mathtt{X}^c\, d\mathtt{X} = d\mathbf{X}, \qquad \int_{\mathcal{B}_0} g(\mathbf{X})\, d\mathbf{X} = \int_{\Omega} g_1(\mathtt{X}) \int_{\Omega^c} g_2(\mathtt{X}^c)\, d\mathtt{X}^c\, d\mathtt{X}.$$

Note that for 3D elasticity (see Fig. II.3a), we have $\mathtt{X} = \mathbf{X}$, $\mathtt{X}^c = \{\emptyset\}$, $\mathcal{B}_0 = \Omega$ and $d\mathbf{X} = d\mathtt{X}$, which implies $\int_{\mathcal{B}_0} g(\mathbf{X})\, d\mathbf{X} = \int_{\Omega} g(\mathbf{X})\, d\mathtt{X}$, then $\int_{\Omega^c} g(\mathbf{X})\, d\mathtt{X}^c = g(\mathbf{X})$.

Additionally, following the Voigt-Kelvin notation, the nonzero components of $\vec{\boldsymbol{\varepsilon}}(\mathbf{X},t) \in \mathbb{R}^6$ will be grouped into the vector $\boldsymbol{\varepsilon}(\mathbf{X},t) \in \mathbb{R}^d$, where $6 \geq d \in \mathbb{N}_+$ is the number of nonzero components. This vector $\vec{\boldsymbol{\varepsilon}}(\mathbf{X},t)$ represents the Voigt-strain vector for either the Green-Lagrange strain tensor $\underline{\mathbf{E}}$ or the infinitesimal strain tensor $\underline{\boldsymbol{\varepsilon}}$, depending on the context. Similarly, $\boldsymbol{\sigma}(\mathbf{X},t) \in \mathbb{R}^d$ denotes the corresponding nonzero components of the Voigt-stress vector $\vec{\boldsymbol{\sigma}}(\mathbf{X},t) \in \mathbb{R}^6$ for the second Piola-Kirchhoff stress tensor $\underline{\mathbf{S}}$.

Lastly, using the notation introduced, the extended elastic potential energy $\mathcal{U}_{\mathcal{E}} \in \mathbb{R}$ and the extended constraint functional $\mathcal{C}_{\mathcal{E}} \in \mathbb{R}$ of the generalized extended Hamilton's principle in Definition II.3 are rewritten as:

$$\mathcal{U}_{\mathcal{E}} = \int_{\mathcal{B}_0} \{\boldsymbol{\sigma}(\mathbf{X},t) \cdot [\boldsymbol{\varepsilon}(\mathbf{u}) - \boldsymbol{\varepsilon}(\mathbf{X},t)] + W(\boldsymbol{\varepsilon}(\mathbf{X},t))\}\, d\mathbf{X}, \tag{II.43}$$

$$\mathcal{C}_{\mathcal{E}} = \int_{\mathcal{B}_0} \Lambda(\mathbf{X},t) \cdot \Gamma(\boldsymbol{\varepsilon}(\mathbf{X},t))\, d\mathbf{X}, \tag{II.44}$$

where $\boldsymbol{\varepsilon}(\mathbf{u})$ denotes the nonzero components of the Voigt-strain vector expressed in terms of the displacement field $\mathbf{u}(\mathbf{X},t)$. Therefore, $\boldsymbol{\varepsilon}(\mathbf{u})$ is not considered as an independent field and its variation must be expressed in terms of $\delta\mathbf{u}$.

Considered class of systems

The class of systems under consideration must satisfy the following set of assumptions, which serve as pillars to characterize the proposed modeling framework.

Assumption II.1. *We consider three-dimensional bodies with volume $\mathcal{B}_0 \subset \mathbb{R}^3$ in the reference configuration and density $\rho_0(\mathtt{X}) \in \mathbb{R}$, and whose kinematic assumptions are represented by a displacement field $\boldsymbol{u}(\boldsymbol{X},t) \in \mathbb{R}^3$ with the following structure:*

$$\boldsymbol{u}(\boldsymbol{X},t) = \bar{M}_1(\mathtt{X}^c)\, r(\mathtt{X},t), \tag{II.45}$$

where $\bar{M}_1(\mathtt{X}^c) \in \mathbb{R}^{3\times n}$ is a full rank matrix, and $r(\mathtt{X},t) = [r_1(\mathtt{X},t) \cdots r_n(\mathtt{X},t)]^\top \in \mathbb{R}^n$ is defined as the vector of generalized displacements or primary unknowns.

Assumption II.2. *The nonzero components of the Voigt-strain vector, that is $\boldsymbol{\varepsilon}(\boldsymbol{X},t) \in \mathbb{R}^d$, can be written as:*

$$\boldsymbol{\varepsilon}(\boldsymbol{X},t) = \bar{M}_2(\mathtt{X}^c)\epsilon(\mathtt{X},t), \tag{II.46}$$

where $\bar{M}_2(\mathtt{X}^c) \in \mathbb{R}^{d\times m}$ is a full rank matrix, and $\epsilon(\mathtt{X},t) = [\epsilon_1(\mathtt{X},t) \cdots \epsilon_m(\mathtt{X},t)]^\top \in \mathbb{R}^m$ is defined as the vector of generalized strains or secondary unknowns. Additionally, we assume that the strain energy density function $W(\boldsymbol{\varepsilon}) \in \mathbb{R}$ is integrable over the complementary domain Ω^c and results in:

$$\Psi(\epsilon) = \int_{\Omega^c} W(\boldsymbol{\varepsilon})\, d\mathtt{X}^c, \tag{II.47}$$

where $\Psi(\epsilon) \in \mathbb{R}$ is defined as the generalized strain energy density function.

Assumption II.3. *In case of constrained systems, we assume that the Lagrange multiplier $\Lambda(\boldsymbol{X}, t) \in \mathbb{R}$ is distributed on the spatial domain $\Omega \subset \mathbb{R}^\ell$, that is, $\Lambda(\boldsymbol{X}, t) = \lambda(\mathtt{X}, t)$. In addition, we assume that the algebraic constraint $\Gamma(\boldsymbol{\varepsilon}) = 0 \in \mathbb{R}$ is integrable over the complementary domain Ω^c and results in:*

$$\gamma(\epsilon) = \int_{\Omega^c} \Gamma(\boldsymbol{\varepsilon})\, d\mathtt{X}^c = 0, \tag{II.48}$$

where $\gamma(\epsilon) = 0 \in \mathbb{R}$ is defined as the generalized algebraic constraint.

Remark II.7. *The class of displacement field $\boldsymbol{u}(\boldsymbol{X}, t)$ in Assumption II.1 encompasses a wide range of models found in current literature. For instance, for the Timoshenko beam model presented as example in Section I.2.3.c, its displacement field is given by:*

$$\boldsymbol{u}(\boldsymbol{X}, t) = \begin{bmatrix} -X_3\, \psi(X_1, t) \\ 0 \\ w(X_1, t) \end{bmatrix} = \underbrace{\begin{bmatrix} -X_3 & 0 \\ 0 & 0 \\ 0 & 1 \end{bmatrix}}_{\bar{M}_1(\mathtt{X}^c)} \underbrace{\begin{bmatrix} \psi(X_1, t) \\ w(X_1, t) \end{bmatrix}}_{r(\mathtt{X}, t)}.$$

On the other hand, the integrability assumption (II.47) is the natural way to define a consistent (average) strain energy density function per unit spatial domain $\Psi(\epsilon)$. Strain energy density functions $W(\boldsymbol{\varepsilon})$ for hyperelastic materials can be found in [Beda 2007; Chagnon 2015; Melly 2021; Khaniki 2022], and a list of displacement fields $\boldsymbol{u}(\boldsymbol{X}, t) \in \mathbb{R}^3$ for typical elasticity problems is provided in Appendix B.

II.3.1 Linear systems

Models based on linear elasticity are developed using the infinitesimal strain tensor $\underline{\boldsymbol{\varepsilon}}(\mathbf{X}, t) \in \mathbb{R}^{3\times3}$ and Hooke's law. In what follows, we present the class of differential operators and their formal adjoints, an integration by parts lemma, and the choices of energy variables, co-energy variables, and boundary inputs and outputs that ensure an infinite-dimensional PHS representation for the considered multidimensional linear mechanical systems.

Class of linear differential operators

Definition II.4. *Let $\mathtt{X} = \{X_1, \ldots, X_\ell\}$ be a set of orthogonal coordinate axes and also the coordinates of an arbitrary point of an open set $\Omega \subset \mathbb{R}^\ell$, $v(\mathtt{X}) \in \mathbb{R}^m$ and $w(\mathtt{X}) \in \mathbb{R}^n$ two vector functions. The linear differential operator $\mathcal{F}_\mathtt{x}$ and its formal adjoint $\mathcal{F}_\mathtt{x}{}^*$ are defined as:*

$$\mathcal{F}_\mathtt{x}\, w(\mathtt{X}) = F_0\, w(\mathtt{X}) + \sum_{k=1}^{\ell} \sum_{i=1}^{N} F_k^i\, \partial_k^i\, w(\mathtt{X}), \tag{II.49}$$

$$\mathcal{F}_\mathtt{x}{}^*\, v(\mathtt{X}) = F_0^\top v(\mathtt{X}) + \sum_{k=1}^{\ell} \sum_{i=1}^{N} (-1)^i (F_k^i)^\top \partial_k^i\, v(\mathtt{X}), \tag{II.50}$$

where $\partial_k^i = \partial^i / \partial X_k^i$, $F_0 \in \mathbb{R}^{m\times n}$ *and* $F_k^i \in \mathbb{R}^{m\times n}$ *are constant matrices, and* N *is the order of the highest derivative with respect to any* X_k*. Note that* $\mathcal{F}_{\mathtt{x}}$ *admits higher-order derivatives but not cross derivatives.*

Lemma II.1. *Consider Definition II.4, the open set* $\Omega \subset \mathbb{R}^\ell$*, its boundary* $\partial\Omega$*, and the closure* $\bar{\Omega} = \Omega \cup \partial\Omega$*. Then, for any pair of smooth functions* $v(\mathtt{X}) \in \mathbb{R}^m$ *and* $w(\mathtt{X}) \in \mathbb{R}^n$ *defined on* $\bar{\Omega}$*, we have that:*

$$\int_\Omega \Big(v(\mathtt{X})^\top \mathcal{F}_{\mathtt{x}}\, w(\mathtt{X}) - w(\mathtt{X})^\top \mathcal{F}_{\mathtt{x}}{}^* v(\mathtt{X}) \Big)\, d\mathtt{X} = \int_{\partial\Omega} \mathcal{B}(w(\mathtt{S}))^\top \mathcal{Q}_\partial(\mathtt{S})\, \mathcal{B}(v(\mathtt{S}))\, d\mathtt{S}, \quad \text{(II.51)}$$

where $\mathcal{B}(\cdot)$ *is a linear differential operator defined as:*

$$\mathcal{B}(\cdot) = \Big[(\cdot) \quad \partial_1(\cdot) \;\cdots\; \partial_\ell(\cdot) \quad \partial_1^2(\cdot) \;\cdots\; \partial_\ell^2(\cdot) \quad \cdots \quad \partial_1^{N-1}(\cdot) \;\cdots\; \partial_\ell^{N-1}(\cdot) \Big]^\top, \quad \text{(II.52)}$$

$\mathcal{Q}_\partial(\mathtt{S}) \in \mathbb{R}^{n+(N-1)n\ell \times m+(N-1)m\ell}$ *is a boundary matrix given by:*

$$\mathcal{Q}_\partial(\mathtt{S}) = \begin{bmatrix} F_\partial(\mathtt{S}) & -W_2(\mathtt{S}) & W_3(\mathtt{S}) & -W_4(\mathtt{S}) & \cdots & (-1)^{N-1} W_N(\mathtt{S}) \\ V_2(\mathtt{S}) & -\Lambda_3(\mathtt{S}) & \Lambda_4(\mathtt{S}) & \iddots & \iddots & 0 \\ V_3(\mathtt{S}) & -\Lambda_4(\mathtt{S}) & \Lambda_5(\mathtt{S}) & \iddots & & \vdots \\ \vdots & \vdots & \iddots & \iddots & & \vdots \\ V_{N-1}(\mathtt{S}) & -\Lambda_N(\mathtt{S}) & 0 & & & \vdots \\ V_N(\mathtt{S}) & 0 & 0 & \cdots & \cdots & 0 \end{bmatrix}, \quad \text{(II.53)}$$

with $F_\partial(\mathtt{S}) \in \mathbb{R}^{n\times m}$, $W_i(\mathtt{S}) \in \mathbb{R}^{n\times m\ell}$, $V_i(\mathtt{S}) \in \mathbb{R}^{n\ell\times m}$*, and* $\Lambda_i(\mathtt{S}) \in \mathbb{R}^{n\ell\times m\ell}$ *defined as:*

$$\begin{aligned} F_\partial(\mathtt{S}) &= \sum_{k=1}^{\ell} (F_k^1)^\top \hat{n}_k(\mathtt{S}) \quad , \quad W_i(\mathtt{S}) = \begin{bmatrix} (F_1^i)^\top \hat{n}_1(\mathtt{S}) & \cdots & (F_\ell^i)^\top \hat{n}_\ell(\mathtt{S}) \end{bmatrix}, \\ V_i(\mathtt{S}) &= \begin{bmatrix} (F_1^i)^\top \hat{n}_1(\mathtt{S}) \\ \vdots \\ (F_\ell^i)^\top \hat{n}_\ell(\mathtt{S}) \end{bmatrix} \quad , \quad \Lambda_i(\mathtt{S}) = \begin{bmatrix} (F_1^i)^\top \hat{n}_1(\mathtt{S}) & & 0 \\ & \ddots & \\ 0 & & (F_\ell^i)^\top \hat{n}_\ell(\mathtt{S}) \end{bmatrix}, \end{aligned} \quad \text{(II.54)}$$

where $\hat{n}_k(\mathtt{S})$ *is the* k*-component of the outward unit normal vector to the boundary* $\partial\Omega$ *projected on the coordinate axis* X_k*.*

Proof. By iteratively applying integration by parts to the left side of (II.51) and employing the identity provided in [Warsewa 2021, Section 3], we obtain:

$$\int_\Omega \Big(v^\top \mathcal{F}_{\mathtt{x}}\, w - w^\top \mathcal{F}_{\mathtt{x}}{}^*\, v \Big) d\mathtt{X} = \sum_{k=1}^{\ell} \sum_{i=1}^{N} \sum_{j=1}^{i} (-1)^{j-1} \int_{\partial\Omega} \partial_k^{i-j} w(\mathtt{S})^\top (F_k^i)^\top \hat{n}_k(\mathtt{S})\, \partial_k^{j-1} v(\mathtt{S})\, d\mathtt{S}.$$

Expanding the terms and grouping them into a quadratic form, following the approach outlined in [Le Gorrec 2005, Theorem 3.1], leads to the expression in (II.51) with $\mathcal{Q}_\partial(\mathtt{S})$ given in (II.53) along with their associated matrices.

□

Corollary II.1. *For $\mathcal{F}_{\mathtt{x}}$ of order $N = 1$, Lemma II.1 leads to:*

$$\int_{\Omega} \left(v(\mathtt{X})^{\top} \mathcal{F}_{\mathtt{x}}\, w(\mathtt{X}) - w(\mathtt{X})^{\top} \mathcal{F}_{\mathtt{x}}{}^{*} v(\mathtt{X}) \right) d\mathtt{X} = \int_{\partial\Omega} w(\mathtt{S})^{\top} F_{\partial}(\mathtt{S})\, v(\mathtt{S})\, d\mathtt{S}, \tag{II.55}$$

since $\mathcal{B}(\cdot)$ becomes the identity and $\mathcal{Q}_{\partial}(\mathtt{S})$ becomes $F_{\partial}(\mathtt{S})$.

Kinetic energy

Proposition II.1. *The generalized momentum $p(\mathtt{X}, t) \in \mathbb{R}^n$, the mass density matrix $\mathcal{M}(\mathtt{X}) = \mathcal{M}(\mathtt{X})^{\top} > 0 \in \mathbb{R}^{n \times n}$, the total kinetic energy $T(p) \in \mathbb{R}$ and the co-energy variable $e_p(\mathtt{X}, t) \in \mathbb{R}^n$ are defined as:*

$$p(\mathtt{X}, t) = \mathcal{M}(\mathtt{X})\, \dot{r}(\mathtt{X}, t), \tag{II.56}$$

$$\mathcal{M}(\mathtt{X}) = \rho_0(\mathtt{X}) \int_{\Omega^c} \bar{M}_1(\mathtt{X}^c)^{\top} \bar{M}_1(\mathtt{X}^c)\, d\mathtt{X}^c, \tag{II.57}$$

$$T(p) = \frac{1}{2} \int_{\Omega} p(\mathtt{X}, t)^{\top} \mathcal{M}(\mathtt{X})^{-1} p(\mathtt{X}, t)\, d\mathtt{X}, \tag{II.58}$$

$$e_p(\mathtt{X}, t) = \mathcal{M}(\mathtt{X})^{-1} p(\mathtt{X}, t). \tag{II.59}$$

Proof. The displacement field $\mathbf{u}(\mathbf{X}, t)$ according to Assumption II.1 implies $\dot{\mathbf{u}}(\mathbf{X}, t) = \bar{M}_1(\mathtt{X}^c)\, \dot{r}(\mathtt{X}, t)$. Then, by the definition of kinetic energy in (II.30) we have:

$$\begin{aligned} \mathcal{T} = & \frac{1}{2} \int_{\mathcal{B}_0} \rho_0(\mathtt{X})\, \dot{\mathbf{u}}(\mathbf{X}, t)^{\top} \dot{\mathbf{u}}(\mathbf{X}, t)\, d\mathbf{X} \\ = & \frac{1}{2} \int_{\Omega} \dot{r}(\mathtt{X}, t)^{\top} \underbrace{\rho_0(\mathtt{X}) \int_{\Omega^c} \bar{M}_1(\mathtt{X}^c)^{\top} \bar{M}_1(\mathtt{X}^c)\, d\mathtt{X}^c}_{\mathcal{M}(\mathtt{X})}\, \dot{r}(\mathtt{X}, t)\, d\mathtt{X}, \end{aligned}$$

but from (II.56) and since $\bar{M}_1(\mathtt{X}^c)$ is full rank, we know that $\dot{r}(\mathtt{X}, t) = \mathcal{M}(\mathtt{X})^{-1} p(\mathtt{X}, t)$, then we can write $\mathcal{T}$ as (II.58). By definition $e_p(\mathtt{X}, t)$ is the variational derivative of $T(p)$ with respect to $p(\mathtt{X}, t)$.

□

Notice that the kinetic energy $T(p)$ is quadratic with respect to the generalized momentum $p(\mathtt{X}, t)$ and the inverse of the mass density matrix $\mathcal{M}(\mathtt{X})$. This arises from the structure of the displacement field $\mathbf{u}(\mathbf{X}, t)$ in Assumption II.1. Additionally, the assumption that $\bar{M}_1(\mathtt{X}^c)$ is full rank ensures an invertible mass density matrix. However, this assumption can be relaxed in many models if the complementary domain Ω^c is symmetric with respect to its centroidal coordinates, which also results in invertible mass density matrices.

Elastic potential energy

In Hooke's law, the strain energy density function $W(\boldsymbol{\varepsilon}) \in \mathbb{R}$ can always be written as a quadratic form between $\boldsymbol{\varepsilon}(\mathbf{X}, t) \in \mathbb{R}^d$ and a constitutive matrix $C_L = C_L^{\top} > 0 \in \mathbb{R}^{d \times d}$. Then, the strain energy density function for generalized Hooke's law is given by:

$$W(\boldsymbol{\varepsilon}(\mathbf{X}, t)) = \frac{1}{2} \boldsymbol{\varepsilon}(\mathbf{X}, t)^{\top} C_L\, \boldsymbol{\varepsilon}(\mathbf{X}, t). \tag{II.60}$$

Proposition II.2. *The generalized strains $\epsilon(\mathtt{X},t) \in \mathbb{R}^m$, the stiffness density matrix $\mathcal{K}_\epsilon(\mathtt{X}) = \mathcal{K}_\epsilon(\mathtt{X})^\top > 0 \in \mathbb{R}^{m\times m}$, the elastic potential energy $U(\epsilon) \in \mathbb{R}$, and the co-energy variable $e_\epsilon(\mathtt{X},t) \in \mathbb{R}^m$ are defined as:*

$$\epsilon(\mathtt{X},t) = \mathcal{F}_{\mathtt{x}} r(\mathtt{X},t), \tag{II.61}$$

$$\mathcal{K}_\epsilon(\mathtt{X}) = \int_{\Omega^c} \bar{M}_2(\mathtt{X}^c)^\top C_L\, \bar{M}_2(\mathtt{X}^c)\, d\mathtt{X}^c, \tag{II.62}$$

$$U(\epsilon) = \int_\Omega \Psi(\epsilon)\, d\mathtt{X} = \frac{1}{2}\int_\Omega \epsilon(\mathtt{X},t)^\top \mathcal{K}_\epsilon(\mathtt{X})\, \epsilon(\mathtt{X},t)\, d\mathtt{X}, \tag{II.63}$$

$$e_\epsilon(\mathtt{X},t) = \frac{\partial \Psi(\epsilon)}{\partial \epsilon} = \mathcal{K}_\epsilon(\mathtt{X})\epsilon(\mathtt{X},t), \tag{II.64}$$

with $\mathcal{F}_{\mathtt{x}}$ a constant differential operator of dimension $(m\times n)$ of the same class as in Definition II.4 with associated constant matrices F_0, $F_k^i \in \mathbb{R}^{m\times n}$.

Proof. Given that the strain measure is the infinitesimal strain tensor $\underline{\boldsymbol{\varepsilon}}(\mathbf{X},t)$, the real strains are linearly related to $\mathbf{u}(\mathbf{X},t)$ through the symmetric gradient operator Grad$(\cdot)$ introduced in (II.19) in page 35. Therefore, we can express the generalized strains as $\epsilon(\mathtt{X},t) = \mathcal{F}_{\mathtt{x}} r(\mathtt{X},t)$ with $\mathcal{F}_{\mathtt{x}}$ a constant differential operator (with associated constant matrices F_0, F_k^i). On the other hand, from Assumption II.2 we have $\boldsymbol{\varepsilon}(\mathbf{X},t) = \bar{M}_2(\mathtt{X}^c)\epsilon(\mathtt{X},t) \in \mathbb{R}^d$, then by the definition of the elastic potential energy in (II.31) we have:

$$\mathcal{U} = \int_{\mathcal{B}_0} W(\boldsymbol{\varepsilon})\, d\mathbf{X} = \frac{1}{2}\int_\Omega \epsilon(\mathtt{X},t)^\top \underbrace{\int_{\Omega^c} \bar{M}_2(\mathtt{X}^c)^\top C_L\, \bar{M}_2(\mathtt{X}^c)\, d\mathtt{X}^c}_{\mathcal{K}_\epsilon(\mathtt{X})} \epsilon(\mathtt{X},t)\, d\mathtt{X} = U(\epsilon).$$

□

Remark II.8. *Note that the structure of $\mathcal{F}_{\mathtt{x}}$ is mainly determined by Grad$(\boldsymbol{u})$, where if there are no differential dependencies between the components of $r(\mathtt{X},t)$, the operator $\mathcal{F}_{\mathtt{x}}$ is of order $N = 1$. Also note that for $N > 1$, the matrix $\mathcal{Q}_\partial(\mathtt{S})$ is not full row rank.*

Proposition II.3. *Consider an arbitrary differential operator $\mathcal{F}_{\mathtt{x}}$ of order N, $\mathcal{B}(\cdot)$ and $\mathcal{Q}_\partial(\mathtt{S})$ defined in (II.52) and (II.53), respectively. Define $T_R \in \mathbb{R}^{n_z\times n+(N-1)n\ell}$ with n_z the number of nonzero rows of $\mathcal{Q}_\partial(\mathtt{S})$, as a constant matrix such that $T_R\mathcal{Q}_\partial(\mathtt{S})$ only retains the nonzero rows of $\mathcal{Q}_\partial(\mathtt{S})$. Assume that $T_R\mathcal{B}(e_p(\mathtt{S},t)) = T_L e_p(\mathtt{S},t)$ with $T_L \in \mathbb{R}^{n_z\times n}$ a constant matrix. Then the following equality holds:*

$$\int_{\partial\Omega} \mathcal{B}(e_p(\mathtt{S},t))^\top \mathcal{Q}_\partial(\mathtt{S})\, \mathcal{B}(e_\epsilon(\mathtt{S},t))\, d\mathtt{S} = \int_{\partial\Omega} e_p(\mathtt{S},t)^\top \bar{\mathcal{Q}}_\partial(\mathtt{S})\, \mathcal{B}(e_\epsilon(\mathtt{S},t))\, d\mathtt{S}, \tag{II.65}$$

with $\bar{\mathcal{Q}}_\partial(\mathtt{S}) = T_L^\top T_R\, \mathcal{Q}_\partial(\mathtt{S}) \in \mathbb{R}^{n\times m+(N-1)m\ell}$.

Proof. Since $T_R\mathcal{Q}_\partial(\mathtt{S})$ only retains non-zero rows, and using $T_R\mathcal{B}(e_p(\mathtt{S},t)) = T_L e_p(\mathtt{S},t)$, then we have:

$$\begin{aligned}
\mathcal{B}(e_p(\mathtt{S},t))^\top \mathcal{Q}_\partial(\mathtt{S})\mathcal{B}(e_\epsilon(\mathtt{S},t)) &= (T_R\mathcal{B}(e_p(\mathtt{S},t)))^\top T_R\mathcal{Q}_\partial(\mathtt{S})\mathcal{B}(e_\epsilon(\mathtt{S},t)) \\
&= e_p(\mathtt{S},t)^\top T_L^\top T_R\, \mathcal{Q}_\partial(\mathtt{s})\mathcal{B}(e_\epsilon(\mathtt{S},t)) \\
&= e_p(\mathtt{S},t)^\top \bar{\mathcal{Q}}_\partial(\mathtt{S})\mathcal{B}(e_\epsilon(\mathtt{S},t)).
\end{aligned}$$

□

Extended work associated to external forces

The extended work $\mathcal{W}_\mathcal{E}$ defined in (II.41) in page 39 involves the imposed body forces $f_V(\mathbf{X},t)$, the imposed surface traction $\mathbf{t}_N(S,t)$ on the Neumann surface $\partial\mathcal{B}_0^N$, the imposed displacements $\mathbf{u}_D(S,t)$ on the Dirichlet surface $\partial\mathcal{B}_0^D$, and their respective reaction traction $\mathbf{t}_D(S,t)$ on $\partial\mathcal{B}_0^D$, as previously illustrated in Fig. II.2 in page 36. In the following proposition, the extended work $\mathcal{W}_\mathcal{E}$ is rewritten to be valid for any spatial domain $\Omega \subset \mathbb{R}^\ell$.

Proposition II.4. *The extended work $\mathcal{W}_\mathcal{E}$ defined in (II.41) is rewritten as:*

$$\begin{aligned}\mathcal{W}_\mathcal{E} = &\int_\Omega r(\mathtt{X},t)^\top \left[B_d\, u_d(\mathtt{X},t) + b(\mathtt{X})\right] d\mathtt{X} + \int_{\partial\Omega_N} r(\mathtt{S},t)^\top \tau_N(\mathtt{S},t)\, d\mathtt{S} \ldots \\ &\ldots + \int_{\partial\Omega_D} \left[r(\mathtt{S},t) - r_D(\mathtt{S},t)\right]^\top \tau_D(\mathtt{S},t)\, d\mathtt{S},\end{aligned} \tag{II.66}$$

where $B_d\, u_d(\mathtt{X},t) \in \mathbb{R}^n$ is defined as the generalized distributed load with B_d an algebraic input map and $u_d(\mathtt{X},t)$ the distributed input, $b(\mathtt{X}) \in \mathbb{R}^n$ is the generalized body force, $\tau_N(\mathtt{S},t) \in \mathbb{R}^n$ is the imposed generalized traction on $\partial\Omega_N$, $\tau_D(\mathtt{S},t) \in \mathbb{R}^n$ is the generalized reaction traction on $\partial\Omega_D$, and $r_D(\mathtt{S},t) \in \mathbb{R}^n$ is the imposed generalized displacement on $\partial\Omega_D$.

Proof. The extended work $\mathcal{W}_\mathcal{E}$ defined in (II.41) is composed of the three terms:

$$\mathcal{W}_\mathcal{E} = \underbrace{\int_{\mathcal{B}_0} f_V \cdot \mathbf{u}\, d\mathbf{X}}_{(a)} + \underbrace{\int_{\partial\mathcal{B}_0^N} \mathbf{t}_N \cdot \mathbf{u}\, dS}_{(b)} + \underbrace{\int_{\partial\mathcal{B}_0^D} \mathbf{t}_D \cdot [\mathbf{u} - \mathbf{u}_D]\, dS}_{(c)}.$$

According to Assumption II.1, for the term (a) we have:

$$(a) = \int_\Omega r(\mathtt{X},t)^\top \int_{\Omega^c} \bar{M}_1(\mathtt{X}^c)^\top f_V(\mathbf{X},t)\, d\mathtt{X}^c\, d\mathtt{X} = \int_\Omega r(\mathtt{X},t)^\top f_\Omega(\mathtt{X},t)\, d\mathtt{X},$$

where considering the partition $f_\Omega(\mathtt{X},t) = B_d\, u_d(\mathtt{X},t) + b(\mathtt{X})$ we recover the first term in (II.66). For the terms (b) and (c) we obtain:

$$\begin{aligned}(b) &= \int_{\partial\Omega_N} r(\mathtt{S},t)^\top \int_{\Omega^c} \bar{M}_1(\mathtt{X}^c)^\top \mathbf{t}_N(S,t)\, d\mathtt{X}^c\, d\mathtt{S} = \int_{\partial\Omega_N} r(\mathtt{S},t)^\top \tau_N(\mathtt{S},t)\, d\mathtt{S}. \\ (c) &= \int_{\partial\Omega_D} \left[r(\mathtt{S},t) - r_D(\mathtt{S},t)\right]^\top \int_{\Omega^c} \bar{M}_1(\mathtt{X}^c)^\top \mathbf{t}_D(S,t)\, d\mathtt{X}^c\, d\mathtt{S} \\ &= \int_{\partial\Omega_D} \left[r(\mathtt{S},t) - r_D(\mathtt{S},t)\right]^\top \tau_D(\mathtt{S},t)\, d\mathtt{S}.\end{aligned}$$

Considering the above, $\mathcal{W}_\mathcal{E}$ in (II.41) is equivalent to the expression in (II.66). □

$\mathcal{W}_\mathcal{E}$ is related to the external loads that interact with the body, either distributed over the spatial domain $\Omega \subset \mathbb{R}^\ell$ or through its boundary $\partial\Omega$. The distributed loads are separated into two parts, where $B_d\, u_d(\mathtt{X},t)$ is the generalized distributed load with $u_d(\mathtt{X},t)$ some external input, and $b(\mathtt{X})$ is the generalized body force,

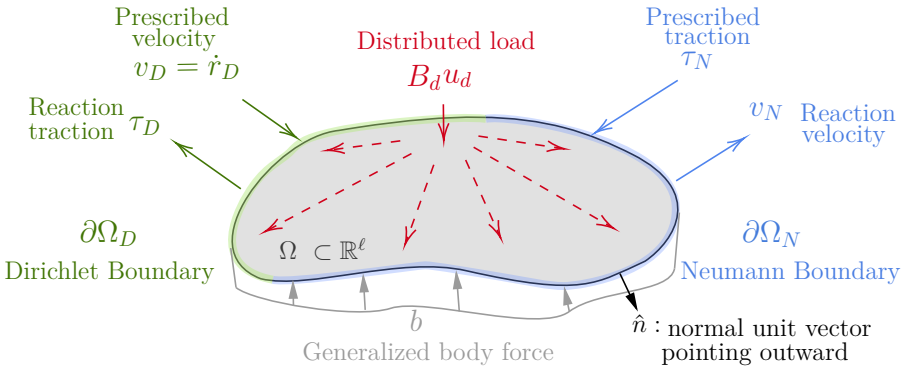

Figure II.4 – Scheme to illustrate the extended work

normally considered as the weight of the body. On the other hand, on $\partial\Omega_N$ we have $\tau_N(\mathtt{S}, t)$ which corresponds to the imposed generalized traction, and its power conjugated reaction is the generalized velocity $v_N(\mathtt{S}, t)$. Finally, on $\partial\Omega_D$ we have $v_D(\mathtt{S}, t) = \dot{r}_D(\mathtt{S}, t)$ which corresponds to the imposed generalized velocity, and its power conjugated reaction is the generalized traction $\tau_D(\mathtt{S}, t)$. For an illustrative representation of the new variables introduced see Figure II.4.

Remark II.9. *Dissipative effects are not included in the formulation of external work. The inclusion of such effects, such as viscous damping, requires special care, particularly in nonlinear systems, as it can complicate the variational formulation. Incorporating dissipation may divert attention from the primary focus of Proposition II.4, which is to introduce the distributed and boundary ports used to express energy conservation. However, viscous damping can be incorporated into the model at a later stage, either in infinite-dimensional or finite-dimensional systems, but it must be studied on a case-by-case basis to avoid compromising the formulation.*

Infinite-dimensional linear PHS

The infinite-dimensional PHS representation of the considered class of linear mechanical systems is presented in the next theorem.

Theorem II.1. *Let consider* $x(\mathtt{X}, t) = [p(\mathtt{X}, t)^\top \ \epsilon(\mathtt{X}, t)^\top \ r(\mathtt{X}, t)^\top]^\top \in \mathbb{R}^{2n+m}$ *as the energy variables, and* $\delta_x H(x) = [e_p(\mathtt{X}, t)^\top \ e_\epsilon(\mathtt{X}, t)^\top - b(\mathtt{X})^\top]^\top \in \mathbb{R}^{2n+m}$ *as the co-energy variables. From Propositions II.1, II.2, II.3 and II.4, the dynamics of the considered linear systems can be written in an explicit PHS form as:*

$$\underbrace{\begin{bmatrix} \dot{p}(\mathtt{X}, t) \\ \dot{\epsilon}(\mathtt{X}, t) \\ \dot{r}(\mathtt{X}, t) \end{bmatrix}}_{\dot{x}} = \underbrace{\begin{bmatrix} 0 & -\mathcal{F}_{\mathtt{x}}^* & -1 \\ \mathcal{F}_{\mathtt{x}} & 0 & 0 \\ 1 & 0 & 0 \end{bmatrix}}_{\mathcal{J} = -\mathcal{J}^*} \underbrace{\begin{bmatrix} e_p(\mathtt{X}, t) \\ e_\epsilon(\mathtt{X}, t) \\ -b(\mathtt{X}) \end{bmatrix}}_{\delta_x H(x)} + \underbrace{\begin{bmatrix} B_d \\ 0 \\ 0 \end{bmatrix}}_{\mathcal{G}} u_d(\mathtt{X}, t) \tag{II.67}$$

$$y_d(\mathtt{X}, t) = \mathcal{G}^* \delta_x H(x) = B_d^\top e_p(\mathtt{X}, t).$$

The boundary inputs and outputs $u_\partial(\mathtt{S},t)$, $y_\partial(\mathtt{S},t) \in \mathbb{R}^{2n}$ *are defined as:*

$$u_\partial(\mathtt{S},t) = \begin{bmatrix} \tau_N(\mathtt{S},t)^\top & v_D(\mathtt{S},t)^\top \end{bmatrix}^\top, \quad y_\partial(\mathtt{S},t) = \begin{bmatrix} v_N(\mathtt{S},t)^\top & \tau_D(\mathtt{S},t)^\top \end{bmatrix}^\top \tag{II.68}$$

where:

$$\begin{aligned} \tau_N(\mathtt{S},t) &= \bar{\mathcal{Q}}_\partial(\mathtt{S})\mathcal{B}(e_\epsilon(\mathtt{S},t)), \quad v_N(\mathtt{S},t) = e_p(\mathtt{S},t) \quad (\textit{on } \partial\Omega_N), \\ \tau_D(\mathtt{S},t) &= \bar{\mathcal{Q}}_\partial(\mathtt{S})\mathcal{B}(e_\epsilon(\mathtt{S},t)), \quad v_D(\mathtt{S},t) = e_p(\mathtt{S},t) \quad (\textit{on } \partial\Omega_D). \end{aligned} \tag{II.69}$$

The total energy function is given by the Hamiltonian:

$$H(x) = \int_\Omega \left(\frac{1}{2}\, p(\mathtt{X},t)^\top \mathcal{M}(\mathtt{X})^{-1} p(\mathtt{X},t) + \frac{1}{2}\, \epsilon(\mathtt{X},t)^\top \mathcal{K}_\epsilon(\mathtt{X})\epsilon(\mathtt{X},t) - r(\mathtt{X},t)^\top b(\mathtt{X}) \right) d\mathtt{X}, \tag{II.70}$$

and the power exchanged with the environment is given by:

$$\dot{H}(x) = \int_\Omega u_d(\mathtt{X},t)^\top y_d(\mathtt{X},t)\, d\mathtt{X} + \int_{\partial\Omega} u_\partial(\mathtt{S},t)^\top y_\partial(\mathtt{S},t)\, d\mathtt{S}. \tag{II.71}$$

Proof. The proof consists of applying the generalized extended Hamilton's principle (without constraints). To improve the readability of the proof, it is divided into four steps and the spatial and temporal dependencies are omitted.

Step 1: From Proposition II.1 we have $\mathcal{T} = \frac{1}{2}\int_\Omega \dot{r}^\top \mathcal{M}\dot{r}\, d\mathtt{X}$, then the term:

$$\delta \int_{t_1}^{t_2} \mathcal{T}\, dt = \int_{t_1}^{t_2} \int_\Omega \delta\dot{r}^\top \mathcal{M}\dot{r}\, d\mathtt{X}\, dt,$$

where integrating by parts with respect to time we obtain:

$$\delta \int_{t_1}^{t_2} \mathcal{T}\, dt = \underbrace{\int_\Omega \delta r^\top \mathcal{M}\dot{r}\, d\mathtt{X}\Big|_{t_1}^{t_2}}_{=0 \text{ due to (II.39)}} - \int_{t_1}^{t_2} \int_\Omega \delta r^\top \mathcal{M}\ddot{r}\, d\mathtt{X}\, dt. \tag{II.72}$$

Step 2: Consider the term:

$$\begin{aligned} \delta \int_{t_1}^{t_2} \mathcal{U}_\mathcal{E}\, dt &= \int_{t_1}^{t_2} \int_{\mathcal{B}_0} \Big[\underbrace{\boldsymbol{\sigma}\cdot\delta\boldsymbol{\varepsilon}(\mathbf{u})}_{\boldsymbol{\sigma}^\top \bar{M}_2 \mathcal{F}_\mathtt{x}\delta r} + \delta\boldsymbol{\sigma}\cdot(\boldsymbol{\varepsilon}(\mathbf{u}) - \boldsymbol{\varepsilon}) - \delta\boldsymbol{\varepsilon}\cdot\left(\boldsymbol{\sigma} - \frac{\partial W(\boldsymbol{\varepsilon})}{\partial \boldsymbol{\varepsilon}}\right) \Big] d\mathbf{X}\, dt \\ &= \int_{t_1}^{t_2} \Big[\int_\Omega \underbrace{\int_{\Omega^c} \boldsymbol{\sigma}^\top \bar{M}_2 d\mathtt{X}^c}_{e_\epsilon^\top} \mathcal{F}_\mathtt{x}\delta r\, d\mathtt{X} + \int_\Omega \underbrace{\int_{\Omega^c} \delta\boldsymbol{\sigma}^\top \bar{M}_2 d\mathtt{X}^c}_{\delta e_\epsilon^\top} (\epsilon(r) - \epsilon)\, d\mathtt{X} \ldots \\ &\quad \ldots - \int_\Omega \delta\epsilon^\top \Big(\underbrace{\int_{\Omega^c} \bar{M}_2^\top \boldsymbol{\sigma}\, d\mathtt{X}^c}_{e_\epsilon} - \underbrace{\int_{\Omega^c} \bar{M}_2^\top \frac{\partial W(\boldsymbol{\varepsilon})}{\partial \boldsymbol{\varepsilon}} d\mathtt{X}^c}_{\frac{\partial \Psi(\epsilon)}{\partial \epsilon} \text{ by Assumption II.2}} \Big) d\mathtt{X} \Big] dt \\ &= \int_{t_1}^{t_2} \Big[\underbrace{\int_\Omega e_\epsilon^\top \mathcal{F}_\mathtt{x}\delta r d\mathtt{X}}_{\text{Lemma II.1}} + \int_\Omega \delta e_\epsilon^\top (\epsilon(r) - \epsilon) d\mathtt{X} - \int_\Omega \delta\epsilon^\top \left(e_\epsilon - \frac{\partial \Psi(\epsilon)}{\partial \epsilon} \right) d\mathtt{X} \Big] dt. \end{aligned}$$

Applying Lemma II.1 and Proposition II.3 to the first term we obtain:

$$\int_\Omega e_\epsilon^\top \mathcal{F}_{\mathtt{x}} \delta r \, d\mathtt{X} = \int_\Omega \delta r^\top {\mathcal{F}_{\mathtt{x}}}^* e_\epsilon d\mathtt{X} + \int_{\partial\Omega_N} \delta r^\top \bar{\mathcal{Q}}_\partial \mathcal{B}(e_\epsilon)\, d\mathtt{S} + \underbrace{\int_{\partial\Omega_D} \delta r^\top \bar{\mathcal{Q}}_\partial \mathcal{B}(e_\epsilon)\, d\mathtt{S}}_{=0 \text{ due to (II.38)}}.$$

Replacing the above into the last expression of $\delta\int_{t_1}^{t_2} \mathcal{U}_\mathcal{E}\, dt$ we obtain:

$$\delta\int_{t_1}^{t_2} \mathcal{U}_\mathcal{E}\, dt = \int_{t_1}^{t_2} \left\{ \int_\Omega \left[\delta r^\top {\mathcal{F}_{\mathtt{x}}}^* e_\epsilon + \delta e_\epsilon^\top (\epsilon(r) - \epsilon) - \delta\epsilon^\top \left(e_\epsilon - \frac{\partial\Psi(\epsilon)}{\partial\epsilon} \right) \right] d\mathtt{X} ... \right.$$
$$\left. ... + \int_{\partial\Omega_N} \delta r^\top \bar{\mathcal{Q}}_\partial \mathcal{B}(e_\epsilon)\, d\mathtt{S} \right\} dt. \tag{II.73}$$

Step 3: From the expression for external work, we derive:

$$\delta\int_{t_1}^{t_2} \mathcal{W}_\mathcal{E}\, dt = \int_{t_1}^{t_2} \left[\int_\Omega \delta r^\top (B_d\, u_d + b) d\mathtt{X} + \int_{\partial\Omega_N} \delta r^\top \tau_N\, d\mathtt{S} + \int_{\partial\Omega_D} \delta\tau_D^\top (r - r_D) d\mathtt{S} \right] dt. \tag{II.74}$$

Step 4: Considering expressions from (II.72) to (II.74), the application of the generalized extended Hamilton's principle leads to:

$$\int_{t_1}^{t_2} \delta(\mathcal{T} - \mathcal{U}_\mathcal{E} + \mathcal{W}_\mathcal{E}) dt = \int_{t_1}^{t_2} \left\{ \int_\Omega \left[\delta r^\top \underbrace{(-\mathcal{M}\ddot{r} - {\mathcal{F}_{\mathtt{x}}}^* e_\epsilon + b + B_d\, u_d)}_{(1)} - \delta e_\epsilon^\top \underbrace{(\epsilon(r) - \epsilon)}_{(2)} ... \right.\right.$$
$$\left.\left. ... \delta\epsilon^\top \underbrace{\left(e_\epsilon - \frac{\partial\Psi(\epsilon)}{\partial\epsilon} \right)}_{(3)} \right] d\mathtt{X} \right\} dt + \int_{t_1}^{t_2} \left[\int_{\partial\Omega_N} \delta r^\top \underbrace{[\tau_N - \bar{\mathcal{Q}}_\partial \mathcal{B}(e_\epsilon)]}_{(4)} d\mathtt{S} ... \right.$$
$$\left. ... + \int_{t_1}^{t_2} \left[\int_{\partial\Omega_D} \delta\tau_D^\top \underbrace{(r - r_D)}_{(5)} d\mathtt{S} \right] dt = 0. \right.$$

So applying the fundamental lemma of variational calculus, each term (i) with $i = \{1, ..., 5\}$ is equal to zero. Then, the following Lagrangian model with Dirichlet and Neumann boundary conditions is obtained:

$$\forall \mathtt{X} \in \Omega: \quad \mathcal{M}\ddot{r} = -{\mathcal{F}_{\mathtt{x}}}^*\, e_\epsilon + b + B_d\, u_d, \tag{II.75}$$
$$\epsilon = \epsilon(r), \tag{II.76}$$
$$e_\epsilon = \frac{\partial\Psi(\epsilon)}{\partial\epsilon}, \tag{II.77}$$
$$\forall \mathtt{S} \in \partial\Omega_N: \quad \tau_N = \bar{\mathcal{Q}}_\partial \mathcal{B}(e_\epsilon), \tag{II.78}$$
$$\forall \mathtt{S} \in \partial\Omega_D: \quad r_D = r. \tag{II.79}$$

Noticing that the time derivative of (II.76) leads to $\dot{\epsilon} = \mathcal{F}_{\mathtt{x}}\dot{r} = \mathcal{F}_{\mathtt{x}} e_p$, the Lagrangian model with Hamiltonian in (II.70) can be written as the explicit PHS in (II.67). The power exchange with the environment is given by:

$$\dot{H}(x) = \int_\Omega \delta_x H^\top \dot{x}\, d\mathtt{X} = \int_\Omega e_p^\top B_d\, u_d\, d\mathtt{X} + \underbrace{\int_\Omega (e_\epsilon^\top \mathcal{F}_{\mathtt{x}} e_p - e_p^\top {\mathcal{F}_{\mathtt{x}}}^* e_\epsilon) d\mathtt{X}}_{\text{Lemma II.1}},$$

so applying Lemma II.1 to the term indicated above we obtain:

$$\dot{H}(x) = \int_\Omega u_d^\top \underbrace{B_d^\top e_p}_{y_d}\, d\mathtt{X} + \underbrace{\int_{\partial\Omega} \mathcal{B}(e_p)^\top \mathcal{Q}_\partial \mathcal{B}(e_\epsilon)\, d\mathtt{S}}_{\text{Proposition II.3}} = \int_\Omega u_d^\top y_d\, d\mathtt{X} + \int_{\partial\Omega} u_\partial^\top y_\partial\, d\mathtt{S},$$

where u_∂ and y_∂ are the boundary inputs and outputs defined in (II.68).

□

Remark II.10. *The PHS obtained in Theorem II.1 has different structure with respect to the one obtained by the Legendre transformation of the Lagrangian system. Furthermore, the latter is a field port-Lagrangian system described by a canonical interconnection matrix, a mass density matrix and a differential stiffness operator.*

Proposition II.5. *The field port-Lagrangian representation of the linear PHS in Theorem II.1 is described by the state variable $z(\mathtt{X},t) = [p(\mathtt{X},t)^\top \;\; r(\mathtt{X},t)^\top]^\top \in \mathbb{R}^{2n}$, where:*

$$\underbrace{\begin{bmatrix}\dot{p}(\mathtt{X},t)\\ \dot{r}(\mathtt{X},t)\end{bmatrix}}_{\dot{z}} = \underbrace{\begin{bmatrix}0 & -1\\ 1 & 0\end{bmatrix}}_{J=-J^\top} \underbrace{\begin{bmatrix}e_p(\mathtt{X},t)\\ e_r(\mathtt{X},t)\end{bmatrix}}_{\delta_z H(z)} + \underbrace{\begin{bmatrix}B_d\\ 0\end{bmatrix}}_{\mathcal{G}} u_d(\mathtt{X},t) \tag{II.80}$$

$$y_d(\mathtt{X},t) = \mathcal{G}^*\delta_z H(z) = B_d^\top e_p(\mathtt{X},t),$$

with Hamiltonian defined as $H(z) = T(p) + U_T(r)$, where $T(p)$ is the kinetic energy defined in Proposition II.1, and $U_T(r)$ is the total potential energy defined as:

$$U_T(r) = \int_\Omega \left[\frac{1}{2}(\mathcal{F}_{\mathtt{x}} r(\mathtt{X},t))^\top \mathcal{K}_\epsilon(\mathtt{X})(\mathcal{F}_{\mathtt{x}} r(\mathtt{X},t)) - r(\mathtt{X},t)^\top b(\mathtt{X})\right] d\mathtt{X}. \tag{II.81}$$

The co-energy variable $e_r(\mathtt{X},t) \in \mathbb{R}^n$ is defined as the variational derivative of the Hamiltonian $H(z)$ with respect to $r(\mathtt{X},t)$ and is given by:

$$e_r(\mathtt{X},t) = \mathcal{F}_{\mathtt{x}}{}^* \left(\mathcal{K}_\epsilon(\mathtt{X})\mathcal{F}_{\mathtt{x}} r(\mathtt{X},t)\right) - b(\mathtt{X}) = \mathcal{K}_r(r(\mathtt{X},t)) - b(\mathtt{X}), \tag{II.82}$$

where $\mathcal{K}_r(\cdot) = \mathcal{F}_{\mathtt{x}}{}^* \left(\mathcal{K}_\epsilon(\mathtt{X})\mathcal{F}_{\mathtt{x}}(\cdot)\right)$ is the differential stiffness operator.

Proof. The dynamic equation for $\dot{p}(\mathtt{X},t)$ in (II.80) is identical to the dynamic equation for $\dot{p}(\mathtt{X},t)$ in (II.67). Therefore, both models equivalently describe the dynamics. What remains to be demonstrated is that the proposed field port-Lagrangian model is obtained via the Legendre transformation of the Lagrangian model. The kinetic energy $T(\dot{r})$ and the total potential energy $U_T(r)$ are given by:

$$T(\dot{r}) = \int_\Omega \mathscr{T}(\dot{r})\, d\mathtt{X} = \frac{1}{2}\int_\Omega \dot{r}^\top \mathcal{M}\, \dot{r}\, d\mathtt{X}, \tag{II.83}$$

$$U_T(r) = \int_\Omega \mathscr{U}_T(r)\, d\mathtt{X} = \int_\Omega \left(\frac{1}{2}(\mathcal{F}_{\mathtt{x}} r)^\top \mathcal{K}_\epsilon\, (\mathcal{F}_{\mathtt{x}} r) - r^\top b\right) d\mathtt{X}. \tag{II.84}$$

The Hamiltonian density $\mathscr{H}(\dot{r}, r)$ is defined as the Legendre transform of the Lagrangian density $\mathscr{L}(\dot{r}, r) = \mathscr{T}(\dot{r}) - \mathscr{U}_T(r)$. So, applying the Legendre operator to $\mathscr{L}(\dot{r}, r)$ we obtain:

$$\mathscr{H}(\dot{r}, r) = \left[\dot{r} \cdot \frac{\partial}{\partial \dot{r}} - 1\right](\mathscr{L}(\dot{r}, r)) = \frac{1}{2}\dot{r}^\top \mathcal{M}\, \dot{r} + \frac{1}{2}(\mathcal{F}_{\mathtt{x}} r)^\top \mathcal{K}_\epsilon\, (\mathcal{F}_{\mathtt{x}} r) - r^\top b.$$

Then, by definition the momentum variable is given by $p = \partial\mathscr{L}/\partial\dot{r} = \mathcal{M}\dot{r}$, which implies $\dot{r} = \mathcal{M}^{-1}\, p$ and the Hamiltonian with respect to $z = [p^\top \;\; r^\top]^\top$ is the total energy defined in (II.81). On the other hand, to prove (II.82), we first consider the following functionals:

$$U_T(r) = \int_\Omega \mathscr{U}_T(\mathtt{X}, r, \mathcal{F}_{\mathtt{x}} r)\, d\mathtt{X}, \quad U_T^\star(r^\star) = U_T(r + \alpha\eta) = \int_\Omega \mathscr{U}_T(\mathtt{X}, r^\star, \mathcal{F}_{\mathtt{x}} r^\star)\, d\mathtt{X},$$

where η is an arbitrary function that vanishes in $\partial\Omega$, and $\alpha \in \mathbb{R}$ is a scalar. By definition the first variation of U_T is given by $\delta U_T = \lim_{\alpha\to 0} dU_T^\star/d\alpha$, then we have:

$$\begin{aligned}
\delta U_T = &\lim_{\alpha\to 0} \frac{d}{d\alpha} \int_\Omega \mathscr{U}_T(\mathtt{X}, r^\star, (\mathcal{F}_{\mathtt{x}} r^\star)) d\mathtt{X} \\
= &\lim_{\alpha\to 0} \int_\Omega \left(\frac{\partial \mathscr{U}_T}{\partial \mathtt{X}} \frac{\partial \mathtt{X}}{\partial \alpha} + \frac{\partial \mathscr{U}_T}{\partial r^\star} \cdot \frac{\partial r^\star}{\partial \alpha} + \frac{\partial \mathscr{U}_T}{\partial (\mathcal{F}_{\mathtt{x}} r^\star)} \cdot \frac{\partial (\mathcal{F}_{\mathtt{x}} r^\star)}{\partial \alpha} \right) d\mathtt{X} \\
= &\lim_{\alpha\to 0} \int_\Omega \Bigg(\frac{\partial \mathscr{U}_T}{\partial r^\star} \cdot \eta + \underbrace{v \cdot \mathcal{F}_{\mathtt{x}} \eta}_{\text{Lemma II.1}} \Bigg) d\mathtt{X},
\end{aligned}$$

with $v = \frac{\partial \mathscr{U}_T}{\partial (\mathcal{F}_{\mathtt{x}} r^\star)}$. So applying Lemma II.1 to the indicated term above we obtain:

$$\delta U_T = \lim_{\alpha\to 0} \left(\int_\Omega \frac{\partial \mathscr{U}_T}{\partial r^\star} \cdot \eta \, d\mathtt{X} + \int_\Omega \eta^\top {\mathcal{F}_{\mathtt{x}}}^* v \, d\mathtt{X} + \int_{\partial\Omega} \mathcal{B}(\eta)^\top \mathcal{Q}_\partial\, \mathcal{B}(v)\, d\mathtt{S} \right),$$

where the last term is equal to zero because $\eta = 0$ in $\partial\Omega$. Then,

$$\begin{aligned}
\delta U_T = &\lim_{\alpha\to 0} \int_\Omega \eta \cdot \left[\frac{\partial \mathscr{U}_T}{\partial r^\star} + {\mathcal{F}_{\mathtt{x}}}^* \left(\frac{\partial \mathscr{U}_T}{\partial (\mathcal{F}_{\mathtt{x}} r^\star)} \right) \right] d\mathtt{X} \\
= &\int_\Omega \delta r \cdot \left[\frac{\partial \mathscr{U}_T}{\partial r} + {\mathcal{F}_{\mathtt{x}}}^* \left(\frac{\partial \mathscr{U}_T}{\partial (\mathcal{F}_{\mathtt{x}} r)} \right) \right] d\mathtt{X} \\
= &\int_\Omega \delta r \cdot \frac{\delta U_T}{\delta r}\, d\mathtt{X}.
\end{aligned}$$

Considering the above, we obtain that $\dfrac{\delta U_T}{\delta r} = \dfrac{\delta H(p, r)}{\delta r} = {\mathcal{F}_{\mathtt{x}}}^*(\mathcal{K}_\epsilon\, \mathcal{F}_{\mathtt{x}} r) - b = e_r$. □

We now propose a procedure for the systematic modeling of linear mechanical systems as explicit PHS. This procedure involves defining the system's state variables, establishing the Hamiltonian function, constructing the interconnection operator, and defining the ports. By following these steps, we ensure a structured approach to capture the dynamics and energy interactions within the system, facilitating both analysis and design.

Methodology 1. *For a flexible mechanical system with density $\rho_0(\mathtt{X})$, whose kinematic assumptions lead to a displacement field $\boldsymbol{u}(\boldsymbol{X},t)$ as in Assumption II.1, using as strain measure the infinitesimal strain tensor $\underline{\boldsymbol{\varepsilon}}(\boldsymbol{X},t)$, and whose constitutive model is defined by the generalized Hooke's law, the procedure to obtain its explicit infinite-dimensional linear PHS representation consists in following the steps below:*

1. *Calculate the mass density matrix $\mathcal{M}(\mathtt{X})$ and define the generalized momentum variables $p(\mathtt{X},t)$, the co-energy variables $e_p(\mathtt{X},t)$ and the kinetic energy $T(p)$. (Proposition II.1).*
2. *Compute the nonzero components of the Voigt-strain vector and define the generalized strain $\epsilon(\mathtt{X},t)$. Then, build the constant differential operator $\mathcal{F}_{\mathtt{x}}$ and its formal adjoint $\mathcal{F}_{\mathtt{x}}{}^*$. (Proposition II.2).*
3. *Calculate the stiffness density matrix $\mathcal{K}_\epsilon(\mathtt{X})$ and define the co-energy variable $e_\epsilon(\mathtt{X},t)$ and the elastic potential energy $U(\epsilon)$. (Proposition II.2).*
4. *If desired, define the generalized distributed load $B_d\,u_d(\mathtt{X},t)$, and the generalized body force $b(\mathtt{X})$. (Proposition II.4).*
5. *Apply Theorem II.1 to obtain the explicit linear PHS, along with the definitions of boundary inputs $u_\partial(\mathtt{S},t)$ and boundary outputs $y_\partial(\mathtt{S},t)$.*

II.3.2 Nonlinear systems

In this section, we develop models considering the Green-Lagrange strain tensor $\underline{\mathbf{E}}(\mathbf{X},t)$ as the measure of the strain, and the constitutive law assuming hyperelastic behavior based on the strain energy density function $W(\boldsymbol{\varepsilon})$ described in Assumption II.2. Unlike the linear case, the class of differential operators $\mathcal{F}_{\mathtt{x}}$ considered for the following models will be non-constant and first-order. This means that their associated matrices are functions of the spatial coordinates, and the highest derivative with respect to any spatial coordinate is of first order.

Class of non-constant differential operators

Let us recall the definition of the mentioned class of operators, and state the integration by parts lemma for these operators.

Definition I.1. *Let $\mathtt{X}=\{X_1,...,X_\ell\}$ be a set of orthogonal coordinate axes, $\Omega\subset\mathbb{R}^\ell$ an open set, $w(\mathtt{X})\in\mathbb{R}^n$ and $v(\mathtt{X})\in\mathbb{R}^m$ two smooth vector functions with compact support on Ω. The first order nonlinear differential operator $\mathcal{F}_{\mathtt{x}}$ and its formal adjoint $\mathcal{F}_{\mathtt{x}}{}^*$ are defined as:*

$$\mathcal{F}_{\mathtt{x}}w(\mathtt{X}) = F_0(\mathtt{X})w(\mathtt{X}) + \textstyle\sum_{k=1}^{\ell} F_k(\mathtt{X})\partial_k w(\mathtt{X}), \tag{I.50}$$

$$\mathcal{F}_{\mathtt{x}}{}^*v(\mathtt{X}) = F_0(\mathtt{X})^\top v(\mathtt{X}) - \textstyle\sum_{k=1}^{\ell} \partial_k\left(F_k(\mathtt{X})^\top v(\mathtt{X})\right), \tag{I.51}$$

with $\partial_k=\partial/\partial X_k$, $F_0(\mathtt{X})\in\mathbb{R}^{m\times n}$ and $F_k(\mathtt{X})\in\mathbb{R}^{m\times n}$ real matrices.

Lemma II.2. *Consider Definition I.1, the open set $\Omega \subset \mathbb{R}^\ell$, its boundary $\partial\Omega$, and the closure $\bar{\Omega} = \Omega \cup \partial\Omega$. Then, for any pair of smooth functions $v(\mathtt{X}) \in \mathbb{R}^m$ and $w(\mathtt{X}) \in \mathbb{R}^n$ defined on $\bar{\Omega}$, we have that:*

$$\int_\Omega \left(v(\mathtt{X})^\top \mathcal{F}_\mathtt{x}\, w(\mathtt{X}) - w(\mathtt{X})^\top \mathcal{F}_\mathtt{x}^{\,*} v(\mathtt{X}) \right) d\mathtt{X} = \int_{\partial\Omega} w(\mathtt{S})^\top F_\partial(\mathtt{S})\, v(\mathtt{S})\, d\mathtt{S}, \tag{II.85}$$

where $F_\partial(\mathtt{S}) \in \mathbb{R}^{n\times m}$ is defined as:

$$F_\partial(\mathtt{S}) = \textstyle\sum_{k=1}^{\ell} F_k(\mathtt{S})^\top \hat{n}_k(\mathtt{S}), \tag{II.86}$$

with $\hat{n}_k(\mathtt{S})$ the k-component of the outward unit normal vector to the boundary $\partial\Omega$ projected on the coordinate axis X_k.

Proof. (II.85) is obtained by integration by parts. □

Elastic potential energy

Note that under Assumptions II.1, the results of Propositions II.1 and II.4 regarding the kinetic energy and external work remain applicable. However, since the systems are now allowed to be geometrically and materially nonlinear, Proposition II.2 for the linear case is extended by the following proposition.

Proposition II.6. *The time derivative of the generalized strains $\dot{\epsilon}(\mathtt{X}, t) \in \mathbb{R}^m$, the elastic potential energy $U(\epsilon) \in \mathbb{R}$, and the co-energy variable $e_\epsilon(\mathtt{X}, t) \in \mathbb{R}^m$ are defined as:*

$$\dot{\epsilon}(\mathtt{X}, t) = \mathcal{F}_\mathtt{x}(r)\dot{r}(\mathtt{X}, t), \tag{II.87}$$

$$U(\epsilon) = \int_\Omega \Psi(\epsilon)\, d\mathtt{X}, \tag{II.88}$$

$$e_\epsilon(\mathtt{X}, t) = \frac{\partial \Psi(\epsilon)}{\partial \epsilon}, \tag{II.89}$$

with $\mathcal{F}_\mathtt{x}(r)$ a differential operator of dimension $(m \times n)$ of the same class as in Definition I.1, with associated matrices $F_0(r)$, $F_k(r) \in \mathbb{R}^{m\times n}$.

Proof. The generalized strain $\epsilon(\mathtt{X}, t)$ is a function of $r(\mathtt{X}, t)$ and its spatial derivatives. Then, by applying the chain rule derivation, it is possible to write $\dot{\epsilon}(\mathtt{X}, t)$ as in (II.87), with $\mathcal{F}_\mathtt{x}(r)$ a differential operator modulated by $r(\mathtt{X}, t)$ and its spatial derivatives. From the definition of elastic potential energy $\mathcal{U}$ in (II.31), and also considering Assumption II.2, we can write $\mathcal{U}$ as (II.88). By definition $e_\epsilon(\mathtt{X}, t)$ is the variational derivative of $U(\epsilon)$ with respect to $\epsilon(\mathtt{X}, t)$.

□

Note that Proposition II.2 in the linear case is a particular case of Proposition II.6 (when $\mathcal{F}_\mathtt{x}$ is of first order). For the nonlinear case, the generalized strain $\epsilon(\mathtt{X}, t)$ is derived from the Green-Lagrange strain tensor, and $\Psi(\epsilon)$ has the same physical interpretation as the strain energy density function. Thus, the co-energy variable $e_\epsilon(\mathtt{X}, t)$ resembles the second Piola-Kirchhoff stress and is defined as generalized stress.

Infinite-dimensional nonlinear PHS

The infinite-dimensional PHS representation of the considered class of nonlinear mechanical systems is presented in the next theorem.

Theorem II.2. *Let consider* $x(\mathtt{X},t) = [p(\mathtt{X},t)^\top \ \epsilon(\mathtt{X},t)^\top \ r(\mathtt{X},t)^\top]^\top \in \mathbb{R}^{2n+m}$ *as the energy variables, and* $\delta_x H(x) = [e_p(\mathtt{X},t)^\top \ e_\epsilon(\mathtt{X},t)^\top - b(\mathtt{X})^\top]^\top \in \mathbb{R}^{2n+m}$ *as the co-energy variables. From Propositions II.1, II.4 and II.6, the dynamics of the nonlinear systems can be written in an explicit PHS form as:*

$$\underbrace{\begin{bmatrix}\dot{p}(\mathtt{X},t)\\ \dot{\epsilon}(\mathtt{X},t)\\ \dot{r}(\mathtt{X},t)\end{bmatrix}}_{\dot{x}} = \underbrace{\begin{bmatrix}0 & -\mathcal{F}_{\mathtt{x}}(r)^* & -1\\ \mathcal{F}_{\mathtt{x}}(r) & 0 & 0\\ 1 & 0 & 0\end{bmatrix}}_{\mathcal{J}(x)=-\mathcal{J}(x)^*} \underbrace{\begin{bmatrix}e_p(\mathtt{X},t)\\ e_\epsilon(\mathtt{X},t)\\ -b(\mathtt{X})\end{bmatrix}}_{\delta_x H(x)} + \underbrace{\begin{bmatrix}B_d\\ 0\\ 0\end{bmatrix}}_{\mathcal{G}} u_d(\mathtt{X},t) \tag{II.90}$$

$$y_d(\mathtt{X},t) = \mathcal{G}^* \delta_x H(x) = B_d^\top e_p(\mathtt{X},t).$$

The boundary inputs and outputs $u_\partial(\mathtt{S},t)$, $y_\partial(\mathtt{S},t) \in \mathbb{R}^{2n}$ *are defined as:*

$$u_\partial(\mathtt{S},t) = \begin{bmatrix}\tau_N(\mathtt{S},t)^\top & v_D(\mathtt{S},t)^\top\end{bmatrix}^\top, \quad y_\partial(\mathtt{S},t) = \begin{bmatrix}v_N(\mathtt{S},t)^\top & \tau_D(\mathtt{S},t)^\top\end{bmatrix}^\top \tag{II.91}$$

where:

$$\begin{aligned}\tau_N(\mathtt{S},t) &= F_\partial(r) e_\epsilon(\mathtt{S},t), \quad v_N(\mathtt{S},t) = e_p(\mathtt{S},t) \quad (\textit{on } \partial\Omega_N),\\ \tau_D(\mathtt{S},t) &= F_\partial(r) e_\epsilon(\mathtt{S},t), \quad v_D(\mathtt{S},t) = e_p(\mathtt{S},t) \quad (\textit{on } \partial\Omega_D),\end{aligned} \tag{II.92}$$

and the boundary matrix $F_\partial(r) \in \mathbb{R}^{n\times m}$ *is defined as:*

$$F_\partial(r) = \textstyle\sum_{k=1}^{\ell} F_k(r)^\top \hat{n}_k(\mathtt{S}), \tag{II.93}$$

with $\hat{n}_k(\mathtt{S}) \in \mathbb{R}$ *the k-component of the normal unit vector pointing outward of the boundary* $\partial\Omega$*. The total energy function is given by the Hamiltonian:*

$$H(x) = \int_\Omega \left(\frac{1}{2} p(\mathtt{X},t)^\top \mathcal{M}(\mathtt{X})^{-1} p(\mathtt{X},t) + \Psi(\epsilon(\mathtt{X},t)) - r(\mathtt{X},t)^\top b(\mathtt{X})\right) d\mathtt{X}, \tag{II.94}$$

and the power exchange with the environment is given by:

$$\dot{H}(x) = \int_\Omega u_d(\mathtt{X},t)^\top y_d(\mathtt{X},t)\, d\mathtt{X} + \int_{\partial\Omega} u_\partial(\mathtt{S},t)^\top y_\partial(\mathtt{S},t)\, d\mathtt{S}. \tag{II.95}$$

Proof. Analogous to the proof of Theorem II.1, the proof consists in applying the generalized extended Hamilton's principle (without constraints). To improve the readability of the proof, it is divided into four steps and the spatial and temporal dependencies are omitted.

Step 1: From the proof of Theorem II.1 we have:

$$\delta \int_{t_1}^{t_2} \mathcal{T}\, dt = \underbrace{\int_\Omega \delta r^\top \mathcal{M} \dot{r}\, d\mathtt{X}\Big|_{t_1}^{t_2}}_{=0 \text{ due to (II.39)}} - \int_{t_1}^{t_2} \int_\Omega \delta r^\top \mathcal{M} \ddot{r}\, d\mathtt{X}\, dt.$$

Step 2: Similarly to the proof of Theorem II.1 we have:

$$\delta\int_{t_1}^{t_2}\mathcal{U}_{\mathcal{E}}\,dt=\int_{t_1}^{t_2}\Big\{\int_{\Omega}\Big[\delta r^{\top}\mathcal{F}_{\mathtt{x}}(r)^{*}e_{\epsilon}+\delta e_{\epsilon}^{\top}(\epsilon(r)-\epsilon)-\delta\epsilon^{\top}\Big(e_{\epsilon}-\frac{\partial\Psi(\epsilon)}{\partial\epsilon}\Big)\Big]\,d\mathtt{X}...$$
$$...+\int_{\partial\Omega_N}\delta r^{\top}F_{\partial}(r)\,e_{\epsilon}\,d\mathtt{S}\Big\}\,dt.$$

Step 3: From the proof of Theorem II.1 we have:

$$\delta\int_{t_1}^{t_2}\mathcal{W}_{\mathcal{E}}\,dt=\int_{t_1}^{t_2}\Big[\int_{\Omega}\delta r^{\top}(B_d\,u_d+b)d\mathtt{X}+\int_{\partial\Omega_N}\delta r^{\top}\tau_N\,d\mathtt{S}+\int_{\partial\Omega_D}\delta\tau_D^{\top}(r-r_D)d\mathtt{S}\Big]\,dt.$$

Step 4: Considering the above expressions, the application of the generalized extended Hamilton's principle leads to:

$$\int_{t_1}^{t_2}\delta(\mathcal{T}-\mathcal{U}_{\mathcal{E}}+\mathcal{W}_{\mathcal{E}})dt=\int_{t_1}^{t_2}\Big\{\int_{\Omega}\Big[\delta r^{\top}\underbrace{(-\mathcal{M}\ddot{r}-\mathcal{F}_{\mathtt{x}}(r)^{*}e_{\epsilon}+b+B_d\,u_d)}_{(1)}-\delta e_{\epsilon}^{\top}\underbrace{(\epsilon(r)-\epsilon)}_{(2)}...$$
$$...\delta\epsilon^{\top}\underbrace{\Big(e_{\epsilon}-\frac{\partial\Psi(\epsilon)}{\partial\epsilon}\Big)}_{(3)}\Big]\,d\mathtt{X}\Big\}\,dt+\int_{t_1}^{t_2}\Big[\int_{\partial\Omega_N}\delta r^{\top}\underbrace{[\tau_N-F_{\partial}(r)e_{\epsilon}]}_{(4)}d\mathtt{S}...$$
$$...+\int_{t_1}^{t_2}\Big[\int_{\partial\Omega_D}\delta\tau_D^{\top}\underbrace{(r-r_D)}_{(5)}d\mathtt{S}\Big]\,dt=0.$$

So applying the fundamental lemma of variational calculus, each term (i) with $i=\{1,...,5\}$ is equal to zero. Then, the following Lagrangian model with Dirichlet and Neumann boundary conditions is obtained:

$$\forall\mathtt{X}\in\Omega:\quad \mathcal{M}\ddot{r}=-\mathcal{F}_{\mathtt{x}}(r)^{*}\,e_{\epsilon}+b+B_d\,u_d, \tag{II.96}$$
$$\epsilon=\epsilon(r), \tag{II.97}$$
$$e_{\epsilon}=\frac{\partial\Psi(\epsilon)}{\partial\epsilon}, \tag{II.98}$$
$$\forall\mathtt{S}\in\partial\Omega_N:\quad \tau_N=F_{\partial}(r)\,e_{\epsilon}, \tag{II.99}$$
$$\forall\mathtt{S}\in\partial\Omega_D:\quad r_D=r. \tag{II.100}$$

Noticing that the time derivative of (II.97) leads to $\dot{\epsilon}=\mathcal{F}_{\mathtt{x}}(r)\dot{r}=\mathcal{F}_{\mathtt{x}}(r)e_p$, the Lagrangian model with Hamiltonian in (II.94) can be written as the explicit PHS in (II.90). The power exchange with the environment is given by:

$$\dot{H}(x)=\int_{\Omega}\delta_x H^{\top}\dot{x}\,d\mathtt{X}=\int_{\Omega}e_p^{\top}B_d\,u_d\,d\mathtt{X}+\underbrace{\int_{\Omega}(e_{\epsilon}^{\top}\mathcal{F}_{\mathtt{x}}(r)e_p-e_p^{\top}\mathcal{F}_{\mathtt{x}}(r)^{*}e_{\epsilon})d\mathtt{X}}_{\text{Lemma II.2}},$$

so applying Lemma II.2 to the term indicated above we obtain:

$$\dot{H}(x)=\int_{\Omega}u_d^{\top}\underbrace{B_d^{\top}e_p}_{y_d}\,d\mathtt{X}+\int_{\partial\Omega}e_p^{\top}F_{\partial}(r)e_{\epsilon}\,d\mathtt{S}=\int_{\Omega}u_d^{\top}y_d\,d\mathtt{X}+\int_{\partial\Omega}u_{\partial}^{\top}y_{\partial}\,d\mathtt{S},$$

where u_{∂} and y_{∂} are the boundary inputs and outputs defined in (II.91). □

Note that the models in Theorem II.2 incorporate geometric nonlinearity through the differential operator $\mathcal{F}_{\mathtt{x}}(r)$, and the material nonlinearity is present only in the generalized stress $e_\epsilon(\mathtt{X},t)$. Additionally, notice that Theorem II.1 for the modeling of linear systems is a particular case of Theorem II.2.

Methodology 2. *In order to obtain an explicit PHS representation for a flexible mechanical system with density $\rho_0(\mathtt{X})$, whose kinematic assumptions lead to a displacement field $\boldsymbol{u}(\boldsymbol{X},t)$ as in Assumption II.1, and whose constitutive laws are defined by a hyperelastic model using a strain energy density function $W(\boldsymbol{\varepsilon})$ satisfying Assumption II.2, follow the steps below:*

1. *Calculate the mass density matrix $\mathcal{M}(\mathtt{X})$ and define the generalized momentum variables $p(\mathtt{X},t)$, the co-energy variables $e_p(\mathtt{X},t)$ and the kinetic energy $T(p)$. (Proposition II.1).*
2. *Compute the nonzero components of the Voigt-strain vector and define the generalized strain $\epsilon(\mathtt{X},t)$. Then, compute its time derivative to build the differential operator $\mathcal{F}_{\mathtt{x}}(r)$ and its formal adjoint $\mathcal{F}_{\mathtt{x}}(r)^*$. (Proposition II.6).*
3. *Compute the generalized strain energy density function $\Psi(\epsilon)$. Then, compute the co-energy variable $e_\epsilon(\mathtt{X},t)$ and the elastic potential energy $U(\epsilon)$. (Proposition II.6).*
4. *If desired, define the generalized distributed load $B_d\,u_d(\mathtt{X},t)$, and the generalized body force $b(\mathtt{X})$. (Proposition II.4).*
5. *Apply Theorem II.2 to obtain the explicit nonlinear PHS, along with the definitions of boundary inputs $u_\partial(\mathtt{S},t)$ and boundary outputs $y_\partial(\mathtt{S},t)$.*

II.3.3 Constrained nonlinear systems

In this section, we formulate models that incorporate algebraic constraints as specified in Assumption II.3. The strain measure employed is the Green-Lagrange strain tensor, and the material's constitutive law is assumed to be hyperelastic, based on the strain energy density function $W(\boldsymbol{\varepsilon})$ as described in Assumption II.2. The class of differential operators and the integration by parts lemma used here remain consistent with those in the previous nonlinear case.

The presentation of constrained nonlinear systems will be divided into two parts: The first approach enforces the constraint using Lagrange multipliers, resulting in infinite-dimensional nonlinear PH-DAEs, while the second approach internally resolves the constraint, leading to an equivalent explicit infinite-dimensional nonlinear PHS.

Constrained systems: Infinite-dimensional PH-DAE

Note that under Assumptions II.1 and II.2, the results of Propositions II.1, II.4 and II.6 regarding the kinetic energy, external work and elastic potential energy remain applicable. What remains pending is to deal with the constraints, which is presented in the following proposition.

Proposition II.7. *The time derivative of the generalized constraint* $\gamma(\epsilon) = 0$ *is equivalently written as:*

$$\dot{\gamma}(\epsilon) = \mathcal{L}_{\mathtt{x}}(\epsilon, r)\dot{r}(\mathtt{X}, t) = 0, \tag{II.101}$$

where $\mathcal{L}_{\mathtt{x}}(\epsilon, r)$ *is a non-constant and first-order differential operator of dimension* $(1 \times n)$ *of the same class as in Definition I.1. This operator is given by:*

$$\mathcal{L}_{\mathtt{x}}(\epsilon, r)(\cdot) = L_0(\epsilon, r)(\cdot) + \textstyle\sum_{k=1}^{\ell} L_k(\epsilon, r)\partial_k(\cdot), \tag{II.102}$$

whose associated matrices $L_0(\epsilon, r)$, $L_k(\epsilon, r) \in \mathbb{R}^{1\times n}$ *are defined as:*

$$L_0(\epsilon, r) = \frac{\partial \gamma(\epsilon)}{\partial \epsilon}^{\top} F_0(r), \qquad L_k(\epsilon, r) = \frac{\partial \gamma(\epsilon)}{\partial \epsilon}^{\top} F_k(r), \tag{II.103}$$

with $F_0(r)$, $F_k(r) \in \mathbb{R}^{m\times n}$ *the associated matrices of the differential operator* $\mathcal{F}_{\mathtt{x}}(r)$ *introduced in Proposition II.6.*

Proof. Applying the chain rule derivation we obtain:

$$\dot{\gamma}(\epsilon) = \frac{\partial \gamma(\epsilon)}{\partial \epsilon}^{\top} \dot{\epsilon}(\mathtt{X}, t) = \frac{\partial \gamma(\epsilon)}{\partial \epsilon}^{\top} \mathcal{F}_{\mathtt{x}}(r)\dot{r}(\mathtt{X}, t) = 0.$$

Since $\mathcal{F}_{\mathtt{x}}(r)$ is of the same class as in Definition I.1, it can be written with respect to its associated matrices $F_0(r)$, $F_k(r) \in \mathbb{R}^{m\times n}$. Then, the expression above is equivalent to:

$$\begin{aligned}\dot{\gamma}(\epsilon) &= \frac{\partial \gamma(\epsilon)}{\partial \epsilon}^{\top} \left[F_0(r)\dot{r}(\mathtt{X}, t) + \textstyle\sum_{k=1}^{\ell} F_k(r)\partial_k\dot{r}(\mathtt{X}, t)\right] \\ &= L_0(\epsilon, r)\dot{r}(\mathtt{X}, t) + \textstyle\sum_{k=1}^{\ell} L_k(\epsilon, r)\partial_k\dot{r}(\mathtt{X}, t) \\ &= \mathcal{L}_{\mathtt{x}}(\epsilon, r)\dot{r}(\mathtt{X}, t) = 0,\end{aligned}$$

which completes the proof.

□

Remark II.11. *Since* $\mathcal{L}_{\mathtt{x}}(\epsilon, r)$ *belongs to the same class of differential operators as defined in Definition I.1, its formal adjoint* $\mathcal{L}_{\mathtt{x}}(\epsilon, r)^*$ *can be derived in the same way. The integration by parts of Lemma II.2 also applies for these operators.*

Considering the above, the infinite-dimensional PH-DAE representation of the considered class of constrained nonlinear mechanical systems is presented in the next theorem.

Theorem II.3. *Let consider* $x(\mathtt{X}, t) = [p(\mathtt{X}, t)^{\top}\ \epsilon(\mathtt{X}, t)^{\top}\ r(\mathtt{X}, t)^{\top}\ \lambda(\mathtt{X}, t)]^{\top} \in \mathbb{R}^{2n+m+1}$ *as the energy variables, and* $\mathcal{Z}(\mathtt{X}, t) = [e_p(\mathtt{X}, t)^{\top}\ e_\epsilon(\mathtt{X}, t)^{\top} - b(\mathtt{X})^{\top}\ \lambda(\mathtt{X}, t)]^{\top} \in \mathbb{R}^{2n+m+1}$ *as the effort function. From Propositions II.1, II.4, II.6 and II.7, the*

dynamics of the constrained nonlinear systems can be written in an implicit PH-DAE form as:

$$\underbrace{\begin{bmatrix}1&0&0&0\\0&1&0&0\\0&0&1&0\\0&0&0&0\end{bmatrix}}_{\mathcal{E}}\underbrace{\begin{bmatrix}\dot{p}(\mathtt{X},t)\\\dot{\epsilon}(\mathtt{X},t)\\\dot{r}(\mathtt{X},t)\\\dot{\lambda}(\mathtt{X},t)\end{bmatrix}}_{\dot{x}}=\underbrace{\begin{bmatrix}0&-\mathcal{F}_{\mathtt{x}}(r)^*&-1&-\mathcal{L}_{\mathtt{x}}(\epsilon,r)^*\\\mathcal{F}_{\mathtt{x}}(r)&0&0&0\\1&0&0&0\\\mathcal{L}_{\mathtt{x}}(\epsilon,r)&0&0&0\end{bmatrix}}_{\mathcal{J}(x)=-\mathcal{J}(x)^*}\underbrace{\begin{bmatrix}e_p(\mathtt{X},t)\\e_\epsilon(\mathtt{X},t)\\-b(\mathtt{X})\\\lambda(\mathtt{X},t)\end{bmatrix}}_{\mathcal{Z}(\mathtt{X},t)}+\underbrace{\begin{bmatrix}B_d\\0\\0\\0\end{bmatrix}}_{\mathcal{G}}u_d(\mathtt{X},t)$$
$$y_d(\mathtt{X},t)=\mathcal{G}^*\mathcal{Z}(\mathtt{X},t)=B_d^\top e_p(\mathtt{X},t). \tag{II.104}$$

The boundary inputs and outputs $u_\partial(\mathtt{S},t)$, $y_\partial(\mathtt{S},t)\in\mathbb{R}^{2n}$ *are defined as:*

$$u_\partial(\mathtt{S},t)=\begin{bmatrix}\tau_N(\mathtt{S},t)^\top & v_D(\mathtt{S},t)^\top\end{bmatrix}^\top,\quad y_\partial(\mathtt{S},t)=\begin{bmatrix}v_N(\mathtt{S},t)^\top & \tau_D(\mathtt{S},t)^\top\end{bmatrix}^\top \tag{II.105}$$

where:

$$\begin{aligned}\tau_N(\mathtt{S},t)&=F_\partial(r)e_\epsilon(\mathtt{S},t)+L_\partial(\epsilon,r)\lambda(\mathtt{S},t),\quad v_N(\mathtt{S},t)=e_p(\mathtt{S},t)\quad(\textit{on }\partial\Omega_N),\\\tau_D(\mathtt{S},t)&=F_\partial(r)e_\epsilon(\mathtt{S},t)+L_\partial(\epsilon,r)\lambda(\mathtt{S},t),\quad v_D(\mathtt{S},t)=e_p(\mathtt{S},t)\quad(\textit{on }\partial\Omega_D),\end{aligned} \tag{II.106}$$

and the boundary matrices $F_\partial(r)\in\mathbb{R}^{n\times m}$ *and* $L_\partial(\epsilon,r)\in\mathbb{R}^{n\times 1}$ *are defined as:*

$$F_\partial(r)=\textstyle\sum_{k=1}^{\ell}F_k(r)^\top\hat{n}_k(\mathtt{S}),\quad L_\partial(\epsilon,r)=\sum_{k=1}^{\ell}L_k(\epsilon,r)^\top\hat{n}_k(\mathtt{S}), \tag{II.107}$$

with $\hat{n}_k(\mathtt{S})\in\mathbb{R}$ *the k-component of the normal unit vector pointing outward of the boundary* $\partial\Omega$*. The total energy function is given by the Hamiltonian:*

$$H(x)=\int_\Omega\left(\frac{1}{2}\,p(\mathtt{X},t)^\top\mathcal{M}(\mathtt{X})^{-1}p(\mathtt{X},t)+\Psi(\epsilon(\mathtt{X},t))-r(\mathtt{X},t)^\top b(\mathtt{X})\right)d\mathtt{X}, \tag{II.108}$$

the co-energy variables are given by $\delta_x H(x)=\mathcal{E}^\top\mathcal{Z}(\mathtt{X},t)$*, and the power exchange with the environment is given by:*

$$\dot{H}(x)=\int_\Omega u_d(\mathtt{X},t)^\top y_d(\mathtt{X},t)\,d\mathtt{X}+\int_{\partial\Omega}u_\partial(\mathtt{S},t)^\top y_\partial(\mathtt{S},t)\,d\mathtt{S}. \tag{II.109}$$

Proof. The proof consists in applying the generalized extended Hamilton's principle with constraints. To improve the readability of the proof, it is divided into five steps and the spatial and temporal dependencies are omitted. The first three steps are the same as in the proof of Theorem II.2.
Step 4: Consider the term:

$$\begin{aligned}\delta\int_{t_1}^{t_2}\mathcal{C}_\mathcal{E}\,dt&=\delta\int_{t_1}^{t_2}\int_{\mathcal{B}_0}\Lambda\cdot\Gamma(\boldsymbol{\varepsilon})\,d\mathbf{X}\,dt=\delta\int_{t_1}^{t_2}\int_\Omega\lambda\underbrace{\int_{\Omega^c}\Gamma(\boldsymbol{\varepsilon})\,d\mathtt{X}^c}_{\gamma(\epsilon)}d\mathtt{X}\,dt\\&=\int_{t_1}^{t_2}\int_\Omega\left(\delta\lambda\,\gamma(\epsilon)+\lambda\frac{\partial\gamma(\epsilon)}{\partial\epsilon}^\top\delta\epsilon\right)d\mathtt{X}\,dt\\&=\int_{t_1}^{t_2}\left[\int_\Omega\delta\lambda\,\gamma(\epsilon)\,d\mathtt{X}+\underbrace{\int_\Omega\lambda\,\mathcal{L}_{\mathtt{x}}(\epsilon,r)\delta r\,d\mathtt{X}}_{\text{Lemma II.2}}\right]dt.\end{aligned}$$

Applying Lemma II.2 to the term indicated above we obtain:

$$\int_\Omega \lambda\, \mathcal{L}_{\mathtt{x}}(\epsilon, r)\delta r\, d\mathtt{X} = \int_\Omega \delta r^\top \mathcal{L}_{\mathtt{x}}(\epsilon, r)^* \lambda\, d\mathtt{X} + \int_{\partial\Omega_N} \delta r^\top L_\partial(\epsilon, r)\lambda\, d\mathtt{S} + \underbrace{\int_{\partial\Omega_D} \delta r^\top L_\partial(\epsilon, r)\lambda\, d\mathtt{S}}_{=0 \text{ due to (II.38)}}.$$

Replacing the above into the last expression for $\delta\int_{t_1}^{t_2} \mathcal{C}_\mathcal{E}\, dt$ we obtain:

$$\delta\int_{t_1}^{t_2} \mathcal{C}_\mathcal{E}\, dt = \int_{t_1}^{t_2} \left[\int_\Omega \left(\delta\lambda\, \gamma(\epsilon) + \delta r^\top \mathcal{L}_{\mathtt{x}}(\epsilon, r)^* \lambda \right) d\mathtt{X} + \int_{\partial\Omega_N} \delta r^\top L_\partial(\epsilon, r)\, \lambda\, d\mathtt{S} \right] dt.$$

Step 5: Considering the above, the application of the generalized extended Hamilton's principle leads to:

$$\begin{aligned}
\int_{t_1}^{t_2} [\delta(\mathcal{T} - \mathcal{U}_\mathcal{E} + \mathcal{W}_\mathcal{E}) - \delta\mathcal{C}_\mathcal{E}]\, dt = \\
\int_{t_1}^{t_2} \Bigg\{ \int_\Omega \Bigg[\delta r^\top \underbrace{(-\mathcal{M}\ddot{r} - \mathcal{F}_{\mathtt{x}}(r)^* e_\epsilon + b - \mathcal{L}_{\mathtt{x}}(\epsilon, r)^*\lambda + B_d\, u_d)}_{(1)} \dots \\
\dots - \delta e_\epsilon^\top \underbrace{(\epsilon(r) - \epsilon)}_{(2)} + \delta\epsilon^\top \underbrace{\left(e_\epsilon - \frac{\partial\Psi(\epsilon)}{\partial\epsilon} \right)}_{(3)} - \delta\lambda \cdot \underbrace{\gamma(\epsilon)}_{(4)} \Bigg] d\mathtt{X} \Bigg\} dt \dots \\
\dots + \int_{t_1}^{t_2} \Bigg[\int_{\partial\Omega_N} \delta r^\top \underbrace{(\tau_N - F_\partial(r) e_\epsilon - L_\partial(\epsilon, r)\lambda)}_{(5)} d\mathtt{S} \dots \\
\dots + \int_{t_1}^{t_2} \Bigg[\int_{\partial\Omega_D} \delta\tau_D^\top \underbrace{(r - r_D)}_{(6)} d\mathtt{S} \Bigg] dt = 0.
\end{aligned}$$

So applying the fundamental lemma of variational calculus to each term in the above expression, all the terms (i) with $i = \{1, ..., 6\}$ are equal to zero. Then, the following constrained Lagrangian model with Dirichlet and Neumann boundary conditions is obtained:

$$\begin{aligned}
\forall \mathtt{X} \in \Omega: \quad & \mathcal{M}\ddot{r} = -\mathcal{F}_{\mathtt{x}}(r)^*\, e_\epsilon + b - \mathcal{L}_{\mathtt{x}}(\epsilon, r)^*\lambda + B_d\, u_d, && \text{(II.110)} \\
& \epsilon = \epsilon(r), && \text{(II.111)} \\
& e_\epsilon = \frac{\partial\Psi(\epsilon)}{\partial\epsilon}, && \text{(II.112)} \\
& \gamma(\epsilon) = 0, && \text{(II.113)} \\
\forall \mathtt{S} \in \partial\Omega_N: \quad & \tau_N = F_\partial(r) e_\epsilon + L_\partial(\epsilon, r)\lambda, && \text{(II.114)} \\
\forall \mathtt{S} \in \partial\Omega_D: \quad & r_D = r. && \text{(II.115)}
\end{aligned}$$

Noticing that the time derivative of (II.111) leads to $\dot{\epsilon} = \mathcal{F}_{\mathtt{x}}(r)\dot{r} = \mathcal{F}_{\mathtt{x}}(r) e_p$ and the time derivative of (II.113) leads to $\dot{\gamma}(\epsilon) = \mathcal{L}_{\mathtt{x}}(\epsilon, r) e_p = 0$, together with the Hamiltonian in (II.108), they define the dynamic equations of the implicit PH-DAE in (II.104). The power exchange with the environment is given by:

$$\begin{aligned}
\dot{H}(x) = \int_\Omega \delta_x H^\top \dot{x}\, d\mathtt{X} = \int_\Omega e_p^\top B_d\, u_d\, d\mathtt{X} + \underbrace{\int_\Omega (e_\epsilon^\top \mathcal{F}_{\mathtt{x}}(r) e_p - e_p^\top \mathcal{F}_{\mathtt{x}}(r)^* e_\epsilon) d\mathtt{X}}_{\text{Lemma II.2}} \dots \\
\dots + \underbrace{\int_\Omega (\lambda\, \mathcal{L}_{\mathtt{x}}(\epsilon, r) e_p - e_p^\top \mathcal{L}_{\mathtt{x}}(\epsilon, r)^* \lambda) d\mathtt{X}}_{\text{Lemma II.2}},
\end{aligned}$$

so applying Lemma II.2 to the two terms indicated above we obtain:

$$\dot{H}(x) = \int_\Omega u_d^\top \underbrace{B_d^\top e_p}_{y_d} \, d\mathtt{X} + \int_{\partial\Omega} e_p^\top [F_\partial(r) e_\epsilon + L_\partial(\epsilon, r)\lambda] \, d\mathtt{S} = \int_\Omega u_d^\top y_d \, d\mathtt{X} + \int_{\partial\Omega} u_\partial^\top y_\partial \, d\mathtt{S},$$

with u_∂ and y_∂ defined in (II.105).

□

Hereafter, we present a systematic methodology for deriving PH-DAE representations of flexible mechanical systems subject to constraints.

Methodology 3. *In order to obtain the implicit PH-DAE representation for a flexible mechanical system with density $\rho_0(\mathtt{X})$, whose kinematic assumptions lead to a displacement field $\boldsymbol{u}(\boldsymbol{X}, t)$ as specified in Assumption II.1, and the constitutive law is defined by a hyperelastic model using a strain energy density function $W(\boldsymbol{\varepsilon})$ satisfying Assumption II.2, along with an algebraic constraint $\Gamma(\boldsymbol{\varepsilon}) = 0$ under Assumption II.3, follow the steps below:*

1. *Calculate the mass density matrix $\mathcal{M}(\mathtt{X})$ and define the generalized momentum variables $p(\mathtt{X}, t)$, the co-energy variables $e_p(\mathtt{X}, t)$ and the kinetic energy $T(p)$. (Proposition II.1).*
2. *Compute the nonzero components of the Voigt-strain vector and define the generalized strain $\epsilon(\mathtt{X}, t)$. Then, compute its time derivative to build the differential operator $\mathcal{F}_\mathtt{x}(r)$ and its formal adjoint $\mathcal{F}_\mathtt{x}(r)^*$. (Proposition II.6).*
3. *Compute the generalized strain energy density function $\Psi(\epsilon)$. Then, compute the co-energy variable $e_\epsilon(\mathtt{X}, t)$ and the elastic potential energy $U(\epsilon)$. (Proposition II.6).*
4. *If desired, define the generalized distributed load $B_d\, u_d(\mathtt{X}, t)$, and the generalized body force $b(\mathtt{X})$. (Proposition II.4).*
5. *Compute the generalized constraint $\gamma(\epsilon) = 0$. Next, compute its time derivative to build the differential operator $\mathcal{L}_\mathtt{x}(\epsilon, r)$ and its formal adjoint $\mathcal{L}_\mathtt{x}(\epsilon, r)^*$. (Proposition II.7).*
6. *Apply Theorem II.3 to obtain the implicit PH-DAE, along with the definitions of boundary inputs $u_\partial(\mathtt{S}, t)$ and boundary outputs $y_\partial(\mathtt{S}, t)$.*

At this point, one might assume that the explicit PHS model without constraints from Theorem II.2 can be directly derived from the constrained model of Theorem II.3 by simply excluding the last row and column associated with the Lagrange multiplier, or conversely, incorporate the constraint by adding the terms related to the operator $\mathcal{L}_\mathtt{x}(\epsilon, r)$ to the explicit PHS. However, depending on the nature of the algebraic constraint, this approach is not always feasible, such as in the case of incompressible deformation where $J_\varepsilon = \det(\underline{\mathbf{F}}) = 1$ is enforced. In such cases, enforcing the constraint via Lagrange multiplier also requires modifying the strain energy density function $W(\boldsymbol{\varepsilon})$. Therefore, transitioning from one model to the other needs changing the energy function as well, making it not straightforward. Given the importance of incompressibility in the modeling of rubber and dielectric elastomer actuators (DEA), among other applications, more details on how to handle this constraint will be provided in the examples of Section II.4.1.

Constrained systems: Infinite-dimensional explicit PHS

In this section, we present the conditions under which an explicit PHS representation equivalent to the constrained system in Theorem II.3 can be obtained, along with the methodology for deriving such a model.

To achieve the equivalent explicit representation of the model in Theorem II.3, the flexible mechanical system must satisfy the following assumption in addition to Assumptions II.1 to II.3.

Assumption II.4. *From the generalized algebraic constraint $\gamma(\epsilon) = 0$, assume that it is possible to express one of the components of the generalized strain $\epsilon(\mathtt{X}, t) \in \mathbb{R}^m$ as a function of the others, that is:*

$$\epsilon_m(\mathtt{X}, t) = f(\bar{\epsilon}(\mathtt{X}, t)), \tag{II.116}$$

where $\epsilon(\mathtt{X}, t) = \left[\bar{\epsilon}(\mathtt{X}, t)^\top \;\; \epsilon_m(\mathtt{X}, t)\right]^\top \in \mathbb{R}^m$ with $\bar{\epsilon}(\mathtt{X}, t) = [\epsilon_1(\mathtt{X}, t) \;\; \dots \;\; \epsilon_{m-1}(\mathtt{X}, t)]^\top \in \mathbb{R}^{m-1}$ being the independent components, and $\epsilon_m(\mathtt{X}, t) \in \mathbb{R}$ the dependent one. Then, assume that the generalized strain energy density function depends explicitly on the dependent component $\epsilon_m(\mathtt{X}, t)$ such that it can be equivalently written as:

$$\bar{\Psi}(\bar{\epsilon}) = \Psi(\epsilon(\bar{\epsilon})), \tag{II.117}$$

where the notation $\epsilon(\bar{\epsilon}) = [\epsilon_1(\mathtt{X}, t) \;\; \dots \;\; \epsilon_{m-1}(\mathtt{X}, t) \;\; f(\bar{\epsilon}(\mathtt{X}, t))]^\top \in \mathbb{R}^m$ represents the generalized strain solely in terms of the independent components.

Given the previous assumption, we propose to adapt Proposition II.6 by considering only the independent components $\bar{\epsilon}(\mathtt{X}, t)$.

Proposition II.8. *The time derivative of the independent components $\dot{\bar{\epsilon}}(\mathtt{X}, t) \in \mathbb{R}^{m-1}$, the elastic potential energy $\bar{U}(\bar{\epsilon}) \in \mathbb{R}$, and the co-energy variable $e_{\bar{\epsilon}}(\mathtt{X}, t) \in \mathbb{R}^{m-1}$ are defined as:*

$$\dot{\bar{\epsilon}}(\mathtt{X}, t) = \bar{\mathcal{F}}_{\mathtt{x}}(r)\dot{r}(\mathtt{X}, t), \tag{II.118}$$

$$\bar{U}(\bar{\epsilon}) = \int_\Omega \bar{\Psi}(\bar{\epsilon})\, d\mathtt{X}, \tag{II.119}$$

$$e_{\bar{\epsilon}}(\mathtt{X}, t) = \frac{\partial \bar{\Psi}(\bar{\epsilon})}{\partial \bar{\epsilon}}, \tag{II.120}$$

with $\bar{\mathcal{F}}_{\mathtt{x}}(r)$ a differential operator of dimension $(m-1 \times n)$ of the same class as in Definition I.1 with associated matrices $\bar{F}_0(r)$, $\bar{F}_k(r) \in \mathbb{R}^{m-1 \times n}$. In addition, considering $e_\epsilon(\mathtt{X}, t)$ in (II.89) and its partition $e_\epsilon(\mathtt{X}, t) = [\bar{e}_\epsilon(\mathtt{X}, t)^\top \; e_{\epsilon_m}(\mathtt{X}, t)]^\top \in \mathbb{R}^m$ with $\bar{e}_\epsilon(\mathtt{X}, t) = [e_{\epsilon_1}(\mathtt{X}, t) \; \dots \; e_{\epsilon_{m-1}}(\mathtt{X}, t)]^\top \in \mathbb{R}^{m-1}$ and $e_{\epsilon_m}(\mathtt{X}, t) \in \mathbb{R}$, the relationship between $e_\epsilon(\mathtt{X}, t)$ and $e_{\bar{\epsilon}}(\mathtt{X}, t)$ is given by:

$$e_{\bar{\epsilon}}(\mathtt{X}, t) = \bar{e}_\epsilon(\mathtt{X}, t) + \frac{\partial f}{\partial \bar{\epsilon}}\, e_{\epsilon_m}(\mathtt{X}, t). \tag{II.121}$$

Proof. The proof of equations (II.118) to (II.120) is analogous to the proof of Proposition II.6. On the other hand, from the right part of (II.117) we have that:

$$e_{\bar{\epsilon}}(\mathtt{X},t) = \frac{\partial \Psi}{\partial \bar{\epsilon}} = \frac{\partial \epsilon}{\partial \bar{\epsilon}}^{\top} \frac{\partial \Psi}{\partial \epsilon} = \frac{\partial \epsilon}{\partial \bar{\epsilon}}^{\top} e_{\epsilon}(\mathtt{X},t), \tag{II.122}$$

with $\frac{\partial \epsilon}{\partial \bar{\epsilon}}^{\top} = \begin{bmatrix} I_{m-1} & \frac{\partial f}{\partial \bar{\epsilon}} \end{bmatrix}$ and $I_{m-1} \in \mathbb{R}^{m-1 \times m-1}$ the identity matrix. Replacing $\frac{\partial \epsilon}{\partial \bar{\epsilon}}^{\top}$ into (II.122) and considering the partition of $e_{\epsilon}(\mathtt{X},t)$ we obtain:

$$e_{\bar{\epsilon}}(\mathtt{X},t) = \begin{bmatrix} I_{m-1} & \frac{\partial f}{\partial \bar{\epsilon}} \end{bmatrix} \begin{bmatrix} \bar{e}_{\epsilon}(\mathtt{X},t) \\ e_{\epsilon_m}(\mathtt{X},t) \end{bmatrix} = \bar{e}_{\epsilon}(\mathtt{X},t) + \frac{\partial f}{\partial \bar{\epsilon}} e_{\epsilon_m}(\mathtt{X},t).$$

□

Theorem II.4. *Let consider* $x(\mathtt{X},t) = [p(\mathtt{X},t)^{\top}\ \bar{\epsilon}(\mathtt{X},t)^{\top}\ r(\mathtt{X},t)^{\top}]^{\top} \in \mathbb{R}^{2n+m-1}$ *as the energy variables,* $\delta_x H(x) = [e_p(\mathtt{X},t)^{\top}\ e_{\bar{\epsilon}}(\mathtt{X},t)^{\top} - b(\mathtt{X})^{\top}]^{\top} \in \mathbb{R}^{2n+m-1}$ *as the co-energy variables,* $\gamma(\epsilon) = 0$ *and* $\epsilon_m(\mathtt{X},t) = f(\bar{\epsilon}(\mathtt{X},t))$*. From Propositions II.1, II.4 and II.8, the implicit PH-DAE in Theorem II.3 is equivalent to the following explicit PHS defined as:*

$$\begin{aligned} \underbrace{\begin{bmatrix} \dot{p}(\mathtt{X},t) \\ \dot{\bar{\epsilon}}(\mathtt{X},t) \\ \dot{r}(\mathtt{X},t) \end{bmatrix}}_{\dot{x}} &= \underbrace{\begin{bmatrix} 0 & -\bar{\mathcal{F}}_{\mathtt{x}}(r)^* & -1 \\ \bar{\mathcal{F}}_{\mathtt{x}}(r) & 0 & 0 \\ 1 & 0 & 0 \end{bmatrix}}_{\mathcal{J}(x) = -\mathcal{J}(x)^*} \underbrace{\begin{bmatrix} e_p(\mathtt{X},t) \\ e_{\bar{\epsilon}}(\mathtt{X},t) \\ -b(\mathtt{X}) \end{bmatrix}}_{\delta_x H(x)} + \underbrace{\begin{bmatrix} B_d \\ 0 \\ 0 \end{bmatrix}}_{\mathcal{G}} u_d(\mathtt{X},t) \\ y_d(\mathtt{X},t) &= \mathcal{G}^* \delta_x H(x) = B_d^{\top} e_p(\mathtt{X},t), \end{aligned} \tag{II.123}$$

if and only if the condition:

$$0 = \left(\frac{\partial \gamma}{\partial \epsilon_i} + \frac{\partial f}{\partial \epsilon_i} \frac{\partial \gamma}{\partial \epsilon_m} \right)_{\epsilon_m = f(\bar{\epsilon})} \tag{II.124}$$

holds for all $i = \{1, ..., m-1\}$*. The boundary inputs and outputs* $u_{\partial}(\mathtt{S},t)$, $y_{\partial}(\mathtt{S},t) \in \mathbb{R}^{2n}$ *are defined as:*

$$u_{\partial}(\mathtt{S},t) = \begin{bmatrix} \tau_N(\mathtt{S},t)^{\top} & v_D(\mathtt{S},t)^{\top} \end{bmatrix}^{\top}, \quad y_{\partial}(\mathtt{S},t) = \begin{bmatrix} v_N(\mathtt{S},t)^{\top} & \tau_D(\mathtt{S},t)^{\top} \end{bmatrix}^{\top} \tag{II.125}$$

where:

$$\begin{aligned} \tau_N(\mathtt{S},t) &= \bar{F}_{\partial}(r) e_{\bar{\epsilon}}(\mathtt{S},t), \quad v_N(\mathtt{S},t) = e_p(\mathtt{S},t) \quad (on\ \partial\Omega_N), \\ \tau_D(\mathtt{S},t) &= \bar{F}_{\partial}(r) e_{\bar{\epsilon}}(\mathtt{S},t), \quad v_D(\mathtt{S},t) = e_p(\mathtt{S},t) \quad (on\ \partial\Omega_D), \end{aligned} \tag{II.126}$$

and the boundary matrix $\bar{F}_{\partial}(r) \in \mathbb{R}^{n \times m-1}$ *is defined as:*

$$\bar{F}_{\partial}(r) = \textstyle\sum_{k=1}^{\ell} \bar{F}_k(r)^{\top} \hat{n}_k(\mathtt{S}), \tag{II.127}$$

with $\hat{n}_k(\mathtt{S}) \in \mathbb{R}$ *the* k*-component of the normal unit vector pointing outward of the boundary* $\partial\Omega$*. The total energy function is given by the Hamiltonian:*

$$H(x) = \int_{\Omega} \left(\frac{1}{2} p(\mathtt{X},t)^{\top} \mathcal{M}(\mathtt{X})^{-1} p(\mathtt{X},t) + \bar{\Psi}(\bar{\epsilon}(\mathtt{X},t)) - r(\mathtt{X},t)^{\top} b(\mathtt{X}) \right) d\mathtt{X}, \tag{II.128}$$

and the power exchange with the environment is given by:

$$\dot{H}(x) = \int_{\Omega} u_d(\mathtt{X},t)^{\top} y_d(\mathtt{X},t)\, d\mathtt{X} + \int_{\partial\Omega} u_{\partial}(\mathtt{S},t)^{\top} y_{\partial}(\mathtt{S},t)\, d\mathtt{S}. \tag{II.129}$$

Proof. Considering Propositions II.1, II.4 and II.8, and applying the generalized Hamilton's principle yields to the presented explicit PHS. To establish their equivalence under condition (II.124), it suffices to demonstrate that the dynamic equation for $\dot{p}(\mathtt{X},t)$ in the implicit PH-DAE matches the dynamic equation for $\dot{p}(\mathtt{X},t)$ in the proposed explicit PHS. Thus, for the dynamic equation of $\dot{p}(\mathtt{X},t)$ in the implicit PH-DAE we have:

$$\dot{p}(\mathtt{X},t) = -\mathcal{F}_{\mathtt{x}}(r)^* e_\epsilon(\mathtt{X},t) + b(\mathtt{X}) - \mathcal{L}_{\mathtt{x}}(\epsilon,r)^*\lambda(\mathtt{X},t) + B_d\, u_d(\mathtt{X},t). \tag{II.130}$$

From the generalized constraint we obtain the following two expressions:

$$\begin{aligned}\dot{\gamma}(\epsilon) =& \frac{\partial\gamma}{\partial\epsilon}^\top \mathcal{F}_{\mathtt{x}}(r)\dot{r}(\mathtt{X},t) = \mathcal{L}_{\mathtt{x}}(\epsilon,r)\dot{r}(\mathtt{X},t) = 0,\\ \dot{\gamma}(\epsilon(\bar{\epsilon})) =& \frac{\partial\gamma}{\partial\epsilon}^\top \frac{\partial\epsilon}{\partial\bar{\epsilon}}\dot{\bar{\epsilon}}(\mathtt{X},t) = \frac{\partial\gamma}{\partial\epsilon}^\top \frac{\partial\epsilon}{\partial\bar{\epsilon}}\bar{\mathcal{F}}_{\mathtt{x}}(r)\dot{r}(\mathtt{X},t) = \bar{\mathcal{L}}_{\mathtt{x}}(\bar{\epsilon},r)\dot{r}(\mathtt{X},t) = 0,\end{aligned}$$

where by association we obtain the equivalences:

$$\mathcal{F}_{\mathtt{x}}(r) = \frac{\partial\epsilon}{\partial\bar{\epsilon}}\bar{\mathcal{F}}_{\mathtt{x}}(r) = \begin{bmatrix}\bar{\mathcal{F}}_{\mathtt{x}}(r)\\ \frac{\partial f}{\partial\bar{\epsilon}}^\top \bar{\mathcal{F}}_{\mathtt{x}}(r)\end{bmatrix}, \tag{II.131}$$

$$\mathcal{L}_{\mathtt{x}}(\epsilon,r) = \frac{\partial\gamma}{\partial\epsilon}^\top \frac{\partial\epsilon}{\partial\bar{\epsilon}}\bar{\mathcal{F}}_{\mathtt{x}}(r) = \bar{\mathcal{L}}_{\mathtt{x}}(\bar{\epsilon},r). \tag{II.132}$$

Then, considering the partition $\frac{\partial\gamma}{\partial\epsilon} = \begin{bmatrix}\frac{\partial\bar{\gamma}}{\partial\bar{\epsilon}}^\top & \frac{\partial\gamma}{\partial\epsilon_m}\end{bmatrix}^\top \in \mathbb{R}^m$, with $\frac{\partial\bar{\gamma}}{\partial\bar{\epsilon}} = \begin{bmatrix}\frac{\partial\gamma}{\partial\epsilon_1}\cdots\frac{\partial\gamma}{\partial\epsilon_{m-1}}\end{bmatrix}^\top \in \mathbb{R}^{m-1}$ and $\frac{\partial\gamma}{\partial\epsilon_m} \in \mathbb{R}$, we obtain:

$$\frac{\partial\gamma}{\partial\epsilon}^\top \frac{\partial\epsilon}{\partial\bar{\epsilon}} = \begin{bmatrix}\frac{\partial\bar{\gamma}}{\partial\bar{\epsilon}}^\top & \frac{\partial\gamma}{\partial\epsilon_m}\end{bmatrix}\begin{bmatrix}I_{m-1}\\ \frac{\partial f}{\partial\bar{\epsilon}}^\top\end{bmatrix} = \left(\frac{\partial\bar{\gamma}}{\partial\bar{\epsilon}}^\top + \frac{\partial\gamma}{\partial\epsilon_m}\frac{\partial f}{\partial\bar{\epsilon}}^\top\right). \tag{II.133}$$

Note that (II.133) is the expression of condition (II.124) in matrix form, therefore, if it is satisfied, then we have $\mathcal{L}_{\mathtt{x}}(\epsilon,r)^*\lambda = \bar{\mathcal{L}}_{\mathtt{x}}(\bar{\epsilon},r)^*\lambda = 0$. So, considering that the condition is satisfied, the partition $e_\epsilon(\mathtt{X},t) = [\bar{e}_\epsilon(\mathtt{X},t)^\top \; e_{\epsilon_m}(\mathtt{X},t)]^\top$, and replacing (II.131) into (II.130) we obtain:

$$\begin{aligned}\dot{p}(\mathtt{X},t) =& -\mathcal{F}_{\mathtt{x}}(r)^* e_\epsilon(\mathtt{X},t) + b(\mathtt{X}) - \mathcal{L}_{\mathtt{x}}(\epsilon,r)^*\lambda(\mathtt{X},t) + B_d\, u_d(\mathtt{X},t)\\ =& -\left[\bar{\mathcal{F}}_{\mathtt{x}}(r)^* \left(\frac{\partial f}{\partial\bar{\epsilon}}^\top \bar{\mathcal{F}}_{\mathtt{x}}(r)\right)^*\right]\begin{bmatrix}\bar{e}_\epsilon(\mathtt{X},t)\\ e_{\epsilon_m}(\mathtt{X},t)\end{bmatrix} + b(\mathtt{X}) + B_d\, u_d(\mathtt{X},t)\\ =& -\bar{\mathcal{F}}_{\mathtt{x}}(r)^*\bar{e}_\epsilon(\mathtt{X},t) - \bar{\mathcal{F}}_{\mathtt{x}}(r)^*\frac{\partial f}{\partial\bar{\epsilon}}\, e_{\epsilon_m}(\mathtt{X},t) + b(\mathtt{X}) + B_d\, u_d(\mathtt{X},t)\\ =& -\bar{\mathcal{F}}_{\mathtt{x}}(r)^*\left(\bar{e}_\epsilon(\mathtt{X},t) + \frac{\partial f}{\partial\bar{\epsilon}}\, e_{\epsilon_m}(\mathtt{X},t)\right) + b(\mathtt{X}) + B_d\, u_d(\mathtt{X},t)\\ =& -\bar{\mathcal{F}}_{\mathtt{x}}(r)^* e_{\bar{\epsilon}}(\mathtt{X},t) + b(\mathtt{X}) + B_d\, u_d(\mathtt{X},t),\end{aligned}$$

where the last line corresponds to the dynamic equation for $\dot{p}(\mathtt{X},t)$ of the explicit PHS in (II.123). □

One can notice that the algebraic constraint $\gamma(\epsilon) = 0$, expressed in terms of $\mathcal{L}_{\mathtt{x}}(\epsilon, r)$ within the interconnection operator of the implicit PH-DAE, is now encoded in the generalized strain energy density function $\bar{\Psi}(\bar{\epsilon})$ and the associated co-energy variables $e_{\bar{\epsilon}}(\mathtt{X}, t)$. This approach simplifies the system by reducing the number of variables and providing a clearer interpretation of dependencies, but it is limited to cases where the constraint, the dependent strain, and the generalized strain energy density function satisfy Assumption II.4 and condition (II.124). In contrast, the Lagrange multiplier method is more versatile, applicable to a broader range of constraints, and ensures that the constraint is always enforced, although it adds complexity by increasing the number of equations and variables in the system.

The methodology for deriving explicit PHS representations of constrained flexible mechanical systems is summarized next.

Methodology 4. *In order to obtain an infinite-dimensional explicit PHS representation of a flexible mechanical system with density $\rho_0(\mathtt{X})$, whose kinematic assumptions lead to a displacement field $\boldsymbol{u}(\boldsymbol{X}, t)$ as in Assumption II.1, whose constitutive law is defined by a strain energy density function $W(\boldsymbol{\varepsilon})$ that satisfies Assumption II.2, and the algebraic constraint $\Gamma(\boldsymbol{\varepsilon}) = 0$ satisfies Assumption II.3, follow the steps hereafter:*

1. *Compute the nonzero components of the Voigt-strain vector and define the generalized strain $\epsilon(\mathtt{X}, t) \in \mathbb{R}^m$. Next, compute the generalized strain energy density function $\Psi(\epsilon)$ and identify the specific components of $\epsilon(\mathtt{X}, t)$ on which it explicitly depends. Then, compute the generalized constraint $\gamma(\epsilon) = 0$ and use this expression to represent one of the components of $\epsilon(\mathtt{X}, t)$ that appears in $\Psi(\epsilon)$ as function of the others, that is, $\epsilon_m(\mathtt{X}, t) = f(\bar{\epsilon}(\mathtt{X}, t))$ (Assumption II.4). Finally, check that condition (II.124) is met for the chosen dependent strain.*
2. *Calculate the mass density matrix $\mathcal{M}(\mathtt{X})$ and define the generalized momentum variables $p(\mathtt{X}, t)$, the co-energy variables $e_p(\mathtt{X}, t)$ and the kinetic energy $T(p)$. (Proposition II.1).*
3. *For the independent components of the generalized strain $\bar{\epsilon}(\mathtt{X}, t) \in \mathbb{R}^{m-1}$, compute its time derivative to build the differential operator $\bar{\mathcal{F}}_{\mathtt{x}}(r)$ and its formal adjoint $\bar{\mathcal{F}}_{\mathtt{x}}(r)^*$. (Proposition II.8).*
4. *Compute the generalized strain energy density function $\bar{\Psi}(\bar{\epsilon})$ expressed solely in terms of the independent components. Then, compute the co-energy variable $e_{\bar{\epsilon}}(\mathtt{X}, t)$ and the elastic potential energy $\bar{U}(\bar{\epsilon})$. (Proposition II.8).*
5. *If desired, define the generalized distributed load $B_d\, u_d(\mathtt{X}, t)$, and the generalized body force $b(\mathtt{X})$. (Proposition II.4).*
6. *Apply Theorem II.4 to obtain the explicit PHS representation of the constrained system, along with the definitions of boundary inputs $u_\partial(\mathtt{S}, t)$ and boundary outputs $y_\partial(\mathtt{S}, t)$.*

II.4 Examples

In this section, we derive models in some practical cases to illustrate the proposed methodologies, demonstrating their practical implementation. The first part focuses on deriving various two-dimensional elasticity models, including linear, nonlinear, and constrained nonlinear systems, with the latter enforcing the incompressibility condition. The second part addresses the derivation of one-dimensional planar beam models, emphasizing the challenges encountered. Additionally, Appendix B provides several definitions of displacement fields which serve as the foundation for model derivation.

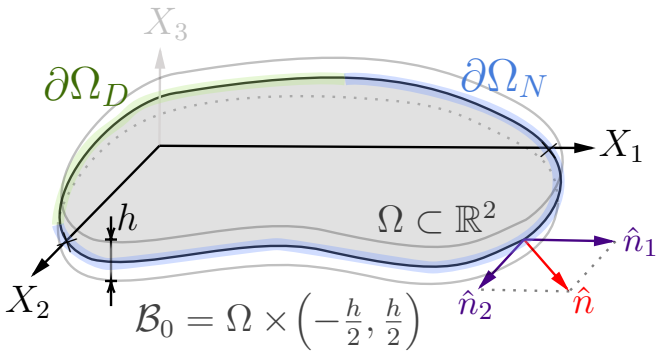

Figure II.5 – Scheme of the 2D domain

II.4.1 Models for two-dimensional general elasticity

In this subsection, we present models for two-dimensional general elasticity, as illustrated in Fig. II.5. We begin with the linear case to establish a foundational understanding of the system's behavior. Next, we explore the unconstrained nonlinear case, followed by the introduction of the incompressible deformation constraint, to derive in a first instance the PH-DAE model. Finally, we derive the equivalent explicit PHS model for the incompressible system, showing the transition between these representations.

Displacement field

Consider a three-dimensional body that can be treated as a two-dimensional one, as shown in Fig. II.5, where $h \in \mathbb{R}$ represents the constant thickness. The displacement field for the two-dimensional elasticity problem is given by:

$$\mathbf{u}(\mathbf{X}, t) = \underbrace{\begin{bmatrix} 1 & 0 \\ 0 & 1 \\ 0 & 0 \end{bmatrix}}_{\bar{M}_1} \underbrace{\begin{bmatrix} u_1(\mathtt{X}, t) \\ u_2(\mathtt{X}, t) \end{bmatrix}}_{r(\mathtt{X},t)}, \tag{II.134}$$

where $\mathtt{X} = \{X_1, X_2\}$, $\mathtt{X}^c = \{X_3\}$, $\Omega \subset \mathbb{R}^2$, $\Omega^c = \left(-\frac{h}{2}, \frac{h}{2}\right) \subset \mathbb{R}$, and $u_1(\mathtt{X}, t) \in \mathbb{R}$ and $u_2(\mathtt{X}, t) \in \mathbb{R}$ are the displacements in the direction of the X_1 and X_2 axes, respectively. Note that the matrix $\bar{M}_1$ does not depend on the coordinates $\mathtt{X}^c$.

Hyperelastic models

For the following examples, we use the Hookean and Neo-Hookean hyperelastic models. The Hookean model, derived from Hooke's law, assumes linear elastic behavior and small deformations, making it suitable for materials such as metals and ceramics under low strain conditions. These materials exhibit nearly linear stress-strain relationships for small deformations. In contrast, the Neo-Hookean model is a nonlinear formulation that accommodates large deformations and is typically used for soft, elastomeric materials, such as rubber and biological tissues, where the strain response is far from linear. The strain energy density functions for the Hookean and Neo-Hookean models are respectively given by:

Hookean model:

$$W(\underline{\boldsymbol{\varepsilon}}) = \frac{\lambda_L}{2}[\mathrm{tr}(\underline{\boldsymbol{\varepsilon}})]^2 + \mu_L \,\mathrm{tr}(\underline{\boldsymbol{\varepsilon}}) = \frac{1}{2}(\underline{\underline{\mathbf{C}_L}} : \underline{\boldsymbol{\varepsilon}}) : \underline{\boldsymbol{\varepsilon}} = \frac{1}{2}\,\boldsymbol{\varepsilon}^\top C_L \boldsymbol{\varepsilon}, \tag{II.135}$$

where $\underline{\boldsymbol{\varepsilon}}(\mathbf{X}, t) \in \mathbb{R}^{3\times 3}$ is the infinitesimal strain tensor. Considering Hooke's law under assumptions of plane strain or plane stress, the constitutive matrix $C_L = C_L^\top > 0 \in \mathbb{R}^{3\times 3}$ for an isotropic material is given by:

$$\underbrace{C_L = \begin{bmatrix} \lambda_L+2\mu_L & \lambda_L & 0 \\ \lambda_L & \lambda_L+2\mu_L & 0 \\ 0 & 0 & \mu_L \end{bmatrix}}_{\text{plane strain}}, \qquad \underbrace{C_L = \frac{E}{1-\nu^2}\begin{bmatrix} 1 & \nu & 0 \\ \nu & 1 & 0 \\ 0 & 0 & \frac{(1-\nu)}{2} \end{bmatrix}}_{\text{plane stress}},$$

where $\lambda_L, \mu_L \in \mathbb{R}_+$ are the Lamé constants of the material and are given by:

$$\lambda_L = \frac{E\nu}{(1+\nu)(1-2\nu)}, \quad \mu_L = \frac{E}{2(1+\nu)} = G,$$

with E Young's modulus, ν Poisson's ratio, and G the shear modulus.

Neo-Hookean model:

$$W(\underline{\mathbf{C}}) = \frac{\mu_L}{2}\left[I_C - 3 - \ln(III_C)\right] + \frac{\lambda_L}{2}\left(\sqrt{III_C} - 1\right)^2, \tag{II.136}$$

where $I_C = \mathrm{tr}(\underline{\mathbf{C}}) \in \mathbb{R}$ and $III_C = \det(\underline{\mathbf{C}}) \in \mathbb{R}$ are the first and third invariant of the right Green-Cauchy tensor $\underline{\mathbf{C}} \in \mathbb{R}^{3\times 3}$, respectively, which is given by $\underline{\mathbf{C}} = 2\underline{\mathbf{E}} + \underline{\mathbf{I}}$, with $\underline{\mathbf{E}} \in \mathbb{R}^{3\times 3}$ the Green-Lagrange strain tensor and $\underline{\mathbf{I}} \in \mathbb{R}^{3\times 3}$ the second order identity tensor (identity matrix).

II.4.1.a Linear model for 2D-elasticity

We introduce the linear PHS representation following the Methodology 1. The linear model employs the infinitesimal strain tensor to measure strain and uses the Hookean model as constitutive law. The spatial and temporal dependencies will be often omitted.

Step 1. From Proposition II.1, $\mathcal{M}(\mathtt{X}) \in \mathbb{R}^{2\times 2}$ is given by:

$$\mathcal{M} = \rho_0 \int_{\Omega^c} \bar{M}_1^\top \bar{M}_1 \, d\mathtt{X}^c = \begin{bmatrix} \rho_0 h & 0 \\ 0 & \rho_0 h \end{bmatrix}.$$

Then, the generalized momentum $p(\mathtt{X}, t) \in \mathbb{R}^2$, the kinetic energy $T(p) \in \mathbb{R}$ and the co-energy variables $e_p(\mathtt{X}, t) \in \mathbb{R}^2$ are completely defined.

Step 2. By definition (II.20), the components of the infinitesimal strain tensor are given by:

$$\varepsilon_{ij} = \frac{1}{2}\left(\frac{\partial u_i}{\partial X_j} + \frac{\partial u_j}{\partial X_i}\right) \quad \text{with } i, j = \{1, 2, 3\}.$$

The nonzero components $\boldsymbol{\varepsilon}(\mathtt{X}, t) \in \mathbb{R}^3$ of the Voigt-strain vector are given by:

$$\begin{aligned} \varepsilon_{11} &= \partial_1 u_1 = \epsilon_1(\mathtt{X}, t) \\ \varepsilon_{22} &= \partial_2 u_2 = \epsilon_3(\mathtt{X}, t) \\ 2\varepsilon_{12} &= \partial_2 u_1 + \partial_1 u_2 = \epsilon_3(\mathtt{X}, t) \end{aligned} \quad \rightarrow \quad \begin{bmatrix} \epsilon_1 \\ \epsilon_2 \\ \epsilon_3 \end{bmatrix} = \underbrace{\begin{bmatrix} \partial_1 & 0 \\ 0 & \partial_2 \\ \partial_2 & \partial_1 \end{bmatrix}}_{\mathcal{F}_{\mathtt{x}}} \begin{bmatrix} u_1 \\ u_2 \end{bmatrix}.$$

The associated matrices of the constant differential operator $\mathcal{F}_{\mathtt{x}}$ are given by:

$$F_0 = 0_{3\times 2}, \quad F_1 = \begin{bmatrix} 1 & 0 \\ 0 & 0 \\ 0 & 1 \end{bmatrix}, \quad F_2 = \begin{bmatrix} 0 & 0 \\ 0 & 1 \\ 1 & 0 \end{bmatrix}, \quad \rightarrow \quad F_\partial = \begin{bmatrix} \hat{n}_1 & 0 \\ 0 & \hat{n}_2 \\ \hat{n}_2 & \hat{n}_1 \end{bmatrix},$$

so, by Definition II.4 the formal adjoint of $\mathcal{F}_{\mathtt{x}}$ is given by:

$$\mathcal{F}_{\mathtt{x}}{}^* = -\begin{bmatrix} \partial_1 & 0 & \partial_2 \\ 0 & \partial_2 & \partial_1 \end{bmatrix}.$$

Step 3. $\boldsymbol{\varepsilon}(\mathbf{X}, t) = \bar{M}_2(\mathtt{X}^c)\epsilon(\mathtt{X}, t) \in \mathbb{R}^3$, where in our case the matrix $\bar{M}_2 = I_3$ with $I_3 \in \mathbb{R}^{3\times 3}$ the identity matrix. With the above, from (II.62) the stiffness density matrix $\mathcal{K}_\epsilon \in \mathbb{R}^{3\times 3}$ is given by $\mathcal{K}_\epsilon = hC_L$. Then, the elastic potential energy $U(\epsilon)$ and the co-energy variables $e_\epsilon(\mathtt{X}, t)$ are completely defined.

Step 4. The generalized distributed load $B_d\, u_d$ and the generalized body force are not included in this example.

Step 5. From Theorem II.1, the infinite-dimensional explicit linear PHS, the Hamiltonian and the boundary inputs and outputs are given by:

$$\underbrace{\begin{bmatrix}\dot{p}\\ \dot{\epsilon}\\ \dot{r}\end{bmatrix}}_{\dot{x}} = \underbrace{\begin{bmatrix}0 & -\mathcal{F}_{\mathtt{x}}{}^* & -1\\ \mathcal{F}_{\mathtt{x}} & 0 & 0\\ 1 & 0 & 0\end{bmatrix}}_{\mathcal{J}=-\mathcal{J}^*}\underbrace{\begin{bmatrix}e_p\\ e_\epsilon\\ 0\end{bmatrix}}_{\delta_x H},$$

$$H(x) = \int_\Omega \left(\frac{1}{2}\, p^\top \mathcal{M}^{-1} p + \frac{1}{2}\,\epsilon^\top \mathcal{K}_\epsilon \epsilon\right) d\mathtt{X},$$

$$u_\partial(\mathtt{S},t) = \begin{bmatrix}\tau_N(\mathtt{S},t)^\top & v_D(\mathtt{S},t)^\top\end{bmatrix}^\top, \quad y_\partial(\mathtt{S},t) = \begin{bmatrix}v_N(\mathtt{S},t)^\top & \tau_D(\mathtt{S},t)^\top\end{bmatrix}^\top,$$

where:

$$\begin{aligned}\tau_N(\mathtt{S},t) &= F_\partial\, e_\epsilon(\mathtt{S},t), \quad v_N(\mathtt{S},t) = e_p(\mathtt{S},t) \quad (\text{on } \partial\Omega_N),\\ \tau_D(\mathtt{S},t) &= F_\partial\, e_\epsilon(\mathtt{S},t), \quad v_D(\mathtt{S},t) = e_p(\mathtt{S},t) \quad (\text{on } \partial\Omega_D).\end{aligned}$$

II.4.1.b Nonlinear model for 2D-elasticity

Here we follow the Methodology 2 to systematically derive the model.

Step 1. Since $\mathbf{u}(\mathbf{X},t)$ does not change with respect to the previous case, the mass density matrix $\mathcal{M}(\mathtt{X})$, the generalized momentum $p(\mathtt{X},t)$, the kinetic energy $T(p)$ and the co-energy variables $e_p(\mathtt{X},t)$ are the same as in the previous case.

Step 2. By definition (II.8), the components of the Green-Lagrange strain tensor are given by:

$$\varepsilon_{ij} = \frac{1}{2}\left(\frac{\partial u_i}{\partial X_j} + \frac{\partial u_j}{\partial X_i} + \sum_{k=1}^{3}\frac{\partial u_k}{\partial X_i}\frac{\partial u_k}{\partial X_j}\right) \quad \text{with } i,j = \{1,2,3\}.$$

The nonzero components $\boldsymbol{\varepsilon}(\mathtt{X},t) \in \mathbb{R}^3$ of the Voigt-strain vector are given by:

$$\begin{aligned}\varepsilon_{11} &= \partial_1 u_1 + \frac{1}{2}(\partial_1 u_1)^2 + \frac{1}{2}(\partial_1 u_2)^2 = \epsilon_1(\mathtt{X},t),\\ \varepsilon_{22} &= \partial_2 u_2 + \frac{1}{2}(\partial_2 u_1)^2 + \frac{1}{2}(\partial_2 u_2)^2 = \epsilon_3(\mathtt{X},t),\\ 2\varepsilon_{12} &= \partial_2 u_1 + \partial_1 u_2 + (\partial_1 u_1\, \partial_2 u_1) + (\partial_1 u_2\, \partial_2 u_2) = \epsilon_3(\mathtt{X},t).\end{aligned}$$

Taking the time derivative of $\epsilon(\mathtt{X},t) \in \mathbb{R}^3$ we obtain:

$$\begin{bmatrix}\dot{\epsilon}_1\\ \dot{\epsilon}_2\\ \dot{\epsilon}_3\end{bmatrix} = \begin{bmatrix}\partial_1\dot{u}_1 + \partial_1 u_1\partial_1\dot{u}_1 + \partial_1 u_2\partial_1\dot{u}_2\\ \partial_2\dot{u}_2 + \partial_2 u_1\partial_2\dot{u}_1 + \partial_2 u_2\partial_2\dot{u}_2\\ \partial_2\dot{u}_1 + \partial_1\dot{u}_2 + (\partial_1\dot{u}_1\partial_2 u_1 + \partial_1 u_1\partial_2\dot{u}_1) + (\partial_1\dot{u}_2\partial_2 u_2 + \partial_1 u_2\partial_2\dot{u}_2)\end{bmatrix},$$

from where we get that:

$$\begin{bmatrix}\dot{\epsilon}_1\\ \dot{\epsilon}_2\\ \dot{\epsilon}_3\end{bmatrix} = \underbrace{\begin{bmatrix}\partial_1 + \partial_1 u_1\partial_1 & \partial_1 u_2\partial_1\\ \partial_2 u_1\partial_2 & \partial_2 + \partial_2 u_2\partial_2\\ \partial_2 + \partial_2 u_1\partial_1 + \partial_1 u_1\partial_2 & \partial_1 + \partial_2 u_2\partial_1 + \partial_1 u_2\partial_2\end{bmatrix}}_{\mathcal{F}_{\mathtt{x}}(r)}\begin{bmatrix}\dot{u}_1\\ \dot{u}_2\end{bmatrix}.$$

The associated matrices of the differential operator $\mathcal{F}_{\mathtt{x}}(r)$ are given by:

$$F_0 = 0_{3\times 2}, \quad F_1(r) = \begin{bmatrix} 1+\partial_1 u_1 & \partial_1 u_2 \\ 0 & 0 \\ \partial_2 u_1 & 1+\partial_2 u_2 \end{bmatrix}, \quad F_2(r) = \begin{bmatrix} 0 & 0 \\ \partial_2 u_1 & 1+\partial_2 u_2 \\ 1+\partial_1 u_1 & \partial_1 u_2 \end{bmatrix},$$

so, by Definition I.1 the formal adjoint of $\mathcal{F}_{\mathtt{x}}(r)$ is given by:

$$\mathcal{F}_{\mathtt{x}}(r)^* = -\begin{bmatrix} \partial_1 + \partial_1(\,\cdot\,\partial_1 u_1) & \partial_2(\,\cdot\,\partial_2 u_1) & \partial_2 + \partial_1(\,\cdot\,\partial_2 u_1) + \partial_2(\,\cdot\,\partial_1 u_1) \\ \partial_1(\,\cdot\,\partial_1 u_2) & \partial_2 + \partial_2(\,\cdot\,\partial_2 u_2) & \partial_1 + \partial_1(\,\cdot\,\partial_2 u_2) + \partial_2(\,\cdot\,\partial_1 u_2) \end{bmatrix}.$$

Step 3. Considering the nonzero components of the Green-Lagrange strain tensor $\underline{\mathbf{E}}$, the right Green-Cauchy tensor $\underline{\mathbf{C}}$ is given by:

$$\underline{\mathbf{C}} = 2\,\underline{\mathbf{E}} + \underline{\mathbf{I}} = \begin{bmatrix} 2\varepsilon_{11}+1 & 2\varepsilon_{12} & 0 \\ 2\varepsilon_{12} & 2\varepsilon_{22}+1 & 0 \\ 0 & 0 & 1 \end{bmatrix} = \begin{bmatrix} 2\epsilon_1+1 & \epsilon_3 & 0 \\ \epsilon_3 & 2\epsilon_2+1 & 0 \\ 0 & 0 & 1 \end{bmatrix} = \underline{\mathbf{C}}(\epsilon),$$

so the invariants expressed in terms of the generalized strains are:

$$\begin{aligned} I_C(\epsilon) &= \mathrm{tr}(\underline{\mathbf{C}}(\epsilon)) = 2\epsilon_1 + 2\epsilon_2 + 3, \\ III_C(\epsilon) &= \det(\underline{\mathbf{C}}(\epsilon)) = (2\epsilon_1+1)(2\epsilon_2+1) - \epsilon_3^2 = 4\epsilon_1\epsilon_2 + 2\epsilon_1 + 2\epsilon_2 + 1 - \epsilon_3^2. \end{aligned}$$

With the above, the generalized strain energy density function $\Psi(\epsilon)$ is given by:

$$\Psi(\epsilon) = hW(\underline{\mathbf{C}}(\epsilon)) = h\frac{\mu_L}{2}\left[I_C(\epsilon) - 3 - \ln(III_C(\epsilon))\right] + h\frac{\lambda_L}{2}\left(\sqrt{III_C(\epsilon)} - 1\right)^2.$$

Now, the co-energy variable $e_\epsilon(\mathtt{X}, t) \in \mathbb{R}^3$ is obtained by differentiation and we have:

$$e_\epsilon(\mathtt{X}, t) = \frac{\partial \Psi}{\partial \epsilon} = h\left[\frac{\mu_L}{2}\frac{\partial I_C}{\partial \epsilon} - \frac{\partial III_C}{\partial \epsilon}\left(\frac{\mu_L}{2III_C} - \frac{\lambda_L}{2} + \frac{\lambda_L}{2\sqrt{III_C}}\right)\right].$$

One can notice that since $\epsilon(\mathtt{X}, t)$ represents the real Voigt-strain vector of the Green-Lagrange strain tensor, then $e_\epsilon(\mathtt{X}, t)$ represents the real Voigt-stress vector of the second Piola-Kirchhoff stress. Also note that at $\epsilon(\mathtt{X}, t) = 0 \rightarrow e_\epsilon(\mathtt{X}, t) = 0$. This means that at zero strain, the stress is also zero, which is expected.

Step 4. The generalized distributed load $B_d\, u_d$ and the generalized body force are not included in this example.

Step 5. From Theorem II.2, the infinite-dimensional explicit nonlinear PHS, the Hamiltonian and the boundary inputs and outputs are given by:

$$\underbrace{\begin{bmatrix}\dot{p}\\ \dot{\epsilon}\\ \dot{r}\end{bmatrix}}_{\dot{x}} = \underbrace{\begin{bmatrix}0 & -\mathcal{F}_{\mathtt{x}}(r)^* & -1\\ \mathcal{F}_{\mathtt{x}}(r) & 0 & 0\\ 1 & 0 & 0\end{bmatrix}}_{\mathcal{J}(x)=-\mathcal{J}(x)^*} \underbrace{\begin{bmatrix}e_p\\ e_\epsilon\\ 0\end{bmatrix}}_{\delta_x H},$$

$$H(x) = \int_\Omega \left(\frac{1}{2}\, p^\top \mathcal{M}^{-1} p + \Psi(\epsilon)\right) d\mathtt{X},$$

$$u_\partial(\mathtt{S},t) = \begin{bmatrix}\tau_N(\mathtt{S},t)^\top & v_D(\mathtt{S},t)^\top\end{bmatrix}^\top, \quad y_\partial(\mathtt{S},t) = \begin{bmatrix}v_N(\mathtt{S},t)^\top & \tau_D(\mathtt{S},t)^\top\end{bmatrix}^\top,$$

where:

$$\tau_N(\mathtt{S},t) = F_\partial(r)\, e_\epsilon(\mathtt{S},t), \quad v_N(\mathtt{S},t) = e_p(\mathtt{S},t) \quad (\text{on } \partial\Omega_N),$$
$$\tau_D(\mathtt{S},t) = F_\partial(r)\, e_\epsilon(\mathtt{S},t), \quad v_D(\mathtt{S},t) = e_p(\mathtt{S},t) \quad (\text{on } \partial\Omega_D).$$

Remark II.12. *Note that if one wants to consider another hyperelastic model, the only thing to do is to apply Step 3 for the new strain energy density function $W(\boldsymbol{\varepsilon})$. Consequently, if the kinematic does not change (that is, $\boldsymbol{u}(\boldsymbol{X},t)$ and the strain measure do not change), Theorem II.2 ensures that the new PHS will have the same interconnection structure.*

II.4.1.c Implicit nonlinear model for incompressible 2D-elasticity

In this section, we impose the constraint of incompressible deformation using Lagrange multipliers, as outlined in Methodology 3. Incompressibility ensures that the volume remains constant during deformation, which is mathematically achieved by enforcing $J_\varepsilon = \sqrt{III_C} = 1$. To address this constraint, special consideration must be taken with the strain energy density function, which will be detailed below in Steps 3 and 5.

Step 1. Since $\mathbf{u}(\mathbf{X},t)$ does not change with respect to the previous case, the mass density matrix $\mathcal{M}(\mathtt{X})$, the generalized momentum $p(\mathtt{X},t)$, the kinetic energy $T(p)$ and the co-energy variables $e_p(\mathtt{X},t)$ are the same as in the previous case.

Step 2. The generalized strains $\epsilon(\mathtt{X},t)$, the differential operator $\mathcal{F}_{\mathtt{x}}(r)$ and its formal adjoint $\mathcal{F}_{\mathtt{x}}(r)^*$ are the same as in the previous case.

Step 3. Since it is desired to impose the incompressibility constraint via Lagrange multiplier, it is necessary to split the strain energy density function $W(\boldsymbol{\varepsilon})$ into two parts: $W_{iso}(\boldsymbol{\varepsilon})$ representing the isochoric part, and $W_{vol}(J_\varepsilon)$ representing the volumetric part. The isochoric part accounts for distortional or shape-changing deformation without any volume change, while the volumetric part accounts for compressional or dilational deformation involving volume change. In this formulation, the volumetric part $W_{vol}(J_\varepsilon) = \Gamma(\boldsymbol{\varepsilon}) = 0$ corresponds to the constraint to be

enforced via Lagrange multiplier and will be treated in Step 5. To facilitate the presentation of the isochoric part W_{iso}, the isochoric right Green-Cauchy tensor is introduced. The isochoric right Green-Cauchy tensor is defined as $\underline{\mathbf{C}}_{iso} = III_C^{-1/3}\underline{\mathbf{C}}$. This tensor normalizes $\underline{\mathbf{C}}$ by its determinant to isolate the distortional part of the deformation, ensuring that the determinant of $\underline{\mathbf{C}}_{iso}$ is always equal to one. Considering the above, the isochoric part of the strain energy density function of the Neo-Hookean model is defined as:

$$\begin{aligned} W_{iso} = W(\underline{\mathbf{C}}_{iso}) &= \frac{\mu_L}{2}\left(I_C^{iso} - 3 - \ln(III_C^{iso})\right) + \frac{\lambda_L}{2}\left(\sqrt{(III_C^{iso})} - 1\right)^2 \\ &= \frac{\mu_L}{2}(III_C^{-\frac{1}{3}} I_C - 3), \end{aligned}$$

where $I_C^{iso} = III_C^{-\frac{1}{3}} I_C$ and $III_C^{iso} = \det(\underline{\mathbf{C}}_{iso}) = 1$ are the first and third invariant of $\underline{\mathbf{C}}_{iso}$, respectively. With the above, the generalized isochoric strain energy density function $\Psi_{iso}(\epsilon)$ reads:

$$\Psi_{iso}(\epsilon) = hW_{iso} = h\frac{\mu_L}{2}\left(III_C(\epsilon)^{-\frac{1}{3}} I_C(\epsilon) - 3\right).$$

Now, the co-energy variable $e_\epsilon^{iso}(\mathtt{X}, t) \in \mathbb{R}^3$ is obtained by differentiation and we obtain:

$$e_\epsilon^{iso}(\mathtt{X}, t) = \frac{\partial \Psi_{iso}}{\partial \epsilon} = \frac{h\mu_L}{6}\left(3III_C^{-\frac{1}{3}}\frac{\partial I_C}{\partial \epsilon} - III_C^{-\frac{4}{3}}\frac{\partial III_C}{\partial \epsilon} I_C\right),$$

where again at $\epsilon(\mathtt{X}, t) = 0 \rightarrow e_\epsilon^{iso}(\mathtt{X}, t) = 0$.

Step 4. The generalized distributed load $B_d\, u_d$ and the generalized body force are not included in this example.

Step 5. Being consistent with the (compressible) Neo-Hookean model in (II.136), the natural choice for the volumetric part $W_{vol}(J_\varepsilon)$ is:

$$\begin{aligned} W_{vol}(J_\varepsilon) &= -\frac{\mu_L}{2}\ln(J_\varepsilon^2) + \frac{\lambda_L}{2}(J_\varepsilon - 1)^2 \\ &= -\frac{\mu_L}{2}\ln(III_C) + \frac{\lambda_L}{2}\left(\sqrt{III_C} - 1\right)^2. \end{aligned}$$

However, there are several ways to choose $W_{vol}(J_\varepsilon)$ such that it enforces the constraint $J_\varepsilon = 1$. Common choices found in the literature are exponential and polynomial functions, respectively given by:

$$\begin{aligned} W_{vol}(J_\varepsilon) &= [\exp(J_\varepsilon - 1) - 1]^2, \\ W_{vol}(J_\varepsilon) &= (J_\varepsilon^\alpha - 1)^\beta, \end{aligned}$$

with $\alpha, \beta \in \mathbb{N}_+$. For the purpose of illustrating the methodology, in this example $W_{vol}(J_\varepsilon)$ is chosen as polynomial with $\alpha = 2$ and $\beta = 1$. Then, the constraint $\Gamma(\boldsymbol{\varepsilon})$ is written as $\Gamma(\boldsymbol{\varepsilon}) = J_\varepsilon^2 - 1 = III_C - 1 = 0$, from which the generalized constraint $\gamma(\epsilon) = 0$ is calculated as:

$$\gamma(\epsilon) = h(III_C(\epsilon) - 1) = h(4\epsilon_1\epsilon_2 + 2\epsilon_1 + 2\epsilon_2 - \epsilon_3^2) = 0.$$

From the above expression we obtain $\frac{\partial \gamma}{\partial \epsilon} = h\begin{bmatrix}(4\epsilon_2+2) & (4\epsilon_1+2) & (-2\epsilon_3)\end{bmatrix}^\top$, so the differential operator $\mathcal{L}_{\mathtt{x}}(\epsilon, r)$ and its formal adjoint are given by:

$$\mathcal{L}_{\mathtt{x}}(\epsilon, r) = \frac{\partial \gamma}{\partial \epsilon}^\top \mathcal{F}_{\mathtt{x}}(r),$$
$$\mathcal{L}_{\mathtt{x}}(\epsilon, r)^* = \mathcal{F}_{\mathtt{x}}(r)^* \frac{\partial \gamma}{\partial \epsilon},$$

where the associated matrices of $\mathcal{L}_{\mathtt{x}}(\epsilon, r)$ are given by $L_0 = 0_{1\times 2}$ and $L_k(\epsilon, r) = \frac{\partial \gamma}{\partial \epsilon}^\top F_k(r) \in \mathbb{R}^{1\times 2}$, with $k = \{1, 2\}$.

Step 6. From Theorem II.3, the infinite-dimensional implicit nonlinear PH-DAE, the Hamiltonian and the boundary inputs and outputs are given by:

$$\underbrace{\begin{bmatrix}1&0&0&0\\0&1&0&0\\0&0&1&0\\0&0&0&0\end{bmatrix}}_{\mathcal{E}}\underbrace{\begin{bmatrix}\dot{p}\\\dot{\epsilon}\\\dot{r}\\\dot{\lambda}\end{bmatrix}}_{\dot{x}} = \underbrace{\begin{bmatrix}0 & -\mathcal{F}_{\mathtt{x}}(r)^* & -1 & -\mathcal{L}_{\mathtt{x}}(\epsilon, r)^*\\ \mathcal{F}_{\mathtt{x}}(r) & 0 & 0 & 0\\ 1 & 0 & 0 & 0\\ \mathcal{L}_{\mathtt{x}}(\epsilon, r) & 0 & 0 & 0\end{bmatrix}}_{\mathcal{J}(x) = -\mathcal{J}(x)^*}\underbrace{\begin{bmatrix}e_p\\e_\epsilon^{iso}\\0\\\lambda\end{bmatrix}}_{\mathcal{Z}(x)},$$

$$H(x) = \int_\Omega \left(\frac{1}{2} p^\top \mathcal{M}^{-1} p + \Psi_{iso}(\epsilon)\right) d\mathtt{X},$$

$$u_\partial(\mathtt{S}, t) = \begin{bmatrix}\tau_N(\mathtt{S}, t)^\top & v_D(\mathtt{S}, t)^\top\end{bmatrix}^\top, \quad y_\partial(\mathtt{S}, t) = \begin{bmatrix}v_N(\mathtt{S}, t)^\top & \tau_D(\mathtt{S}, t)^\top\end{bmatrix}^\top,$$

where:

$$\tau_N(\mathtt{S}, t) = F_\partial(r) e_\epsilon^{iso}(\mathtt{S}, t) + L_\partial(\epsilon, r)\lambda(\mathtt{S}, t), \quad v_N(\mathtt{S}, t) = e_p(\mathtt{S}, t) \quad (\text{on } \partial\Omega_N),$$
$$\tau_D(\mathtt{S}, t) = F_\partial(r) e_\epsilon^{iso}(\mathtt{S}, t) + L_\partial(\epsilon, r)\lambda(\mathtt{S}, t), \quad v_D(\mathtt{S}, t) = e_p(\mathtt{S}, t) \quad (\text{on } \partial\Omega_D).$$

II.4.1.d Explicit nonlinear model for incompressible 2D-elasticity

Lastly, by following the Methodology 4, we derive the explicit PHS representation of the implicit PH-DAE system described above.

Step 1. The generalized strain $\epsilon(\mathtt{X}, t) \in \mathbb{R}^3$ is the same as previously defined. On the other hand, note that by imposing the constraint $III_C = 1$, the generalized strain energy density function reduces to:

$$\bar{\Psi}(\epsilon) = h\frac{\mu_L}{2}(I_C(\epsilon) - 3) = h\mu_L(\epsilon_1 + \epsilon_2),$$

where $\bar{\Psi}(\epsilon)$ depends explicitly only on $\epsilon_1(\mathtt{X}, t)$ and $\epsilon_2(\mathtt{X}, t)$. Therefore, from the previously calculated generalized constraint $\gamma(\epsilon) = 0$, we choose $\epsilon_1(\mathtt{X}, t)$ as the dependent component, given by:

$$\epsilon_1(\mathtt{X}, t) = f(\epsilon_2, \epsilon_3) = \frac{\epsilon_3^2 - 2\epsilon_2}{2(2\epsilon_2 + 1)},$$

from where we get that:

$$\frac{\partial f}{\partial \epsilon_2} = -\frac{\epsilon_3^2+1}{(2\epsilon_2+1)^2}, \quad \frac{\partial f}{\partial \epsilon_3} = \frac{\epsilon_3}{(2\epsilon_2+1)}.$$

Next, we verify that the condition (II.124) is met. For the first independent component $\epsilon_2(\mathtt{X},t)$ we have:

$$\begin{aligned}\left(\frac{\partial \gamma}{\partial \epsilon_2} + \frac{\partial f}{\partial \epsilon_2}\frac{\partial \gamma}{\partial \epsilon_1}\right)_{\epsilon_1 = f(\epsilon_2,\epsilon_3)} &= (4\epsilon_1+2) - \frac{\epsilon_3^2+1}{(2\epsilon_2+1)^2}(2(2\epsilon_2+1)) \\ &= 4f(\epsilon_2,\epsilon_3) + 2 - \frac{2\epsilon_3^2+2}{(2\epsilon_2+1)} \\ &= 2\frac{\epsilon_3^2-2\epsilon_2}{(2\epsilon_2+1)} + 2\frac{(2\epsilon_2+1)}{(2\epsilon_2+1)} - \frac{2\epsilon_3^2+2}{(2\epsilon_2+1)} \\ &= 0.\end{aligned}$$

For the second independent component $\epsilon_3(\mathtt{X},t)$ we have:

$$\left(\frac{\partial \gamma}{\partial \epsilon_3} + \frac{\partial f}{\partial \epsilon_3}\frac{\partial \gamma}{\partial \epsilon_1}\right)_{\epsilon_1 = f(\epsilon_2,\epsilon_3)} = (-2\epsilon_3) + \frac{\epsilon_3}{(2\epsilon_2+1)}(2(2\epsilon_2+1)) = 0.$$

Thus, condition (II.124) is satisfied. (Note that the process is completely analogous if $\epsilon_2(\mathtt{X},t)$ is chosen as the dependent component).

Step 2. Due to the fact that the displacement field $\mathbf{u}(\mathbf{X},t)$ does not change with respect to the previous cases, the mass density matrix $\mathcal{M}(\mathtt{X})$, the generalized momentum $p(\mathtt{X},t)$, the kinetic energy $T(p)$ and the co-energy variables $e_p(\mathtt{X},t)$ are the same as in the previous cases.

Step 3. Since $\bar{\epsilon}(\mathtt{X},t) = [\epsilon_2(\mathtt{X},t)\ \epsilon_3(\mathtt{X},t)]^\top$, the differential operator $\bar{\mathcal{F}}_{\mathtt{x}}(r)$ is composed of the second and third rows of $\mathcal{F}_{\mathtt{x}}(r)$, and its formal adjoint $\bar{\mathcal{F}}_{\mathtt{x}}(r)^*$ is composed of the second and third columns of $\mathcal{F}_{\mathtt{x}}(r)^*$. That is:

$$\bar{\mathcal{F}}_{\mathtt{x}}(r) = \begin{bmatrix} \partial_2 u_1 \partial_2 & \partial_2 + \partial_2 u_2 \partial_2 \\ \partial_2 + \partial_2 u_1 \partial_1 + \partial_1 u_1 \partial_2 & \partial_1 + \partial_2 u_2 \partial_1 + \partial_1 u_2 \partial_2 \end{bmatrix},$$

$$\bar{\mathcal{F}}_{\mathtt{x}}(r)^* = \begin{bmatrix} \partial_2(\,\cdot\,\partial_2 u_1) & \partial_2 + \partial_1(\,\cdot\,\partial_2 u_1) + \partial_2(\,\cdot\,\partial_1 u_1) \\ \partial_2 + \partial_2(\,\cdot\,\partial_2 u_2) & \partial_1 + \partial_1(\,\cdot\,\partial_2 u_2) + \partial_2(\,\cdot\,\partial_1 u_2) \end{bmatrix}.$$

Step 4. The generalized strain energy density function $\bar{\Psi}(\bar{\epsilon})$ expressed solely in terms of the independent components is given by:

$$\bar{\Psi}(\bar{\epsilon}) = h\mu_L\left(\frac{\epsilon_3^2-2\epsilon_2}{2(2\epsilon_2+1)} + \epsilon_2\right) = h\frac{\mu_L}{2}\left(\frac{4\epsilon_2^2+\epsilon_3^2}{2\epsilon_2+1}\right).$$

Now, the co-energy variable $e_{\bar{\epsilon}}(\mathtt{X},t) \in \mathbb{R}^2$ is obtained by differentiation and is given by:

$$e_{\bar{\epsilon}}(\mathtt{X},t)=\begin{bmatrix}e_{\epsilon_2}(\mathtt{X},t)\\ e_{\epsilon_3}(\mathtt{X},t)\end{bmatrix}=\begin{bmatrix}\dfrac{\partial\bar{\Psi}}{\partial\epsilon_2}\\ \dfrac{\partial\bar{\Psi}}{\partial\epsilon_3}\end{bmatrix}=\begin{bmatrix}h\mu_L\dfrac{4\epsilon_2^2+4\epsilon_2-\epsilon_3^2}{(2\epsilon_2+1)^2}\\ h\mu_L\dfrac{\epsilon_3}{2\epsilon_2+1}\end{bmatrix},$$

where again at $\bar{\epsilon}(\mathtt{X},t)=0\rightarrow e_{\bar{\epsilon}}(\mathtt{X},t)=0$.

Step 5. The generalized distributed load $B_d\,u_d$ and the generalized body force are not included in this example.

Step 6. From Theorem II.4, the infinite-dimensional explicit nonlinear PHS representation of the constrained system, the Hamiltonian and the boundary inputs and outputs are given by:

$$\underbrace{\begin{bmatrix}\dot{p}\\ \dot{\bar{\epsilon}}\\ \dot{r}\end{bmatrix}}_{\dot{x}}=\underbrace{\begin{bmatrix}0 & -\bar{\mathcal{F}}_{\mathtt{x}}(r)^* & -1\\ \bar{\mathcal{F}}_{\mathtt{x}}(r) & 0 & 0\\ 1 & 0 & 0\end{bmatrix}}_{\mathcal{J}(x)=-\mathcal{J}(x)^*}\underbrace{\begin{bmatrix}e_p\\ e_{\bar{\epsilon}}\\ 0\end{bmatrix}}_{\delta_x H},$$

$$H(x)=\int_\Omega\left(\frac{1}{2}\,p^\top\mathcal{M}^{-1}p+\bar{\Psi}(\bar{\epsilon})\right)d\mathtt{X},$$

$$u_\partial(\mathtt{S},t)=\begin{bmatrix}\tau_N(\mathtt{S},t)^\top & v_D(\mathtt{S},t)^\top\end{bmatrix}^\top,\quad y_\partial(\mathtt{S},t)=\begin{bmatrix}v_N(\mathtt{S},t)^\top & \tau_D(\mathtt{S},t)^\top\end{bmatrix}^\top,$$

where:

$$\begin{aligned}\tau_N(\mathtt{S},t)&=\bar{F}_\partial(r)\,e_{\bar{\epsilon}}(\mathtt{S},t),\quad v_N(\mathtt{S},t)=e_p(\mathtt{S},t)\quad(\text{on }\partial\Omega_N),\\ \tau_D(\mathtt{S},t)&=\bar{F}_\partial(r)\,e_{\bar{\epsilon}}(\mathtt{S},t),\quad v_D(\mathtt{S},t)=e_p(\mathtt{S},t)\quad(\text{on }\partial\Omega_D).\end{aligned}$$

Remark II.13. *Notice that in Step 4, the co-energy variable $e_{\bar{\epsilon}}(\mathtt{X},t)$ is also obtainable from (II.121). That is:*

$$\begin{aligned}e_{\bar{\epsilon}}(\mathtt{X},t)&=\bar{e}_\epsilon(\mathtt{X},t)+\frac{\partial f}{\partial\bar{\epsilon}}e_{\epsilon_1}(\mathtt{X},t),\\ &=\bar{e}_\epsilon^{iso}(\mathtt{X},t)+\frac{\partial f}{\partial\bar{\epsilon}}e_{\epsilon_1}^{iso}(\mathtt{X},t),\end{aligned}$$

where in the first line above, $e_{\epsilon_1}(\mathtt{X},t)$ and $\bar{e}_\epsilon(\mathtt{X},t)=[e_{\epsilon_2}(\mathtt{X},t)\;\;e_{\epsilon_3}(\mathtt{X},t)]^\top$ are the co-energy variables of the unconstrained PHS derived in Section II.4.1.b, and in the second line, $e_{\epsilon_1}^{iso}(\mathtt{X},t)$ and $\bar{e}_\epsilon^{iso}(\mathtt{X},t)=[e_{\epsilon_2}^{iso}(\mathtt{X},t)\;\;e_{\epsilon_3}^{iso}(\mathtt{X},t)]^\top$ are the co-energy variables of the constrained PH-DAE derived in Section II.4.1.c.

II.4.2 Models for one-dimensional planar beams

In this subsection, we present models for one-dimensional planar beams, as illustrated in Fig. II.6. We begin with the linear case to establish a fundamental understanding of the system's behavior. Next, we explore the unconstrained geometrically nonlinear case, using von-Kármán strains and discuss issues related

to the choice of the hyperelastic model. We then introduce the incompressible deformation constraint to derive a PH-DAE system, addressing concerns related to the hyperelastic model and the constraint. Finally, we derive an explicit PHS for the incompressible system, which addresses these issues effectively.

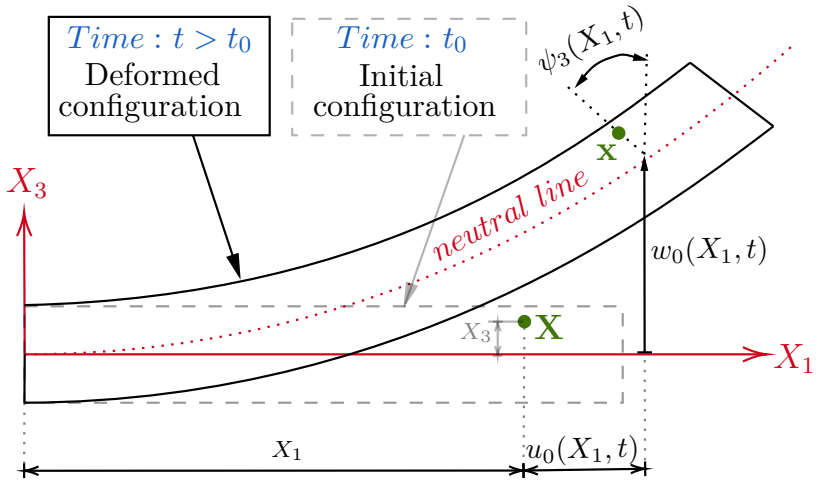

Figure II.6 – Scheme of the one-dimensional planar beam

Displacement field

Consider a three-dimensional body that can be treated as a one-dimensional one, as shown in Fig. II.6. The displacement field for the planar beam is given by:

$$\mathbf{u}(\mathbf{X},t) = \begin{bmatrix} u_1(\mathbf{X},t) \\ u_2(\mathbf{X},t) \\ u_3(\mathbf{X},t) \end{bmatrix} = \underbrace{\begin{bmatrix} 1 & -X_3 & 0 \\ 0 & 0 & 0 \\ 0 & 0 & 1 \end{bmatrix}}_{\bar{M}_1(\mathtt{X}^c)} \underbrace{\begin{bmatrix} u_0(\mathtt{X},t) \\ \psi_3(\mathtt{X},t) \\ w_0(\mathtt{X},t) \end{bmatrix}}_{r(\mathtt{X},t)}, \tag{II.137}$$

where $\mathtt{X} = \{X_1\}$, $\mathtt{X}^c = \{X_2, X_3\}$, $\Omega = (0, L_0) \subset \mathbb{R}$ with L_0 the initial length of the beam, $\Omega^c = A_0 \subset \mathbb{R}^2$ with A_0 the initial cross section area, $u_0(\mathtt{X},t) \in \mathbb{R}$, and $w_0(\mathtt{X},t) \in \mathbb{R}$ are the axial and vertical displacements of points belonging to the neutral line, respectively, and $\psi_3(\mathtt{X},t) \in \mathbb{R}$ is the angle of rotation of the cross section. Note that in this case the matrix $\bar{M}_1(\mathtt{X}^c)$ depends on the coordinates $\mathtt{X}^c$ and is not full rank.

Hyperelastic models

For the following examples, we use the Hookean and Neo-Hookean hyperelastic models. The Hookean model assumes linear elasticity for small deformations, suitable for materials like metals and ceramics. In contrast, the Neo-Hookean model handles large deformations and is used for elastomers and biological tissues. The

strain energy density functions for the Hookean and Neo-Hookean models are respectively given by:

Hookean model:

$$W(\underline{\boldsymbol{\varepsilon}}) = \frac{1}{2}\,\boldsymbol{\varepsilon}^\top C_L \boldsymbol{\varepsilon}, \tag{II.138}$$

where $C_L = C_L^\top > 0 \in \mathbb{R}^{2\times 2}$ for an isotropic material is given by:

$$C_L = \begin{bmatrix} E & 0 \\ 0 & \kappa\, G \end{bmatrix},$$

where $E \in \mathbb{R}_+$ is Young's modulus, $G = \frac{E}{2(1+\nu)} = \mu_L \in \mathbb{R}_+$ is the shear modulus, $\nu \in \mathbb{R}_+$ is Poisson's ratio, and κ is a correction factor.

Neo-Hookean model:

$$W(\underline{\mathbf{C}}) = \frac{\mu_L}{2}\left[I_C - 3 - \ln(III_C)\right] + \frac{\lambda_L}{2}\left(\sqrt{III_C} - 1\right)^2, \tag{II.139}$$

where $I_C = \mathrm{tr}(\underline{\mathbf{C}}) \in \mathbb{R}$ and $III_C = \det(\underline{\mathbf{C}}) \in \mathbb{R}$ are the first and third invariant of the right Green-Cauchy tensor $\underline{\mathbf{C}} \in \mathbb{R}^{3\times 3}$, respectively, which is given by $\underline{\mathbf{C}} = 2\,\underline{\mathbf{E}} + \underline{\mathbf{I}}$, with $\underline{\mathbf{E}} \in \mathbb{R}^{3\times 3}$ the Green-Lagrange strain tensor and $\underline{\mathbf{I}} \in \mathbb{R}^{3\times 3}$ the second order identity tensor (identity matrix).

II.4.2.a Linear model

We introduce the linear PHS representation following the Methodology 1. The linear model employs the infinitesimal strain tensor to measure strain and uses the Hookean model for the constitutive law. The spatial and temporal dependencies will be often omitted.

Step 1. From Proposition II.1 and assuming that the cross section is symmetric with respect to its centroidal coordinates, the mass density matrix $\mathcal{M}(\mathtt{X}) \in \mathbb{R}^{3\times 3}$ is given by:

$$\mathcal{M} = \rho_0 \int_{\Omega^c} \bar{M}_1(\mathtt{X}^c)^\top \bar{M}_1(\mathtt{X}^c)\, d\mathtt{X}^c = \rho_0 \int_{\Omega^c} \begin{bmatrix} 1 & -X_3 & 0 \\ -X_3 & X_3^2 & 0 \\ 0 & 0 & 1 \end{bmatrix} d\mathtt{X}^c = \rho_0 \begin{bmatrix} A_0 & 0 & 0 \\ 0 & \bar{I}_0 & 0 \\ 0 & 0 & A_0 \end{bmatrix},$$

where $\bar{I}_0$ is the second moment of inertia of the cross section. Then, the generalized momentum $p(\mathtt{X}, t) \in \mathbb{R}^3$, the kinetic energy $T(p) \in \mathbb{R}$ and the co-energy variables $e_p(\mathtt{X}, t) \in \mathbb{R}^3$ are completely defined.

Step 2. By definition (II.20), the components of the infinitesimal strain tensor are given by:

$$\varepsilon_{ij} = \frac{1}{2}\left(\frac{\partial u_i}{\partial X_j} + \frac{\partial u_j}{\partial X_i}\right) \quad \text{with } i, j = \{1, 2, 3\}.$$

The nonzero components $\boldsymbol{\varepsilon}(\mathtt{X},t) \in \mathbb{R}^2$ of the Voigt-strain vector are given by:

$$\begin{aligned} \varepsilon_{11} &= \partial_1 u_0 - X_3 \partial_1 \psi_3 = \epsilon_1(\mathtt{X},t) - X_3 \epsilon_2(\mathtt{X},t) \\ 2\varepsilon_{12} &= \partial_1 w_0 - \psi_3 = \epsilon_3(\mathtt{X},t) \end{aligned} \quad \rightarrow \quad \begin{bmatrix} \epsilon_1 \\ \epsilon_2 \\ \epsilon_3 \end{bmatrix} = \underbrace{\begin{bmatrix} \partial_1 & 0 & 0 \\ 0 & \partial_1 & 0 \\ 0 & -1 & \partial_1 \end{bmatrix}}_{\mathcal{F}_{\mathtt{x}}} \begin{bmatrix} u_0 \\ \psi_3 \\ w_0 \end{bmatrix}.$$

The formal adjoint operator ${\mathcal{F}_{\mathtt{x}}}^*$ and the boundary matrix F_∂ are completely defined from $\mathcal{F}_{\mathtt{x}}$.

Step 3. $\boldsymbol{\varepsilon}(\mathbf{X},t) = \bar{M}_2(\mathtt{X}^c)\epsilon(\mathtt{X},t) \in \mathbb{R}^2$, where in this case the matrix $\bar{M}_2(\mathtt{X}^c)$ is given by:

$$\underbrace{\begin{bmatrix} \varepsilon_{11} \\ 2\varepsilon_{12} \end{bmatrix}}_{\boldsymbol{\varepsilon}(\mathbf{X},t)} = \underbrace{\begin{bmatrix} 1 & -X_3 & 0 \\ 0 & 0 & 1 \end{bmatrix}}_{\bar{M}_2(\mathtt{X}^c)} \begin{bmatrix} \epsilon_1 \\ \epsilon_2 \\ \epsilon_3 \end{bmatrix}.$$

With the above and from (II.62), the stiffness density matrix $\mathcal{K}_\epsilon \in \mathbb{R}^{3\times 3}$ is given by:

$$\mathcal{K}_\epsilon = \int_{\Omega^c} \bar{M}_2^\top C_L \bar{M}_2 \, d\mathtt{X}^c = \int_{\Omega^c} \begin{bmatrix} E & -EX_3 & 0 \\ -EX_3 & EX_3^2 & 0 \\ 0 & 0 & \kappa G \end{bmatrix} d\mathtt{X}^c = \begin{bmatrix} EA_0 & 0 & 0 \\ 0 & E\bar{I}_0 & 0 \\ 0 & 0 & \kappa G A_0 \end{bmatrix}.$$

Then, the elastic potential energy $U(\epsilon)$ and the co-energy variables $e_\epsilon(\mathtt{X},t)$ are completely defined.

Step 4. The generalized distributed load $B_d\, u_d$ is not included in this example. The generalized body force b is considered as the weight of the beam (per unit length), acting in the negative direction of the X_3 axis. Then, the generalized body force is given by $b = [0 \;\; 0 \;\; -\rho_0\, g\, A_0]^\top$, with g the magnitude of the gravitational acceleration.

Step 5. From Theorem II.1, the infinite-dimensional explicit linear PHS, the Hamiltonian and the boundary inputs and outputs are given by:

$$\underbrace{\begin{bmatrix} \dot{p} \\ \dot{\epsilon} \\ \dot{r} \end{bmatrix}}_{\dot{x}} = \underbrace{\begin{bmatrix} 0 & -{\mathcal{F}_{\mathtt{x}}}^* & -1 \\ \mathcal{F}_{\mathtt{x}} & 0 & 0 \\ 1 & 0 & 0 \end{bmatrix}}_{\mathcal{J}=-\mathcal{J}^*} \underbrace{\begin{bmatrix} e_p \\ e_\epsilon \\ -b \end{bmatrix}}_{\delta_x H},$$

$$H(x) = \int_\Omega \left(\frac{1}{2}\, p^\top \mathcal{M}^{-1} p + \frac{1}{2}\, \epsilon^\top \mathcal{K}_\epsilon \epsilon - r^\top b \right) d\mathtt{X},$$

$$u_\partial(\mathtt{S},t) = \begin{bmatrix} \tau_N(\mathtt{S},t)^\top & v_D(\mathtt{S},t)^\top \end{bmatrix}^\top, \quad y_\partial(\mathtt{S},t) = \begin{bmatrix} v_N(\mathtt{S},t)^\top & \tau_D(\mathtt{S},t)^\top \end{bmatrix}^\top,$$

where:

$$\begin{aligned} \tau_N(\mathtt{S},t) &= F_\partial\, e_\epsilon(\mathtt{S},t), \quad v_N(\mathtt{S},t) = e_p(\mathtt{S},t) \quad (\text{on } \partial\Omega_N), \\ \tau_D(\mathtt{S},t) &= F_\partial\, e_\epsilon(\mathtt{S},t), \quad v_D(\mathtt{S},t) = e_p(\mathtt{S},t) \quad (\text{on } \partial\Omega_D). \end{aligned}$$

II.4.2.b Geometrically nonlinear model

Here we follow the Methodology 2 to systematically derive the model, and we use the von-Kármán strains to measure the deformation.

Step 1. Since $\mathbf{u}(\mathbf{X}, t)$ does not change with respect to the previous case, the mass density matrix $\mathcal{M}(\mathtt{X})$, the generalized momentum $p(\mathtt{X}, t)$, the kinetic energy $T(p)$ and the co-energy variables $e_p(\mathtt{X}, t)$ are the same as in the previous case.

Step 2. By definition (II.8), the components of the Green-Lagrange strain tensor are given by:

$$\varepsilon_{ij} = \frac{1}{2}\left(\frac{\partial u_i}{\partial X_j} + \frac{\partial u_j}{\partial X_i} + \sum_{k=1}^{3} \frac{\partial u_k}{\partial X_i}\frac{\partial u_k}{\partial X_j}\right) \quad \text{with } i, j = \{1, 2, 3\}.$$

The nonzero components $\boldsymbol{\varepsilon}(\mathtt{X}, t) \in \mathbb{R}^3$ of the Voigt-strain vector are given by:

$$\begin{aligned}
\varepsilon_{11} &= \partial_1 u_0 - X_3 \partial_1 \psi_3 + \frac{1}{2}(\partial_1 w_0)^2 + \frac{1}{2}(\partial_1 u_0 - X_3 \partial_1 \psi_3)^2 \\
2\varepsilon_{13} &= \partial_1 w_0 - \psi_3 + \psi_3(\partial_1 u_0 - X_3 \partial_1 \psi_3) \\
\varepsilon_{33} &= \frac{1}{2}(\psi_3)^2.
\end{aligned}$$

Using von-Kármán strains (neglecting nonlinear stretching terms) we obtain:

$$\begin{aligned}
\varepsilon_{11} &= \partial_1 u_0 + \frac{1}{2}(\partial_1 w_0)^2 - X_3 \partial_1 \psi_3 = \epsilon_1(\mathtt{X}, t) - X_3 \epsilon_2(\mathtt{X}, t) \\
2\varepsilon_{13} &= \partial_1 w_0 - \psi_3 = \epsilon_3(\mathtt{X}, t),
\end{aligned}$$

where the real strain ε_{33} was neglected. Taking the time derivative of $\epsilon(\mathtt{X}, t) \in \mathbb{R}^3$ we obtain:

$$\begin{bmatrix} \dot{\epsilon}_1 \\ \dot{\epsilon}_2 \\ \dot{\epsilon}_3 \end{bmatrix} = \underbrace{\begin{bmatrix} \partial_1 & 0 & \partial_1 w_0 \partial_1 \\ 0 & \partial_1 & 0 \\ 0 & -1 & \partial_1 \end{bmatrix}}_{\mathcal{F}_{\mathtt{x}}(r)} \begin{bmatrix} \dot{u}_0 \\ \dot{\psi}_3 \\ \dot{w}_0 \end{bmatrix}.$$

The formal adjoint operator $\mathcal{F}_{\mathtt{x}}(r)^*$ and the boundary matrix $F_\partial(r)$ are completely defined from $\mathcal{F}_{\mathtt{x}}(r)$.

Step 3. Since the model is only geometrically nonlinear and $\bar{M}_2(\mathtt{X}^c)$ is the same as in the previous case, the elastic potential energy is expressed with respect to the same stiffness density matrix $\mathcal{K}_\epsilon(\mathtt{X})$ as before.

Step 4. The generalized distributed load $B_d\, u_d$ is not considered in this example and the generalized body force is the same as in the previous case, that is, $b = [0 \;\; 0 \;\; -\rho_0\, g\, A_0]^\top$, with g the magnitude of the gravitational acceleration.

Step 5. From Theorem II.2, the infinite-dimensional geometrically nonlinear explicit PHS, the Hamiltonian and the boundary inputs and outputs are given by:

$$\underbrace{\begin{bmatrix}\dot{p}\\ \dot{\epsilon}\\ \dot{r}\end{bmatrix}}_{\dot{x}} = \underbrace{\begin{bmatrix}0 & -\mathcal{F}_{\mathtt{x}}(r)^* & -1\\ \mathcal{F}_{\mathtt{x}}(r) & 0 & 0\\ 1 & 0 & 0\end{bmatrix}}_{\mathcal{J}(x)=-\mathcal{J}(x)^*}\underbrace{\begin{bmatrix}e_p\\ e_\epsilon\\ -b\end{bmatrix}}_{\delta_x H},$$

$$H(x) = \int_\Omega \left(\frac{1}{2}\, p^\top \mathcal{M}^{-1} p + \frac{1}{2}\,\epsilon^\top \mathcal{K}_\epsilon \epsilon - r^\top b\right) d\mathtt{X},$$

$$u_\partial(\mathtt{S},t) = \begin{bmatrix}\tau_N(\mathtt{S},t)^\top & v_D(\mathtt{S},t)^\top\end{bmatrix}^\top, \quad y_\partial(\mathtt{S},t) = \begin{bmatrix}v_N(\mathtt{S},t)^\top & \tau_D(\mathtt{S},t)^\top\end{bmatrix}^\top,$$

where:

$$\begin{aligned}\tau_N(\mathtt{S},t) &= F_\partial(r)\, e_\epsilon(\mathtt{S},t), \quad v_N(\mathtt{S},t) = e_p(\mathtt{S},t) \quad (\text{on } \partial\Omega_N),\\ \tau_D(\mathtt{S},t) &= F_\partial(r)\, e_\epsilon(\mathtt{S},t), \quad v_D(\mathtt{S},t) = e_p(\mathtt{S},t) \quad (\text{on } \partial\Omega_D).\end{aligned}$$

Remark II.14. *Note that considering the neo-Hookean model is not straightforward since the terms $ln(III_C)$ and $\sqrt{III_C}$ are not integrable over Ω^c, leading to a failure of the integrability assumption (II.47). Possible solutions include approximating these terms with polynomials that are easier to integrate or considering incompressibility.*

II.4.2.c Implicit nonlinear model for incompressible planar beam

Incompressible deformation is typically applied in 2D and 3D models for general elasticity, as previously discussed in Sections II.4.1.c and II.4.1.d. In these models, generalized strains coincide with the real strains, meaning that the matrix $\bar{M}_2(\mathtt{X}^c)$ does not depend on the coordinates $\mathtt{X}^c$ and the strain energy density function can be integrated over Ω^c. This section addresses the challenges of imposing the incompressibility constraint in a 1D system where $\bar{M}_2(\mathtt{X}^c)$ does depend on $\mathtt{X}^c$. As examples, we will approach this by using Lagrange multipliers, as outlined in Methodology 3, with a focus on the neo-Hookean model and von-Kármán strains.

Step 1. Since $\mathbf{u}(\mathbf{X},t)$ does not change with respect to the previous case, the mass density matrix $\mathcal{M}(\mathtt{X})$, the generalized momentum $p(\mathtt{X},t)$, the kinetic energy $T(p)$ and the co-energy variables $e_p(\mathtt{X},t)$ are the same as in the previous case.

Step 2. The generalized strains $\epsilon(\mathtt{X},t)$, the differential operator $\mathcal{F}_{\mathtt{x}}(r)$ and its formal adjoint $\mathcal{F}_{\mathtt{x}}(r)^*$ are the same as in the previous case.

Step 3. Since it is desired to impose the incompressibility constraint via Lagrange multipliers, it is necessary to split the strain energy density function $W(\boldsymbol{\varepsilon})$ into two parts: $W_{iso}(\boldsymbol{\varepsilon})$ representing the isochoric part, and $W_{vol}(J_\varepsilon)$ representing the

volumetric part. The isochoric part of the strain energy density function of the neo-Hookean model is defined as:

$$W_{iso} = \frac{\mu_L}{2}(III_C^{-\frac{1}{3}} I_C - 3),$$

where $I_C = \mathrm{tr}(\underline{\mathbf{C}}) = 2\varepsilon_{11} + 3$ and $III_C = det(\underline{\mathbf{C}}) = 2\varepsilon_{11} + 1 - 4\varepsilon_{13}^2$. Note that W_{iso} is not integrable over Ω^c, then we approximate it by considering the initial terms of the Taylor series expansion around ε_{11}, resulting in:

$$W_{iso} \approx \frac{\mu_L}{2}\left(\frac{3}{(1-4\varepsilon_{13}^2)^{1/3}} - \frac{8\varepsilon_{11}\varepsilon_{13}^2}{(1-4\varepsilon_{13}^2)^{4/3}} + \frac{4\varepsilon_{11}^2(4\varepsilon_{13}^2+1)}{3(1-4\varepsilon_{13}^2)^{7/3}} - 3\right).$$

With the above, the generalized isochoric strain energy density function $\Psi_{iso}(\epsilon)$ is given by:

$$\Psi_{iso}(\epsilon) = \frac{A_0\mu_L}{2}\left(\frac{3}{(1-\epsilon_3^2)^{1/3}} - \frac{2\epsilon_3^2\epsilon_1}{(1-\epsilon_3^2)^{4/3}} + \frac{4\epsilon_1^2(\epsilon_3^2+1)}{3(1-\epsilon_3^2)^{7/3}} - 3\right) + \frac{2\bar{I}_0\mu_L}{3}\left(\frac{\epsilon_2^2(\epsilon_3^2+1)}{(1-\epsilon_3^2)^{7/3}}\right).$$

The co-energy variable $e_\epsilon^{iso}(\mathtt{X}, t) = \partial\Psi_{iso}/\partial\epsilon \in \mathbb{R}^3$ is obtained through differentiation, and it satisfies $e_\epsilon^{iso}(\mathtt{X}, t) = 0$ when $\epsilon(\mathtt{X}, t) = 0$.

Step 4. The generalized distributed load $B_d\, u_d$ is not considered in this example and the generalized body force is the same as in the previous case, that is, $b = [0 \;\; 0 \;\; -\rho_0\, g\, A_0]^\top$, with g the magnitude of the gravitational acceleration.

Step 5. In this example we model $W_{vol}(J_\epsilon)$ as:

$$W_{vol}(J_\varepsilon) = J_\varepsilon^2 - 1 = III_C - 1 = \Gamma(\boldsymbol{\varepsilon}) = 0,$$

from which it is calculated the generalized constraint $\gamma(\epsilon) = 0$ as:

$$\gamma(\epsilon) = A_0(III_C(\epsilon) - 1) = A_0(2\epsilon_1 - \epsilon_3^2) = 0.$$

From the above expression we obtain $\dfrac{\partial\gamma}{\partial\epsilon} = A_0\begin{bmatrix}2 & 0 & -2\epsilon_3\end{bmatrix}^\top$, so the differential operator $\mathcal{L}_{\mathtt{x}}(\epsilon, r)$ and its formal adjoint are given by:

$$\mathcal{L}_{\mathtt{x}}(\epsilon, r) = \frac{\partial\gamma}{\partial\epsilon}^\top \mathcal{F}_{\mathtt{x}}(r), \quad \mathcal{L}_{\mathtt{x}}(\epsilon, r)^* = \mathcal{F}_{\mathtt{x}}(r)^* \frac{\partial\gamma}{\partial\epsilon},$$

where the boundary matrix $L_\partial(\epsilon, r)$ is completely defined with $\mathcal{L}_{\mathtt{x}}(\epsilon, r)$ above.

Step 6. From Theorem II.3, the infinite-dimensional implicit nonlinear PH-DAE, the Hamiltonian and the boundary inputs and outputs are given by:

$$\underbrace{\begin{bmatrix}1&0&0&0\\0&1&0&0\\0&0&1&0\\0&0&0&0\end{bmatrix}}_{\mathcal{E}}\underbrace{\begin{bmatrix}\dot{p}\\\dot{\epsilon}\\\dot{r}\\\dot{\lambda}\end{bmatrix}}_{\dot{x}} = \underbrace{\begin{bmatrix}0 & -\mathcal{F}_{\mathtt{x}}(r)^* & -1 & -\mathcal{L}_{\mathtt{x}}(\epsilon,r)^*\\ \mathcal{F}_{\mathtt{x}}(r) & 0 & 0 & 0\\ 1 & 0 & 0 & 0\\ \mathcal{L}_{\mathtt{x}}(\epsilon,r) & 0 & 0 & 0\end{bmatrix}}_{\mathcal{J}(x)=-\mathcal{J}(x)^*}\underbrace{\begin{bmatrix}e_p\\ e_\epsilon^{iso}\\ -b\\ \lambda\end{bmatrix}}_{\mathcal{Z}(x)},$$

$$H(x) = \int_\Omega \left(\frac{1}{2}\, p^\top \mathcal{M}^{-1} p + \Psi_{iso}(\epsilon) - r^\top b\right) d\mathtt{X},$$

$$u_\partial(\mathtt{S}, t) = \begin{bmatrix}\tau_N(\mathtt{S}, t)^\top & v_D(\mathtt{S}, t)^\top\end{bmatrix}^\top, \quad y_\partial(\mathtt{S}, t) = \begin{bmatrix}v_N(\mathtt{S}, t)^\top & \tau_D(\mathtt{S}, t)^\top\end{bmatrix}^\top,$$

where:

$$\tau_N(\mathtt{S},t) = F_\partial(r)e_\epsilon^{iso}(\mathtt{S},t) + L_\partial(\epsilon,r)\lambda(\mathtt{S},t), \quad v_N(\mathtt{S},t) = e_p(\mathtt{S},t) \quad (\text{on } \partial\Omega_N),$$
$$\tau_D(\mathtt{S},t) = F_\partial(r)e_\epsilon^{iso}(\mathtt{S},t) + L_\partial(\epsilon,r)\lambda(\mathtt{S},t), \quad v_D(\mathtt{S},t) = e_p(\mathtt{S},t) \quad (\text{on } \partial\Omega_D).$$

Remark II.15. *Note that due to the simplifications, the constraint $\Gamma(\boldsymbol{\varepsilon}) = 0$ does not depend on ε_{33}, as this component is neglected. Consequently, the incompressibility constraint does not relate the strains ε_{11} and ε_{33}, which measure the deformation along the X_1 and X_3 axes, respectively. Therefore, imposing the constraint $\gamma(\epsilon) = 0$ is insufficient to ensure volume-preserving deformation. This will be verified in simulations later in Chapter III.*

II.4.2.d Explicit nonlinear model for incompressible planar beam

To address the issue in the previous PH-DAE model, where the constraint does not link the strains ε_{11} and ε_{33}, this section derives an explicit PHS for the incompressible planar beam (not equivalent to the previous PH-DAE) by incorporating the real strain ε_{33} as a generalized strain. Consequently, the incompressibility constraint will connect all nonzero strains, that is, ε_{11}, ε_{13} and ε_{33}. Lastly, following the Methodology 4, we choose ε_{33} as the dependent component to maintain the interconnection operator of the previously discussed models.

Step 1. Using von-Kármán strains (neglecting nonlinear stretching terms) and keeping ε_{33} we obtain:

$$\begin{aligned}
\varepsilon_{11} &= \partial_1 u_0 + \frac{1}{2}(\partial_1 w_0)^2 - X_3\partial_1\psi_3 = \epsilon_1(\mathtt{X},t) - X_3\epsilon_2(\mathtt{X},t)\\
2\varepsilon_{13} &= \partial_1 w_0 - \psi_3 = \epsilon_3(\mathtt{X},t),\\
\varepsilon_{33} &= \frac{1}{2}(\psi_3)^2 = \epsilon_4(\mathtt{X},t).
\end{aligned}$$

In comparison with the previous case, the generalized strain $\epsilon(\mathtt{X},t) \in \mathbb{R}^4$ incorporates the real strain $\varepsilon_{33}(\mathtt{X},t)$ as the generalized strain component $\epsilon_4(\mathtt{X},t)$. Imposing the constraint $III_C = 1$, the strain energy density function of the neo-Hookean model is given by:

$$W = \frac{\mu_L}{2}(I_C - 3) = \mu_L(\varepsilon_{11} + \varepsilon_{33}),$$

where ε_{11} and ε_{33} can be used as dependent strains. The incompressibility constraint $\Gamma(\boldsymbol{\varepsilon}) = III_C - 1 = 0$, leads to:

$$\Gamma(\boldsymbol{\varepsilon}) = (2\varepsilon_{11}+1)(2\varepsilon_{33}+1) - 4\varepsilon_{13}^2 - 1 = 0 \quad \rightarrow \quad \varepsilon_{33} = \frac{2\varepsilon_{13}^2 - \varepsilon_{11}}{2\varepsilon_{11}+1}.$$

Similar to the approach discussed in [Azarniya 2023], we approximate ε_{33} by considering the initial terms of the Taylor series expansion around $\varepsilon_{11} = 0$, resulting in:

$$\varepsilon_{33} \approx -\varepsilon_{11} + 2\varepsilon_{11}^2 + 2\varepsilon_{13}^2 - 4\varepsilon_{11}^3 - 4\varepsilon_{11}\varepsilon_{13}^2,$$

then, $\Gamma(\boldsymbol{\varepsilon}) \approx -\varepsilon_{11} + 2\varepsilon_{11}^2 + 2\varepsilon_{13}^2 - 4\varepsilon_{11}^3 - 4\varepsilon_{11}\varepsilon_{13}^2 - \varepsilon_{33} \approx 0$, which leads to:

$$\gamma(\epsilon) = A_0\Theta_0(\bar{\epsilon}) + \bar{I}_0\Theta_2(\bar{\epsilon}) - A_0\epsilon_4 = 0 \quad \rightarrow \quad \epsilon_4 = f(\bar{\epsilon}) = \Theta_0(\bar{\epsilon}) + \frac{\bar{I}_0}{A_0}\Theta_2(\bar{\epsilon}),$$

with $\bar{\epsilon} = [\epsilon_1 \ \epsilon_2 \ \epsilon_3]^\top$ the independent components, $\epsilon_m = \epsilon_4 = f(\bar{\epsilon})$ the dependent one, and:

$$\Theta_0(\bar{\epsilon}) = 2\epsilon_1^2 - \epsilon_1 + \tfrac{1}{2}\epsilon_3^2 - \epsilon_1^2\epsilon_3^2 - 4\epsilon_1^3, \quad \Theta_2(\bar{\epsilon}) = 2\epsilon_2^2 - \epsilon_2^2\epsilon_3^2 - 12\epsilon_1\epsilon_2^2.$$

Since the goal is not to find a model equivalent to the previous PH-DAE system, and $\gamma(\epsilon) = 0$ is different in this case, it is not relevant to verify condition (II.124).

Step 2. Due to the displacement field $\mathbf{u}(\mathbf{X}, t)$ does not change with respect to the previous cases, the mass density matrix $\mathcal{M}(\mathtt{X})$, the generalized momentum $p(\mathtt{X}, t)$, the kinetic energy $T(p)$ and the co-energy variables $e_p(\mathtt{X}, t)$ are the same as in the previous cases.

Step 3. Since $\bar{\epsilon}(\mathtt{X}, t) = [\epsilon_1(\mathtt{X}, t) \ \epsilon_2(\mathtt{X}, t) \ \epsilon_3(\mathtt{X}, t)]^\top$, we have $\bar{\mathcal{F}}_{\mathtt{x}}(r) = \mathcal{F}_{\mathtt{x}}(r)$, with $\mathcal{F}_{\mathtt{x}}(r)$ the differential operator of the previous PH-DAE system.

Step 4. The generalized strain energy density function $\bar{\Psi}(\bar{\epsilon})$ expressed solely in terms of the independent components is given by:

$$\bar{\Psi}(\bar{\epsilon}) = A_0\mu_L(\Theta_0(\bar{\epsilon}) + \epsilon_1) + \bar{I}_0\mu_L\Theta_2(\bar{\epsilon}).$$

The co-energy variable $e_{\bar{\epsilon}}(\mathtt{X}, t) = \partial\bar{\Psi}/\partial\bar{\epsilon} \in \mathbb{R}^3$ is obtained through differentiation, and it satisfies $e_{\bar{\epsilon}}(\mathtt{X}, t) = 0$ when $\bar{\epsilon}(\mathtt{X}, t) = 0$.

Step 5. The generalized distributed load $B_d\, u_d$ is not considered in this example and the generalized body force is the same as in the previous case, that is, $b = [0 \ \ 0 \ \ -\rho_0\, g\, A_0]^\top$, with g the magnitude of the gravitational acceleration.

Step 6. From Theorem II.4, the infinite-dimensional explicit nonlinear PHS representation of the constrained planar beam, the Hamiltonian and the boundary inputs and outputs are given by:

$$\underbrace{\begin{bmatrix} \dot{p} \\ \dot{\bar{\epsilon}} \\ \dot{r} \end{bmatrix}}_{\dot{x}} = \underbrace{\begin{bmatrix} 0 & -\bar{\mathcal{F}}_{\mathtt{x}}(r)^* & -1 \\ \bar{\mathcal{F}}_{\mathtt{x}}(r) & 0 & 0 \\ 1 & 0 & 0 \end{bmatrix}}_{\mathcal{J}(x) = -\mathcal{J}(x)^*} \underbrace{\begin{bmatrix} e_p \\ e_{\bar{\epsilon}} \\ -b \end{bmatrix}}_{\delta_x H},$$

$$H(x) = \int_\Omega \left(\frac{1}{2}\, p^\top \mathcal{M}^{-1} p + \bar{\Psi}(\bar{\epsilon}) - r^\top b \right) d\mathtt{X},$$

$$u_\partial(\mathtt{S}, t) = \begin{bmatrix} \tau_N(\mathtt{S}, t)^\top & v_D(\mathtt{S}, t)^\top \end{bmatrix}^\top, \quad y_\partial(\mathtt{S}, t) = \begin{bmatrix} v_N(\mathtt{S}, t)^\top & \tau_D(\mathtt{S}, t)^\top \end{bmatrix}^\top,$$

where:

$$\tau_N(\mathtt{S},t) = \bar{F}_\partial(r)\, e_{\bar{\epsilon}}(\mathtt{S},t), \quad v_N(\mathtt{S},t) = e_p(\mathtt{S},t) \quad (\text{on } \partial\Omega_N),$$
$$\tau_D(\mathtt{S},t) = \bar{F}_\partial(r)\, e_{\bar{\epsilon}}(\mathtt{S},t), \quad v_D(\mathtt{S},t) = e_p(\mathtt{S},t) \quad (\text{on } \partial\Omega_D).$$

Remark II.16. *Deriving a PH-DAE system using $\gamma(\epsilon) = 0$ from this model requires extending the differential operator $\mathcal{F}_{\mathtt{x}}(r)$ to include the contribution of $\epsilon_4(\mathtt{X},t)$. Making this adjustment and accordingly modifying the isochoric part of the strain energy density function, W_{iso} remains non-integrable over Ω^c. Approximating W_{iso} with a Taylor series expansion leads to $e_\epsilon^{iso}(\mathtt{X},t) \neq 0$ when $\epsilon(\mathtt{X},t) = 0$. Therefore, this model was discarded and its derivation is not presented.*

II.5 Conclusion

In this chapter, methodologies for modeling both linear and nonlinear PHS systems were proposed, including cases with constraints that admit a PH-DAE representation. As illustrated in the examples section, these methodologies prove effective for deriving PHS models, where the process is straightforward when the specified assumptions are satisfied. However, when these assumptions do not hold, the methodologies still offer flexibility by allowing for approximations while maintaining the ability to derive PHS models. While these approaches do not replace the specialized knowledge required to formulate each specific model, they provide a structured pathway that can be adapted and expanded upon for individual cases.

Chapter III
Structure-preserving spatial discretization

III.1 Introduction

In computational mechanics, classical numerical methods such as finite difference, finite volume, and finite element methods often do not adequately capture the fundamental properties of systems, such as energy and symmetry, particularly when applied to infinite-dimensional PHS [Seslija 2012]. To overcome these limitations, specialized structure-preserving discretization techniques are essential to ensure that the finite-dimensional models accurately reflect the characteristics of the original systems. Initial structure-preserving methods using finite differences were proposed in [Clemente-Gallardo 2002; Lopezlena 2004], but these approaches were limited to uniform meshes. The use of staggered-grid finite differences addressed this issue [Trenchant 2018], while finite volume methods based on the generalized leapfrog approach were developed for both one-dimensional and two-dimensional systems [Kotyczka 2016; Serhani 2018].

Standard finite element methods (sFEM) typically approximate the displacement field independently [Cook 2007; Reddy 2014]. By employing Hamilton's principle and Galerkin method, these methods preserve the Lagrangian structure [Reddy 2017], facilitating the representation as finite-dimensional PHS by means of a suitable change of variables. The partitioned FEM (pFEM) approach, introduced in [Cardoso-Ribeiro 2018], separates the discretization of interconnection structures and constitutive equations, making it suitable for parabolic and nonlinear systems while resulting in finite-dimensional PH-DAE systems. This approach has been successfully applied to the discretization and simulation of various plate models [Brugnoli 2019a; Brugnoli 2019b] and demonstrated that complex structures can be assembled from discretized components [Warsewa 2021], confirming the equivalence of discretization methods when consistent approximation bases are used [Brugnoli 2024]. Additionally, improvements such as exterior calculus FEM [Brugnoli 2022b] and mixed FEM (mFEM) [Golo 2004] have further enhanced discretization capabilities. mFEM effectively addresses the discretization of the interconnection structure and constitutive equations, showing success in both one-dimensional and two-dimensional problems [Hamroun 2010; Golo 2002; Wu 2015; Eberard 2007]. Pseudospectral methods have also been developed to achieve higher accuracy with lower-order approximations [Moulla 2012]. Furthermore, two-fields-based [1] mFEM approaches, aligned with the Hellinger-Reissner (H-R) variational principle, have facilitated weak imposition of boundary conditions, resulting in explicit finite-dimensional PHS representations [Thoma 2022b; Thoma 2022a]. Lastly, a three-fields-based mFEM method has been introduced to include material nonlinearities [Kinon 2023], based on the Hu-Washizu principle.

1. Two-fields-based means that the approach discretizes two fields independently. In [Thoma 2022b; Thoma 2022a], these fields are displacement and stress.

In this chapter, we focus on the structure-preserving mixed FEM discretization of the class of flexible mechanical systems discussed in Chapter II. The chapter is organized into several sections, each building on the development of structure-preserving mixed FEM discretization for flexible mechanical systems. It begins with a review of the essential background on FEM, followed by an overview of existing FEM approaches applied to infinite-dimensional PHS representations of linear mechanical systems. The first main contribution of this chapter is a structure-preserving mixed FEM strategy for linear mechanical systems, based on two fields and using the modified Linked Lagrange Multiplier (mLLM) method. The mLLM method expresses elastic potential energy through generalized displacements and strains, while also introducing independent variations of the stress field, acting as a Lagrange multiplier to weakly enforce Dirichlet boundary conditions. To ensure a symmetric formulation, an additional term is included, representing the weak imposition of the constitutive law, which connects the displacement and stress fields near the Dirichlet boundary in a least-squares sense. The mLLM method, akin to the H-R method, allows for the imposition of power-conjugated inputs. However, the condensation process [2] in the mLLM method results in an invertible stiffness matrix, a significant advantage over the H-R method, does not always guarantee an invertible matrix. This characteristic makes the mLLM method more advantageous for control applications, preserving the interconnection properties of the H-R approach while enhancing the stiffness matrix's attributes for control purposes. The second contribution involves the discretization of geometrically nonlinear and hyperelastic systems, introducing a three-field FEM scheme derived from a virtual power principle similar to the generalized Hamilton's principle (GHP). The third and final contribution presents a further extension of the mixed FEM scheme to handle algebraic constraints using a virtual power principle akin to the generalized extended Hamilton's principle, resulting in a four-field discretization. These contributions are motivated by the need to preserve the structure of the PHS or PH-DAE while effectively dealing with material nonlinearities and algebraic constraints, as well as weakly imposing both Dirichlet and Neumann boundary conditions. These methods represent an advancement over existing structure-preserving methods based on the H-R principle [Thoma 2022b; Thoma 2022a] and the Hu-Washizu principle [Kinon 2023]. These methods are then applied to various simulated examples, demonstrating the effectiveness of the proposed mixed FEM strategies for linear, nonlinear, and constrained nonlinear systems. The chapter concludes with a summary of the key results and a discussion of the broader implications of the developed methods.

2. Condensation refers to the process of eliminating the explicit dependency of the system on the strains by expressing them as functions of the displacements. This implies that the elastic potential energy is reformulated in terms of displacements, which, for linear systems, results in a quadratic function of the displacements and the stiffness matrix. Consequently, the state of the condensed model is characterized solely by momenta and displacements as state variables.

III.2 Preliminaries

Weighted residual methods are a family of numerical techniques used to approximate solutions of PDEs [Kwon 2018, Chapter 2]. These methods transform a continuous problem into a discrete one by applying a weighted integral approach to ensure that the approximate solution satisfies the PDE in an integral sense. In order to present the main idea, consider a general PDE of the form: $\frac{\partial^2 u}{\partial t^2} + \mathcal{D}(u) - f = 0$, where $\mathcal{D}$ is a differential operator, $u(\mathtt{X}, t)$ is the unknown solution, and $f(\mathtt{X}, t)$ is a known function. The residual $R(\tilde{u})$ is defined as the PDE evaluated in the approximate solution $\tilde{u}(\mathtt{X}, t) = \sum_{j=1}^{N} N_{u_j}(\mathtt{X})\hat{u}_j(t)$, where $N_{u_j}(\mathtt{X})$ are the shape functions, $\hat{u}_j(t)$ are the unknown coefficients, which, in specific cases, represent the local approximate solution at specific points within the domain of interest Ω, and N is the number of independent functions used for the approximation. In weighted residual methods, the goal is to ensure that this residual, when integrated over the domain Ω and weighted by arbitrary test functions $w_j(\mathtt{X})$, satisfies:

$$\int_{\Omega} w_j \, R(\tilde{u}) \, d\mathtt{X} = 0, \quad \text{for } j = \{1, ..., N\}. \tag{III.1}$$

Various types of weighted residual methods use different approaches for choosing the test functions $w_j(\mathtt{X})$. Two of the most used approaches are the Galerkin method, which employs $w_j(\mathtt{X}) = N_{u_j}(\mathtt{X})$, and the subdomains method, which uses test functions $w_j(\mathtt{X})$ defined over smaller regions $\Omega_j \subset \Omega$ (the subdomains), that is, $w_j(\mathtt{X}) = \begin{cases} 1; \text{ for all } \mathtt{X} \in \Omega_j \\ 0; \text{ othercase} \end{cases}$.

Remark III.1. *Note that (III.1) shares the structure with the final step when applying variational principles. For instance, in Hamilton's principle, $w_j = \delta u$ represents the arbitrary test function (similar to the Galerkin approach), and due to the fundamental lemma of variational calculus $R(\tilde{u}) = 0$, which implies $\tilde{u}(\mathtt{X}, t) = u(\mathtt{X}, t)$ and defines the PDE. This is the key feature of using variational principles to find approximate solutions to PDEs. The FEM is a specific weighted residual method that combines the subdomains method with the Galerkin approach, and the residual is defined in the weak form of the PDE, achieved by applying integration by parts.*

III.2.1 The finite element method

This section aims to present the key concepts used in FEM, including the mesh and local finite elements, the local shape functions used to approximate the solution within each element, and the location matrices (also called assembly matrices) required to formulate the final system of equations over the entire domain. The discussion is illustrated with 1D and 2D domains. For more details, the reader is referred to [Larson 2010; Kwon 2018].

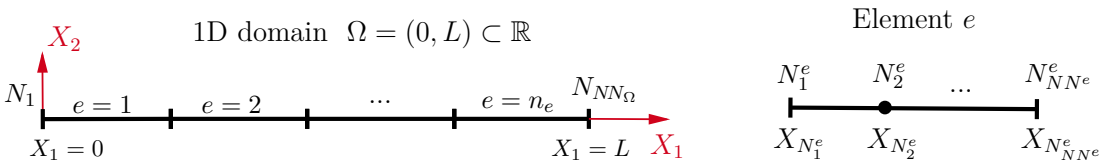

(a) 1D domain (b) 1D finite element

Figure III.1 – 1D mesh and finite elements.

One-dimensional domain

Mesh: Consider the 1D domain $\Omega = (0, L) \subset \mathbb{R}$ along the coordinate axis X_1 as illustrated in Fig. III.1, and its partition in n_e finite elements. In addition, consider that each element is composed of NN^e nodes and the entire domain contains NN_Ω nodes. The mesh is the set of all finite elements, all the nodes on Ω, and the connectivity topology of them.

Shape functions: Consider the one-dimensional unknown field $u(X_1, t) \in \mathbb{R}^n$ and its local approximate solution $\tilde{u}^e(X_1, t) = N_u^e(X_1)\,\hat{u}^e(t) \in \mathbb{R}^n$, where $N_u^e(X_1) \in \mathbb{R}^{n \times nNN^e}$ is the shape function and $\hat{u}^e(t) \in \mathbb{R}^{nNN^e}$ is the vector of local approximations of $u(X_1, t)$ evaluated at the nodes within the finite element. One of the most common choices of shape functions are the Canonical ones. The process to build these shape functions is illustrated below. Consider the 1D finite element in Fig. III.1b. The approximate local solution of the component $\tilde{u}_i^e(X_1, t) \in \mathbb{R}$ with $i = \{1, ..., n\}$, is assumed to be a polynomial of order $or = (NN^e - 1)$ of the form:

$$\tilde{u}_i^e(X_1, t) = \begin{bmatrix} 1 & X_1 & \cdots & X_1^{or} \end{bmatrix} \begin{bmatrix} (\alpha_0)_i^e(t) \\ \vdots \\ (\alpha_{or})_i^e(t) \end{bmatrix} = P(X_1)\alpha_i^e(t), \tag{III.2}$$

where $P(X_1) \in \mathbb{R}^{1 \times NN^e}$ is the canonical polynomial basis and $\alpha_i^e(t) \in \mathbb{R}^{NN^e}$ are unknown coefficients. Then, evaluating $P(X_1)$ at the coordinates of each node within the finite element we obtain the relation:

$$\underbrace{\begin{bmatrix} (\hat{u}_i^e)_1(t) \\ \vdots \\ (\hat{u}_i^e)_{NN^e}(t) \end{bmatrix}}_{\hat{u}_i^e(t)} = \underbrace{\begin{bmatrix} P(X_{N_1^e}) \\ \vdots \\ P(X_{N_{NN^e}^e}) \end{bmatrix}}_{C^e} \underbrace{\begin{bmatrix} (\alpha_0)_i^e(t) \\ \vdots \\ (\alpha_{or})_i^e(t) \end{bmatrix}}_{\alpha_i^e(t)}, \tag{III.3}$$

where $C^e \in \mathbb{R}^{NN^e \times NN^e}$ is an invertible matrix and $\hat{u}_i^e(t)$ are the local approximations of $u_i(X_1, t)$ at the nodes within the finite element. With the above we get:

$$\tilde{u}_i^e(X_1, t) = \underbrace{P(X_1)(C^e)^{-1}}_{N^e(X_1)}\,\hat{u}_i^e(t), \tag{III.4}$$

with $N^e(X_1) \in \mathbb{R}^{1\times NN^e}$ the local shape function of one component of $\tilde{u}(X_1,t)$. Repeating the process for each component $i = \{1,...,n\}$ we obtain:

$$\underbrace{\begin{bmatrix}\tilde{u}_1^e(X_1,t)\\ \vdots \\ \tilde{u}_n^e(X_1,t)\end{bmatrix}}_{\tilde{u}^e(X_1,t)} = \underbrace{\begin{bmatrix}N^e(X_1) & & 0\\ & \ddots & \\ 0 & & N^e(X_1)\end{bmatrix}}_{N_u^e(X_1)} \underbrace{\begin{bmatrix}\hat{u}_1^e(t)\\ \vdots \\ \hat{u}_n^e(t)\end{bmatrix}}_{\hat{u}^e(t)}. \tag{III.5}$$

Location matrices: Location matrices $L_u^e \in \mathbb{R}^{nNN^e\times N_\Omega}$ with $N_\Omega = nNN_\Omega$ the total number of unknowns, are mappings between the local sorting of unknowns $\hat{u}^e(t) \in \mathbb{R}^{nNN^e}$ in each element and the global sorting of unknowns $\hat{u}(t) \in \mathbb{R}^{N_\Omega}$ over the entire domain Ω. This mapping is given by:

$$\hat{u}^e(t) = L_u^e\,\hat{u}(t). \tag{III.6}$$

Note that $\hat{u}(t) \in \mathbb{R}^{N_\Omega}$ gather all the unknowns over the entire domain Ω and its sorting is arbitrary. However, once this sorting is fixed, the location matrices have to be defined for each element such that they satisfy the relation (III.6).

Two-dimensional domain

Mesh: Analogous to the 1D domain, the mesh is the set of all finite elements, all nodes on Ω, and their connectivity topology. In the 2D case, finite elements are simple 2D regions, typically considered as rectangles or triangles. Fig. III.2a illustrates a 2D rectangular domain $\Omega \subset \mathbb{R}^2$ with a triangular mesh, where each element could be of arbitrary order. For the purposes of this section, only first-order and second-order triangular elements are illustrated in Fig. III.2b and III.2c, respectively.

Shape functions: Consider the two-dimensional unknown field $u(\mathtt{X},t) \in \mathbb{R}^n$ with $\mathtt{X} = \{X_1, X_2\} \in \Omega$ a point of the 2D domain, and its local approximate solution $\tilde{u}^e(\mathtt{X},t) = N_u^e(\mathtt{X})\,\hat{u}^e(t) \in \mathbb{R}^n$, where $N_u^e(\mathtt{X}) \in \mathbb{R}^{n\times nNN^e}$ is the shape function and $\hat{u}^e(t) \in \mathbb{R}^{nNN^e}$ is the vector of local approximations of $u(\mathtt{X},t)$ evaluated at the nodes within the finite element. Note that for first-order and second-order triangular

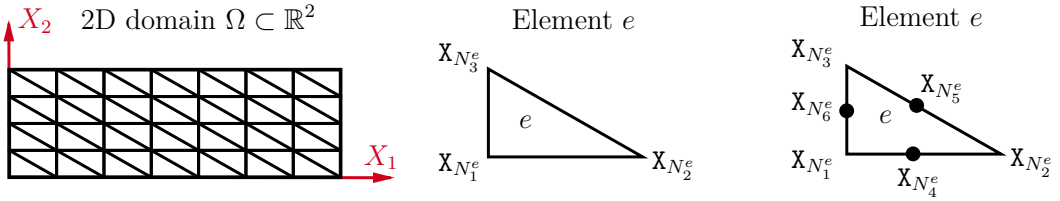

(a) 2D domain: Triangular mesh (b) First-order triangular element (c) Second-order triangular element

Figure III.2 – 2D triangular mesh and finite elements.

elements we have $NN^e = 3$ and $NN^e = 6$, respectively. The process to build canonical shape functions based on 2D triangular elements is illustrated below. Consider both finite elements in Fig. III.2b and III.2c. The approximate local solution of the component $\tilde{u}_i^e(\mathtt{X}, t) \in \mathbb{R}$ with $i = \{1, ..., n\}$, is assumed to be a polynomial of the form:

$$\text{First-order element} \quad : \quad \tilde{u}_i^e(\mathtt{X}, t) = \underbrace{\begin{bmatrix} 1 & X_1 & X_2 \end{bmatrix}}_{P(\mathtt{X})} \underbrace{\begin{bmatrix} (\alpha_0)_i^e(t) \\ (\alpha_1)_i^e(t) \\ (\alpha_2)_i^e(t) \end{bmatrix}}_{\alpha_i^e(t)}, \tag{III.7}$$

$$\text{Second-order element} \quad : \quad \tilde{u}_i^e(\mathtt{X}, t) = \underbrace{\begin{bmatrix} 1 & X_1 & X_2 & X_1^2 & X_1X_2 & X_2^2 \end{bmatrix}}_{P(\mathtt{X})} \underbrace{\begin{bmatrix} (\alpha_0)_i^e(t) \\ \vdots \\ (\alpha_5)_i^e(t) \end{bmatrix}}_{\alpha_i^e(t)}, \tag{III.8}$$

where $P(\mathtt{X}) \in \mathbb{R}^{1 \times NN^e}$ is the canonical 2D polynomial basis and $\alpha_i^e(t) \in \mathbb{R}^{NN^e}$ are unknown coefficients. Then, evaluating $P(\mathtt{X})$ at the coordinates of each node within the finite element we obtain the relations:

$$\text{First-order element} \quad : \quad \underbrace{\begin{bmatrix} (\hat{u}_i^e)_1(t) \\ (\hat{u}_i^e)_2(t) \\ (\hat{u}_i^e)_3(t) \end{bmatrix}}_{\hat{u}_i^e(t)} = \underbrace{\begin{bmatrix} P(\mathtt{X}_{N_1^e}) \\ P(\mathtt{X}_{N_2^e}) \\ P(\mathtt{X}_{N_3^e}) \end{bmatrix}}_{C^e} \underbrace{\begin{bmatrix} (\alpha_0)_i^e(t) \\ (\alpha_1)_i^e(t) \\ (\alpha_2)_i^e(t) \end{bmatrix}}_{\alpha_i^e(t)}, \tag{III.9}$$

$$\text{Second-order element} \quad : \quad \underbrace{\begin{bmatrix} (\hat{u}_i^e)_1(t) \\ \vdots \\ (\hat{u}_i^e)_6(t) \end{bmatrix}}_{\hat{u}_i^e(t)} = \underbrace{\begin{bmatrix} P(\mathtt{X}_{N_1^e}) \\ \vdots \\ P(\mathtt{X}_{N_6^e}) \end{bmatrix}}_{C^e} \underbrace{\begin{bmatrix} (\alpha_0)_i^e(t) \\ \vdots \\ (\alpha_5)_i^e(t) \end{bmatrix}}_{\alpha_i^e(t)}, \tag{III.10}$$

where $C^e \in \mathbb{R}^{NN^e \times NN^e}$ is an invertible matrix and $\hat{u}_i^e(t)$ are the local approximations of $u_i(\mathtt{X}, t)$ at the nodes within the finite element. With the above we get:

$$\tilde{u}_i^e(\mathtt{X}, t) = P(\mathtt{X})(C^e)^{-1}\hat{u}_i^e(t) = N^e(\mathtt{X})\,\hat{u}_i^e(t), \tag{III.11}$$

with $N^e(\mathtt{X}) \in \mathbb{R}^{1 \times NN^e}$ the local 2D shape function of one component of $\tilde{u}(\mathtt{X}, t)$. Repeating the process for each component $i = \{1, ..., n\}$ we obtain:

$$\underbrace{\begin{bmatrix} \tilde{u}_1^e(\mathtt{X}, t) \\ \vdots \\ \tilde{u}_n^e(\mathtt{X}, t) \end{bmatrix}}_{\tilde{u}^e(\mathtt{X}, t)} = \underbrace{\begin{bmatrix} N^e(\mathtt{X}) & & 0 \\ & \ddots & \\ 0 & & N^e(\mathtt{X}) \end{bmatrix}}_{N_u^e(\mathtt{X})} \underbrace{\begin{bmatrix} \hat{u}_1^e(t) \\ \vdots \\ \hat{u}_n^e(t) \end{bmatrix}}_{\hat{u}^e(t)}. \tag{III.12}$$

Location matrices: Analogously to the 1D domain, location matrices $L_u^e \in \mathbb{R}^{nNN^e \times N_\Omega}$ define the mapping between the local and global sorting of unknowns, satisfying the relation (III.6).

III.2.2 Overview of FEM approaches

In Section I.3.2, we provided a comprehensive review of existing structure-preserving FEM approaches applicable to infinite-dimensional PHS. In this section, we only provide an overview of the discretization of linear PHS based on standard FEM, following the extended Hamilton's principle, while imposing Dirichlet boundary conditions using Lagrange multipliers [Babuška 1973a] and a penalty functional [Babuška 1973b]. Additionally, we present the mixed FEM structure-preserving discretization following the Hellinger-Reissner principle as proposed in [Thoma 2022b]. This discussion serves as motivation and foundation for the forthcoming proposed approaches in Section III.3.

The discussion is focused on linear PHS associated with first-order differential operators. So, to contextualize, we begin by recalling the class of differential operators and the associated integration by parts lemma, which is crucial for transforming the strong form of the PDEs into their weak form, suitable for FEM. Following this, we revisit the class of linear PHS under consideration.

III.2.2.a Reminder: Considered class of infinite-dimensional linear PHS

From Definition II.4, we recall the class of first-order linear differential operators and their formal adjoints.

(From Definition II.4.) Let $\mathtt{X} = \{X_1, \dots, X_\ell\}$ be a Cartesian basis, $\Omega \subset \mathbb{R}^\ell$ an open set, $v(\mathtt{X}) \in \mathbb{R}^m$ and $w(\mathtt{X}) \in \mathbb{R}^n$ two smooth vector functions. The first-order linear differential operator $\mathcal{F}_\mathtt{x}$ and its formal adjoint $\mathcal{F}_\mathtt{x}{}^*$ are given by:

$$\mathcal{F}_\mathtt{x}\, w(\mathtt{X}) = F_0\, w(\mathtt{X}) + \textstyle\sum_{k=1}^{\ell} F_k\, \partial_k w(\mathtt{X}), \tag{III.13}$$

$$\mathcal{F}_\mathtt{x}{}^* v(\mathtt{X}) = F_0^\top v(\mathtt{X}) - \textstyle\sum_{k=1}^{\ell} F_k^\top \partial_k v(\mathtt{X}), \tag{III.14}$$

with $\partial_k = \partial/\partial X_k$ and F_0, $F_k \in \mathbb{R}^{m\times n}$ constant matrices.

From Lemma II.1 and Corollary II.1, we recall the integration by parts lemma for these differential operators.

(From Lemma II.1 and Corollary II.1.) Consider the above definition of first-order differential operators, the open set $\Omega \subset \mathbb{R}^\ell$, its boundary $\partial\Omega$, and the closure $\bar{\Omega} = \Omega \cup \partial\Omega$, such that $\mathtt{X} \in \Omega$ and $\mathtt{S} \in \partial\Omega$. Then for any pair of smooth functions $v(\mathtt{X}) \in \mathbb{R}^m$ and $w(\mathtt{X}) \in \mathbb{R}^n$ defined on $\bar{\Omega}$, we have that:

$$\int_\Omega \left(v(\mathtt{X})^\top \mathcal{F}_\mathtt{x} w(\mathtt{X}) - w(\mathtt{X})^\top \mathcal{F}_\mathtt{x}{}^* v(\mathtt{X}) \right) d\mathtt{X} = \int_{\partial\Omega} w(\mathtt{S})^\top F_\partial(\mathtt{S}) v(\mathtt{S}) d\mathtt{S}, \tag{III.15}$$

with $F_\partial(\mathtt{S}) \in \mathbb{R}^{n\times m}$ a boundary valued matrix given by:

$$F_\partial(\mathtt{S}) = \textstyle\sum_{k=1}^{\ell} F_k^\top \hat{n}_k(\mathtt{S}), \tag{III.16}$$

where $\hat{n}_k(\mathtt{S})$ is the k-component of the outward unit normal vector to the boundary $\partial\Omega$ projected on the axis X_k.

Assuming a mixed boundary problem with $\partial\Omega = \partial\Omega_D \cup \partial\Omega_N$, where $\partial\Omega_D$ and $\partial\Omega_N$ are the boundary portions where Dirichlet and Neumann boundary conditions are imposed, respectively, from Theorem II.1, we recall the class of infinite-dimensional linear PHS representation of flexible mechanical systems.

(From Theorem II.1.) Let $x(\mathtt{X},t) = [p(\mathtt{X},t)^\top \ \epsilon(\mathtt{X},t)^\top \ r(\mathtt{X},t)^\top]^\top \in \mathbb{R}^{2n+m}$ be the energy variables, and $\delta_x H(x) = [e_p(\mathtt{X},t)^\top \ e_\epsilon(\mathtt{X},t)^\top \ -b(\mathtt{X})^\top]^\top \in \mathbb{R}^{2n+m}$ be the co-energy variables. The system's dynamics defines an infinite-dimensional linear PHS of the form:

$$\underbrace{\begin{bmatrix}\dot{p}(\mathtt{X},t)\\ \dot{\epsilon}(\mathtt{X},t)\\ \dot{r}(\mathtt{X},t)\end{bmatrix}}_{\dot{x}} = \underbrace{\begin{bmatrix}0 & -\mathcal{F}_{\mathtt{x}}^* & -1\\ \mathcal{F}_{\mathtt{x}} & 0 & 0\\ 1 & 0 & 0\end{bmatrix}}_{\mathcal{J}=-\mathcal{J}^*} \underbrace{\begin{bmatrix}e_p(\mathtt{X},t)\\ e_\epsilon(\mathtt{X},t)\\ -b(\mathtt{X})\end{bmatrix}}_{\delta_x H(x)} + \underbrace{\begin{bmatrix}B_d\\ 0\\ 0\end{bmatrix}}_{\mathcal{G}} u_d(\mathtt{X},t) \tag{III.17}$$

$$y_d(\mathtt{X},t) = \mathcal{G}^* \delta_x H(x) = B_d^\top e_p(\mathtt{X},t).$$

$$H(x) = \int_\Omega \left(\frac{1}{2}\, p(\mathtt{X},t)^\top \mathcal{M}(\mathtt{X})^{-1} p(\mathtt{X},t) + \frac{1}{2}\, \epsilon(\mathtt{X},t)^\top \mathcal{K}_\epsilon(\mathtt{X}) \epsilon(\mathtt{X},t) - r(\mathtt{X},t)^\top b(\mathtt{X})\right) d\mathtt{X}, \tag{III.18}$$

$$\dot{H}(x) = \int_\Omega u_d(\mathtt{X},t)^\top y_d(\mathtt{X},t)\, d\mathtt{X} + \int_{\partial\Omega} u_\partial(\mathtt{S},t)^\top y_\partial(\mathtt{S},t)\, d\mathtt{S}, \tag{III.19}$$

where $u_\partial(\mathtt{S},t)$, $y_\partial(\mathtt{S},t) \in \mathbb{R}^{2n}$ are the boundary inputs and outputs, respectively, defined as:

$$u_\partial(\mathtt{S},t) = \begin{bmatrix}\tau_N(\mathtt{S},t)^\top & v_D(\mathtt{S},t)^\top\end{bmatrix}^\top, \quad y_\partial(\mathtt{S},t) = \begin{bmatrix}v_N(\mathtt{S},t)^\top & \tau_D(\mathtt{S},t)^\top\end{bmatrix}^\top \tag{III.20}$$

where:

$$\begin{aligned}\tau_N(\mathtt{S},t) &= F_\partial(\mathtt{S}) e_\epsilon(\mathtt{S},t), \quad v_N(\mathtt{S},t) = e_p(\mathtt{S},t) \quad (\text{on } \partial\Omega_N),\\ \tau_D(\mathtt{S},t) &= F_\partial(\mathtt{S}) e_\epsilon(\mathtt{S},t), \quad v_D(\mathtt{S},t) = e_p(\mathtt{S},t) \quad (\text{on } \partial\Omega_D).\end{aligned} \tag{III.21}$$

In the infinite-dimensional linear PHS above, $\mathcal{J} = -\mathcal{J}^*$ is the skew-adjoint linear differential operator (interconnection operator), $\delta_x H(x)$ denotes the variational derivative of $H(x)$ with respect to $x(\mathtt{X},t)$, and $\dot{H}$ is the energy balance. The total energy is given by the Hamiltonian $H(x)$, where $\mathcal{M}(\mathtt{X}) = \mathcal{M}(\mathtt{X})^\top > 0 \in \mathbb{R}^{n\times n}$ is the mass density matrix, and $\mathcal{K}_\epsilon(\mathtt{X}) = \mathcal{K}_\epsilon(\mathtt{X})^\top > 0 \in \mathbb{R}^{m\times m}$ is the stiffness density matrix. From energy variables, $p(\mathtt{X},t) = \mathcal{M}(\mathtt{X})\dot{r}(\mathtt{X},t) \in \mathbb{R}^n$ is the generalized momentum with $r(\mathtt{X},t) \in \mathbb{R}^n$ the generalized displacement, and $\epsilon(\mathtt{X},t) = \mathcal{F}_{\mathtt{x}}\, r(\mathtt{X},t) \in \mathbb{R}^m$ is the generalized strain (representing kinematics, strain-displacement relation). From co-energy variables, $e_p(\mathtt{X},t) = \mathcal{M}(\mathtt{X})^{-1}\, p(\mathtt{X},t) = \dot{r}(\mathtt{X},t)$ is the generalized velocity, $e_\epsilon(\mathtt{X},t) = \mathcal{K}_\epsilon(\mathtt{X})\, \epsilon(\mathtt{X},t)$ is the generalized stress (representing Hooke's law, stress-strain relation), and $b(\mathtt{X})$ is the generalized body force, usually considered

as the weight of the body. From boundary inputs and outputs, $\tau_D(\mathtt{S},t)$, $\tau_N(\mathtt{S},t)$ and $v_D(\mathtt{S},t)$, $v_N(\mathtt{S},t) \in \mathbb{R}^n$ are the generalized boundary tractions and velocities, respectively.

Lastly, from Proposition II.5, we recall the field port-Lagrangian system (PLS) representation of the above infinite-dimensional linear PHS.

(From Proposition II.5.) The infinite-dimensional linear PLS representation of the linear PHS in Theorem II.1 is described by the state variable $z(\mathtt{X},t) = [p(\mathtt{X},t)^\top \;\; r(\mathtt{X},t)^\top]^\top \in \mathbb{R}^{2n}$, and the dynamic equation:

$$\begin{aligned}
\underbrace{\begin{bmatrix}\dot{p}(\mathtt{X},t)\\ \dot{r}(\mathtt{X},t)\end{bmatrix}}_{\dot{z}} &= \underbrace{\begin{bmatrix}0 & -1\\ 1 & 0\end{bmatrix}}_{J=-J^\top}\underbrace{\begin{bmatrix}e_p(\mathtt{X},t)\\ e_r(\mathtt{X},t)\end{bmatrix}}_{\delta_z H(z)} + \underbrace{\begin{bmatrix}B_d\\ 0\end{bmatrix}}_{\mathcal{G}} u_d(\mathtt{X},t)\\
y_d(\mathtt{X},t) &= \mathcal{G}^*\delta_z H(z) = B_d^\top e_p(\mathtt{X},t),\\
u_\partial(\mathtt{S},t) &= \begin{bmatrix}\tau_N(\mathtt{S},t)^\top & r_D(\mathtt{S},t)^\top\end{bmatrix}^\top,\\
y_\partial(\mathtt{S},t) &= \begin{bmatrix}v_N(\mathtt{S},t)^\top & \dot{\tau}_D(\mathtt{S},t)^\top\end{bmatrix}^\top,
\end{aligned} \tag{III.22}$$

where the total energy is given by the Hamiltonian $H(z) = T(p) + U_T(r)$, where $T(p) = \frac{1}{2}p(\mathtt{X},t)^\top \mathcal{M}(\mathtt{X})^{-1} p(\mathtt{X},t)$ is the kinetic energy, and $U_T(r)$ is the total potential energy defined as:

$$U_T(r) = \int_\Omega \left[\frac{1}{2}(\mathcal{F}_{\mathtt{x}} r(\mathtt{X},t))^\top \mathcal{K}_\epsilon(\mathtt{X})(\mathcal{F}_{\mathtt{x}} r(\mathtt{X},t)) - r(\mathtt{X},t)^\top b(\mathtt{X})\right] d\mathtt{X}. \tag{III.23}$$

The co-energy variable $e_r(\mathtt{X},t) \in \mathbb{R}^n$ is defined as the variational derivative of the Hamiltonian $H(z)$ with respect to $r(\mathtt{X},t)$ and is given by:

$$e_r(\mathtt{X},t) = \mathcal{F}_{\mathtt{x}}{}^*\left(\mathcal{K}_\epsilon(\mathtt{X})\mathcal{F}_{\mathtt{x}} r(\mathtt{X},t)\right) - b(\mathtt{X}) = \mathcal{K}_r(r(\mathtt{X},t)) - b(\mathtt{X}), \tag{III.24}$$

where $\mathcal{K}_r(\cdot) = \mathcal{F}_{\mathtt{x}}{}^*\left(\mathcal{K}_\epsilon(\mathtt{X})\mathcal{F}_{\mathtt{x}}(\cdot)\right)$ is the differential stiffness operator.

III.2.2.b Dimensions of the discretized variables

In this section, we detail the dimensions of the main variables involved in the discretization process using FEM-based approaches. Each variable, previously introduced in the continuous formulation, will be assigned specific dimensions based on canonical shape functions. While the methods presented are not limited to this specific choice of shape functions, we focus on canonical ones for simplicity. If other shape functions were used, the dimensions of the variables would need to be redefined accordingly. For more information on the types of shape functions and their respective advantages, please refer to [Zienkiewicz 2005, Chapter 8] and [Reddy 2005, Chapter 9].

First of all, let us remember that the main variables $r(\mathtt{X},t)$, $e_p(X,t) \in \mathbb{R}^n$ and $\epsilon(\mathtt{X},t)$, $e_\epsilon(\mathtt{X},t) \in \mathbb{R}^m$ are defined on Ω, $r_D(\mathtt{S},t)$, $v_D(\mathtt{S},t) \in \mathbb{R}^n$ are defined on $\partial\Omega_D$, and $\tau_N(\mathtt{S},t) \in \mathbb{R}^n$ is defined on $\partial\Omega_N$.

Consider a mesh composed of:

- n_e: Total number of finite elements in Ω,
- NN_Ω: Total number of nodes in Ω,
- $NN_{\partial\Omega_D}$: Total number of nodes on $\partial\Omega_D$,
- $NN_{\partial\Omega_N}$: Total number of nodes on $\partial\Omega_N$,

and each finite element consisting of:

- Ω^e: The local domain of the finite element,
- $\partial\Omega_D^e$: The portion of the boundary of Ω^e that coincides with the Dirichlet boundary $\partial\Omega_D$ of the overall domain Ω,
- $\partial\Omega_N^e$: The portion of the boundary of Ω^e that coincides with the Neumann boundary $\partial\Omega_N$ of the overall domain Ω,
- NN^e: Total number of nodes in Ω^e.

Then, the dimensions of the global discrete variables are given by:

- $N_\Omega = nNN_\Omega$: Total number of discrete variables associated with continuous variables in $\mathbb{R}^n$ and defined on Ω,
- $M_\Omega = mNN_\Omega$: Total number of discrete variables associated with continuous variables in $\mathbb{R}^m$ and defined on Ω,
- $N_{\partial\Omega_D} = nNN_{\partial\Omega_D}$: Total number of discrete Dirichlet boundary conditions on $\partial\Omega_D$,
- $N_{\partial\Omega_N} = nNN_{\partial\Omega_N}$: Total number of discrete Neumann boundary conditions on $\partial\Omega_N$.

Depending on the specific approach, the local approximations of the main variables might be given by:

$$\tilde{r}_D^e(\mathtt{S},t) = N_{r_D}^e(\mathtt{S})\,\hat{r}_D^e(t), \qquad \tilde{r}^e(\mathtt{X},t) = N_r^e(\mathtt{X})\,\hat{r}^e(t), \qquad \tilde{\epsilon}^e(\mathtt{X},t) = N_\epsilon^e(\mathtt{X})\,\hat{\epsilon}^e(t),$$
$$\tilde{v}_D^e(\mathtt{S},t) = N_{r_D}^e(\mathtt{S})\,\hat{v}_D^e(t), \qquad \tilde{e}_p^e(\mathtt{X},t) = N_r^e(\mathtt{X})\,\hat{e}_p^e(t), \qquad \tilde{e}_\epsilon^e(\mathtt{X},t) = N_e^e(\mathtt{X})\,\hat{e}_\epsilon^e(t),$$
$$\tilde{\tau}_N^e(\mathtt{S},t) = N_{\tau_N}^e(\mathtt{S})\,\hat{\tau}_N^e(t),$$

where $N_r^e(\mathtt{X})$, $N_{r_D}^e(\mathtt{S})$, $N_{\tau_N}^e(\mathtt{S}) \in \mathbb{R}^{n\times nNN^e}$ and $N_\epsilon^e(\mathtt{X})$, $N_e^e(\mathtt{X}) \in \mathbb{R}^{m\times mNN^e}$ are the local shape functions, $\hat{r}^e(t)$, $\hat{e}_p^e(t) \in \mathbb{R}^{nNN^e}$ and $\hat{\epsilon}^e(t)$, $\hat{e}_\epsilon^e(t) \in \mathbb{R}^{mNN^e}$ are the local discrete variables on Ω^e, $\hat{r}_D^e(t)$, $\hat{v}_D(t) \in \mathbb{R}^{nNN^e}$ are the local discrete Dirichlet boundary conditions on $\partial\Omega_D^e$, and $\hat{\tau}_N^e(t) \in \mathbb{R}^{nNN^e}$ is the local discrete Neumann boundary condition on $\partial\Omega_N^e$. Lastly, the mapping between global and local discrete variables is established through the location (assembly) matrices, following the relations:

$$\hat{r}_D^e(t) = L_{r_D}^e\,\hat{r}_D(t), \qquad \hat{r}^e(t) = L_r^e\,\hat{r}(t), \qquad \hat{\epsilon}^e(t) = L_\epsilon^e\,\hat{\epsilon}(t),$$
$$\hat{v}_D^e(t) = L_{r_D}^e\,\hat{v}_D(t), \qquad \hat{e}_p^e(t) = L_r^e\,\hat{e}_p(t), \qquad \hat{e}_\epsilon^e(t) = L_e^e\,\hat{e}_\epsilon(t),$$
$$\hat{\tau}_N^e(t) = L_{\tau_N}^e\,\hat{\tau}_N(t),$$

with $\hat{r}(t)$, $\hat{e}_p(t) \in \mathbb{R}^{N_\Omega}$, $\hat{\epsilon}(t)$, $\hat{e}_\epsilon(t) \in \mathbb{R}^{M_\Omega}$, $\hat{r}_D(t)$, $\hat{v}_D(t) \in \mathbb{R}^{N_{\partial\Omega_D}}$ and $\hat{\tau}_N(t) \in \mathbb{R}^{N_{\partial\Omega_N}}$ the global discrete variables; and $L_r^e \in \mathbb{R}^{nNN^e\times N_\Omega}$, L_e^e and $L_\epsilon^e \in \mathbb{R}^{mNN^e\times M_\Omega}$, $L_{r_D}^e \in \mathbb{R}^{nNN^e\times N_{\partial\Omega_D}}$, and $L_{\tau_N}^e \in \mathbb{R}^{nNN^e\times N_{\partial\Omega_N}}$ the location (assembly) matrices.

III.2.2.c Standard FEM with extended Hamilton's principle

In this section, we present two discretization approaches based on standard FEM using the extended Hamilton's principle, where Dirichlet boundary conditions are imposed through the use of Lagrange multipliers [Babuška 1973a] and the Penalty method [Babuška 1973b]. These methods, along with the H-R based approach introduced in Section III.2.2.d, are presented as a foundation for the FEM applied to the considered class of systems. They help define key matrices and clarify the characteristics and limitations of these approaches, providing a more structured understanding of their behavior. This groundwork enables a clearer introduction of the proposed methods in Section III.3, by illustrating shared features and emphasizing the specific advantages of the new approaches over these existing methods.

Extended Hamilton's principle states that the true evolution of $r(\mathtt{X}, t)$, subject to algebraic constraints of the form $\gamma(r) = 0 \in \mathbb{R}^{n_\lambda}$, between two specific times t_1 and t_2, is a stationary point of the extended action functional under admissible small variations of δr and $\delta\lambda$, with $\lambda(\mathtt{X}, t) \in \mathbb{R}^{n_\lambda}$ the Lagrange multiplier. Mathematically [Bedford 1985]:

$$\int_{t_1}^{t_2} \left[\delta(\mathcal{T} - \mathcal{U}) + \delta\mathcal{W}_E - \delta\mathcal{C}_\lambda\right] dt = 0, \tag{III.25}$$

$$\delta r(\mathtt{S}, t) = 0 \text{ on } \partial\Omega_D \text{ for all } t, \tag{III.26}$$

$$\delta r(\mathtt{X}, t_1) = \delta r(\mathtt{X}, t_2) = 0 \text{ for all } \mathtt{X}, \tag{III.27}$$

where δ is the variational operator, $\mathcal{T} \in \mathbb{R}$ is the kinetic energy, $\mathcal{U} \in \mathbb{R}$ is the elastic potential energy, $\delta\mathcal{W}_E \in \mathbb{R}$ is the virtual work associated to the external forces, and $\mathcal{C}_\lambda$ is the constraint functional. For the considered class of linear PHS we have:

$$\mathcal{T}(\dot{r}) = \frac{1}{2}\int_\Omega \dot{r}(\mathtt{X}, t)^\top \mathcal{M}(\mathtt{X})\, \dot{r}(\mathtt{X}, t)\, d\mathtt{X}, \tag{III.28}$$

$$\mathcal{U}(r) = \frac{1}{2}\int_\Omega (\mathcal{F}_{\mathtt{x}} r(\mathtt{X}, t))^\top \mathcal{K}_\epsilon(\mathtt{X})\, (\mathcal{F}_{\mathtt{x}} r(\mathtt{X}, t))\, d\mathtt{X}, \tag{III.29}$$

$$\delta\mathcal{W}_E(r) = \int_\Omega \delta r(\mathtt{X}, t)^\top \left(B_d u_d(\mathtt{X}, t) + b(\mathtt{X})\right) d\mathtt{X} + \int_{\partial\Omega_N} \delta r(\mathtt{S}, t)^\top \tau_N(\mathtt{S}, t)\, d\mathtt{S}, \tag{III.30}$$

$$\mathcal{C}_\lambda(r, \lambda) = \int_\Omega \lambda(\mathtt{X}, t)^\top \gamma(r)\, d\mathtt{X}. \tag{III.31}$$

Imposition of Dirichlet boundary conditions via Lagrange multipliers

Following the approach originally proposed in [Babuška 1973a], the algebraic constraint is given by $\gamma(r) = (r(\mathtt{S}, t) - r_D(\mathtt{S}, t)) = 0 \in \mathbb{R}^n$, where $r_D(\mathtt{S}, t) \in \mathbb{R}^n$ is the Dirichlet boundary condition satisfying $v_D(\mathtt{S}, t) = \dot{r}_D(\mathtt{S}, t)$ on $\partial\Omega_D$. Then, the constraint functional in (III.31) takes the form:

$$\mathcal{C}_\lambda(r, \lambda) = \int_{\partial\Omega_D} \lambda(\mathtt{S}, t)^\top (r(\mathtt{S}, t) - r_D(\mathtt{S}, t))\, d\mathtt{S}. \tag{III.32}$$

Proposition III.1. *The standard FEM discretization of (III.17) based on the extended Hamilton's principle with Lagrange multipliers, using local approximations:*

$$\begin{aligned}
&\tilde{r}^e(\mathtt{X},t) = N_r^e(\mathtt{X})\,\hat{r}^e(t), && \delta\tilde{r}^e(\mathtt{X},t) = N_r^e(\mathtt{X})\,\delta\hat{r}^e(t), && r_D^e(\mathtt{S},t) = N_{r_D}^e(\mathtt{S})\,\hat{r}_D^e(t),\\
&\tilde{\lambda}^e(\mathtt{S},t) = N_\lambda^e(\mathtt{S})\,\hat{\lambda}^e(t), && \delta\tilde{\lambda}^e(\mathtt{S},t) = N_\lambda^e(\mathtt{S})\,\delta\hat{\lambda}^e(t), && \tau_N^e(\mathtt{S},t) = N_{\tau_N}^e(\mathtt{S})\,\hat{\tau}_N^e(t),\\
&u_d^e(\mathtt{X},t) = N_{u_d}^e(\mathtt{X})\,\hat{u}_d^e(t),
\end{aligned}$$

leads to the following finite-dimensional linear PLS-DAE:

$$\underbrace{\begin{bmatrix} I_{N_\Omega} & 0 & 0\\ 0 & I_{N_\Omega} & 0\\ 0 & 0 & 0 \end{bmatrix}}_{\hat{E}} \underbrace{\begin{bmatrix} \dot{\hat{p}}(t)\\ \dot{\hat{r}}(t)\\ \dot{\hat{\lambda}}(t) \end{bmatrix}}_{\dot{\hat{z}}(t)} = \underbrace{\begin{bmatrix} 0 & -I_{N_\Omega} & -\hat{B}_\lambda^\top\\ I_{N_\Omega} & 0 & 0\\ \hat{B}_\lambda & 0 & 0 \end{bmatrix}}_{\hat{J}=-\hat{J}^\top} \underbrace{\begin{bmatrix} \hat{e}_p(t)\\ \hat{e}_r(t)\\ \hat{\lambda}(t) \end{bmatrix}}_{\hat{Z}(\hat{z})} + \underbrace{\begin{bmatrix} \hat{B}_d & \hat{B}_{\tau_N} & 0\\ 0 & 0 & 0\\ 0 & 0 & -\hat{B}_{LM} \end{bmatrix}}_{\hat{G}} \underbrace{\begin{bmatrix} \hat{u}_d(t)\\ \hat{\tau}_N(t)\\ \hat{v}_D(t) \end{bmatrix}}_{\hat{u}(t)} \tag{III.33}$$

$$\begin{aligned}
\hat{y}(t) &= \hat{G}^\top \hat{Z}(\hat{z})\\
\hat{H}_{LM}(\hat{z}) &= \frac{1}{2}\,\hat{p}(t)^\top \hat{M}^{-1}\hat{p}(t) + \frac{1}{2}\,\hat{r}(t)^\top \hat{K}_r\,\hat{r}(t) - \hat{r}(t)^\top \hat{b},
\end{aligned} \tag{III.34}$$

where $\hat{p}(t) = \hat{M}\dot{\hat{r}}(t)$ is the discrete generalized momentum, $\hat{e}_r(t) = \hat{K}_r\,\hat{r}(t) - \hat{b}$ is the gradient of the Hamiltonian $\hat{H}_{LM}(\hat{z})$ with respect to $\hat{r}(t)$, and I_{N_Ω} is an identity matrix. The involved matrices and vectors are given by:

$$\hat{M} = \sum_{e=1}^{n_e} (L_r^e)^\top \int_{\Omega^e} N_r^e(\mathtt{X})^\top \mathcal{M}(\mathtt{X}) N_r^e(\mathtt{X})\,d\mathtt{X}\,L_r^e, \tag{III.35}$$

$$\hat{K}_r = \sum_{e=1}^{n_e} (L_r^e)^\top \int_{\Omega^e} (\mathcal{F}_{\mathtt{x}} N_r^e(\mathtt{X}))^\top \mathcal{K}_\epsilon(\mathtt{X})(\mathcal{F}_{\mathtt{x}} N_r^e(\mathtt{X}))\,d\mathtt{X}\,L_r^e, \tag{III.36}$$

$$\hat{b} = \sum_{e=1}^{n_e} (L_r^e)^\top \int_{\Omega^e} N_r^e(\mathtt{X})^\top b(\mathtt{X})\,d\mathtt{X}, \tag{III.37}$$

$$\hat{B}_d = \sum_{e=1}^{n_e} (L_r^e)^\top \int_{\Omega^e} N_r^e(\mathtt{X})^\top B_d N_{u_d}^e(\mathtt{X})\,d\mathtt{X}\,L_{u_d}^e, \tag{III.38}$$

$$\hat{B}_{\tau_N} = \sum_{e=1}^{n_e} (L_r^e)^\top \int_{\partial\Omega_N^e} N_r^e(\mathtt{S})^\top N_{\tau_N}^e(\mathtt{S})\,d\mathtt{S}\,L_{\tau_N}^e, \tag{III.39}$$

$$\hat{B}_\lambda = \sum_{e=1}^{n_e} (L_\lambda^e)^\top \int_{\partial\Omega_D^e} N_\lambda^e(\mathtt{S})^\top N_r^e(\mathtt{S})\,d\mathtt{S}\,L_r^e, \tag{III.40}$$

$$\hat{B}_{LM} = \sum_{e=1}^{n_e} (L_\lambda^e)^\top \int_{\partial\Omega_D^e} N_\lambda^e(\mathtt{S})^\top N_{r_D}^e(\mathtt{S})\,d\mathtt{S}\,L_{r_D}^e. \tag{III.41}$$

Proof. (III.33) is obtained by applying the extended Hamilton's principle with the considered local approximations and constraint functional. For simplicity the spatial and temporal dependencies are omitted. First, from kinetic energy:

$$\delta\mathcal{T}^e = (\delta\dot{\hat{r}}^e)^\top \int_{\Omega^e} (N_r^e)^\top \mathcal{M} N_r^e\,d\mathtt{X}\,\dot{\hat{r}}^e = (\delta\dot{\hat{r}}^e)^\top \hat{M}^e\,\dot{\hat{r}}^e,$$

where, by assembling with the location matrices, we obtain:

$$\delta\mathcal{T} = \sum_{e=1}^{n_e} \delta\mathcal{T}^e = (\delta\dot{\hat{r}})^\top \sum_{e=1}^{n_e} (L_r^e)^\top \hat{M}^e \, L_r^e \, \dot{\hat{r}} = (\delta\dot{\hat{r}})^\top \hat{M} \, \dot{\hat{r}}.$$

Thus, we have $\int_{t_1}^{t_2} \delta\mathcal{T} \, dt = -\int_{t_1}^{t_2} (\delta\hat{r})^\top \hat{M} \, \ddot{\hat{r}} \, dt + (\delta\hat{r})^\top \hat{M} \, \dot{\hat{r}}|_{t_1}^{t_2}$, where the last term is equal to zero due to (III.27). Next, from the elastic potential energy:

$$\delta\mathcal{U}^e = (\delta\hat{r}^e)^\top \int_{\Omega^e} (\mathcal{F}_{\mathtt{x}} N_r^e)^\top \mathcal{K}_\epsilon (\mathcal{F}_{\mathtt{x}} N_r^e) \, d\mathtt{X} \, \hat{r}^e = (\delta\hat{r}^e)^\top \hat{K}_r^e \, \hat{r}^e,$$

where assembling gives us: $\delta\mathcal{U} = (\delta\hat{r})^\top \hat{K}_r \, \hat{r}$. Third, from the virtual work:

$$\begin{aligned}
\delta\mathcal{W}_E{}^e &= (\delta\hat{r}^e)^\top \left[\int_{\Omega^e} (N_r^e)^\top B_d \, N_{u_d}^e \, d\mathtt{X} \, \hat{u}_d^e + \int_{\Omega^e} (N_r^e)^\top b \, d\mathtt{X} + \int_{\partial\Omega_N^e} (N_r^e)^\top N_{\tau_N}^e \, d\mathtt{S} \, \hat{\tau}_N^e \right] \\
&= (\delta\hat{r}^e)^\top \left[\hat{B}_d^e \hat{u}_d^e + \hat{b}^e + \hat{B}_{\tau_N}^e \hat{\tau}_N^e \right],
\end{aligned}$$

which leads to: $\delta\mathcal{W}_E = (\delta\hat{r})^\top \left[\hat{B}_d \, \hat{u}_d + \hat{b} + \hat{B}_{\tau_N} \hat{\tau}_N \right]$. Fourth, from the algebraic constraint:

$$\begin{aligned}
\delta\mathcal{C}_\lambda^e &= \int_{\partial\Omega_D^e} (\delta\tilde{\lambda}^e)^\top (\tilde{r}^e - \tilde{r}_D) \, d\mathtt{S} + \int_{\partial\Omega_D^e} (\delta\tilde{r}^e)^\top \tilde{\lambda}^e \, d\mathtt{S} \\
&= (\delta\hat{\lambda}^e)^\top \left[\int_{\partial\Omega_D^e} (N_\lambda^e)^\top N_r^e \, d\mathtt{S} \, \hat{r}^e - \int_{\partial\Omega_D^e} (N_\lambda^e)^\top N_{r_D}^e \, d\mathtt{S} \, \hat{r}_D^e \right] + (\delta\hat{r}^e)^\top \int_{\partial\Omega_D^e} (N_r^e)^\top N_\lambda^e \, d\mathtt{S} \, \hat{\lambda}^e \\
&= (\delta\hat{\lambda}^e)^\top \left[\hat{B}_\lambda^e \, \hat{r}^e - \hat{B}_{LM}^e \hat{r}_D^e \right] + (\delta\hat{r}^e)^\top (\hat{B}_\lambda^e)^\top \hat{\lambda}^e,
\end{aligned}$$

which assembles to give: $\delta\mathcal{C}_\lambda = (\delta\hat{\lambda})^\top \left[\hat{B}_\lambda \, \hat{r} - \hat{B}_{LM} \hat{r}_D \right] + (\delta\hat{r})^\top (\hat{B}_\lambda)^\top \hat{\lambda}$. Note that $\delta\tilde{r}^e \neq 0$ on $\partial\Omega_D^e$, since the shape function $N_r(\mathtt{S})$ does not necessarily satisfy the Dirichlet boundary condition strongly on $\partial\Omega_D$, instead, these boundary conditions are enforced through Lagrange multipliers. Applying the extended Hamilton's principle, we obtain:

$$\begin{aligned}
\int_{t_1}^{t_2} [\delta(\mathcal{T} - \mathcal{U}) + \delta\mathcal{W}_E - \delta\mathcal{C}_\lambda] \, dt = \delta r^\top [-\hat{M}\ddot{\hat{r}} - \hat{K}_r \hat{r} + \hat{B}_d \hat{u}_d + \hat{b} + \hat{B}_{\tau_N} \hat{\tau}_N - \hat{B}_\lambda^\top \hat{\lambda}] \\
- \delta\lambda^\top [\hat{B}_\lambda \hat{r} - \hat{B}_{LM} \hat{r}_D] = 0.
\end{aligned}$$

So, applying the fundamental lemma of variational calculus to each term above, we obtain:

$$\begin{aligned}
\hat{M}\ddot{\hat{r}} &= -\hat{K}_r \hat{r} + \hat{B}_d \hat{u}_d + \hat{b} + \hat{B}_{\tau_N} \hat{\tau}_N - \hat{B}_\lambda^\top \hat{\lambda}, \\
0 &= \hat{B}_\lambda \hat{r} - \hat{B}_{LM} \hat{r}_D.
\end{aligned}$$

The first equation above (the dynamic equation) and the time derivative of the second equation (the algebraic constraint), along with $\hat{p} = \hat{M}\dot{r}$ and $\hat{e}_p = \hat{M}^{-1}\hat{p} = \dot{\hat{r}}$, define the finite-dimensional PH-DAE as presented in (III.33).

□

Note that this model has the structure of a PLS and it is a DAE system. The inclusion of Lagrange multipliers enables the imposition of Dirichlet boundary conditions as velocities $\hat{v}_D(t)$ on $\partial\Omega_D$, making it suitable for power-preserving interconnection within the PHS framework. Furthermore, the discretized stiffness matrix $\hat{K}_r$ is symmetric and positive semi-definite (not invertible), which could be inconvenient for control design purposes, as discussed later in Chapter IV. Lastly, the Hamiltonian $H_{LM}(\hat{z})$ preserves the structure of the infinite-dimensional PLS in (III.22), where the elastic potential energy is expressed in terms of the differential stiffness operator $\mathcal{K}_r(\cdot)$.

Imposition of Dirichlet boundary conditions via Penalty method

To avoid the resulting DAE system of the previous approach, with the Penalty method proposed in [Babuška 1973b], the Lagrange multiplier is substituted by a penalty factor $\beta_\infty \to \infty$, and the algebraic constraint take the quadratic form $\gamma(r) = \frac{1}{2}(r(\mathtt{S},t) - r_D(\mathtt{S},t)) \cdot (r(\mathtt{S},t) - r_D(\mathtt{S},t))$ on $\partial\Omega_D$. Then, the constraint functional in (III.31) becomes the Penalty functional and takes the form:

$$\mathcal{C}_\lambda(r) = \frac{\beta_\infty}{2} \int_{\partial\Omega_D} (r(\mathtt{S},t) - r_D(\mathtt{S},t)) \cdot (r(\mathtt{S},t) - r_D(\mathtt{S},t))\, d\mathtt{S}. \tag{III.42}$$

Proposition III.2. *The standard FEM discretization of (III.17) based on the extended Hamilton's principle with Penalty method, using local approximations:*

$$\begin{aligned}
&\tilde{r}^e(\mathtt{X},t) = N_r^e(\mathtt{X})\,\hat{r}^e(t), \qquad \delta\tilde{r}^e(\mathtt{X},t) = N_r^e(\mathtt{X})\,\delta\hat{r}^e(t), \qquad r_D^e(\mathtt{S},t) = N_{r_D}^e(\mathtt{S})\,\hat{r}_D^e(t),\\
&u_d^e(\mathtt{X},t) = N_{u_d}^e(\mathtt{X})\,\hat{u}_d^e(t), \qquad \tau_N^e(\mathtt{S},t) = N_{\tau_N}^e(\mathtt{S})\,\hat{\tau}_N^e(t),
\end{aligned}$$

leads to the following finite-dimensional linear PLS:

$$\underbrace{\begin{bmatrix}\dot{\hat{p}}(t)\\ \dot{\hat{r}}(t)\end{bmatrix}}_{\dot{\hat{z}}(t)} = \underbrace{\begin{bmatrix}0 & -I_{N_\Omega}\\ I_{N_\Omega} & 0\end{bmatrix}}_{\hat{J}=-\hat{J}^\top}\underbrace{\begin{bmatrix}\hat{e}_p(t)\\ \hat{e}_r(t)\end{bmatrix}}_{\nabla_{\hat{z}}\hat{H}_{PM}(\hat{z})} + \underbrace{\begin{bmatrix}\hat{B}_d & \hat{B}_{\tau_N} & \hat{B}_{PM}\\ 0 & 0 & 0\end{bmatrix}}_{\hat{G}}\underbrace{\begin{bmatrix}\hat{u}_d(t)\\ \hat{\tau}_N(t)\\ \hat{r}_D(t)\end{bmatrix}}_{\hat{u}(t)} \tag{III.43}$$

$$\begin{aligned}
\hat{y}(t) &= \hat{G}^\top \nabla_{\hat{z}}\hat{H}_{PM}(\hat{z})\\
\hat{H}_{PM}(\hat{z}) &= \frac{1}{2}\,\hat{p}(t)^\top \hat{M}^{-1}\hat{p}(t) + \frac{1}{2}\,\hat{r}(t)^\top \hat{K}_{PM}\,\hat{r}(t) - \hat{r}(t)^\top \hat{b},
\end{aligned} \tag{III.44}$$

where $\hat{p}(t) = \hat{M}\dot{\hat{r}}(t)$ is the discrete generalized momentum, $\hat{e}_r(t) = \hat{K}_{PM}\,\hat{r}(t) - \hat{b}$ is the gradient of the Hamiltonian $\hat{H}_{PM}(\hat{z})$ with respect to $\hat{r}(t)$, and $\hat{K}_{PM} = \hat{K}_r + \hat{K}_\infty$. The other involved matrices are given by:

$$\hat{K}_\infty = \beta_\infty \sum_{e=1}^{n_e} (L_r^e)^\top \int_{\partial\Omega_D^e} N_r^e(\mathtt{S})^\top N_r^e(\mathtt{S})\, d\mathtt{S}\, L_r^e, \tag{III.45}$$

$$\hat{B}_{PM} = \beta_\infty \sum_{e=1}^{n_e} (L_r^e)^\top \int_{\partial\Omega_D^e} N_r^e(\mathtt{S})^\top N_{r_D}^e(\mathtt{S})\, d\mathtt{S}\, L_{r_D}^e. \tag{III.46}$$

Proof. (III.43) is obtained by applying the extended Hamilton's principle with the considered local approximations and penalty functional. Analogous to the proof of Proposition III.1, from kinetic energy, elastic potential energy and virtual work, we obtain:

$$\delta\mathcal{T} = (\delta\dot{\hat{r}})^\top \hat{M}\,\dot{\hat{r}}, \quad \delta\mathcal{U} = (\delta\hat{r})^\top \hat{K}_r\,\hat{r}, \quad \delta\mathcal{W}_E = (\delta\hat{r})^\top \left[\hat{B}_d\,\hat{u}_d + \hat{b} + \hat{B}_{\tau_N}\hat{\tau}_N\right].$$

From the algebraic constraint we obtain: $\delta\mathcal{C}_\lambda^e = \beta_\infty \int_{\partial\Omega_D^e} (\delta\tilde{r}^e)^\top (\tilde{r}^e - \tilde{r}_D)\, d\mathtt{S}$, where $\delta\tilde{r}^e \neq 0$ on $\partial\Omega_D^e$ since the shape function $N_r(\mathtt{S})$ does not necessarily strongly satisfy the Dirichlet boundary condition; instead, these conditions are enforced through the penalty function. Then:

$$\delta\mathcal{C}_\lambda^e = (\delta\hat{r}^e)^\top \beta_\infty \left[\int_{\partial\Omega_D^e} (N_r^e)^\top N_r^e\, d\mathtt{S}\,\hat{r}^e - \int_{\partial\Omega_D^e} (N_r^e)^\top N_{r_D}^e\, d\mathtt{S}\,\hat{r}_D^e\right] = (\delta\hat{r}^e)^\top \left[\hat{K}_\infty^e\,\hat{r}^e - \hat{B}_{PM}^e \hat{r}_D^e\right],$$

which assembles to give: $\delta\mathcal{C}_\lambda = (\delta\hat{r})^\top \left[\hat{K}_\infty \hat{r} - \hat{B}_{PM}\hat{r}_D\right]$. Applying the extended Hamilton's principle, we obtain:

$$\int_{t_1}^{t_2} [\delta(\mathcal{T} - \mathcal{U}) + \delta\mathcal{W}_E - \delta\mathcal{C}_\lambda]\, dt = \\ \delta r^\top [-\hat{M}\ddot{\hat{r}} - (\hat{K}_r + \hat{K}_\infty)\hat{r} + \hat{B}_d\hat{u}_d + \hat{b} + \hat{B}_{\tau_N}\hat{\tau}_N + \hat{B}_{PM}\hat{r}_D] = 0.$$

So, applying the fundamental lemma of variational calculus we obtain the first dynamic equation in (III.43). This equation, along with $\hat{p} = \hat{M}\dot{r}$ and $\hat{e}_p = \hat{M}^{-1}\hat{p} = \dot{\hat{r}}$, define the finite-dimensional PHS as presented in (III.43). □

The model in Proposition III.2 has the structure of an explicit PLS where the Dirichlet boundary conditions are imposed as displacements $\hat{r}_D(t)$ on $\partial\Omega_D$. Unlike the previous case, the boundary inputs $(\hat{\tau}_N, \hat{r}_D)$ are work-conjugated and are not suitable for power-preserving interconnection between subsystems within the PHS framework. If traction is applied as input, the power-conjugate output will be velocity, which does not represent the physical input of the system. Additionally, note that the discretized stiffness matrix $\hat{K}_{PM}$ is symmetric and positive definite (invertible) due the penalty term $\hat{K}_\infty$. However, this term also appears in the Hamiltonian and changes the real energy of the system in case of non-homogeneous Dirichlet boundary conditions. As $\beta_\infty \to \infty$, the matrix $\hat{K}_{PM}$ can become ill-conditioned, which may affect the numerical stability and accuracy [Lu 2019].

III.2.2.d Mixed FEM based on Hellinger-Reissner principle

Mixed FEM formulations based on the Hellinger-Reissner (H-R) variational principle maintain consistency with power-conjugated boundary inputs enforced as tractions and velocities. These approaches are considered as two-fields based formulations because they involve independent variations of the generalized velocity field $e_p(\mathtt{X}, t) = \dot{r}(\mathtt{X}, t) \in \mathbb{R}^n$ and the generalized stress field $e_\epsilon(\mathtt{X}, t) \in \mathbb{R}^m$. In this framework, the generalized strains are expressed as $\epsilon(\mathtt{X}, t) = \mathcal{C}_\epsilon(\mathtt{X}) e_\epsilon(\mathtt{X}, t)$, where $\mathcal{C}_\epsilon(\mathtt{X}) = \mathcal{K}_\epsilon(\mathtt{X})^{-1}$ is the compliance density matrix. These methods offer

improved accuracy for bending-dominated problems, as they are shear-locking free [Yunhua 1998], and also performs well for nearly incompressible materials [Viebahn 2018]. Let us remind you that shear-locking is a numerical issue in FEM that predominantly affects bending-dominated problems, particularly when low-order polynomials are employed in the element's shape functions. It occurs when displacement-based elements inaccurately represent shear deformation, leading to an overestimation of stiffness. This results from the shape functions constraining shear strain and violating kinematic assumptions, ultimately causing an artificially stiff response and reducing accuracy in stress distributions and deformation patterns.

Remark III.2. *For any infinite-dimensional linear mechanical PHS as in* (III.17)*, with* $\mathcal{F}_{\mathtt{x}}$ *of first-order and dimension* $(m \times n)$*, a necessary condition to apply two-fields based mixed FEM approaches is that* $m \geq n$*. See [Zienkiewicz 2005, Chapter 10.4.3] for the details.*

The scheme presented here is built upon the weak form of (III.17) introduced in [Thoma 2022b]. The local weak form (defined in each element) is given by:

$$\delta P_p^e(e_p^e, e_\epsilon^e) = \int_{\Omega^e} \delta e_p^e(\mathtt{X}, t) \cdot (\dot{p}^e(\mathtt{X}, t) + \mathcal{F}_{\mathtt{x}}{}^* e_\epsilon^e(\mathtt{X}, t) - b^e(\mathtt{X}) - B_d u_d^e(\mathtt{X}, t))\, d\mathtt{X} \ldots \tag{III.47}$$
$$\ldots + \int_{\partial\Omega_N^e} \delta e_p^e(\mathtt{S}, t) \cdot (F_\partial(\mathtt{S})\, e_\epsilon^e(\mathtt{S}, t) - \tau_N^e(\mathtt{S}, t))\, d\mathtt{S},$$

$$\delta P_e^e(e_p^e, e_\epsilon^e) = \int_{\Omega^e} \delta e_\epsilon^e(\mathtt{X}, t) \cdot (\dot{\epsilon}^e(\mathtt{X}, t) - \mathcal{F}_{\mathtt{x}} e_p^e(\mathtt{X}, t))\, d\mathtt{X} \ldots \tag{III.48}$$
$$\ldots + \int_{\partial\Omega_D^e} \delta e_\epsilon^e(\mathtt{S}, t) \cdot F_\partial(\mathtt{S})^\top (e_p^e(\mathtt{S}, t) - v_D^e(\mathtt{S}, t))\, d\mathtt{S}.$$

Note that the Dirichlet boundary conditions are weakly imposed through the boundary term in (III.48), where the generalized stress field $e_\epsilon^e(\mathtt{S}, t)$ acts as a Lagrange multiplier to enforce the constraint $F_\partial(\mathtt{S})^\top (e_p^e(\mathtt{S}, t) - v_D^e(\mathtt{S}, t)) = 0$ on $\partial\Omega_D^e$ [Lu 2019]. Additionally, $\delta P_p^e(e_p^e, e_\epsilon^e)$ and $\delta P_e^e(e_p^e, e_\epsilon^e)$ represent the virtual power due to virtual velocities δe_p^e and virtual stresses δe_ϵ^e, respectively.

Theorem III.1. *[Thoma 2022b]. The structure-preserving mixed FEM discretization of* (III.17) *based on the weak formulation* (III.47)−(III.48)*, using local approximations:*

$$\begin{aligned}
&\tilde{e}_p^e(\mathtt{X}, t) = N_r^e(\mathtt{X})\, \hat{e}_p^e(t), \qquad \delta\tilde{e}_p^e(\mathtt{X}, t) = N_r^e(\mathtt{X})\, \delta\hat{e}_p^e(t), \qquad v_D^e(\mathtt{S}, t) = N_{r_D}^e(\mathtt{S})\, \hat{v}_D^e(t),\\
&\tilde{e}_\epsilon^e(\mathtt{X}, t) = N_e^e(\mathtt{X})\, \hat{e}_\epsilon^e(t), \qquad \delta\tilde{e}_\epsilon^e(\mathtt{X}, t) = N_e^e(\mathtt{X})\, \delta\hat{e}_\epsilon^e(t), \qquad \tau_N^e(\mathtt{S}, t) = N_{\tau_N}^e(\mathtt{S})\, \hat{\tau}_N^e(t),\\
&u_d^e(\mathtt{X}, t) = N_{u_d}^e(\mathtt{X})\, \hat{u}_d^e(t),
\end{aligned}$$

leads to the finite-dimensional linear PHS of the form:

$$\underbrace{\begin{bmatrix} \dot{\hat{p}}(t) \\ \dot{\hat{\epsilon}}(t) \\ \dot{\hat{r}}(t) \end{bmatrix}}_{\dot{\hat{x}}(t)} = \underbrace{\begin{bmatrix} 0 & -\hat{F}^\top & -I_{N_\Omega} \\ \hat{F} & 0 & 0 \\ I_{N_\Omega} & 0 & 0 \end{bmatrix}}_{\hat{J}=-\hat{J}^\top} \underbrace{\begin{bmatrix} \hat{e}_p(t) \\ \hat{e}_\epsilon(t) \\ -\hat{b} \end{bmatrix}}_{\nabla_{\hat{x}}\hat{H}_{HR}(\hat{x})} + \underbrace{\begin{bmatrix} \hat{B}_d & \hat{B}_{\tau_N} & 0 \\ 0 & 0 & \hat{B}_{v_D} \\ 0 & 0 & 0 \end{bmatrix}}_{\hat{G}} \underbrace{\begin{bmatrix} \hat{u}_d(t) \\ \hat{\tau}_N(t) \\ \hat{v}_D(t) \end{bmatrix}}_{\hat{u}(t)} \tag{III.49}$$

$$\begin{aligned}\hat{y}(t) &= \hat{G}^\top \nabla_{\hat{x}} \hat{H}_{HR}(\hat{x}) \\ \hat{H}_{HR}(\hat{x}) &= \frac{1}{2}\,\hat{p}(t)^\top \hat{M}^{-1}\hat{p}(t) + \frac{1}{2}\,\hat{\epsilon}(t)^\top \hat{C}_\epsilon^{-1}\,\hat{\epsilon}(t) - \hat{r}(t)^\top \hat{b},\end{aligned} \tag{III.50}$$

where $\hat{p}(t) = \hat{M}\hat{e}_p(t)$ *is the discrete generalized momentum,* $\hat{\epsilon}(t) = \hat{C}_\epsilon\,\hat{e}_\epsilon(t)$ *is the discrete generalized strain,* $\hat{F}$ *is the discretized differential operator, and* $\hat{C}_\epsilon$ *is the discrete compliance matrix. The other involved matrices are given by:*

$$\hat{C}_\epsilon = \sum_{e=1}^{n_e} (L_e^e)^\top \int_{\Omega^e} N_e^e(\mathtt{X})^\top \mathcal{K}_\epsilon(\mathtt{X})^{-1} N_e^e(\mathtt{X})\, d\mathtt{X}\, L_e^e, \tag{III.51}$$

$$\hat{F}^\top = \sum_{e=1}^{n_e} (L_r^e)^\top \left(\int_{\Omega^e} (\mathcal{F}_{\mathtt{x}} N_r^e(\mathtt{X}))^\top N_e^e(\mathtt{X})\, d\mathtt{X} - \int_{\partial\Omega_D^e} N_r^e(\mathtt{S})^\top F_\partial(\mathtt{S}) N_e^e(\mathtt{S})\, d\mathtt{S} \right) L_e^e, \tag{III.52}$$

$$\hat{B}_{v_D} = \sum_{e=1}^{n_e} (L_e^e)^\top \int_{\partial\Omega_D^e} N_e^e(\mathtt{S})^\top F_\partial(\mathtt{S})^\top N_{r_D}^e(\mathtt{S})\, d\mathtt{S}\, L_{r_D}^e. \tag{III.53}$$

Proof. (III.49) is obtained by replacing the considered local approximations into the weak formulation (III.47)−(III.48). For the details refer to [Thoma 2022b]. □

The Hamiltonian $H_{HR}(\hat{x})$ preserved in this finite-dimensional model aligns with that of the infinite-dimensional PHS in (III.18), where the elastic potential energy is quadratic in the generalized strains $\epsilon(t)$. Although $\hat{C}_\epsilon$ is symmetric and positive definite, expressing the elastic potential energy in terms of generalized strains $\hat{\epsilon}(t)$ poses additional challenges for energy-based shape control design, since the desired shapes are expressed in terms of the displacements. To address this issue, the following proposition introduces a condensation process that reformulates the elastic potential energy in terms of generalized displacements, providing a more suitable framework for energy-based shape control applications.

Proposition III.3. *The finite-dimensional linear PHS in Theorem III.1 leads to the following finite-dimensional linear PLS:*

$$\underbrace{\begin{bmatrix}\dot{\hat{p}}(t)\\ \dot{\hat{r}}(t)\end{bmatrix}}_{\dot{\hat{z}}(t)} = \underbrace{\begin{bmatrix}0 & -I_{N_\Omega}\\ I_{N_\Omega} & 0\end{bmatrix}}_{\hat{J}=-\hat{J}^\top} \underbrace{\begin{bmatrix}\hat{e}_p(t)\\ \hat{e}_r(t)\end{bmatrix}}_{\nabla_{\hat{z}}\hat{H}_{HR}(\hat{z})} + \underbrace{\begin{bmatrix}\hat{B}_d & \hat{B}_{\tau_N} & \hat{B}_{HR}\\ 0 & 0 & 0\end{bmatrix}}_{\hat{G}} \underbrace{\begin{bmatrix}\hat{u}_d(t)\\ \hat{\tau}_N(t)\\ \hat{r}_D(t)\end{bmatrix}}_{\hat{u}(t)} \tag{III.54}$$

$$\begin{aligned}\hat{y}(t) &= \hat{G}^\top \nabla_{\hat{z}} \hat{H}_{HR}(\hat{z}) \\ \hat{H}_{HR}(\hat{z}) &= \frac{1}{2}\,\hat{p}(t)^\top \hat{M}^{-1}\hat{p}(t) + \frac{1}{2}\,\hat{r}(t)^\top \hat{K}_{HR}\,\hat{r}(t) - \hat{r}(t)^\top \hat{b},\end{aligned} \tag{III.55}$$

where $\hat{e}_r(t) = \hat{K}_{HR}\,\hat{r}(t) - \hat{b}$, $\hat{K}_{HR} = \hat{F}^\top \hat{C}_\epsilon^{-1}\hat{F}$, *and* $\hat{B}_{HR} = -\hat{F}^\top \hat{C}_\epsilon^{-1}\hat{B}_{v_D}$.

Proof. From (III.49) we have: $\dot{\hat{\epsilon}}(t) = \hat{F}\,\hat{e}_p(t) + \hat{B}_{v_D}\hat{v}_D(t)$, where integrating with respect to time we get: $\hat{\epsilon}(t) = \hat{F}\,\hat{r}(t) + \hat{B}_{v_D}\hat{r}_D(t)$, then $\hat{e}_\epsilon(t) = \hat{C}_\epsilon^{-1}\hat{\epsilon}(t) = \hat{C}_\epsilon^{-1}(\hat{F}\,\hat{r}(t) + \hat{B}_{v_D}\hat{r}_D(t))$. Replacing the above into the first equation of (III.49) we

obtain:

$$\begin{aligned}\dot{\hat{p}}(t) &= -\hat{F}^\top(\hat{C}_\epsilon^{-1}\,\hat{F}\,\hat{r}(t) + \hat{C}_\epsilon^{-1}\hat{B}_{v_D}\hat{r}_D(t)) + \hat{b} + \hat{B}_d\,\hat{u}_d(t) + \hat{B}_{\tau_N}\hat{\tau}_N(t)\\ &= -\hat{K}_{HR}\,\hat{r}(t) + \hat{b} + \hat{B}_d\,\hat{u}_d(t) + \hat{B}_{\tau_N}\hat{\tau}_N(t) + \hat{B}_{HR}\,\hat{r}_D(t)\\ &= -\hat{e}_r(t) + \hat{B}_d\,\hat{u}_d(t) + \hat{B}_{\tau_N}\hat{\tau}_N(t) + \hat{B}_{HR}\,\hat{r}_D(t),\end{aligned}$$

where the last line above corresponds to the first equation of (III.54). Regarding the Hamiltonian, replacing $\hat{\epsilon}(t) = \hat{F}\,\hat{r}(t) + \hat{B}_{v_D}\hat{r}_D(t)$ into (III.50) we obtain:

$$\begin{aligned}\hat{H}_{HR}(\hat{x}) &= \frac{1}{2}\,\hat{p}(t)^\top\hat{M}^{-1}\hat{p}(t) + \frac{1}{2}\begin{bmatrix}\hat{r}(t)\\ \hat{r}_D(t)\end{bmatrix}^\top\begin{bmatrix}\hat{K}_{HR} & -\hat{B}_{HR}\\ -\hat{B}_{HR}^\top & \hat{V}_{HR}\end{bmatrix}\begin{bmatrix}\hat{r}(t)\\ \hat{r}_D(t)\end{bmatrix},\\ &= \hat{H}_{HR}(\hat{z}) + \hat{E}_{HR}(\hat{r},\hat{r}_D),\end{aligned}$$

with $\hat{E}_{HR}(\hat{r},\hat{r}_D) = \frac{1}{2}\hat{r}_D(t)^\top\hat{V}_{HR}\,\hat{r}_D(t) - \hat{r}(t)^\top\hat{B}_{HR}\,\hat{r}_D(t)$, and $\hat{V}_{HR} = \hat{B}_{v_D}^\top\hat{C}_\epsilon^{-1}\hat{B}_{v_D}$. □

Note that when $\hat{r}_D(t) = 0 \to \hat{E}_{HR}(\hat{r},\hat{r}_D) = 0$, then $\hat{H}_{HR}(\hat{x}) = \hat{H}_{HR}(\hat{z})$. Additionally, $\hat{K}_{HR}$ is symmetric and, depending on the model and the choice of shape functions, can be positive semi-definite (non-invertible), as $\hat{F}$ might lose rank due to the weak imposition of the Dirichlet boundary conditions. Therefore, even after the condensation process, the model from Proposition III.3 may not be suitable for energy-based shape control design.

III.2.2.e Summary of revised FEM approaches

The summary of the different approaches discussed is provided in the following Table III.1. The table presents key properties and characteristics of the respective FEM approach, including type of system, boundary inputs, elastic potential energy formulation, and stiffness matrix properties.

Property	sFEM (LM)	sFEM (Penalty)	mFEM (H-R)
1. Type of system	DAE system	ODE system	ODE system
2. Boundary inputs	Power-conjugated	Work-conjugated	Power-conjugated
3. Elastic energy	In terms of $\hat{r}(t)$	In terms of $\hat{r}(t)$	In terms of $\hat{\epsilon}(t)$
4. Stiffness matrix	$\hat{K}_{LM}$ non-invertible	$\hat{K}_{PM}$ invertible but may become ill-conditioned	$\hat{K}_{HR}$ could be non-invertible

Table III.1 – Summary of revised FEM approaches.

Motivated by the need for models that are suitable for shape control design, the following section introduces a mixed FEM scheme for the structure-preserving discretization of linear PHS, using the modified Linked Lagrange Multiplier (mLLM) method. This approach integrates features from the previously discussed methods, with key characteristics summarized as follows: 1. Type of system: ODE system, 2. Boundary inputs: Power-conjugated, 3. Elastic energy: In terms of $\hat{r}(t)$ and $\hat{\epsilon}(t)$, 4. Stiffness matrix: $\hat{K}_{LLM}$ invertible and well-conditioned.

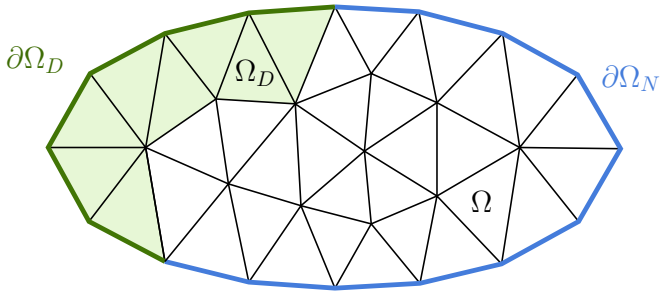

Figure III.3 – Spatial domain Ω, Dirichlet domain Ω_D, Dirichlet boundary $\partial\Omega_D$ and Neumann boundary $\partial\Omega_N$.

III.3 Mixed finite element discretization

In this section, we propose structure-preserving mixed FEM schemes. We begin with the linear case by introducing a scheme based on the modified Linked Lagrange Multiplier (mLLM) method, which shares characteristics with both standard and mixed FEM approaches derived from Hamilton's principle and the Hellinger-Reissner formulation. Subsequently, to address both geometrical and material nonlinearities, we present a different scheme based on the generalized Hamilton's principle (GHP), which is then extended to incorporate algebraic constraints.

III.3.1 Linear systems

The mLLM method is a mixed FEM strategy that allows us to impose non-homogeneous Dirichlet boundary conditions in linear elastostatic systems [Baiges 2012]. Similar to Hamilton's principle, it expresses the elastic potential energy in terms of generalized displacements. In line with the Hellinger-Reissner principle, it also involves independent variations of the generalized stress field, serving as a Lagrange multiplier to enforce a boundary constraint on $\partial\Omega_D$. To ensure symmetry, an additional term is introduced, representing the weak imposition of the constitutive law. This term links both displacement and stress fields near the Dirichlet boundary (within Ω_D) in a least-squares sense [Lu 2019]. Here, $\Omega_D \subset \Omega$ refers to the Dirichlet domain, encompassing all finite elements that share nodes with the Dirichlet boundary $\partial\Omega_D$. For an illustration see Fig. III.3.

Following the mLLM method and adding the dynamic terms, the local weak form of the infinite-dimensional linear PHS in (III.17) is given by:

$$\begin{aligned}\delta P_p^e(\dot{r}^e, e_\epsilon^e) = &\int_{\Omega^e} \delta\dot{r}^e(\mathtt{X},t)\cdot(\dot{p}^e(\mathtt{X},t) + \mathcal{F}_{\mathtt{x}}{}^* e_\epsilon^e(\mathtt{X},t) - b^e(\mathtt{X}) - B_d u_d^e(\mathtt{X},t))\, d\mathtt{X} \ldots \\ &\ldots + \int_{\partial\Omega_N^e} \delta\dot{r}^e(\mathtt{S},t)\cdot(F_\partial(\mathtt{S}) e_\epsilon^e(\mathtt{S},t) - \tau_N^e(\mathtt{S},t))\, d\mathtt{S} \ldots \\ &\ldots + \frac{1}{\beta}\int_{\Omega_D^e} \delta\dot{\epsilon}^e(\mathtt{X},t)\cdot(e_\epsilon^e(\mathtt{X},t) - \mathcal{K}_\epsilon(\mathtt{X})\,\epsilon^e(\mathtt{X},t))\, d\mathtt{X},\end{aligned} \tag{III.56}$$

$$\delta P_e^e(\dot{r}^e, e_\epsilon^e) = \frac{1}{\beta}\int_{\Omega_D^e} \delta e_\epsilon^e(\mathtt{X},t)\cdot(\dot{\epsilon}^e(\mathtt{X},t) - \mathcal{F}_{\mathtt{x}}\dot{r}^e(\mathtt{X},t))\,d\mathtt{X}... \tag{III.57}$$
$$... + \int_{\partial\Omega_D^e} \delta e_\epsilon^e(\mathtt{S},t)\cdot F_\partial(\mathtt{S})^\top(\dot{r}^e(\mathtt{S},t) - v_D^e(\mathtt{S},t))\,d\mathtt{S},$$

where $\beta > 1$ is the link factor. Additionally, the Hamiltonian in each element is written as:

$$H^e(\dot{r}^e, r^e, e_\epsilon^e) = T^e(\dot{r}^e) + U_T^e(r^e) + \Delta U_{\Omega_D^e}^e(r^e, e_\epsilon^e), \tag{III.58}$$

where $T^e(\dot{r}^e)$ and $U_T^e(r^e)$ represent the kinetic energy and total elastic potential energy, respectively, and $\Delta U_{\Omega_D^e}^e(r^e, e_\epsilon^e)$ represent the linked elastic potential energy on Ω_D, which is given by:

$$\Delta U_{\Omega_D^e}^e(r^e, e_\epsilon^e) = \frac{1}{\beta}\left[U^e(e_\epsilon^e) - U^e(r^e)\right]_{\Omega_D^e} = 0, \tag{III.59}$$

with $U^e(r^e)$ the elastic potential energy expressed in terms of $r(\mathtt{X},t)$ (as in Hamilton's principle), and $U^e(e_\epsilon^e)$ the elastic potential energy expressed in terms of $e_\epsilon(\mathtt{X},t)$ and the compliance density matrix $\mathcal{C}_\epsilon(\mathtt{X}) = \mathcal{K}_\epsilon(\mathtt{X})^{-1}$ (as in the Hellinger-Reissner principle).

Remark III.3. *The mLLM method has been proven to be stable for any link factor $\beta > 1$ under the following conditions [Codina 2015]: a) when the shape functions pairs $N_r^e(\mathtt{X})$ and $N_e^e(\mathtt{X})$ are of equal order, and b) when they are piecewise linear and piecewise constant, respectively.*

Theorem III.2. *The structure-preserving mixed FEM discretization of (III.17) based on the weak formulation (III.56)−(III.57) and Hamiltonian (III.58), using local approximations:*

$$\begin{aligned}
&\tilde{r}^e(\mathtt{X},t) = N_r^e(\mathtt{X})\,\hat{r}^e(t), \quad && \delta\tilde{r}^e(\mathtt{X},t) = N_r^e(\mathtt{X})\,\delta\hat{r}^e(t), \quad && v_D^e(\mathtt{S},t) = N_{r_D}^e(\mathtt{S})\,\hat{v}_D^e(t),\\
&\tilde{e}_\epsilon^e(\mathtt{X},t) = N_e^e(\mathtt{X})\,\hat{e}_{\epsilon_D}^e(t), \quad && \delta\tilde{e}_\epsilon^e(\mathtt{X},t) = N_e^e(\mathtt{X})\,\delta\hat{e}_{\epsilon_D}^e(t), \quad && \tau_N^e(\mathtt{S},t) = N_{\tau_N}^e(\mathtt{S})\,\hat{\tau}_N^e(t),\\
&u_d^e(\mathtt{X},t) = N_{u_d}^e(\mathtt{X})\,\hat{u}_d^e(t),
\end{aligned}$$

with $\hat{e}_{\epsilon_D}^e(t) \in \mathbb{R}^{mNN^e}$ the local generalized stress vector only defined on Ω_D^e, leads to the finite-dimensional linear PHS of the form:

$$\underbrace{\begin{bmatrix}\dot{\hat{p}}(t)\\ \dot{\hat{\epsilon}}_D(t)\\ \dot{\hat{r}}(t)\end{bmatrix}}_{\dot{\hat{x}}(t)} = \underbrace{\begin{bmatrix}0 & -\hat{F}_D^\top & -I_{N_\Omega}\\ \hat{F}_D & 0 & 0\\ I_{N_\Omega} & 0 & 0\end{bmatrix}}_{\hat{J}=-\hat{J}^\top}\underbrace{\begin{bmatrix}\hat{e}_p(t)\\ \hat{e}_{\epsilon_D}(t)\\ \hat{e}_r(t)\end{bmatrix}}_{\nabla_{\hat{x}}\hat{H}_{LLM}(\hat{x})} + \underbrace{\begin{bmatrix}\hat{B}_d & \hat{B}_{\tau_N} & 0\\ 0 & 0 & \hat{B}_D\\ 0 & 0 & 0\end{bmatrix}}_{\hat{G}}\underbrace{\begin{bmatrix}\hat{u}_d(t)\\ \hat{\tau}_N(t)\\ \hat{v}_D(t)\end{bmatrix}}_{\hat{u}(t)} \tag{III.60}$$
$$\hat{y}(t) = \hat{G}^\top\nabla_{\hat{x}}\hat{H}_{LLM}(\hat{x})$$

$$\hat{H}_{LLM}(\hat{x}) = \frac{1}{2}\hat{p}(t)^\top\hat{M}^{-1}\hat{p}(t) + \frac{1}{2}\hat{r}(t)^\top\hat{K}_r\,\hat{r}(t) - \hat{r}(t)^\top\hat{b} + \Delta\hat{U}_{\Omega_D}(\hat{r},\hat{\epsilon}_D), \tag{III.61}$$

$$\Delta\hat{U}_{\Omega_D}(\hat{r},\hat{\epsilon}_D) = \frac{1}{2}\hat{\epsilon}_D(t)^\top\hat{C}_{\epsilon_D}^{-1}\,\hat{\epsilon}_D(t) - \frac{1}{2}\hat{r}(t)^\top\hat{K}_D\,\hat{r}(t), \tag{III.62}$$

where $\hat{p}(t) = \hat{M}\dot{\hat{r}}(t)$ and $\hat{\epsilon}_D(t) = \hat{C}_{\epsilon_D}\,\hat{e}_{\epsilon_D}(t)$ are the discrete generalized momentum and strain variables, and $\hat{e}_r(t) = (\hat{K}_r - \hat{K}_D)\,\hat{r}(t) - \hat{b}$ is the gradient of $\hat{H}_{LLM}(\hat{x})$ with respect to $\hat{r}(t)$. The other involved matrices are given by:

$$\hat{C}_{\epsilon_D} = \sum_{e=1}^{n_e} (L_D^e)^\top \frac{1}{\beta} \int_{\Omega_D^e} N_e^e(\mathtt{X})^\top \mathcal{K}_\epsilon(\mathtt{X})^{-1} N_e^e(\mathtt{X})\, d\mathtt{X}\, L_D^e, \tag{III.63}$$

$$\hat{K}_D = \sum_{e=1}^{n_e} (L_r^e)^\top \frac{1}{\beta} \int_{\Omega_D^e} (\mathcal{F}_\mathtt{x} N_r^e(\mathtt{X}))^\top \mathcal{K}_\epsilon(\mathtt{X}) (\mathcal{F}_\mathtt{x} N_r^e(\mathtt{X}))\, d\mathtt{X}\, L_r^e, \tag{III.64}$$

$$\hat{F}_D^\top = \sum_{e=1}^{n_e} (L_r^e)^\top \left(\frac{1}{\beta} \int_{\Omega_D^e} (\mathcal{F}_\mathtt{x} N_r^e(\mathtt{X}))^\top N_e^e(\mathtt{X})\, d\mathtt{X} - \int_{\partial\Omega_D^e} N_r^e(\mathtt{S})^\top F_\partial(\mathtt{S}) N_e^e(\mathtt{S})\, d\mathtt{S} \right) L_D^e, \tag{III.65}$$

$$\hat{B}_D = \sum_{e=1}^{n_e} (L_D^e)^\top \int_{\partial\Omega_D^e} N_e^e(\mathtt{S})^\top F_\partial(\mathtt{S})^\top N_{r_D}^e(\mathtt{S})\, d\mathtt{S}\, L_{r_D}^e, \tag{III.66}$$

where $L_D^e \in \mathbb{R}^{mNN^e \times mNN_{\Omega_D}}$ is a location (assembly) matrix and NN_{Ω_D} is the total number of nodes on Ω_D.

Proof. For simplicity the spatial and temporal dependencies are omitted. From $\delta P_p^e(\dot{r}^e, e_\epsilon^e)$ in (III.56) and the integration lemma in (III.15) we have:

$$\int_{\Omega^e} \delta\dot{\tilde{r}}^e \cdot \mathcal{F}_\mathtt{x}{}^* \tilde{e}_\epsilon^e\, d\mathtt{X} = \int_{\Omega^e} \tilde{e}_\epsilon^e \cdot \mathcal{F}_\mathtt{x}\, \delta\dot{\tilde{r}}^e\, d\mathtt{X} - \left(\int_{\partial\Omega_D^e} \delta\dot{\tilde{r}}^e \cdot F_\partial\, \tilde{e}_\epsilon^e d\mathtt{S} + \int_{\partial\Omega_N^e} \delta\dot{\tilde{r}}^e \cdot F_\partial\, \tilde{e}_\epsilon^e d\mathtt{S} \right),$$

where replacing the above expression in (III.56) we obtain:

$$\begin{aligned} \delta P_p^e = (\delta\dot{\hat{r}}^e)^\top \Bigg[& \int_{\Omega^e} (N_r^e)^\top \mathcal{M} N_r^e\, d\mathtt{X}\, \ddot{\hat{r}}^e - \int_{\Omega^e} (N_r^e)^\top B_d\, N_{u_d}^e\, d\mathtt{X}\, \hat{u}_d^e - \int_{\Omega^e} (N_r^e)^\top b^e\, d\mathtt{X} \ldots \\ \ldots + & \left(\frac{1}{\beta} \int_{\Omega_D^e} (\mathcal{F}_\mathtt{x} N_r^e)^\top N_e^e\, d\mathtt{X} - \int_{\partial\Omega_D^e} (N_r^e)^\top F_\partial\, N_e^e\, d\mathtt{S} \right) \hat{e}_{\epsilon_D}^e - \int_{\partial\Omega_N^e} (N_r^e)^\top N_{\tau_N}^e d\mathtt{S}\, \hat{\tau}_N^e \ldots \\ & \ldots + \left(\int_{\Omega^e} (\mathcal{F}_\mathtt{x} N_r^e)^\top \mathcal{K}_\epsilon (\mathcal{F}_\mathtt{x} N_r^e)\, d\mathtt{X} - \frac{1}{\beta} \int_{\Omega_D^e} (\mathcal{F}_\mathtt{x} N_r^e)^\top \mathcal{K}_\epsilon (\mathcal{F}_\mathtt{x} N_r^e)\, d\mathtt{X} \right) \hat{r}^e \Bigg]. \end{aligned}$$

Assembling using the location matrices, the global form of (III.56) becomes $\delta P_p = \sum_{e=1}^{n_e} \delta P_p^e = 0$ and is given by:

$$\delta P_p = \delta\dot{\hat{r}}^\top [\hat{M}\ddot{\hat{r}} - \hat{B}_d\, \hat{u}_d - \hat{b} + \hat{F}_D^\top\, \hat{e}_{\epsilon_D} - \hat{B}_{\tau_N} \hat{\tau}_N + (\hat{K}_r - \hat{K}_D)\, \hat{r}] = 0. \tag{III.67}$$

Similarly, $\delta P_e = \sum_{e=1}^{n_e} \delta P_e^e = 0$ is given by:

$$\delta P_e = \delta\hat{e}_{\epsilon_D}^\top [\hat{C}_{\epsilon_D} \dot{\hat{e}}_{\epsilon_D} - \hat{F}_D\, \dot{\hat{r}} - \hat{B}_D \hat{v}_D] = 0, \tag{III.68}$$

and the total energy $\hat{H}(\dot{\hat{r}}, \hat{r}, \hat{e}_{\epsilon_D}) = \sum_{e=1}^{n_e} \hat{H}^e(\dot{\hat{r}}^e, \hat{r}^e, \hat{e}_{\epsilon_D}^e)$ is expressed according to (III.58) as:

$$\hat{H}(\dot{\hat{r}}, \hat{r}, \hat{e}_{\epsilon_D}) = \frac{1}{2}\, \dot{\hat{r}}^\top \hat{M}\, \dot{\hat{r}} + \frac{1}{2}\, \hat{e}_{\epsilon_D}^\top \hat{C}_{\epsilon_D}\, \hat{e}_{\epsilon_D} + \frac{1}{2}\, \hat{r}^\top (\hat{K}_r - \hat{K}_D)\, \hat{r} - \hat{r}^\top \hat{b}. \tag{III.69}$$

Finally, $\hat{p} = \hat{M}\dot{\hat{r}}$, $\hat{\epsilon}_D = \hat{C}_{\epsilon_D} \hat{e}_{\epsilon_D}$, $\hat{e}_p = \dot{\hat{r}}$ and the Hamiltonian in (III.69) define the finite-dimensional PHS of Theorem III.2. □

In the finite-dimensional PHS from Theorem III.2, only $\hat{p}(t)$, $\hat{r}(t)$, $\hat{M}$ and $\hat{K}_r$ are defined over the entire domain Ω, while $\hat{\epsilon}_D(t)$, $\hat{K}_D$, $\hat{C}_{\epsilon_D}$ and $\hat{F}_D$ are defined over $\Omega_D \subset \Omega$. Also, note that $\hat{\epsilon}_D(t)$ allows the imposition of boundary velocities $\hat{v}_D(t)$ in the same manner as in the Hellinger-Reissner principle, $\hat{\epsilon}_D(t)$ being the generalized strains on Ω_D scaled by $1/\beta$. Lastly, from (III.62) we have that $\Delta\hat{U}_{\Omega_D}(\hat{r}, \hat{\epsilon}_D) \approx 0$, so $\hat{H}_{LLM}(\hat{x}) \approx \hat{H}_{LM}(\hat{z})$, with equality achieved only when $\Delta\hat{U}_{\Omega_D}(\hat{r}, \hat{\epsilon}_D) = 0$.

In the next Proposition III.4 we present the finite-dimensional PLS that admits Dirichlet boundary conditions imposed as displacements $\hat{r}_D(t)$ on $\partial\Omega_D$. Similar to Proposition III.3, when $\hat{r}_D(t) = 0 \rightarrow \hat{E}_{LLM}(\hat{r}, \hat{r}_D) = 0$, then $\hat{H}_{LLM}(\hat{x}) = \hat{H}_{LLM}(\hat{z})$. Additionally, the (condensated) stiffness matrix $\hat{K}_{LLM}$ is symmetric and positive definite (invertible) due to the link matrix $\hat{K}_D$, so this model is convenient for energy-based shape control design. Furthermore, since it is not necessary to choose $\beta \rightarrow \infty$, the discrete stiffness matrix $\hat{K}_{LLM}$ will not be ill-conditioned.

Proposition III.4. *The finite-dimensional linear PHS in Theorem III.2 leads to the following finite-dimensional linear PLS:*

$$\underbrace{\begin{bmatrix}\dot{\hat{p}}(t)\\ \dot{\hat{r}}(t)\end{bmatrix}}_{\dot{\hat{z}}(t)} = \underbrace{\begin{bmatrix}0 & -I_{N_\Omega}\\ I_{N_\Omega} & 0\end{bmatrix}}_{\hat{J}=-\hat{J}^\top} \underbrace{\begin{bmatrix}\hat{e}_p(t)\\ \hat{e}_r(t)\end{bmatrix}}_{\nabla_{\hat{z}}\hat{H}_{LLM}(\hat{z})} + \underbrace{\begin{bmatrix}\hat{B}_d & \hat{B}_{\tau_N} & \hat{B}_{LLM}\\ 0 & 0 & 0\end{bmatrix}}_{\hat{G}} \underbrace{\begin{bmatrix}\hat{u}_d(t)\\ \hat{\tau}_N(t)\\ \hat{r}_D(t)\end{bmatrix}}_{\hat{u}(t)} \tag{III.70}$$

$$\hat{y}(t) = \hat{G}^\top \nabla_{\hat{z}}\hat{H}_{LLM}(\hat{z})$$

$$\hat{H}_{LLM}(\hat{z}) = \frac{1}{2}\hat{p}(t)^\top \hat{M}^{-1}\hat{p}(t) + \frac{1}{2}\hat{r}(t)^\top \hat{K}_{LLM}\,\hat{r}(t) - \hat{r}(t)^\top \hat{b}, \tag{III.71}$$

where $\hat{e}_r(t) = \hat{K}_{LLM}\,\hat{r}(t) - \hat{b}$, $\hat{K}_{LLM} = (\hat{K}_r - \hat{K}_D + \hat{F}_D^\top \hat{C}_{\epsilon_D}^{-1}\hat{F}_D)$, *and* $\hat{B}_{LLM} = -\hat{F}_D^\top \hat{C}_{\epsilon_D}^{-1}\hat{B}_D$. *The relation between* $\hat{H}_{LLM}(\hat{x})$ *and* $\hat{H}_{LLM}(\hat{z})$ *is given by:*

$$\hat{H}_{LLM}(\hat{x}) = \hat{H}_{LLM}(\hat{z}) + \hat{E}_{LLM}(\hat{r}, \hat{r}_D), \tag{III.72}$$

where $\hat{E}_{LLM}(\hat{r}, \hat{r}_D) = \frac{1}{2}\hat{r}_D(t)^\top \hat{B}_{LLM}\,\hat{r}_D(t) - \hat{r}(t)^\top \hat{V}_{LLM}\,\hat{r}_D(t)$, *and* $\hat{V}_{LLM} = \hat{B}_D^\top \hat{C}_{\epsilon_D}^{-1}\hat{B}_D$.

Proof. The proof is analogous to the proof of Proposition III.3. □

It is worth mentioning that the Hellinger-Reissner-based mixed FEM approach [Thoma 2022b] has been effectively used for the structure-preserving discretization of geometrically nonlinear PHS, as demonstrated in [Thoma 2022a]. Similarly, the proposed mixed FEM approach based on the mLLM method can be extended for structure-preserving discretization of geometrically nonlinear PHS as well. However, it is important to note that neither the Hellinger-Reissner-based method nor the mLLM-based approach are suitable for discretizing materially nonlinear PHS. This is because materially nonlinear systems lack a well-defined stiffness density matrix $\mathcal{K}_\epsilon(\mathtt{X})$, making it impossible to establish a compliance density matrix $\mathcal{C}_\epsilon(\mathtt{X}) = \mathcal{K}_\epsilon(\mathtt{X})^{-1}$, which is crucial for applying the mixed FEM approaches discussed in this section. To address this limitation, in the next section we propose

a structure-preserving mixed FEM approach based on the generalized Hamilton's principle [Yi-Yuan 1964], which generalizes the Hu-Washizu variational principle used in elastostatics and Hamilton's principle used in elastodynamics.

III.3.2 Nonlinear systems

This section proposes a Total Lagrangian FEM approach for discretizing nonlinear PHS, where models are described in material coordinates and referred to the reference configuration. In this method, matrices are integrated over the reference domain. The Updated Lagrangian FEM, by contrast, recalculates the current configuration at each step and integrates over the current spatial domain; however, it is not addressed here. We adopt the Total Lagrangian approach since our models are inherently formulated in this framework. Applying the Updated Lagrangian approach would require all quantities to be referred to the current configuration, and it remains unclear whether the PHS structure would be preserved in both the infinite and finite-dimensional settings [Roze 2024], necessitating further investigation. Numerically, the Total Lagrangian method offers more stability for large deformations by avoiding the need to frequently update the configuration, though it can be more computationally expensive for incremental updates. Conversely, the Updated Lagrangian method efficiently handles incremental deformations but can encounter numerical instability in geometrically nonlinear problems [Belytschko 2014, Chapters 2, 4, and 6].

To begin, we recall the definition of non-constant differential operators and their integration by parts lemma, along with the class of nonlinear PHS considered.

Definition I.1. *Let* $\mathtt{X} = \{X_1, ..., X_\ell\}$ *be a set of orthogonal coordinate axes,* $\Omega \subset \mathbb{R}^\ell$ *an open set,* $w(\mathtt{X}) \in \mathbb{R}^n$ *and* $v(\mathtt{X}) \in \mathbb{R}^m$ *two smooth vector functions with compact support on* Ω*. The first order nonlinear differential operator* $\mathcal{F}_\mathtt{x}$ *and its formal adjoint* ${\mathcal{F}_\mathtt{x}}^*$ *are defined as:*

$$\mathcal{F}_\mathtt{x} w(\mathtt{X}) = F_0(\mathtt{X}) w(\mathtt{X}) + \textstyle\sum_{k=1}^{\ell} F_k(\mathtt{X}) \partial_k w(\mathtt{X}), \tag{I.50}$$

$${\mathcal{F}_\mathtt{x}}^* v(\mathtt{X}) = F_0(\mathtt{X})^\top v(\mathtt{X}) - \textstyle\sum_{k=1}^{\ell} \partial_k \left(F_k(\mathtt{X})^\top v(\mathtt{X}) \right), \tag{I.51}$$

with $\partial_k = \partial / \partial X_k$*,* $F_0(\mathtt{X}) \in \mathbb{R}^{m \times n}$ *and* $F_k(\mathtt{X}) \in \mathbb{R}^{m \times n}$ *real matrices.*

Lemma II.2. *Consider Definition I.1, the open set* $\Omega \subset \mathbb{R}^\ell$*, its boundary* $\partial\Omega$*, and the closure* $\bar{\Omega} = \Omega \cup \partial\Omega$*. Then, for any pair of smooth functions* $v(\mathtt{X}) \in \mathbb{R}^m$ *and* $w(\mathtt{X}) \in \mathbb{R}^n$ *defined on* $\bar{\Omega}$*, we have that:*

$$\int_\Omega \left(v(\mathtt{X})^\top \mathcal{F}_\mathtt{x}\, w(\mathtt{X}) - w(\mathtt{X})^\top {\mathcal{F}_\mathtt{x}}^* v(\mathtt{X}) \right) d\mathtt{X} = \int_{\partial\Omega} w(\mathtt{S})^\top F_\partial(\mathtt{S})\, v(\mathtt{S})\, d\mathtt{S}, \tag{II.85}$$

where $F_\partial(\mathtt{S}) \in \mathbb{R}^{n \times m}$ *is defined as:*

$$F_\partial(\mathtt{S}) = \textstyle\sum_{k=1}^{\ell} F_k(\mathtt{S})^\top \hat{n}_k(\mathtt{S}), \tag{II.86}$$

with $\hat{n}_k(\mathtt{S})$ *the* k*-component of the outward unit normal vector to the boundary* $\partial\Omega$ *projected on the coordinate axis* X_k*.*

(From Theorem II.2.) Let $x(\mathtt{X},t) = [p(\mathtt{X},t)^\top\ \epsilon(\mathtt{X},t)^\top\ r(\mathtt{X},t)^\top]^\top \in \mathbb{R}^{2n+m}$ be the energy variables, and $\delta_x H(x) = [e_p(\mathtt{X},t)^\top\ e_\epsilon(\mathtt{X},t)^\top\ -b(\mathtt{X})^\top]^\top \in \mathbb{R}^{2n+m}$ be the co-energy variables. The system's dynamics defines an infinite-dimensional nonlinear PHS of the form:

$$\begin{aligned}\underbrace{\begin{bmatrix}\dot{p}(\mathtt{X},t)\\ \dot{\epsilon}(\mathtt{X},t)\\ \dot{r}(\mathtt{X},t)\end{bmatrix}}_{\dot{x}} &= \underbrace{\begin{bmatrix}0 & -\mathcal{F}_{\mathtt{x}}(r)^* & -1\\ \mathcal{F}_{\mathtt{x}}(r) & 0 & 0\\ 1 & 0 & 0\end{bmatrix}}_{\mathcal{J}(x)=-\mathcal{J}(x)^*}\underbrace{\begin{bmatrix}e_p(\mathtt{X},t)\\ e_\epsilon(\mathtt{X},t)\\ -b(\mathtt{X})\end{bmatrix}}_{\delta_x H(x)} + \underbrace{\begin{bmatrix}B_d\\ 0\\ 0\end{bmatrix}}_{\mathcal{G}} u_d(\mathtt{X},t)\\ y_d(\mathtt{X},t) &= \mathcal{G}^*\delta_x H(x) = B_d^\top e_p(\mathtt{X},t).\end{aligned} \tag{III.73}$$

$$H(x) = \int_\Omega \left(\frac{1}{2}\, p(\mathtt{X},t)^\top \mathcal{M}(\mathtt{X})^{-1} p(\mathtt{X},t) + \Psi(\epsilon(\mathtt{X},t)) - r(\mathtt{X},t)^\top b(\mathtt{X})\right) d\mathtt{X}, \tag{III.74}$$

$$\dot{H}(x) = \int_\Omega u_d(\mathtt{X},t)^\top y_d(\mathtt{X},t)\, d\mathtt{X} + \int_{\partial\Omega} u_\partial(\mathtt{S},t)^\top y_\partial(\mathtt{S},t)\, d\mathtt{S}, \tag{III.75}$$

with $u_\partial(\mathtt{S},t) = [\tau_N(\mathtt{S},t)^\top\ v_D(\mathtt{S},t)^\top]^\top \in \mathbb{R}^{2n}$, $y_\partial(\mathtt{S},t) = [v_N(\mathtt{S},t)^\top\ \tau_D(\mathtt{S},t)^\top]^\top \in \mathbb{R}^{2n}$ the boundary inputs and outputs, respectively, where:

$$\begin{aligned}\tau_N(\mathtt{S},t) &= F_\partial(r) e_\epsilon(\mathtt{S},t), \quad v_N(\mathtt{S},t) = e_p(\mathtt{S},t) \quad (\text{on } \partial\Omega_N),\\ \tau_D(\mathtt{S},t) &= F_\partial(r) e_\epsilon(\mathtt{S},t), \quad v_D(\mathtt{S},t) = e_p(\mathtt{S},t) \quad (\text{on } \partial\Omega_D).\end{aligned} \tag{III.76}$$

Unlike in the linear case, in the infinite-dimensional nonlinear PHS described above, the elastic potential energy can be non-quadratic and is given by $\Psi(\epsilon) \in \mathbb{R}$, which is the generalized strain energy density function and accounts for material nonlinearity. Additionally, $\dot{\epsilon}(\mathtt{X},t) = \mathcal{F}_{\mathtt{x}}(r)\, e_p(\mathtt{X},t) \in \mathbb{R}^m$ is the time derivative of the generalized strain, which is derived from the Green-Lagrange strain tensor and incorporates geometric nonlinearities.

In what follows, we propose a mixed FEM approach based on the virtual power principle derived from the generalized Hamilton's principle (GHP) [Yi-Yuan 1964]. The GHP, which extends the Hu-Washizu principle to dynamic systems, incorporates kinetic energy contributions and independent variations of displacement, strain, and stress fields, effectively addressing geometrical and material nonlinearities. The weak form directly based on the GHP physically expresses virtual work, but to preserve the PHS structure, it must be consistently extended as a virtual power principle, as in the weak form based on the H-R principle in (III.47)-(III.48) proposed by [Thoma 2022b], or the weak form based on the mLLM method in (III.56)-(III.57) proposed in the previous section.

Proposition III.5. *The local weak form of the infinite-dimensional nonlinear PHS in (III.73), following the virtual power principle derived from the generalized Hamilton's principle, is given by:*

$$\begin{aligned}\delta P_p^e = \int_{\Omega^e} \delta\dot{r}^e(\mathtt{X},t) \cdot (\dot{p}^e(\mathtt{X},t) + \mathcal{F}_{\mathtt{x}}(r^e)^* e_\epsilon^e(\mathtt{X},t) - b^e(\mathtt{X}) - B_d u_d^e(\mathtt{X},t))\, d\mathtt{X} \ldots\\ \ldots + \int_{\partial\Omega_N^e} \delta\dot{r}^e(\mathtt{S},t) \cdot (F_\partial(r^e) e_\epsilon^e(\mathtt{S},t) - \tau_N^e(\mathtt{S},t))\, d\mathtt{S},\end{aligned} \tag{III.77}$$

$$\delta P_e^e = \int_{\Omega^e} \delta e_\epsilon^e(\mathtt{X},t)\cdot(\dot\epsilon^e(\mathtt{X},t) - \mathcal{F}_{\mathtt{x}}(r^e)\dot r^e(\mathtt{X},t))\,d\mathtt{X}... \tag{III.78}$$
$$... + \int_{\partial\Omega_D^e} \delta e_\epsilon^e(\mathtt{S},t)\cdot F_\partial(r^e)^\top(\dot r^e(\mathtt{S},t) - v_D^e(\mathtt{S},t))\,d\mathtt{S},$$
$$\delta P_\epsilon^e = \int_{\Omega^e} \delta\dot\epsilon^e(\mathtt{X},t)\cdot\left(e_\epsilon^e(\mathtt{X},t) - \frac{\partial\Psi}{\partial\epsilon}\Big|_{\epsilon=\tilde\epsilon^e(\mathtt{X},t)}\right)d\mathtt{X}. \tag{III.79}$$

Proof. From Step 4 in the proof of Theorem II.2, where the GHP has been used to derive the infinite-dimensional nonlinear PHS in (III.73), we have:

$$\int_{t_1}^{t_2}\delta(\mathcal{T}-\mathcal{U}_\mathcal{E}+\mathcal{W}_\mathcal{E})dt = \int_{t_1}^{t_2}\Big\{\int_\Omega\Big[\delta r^\top\underbrace{(-\mathcal{M}\ddot r-\mathcal{F}_{\mathtt{x}}(r)^* e_\epsilon+b+B_d\,u_d)}_{(1)} - \delta e_\epsilon^\top\underbrace{(\epsilon(r)-\epsilon)}_{(2)}...$$
$$...\delta\epsilon^\top\underbrace{\left(e_\epsilon - \frac{\partial\Psi(\epsilon)}{\partial\epsilon}\right)}_{(3)}\Big]\,d\mathtt{X}\Big\}\,dt + \int_{t_1}^{t_2}\Big[\int_{\partial\Omega_N}\delta r^\top\underbrace{[\tau_N - F_\partial(r)e_\epsilon]}_{(4)}\,d\mathtt{S}...$$
$$... + \int_{t_1}^{t_2}\Big[\int_{\partial\Omega_D}\delta\tau_D^\top\underbrace{(r-r_D)}_{(5)}\,d\mathtt{S}\Big]\,dt = 0.$$

Note that each term (i) with $i=\{1,...,5\}$ is multiplied by a virtual displacement, virtual strain, virtual stress or virtual traction, and these products define virtual work. In addition, from (III.76) we get $\delta\tau_D(\mathtt{S},t) = F_\partial(r)\delta e_\epsilon(\mathtt{S},t)$, where there is no contribution of δr since it vanishes on $\partial\Omega_D$. Gathering (1) and (4) and multiplying them by $\delta\dot r$, and defining it in local form, we get the virtual power expression in (III.77). Similarly, gathering the time derivative of (2) and (5) and multiplying them by δe_ϵ and $\delta\tau_D$, respectively, and defining it in local form, we get the virtual power expression in (III.78). Lastly, multiplying (3) by $\delta\dot\epsilon$ and defining it in local form, we get the virtual power expression in (III.79). □

In Theorem III.3, we present the discretized model of the infinite-dimensional nonlinear PHS in (III.73), employing the weak form proposed in Proposition III.5 to preserve the PHS structure.

Theorem III.3. *The structure-preserving mixed FEM discretization of* (III.73) *based on the weak formulation* (III.77)−(III.79)*, using local approximations:*

$$\begin{aligned}
&\tilde r^e(\mathtt{X},t) = N_r^e(\mathtt{X})\,\hat r^e(t), && \delta\tilde r^e(\mathtt{X},t) = N_r^e(\mathtt{X})\,\delta\hat r^e(t), && v_D^e(\mathtt{S},t) = N_{r_D}^e(\mathtt{S})\,\hat v_D^e(t),\\
&\tilde e_\epsilon^e(\mathtt{X},t) = N_e^e(\mathtt{X})\,\hat e^e(t), && \delta\tilde e_\epsilon^e(\mathtt{X},t) = N_e^e(\mathtt{X})\,\delta\hat e^e(t), && \tau_N^e(\mathtt{S},t) = N_{\tau_N}^e(\mathtt{S})\,\hat\tau_N^e(t),\\
&\tilde\epsilon^e(\mathtt{X},t) = N_\epsilon^e(\mathtt{X})\,\hat\epsilon^e(t), && \delta\tilde\epsilon^e(\mathtt{X},t) = N_\epsilon^e(\mathtt{X})\,\delta\hat\epsilon^e(t), && u_d^e(\mathtt{X},t) = N_{u_d}^e(\mathtt{X})\,\hat u_d^e(t),
\end{aligned}$$

leads to the finite-dimensional nonlinear PHS of the form:

$$\underbrace{\begin{bmatrix}\dot{\hat p}(t)\\ \dot{\hat\epsilon}(t)\\ \dot{\hat r}(t)\end{bmatrix}}_{\dot{\hat x}(t)} = \underbrace{\begin{bmatrix}0 & -\hat F_x(\hat r)^\top & -I_{N_\Omega}\\ \hat F_x(\hat r) & 0 & 0\\ I_{N_\Omega} & 0 & 0\end{bmatrix}}_{\hat J(\hat x)=-\hat J(\hat x)^\top}\underbrace{\begin{bmatrix}\hat e_p(t)\\ \hat e_\epsilon(\hat\epsilon)\\ -\hat b\end{bmatrix}}_{\nabla_{\hat x}\hat H_{GHP}(\hat x)} + \underbrace{\begin{bmatrix}\hat B_d & \hat B_{\tau_N} & 0\\ 0 & 0 & \hat B_v(\hat r)\\ 0 & 0 & 0\end{bmatrix}}_{\hat G(\hat x)}\underbrace{\begin{bmatrix}\hat u_d(t)\\ \hat\tau_N(t)\\ \hat v_D(t)\end{bmatrix}}_{\hat u(t)} \tag{III.80}$$
$$\hat y(t) = \hat G(\hat x)^\top\nabla_{\hat x}\hat H_{GHP}(\hat x)$$

$$\hat H_{GHP}(\hat x) = \frac{1}{2}\,\hat p(t)^\top\hat M^{-1}\hat p(t) + \hat U(\hat\epsilon) - \hat r(t)^\top\hat b, \tag{III.81}$$

where $\hat{p}(t) = \hat{M}\dot{\hat{r}}(t)$ *is the discrete generalized momentum, and* $\hat{e}_\epsilon(\hat{\epsilon}) = \nabla_{\hat{\epsilon}}\hat{U}(\hat{\epsilon})$ *is the discrete generalized stress. The discrete elastic potential energy* $\hat{U}(\hat{\epsilon})$ *and the rest of involved matrices and vectors are defined as:*

$$\hat{U}(\hat{\epsilon}) = \sum_{e=1}^{n_e} \int_{\Omega^e} \Psi(N_\epsilon^e(\mathtt{X})\,\hat{\epsilon}^e(t))\,d\mathtt{X}, \tag{III.82}$$

$$\hat{M}_\epsilon = \sum_{e=1}^{n_e} (L_e^e)^\top \int_{\Omega^e} N_e^e(\mathtt{X})^\top N_\epsilon^e(\mathtt{X})\,d\mathtt{X}\,L_\epsilon^e, \tag{III.83}$$

$$\hat{e}_\epsilon(\hat{\epsilon}) = \sum_{e=1}^{n_e} (L_\epsilon^e)^\top \int_{\Omega^e} N_\epsilon^e(\mathtt{X})^\top \frac{\partial \Psi}{\partial \epsilon}\Big|_{\epsilon = \tilde{\epsilon}^e(\mathtt{X},t)}\,d\mathtt{X}, \tag{III.84}$$

$$\hat{F}_x(\hat{r}) = \hat{M}_\epsilon^{-1} \sum_{e=1}^{n_e} (L_e^e)^\top \left(\int_{\Omega^e} N_e^e(\mathtt{X})^\top (\mathcal{F}_{\mathtt{x}}(\tilde{r}^e(\mathtt{X},t)) N_r^e(\mathtt{X}))\,d\mathtt{X} \ldots \right. \tag{III.85}$$
$$\left. \ldots - \int_{\partial\Omega_D^e} N_e^e(\mathtt{S})^\top F_\partial(\tilde{r}^e(\mathtt{S},t))^\top N_r^e(\mathtt{S})\,d\mathtt{S} \right) L_r^e,$$

$$\hat{B}_v(\hat{r}) = \hat{M}_\epsilon^{-1} \sum_{e=1}^{n_e} (L_e^e)^\top \int_{\partial\Omega_D^e} N_e^e(\mathtt{S})^\top F_\partial(\tilde{r}^e(\mathtt{S},t))^\top N_{r_D}^e(\mathtt{S})\,d\mathtt{S}\,L_{r_D}^e. \tag{III.86}$$

Proof. For simplicity the spatial and temporal dependencies are omitted. From δP_p^e in (III.77) and the integration Lemma II.2 we have:

$$\int_{\Omega^e} (\delta\dot{\tilde{r}}^e)^\top \mathcal{F}_{\mathtt{x}}(\tilde{r}^e)^* \tilde{e}_\epsilon^e\,d\mathtt{X} = \int_{\Omega^e} (\tilde{e}_\epsilon^e)^\top \mathcal{F}_{\mathtt{x}}(\tilde{r}^e)\,\delta\dot{\tilde{r}}^e\,d\mathtt{X} \ldots$$
$$\ldots - \left(\int_{\partial\Omega_D^e} (\delta\dot{\tilde{r}}^e)^\top F_\partial(\tilde{r}^e)\,\tilde{e}_\epsilon^e\,d\mathtt{S} + \int_{\partial\Omega_N^e} (\delta\dot{\tilde{r}}^e)^\top F_\partial(\tilde{r}^e)\,\tilde{e}_\epsilon^e\,d\mathtt{S} \right),$$

where replacing the above expression in (III.77) we obtain:

$$\delta P_p^e = (\delta\dot{\hat{r}}^e)^\top \left[\int_{\Omega^e} (N_r^e)^\top \mathcal{M} N_r^e\,d\mathtt{X}\,\ddot{\hat{r}}^e - \int_{\Omega^e} (N_r^e)^\top B_d\,N_{u_d}^e\,d\mathtt{X}\,\hat{u}_d^e - \int_{\Omega^e} (N_r^e)^\top b^e\,d\mathtt{X} \ldots \right.$$
$$\left. \ldots + \underbrace{\left(\int_{\Omega^e} (\mathcal{F}_{\mathtt{x}}(\tilde{r}^e) N_r^e)^\top N_e^e\,d\mathtt{X} - \int_{\partial\Omega_D^e} (N_r^e)^\top F_\partial(\tilde{r}^e)\,N_e^e d\mathtt{S} \right)}_{\hat{\Sigma}^e(\hat{r}^e)^\top} \hat{e}^e - \int_{\partial\Omega_N^e} (N_r^e)^\top N_{\tau_N}^e d\mathtt{S}\,\hat{\tau}_N^e \right].$$

Assembling using the location matrices, the global form of (III.77) becomes $\delta P_p = \sum_{e=1}^{n_e} \delta P_p^e = 0$ and is given by: $\delta P_p = \delta\dot{\hat{r}}^\top [\hat{M}\ddot{\hat{r}} - \hat{B}_d\,\hat{u}_d - \hat{b} + \hat{\Sigma}(\hat{r})^\top \hat{e} - \hat{B}_{\tau_N}\hat{\tau}_N] = 0$, which leads to:

$$\dot{\hat{p}} = -\hat{\Sigma}(\hat{r})^\top \hat{e} + \hat{b} + \hat{B}_d\,\hat{u}_d + \hat{B}_{\tau_N}\hat{\tau}_N, \tag{III.87}$$

where $\hat{p} = \hat{M}\dot{\hat{r}}$ and $\hat{\Sigma}(\hat{r})^\top = \sum_{e=1}^{n_e} (L_r^e)^\top \hat{\Sigma}^e(\hat{r}^e)^\top L_e^e$. From δP_e^e in (III.78) we have:

$$\delta P_e^e = (\delta\hat{e}^e)^\top \left[\int_{\Omega^e} (N_e^e)^\top N_\epsilon^e\,d\mathtt{X}\,\dot{\hat{\epsilon}}^e - \left(\int_{\Omega^e} (N_e^e)^\top \mathcal{F}_{\mathtt{x}}(\tilde{r}^e) N_r^e\,d\mathtt{X} - \int_{\partial\Omega_D^e} (N_e^e)^\top F_\partial(\tilde{r}^e)^\top N_r^e\,d\mathtt{X} \right) \dot{\hat{r}}^e \ldots \right.$$
$$\left. \ldots - \underbrace{\int_{\partial\Omega_D^e} (N_e^e)^\top F_\partial(\tilde{r}^e)^\top\,N_{r_D}^e\,d\mathtt{S}}_{\hat{V}^e(\hat{r}^e)}\,\hat{v}_D^e \right],$$

where using the location matrices, the global form of (III.78) becomes $\delta P_e = \sum_{e=1}^{n_e} \delta P_e^e = 0$ and is given by: $\delta P_e = \delta\hat{e}^\top[\hat{M}_\epsilon\,\dot{\hat{\epsilon}} - \hat{\Sigma}(\hat{r})\dot{\hat{r}} - \hat{V}(\hat{r})\hat{v}_D] = 0$, which leads to:

$$\dot{\hat{\epsilon}} = \hat{M}_\epsilon^{-1}\hat{\Sigma}(\hat{r})\dot{\hat{r}} + \hat{M}_\epsilon^{-1}\hat{V}(\hat{r})\hat{v}_D = \hat{F}_x(\hat{r})\hat{e}_p + \hat{B}_v(\hat{r})\hat{v}_D, \tag{III.88}$$

where $\hat{e}_p = \hat{M}^{-1}\hat{p} = \dot{\hat{r}}$ and $\hat{V}(\hat{r}) = \sum_{e=1}^{n_e}(L_e^e)^\top \hat{V}^e(\hat{r}^e)L_{r_D}^e$. From δP_ϵ^e in (III.79) we have:

$$\delta P_\epsilon^e = (\delta\dot{\hat{\epsilon}}^e)^\top\left[\int_{\Omega^e}(N_\epsilon^e)^\top N_e^e\, d\mathtt{X}\,\hat{e}^e - \int_{\Omega^e}(N_\epsilon^e)^\top \frac{\partial\Psi}{\partial\epsilon}\Big|_{\epsilon=\tilde{\epsilon}^e} d\mathtt{X}\right].$$

Assembling using the location matrices, the global form of (III.79) becomes $\delta P_\epsilon = \sum_{e=1}^{n_e}\delta P_\epsilon^e = 0$ and is given by: $\delta P_\epsilon = \delta\dot{\hat{\epsilon}}^\top[\hat{M}_\epsilon^\top\hat{e} - \hat{e}_\epsilon(\hat{\epsilon})] = 0$, which leads to:

$$\hat{e} = \hat{M}_\epsilon^{-\top}\hat{e}_\epsilon(\hat{\epsilon}). \tag{III.89}$$

Replacing (III.89) into (III.87), together with (III.88) and $\dot{\hat{r}} = \hat{e}_p$, define the finite-dimensional PHS in (III.80). Regarding the elastic potential energy, it is trivial that $\hat{U}(\hat{\epsilon}) = \sum_{e=1}^{n_e}\int_{\Omega^e}\Psi(\tilde{\epsilon}^e)\,d\mathtt{X}$. Lastly, using $\tilde{\epsilon}^e = N_\epsilon^e\,\hat{\epsilon}^e = N_\epsilon^e L_\epsilon^e\,\hat{\epsilon}$ we get:

$$\nabla_{\hat{\epsilon}}\hat{U}(\hat{\epsilon}) = \frac{\partial}{\partial\hat{\epsilon}}\sum_{e=1}^{n_e}\int_{\Omega^e}\Psi(N_\epsilon^e L_\epsilon^e\,\hat{\epsilon})\,d\mathtt{X} = \sum_{e=1}^{n_e}(L_\epsilon^e)^\top\int_{\Omega^e}(N_\epsilon^e)^\top\frac{\partial\Psi}{\partial\epsilon}\Big|_{\epsilon=\tilde{\epsilon}^e} d\mathtt{X} = \hat{e}_\epsilon(\hat{\epsilon}).$$

□

In Corollary III.1, we specialize the GHP-based structure-preserving mixed FEM discretization for the class of linear PHS in (III.17).

Corollary III.1. *The structure-preserving mixed FEM discretization of linear PHS as in (III.17), based on the weak formulation (III.77)−(III.79), leads to the finite-dimensional linear PHS of the form:*

$$\underbrace{\begin{bmatrix}\dot{\hat{p}}(t)\\ \dot{\hat{\epsilon}}(t)\\ \dot{\hat{r}}(t)\end{bmatrix}}_{\dot{\hat{x}}(t)} = \underbrace{\begin{bmatrix}0 & -\hat{F}_x^\top & -I_{N_\Omega}\\ \hat{F}_x & 0 & 0\\ I_{N_\Omega} & 0 & 0\end{bmatrix}}_{\hat{J}=-\hat{J}^\top}\underbrace{\begin{bmatrix}\hat{e}_p(t)\\ \hat{e}_\epsilon(t)\\ -\hat{b}\end{bmatrix}}_{\nabla_{\hat{x}}\hat{H}_{GHP}(\hat{x})} + \underbrace{\begin{bmatrix}\hat{B}_d & \hat{B}_{\tau_N} & 0\\ 0 & 0 & \hat{B}_v\\ 0 & 0 & 0\end{bmatrix}}_{\hat{G}}\underbrace{\begin{bmatrix}\hat{u}_d(t)\\ \hat{\tau}_N(t)\\ \hat{v}_D(t)\end{bmatrix}}_{\hat{u}(t)} \tag{III.90}$$

$$\hat{y}(t) = \hat{G}^\top\nabla_{\hat{x}}\hat{H}_{GHP}(\hat{x})$$

$$\hat{H}_{GHP}(\hat{x}) = \frac{1}{2}\,\hat{p}(t)^\top\hat{M}^{-1}\hat{p}(t) + \frac{1}{2}\,\hat{\epsilon}(t)^\top\hat{K}_\epsilon\,\hat{\epsilon}(t) - \hat{r}(t)^\top\hat{b}, \tag{III.91}$$

where $\hat{p}(t) = \hat{M}\dot{\hat{r}}(t)$ is the discrete generalized momentum, and $\hat{e}_\epsilon(t) = \hat{K}_\epsilon\,\hat{\epsilon}(t)$ is the discrete generalized stress. The discrete stiffness matrix is given by:

$$\hat{K}_\epsilon = \sum_{e=1}^{n_e}(L_\epsilon^e)^\top\int_{\Omega^e}N_\epsilon^e(\mathtt{X})^\top\mathcal{K}_\epsilon(\mathtt{X})\,N_\epsilon^e(\mathtt{X})\,d\mathtt{X}\,L_\epsilon^e, \tag{III.92}$$

and the matrices $\hat{F}_x = \hat{M}_\epsilon^{-1}\hat{F}$ and $\hat{B}_v = \hat{M}_\epsilon^{-1}\hat{B}_{v_D}$ are related to $\hat{F}$ and $\hat{B}_{v_D}$, which were previously defined in the mixed FEM approach based on the Hellinger-Reissner principle in Theorem III.1.

It has been shown in [Stolarski 1987] that if the spaces for stresses and strains satisfy the inclusion $S_h \subset C_L D_h$, where S_h and D_h are the finite-dimensional spaces in which stresses and strains are discretized, and C_L is the constant constitutive matrix in linear elasticity, the FEM discretization based on the classical Hu-Washizu principle is equivalent to the FEM discretization based on the classical Hellinger-Reissner principle. Following this reasoning, if equal shape functions are selected for generalized strains and stresses, i.e., $N_\epsilon^e(\mathtt{X}) = N_e^e(\mathtt{X})$, it can be expected that the structure-preserving mixed FEM discretizations of linear PHS based on the H-R approach proposed in [Thoma 2022b] and the GHP-based approach presented in Corollary III.1 would be equivalent.

In order to compare with previous linear PHS models, the condensation process employed in Propositions III.3 and III.4 is applied to the GHP-based model presented in Corollary III.1.

Proposition III.6. *The finite-dimensional linear PHS in Corollary III.1 leads to the following finite-dimensional linear PLS:*

$$\underbrace{\begin{bmatrix}\dot{\hat{p}}(t)\\ \dot{\hat{r}}(t)\end{bmatrix}}_{\dot{\hat{z}}(t)} = \underbrace{\begin{bmatrix}0 & -I_{N_\Omega}\\ I_{N_\Omega} & 0\end{bmatrix}}_{\hat{J}=-\hat{J}^\top} \underbrace{\begin{bmatrix}\hat{e}_p(t)\\ \hat{e}_r(t)\end{bmatrix}}_{\nabla_{\hat{z}}\hat{H}_{GHP}(\hat{z})} + \underbrace{\begin{bmatrix}\hat{B}_d & \hat{B}_{\tau_N} & \hat{B}_{GHP}\\ 0 & 0 & 0\end{bmatrix}}_{\hat{G}} \underbrace{\begin{bmatrix}\hat{u}_d(t)\\ \hat{\tau}_N(t)\\ \hat{r}_D(t)\end{bmatrix}}_{\hat{u}(t)} \tag{III.93}$$

$$\hat{y}(t) = \hat{G}^\top \nabla_{\hat{z}} \hat{H}_{GHP}(\hat{z})$$

$$\hat{H}_{GHP}(\hat{z}) = \frac{1}{2}\,\hat{p}(t)^\top \hat{M}^{-1}\hat{p}(t) + \frac{1}{2}\,\hat{r}(t)^\top \hat{K}_{GHP}\,\hat{r}(t) - \hat{r}(t)^\top \hat{b}, \tag{III.94}$$

where $\hat{e}_r(t) = \hat{K}_{GHP}\,\hat{r}(t) - \hat{b}$, $\hat{K}_{GHP} = \hat{F}_x^\top \hat{K}_\epsilon \hat{F}_x$, *and* $\hat{B}_{GHP} = -\hat{F}_x^\top \hat{K}_\epsilon \hat{B}_v$. *The relation between* $\hat{H}_{GHP}(\hat{x})$ *and* $\hat{H}_{GHP}(\hat{z})$ *is given by:*

$$\hat{H}_{GHP}(\hat{x}) = \hat{H}_{GHP}(\hat{z}) + \hat{E}_{GHP}(\hat{r}, \hat{r}_D), \tag{III.95}$$

where $\hat{E}_{GHP}(\hat{r}, \hat{r}_D) = \frac{1}{2}\hat{r}_D(t)^\top \hat{B}_{GHP}\,\hat{r}_D(t) - \hat{r}(t)^\top \hat{V}_{GHP}\,\hat{r}_D(t)$, *and* $\hat{V}_{GHP} = \hat{B}_v^\top \hat{K}_\epsilon \hat{B}_v$.

Proof. The proof is analogous to the proof of Proposition III.3. □

Note that, as in the Hellinger-Reissner-based models in Theorem III.1 and Proposition III.3, the Hamiltonian $\hat{H}_{GHP}(\hat{x})$ is preserved, and the matrix $\hat{K}_\epsilon$ is symmetric and positive definite. However, the elastic potential energy is quadratic in the generalized strains $\hat{\epsilon}(t)$, which poses additional challenges for energy-based shape control design. In addition, $\hat{r}_D(t) = 0$ implies $\hat{E}_{GHP}(\hat{r}, \hat{r}_D) = 0$ and $\hat{H}_{GHP}(\hat{x}) = \hat{H}_{GHP}(\hat{z})$. Furthermore, $\hat{K}_{GHP}$ is symmetric and, depending on the model and the choice of shape functions, can be positive semi-definite (non-invertible), since $\hat{F}_x$ might lose rank due to the weak imposition of the Dirichlet boundary conditions. Therefore, the suitability of the linear models based on the generalized Hamilton's principle for energy-based shape control design is comparable to that of the models based on the Hellinger-Reissner principle.

III.3.3 Constrained nonlinear systems

To properly handle the constraints while preserving the PH-DAE structure, in this section we propose a structure-preserving mixed FEM approach based on the virtual power principle derived from the generalized extended Hamilton's principle (as defined in Definition II.3), which extends the GHP to accomodate algebraic constraints. Before presenting the weak form and the discretized model, let us recall the considered class of infinite-dimensional PH-DAE systems.

(From Theorem II.3.) Let $x(\mathtt{X},t) = [p(\mathtt{X},t)^\top \ \epsilon(\mathtt{X},t)^\top \ r(\mathtt{X},t)^\top \ \lambda(\mathtt{X},t)]^\top \in \mathbb{R}^{2n+m+1}$ be the energy variables, and $\mathcal{Z}(\mathtt{X},t) = [e_p(\mathtt{X},t)^\top \ e_\epsilon(\mathtt{X},t)^\top \ -b(\mathtt{X})^\top \ \lambda(\mathtt{X},t)]^\top \in \mathbb{R}^{2n+m+1}$ be the effort function. The system's dynamics defines an infinite-dimensional nonlinear PH-DAE of the form:

$$\underbrace{\begin{bmatrix} 1 & 0 & 0 & 0 \\ 0 & 1 & 0 & 0 \\ 0 & 0 & 1 & 0 \\ 0 & 0 & 0 & 0 \end{bmatrix}}_{\mathcal{E}} \underbrace{\begin{bmatrix} \dot{p}(\mathtt{X},t) \\ \dot{\epsilon}(\mathtt{X},t) \\ \dot{r}(\mathtt{X},t) \\ \dot{\lambda}(\mathtt{X},t) \end{bmatrix}}_{\dot{x}} = \underbrace{\begin{bmatrix} 0 & -\mathcal{F}_{\mathtt{x}}(r)^* & -1 & -\mathcal{L}_{\mathtt{x}}(\epsilon,r)^* \\ \mathcal{F}_{\mathtt{x}}(r) & 0 & 0 & 0 \\ 1 & 0 & 0 & 0 \\ \mathcal{L}_{\mathtt{x}}(\epsilon,r) & 0 & 0 & 0 \end{bmatrix}}_{\mathcal{J}(x)=-\mathcal{J}(x)^*} \underbrace{\begin{bmatrix} e_p(\mathtt{X},t) \\ e_\epsilon(\mathtt{X},t) \\ -b(\mathtt{X}) \\ \lambda(\mathtt{X},t) \end{bmatrix}}_{\mathcal{Z}(\mathtt{X},t)} + \underbrace{\begin{bmatrix} B_d \\ 0 \\ 0 \\ 0 \end{bmatrix}}_{\mathcal{G}} u_d(\mathtt{X},t)$$

$$y_d(\mathtt{X},t) = \mathcal{G}^*\mathcal{Z}(\mathtt{X},t) = B_d^\top e_p(\mathtt{X},t). \tag{III.96}$$

$$H(x) = \int_\Omega \left(\frac{1}{2} p(\mathtt{X},t)^\top \mathcal{M}(\mathtt{X})^{-1} p(\mathtt{X},t) + \Psi(\epsilon(\mathtt{X},t)) - r(\mathtt{X},t)^\top b(\mathtt{X}) \right) d\mathtt{X}, \tag{III.97}$$

$$\dot{H}(x) = \int_\Omega u_d(\mathtt{X},t)^\top y_d(\mathtt{X},t)\, d\mathtt{X} + \int_{\partial\Omega} u_\partial(\mathtt{S},t)^\top y_\partial(\mathtt{S},t)\, d\mathtt{S}, \tag{III.98}$$

with $u_\partial(\mathtt{S},t) = [\tau_N(\mathtt{S},t)^\top \ v_D(\mathtt{S},t)^\top]^\top \in \mathbb{R}^{2n}$, $y_\partial(\mathtt{S},t) = [v_N(\mathtt{S},t)^\top \ \tau_D(\mathtt{S},t)^\top]^\top \in \mathbb{R}^{2n}$ the boundary inputs and outputs, respectively, where:

$$\begin{aligned} \tau_N(\mathtt{S},t) &= F_\partial(r)e_\epsilon(\mathtt{S},t) + L_\partial(\epsilon,r)\lambda(\mathtt{S},t), \quad v_N(\mathtt{S},t) = e_p(\mathtt{S},t) \quad (\text{on } \partial\Omega_N), \\ \tau_D(\mathtt{S},t) &= F_\partial(r)e_\epsilon(\mathtt{S},t) + L_\partial(\epsilon,r)\lambda(\mathtt{S},t), \quad v_D(\mathtt{S},t) = e_p(\mathtt{S},t) \quad (\text{on } \partial\Omega_D). \end{aligned} \tag{III.99}$$

In the infinite-dimensional nonlinear PH-DAE described above, the interconnection operator $\mathcal{J}(x) = -\mathcal{J}(x)^\top$ contains the differential operator $\mathcal{L}_{\mathtt{x}}(\epsilon,r)$ and its formal adjoint, both belonging to the same class of operators defined in Definition I.1. Therefore, the integration Lemma II.2 also applies to them.

Building on the weak form of nonlinear PHS presented in Proposition III.5, in Proposition III.7 we extend these results to propose the weak form for PH-DAE systems, using a virtual power principle derived from the generalized extended Hamilton's principle. Following this, Theorem III.4 presents the discretized model for the infinite-dimensional nonlinear PH-DAE system introduced in (III.96), ensuring that its structure is preserved.

Proposition III.7. *The local weak form of the infinite-dimensional nonlinear PH-DAE in (III.96), following the virtual power principle derived from the generalized extended Hamilton's principle, is given by:*

$$\delta P_p^e = \int_{\partial\Omega_N^e} \delta\dot{r}^e(\mathtt{S},t)\cdot(F_\partial(r^e)e_\epsilon^e(\mathtt{S},t) + L_\partial(\epsilon^e,r^e)\lambda^e(\mathtt{S},t) - \tau_N^e(\mathtt{S},t))\,d\mathtt{S}... \tag{III.100}$$

$$...+\int_{\Omega^e} \delta\dot{r}^e(\mathtt{X},t)\cdot(\dot{p}^e(\mathtt{X},t)+\mathcal{F}_\mathtt{x}(r^e)^* e_\epsilon^e(\mathtt{X},t)-b^e(\mathtt{X})+\mathcal{L}_\mathtt{x}(\epsilon^e,r^e)^*\lambda^e(\mathtt{X},t)-B_d u_d^e(\mathtt{X},t))\,d\mathtt{X},$$

$$\delta P_e^e = \int_{\Omega^e} \delta e_\epsilon^e(\mathtt{X},t)\cdot(\dot{\epsilon}^e(\mathtt{X},t) - \mathcal{F}_\mathtt{x}(r^e)\dot{r}^e(\mathtt{X},t))\,d\mathtt{X}... \tag{III.101}$$

$$... + \int_{\partial\Omega_D^e} \delta e_\epsilon^e(\mathtt{S},t)\cdot F_\partial(r^e)^\top(\dot{r}^e(\mathtt{S},t) - v_D^e(\mathtt{S},t))\,d\mathtt{S},$$

$$\delta P_\epsilon^e = \int_{\Omega^e} \delta\dot{\epsilon}^e(\mathtt{X},t)\cdot\left(e_\epsilon^e(\mathtt{X},t) - \frac{\partial\Psi}{\partial\epsilon}\Big|_{\epsilon=\tilde{\epsilon}^e(\mathtt{X},t)}\right)d\mathtt{X}, \tag{III.102}$$

$$\delta P_\lambda^e = -\int_{\Omega^e} \delta\lambda^e(\mathtt{X},t)\cdot\mathcal{L}_\mathtt{x}(\epsilon^e,r^e)\dot{r}^e(\mathtt{X},t))\,d\mathtt{X}... \tag{III.103}$$

$$... + \int_{\partial\Omega_D^e} \delta\lambda^e(\mathtt{S},t)\cdot L_\partial(\epsilon^e,r^e)^\top(\dot{r}^e(\mathtt{S},t) - v_D^e(\mathtt{S},t))\,d\mathtt{S},$$

Proof. From Step 5 in the proof of Theorem II.3, where the generalized extended Hamilton's principle has been used to derive the PH-DAE in (III.96), we have:

$$\begin{aligned}
\int_{t_1}^{t_2}[\delta(\mathcal{T}-\mathcal{U}_\mathcal{E}+\mathcal{W}_\mathcal{E})-\delta\mathcal{C}_\mathcal{E}]\,dt = \\
\int_{t_1}^{t_2}\Big\{\int_\Omega\Big[\delta r^\top\underbrace{(-\mathcal{M}\ddot{r}-\mathcal{F}_\mathtt{x}(r)^* e_\epsilon + b - \mathcal{L}_\mathtt{x}(\epsilon,r)^*\lambda + B_d\,u_d)}_{(1)}... \\
... - \delta e_\epsilon^\top\underbrace{(\epsilon(r)-\epsilon)}_{(2)} + \delta\epsilon^\top\underbrace{\left(e_\epsilon - \frac{\partial\Psi(\epsilon)}{\partial\epsilon}\right)}_{(3)} - \delta\lambda\cdot\underbrace{\gamma(\epsilon)}_{(4)}\Big]\,d\mathtt{X}\Big\}\,dt... \\
... + \int_{t_1}^{t_2}\Big[\int_{\partial\Omega_N}\delta r^\top\underbrace{(\tau_N - F_\partial(r)e_\epsilon - L_\partial(\epsilon,r)\lambda)}_{(5)}\,d\mathtt{S}... \\
... + \int_{t_1}^{t_2}\Big[\int_{\partial\Omega_D}\delta\tau_D^\top\underbrace{(r-r_D)}_{(6)}\,d\mathtt{S}\Big]\,dt = 0.
\end{aligned}$$

Note that each term (i) with $i=\{1,...,6\}$ is multiplied by a virtual quantity and these products define virtual work. In addition, from (III.99) we get $\delta\tau_D(\mathtt{S},t) = F_\partial(r)\delta e_\epsilon(\mathtt{S},t)+L_\partial(\epsilon,r)\delta\lambda(\mathtt{S},t)$, where there is no contribution of δr since it vanishes on $\partial\Omega_D$. Gathering (1) and (5) and multiplying them by $\delta\dot{r}$, and defining it in local form, we get the virtual power expression in (III.100). Gathering the time derivative of (2) and (6) and multiplying them by δe_ϵ and $F_\partial(r)\delta e_\epsilon$, respectively, and defining it in local form, we get the virtual power expression in (III.101). Similarly, multiplying (3) by $\delta\dot{\epsilon}$ and defining it in local form, we get the virtual power expression in (III.102). Lastly, gathering the time derivative of (4) and (6) and multiplying them by $\delta\lambda$ and $L_\partial(\epsilon,r)\delta\lambda$, respectively, and defining it in local form, we get the virtual power expression in (III.103).

□

Theorem III.4. *The structure-preserving mixed FEM discretization of* (III.96) *based on the weak formulation* (III.100)−(III.103)*, using local approximations:*

$$
\begin{aligned}
&\tilde{r}^e(\mathtt{X},t) = N_r^e(\mathtt{X})\,\hat{r}^e(t), && \delta\tilde{r}^e(\mathtt{X},t) = N_r^e(\mathtt{X})\,\delta\hat{r}^e(t), && v_D^e(\mathtt{S},t) = N_{r_D}^e(\mathtt{S})\,\hat{v}_D^e(t),\\
&\tilde{e}_\epsilon^e(\mathtt{X},t) = N_e^e(\mathtt{X})\,\hat{e}^e(t), && \delta\tilde{e}_\epsilon^e(\mathtt{X},t) = N_e^e(\mathtt{X})\,\delta\hat{e}^e(t), && \tau_N^e(\mathtt{S},t) = N_{\tau_N}^e(\mathtt{S})\,\hat{\tau}_N^e(t),\\
&\tilde{\epsilon}^e(\mathtt{X},t) = N_\epsilon^e(\mathtt{X})\,\hat{\epsilon}^e(t), && \delta\tilde{\epsilon}^e(\mathtt{X},t) = N_\epsilon^e(\mathtt{X})\,\delta\hat{\epsilon}^e(t), && u_d^e(\mathtt{X},t) = N_{u_d}^e(\mathtt{X})\,\hat{u}_d^e(t),\\
&\tilde{\lambda}^e(\mathtt{X},t) = N_\lambda^e(\mathtt{X})\,\hat{\lambda}^e(t), && \delta\tilde{\lambda}^e(\mathtt{X},t) = N_\lambda^e(\mathtt{X})\,\delta\hat{\lambda}^e(t),
\end{aligned}
$$

leads to the finite-dimensional nonlinear PH-DAE of the form:

$$
\begin{aligned}
\big[\hat{E}\big]\underbrace{\begin{bmatrix}\dot{\hat{p}}(t)\\ \dot{\hat{\epsilon}}(t)\\ \dot{\hat{r}}(t)\\ \dot{\hat{\lambda}}(t)\end{bmatrix}}_{\dot{\hat{x}}(t)} &= \underbrace{\begin{bmatrix} 0 & -\hat{F}_x(\hat{r})^\top & -I_{N_\Omega} & -\hat{L}_x(\hat{\epsilon},\hat{r})^\top\\ \hat{F}_x(\hat{r}) & 0 & 0 & 0\\ I_{N_\Omega} & 0 & 0 & 0\\ \hat{L}_x(\hat{\epsilon},\hat{r}) & 0 & 0 & 0\end{bmatrix}}_{\hat{J}(\hat{x})=-\hat{J}(\hat{x})^\top}\underbrace{\begin{bmatrix}\hat{e}_p(t)\\ \hat{e}_\epsilon(\hat{\epsilon})\\ -\hat{b}\\ \hat{\lambda}(t)\end{bmatrix}}_{\hat{Z}(\hat{x})} + \underbrace{\begin{bmatrix}\hat{B}_d & \hat{B}_{\tau_N} & 0\\ 0 & 0 & \hat{B}_v(\hat{r})\\ 0 & 0 & 0\\ 0 & 0 & \hat{B}_L(\hat{\epsilon},\hat{r})\end{bmatrix}}_{\hat{G}(\hat{x})}\underbrace{\begin{bmatrix}\hat{u}_d(t)\\ \hat{\tau}_N(t)\\ \hat{v}_D(t)\end{bmatrix}}_{\hat{u}(t)}\\
\hat{y}(t) &= \hat{G}(\hat{x})^\top\hat{Z}(\hat{x})
\end{aligned}
\tag{III.104}
$$

$$
\hat{H}_{GHP}(\hat{x}) = \frac{1}{2}\,\hat{p}(t)^\top\hat{M}^{-1}\hat{p}(t) + \hat{U}(\hat{\epsilon}) - \hat{r}(t)^\top\hat{b}, \tag{III.105}
$$

where $\hat{p}(t) = \hat{M}\dot{\hat{r}}(t)$ *is the discrete generalized momentum,* $\hat{e}_\epsilon(\hat{\epsilon}) = \nabla_{\hat{\epsilon}}\hat{U}(\hat{\epsilon})$ *is the discrete generalized stress, and* $\nabla_{\hat{x}}\hat{H}_{GHP}(\hat{x}) = \hat{E}^\top\hat{Z}(\hat{x})$ *define the discrete co-energy variables. The other involved matrices are defined as:*

$$
\hat{E} = diag\,(I_{N_\Omega},\, I_{M_\Omega},\, I_{N_\Omega},\, 0_{NN_\Omega}), \tag{III.106}
$$

$$
\begin{aligned}
\hat{L}_x(\hat{\epsilon},\hat{r}) = \sum_{e=1}^{n_e}(L_\lambda^e)^\top\Big(&\int_{\Omega^e} N_\lambda^e(\mathtt{X})^\top(\mathcal{L}_{\mathtt{x}}(\tilde{\epsilon}^e(\mathtt{X},t),\tilde{r}^e(\mathtt{X},t))N_r^e(\mathtt{X}))\,d\mathtt{X}\ldots\\
&\ldots - \int_{\partial\Omega_D^e} N_\lambda^e(\mathtt{S})^\top L_\partial(\tilde{\epsilon}^e(\mathtt{S},t),\tilde{r}^e(\mathtt{S},t))^\top N_r^e(\mathtt{S})\,d\mathtt{S}\Big)L_r^e,
\end{aligned}
\tag{III.107}
$$

$$
\hat{B}_L(\hat{\epsilon},\hat{r}) = \sum_{e=1}^{n_e}(L_\lambda^e)^\top\int_{\partial\Omega_D^e} N_\lambda^e(\mathtt{S})^\top L_\partial(\tilde{\epsilon}^e(\mathtt{S},t),\tilde{r}^e(\mathtt{S},t))^\top N_{r_D}^e(\mathtt{S})\,d\mathtt{S}\,L_{r_D}^e. \tag{III.108}
$$

Proof. For simplicity the spatial and temporal dependencies are omitted. From δP_p^e in (III.100) and the integration Lemma II.2 we have:

$$
\begin{aligned}
\int_{\Omega^e}(\delta\dot{\tilde{r}}^e)^\top\mathcal{F}_{\mathtt{x}}(\tilde{r}^e)^*\tilde{e}_\epsilon^e\,d\mathtt{X} = &\int_{\Omega^e}(\tilde{e}_\epsilon^e)^\top\mathcal{F}_{\mathtt{x}}(\tilde{r}^e)\,\delta\dot{\tilde{r}}^e\,d\mathtt{X}\ldots\\
&\ldots - \left(\int_{\partial\Omega_D^e}(\delta\dot{\tilde{r}}^e)^\top F_\partial(\tilde{r}^e)\,\tilde{e}_\epsilon^e\,d\mathtt{S} + \int_{\partial\Omega_N^e}(\delta\dot{\tilde{r}}^e)^\top F_\partial(\tilde{r}^e)\,\tilde{e}_\epsilon^e\,d\mathtt{S}\right),
\end{aligned}
$$

and

$$
\begin{aligned}
\int_{\Omega^e}(\delta\dot{\tilde{r}}^e)^\top\mathcal{L}_{\mathtt{x}}(\tilde{\epsilon}^e,\tilde{r}^e)^*\tilde{\lambda}^e\,d\mathtt{X} = &\int_{\Omega^e}(\tilde{\lambda}^e)^\top\mathcal{L}_{\mathtt{x}}(\tilde{\epsilon}^e,\tilde{r}^e)\,\delta\dot{\tilde{r}}^e\,d\mathtt{X}\ldots\\
&\ldots - \left(\int_{\partial\Omega_D^e}(\delta\dot{\tilde{r}}^e)^\top L_\partial(\tilde{\epsilon}^e,\tilde{r}^e)\,\tilde{\lambda}^e\,d\mathtt{S} + \int_{\partial\Omega_N^e}(\delta\dot{\tilde{r}}^e)^\top L_\partial(\tilde{\epsilon}^e,\tilde{r}^e)\,\tilde{\lambda}^e\,d\mathtt{S}\right),
\end{aligned}
$$

where replacing the above expression in (III.100) we obtain:

$$\delta P_p^e = (\delta\dot{\hat{r}}^e)^\top \Bigg[\int_{\Omega^e}(N_r^e)^\top \mathcal{M} N_r^e \, d\mathtt{X}\, \ddot{\hat{r}}^e - \int_{\Omega^e}(N_r^e)^\top B_d\, N_{u_d}^e \, d\mathtt{X}\, \hat{u}_d^e - \int_{\Omega^e}(N_r^e)^\top b^e \, d\mathtt{X} \ldots$$
$$\ldots + \underbrace{\left(\int_{\Omega^e}(\mathcal{F}_{\mathtt{x}}(\tilde{r}^e)N_r^e)^\top N_e^e \, d\mathtt{X} - \int_{\partial\Omega_D^e}(N_r^e)^\top F_\partial(\tilde{r}^e)\, N_e^e d\mathtt{S}\right)}_{\hat{\Sigma}^e(\hat{r}^e)^\top}\hat{e}^e - \int_{\partial\Omega_N^e}(N_r^e)^\top N_{\tau_N}^e d\mathtt{S}\, \hat{\tau}_N^e \ldots$$
$$\ldots + \left(\int_{\Omega^e}(\mathcal{L}_{\mathtt{x}}(\tilde{\epsilon}^e,\tilde{r}^e)N_r^e)^\top N_\lambda^e \, d\mathtt{X} - \int_{\partial\Omega_D^e}(N_r^e)^\top L_\partial(\tilde{\epsilon}^e,\tilde{r}^e)\, N_\lambda^e \, d\mathtt{S}\right)\hat{\lambda}^e\Bigg].$$

Assembling using the location matrices, the global form of (III.100) becomes $\delta P_p = \sum_{e=1}^{n_e}\delta P_p^e = 0$ and is given by: $\delta P_p = \delta\dot{\hat{r}}^\top[\hat{M}\ddot{\hat{r}} - \hat{B}_d\,\hat{u}_d - \hat{b} + \hat{\Sigma}(\hat{r})^\top\hat{e} - \hat{B}_{\tau_N}\hat{\tau}_N + \hat{L}_x(\hat{\epsilon},\hat{r})^\top\hat{\lambda}] = 0$, which leads to:

$$\dot{\hat{p}} = -\hat{\Sigma}(\hat{r})^\top\hat{e} + \hat{b} - \hat{L}_x(\hat{\epsilon},\hat{r})^\top\hat{\lambda} + \hat{B}_d\,\hat{u}_d + \hat{B}_{\tau_N}\hat{\tau}_N, \tag{III.109}$$

where $\hat{p} = \hat{M}\dot{\hat{r}}$ and $\hat{\Sigma}(\hat{r})^\top = \sum_{e=1}^{n_e}(L_r^e)^\top\hat{\Sigma}^e(\hat{r}^e)^\top L_e^e$. From δP_e^e in (III.101) we have:

$$\delta P_e^e = (\delta\hat{e}^e)^\top\Bigg[\int_{\Omega^e}(N_e^e)^\top N_\epsilon^e \, d\mathtt{X}\, \dot{\hat{\epsilon}}^e - \left(\int_{\Omega^e}(N_e^e)^\top\mathcal{F}_{\mathtt{x}}(\tilde{r}^e)N_r^e \, d\mathtt{X} - \int_{\partial\Omega_D^e}(N_e^e)^\top F_\partial(\tilde{r}^e)^\top N_r^e \, d\mathtt{X}\right)\dot{\hat{r}}^e \ldots$$
$$\ldots - \underbrace{\int_{\partial\Omega_D^e}(N_e^e)^\top F_\partial(\tilde{r}^e)^\top\, N_{r_D}^e \, d\mathtt{S}}_{\hat{V}^e(\hat{r}^e)}\hat{v}_D^e\Bigg],$$

where using the location matrices, the global form of (III.101) becomes $\delta P_e = \sum_{e=1}^{n_e}\delta P_e^e = 0$ and is given by: $\delta P_e = \delta\hat{e}^\top[\hat{M}_\epsilon\,\dot{\hat{\epsilon}} - \hat{\Sigma}(\hat{r})\dot{\hat{r}} - \hat{V}(\hat{r})\hat{v}_D] = 0$, which leads to:

$$\dot{\hat{\epsilon}} = \hat{M}_\epsilon^{-1}\hat{\Sigma}(\hat{r})\dot{\hat{r}} + \hat{M}_\epsilon^{-1}\hat{V}(\hat{r})\hat{v}_D = \hat{F}_x(\hat{r})\hat{e}_p + \hat{B}_v(\hat{r})\hat{v}_D, \tag{III.110}$$

where $\hat{e}_p = \hat{M}^{-1}\hat{p} = \dot{\hat{r}}$ and $\hat{V}(\hat{r}) = \sum_{e=1}^{n_e}(L_e^e)^\top\hat{V}^e(\hat{r}^e)L_{r_D}^e$. From δP_ϵ^e in (III.102) we have:

$$\delta P_\epsilon^e = (\delta\dot{\hat{\epsilon}}^e)^\top\left[\int_{\Omega^e}(N_\epsilon^e)^\top N_e^e \, d\mathtt{X}\, \hat{e}^e - \int_{\Omega^e}(N_\epsilon^e)^\top\frac{\partial\Psi}{\partial\epsilon}\Big|_{\epsilon=\tilde{\epsilon}^e} d\mathtt{X}\right].$$

Assembling using the location matrices, the global form of (III.102) becomes $\delta P_\epsilon = \sum_{e=1}^{n_e}\delta P_\epsilon^e = 0$ and is given by: $\delta P_\epsilon = \delta\dot{\hat{\epsilon}}^\top[\hat{M}_\epsilon^\top\hat{e} - \hat{e}_\epsilon(\hat{\epsilon})] = 0$, which leads to:

$$\hat{e} = \hat{M}_\epsilon^{-\top}\hat{e}_\epsilon(\hat{\epsilon}). \tag{III.111}$$

Lastly, from δP_λ^e in (III.103) we have:

$$\delta P_\lambda^e = -(\delta\hat{\lambda}^e)^\top\Bigg[\left(\int_{\Omega^e}(N_\lambda^e)^\top\mathcal{L}_{\mathtt{x}}(\tilde{\epsilon}^e,\tilde{r}^e)N_r^e \, d\mathtt{X} - \int_{\partial\Omega_D^e}(N_\lambda^e)^\top L_\partial(\tilde{\epsilon}^e,\tilde{r}^e)^\top N_r^e \, d\mathtt{X}\right)\dot{\hat{r}}^e \ldots$$
$$\ldots + \int_{\partial\Omega_D^e}(N_\lambda^e)^\top L_\partial(\tilde{\epsilon}^e,\tilde{r}^e)^\top\, N_{r_D}^e \, d\mathtt{S}\Bigg],$$

where using the location matrices, the global form of (III.103) becomes $\delta P_\lambda = \sum_{e=1}^{n_e}\delta P_\lambda^e = 0$ and is given by: $\delta P_\lambda = -\delta\hat{\lambda}^\top[\hat{L}_x(\hat{\epsilon},\hat{r})\dot{\hat{r}} + \hat{B}_L(\hat{\epsilon},\hat{r})\hat{v}_D] = 0$, which leads to:

$$0 = \hat{L}_x(\hat{\epsilon},\hat{r})\hat{e}_p + \hat{B}_L(\hat{\epsilon},\hat{r})\hat{v}_D. \tag{III.112}$$

Replacing (III.111) into (III.109), together with (III.110), (III.112) and $\dot{\hat{r}} = \hat{e}_p$, define the finite-dimensional PH-DAE in (III.104). □

The theoretical development of the structure-preserving mixed FEM discretization of infinite-dimensional PHS and PH-DAE systems has been presented. The next section will focus on simulations of various physical examples to assess the behavior of the finite-dimensional approximations.

III.4 Examples

This section presents simulations using the previously discussed mixed FEM approaches for both linear and nonlinear PHS, focusing on 1D and 2D cases. Results are often compared with those obtained from the software *Autodesk Inventor ®*, which serves as a reference. Additionally, key challenges such as shear locking are addressed, and well-known strategies for its mitigation are discussed.

III.4.1 Linear systems

In this section, we simulate discretized linear PHS using a one-dimensional planar beam and a two-dimensional elastic body as examples. The infinite-dimensional linear PHS models were derived in Section II.4, following the modeling Methodology 1 in page 53, so the details on the models are omitted here. As a reminder, infinite-dimensional linear PHS models have the form:

$$\underbrace{\begin{bmatrix}\dot{p}(\mathtt{X},t)\\ \dot{\epsilon}(\mathtt{X},t)\\ \dot{r}(\mathtt{X},t)\end{bmatrix}}_{\dot{x}(\mathtt{X},t)} = \underbrace{\begin{bmatrix}0 & -\mathcal{F}_{\mathtt{x}}{}^* & -1\\ \mathcal{F}_{\mathtt{x}} & 0 & 0\\ 1 & 0 & 0\end{bmatrix}}_{\mathcal{J}=-\mathcal{J}^*} \underbrace{\begin{bmatrix}e_p(\mathtt{X},t)\\ e_\epsilon(\mathtt{X},t)\\ -b\end{bmatrix}}_{\delta_x H},$$

$$H(x) = \int_\Omega \left(\frac{1}{2}\, p(\mathtt{X},t)^\top \mathcal{M}^{-1} p(\mathtt{X},t) + \frac{1}{2}\, \epsilon(\mathtt{X},t)^\top \mathcal{K}_\epsilon\, \epsilon(\mathtt{X},t) - r(\mathtt{X},t)^\top b\right) d\mathtt{X},$$

$$u_\partial(\mathtt{S},t) = \begin{bmatrix}\tau_N(\mathtt{S},t)^\top & v_D(\mathtt{S},t)^\top\end{bmatrix}^\top, \quad y_\partial(\mathtt{S},t) = \begin{bmatrix}v_N(\mathtt{S},t)^\top & \tau_D(\mathtt{S},t)^\top\end{bmatrix}^\top,$$

with:

$$\tau_N(\mathtt{S},t) = F_\partial(\mathtt{S})\, e_\epsilon(\mathtt{S},t), \quad v_N(\mathtt{S},t) = e_p(\mathtt{S},t) \quad (\text{on } \partial\Omega_N),$$
$$\tau_D(\mathtt{S},t) = F_\partial(\mathtt{S})\, e_\epsilon(\mathtt{S},t), \quad v_D(\mathtt{S},t) = e_p(\mathtt{S},t) \quad (\text{on } \partial\Omega_D).$$

III.4.1.a Planar beam

The infinite-dimensional explicit linear PHS of the planar beam was derived in Section II.4.2 in page 75. The key variables of the PHS are given by:

$$\mathcal{F}_{\mathtt{x}} = \begin{bmatrix}\partial_1 & 0 & 0\\ 0 & \partial_1 & 0\\ 0 & -1 & \partial_1\end{bmatrix}, \quad \mathcal{M} = \rho_0 \begin{bmatrix}A_0 & 0 & 0\\ 0 & \bar{I}_0 & 0\\ 0 & 0 & A_0\end{bmatrix}, \quad \mathcal{K}_\epsilon = \begin{bmatrix}EA_0 & 0 & 0\\ 0 & E\bar{I}_0 & 0\\ 0 & 0 & \kappa G A_0\end{bmatrix}, \quad b = \begin{bmatrix}0\\ 0\\ -\rho_0 g A_0\end{bmatrix},$$

where A_0 is the cross section area, $\bar{I}_0$ is the second moment of inertia of the cross section, ρ_0 is the density of the material, g is the gravitational acceleration, E is Young's modulus, $G = \mu_L = \frac{E}{2(1+\nu)}$ is the shear modulus, ν is Poisson's ra-

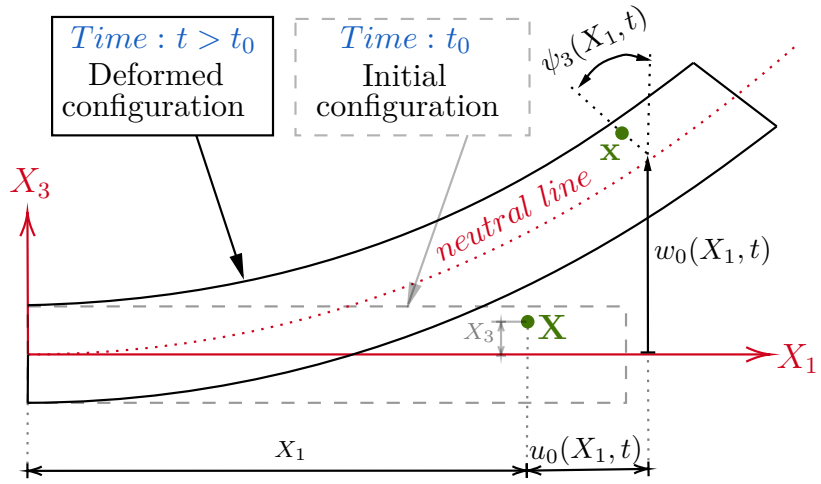

Figure III.4 – Scheme of the one-dimensional planar beam

tio, and κ is a correction factor. The generalized displacement field is given by $r(\mathtt{X}, t) = [u_0(\mathtt{X}, t)\ \psi_3(\mathtt{X}, t)\ w_0(\mathtt{X}, t)]^\top \in \mathbb{R}^3$, where $u_0(\mathtt{X}, t)$ and $w_0(\mathtt{X}, t)$ are the axial and vertical displacements of points on the neutral line, respectively, and $\psi_3(\mathtt{X}, t)$ is the angle of rotation of the cross section, as illustrated in Fig. III.4. For this case, $\mathtt{X} = X_1 \in \Omega = (0, L_0) \subset \mathbb{R}$ with L_0 the length of the beam in the reference configuration, $\mathtt{S} = \{0, L_0\}$ where it is assumed that $\mathtt{S} = 0 \in \partial\Omega_D$ and $\mathtt{S} = L_0 \in \partial\Omega_N$.

To validate the effectiveness of the proposed methods in capturing the dynamics of the infinite-dimensional planar beam, the natural frequencies (imaginary parts of the eigenvalues) were computed and compared against the results provided by the software *Autodesk Inventor ®*[3]. For this analysis, Dirichlet and Neumman boundary conditions are specified as homogeneous, i.e., $\hat{v}_D(t) = 0$ and $\hat{\tau}_N(t) = 0$, and the gravitational effect is not considered, i.e., $\hat{b} = 0$. The numerical values used are listed in the Table III.2. The shape functions were selected as equal-order canonical, and various combinations of the number of elements n_e, polynomial order or, and link factor β for the mLLM method were tested. The results are presented in Table III.3.

Symbol	Value	Unit	Symbol	Value	Unit	Symbol	Value	Unit
E	210	$[GPa]$	L_0	50	$[cm]$	ρ_0	7800	$[kg/m^3]$
ν	0.3	$[-]$	A_0	$3 \cdot 10^{-5}$	$[m^2]$	g	9.806	$[m/s^2]$
G, μ_L	80.77	$[GPa]$	$\bar{I}_0$	$2.5 \cdot 10^{-12}$	$[m^4]$	κ	5/6	$[-]$

Table III.2 – Numerical values for planar beam.

3. Autodesk Inventor is a Computer-Aided Design (CAD) software used for 3D mechanical design and simulation. It employs standard displacement-based FEM, modeling solids as 3D bodies discretized using first-order tetrahedral elements, while applying strong imposition of Dirichlet boundary conditions.

	Mode N°	1	2	3	4	5	6	7
	Software [Hz]	3.34	20.96	58.70	115.05	190.40	284.70	398.08
H–R and *GHP*	$n_e = 1$, $or = 1$	3.06	10.69	2718	6021	$1.62{\cdot}10^{6}$	$1.62{\cdot}10^{6}$	-
	$n_e = 1$, $or = 2$	3.37	21.24	43.61	2591.1	9100.4	$1.14{\cdot}10^{4}$	$1.62{\cdot}10^{6}$
	$n_e = 1$, $or = 3$	3.35	21.42	71.17	114.13	2594.4	7638.7	$1.69{\cdot}10^{4}$
	$n_e = 1$, $or = 4$	3.35	21.02	60.82	170.28	246.33	2594.4	7793.5
	$n_e = 10$, $or = 1$	3.35	20.99	29.39	58.57	112.91	142.14	179.71
	$n_e = 10$, $or = 2$	3.35	21.01	58.84	115.35	190.85	285.54	399.73
	$n_e = 10$, $or = 3$	3.35	21.01	58.83	115.28	162.49	190.56	284.60
	$n_e = 10$, $or = 4$	3.35	21.01	58.83	115.28	190.55	268.96	284.63
	$n_e = 30$, $or = 1$	3.35	21.01	30.09	58.82	115.25	182.81	190.44
	$n_e = 30$, $or = 2$	3.35	21.01	58.83	83.69	115.28	190.55	284.64
	$n_e = 30$, $or = 3$	3.35	21.01	58.83	115.28	164.07	190.55	284.63
	$n_e = 30$, $or = 4$	3.34	21.01	58.83	115.28	190.55	271.23	284.63
mLLM, $\beta{=}10$	$n_e = 1$, $or = 1$	9.05	2824.6	9717.3	$1.73{\cdot}10^{4}$	$1.53{\cdot}10^{6}$	$1.62{\cdot}10^{6}$	-
	$n_e = 1$, $or = 2$	4.06	57.01	2536.8	9020.1	$2.30{\cdot}10^{4}$	$4.11{\cdot}10^{4}$	$1.53{\cdot}10^{6}$
	$n_e = 1$, $or = 3$	3.28	30.89	187.84	2501.2	7732.5	$1.64{\cdot}10^{4}$	$4.06{\cdot}10^{4}$
	$n_e = 1$, $or = 4$	3.25	20.41	104.72	451.98	2489.2	7490.5	$1.32{\cdot}10^{4}$
	$n_e = 10$, $or = 1$	27.42	429.41	1405.4	2587.8	3037.2	5463.3	7829.8
	$n_e = 10$, $or = 2$	3.31	21.08	60.36	121.92	209.49	328.15	484.5
	$n_e = 10$, $or = 3$	3.30	20.81	58.51	114.98	190.54	285.41	400.15
	$n_e = 10$, $or = 4$	3.30	20.79	58.44	114.8	189.99	283.89	396.45
	$n_e = 30$, $or = 1$	26.85	175.37	504.5	1010.7	1702.9	2589.3	2591.6
	$n_e = 30$, $or = 2$	3.33	20.94	58.77	115.57	191.84	288.00	404.59
	$n_e = 30$, $or = 3$	3.33	20.91	58.58	114.85	189.96	283.89	396.66
	$n_e = 30$, $or = 4$	3.33	20.90	58.55	114.80	189.88	283.77	396.47
mLLM, $\beta{=}50$	$n_e = 1$, $or = 1$	20.22	2853.5	$2.26{\cdot}10^{4}$	$4.01{\cdot}10^{4}$	$1.60{\cdot}10^{6}$	$1.60{\cdot}10^{6}$	-
	$n_e = 1$, $or = 2$	4.22	127.7	2591.3	9300.5	$5.37{\cdot}10^{4}$	$9.51{\cdot}10^{4}$	$1.60{\cdot}10^{6}$
	$n_e = 1$, $or = 3$	3.35	32.71	420.55	2576.6	7938.3	$1.71{\cdot}10^{4}$	$9.48{\cdot}10^{4}$
	$n_e = 1$, $or = 4$	3.33	21.04	111.04	1013.9	2574.1	7742.8	$1.36{\cdot}10^{4}$
	$n_e = 10$, $or = 1$	53.21	458.85	1443.0	2595.3	3084.3	5527.6	7850.5
	$n_e = 10$, $or = 2$	3.34	21.25	60.69	122.39	210.08	328.96	485.76
	$n_e = 10$, $or = 3$	3.34	20.97	58.78	115.31	190.93	286.00	401.18
	$n_e = 10$, $or = 4$	3.34	20.97	58.75	115.18	190.45	284.52	397.42
	$n_e = 30$, $or = 1$	30.60	192.53	541.76	1068.7	1781.2	2594.1	2687.0
	$n_e = 30$, $or = 2$	3.35	21.02	58.98	115.92	192.35	288.67	405.42
	$n_e = 30$, $or = 3$	3.34	20.99	58.78	115.20	190.44	284.50	397.38
	$n_e = 30$, $or = 4$	3.34	20.99	58.77	115.19	190.42	284.46	397.31
mLLM, $\beta{=}100$	$n_e = 1$, $or = 1$	28.59	2857.1	$3.22{\cdot}10^{4}$	$5.69{\cdot}10^{4}$	$1.61{\cdot}10^{6}$	$1.61{\cdot}10^{6}$	-
	$n_e = 1$, $or = 2$	4.24	180.30	2597.7	9335.0	$7.64{\cdot}10^{4}$	$1.35{\cdot}10^{5}$	$1.61{\cdot}10^{6}$
	$n_e = 1$, $or = 3$	3.35	32.95	591.81	2585.6	7963.3	$1.71{\cdot}10^{4}$	$1.34{\cdot}10^{5}$
	$n_e = 1$, $or = 4$	3.34	21.12	111.84	1418.6	2584.3	7773.1	$1.37{\cdot}10^{4}$
	$n_e = 10$, $or = 1$	65.71	484.08	1478.4	2596.2	3126.1	5575.0	7852.9
	$n_e = 10$, $or = 2$	3.35	21.27	60.73	122.44	210.16	329.07	485.89
	$n_e = 10$, $or = 3$	3.34	20.99	58.81	115.35	190.98	286.07	401.30
	$n_e = 10$, $or = 4$	3.34	20.99	58.79	115.23	190.50	284.59	397.54
	$n_e = 30$, $or = 1$	31.19	195.86	550.34	1084.2	1804.9	2594.4	2720.0
	$n_e = 30$, $or = 2$	3.35	21.03	59.00	115.96	192.41	288.76	405.52
	$n_e = 30$, $or = 3$	3.35	21.00	58.80	115.24	190.50	284.57	397.47
	$n_e = 30$, $or = 4$	3.35	21.00	58.80	115.23	190.49	284.55	397.41

Table III.3 – Comparison: Software vs discretized beam models.

We can remark that as the number of elements and the order increase, the predicted natural frequencies become more accurate compared to those provided by the software. However, this is not observed in models based on the mLLM method when first-order elements are used. Regardless the number of elements or the value of the link factor, these models tend to overestimate the frequencies. This issue is attributed to shear locking, a well-known numerical problem in Timoshenko beam (and Mindlin plate) models when discretized using standard FEM with first-order elements. Shear locking occurs when the finite element formulation overly restricts the beam's shear deformation, causing the model to behave as if it were stiffer than it actually is, particularly in bending-dominated scenarios. Since the elastic potential energy in mLLM-based models closely resembles that of standard FEM, the problem is primarily attributed to shear locking effects. Common strategies to mitigate this problem include increasing the polynomial order, employing mixed FEM strategies based on the Hellinger-Reissner (H-R) or Hu-Washizu variational principles, or applying reduced integration [4] in the terms related to the elastic potential energy due to shearing strains [Suri 1996]. As observed in Table III.3, increasing the element order resolves the shear locking issue in mLLM models, while models based on the H-R and GHP principles are inherently free from this problem.

To visualize the impact of shear locking and validate the static solutions of the models, the static deflection profiles $w_0(X_1)$ of the beam under gravitational effects are shown in the Figs. III.5 - III.7. We observe several relevant trends regarding the accuracy and behavior of the static deflection of the beam for different methods and numbers of elements n_e, as well as varying polynomial orders or.

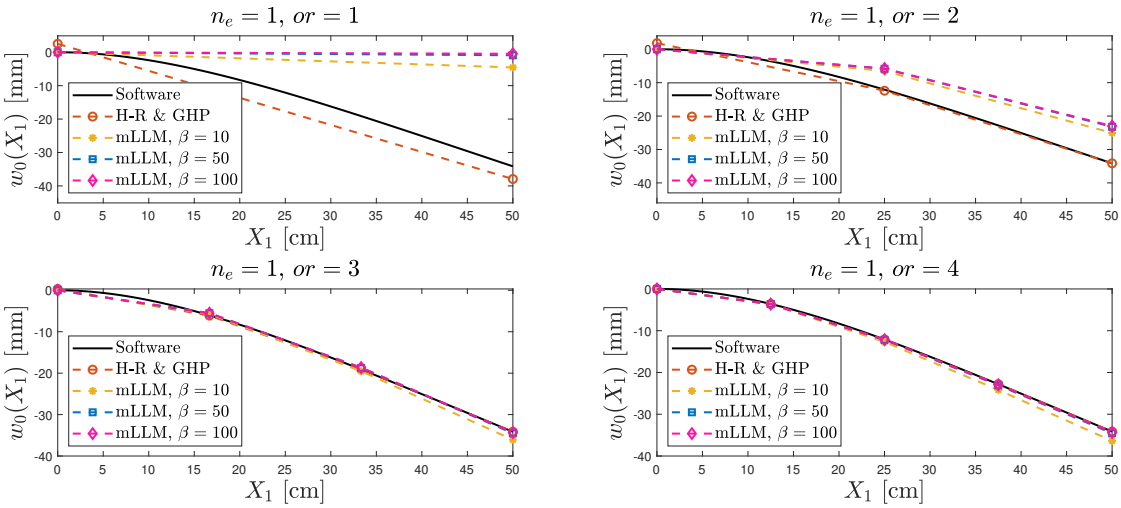

Figure III.5 – Static solution of the beam with $n_e = 1$.

4. Reduced integration involves computing stiffness matrices using fewer Gauss-quadrature points than required for an exact solution.

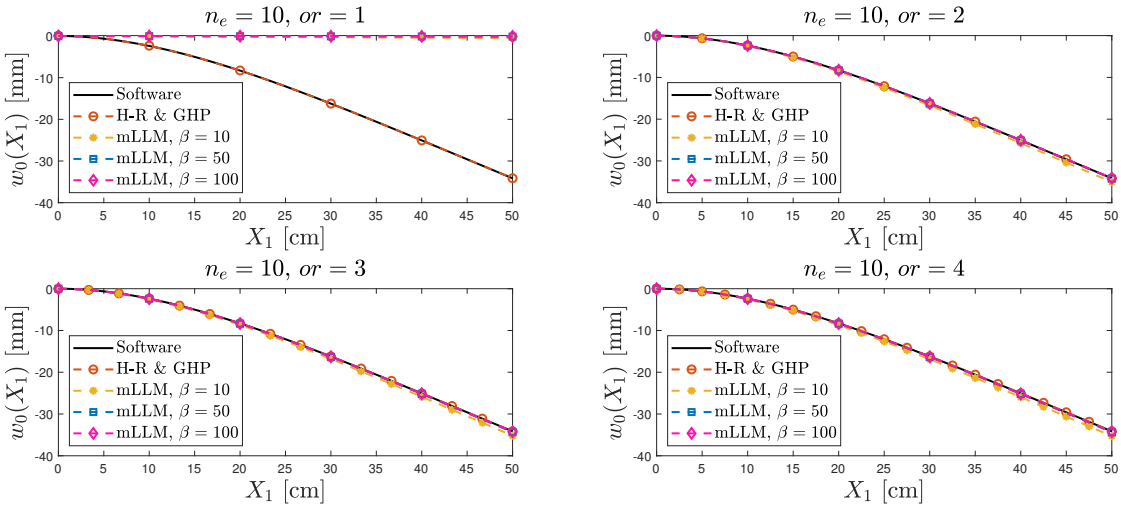

Figure III.6 – Static solution of the beam with $n_e = 10$.

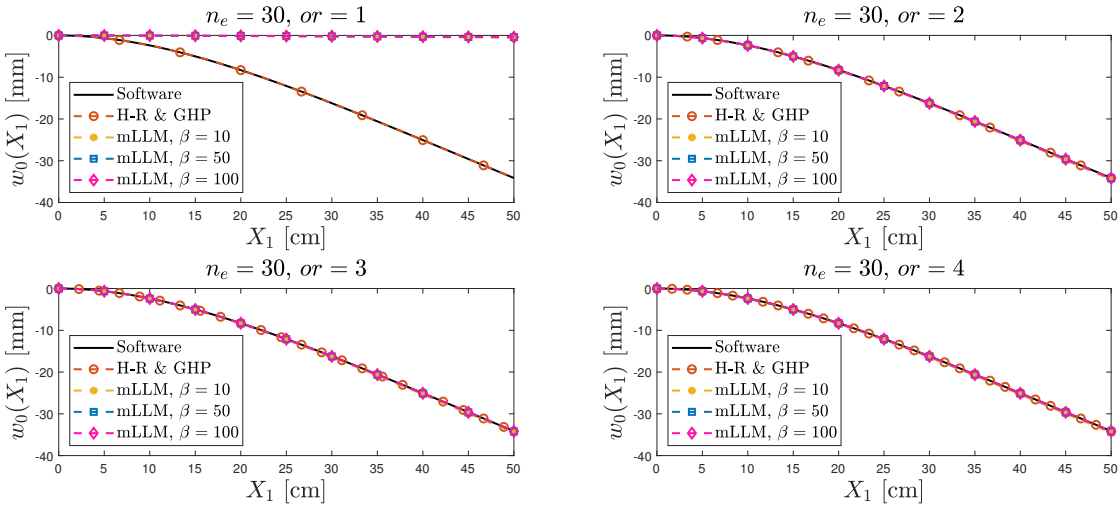

Figure III.7 – Static solution of the beam with $n_e = 30$.

Starting from Fig. III.5 where $n_e = 1$, the top-left plot (for $or = 1$) clearly shows that the mLLM methods do not accurately predict the static deflection, demonstrating significant deviations due to shear locking. This issue persists across different values of β. However, in the subsequent plots for higher polynomial orders ($or = 2, 3, 4$), we observe that the accuracy of the mLLM methods improves substantially, aligning more closely with the H-R and GHP-based results. This indicates that using only one element but with higher-order polynomials effectively mitigates the shear locking issue, resulting in good approximations for all methods. From Figs. III.6 and III.7, where $n_e = 10$ and $n_e = 30$, respectively, similar observations can be made. For $or = 1$, the H-R and GHP-based models provide accurate predictions, while the mLLM methods continue to be affected by shear locking, regardless of the choice of β. However, the results indicate that as the number of elements increases, the differences between methods diminish, even for lower polynomial orders ($or \geq 2$). Across all figures, the accuracy of the mLLM

methods appears to improve with increasing β until a certain limit is reached, beyond which no further gains in accuracy are observed. The underlying cause of this behavior is not analyzed here and will be the subject of future research.

Now, we test the models by applying homogeneous Dirichlet boundary conditions at $X_1 = 0$, i.e., $\hat{v}_D(t) = 0$, and Neumann boundary conditions at $X_1 = L_0$ where a vertical force is considered. The input is defined as:

$$\hat{\tau}_N(t) = \begin{bmatrix} 0 & 0 & 10\sin(40\pi t) \end{bmatrix}^\top [N] \quad ; \text{ for } 0 \leq t \leq 0.2\,[s].$$

Rayleigh damping is introduced to the H−R, GHP and mLLM models, with the damping coefficients set to $a_M = 4$ and $a_K = 1 \cdot 10^{-3}$. The dissipation matrices for the models are given by:

$$\hat{R}_{HR} = \begin{bmatrix} \hat{D}_{HR} & 0 & 0 \\ 0 & 0 & 0 \\ 0 & 0 & 0 \end{bmatrix}, \quad \hat{R}_{GHP} = \begin{bmatrix} \hat{D}_{GHP} & 0 & 0 \\ 0 & 0 & 0 \\ 0 & 0 & 0 \end{bmatrix}, \quad \hat{R}_{LLM} = \begin{bmatrix} \hat{D}_{LLM} & 0 & 0 \\ 0 & 0 & 0 \\ 0 & 0 & 0 \end{bmatrix}, \quad \text{(III.113)}$$

where $\hat{D}_{HR} = a_M\hat{M} + a_K\hat{K}_{HR}$, $\hat{D}_{GHP} = a_M\hat{M} + a_K\hat{K}_{GHP}$ and $\hat{D}_{LLM} = a_M\hat{M} + a_K\hat{K}_{LLM}$ are the corresponding damping matrices. The simulated results for the dynamic response at the tip end of the beam are presented in Fig. III.8, and the evolution of the Hamiltonian functions are shown in Fig. III.9 .

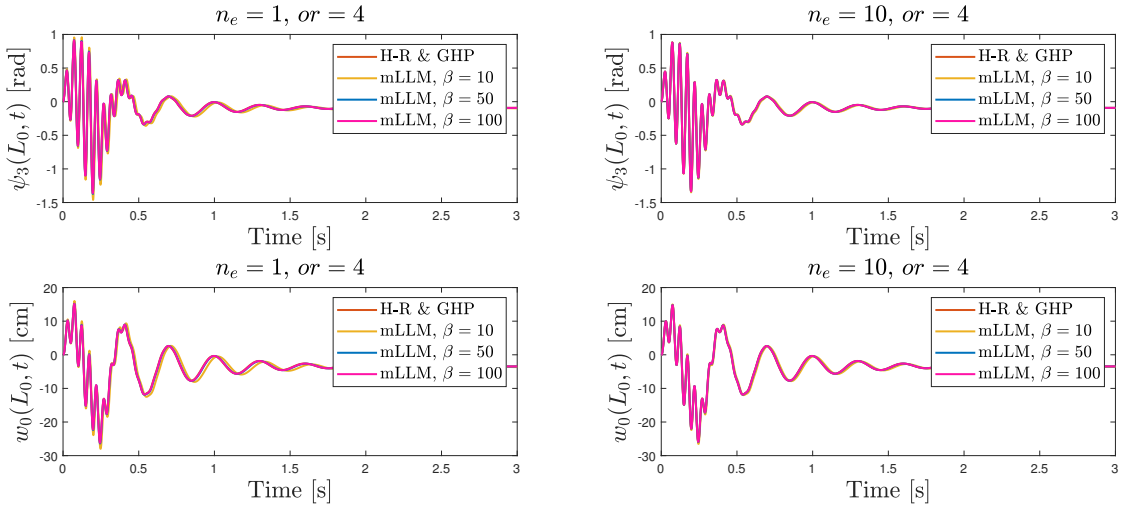

Figure III.8 – Dynamic response of the beam.

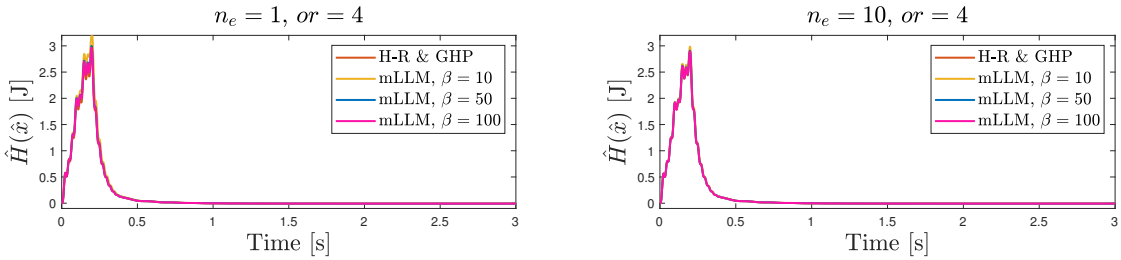

Figure III.9 – Hamiltonian of the beam.

From Fig. III.9, the evolution of the Hamiltonian functions is similar across the mLLM models and the H-R and GHP-based models. For $n_e = 1$, the Hamiltonians show noticeable differences for varying values of β, with $\beta = 50$ and $\beta = 100$ yielding results closest to those of the H-R and GHP models. This trend aligns with the observations in Fig. III.5 (bottom-left plot), which illustrates the static deflections. In contrast, for $n_e = 10$, the Hamiltonians remain nearly identical across all models. The minimum of the Hamiltonian, located at $\hat{r} \neq 0$, corresponds to the equilibrium configuration (static deflection) shown in Fig. III.5, leading to the Hamiltonian converging to a negative value rather than zero, which reflects the gravitational potential energy at the equilibrium configuration. From Fig. III.8, the dynamic response is nearly identical between the discretized models of order four, whether using one or ten finite elements. The axial response $u_0(\mathtt{X}, t)$ remains zero along the domain and at all times, as the axial and vertical directions are not coupled in this linear model, and the input is applied solely in the vertical direction. The dynamic behavior of planar beams with coupled directions will be analyzed later when we discuss nonlinear and constrained nonlinear systems. Finally, the dynamic response of the beam with non-homogeneous Dirichlet boundary conditions (velocity applied as input) is not shown here and will be addressed in the next example involving a two-dimensional body.

III.4.1.b Two-dimensional general elasticity

The infinite-dimensional explicit linear PHS of the two-dimensional general elasticity was derived in Section II.4.1.a in page 68. The key variables of the PHS are given by:

$$\mathcal{F}_{\mathtt{x}} = \begin{bmatrix} \partial_1 & 0 \\ 0 & \partial_2 \\ \partial_2 & \partial_1 \end{bmatrix}, \quad \mathcal{M} = \begin{bmatrix} \rho_0 h & 0 \\ 0 & \rho_0 h \end{bmatrix}, \quad \mathcal{K}_\epsilon = \frac{hE}{1-\nu^2} \begin{bmatrix} 1 & \nu & 0 \\ \nu & 1 & 0 \\ 0 & 0 & \frac{1-\nu}{2} \end{bmatrix}, \quad b = \begin{bmatrix} 0 \\ 0 \\ 0 \end{bmatrix},$$

where $h = 10\,[mm]$ is the thickness, $\rho_0 = 5500\,[kg/m^3]$ is the density of the material, $E = 10\,[kPa]$ is Young's modulus, and $\nu = 0.3\,[-]$ is Poisson's ratio. The generalized displacement field $r(\mathtt{X}, t) = [u_1(\mathtt{X}, t)\ u_2(\mathtt{X}, t)]^\top \in \mathbb{R}^2$, where $u_1(\mathtt{X}, t)$ and $u_2(\mathtt{X}, t)$ are the horizontal and vertical displacements of points within the domain, respectively. For this case, $\mathtt{X} = \{X_1, X_2\} \in \Omega \subset \mathbb{R}^2$, where the domain Ω represents a frame structure, as depicted in Fig. III.10. The geometric parameters of the structure are defined by a horizontal length $L_h = 30\,[cm]$, a vertical length $L_v = 11\,[cm]$, and the frame thickness $t_h = 2\,[cm]$.

To validate the effectiveness of the proposed methods in capturing the dynamics of the infinite-dimensional two-dimensional elasticity problem, the natural frequencies were computed and compared against the results provided by the software *Autodesk Inventor ®*. For this analysis, Dirichlet and Neumman boundary conditions are specified as homogeneous, i.e., $\hat{v}_D(t) = 0$ in $\partial\Omega_D$ and $\hat{\tau}_N(t) = 0$ in $\partial\Omega_N$. For simplicity, a single mesh was used, corresponding to the one shown in Fig. III.10, where the shape functions were selected as second-order canonical. The results are presented graphically in Fig. III.11.

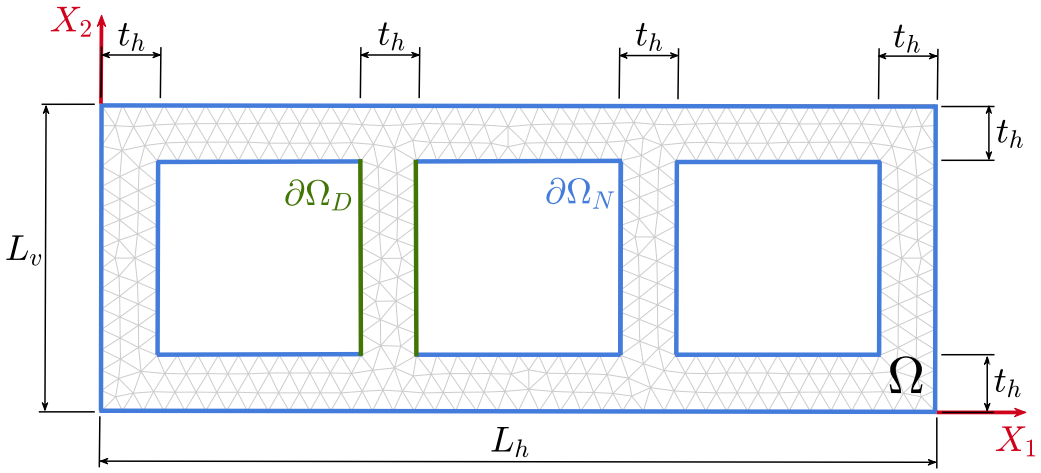

Figure III.10 – Two-dimensional domain.

The eigenmodes displayed in Fig. III.11 demonstrate the effectiveness of the proposed FEM-based approaches in capturing the key dynamic characteristics of the flexible body. All methods exhibit visually consistent mode shapes, confirming that the discretized models provide an adequate approximation of the system's physical behavior. However, slight variations in natural frequencies are noted across the methods. Specifically, the mLLM model with $\beta = 50$, closely aligns with the frequencies computed by the software, particularly in the higher modes. In contrast, the H-R and GHP models tend to underestimate these frequencies. This result is not surprising, as Autodesk Inventor employs a standard FEM approach, and despite mLLM being a mixed FEM, it is structurally closer to sFEM than the H-R and GHP approaches. Despite these differences, all models provide reasonable approximations of the system's eigenfrequencies, with the mLLM offering a marginally better fit to the software results.

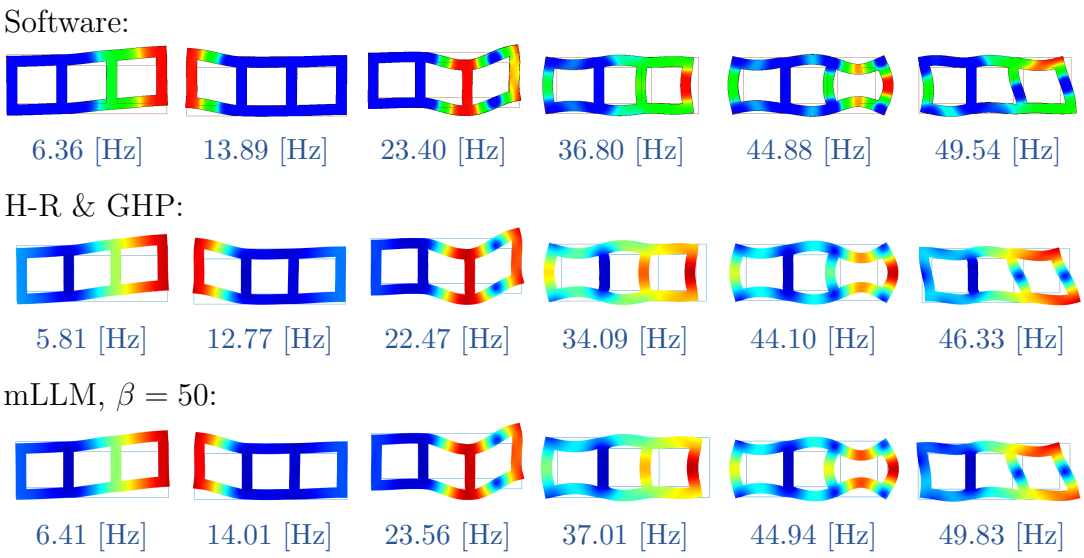

Figure III.11 – Comparison eigenmodes: Software vs discretized models.

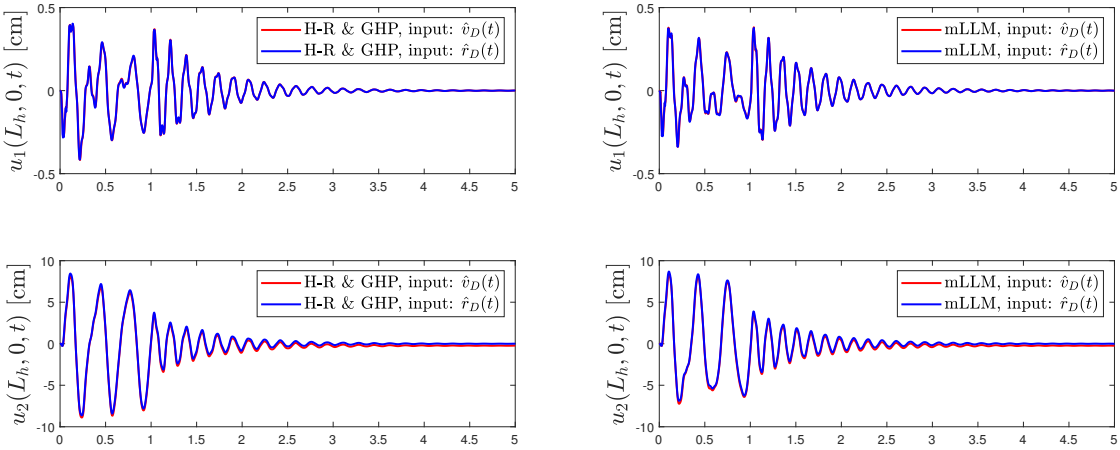

Figure III.12 – Dynamic response of the two-dimensional body.

Now, we test the models by applying Dirichlet boundary conditions, either in the form of displacements $\hat{r}_D(t)$ or velocities $\hat{v}_D(t)$. In this example, the same boundary velocity or boundary displacement, depending on the case, is imposed uniformly at each point along the Dirichlet boundary portion $\partial\Omega_D$. The inputs are defined as follows:

$$\hat{r}_D(t) = \begin{bmatrix} 0 \\ 0.05\sin(6\pi t) \end{bmatrix} [m] \text{ for } 0 \leq t \leq 1\,[s]; \quad \hat{v}_D(t) = \dot{\hat{r}}_D(t)\,[m/s].$$

Rayleigh damping is introduced to the H−R, GHP and mLLM models, with the damping coefficients set to $a_M = 3$ and $a_K = 1 \cdot 10^{-4}$. The simulated results for the dynamic response at the bottom-right corner point $\mathtt{X} = (L_h, 0)$ are presented in Fig. III.12. The responses follow very similar trajectories regardless of whether the H−R, GHP, or mLLM approaches are used for discretizing the system. In addition to the differences between models, slight variations arise within the same approach depending on whether a velocity or displacement input is applied. When the displacement input $\hat{r}_D(t)$ is imposed, the system is expected to settle at zero after the transients decay, and this behavior is indeed observed. In contrast, when the velocity input is applied, the system does not converge to the same vertical position, despite the fact that the imposed velocity $\hat{v}_D(t)$ is defined as the time derivative of $\hat{r}_D(t)$. This discrepancy underscores how the choice of input affects the final steady-state configuration, with the displacement input enabling the system to more accurately follow the intended displacement trajectories. At this stage, it is unclear whether this discrepancy is due to numerical errors during time integration. This issue will be investigated further in future research.

III.4.2 Nonlinear systems

In this section, we present the simulation results of a geometrically nonlinear planar beam model using the proposed approach based on the GHP. The results highlight the coupling between the vertical and axial displacements, illustrating

the inherent nonlinearities of the system. However, it is important to note that no explicit constraint is imposed to preserve the beam's length over time. Examples incorporating such constraints will be presented in the following section. The infinite-dimensional geometrically nonlinear PHS model of the planar beam was derived in Section II.4.2.b, following the modeling Methodology 2 in page 57, so the details on this model are omitted here. The key variables of the geometrically nonlinear planar beam remain the same as those presented in the linear case. The primary difference lies in the differential operator, which is now modulated by the generalized displacement field. The non-constant differential operator $\mathcal{F}_{\mathbf{x}}(r)$ is given by:

$$\mathcal{F}_{\mathbf{x}}(r) = \begin{bmatrix} \partial_1 & 0 & \partial_1 w_0 \\ 0 & \partial_1 & 0 \\ 0 & -1 & \partial_1 \end{bmatrix}.$$

The numerical values used are the same as previously listed in Table III.2. Damping is introduced into the system through the dissipation matrix $\hat{R}_{GHP}$ defined in (III.113), where now the damping matrix is given by $\hat{D}_{GHP} = 2 \cdot 10^{-3} I_{N_\Omega}$. Since the simulated results will be compared with upcoming constrained nonlinear systems, which lack a properly defined stiffness matrix, Rayleigh damping was not chosen. Moreover, special considerations must be taken into account for Rayleigh damping in nonlinear systems. Now, we test the model by applying Neumann boundary conditions at $X_1 = L_0$, where a vertical force is considered. The input is defined as:

$$\hat{\tau}_N(t) = \begin{bmatrix} 0 & 0 & 10\sin(40\pi t) \end{bmatrix}^\top [N] \quad ; \text{ for } 0 \leq t \leq 0.2\,[s].$$

The shape functions are selected as canonical of order $or = 10$, using a mesh consisting of a single element. The simulated results for the dynamic response at the tip end of the beam are presented in Fig. III.13, and the evolution of the Hamiltonian and their components are shown in Fig. III.14. It is important to note that, unlike in the linear case, the vertical input force induces axial motion.

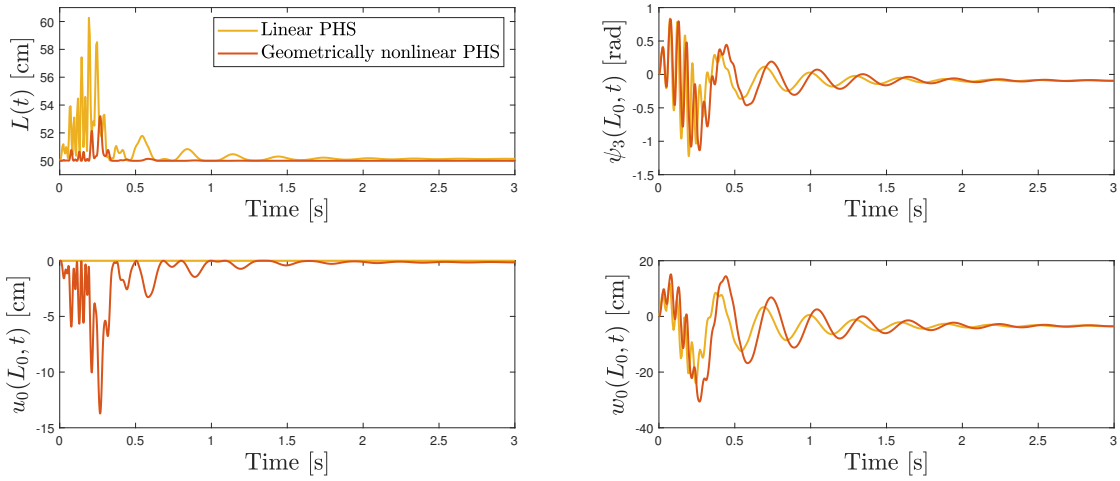

Figure III.13 – Dynamic response of geometrically nonlinear planar beam.

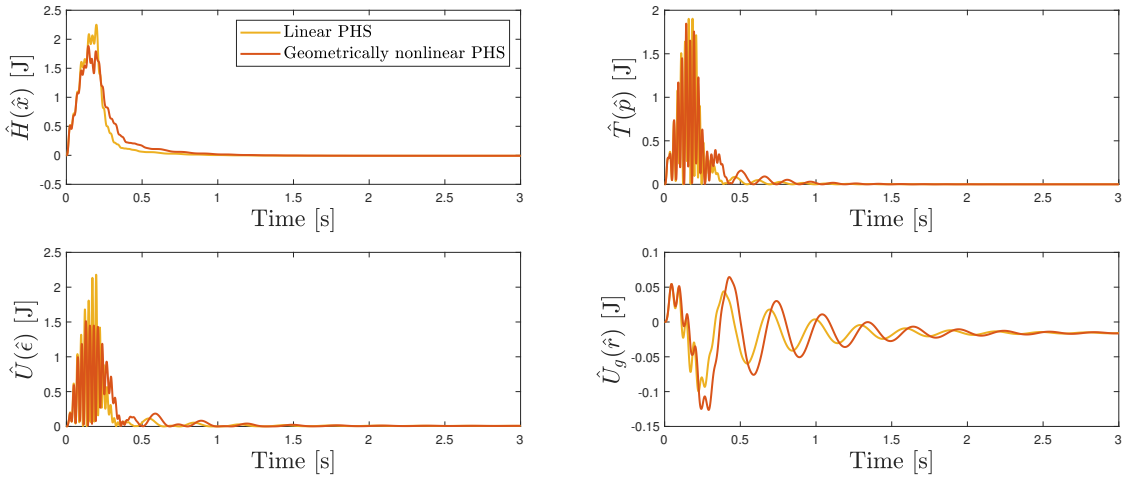

Figure III.14 – Energy of geometrically nonlinear beam.

This occurs because, in the geometrically nonlinear beam, both directions are coupled through the differential operator $\mathcal{F}_{\mathbf{x}}(r)$. Additionally, due to this coupling, the beam's current length $L(t)$ remains closer to its original length, compared to the linear case. However, as previously mentioned, no constraint is imposed to ensure that $L(t) = L_0 = 50\,[cm]$. In Fig. III.14, we present the contributions of the kinetic energy $\hat{T}(\hat{p})$, the elastic potential energy $\hat{U}(\hat{\epsilon})$, and the gravitational potential energy $\hat{U}_g(\hat{r})$. The sum of these components yields the Hamiltonian $\hat{H}(\hat{x})$, which represents the total energy of the system. The Hamiltonian $\hat{H}(\hat{x})$ decays over time due to dissipation, as expected. The kinetic energy $\hat{T}(\hat{p})$ and elastic potential energy $\hat{U}(\hat{\epsilon})$ are both positive definite throughout the simulation. The gravitational potential energy $\hat{U}_g(\hat{r})$, while smaller in magnitude compared to the other components, contributes to the total energy as well. The comparison between the linear and geometrically nonlinear cases shows similar energy decay trends, indicating that both systems exhibit consistent dissipative behavior.

III.4.3 Constrained nonlinear systems

So far, the examples in the previous sections have illustrated the GHP-based approach for handling both linear and nonlinear systems, with the latter addressing nonlinearities in the interconnection operator $\mathcal{F}_{\mathbf{x}}(r)$. To further evaluate the method in the context of both geometrically and materially nonlinear systems, as well as nonlinear systems formulated as PH-DAE systems, this section deals with two different planar beam models. These models both consider the incompressibility constraint, aiming to ensure volume preservation during deformation. The exact constraint that the beam models must satisfy to impose incompressibility is given by:

$$J_\epsilon(\mathbf{X}, t) = \sqrt{III_C(\mathbf{X}, t)} = \sqrt{(2\varepsilon_{11} + 1)(2\varepsilon_{33} + 1) - 4\varepsilon_{13}^2} = 1,$$

where $\varepsilon_{11}(\mathbf{X}, t) = \epsilon_1(X_1, t) - X_3\,\epsilon_2(X_1, t)$, $\varepsilon_{33}(\mathbf{X}, t) = \frac{1}{2}\psi_3(X_1, t)^2$, and $2\varepsilon_{13}(\mathbf{X}, t) = \epsilon_3(X_1, t)$. Note that $J_\epsilon(\mathbf{X}, t)$ is valid for each point $\mathbf{X} \in \mathcal{B}_0$, where $\mathcal{B}_0 \subset \mathbb{R}^3$ denotes

the three-dimensional beam in the reference configuration. To check how effective are the models to impose the incompressibility, we will evaluate $J_\epsilon(\mathbf{X}, t)$ along the neutral line. Then, we define:

$$J^0_\epsilon(X_1, t) = J_\epsilon(X_1, X_2 = 0, X_3 = 0, t) = \sqrt{(2\epsilon_1 + 1)(\psi_3^2 + 1) - \epsilon_3^2} = 1.$$

III.4.3.a Constrained nonlinear beam as a PH-DAE system

The PH-DAE beam is defined with respect to the same non-constant differential operator $\mathcal{F}_{\mathtt{x}}(r)$ as in the geometrically nonlinear case. This model accounts for material nonlinearities by employing an incompressible neo-Hookean model to represent the elastic potential energy. The isochoric-generalized strain energy density function, $\Psi_{iso}(\epsilon)$, is derived from this neo-Hookean model and is given by:

$$\Psi_{iso}(\epsilon) = \frac{A_0\mu_L}{2}\left(\frac{3}{(1-\epsilon_3^2)^{1/3}} - \frac{2\epsilon_3^2\epsilon_1}{(1-\epsilon_3^2)^{4/3}} + \frac{4\epsilon_1^2(\epsilon_3^2+1)}{3(1-\epsilon_3^2)^{7/3}} - 3\right) + \frac{2\bar{I}_0\mu_L}{3}\left(\frac{\epsilon_2^2(\epsilon_3^2+1)}{(1-\epsilon_3^2)^{7/3}}\right).$$

In this case, incompressible deformation is attempted to be imposed through the generalized constraint $\gamma(\epsilon) = A_0(2\epsilon_1 - \epsilon_3^2) = 0$, then, the associated differential operator is then obtained as $\mathcal{L}_{\mathtt{x}}(\epsilon, r) = \frac{\partial\gamma}{\partial\epsilon}^\top \mathcal{F}_{\mathtt{x}}(r)$.

In order to compare the results with those of the previous geometrically nonlinear beam, the shape functions are selected as canonical of order $or = 10$, using a mesh consisting of a single element. The numerical values are those indicated in Table III.2, with artificial damping $\hat{D}_{GHP} = 1{\cdot}10^{-3}$. The Neumman boundary input is the same as before defined as: $\hat{\tau}_N(t) = \begin{bmatrix}0 & 0 & 10\sin(40\pi t)\end{bmatrix}^\top [N]$, for $0 \leq t \leq 0.2\,[s]$. The dynamic response at the tip end of the beam, along with the evaluation of $J^0_\epsilon(X_1, t)$ and $\gamma(\epsilon)$, are presented in Figs. III.15 and III.17, and the evolution of the Hamiltonian and their components are shown in Fig. III.16.

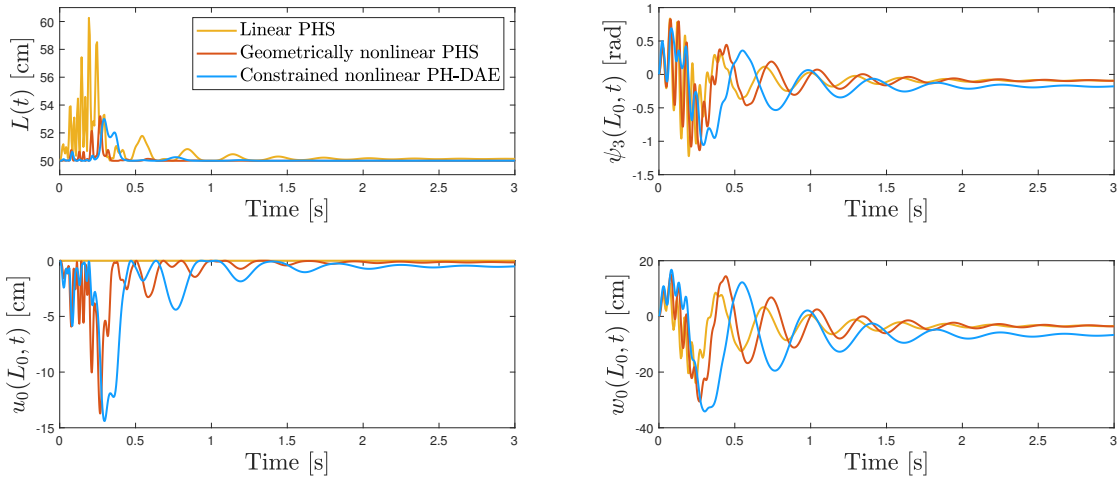

Figure III.15 – Dynamic response of constrained nonlinear beam as PH-DAE.

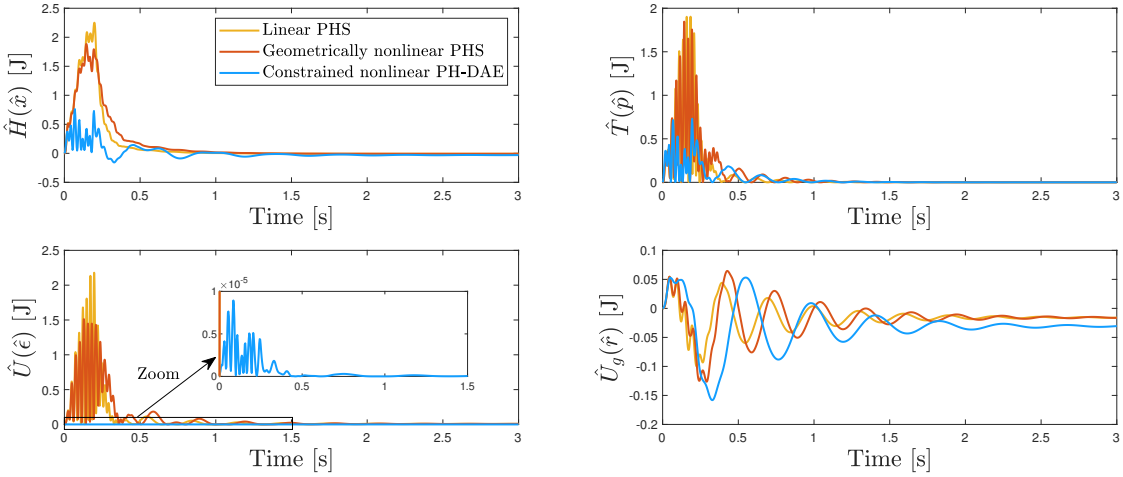

Figure III.16 – Energy of constrained nonlinear beam as PH-DAE.

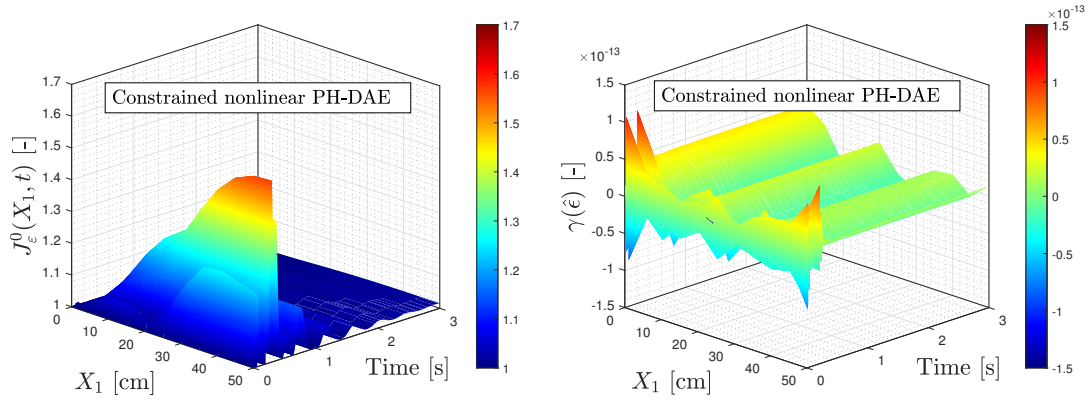

(a) Evaluation of $J^0_\epsilon(X_1,t)$ (b) Evaluation of $\gamma(\epsilon)$

Figure III.17 – Evaluation of constraints: PH-DAE planar beam.

From Fig. III.17a, it can be observed that the discretized PH-DAE model fails to enforce incompressibility, since $J^0_\epsilon(X_1,t) \neq 1$. This issue is attributed to the infinite-dimensional PH-DAE model, where the constraint $\gamma(\epsilon) = 0$ does not couple the real strains ε_{11} and ε_{33}. Consequently, the beam's current length $L(t)$ is not better preserved compared to the unconstrained geometrically nonlinear case, as shown in Fig. III.15. On the other hand, the discretized PH-DAE model accurately enforces the constraint $\gamma(\epsilon) = 0$, as observed in Fig. III.17b, where $\gamma(\hat{\epsilon})$ is almost equal to zero for all $X_1 \in \Omega$ and time. This demonstrates that the proposed approach is capable of approximating the algebraic constraint at the finite-dimensional level. Fig. III.16 reveals that the Hamiltonian $\hat{H}(\hat{x})$ in this case is lower in magnitude, primarily due to the reduced kinetic energy $\hat{T}(\hat{p})$ compared to both the linear and geometrically nonlinear cases, and the elastic potential energy $\hat{U}(\hat{\epsilon})$ being nearly zero. It is important to note that the beam's constitutive model here is an incompressible neo-Hookean solid, which accounts only for the isochoric part, making it not directly comparable to the previous cases where the

constitutive model followed Hooke's law for the linear model, or Saint-Venant-Kirchhoff material for the geometrically nonlinear model. Despite the near-zero values of $\hat{U}(\hat{\epsilon})$, the dynamic behavior remains similar to that observed in the linear and geometrically nonlinear cases, as shown in Fig. III.15.

III.4.3.b Constrained nonlinear beam as an explicit PHS

The explicit PHS formulation of the constrained nonlinear beam model is defined with respect to the non-constant differential operator $\bar{\mathcal{F}}_{\mathbf{x}}(r) = \mathcal{F}_{\mathbf{x}}(r)$, where $\mathcal{F}_{\mathbf{x}}(r)$ is the same as in the geometrically nonlinear case. This model also accounts for material nonlinearities by employing an incompressible neo-Hookean model to represent the elastic potential energy. The strain energy density function $\bar{\Psi}(\bar{\epsilon})$ in this model, is derived from this neo-Hookean model and is given by:

$$\bar{\Psi}(\bar{\epsilon}) = A_0\mu_L(\Theta_0(\bar{\epsilon}) + \epsilon_1) + \bar{I}_0\mu_L\Theta_2(\bar{\epsilon}),$$

where $\Theta_0(\bar{\epsilon}) = 2\epsilon_1^2 - \epsilon_1 + \frac{1}{2}\epsilon_3^2 - \epsilon_1^2\epsilon_3^2 - 4\epsilon_1^3$, and $\Theta_2(\bar{\epsilon}) = 2\epsilon_2^2 - \epsilon_2^2\epsilon_3^2 - 12\epsilon_1\epsilon_2^2$. In this case, incompressible deformation is attempted to be imposed through the generalized constraint $\gamma(\epsilon) = 0$, given by:

$$\gamma(\epsilon) = A_0\Theta_0(\bar{\epsilon}) + \bar{I}_0\Theta_2(\bar{\epsilon}) - A_0\epsilon_4 = 0,$$

where $\epsilon_4(X_1, t) = \frac{1}{2}\psi_3(X_1, t)^2 = \varepsilon_{33}(\mathbf{X}, t)$. Using the same shape functions of order $or = 10$ and a single element, the same numerical values, damping, and Neumann boundary input, the dynamic response at the tip end of the beam, along with the evaluation of $J_\epsilon^0(X_1, t)$ and $\gamma(\epsilon)$ in this case, are presented in Figs. III.18 and III.20, and the evolution of the Hamiltonian and their components in Fig. III.19.

In contrast with the PH-DAE model, from Fig. III.20a, it can be observed that the discretized explicit PHS model is able to enforce incompressibility, since $J_\epsilon^0(X_1, t) \approx 1$ due to the imposition of the constraint $\gamma(\epsilon) = 0$, as observed in Fig.

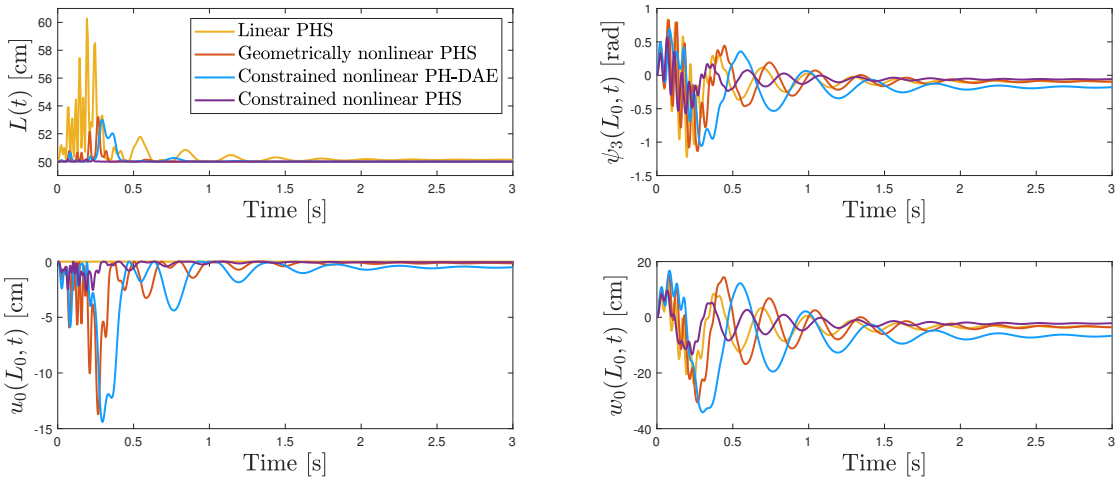

Figure III.18 – Dynamic response of constrained nonlinear beam as PHS.

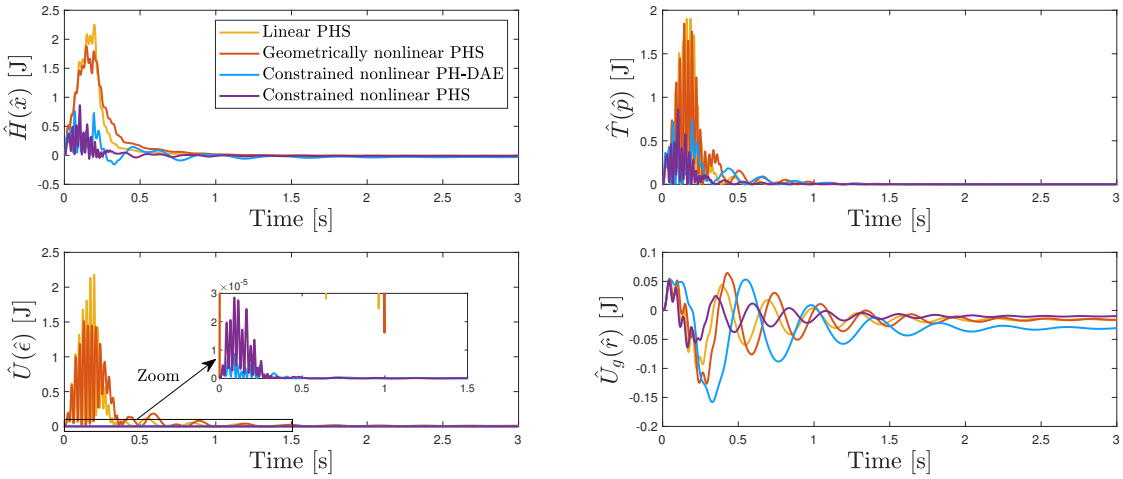

Figure III.19 – Energy of constrained nonlinear beam as PHS.

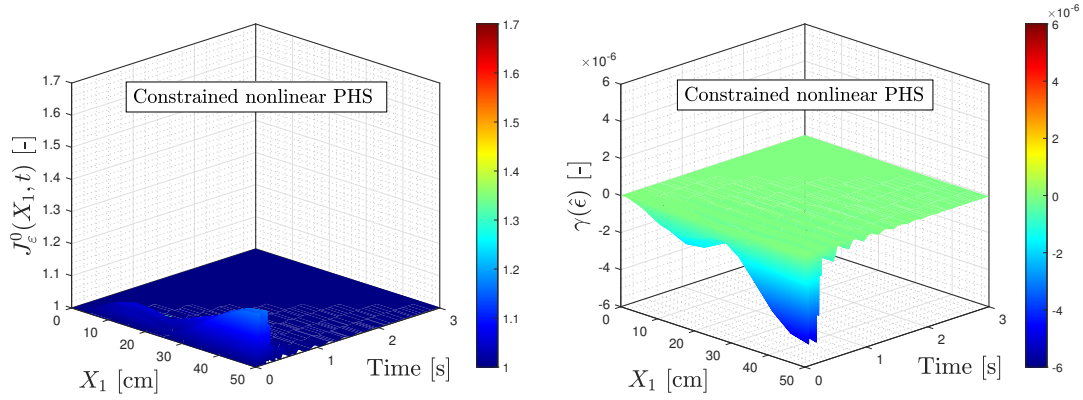

(a) Evaluation of $J^0_\epsilon(X_1, t)$ (b) Evaluation of $\gamma(\epsilon)$

Figure III.20 – Evaluation of constraints: PH-DAE planar beam.

III.20b, where $\gamma(\hat{\epsilon}) \approx 0$ for all $X_1 \in \Omega$ and time. Consequently, the beam's current length $L(t) \approx L_0$ for all time, as shown in Fig. III.18. Lastly, Fig. III.19 shows that the Hamiltonian $\hat{H}(\hat{x})$, kinetic energy $\hat{T}(\hat{p})$, elastic potential energy $\hat{U}(\hat{\epsilon})$, and gravitational potential energy $\hat{U}_g(\hat{r})$ are comparable in magnitude to those of the constrained nonlinear PH-DAE. In this case, the beam's constitutive model is also an incompressible neo-Hookean solid; however, the isochoric part is obtained through a different approach, as discussed in Section II.4.2.d in page 82, where the infinite-dimensional was derived. Therefore, it is not surprising that both models, the constrained nonlinear PH-DAE and the constrained nonlinear PHS, exhibit similar energetic behavior.

Remarks on simulation examples

All simulations were carried out in MATLAB , with custom code developed for the FEM discretization of both 1D and 2D systems. Time integration of the linear systems was performed using the `lsim` command, while the nonlinear systems were simulated using the `ode15s` solver. For the PH-DAE systems, an implicit midpoint rule was employed via a custom implementation. Regarding computational performance, for the 1D linear beam model with $n_e = 30$ finite elements and shape functions of polynomial order $or = 4$, simulation times ranged from 3-4 seconds. For the 2D linear elasticity model, using the mesh illustrated in Fig. III.10 and second-order triangular elements, simulations required 1-2 seconds. In the nonlinear 1D beam models, with $n_e = 1$ and $or = 10$, the geometrically nonlinear case took approximately 10 seconds, while systems with both geometric and material nonlinearities took up to 20 seconds. However, PH-DAE simulations were significantly more time-consuming, taking around 1.5 hours. The simulation times increased further for nonlinear systems with additional elements ($n_e \geq 2$), reaching around 6-7 hours for $n_e = 3$ elements of order $or = 2$, and more than 2 days for the PH-DAE system. This increase in simulation time is likely due to the assembly process that must be performed at each time step, which is not necessary for a single element. We believe these times can be substantially reduced with optimized code, as the current implementation was developed for model testing rather than efficient simulation. Future work will focus on enhancing computational efficiency to make these models suitable for real-time control applications.

III.5 Conclusion

In this chapter we have proposed and numerically tested the mixed FEM discretization approaches for both linear and nonlinear PHS and PH-DAE systems. The mLLM and GHP-based methods were validated using 1D and 2D linear examples, with comparisons to the commercial software *Autodesk Inventor ®*, while the GHP approach was applied to 1D nonlinear PHS and PH-DAE systems. The results demonstrated that these methods effectively capture the dynamic behavior of infinite-dimensional systems.

Simulations of nonlinear systems were limited to 1D due to the increased computational complexity of implementing the nonlinear mixed FEM in 2D. Moreover, simulations of discretized nonlinear systems are significantly more time-consuming than their linear counterparts, as the nonlinear terms require assembly and numerical integration at each time step. While simulations of 2D nonlinear systems remain pending, we expect that the proposed GHP-based approach will perform as well as in the 1D cases. This expectation stems from the fact that the discretization is based on the well-established GHP, with only slight modifications

to preserve the PHS structure. Nonetheless, it is crucial to extend this work by testing 2D and 3D nonlinear systems to fully confirm these insights.

Since the finite-dimensional models have been validated, the next chapter will focus on using them for energy-based shape control design.

Chapter IV
Linear energy-based shape control design

IV.1 Introduction

The concept of shape control has first appeared in [Haftka 1985], where an analytical method was introduced for using thermal actuators to manage quasi-static deformations of large flexible structures. Static shape control deals with achieving a desired configuration using static models, while dynamic shape control addresses systems governed by dynamic models. In mechatronics, shape control finds applications in the development of robotic manipulators and other devices designed for continuous deformation [Dupont 2022; Shintake 2018]. Dynamic shape control design using PHS, leveraging passivity, involves shaping the closed-loop energy function and assigning its dissipation rate. This approach influences both the system's transient response and its steady-state deformation. There are two main methodologies for controller design in this context: (i) those based on finite-dimensional approximations or early lumping approaches, as in [Liu 2024; Yeh 2022; Zhou 2021], and (ii) those using infinite-dimensional models, known as late lumping approaches, as in [Malzer 2019; Voß 2011]. In this chapter we address the dynamic shape control of linear PHS using the early lumping approach. A class of PHS controllers for a class of linear PHS is proposed, enabling the optimal design of dynamic shape control with distributed and pointwise actuation within the domain. The controllers are applicable whether they are derived from low-order discretized models [1] or reduced-order models [2]. The chapter begins with the control design based on the full-order linear PHS using Energy Shaping (ES) and Control by Interconnection (CbI), providing a parametrization of the closed-loop equilibrium points and conditions on the controller parameters that ensure asymptotic stability for arbitrary input mappings. Then, two alternative controllers are developed, one derived from a low-dimensional discretized model and the other from a reduced-order model, both designed based on structural invariants. In each case, the controllers are parametrized to offer clear physical interpretations and to modify both the transient dynamics and the steady-state shape of the system. An error metric is defined as a criterion for achieving the closest possible (optimal) equilibrium configuration relative to an arbitrary desired shape.

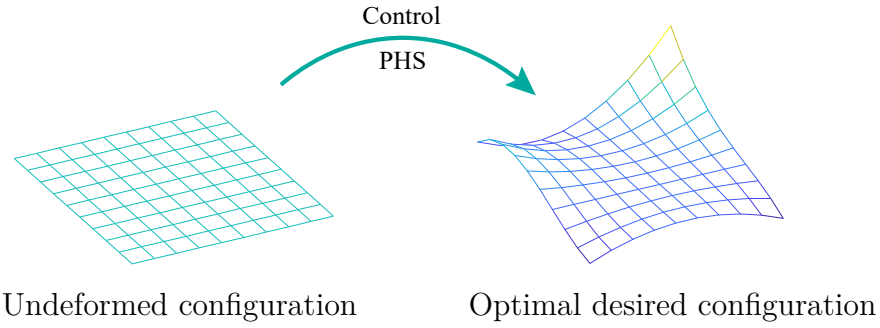

Figure IV.1 – Scheme of dynamic shape control of PHS.

1. Models created using fewer elements than a full-order model that uses many elements.
2. Models obtained through a model-order reduction process applied to a full-order model.

IV.2 Preliminaries

In this section, we discuss the structure-preserving model reduction via modal truncation, a technique that reduces the system's complexity while retaining its essential dynamic properties. Additionally, we introduce the fundamental passivity-based control (PBC) techniques that form the basis for the proposed controllers for dynamic shape control of linear PHS. They are the Energy Shaping (ES) and Control by Interconnection (CbI), which are widely used to shape the energy (Hamiltonian) of PHS to achieve desired control objectives. These foundations will support the development of the controllers for the dynamic shape control presented in the subsequent sections.

IV.2.1 Structure-preserving modal truncation

The considered class of linear PHS and the structure-preserving model reduction via modal truncation are presented here. First, we consider finite-dimensional linear PHS with the following structure, stemming from the modeling and discretization of flexible mechanical systems:

$$\begin{aligned} \underbrace{\begin{bmatrix} \dot{p} \\ \dot{r} \end{bmatrix}}_{\dot{x}} &= \Big(\underbrace{\begin{bmatrix} 0 & -I_n \\ I_n & 0 \end{bmatrix}}_{J} - \underbrace{\begin{bmatrix} D & 0 \\ 0 & 0 \end{bmatrix}}_{R} \Big) \underbrace{\begin{bmatrix} M^{-1} & 0 \\ 0 & K \end{bmatrix}}_{Q} \underbrace{\begin{bmatrix} p \\ r \end{bmatrix}}_{x} + \underbrace{\begin{bmatrix} B \\ 0 \end{bmatrix}}_{G} u \\ y &= G^\top Q\, x, \end{aligned} \tag{IV.1}$$

where $r \in \mathbb{R}^n$ is the vector of generalized displacements, $p \in \mathbb{R}^n$ is the vector of generalized momenta, $M = M^\top > 0 \in \mathbb{R}^{n\times n}$ is the mass matrix, $K = K^\top > 0 \in \mathbb{R}^{n\times n}$ is the stiffness matrix, $D = D^\top \geq 0 \in \mathbb{R}^{n\times n}$ is the damping matrix, $B \in \mathbb{R}^{n\times m}$ is the input map, $u \in \mathbb{R}^m$ is the input vector, $y \in \mathbb{R}^m$ is the output vector, and $I_n \in \mathbb{R}^{n\times n}$ is an identity matrix. The Hamiltonian of (IV.1) is given by:

$$H(x) = \frac{1}{2}\, x^\top Q\, x = \frac{1}{2}\, p^\top M^{-1} p + \frac{1}{2}\, r^\top K\, r > 0, \tag{IV.2}$$

which is the sum of the kinetic and the elastic potential energy. The equilibrium points of (IV.1), denoted as $x^* = [p^{*\top}\ r^{*\top}]^\top$, are given by:

$$p^* = 0, \quad r^* = K^{-1} B\, u^*, \tag{IV.3}$$

where u^* denotes an arbitrary steady-state input, and r^* defines the achievable steady-state deformed configurations (deformed shapes).

Remark IV.1. *The class of linear PHS considered in (IV.1) shares the same structural form as the discretized PLS introduced in Chapter III, excluding the generalized body force term, $\hat{b}$. Specifically, this includes the PLS derived from the standard FEM with the Penalty method, the PLS resulting from mixed FEM using the mLLM method, and the PLS obtained from mixed FEM using H-R-based or GHP-based approaches, in the cases when the stiffness matrices $\hat{K}_{HR}$ and $\hat{K}_{GHP}$ are invertible, respectively.*

Since KM^{-1} is the product of two symmetric positive definite matrices, both matrices are diagonalizable and the product has positive real eigenvalues [Zhou 1996], hence:

$$(KM^{-1})V_p = \Theta^2 V_p,$$

where $\Theta = \text{diag}\{\omega_1, \dots, \omega_n\} \in \mathbb{R}^{n\times n}$ is the eigenfrequencies matrix with $\omega_1 < \omega_2 < \cdots < \omega_n$, $V_p = [V_1^p \dots V_n^p] \in \mathbb{R}^{n\times n}$ is the right eigenvectors matrix, and $V_r = V_p^{-\top} = [V_1^r \dots V_n^r] \in \mathbb{R}^{n\times n}$ is the left eigenvectors matrix. Let define the transformation matrices:

$$T_M = \begin{bmatrix} V_p & 0 \\ 0 & V_r \end{bmatrix}, \quad T_M^{-1} = \begin{bmatrix} V_r^\top & 0 \\ 0 & V_p^\top \end{bmatrix},$$

such that the original state $x \in \mathbb{R}^{2n}$ is related to the modal state $x_M \in \mathbb{R}^{2n}$ by $x = T_M\, x_M$. Then, the modal realization of (IV.1) is written as a PHS with respect to the matrices $J_M = T_M^{-1} J\, T_M^{-\top} = J$, $R_M = T_M^{-1} R\, T_M^{-\top}$, $Q_M = T_M^\top Q\, T_M$, and $G_M = T_M^{-1} G$. Structure-preserving model reduction based on modal truncation, [Mourllion 2013] and [Clough 2003, Chapter 12], consists in truncating the modal realization up to the first $n_r < n$ eigenfrequencies and eigenvectors, that is, $\Theta_{n_r} = \text{diag}\{\omega_1, \dots, \omega_{n_r}\} \in \mathbb{R}^{n_r\times n_r}$. Defining the transformation matrices:

$$\begin{aligned} T_p &= \begin{bmatrix} V_1^p & \dots & V_{n_r}^p \end{bmatrix}, & T_r &= \begin{bmatrix} V_1^r & \dots & V_{n_r}^r \end{bmatrix}, \\ T_R &= \begin{bmatrix} T_p & 0 \\ 0 & T_r \end{bmatrix}, & T_{Ri} &= \begin{bmatrix} T_r^\top & 0 \\ 0 & T_p^\top \end{bmatrix}, \end{aligned} \tag{IV.4}$$

with $T_p, T_r \in \mathbb{R}^{n\times n_r}$, the reduced PHS model is given by:

$$\begin{aligned} \underbrace{\begin{bmatrix} \dot{p}_r \\ \dot{r}_r \end{bmatrix}}_{\dot{x}_r} &= \Big(\underbrace{\begin{bmatrix} 0 & -I_{n_r} \\ I_{n_r} & 0 \end{bmatrix}}_{J_r} - \underbrace{\begin{bmatrix} D_r & 0 \\ 0 & 0 \end{bmatrix}}_{R_r} \Big) \underbrace{\begin{bmatrix} M_r^{-1} & 0 \\ 0 & K_r \end{bmatrix}}_{Q_r} \underbrace{\begin{bmatrix} p_r \\ r_r \end{bmatrix}}_{x_r} + \underbrace{\begin{bmatrix} B_r \\ 0 \end{bmatrix}}_{G_r} u \\ y_r &= G_r^\top Q_r\, x_r, \end{aligned} \tag{IV.5}$$

with $J_r = T_{Ri} J\, T_{Ri}^\top$, $R_r = T_{Ri} R\, T_{Ri}^\top$, $Q_r = T_R^\top Q\, T_R$, $G_r = T_{Ri}\, G$, I_{n_r} an identity matrix, and the reduced modal matrices given by:

$$M_r = T_r^\top M\, T_r = \text{diag}\{\hat{m}_1, \dots, \hat{m}_{n_r}\}, \tag{IV.6}$$

$$K_r = T_r^\top K\, T_r = \text{diag}\{\hat{k}_1, \dots, \hat{k}_{n_r}\}, \tag{IV.7}$$

$$D_r = T_r^\top D\, T_r, \tag{IV.8}$$

$$B_r = T_r^\top B, \tag{IV.9}$$

with $M_r, K_r, D_r \in \mathbb{R}^{n_r\times n_r}$, $B_r \in \mathbb{R}^{n_r\times m}$, and:

$$p_r = T_r^\top p, \quad r_r = T_p^\top r. \tag{IV.10}$$

The equilibrium point of (IV.5) is given by $r_r^* = K_r^{-1} B_r u^*$ and is equivalent to (IV.3) mapped to the reduced order model coordinates, that is, $r_r^* = T_p^\top r^*$.

IV.2.2 Energy shaping using control by interconnection

The ES using CbI is a PBC technique that consists in interconnecting in a power-preserving way a PHS plant with a PHS controller, as illustrated in Fig. IV.2. In this setup, the Hamiltonian H_c of the controller is designed to shape the closed-loop energy function H_{cl} using structural invariants called Casimir functions [van der Schaft 2017], where the objective is to ensure that the minimum of H_{cl} aligns with the desired equilibrium configuration and the closed-loop system behaves with desired dynamic properties. Consider a finite-dimensional plant with PHS structure as:

$$\begin{aligned} \dot{x} &= (J - R)\nabla_x H(x) + G\,u \\ y &= G^\top \nabla_x H(x), \end{aligned} \tag{IV.11}$$

with $x \in \mathbb{R}^{2n}$ the state of the plant, and the finite-dimensional PHS controller:

$$\begin{aligned} \dot{x}_c &= (J_c - R_c)\nabla_{x_c} H_c(x_c) + G_c\,u_c \\ y_c &= G_c^\top \nabla_{x_c} H_c(x_c) + D_c\,u_c, \end{aligned} \tag{IV.12}$$

with $x_c \in \mathbb{R}^m$ the state of the controller and $D_c = D_c^\top \in \mathbb{R}^{m\times m}$ a feedthrough matrix. As illustrated in Fig. IV.2, a power-preserving interconnection between the PHS plant and the PHS controller is given by $u = -y_c$ and $y = u_c$. Then, the interconnected closed-loop system is given by:

$$\begin{bmatrix} \dot{x} \\ \dot{x}_c \end{bmatrix} = \left(\begin{bmatrix} J & -G\,G_c^\top \\ G_c\,G^\top & J_c \end{bmatrix} - \begin{bmatrix} R + G\,D_c\,G^\top & 0 \\ 0 & R_c \end{bmatrix} \right) \begin{bmatrix} \nabla_x H(x) \\ \nabla_{x_c} H_c(x_c) \end{bmatrix}, \tag{IV.13}$$

which is again a PHS with respect to the closed-loop Hamiltonian $H_{cl}(x, x_c) = H(x) + H_c(x_c)$. In ES using CbI, the matrices of the controller are chosen such that there exists a structural invariant linking the state of the controller and the state of the plant [van der Schaft 2017]. The structural invariants are called Casimir functions and are defined in terms of the vector function $F(x) = [F_1(x)^\top\ F_2(x)^\top\ ...\ F_m(x)^\top]^\top$, such that:

$$C = F(x) - x_c, \tag{IV.14}$$

with $C \in \mathbb{R}^m$ a constant on the invariant submanifold.

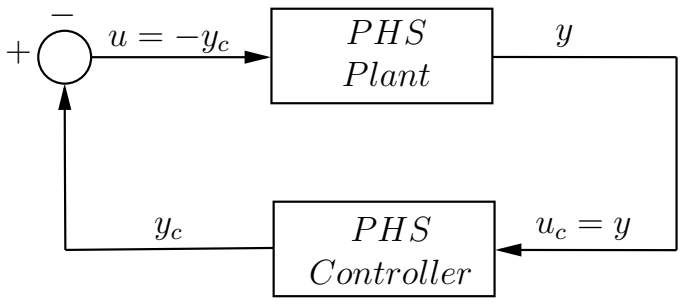

Figure IV.2 – Power-preserving interconnection between PHS.

The necessary and sufficient conditions for the existence of Casimir functions are characterized by the following matching equations (ME) [van der Schaft 2017]:

$$\frac{\partial F^\top}{\partial x} J \frac{\partial F}{\partial x} = J_c, \tag{IV.15}$$

$$R_c = 0, \tag{IV.16}$$

$$(R + G\, D_c\, G^\top) \frac{\partial F}{\partial x} = 0, \tag{IV.17}$$

$$\frac{\partial F^\top}{\partial x} J = G_c\, G^\top. \tag{IV.18}$$

Solving the ME the closed-loop Hamiltonian becomes:

$$H_{cl}(x) = H(x) + H_c(F(x) - C), \tag{IV.19}$$

and (IV.13) restricted to the invariant submanifold is equivalently written as:

$$\begin{aligned} \dot{x} = &\left[J - (R + G\, D_c\, G^\top)\right] \nabla_x H_{cl}(x) \\ y = &\; G^\top \nabla_x H_{cl}(x), \end{aligned} \tag{IV.20}$$

where the dynamic of the state $x \in \mathbb{R}^{2n}$ is characterized by the closed-loop energy function $H_{cl}(x)$ and the closed-loop dissipation matrix $(R + G\, D_c\, G^\top)$. If in addition $H_{cl}(x)$ is designed to be positive definite with strict minimum at the desired equilibrium point x^*, due to:

$$\dot{H}_{cl}(x) = -\nabla_x H_{cl}(x)^\top (R + G\, D_c\, G^\top) \nabla_x H_{cl}(x) < 0, \tag{IV.21}$$

and invoking La Salle's invariance principle, H_{cl} is a Lyapunov function and the closed-loop PHS in (IV.20) is asymptotically stable around x^* [van der Schaft 2017].

IV.3 Dynamic shape control design

In this section, we present a class of controllers for the considered class of linear PHS. The first part focuses on the general setting, where the controller is designed based on the full-order model of the PHS plant. The second part addresses reduced-order control of the full-order plant, where the controller is designed for the full-order system but based on a reduced-order model. This reduced-order model can arise from either a lower-order discretization or structure-preserving modal truncation.

IV.3.1 Full-order energy shaping control

The finite-dimensional PHS controller for the full-order finite-dimensional PHS plant, following the ES approach via CbI, is presented in the following proposition.

Proposition IV.1. *The finite-dimensional PHS controller:*

$$\begin{aligned} \dot{x}_c &= u_c \\ y_c &= \Sigma_c(x_c + C) - \Gamma_c\,\eta_c + D_c\,u_c, \end{aligned} \tag{IV.22}$$

with $C = (B^\top r - x_c)|_{t_0}$, *where* $D_c = D_c^\top \in \mathbb{R}^{m\times m}$ *and* $\Sigma_c = \Sigma_c^\top \in \mathbb{R}^{m\times m}$ *are design parameters which satisfy:*

$$K + B\,\Sigma_c B^\top > 0, \tag{IV.23}$$

$$D + B\,D_c B^\top > 0, \tag{IV.24}$$

and $\Gamma_c \in \mathbb{R}^{m\times n}$, $\eta_c \in \mathbb{R}^n$ *other design parameters associated with the closed-loop steady state, asymptotically stabilizes the linear PHS in* (IV.1) *at the equilibrium configuration:*

$$\begin{aligned} p^* &= 0, \\ r^* &= (K + B\,\Sigma_c B^\top)^{-1} B\,\Gamma_c\,\eta_c. \end{aligned} \tag{IV.25}$$

Proof. From (IV.17), $(D+BD_cB^\top)\frac{\partial F}{\partial p} = 0$, implying that $F(x)$ is only a function of r. Choosing $G_c = I_m$ with $I_m \in \mathbb{R}^{m\times m}$ an identity matrix, and solving (IV.18) it is obtained that $F(x) = B^\top r$, and from the remaining ME we get: $J_c = 0$, $R_c = 0$ and $D_c = D_c^\top$, which are a solution for the ME and defines the controller $\dot{x}_c = u_c$, $y_c = \nabla_{x_c} H_c(x_c) + D_c\,u_c$. Defining the following Hamiltonian for the controller:

$$H_c(x_c) = \frac{1}{2}\begin{bmatrix} x_c + C \\ \eta_c \end{bmatrix}^\top \begin{bmatrix} \Sigma_c & -\Gamma_c \\ -\Gamma_c^\top & \Lambda_c \end{bmatrix} \begin{bmatrix} x_c + C \\ \eta_c \end{bmatrix}, \tag{IV.26}$$

with $\Lambda_c \in \mathbb{R}^{n\times n}$ a constant matrix leads to $\nabla_{x_c} H_c = \Sigma_c(x_c + C) - \Gamma_c\,\eta_c$ and hence to the control system (IV.22) where the Casimir constant C is calculated from the initial conditions of (IV.1) and the initial conditions of the controller. The closed-loop Hamiltonian restricted to the invariant submanifold is given by $H_{cl}(x) = H(x) + H_c(F(x) - C)$, which is equivalently written as:

$$H_{cl}(x) = \frac{1}{2}\begin{bmatrix} p \\ r \\ \eta_c \end{bmatrix}^\top \begin{bmatrix} M^{-1} & 0 & 0 \\ 0 & K + B\,\Sigma_c B^\top & -B\,\Gamma_c \\ 0 & -\Gamma_c^\top B^\top & \Lambda_c \end{bmatrix} \begin{bmatrix} p \\ r \\ \eta_c \end{bmatrix}. \tag{IV.27}$$

Computing the gradient of $H_{cl}(x)$ and setting it equal to zero yields:

$$\nabla_x H_{cl}(x^*) = \begin{bmatrix} M^{-1}p^* \\ (K + B\,\Sigma_c B^\top)r^* - B\,\Gamma_c\,\eta_c \end{bmatrix} = \begin{bmatrix} 0 \\ 0 \end{bmatrix},$$

which leads to $p^* = 0$ and r^* given in (IV.25). To verify that (IV.25) is an equilibrium configuration of (IV.1), the following identity of the inverse of a sum of matrices is used [Henderson 1981]:

$$(A + UWU^\top)^{-1} = A^{-1} - A^{-1}UW(I + U^\top A^{-1}UW)^{-1}U^\top A^{-1},$$

to write (IV.25) as:

$$r^* = -K^{-1}B\,\Sigma_c(I_m + B^\top K^{-1}B\,\Sigma_c)^{-1}B^\top K^{-1}B\,\Gamma_c\,\eta_c + K^{-1}B\,\Gamma_c\,\eta_c,$$

and from (IV.3) it is seen that (IV.25) corresponds to the equilibrium configuration of the input:

$$u^* = (I_m - \Sigma_c(I_m + B^\top K^{-1}B\Sigma_c)^{-1}B^\top K^{-1}B)\,\Gamma_c\,\eta_c. \tag{IV.28}$$

Now, choosing $\Lambda_c = \Gamma_c^\top B^\top (K + B\,\Sigma_c B^\top)^{-1}B\,\Gamma_c$, $H_{cl}(x)$ is equivalently written as:

$$H_{cl}(x) = \frac{1}{2}\begin{bmatrix} p \\ r - r^* \end{bmatrix}^\top \begin{bmatrix} M^{-1} & 0 \\ 0 & K + B\,\Sigma_c B^\top \end{bmatrix} \begin{bmatrix} p \\ r - r^* \end{bmatrix}, \tag{IV.29}$$

which is positive definite if (IV.23) holds. If in addition (IV.24) holds, from (IV.21) $\dot{H}_{cl} = -p^\top(D + B\,D_c B^\top)\,p < 0$, then by LaSalle's invariance principle x^* is asymptotically stable.

□

Note that the PHS controller exhibits the structure of an integrator. The design parameter Σ_c plays a key role in modifying the closed-loop stiffness matrix $K_{cl} = K + B\Sigma_c B^\top$, and is primarily responsible for altering the dynamic properties of the system, that is, its eigenfrequencies. Additionally, the parameter D_c governs the decay rate, while Γ_c and η_c must be carefully chosen to ensure that r^* provides the best possible approximation to an arbitrary desired shape. The criteria for selecting these controller parameters Σ_c, Γ_c and η_c, to achieve the intended optimal deformed configurations will be developed in the following section. Although the upcoming section focuses on reduced-order energy shaping control, the results remain applicable when the controller is designed using the full-order model.

IV.3.2 Reduced-order energy shaping control

In this section, we consider two types of reduced-order representations of the linear PHS for control design. The first approach involves a low-dimensional model, as the one in (IV.1), but using a reduced number of finite elements in the discretization, with the variables denoted by the subscript ℓ. The second approach is based on structure-preserving modal truncation applied to the full-order model in (IV.1), with the variables denoted by the subscript r. As we will see later, the main distinction in their structure is that the matrices of the reduced models considered here are diagonal. For each, we provide an optimal design criterion based on the error between the desired arbitrary steady-state configuration and the achievable configuration. The choice between low-order and reduced-order models depends on the specific goals of preservation: low-order models, derived from discretizing an infinite-dimensional system, retain the structure of the matrices and physical interpretation of the state variables, while reduced-order models better preserve frequency information but lose direct state interpretation as they become modal coordinates. To aid the reader, we will later provide guidance on choosing the appropriate dimensions for both low and reduced-order models.

IV.3.2.a Design based on a low/reduced order model of the system

It is key to notice that the finite-dimensional PHS controller in (IV.22) generates Casimir functions with the same structure ($F(x) = B^\top r$) for any order of dimension of the linear PHS plant in (IV.1), or the reduced-order model in (IV.5). Hence, the PHS controller in (IV.22) can be designed using a low-order approximation of (IV.1) as long as the conditions (IV.23) and (IV.24) hold. Proposition IV.2 and Corollary IV.1 give the conditions on the controller parameters that ensure closed-loop stability when it is designed from the low-order version of (IV.1), or from a reduced-order model, respectively.

Proposition IV.2. *Consider (IV.1) of order $\ell < n$, $K_c = \alpha K_\ell$ with $\alpha \in \mathbb{R} > 0$, the parametrization:*

$$\Sigma_c = B_\ell^\dagger (K_c - K_\ell)(B_\ell^\dagger)^\top \qquad (\Sigma_c \in \mathbb{R}^{m\times m}), \tag{IV.30}$$

$$\Gamma_c = B_\ell^\dagger K_c \qquad (\Gamma_c \in \mathbb{R}^{m\times \ell}), \tag{IV.31}$$

$$\alpha > 1 - 1/\lambda_{max}(BY_\ell B^\top K^{-1}), \tag{IV.32}$$

with $(\cdot)^\dagger$ the pseudo-inverse, $Y_\ell = B_\ell^\dagger K_\ell (B_\ell^\dagger)^\top \in \mathbb{R}^{m\times m}$ and $\lambda_{max}(\cdot)$ the largest eigenvalue, then (IV.23) holds.

Proof. (IV.30) implies $\Sigma_c = (\alpha - 1)Y_\ell$ and the condition (IV.23) is equivalent to $(\alpha - 1)^{-1} I_n + BY_\ell B^\top K^{-1} > 0$. So a sufficient condition for the above inequality to be satisfied is that its lowest eigenvalue is positive, which implies $\det\Big((s - (\alpha - 1)^{-1})I_n - BY_\ell B^\top K^{-1}\Big) = 0$, where the term $(s - (\alpha - 1)^{-1}) = \lambda$ is an eigenvalue of $BY_\ell B^\top K^{-1}$. Then, $s > 0$ implies $\alpha > 1 - 1/\lambda$, where noticing that $BY_\ell B^\top K^{-1} > 0$, the smallest α that satisfies (IV.23) is given by (IV.32). □

Corollary IV.1. *Consider (IV.5) of order $n_r < n$, $K_c = \alpha K_r$ with $\alpha \in \mathbb{R} > 0$, and the parametrization:*

$$\Sigma_c = B_r^\dagger (K_c - K_r)(B_r^\dagger)^\top \qquad (\Sigma_c \in \mathbb{R}^{m\times m}), \tag{IV.33}$$

$$\Gamma_c = B_r^\dagger K_c \qquad (\Gamma_c \in \mathbb{R}^{m\times n_r}), \tag{IV.34}$$

$$\alpha > 1 - 1/\lambda_{max}(BY_r B^\top K^{-1}), \tag{IV.35}$$

with $Y_r = B_r^\dagger K_r (B_r^\dagger)^\top \in \mathbb{R}^{m\times m}$, then (IV.23) holds. If $K_c = (\alpha I' + I'')K_r$ where $I' = \left[\begin{smallmatrix} I_j & 0 \\ 0 & 0 \end{smallmatrix}\right] \in \mathbb{R}^{n_r\times n_r}$, $I'' = \left[\begin{smallmatrix} 0 & 0 \\ 0 & I_{n_r - j} \end{smallmatrix}\right] \in \mathbb{R}^{n_r\times n_r}$ with $j < n_r$,

$$\alpha > 1 - 1/\lambda_{max}(BY_{rj} B^\top K^{-1}), \tag{IV.36}$$

with $Y_{rj} = B_r^\dagger I' K_r (B_r^\dagger)^\top \in \mathbb{R}^{m\times m}$, then (IV.23) holds.

Note that in the second parametrization of K_c in Corollary IV.1, the additional degree of freedom j allows us to scale by α only the first j^{th} components of the modal stiffness matrix K_r, which is diagonal and each component is directly related to an eigenfrequency. So, j gives us more control over the frequency range that is modified by α in the closed-loop system.

In the previous cases, the input maps of the full-order, low-order and reduced-order systems, denoted as B, B_ℓ and B_r, respectively, are not restricted to any particular structure, allowing them to map distributed inputs within the spatial domain. While this general formulation also accommodates pointwise inputs, this case is addressed separately in Proposition IV.3. This is done to better characterize the controller parameters and establish new bounds for α when the desired shape is defined by imposing specific values at the coordinates where pointwise inputs are applied. To achieve this, we first need to describe the structure of the input map B (and B_ℓ) when pointwise inputs are considered.

Assumption IV.1. *The input map of* (IV.1) *is of the form* $B = \begin{bmatrix} 0_{(n-m)\times m} & I_m \end{bmatrix}^\top$ *with* $I_m \in \mathbb{R}^{m\times m}$ *the identity matrix.*

For this class of input map the equilibrium points can be written considering the partitions:

$$r = \begin{bmatrix} r_u \\ r_k \end{bmatrix}, \quad K = \begin{bmatrix} K_{uu} & K_{uk} \\ K_{ku} & K_{kk} \end{bmatrix}, \tag{IV.37}$$

where $r_k \in \mathbb{R}^m$ are the generalized displacements at the coordinates where the inputs are applied (assumed to be known), and $r_u \in \mathbb{R}^{n-m}$ the remaining coordinates (unknown), then (IV.3) leads to:

$$r_u^* = -K_{uu}^{-1} K_{uk} r_k^*, \quad r^* = T_K r_k^*, \quad u^* = K_{Sch} r_k^*, \tag{IV.38}$$

with $T_K = \begin{bmatrix} -K_{uu}^{-1}K_{uk} \\ I_m \end{bmatrix} \in \mathbb{R}^{n\times m}$ and $K_{Sch} = K_{kk} - K_{ku}K_{uu}^{-1}K_{uk} \in \mathbb{R}^{m\times m}$ Schur's complement of $K_{kk} \in \mathbb{R}^{m\times m}$. It is important to underline that K_{Sch} represents the set of springs that have to be interconnected to bring the system to the equilibrium that results from imposing the displacements r_k, which is clearly seen in (IV.38). Furthermore, from the Casimir function, we have $F(x) = B^\top r = r_k$, leading to: $x_c = F(x) - C = r_k - C$. When both the controller and plant states are initialized at zero, we have $C = 0$ and the state of the controller physically represents the displacements at the points where inputs are applied.

Proposition IV.3. *Consider* (IV.1) *of order* $\ell < n$*, the input map* B *as in Assumption IV.1,* $K_c = \alpha K_\ell$ *with* $\alpha \in \mathbb{R} > 0$*, the parametrization:*

$$\Sigma_c = T_{K_\ell}^\top (K_c - K_\ell) T_{K_\ell} \qquad (\Sigma_c \in \mathbb{R}^{m\times m}), \tag{IV.39}$$

$$\Gamma_c = T_{K_\ell}^\top K_c \qquad (\Gamma_c \in \mathbb{R}^{m\times \ell}), \tag{IV.40}$$

$$\alpha > 1 - 1/\lambda_{max}(K_{\ell_{Sch}} K_{Sch}^{-1}), \tag{IV.41}$$

then (IV.23) *holds.*

Proof. Due to the structure of B and since $(K + B\,\Sigma_c B^\top)$ is symmetric with K_{uu} invertible, the condition $\Sigma_c + K_{Sch} > 0$ is sufficient for (IV.23) to hold (see [Boyd 2004, Appendix 5.5]). (IV.39) and (IV.40) imply $\Sigma_c = (\alpha - 1)K_{\ell_{Sch}}$, $\Gamma_c =$

$[0_{m\times(\ell-m)}\ \alpha K_{\ell_{Sch}}]$, and $\Sigma_c + K_{Sch} > 0$ is equivalent to $(\alpha-1)^{-1} I_m + (K_{\ell_{Sch}} K_{Sch}^{-1}) > 0$. So, a sufficient condition for the above inequality to be satisfied is that its lowest eigenvalue is positive. The rest is analogous to the proof of Proposition IV.2. □

The parametrizations provided in Proposition IV.2, Proposition IV.3 and Corollary IV.1 allows to express the stability conditions in terms of the low/reduced-order stiffness matrices, while also establishing bounds for α, where α must be greater than a limiting value, denoted as α_{min}. Additionally, it is evident that K_c can be interpreted as a low/reduced-order stiffness matrix, where $\alpha > 1$ amplifies its effect, and $0 < \alpha < 1$ reduces it. Given that the closed-loop stiffness matrix is defined as $K_{cl} = (K + B\,\Sigma_c B^\top)$, varying α directly influences the closed-loop eigenfrequencies. Specifically, when $0 < \alpha < 1$ (i.e. $\Sigma_c < 0$), the closed-loop stiffness matrix K_{cl} becomes less stiff compared to the open-loop stiffness matrix K. Conversely, when $\alpha > 1$ (i.e. $\Sigma_c > 0$), K_{cl} becomes stiffer. In the case where $\alpha = 1$, it implies that $\Sigma_c = 0$ and $K_{cl} = K$, and no energy shaping occurs.

Remark IV.2. *Note that the limiting value of α, denoted as α_{min}, is the minimum to ensure asymptotic stability and varies depending on the dimensions of the models. Therefore, for a given α, the model orders can be chosen as the minimum orders that guarantee $\alpha > \alpha_{min}$.*

IV.3.2.b Achievable equilibrium shapes

In Proposition IV.1, the equilibrium point r^* is determined by the control parameters Σ_c, Γ_c and η_c. Since the matrices Σ_c and Γ_c have already been designed, the remaining task is to design the parameter η_c, which is used to match the desired equilibrium configurations of the low/reduced order models with the one of the full-order model. Proposition IV.4 and Corollary IV.2 below provide expressions for matching both equilibrium points when the input map B is arbitrary, where it is desired to impose a desired shape $r_d = K^{-1} B\, u^* \in \mathbb{R}^n$ from (IV.3) for a given steady-state input u^*.

Proposition IV.4. *Consider (IV.1) of order $\ell < n$ and the matrices of Proposition IV.2. If $\eta_c = r_\ell^* = K_\ell^{-1} B_\ell\, u_\ell^*$, then:*

$$u_\ell^* = T_u^{-1} u^*, \tag{IV.42}$$

where $T_u \in \mathbb{R}^{m\times m}$ is an invertible matrix defined as:

$$T_u = (I_m - A)\,\Gamma_c\, K_\ell^{-1} B_\ell, \tag{IV.43}$$

where $A = \Sigma_c (I_m + B^\top K^{-1} B \Sigma_c)^{-1} B^\top K^{-1} B \in \mathbb{R}^{m\times m}$.

Proof. From (IV.28) and $\eta_c = K_\ell^{-1} B_\ell\, u_\ell^*$ we have $u^* = (I_m - A)\,\Gamma_c\, K_\ell^{-1} B_\ell\, u_\ell^* = T_u\, u_\ell^*$. Thus for a given u^*, the parameter η_c is an equilibrium configuration of (IV.1) of order $\ell < n$ with u_ℓ^* in (IV.42), and the closed-loop converges exactly to the desired shape $r_d = K^{-1} B u^*$. □

Corollary IV.2. *Consider* (IV.5) *of order* $n_r < n$ *and the matrices of Corollary IV.1. If* $\eta_c = r_r^* = K_r^{-1} B_r \, u_r^*$, *then* $u_r^* = T_u^{-1} u^*$ *with* $T_u = (I_m - A)\,\Gamma_c\, K_r^{-1} B_r$.

Proposition IV.5 and Proposition IV.6 establish similar results but when the input map B is like in Assumption IV.1, and it is desired to impose a desired shape $r_d = T_K \, r_k^* \in \mathbb{R}^n$ from (IV.38) for given generalized displacements r_k^*.

Proposition IV.5. *Consider* (IV.1) *of order* $\ell < n$ *and the matrices of Proposition IV.3. If* $\eta_c = r_\ell^* = T_{K_\ell} r_{\ell_k}^*$, *then:*

$$r_{\ell_k}^* = T_c^{-1} r_k^*, \tag{IV.44}$$

where $T_c \in \mathbb{R}^{m \times m}$ *is an invertible matrix defined as:*

$$T_c = (\Sigma_c + K_{Sch})^{-1} (\Gamma_{c_k} - \Gamma_{c_u} K_{\ell_{uu}}^{-1} K_{\ell_{uk}}), \tag{IV.45}$$

where $\Gamma_{c_u} \in \mathbb{R}^{m \times (\ell - m)}$ *and* $\Gamma_{c_k} \in \mathbb{R}^{m \times m}$ *correspond to the partitions:*

$$\Gamma_c = \begin{bmatrix} \Gamma_{c_u} & \Gamma_{c_k} \end{bmatrix}. \tag{IV.46}$$

Proof. From Assumption IV.1 and (IV.37) the closed-loop equilibrium configuration (IV.25) can be written as:

$$\begin{aligned} r_u^* &= - K_{uu}^{-1} K_{uk} r_k^*, \\ r_k^* &= (\Sigma_c + K_{Sch})^{-1} \Gamma_c \, \eta_c. \end{aligned}$$

Using (IV.38), (IV.46) and $r_\ell^* = [r_{\ell_u}^{*\top} \; r_{\ell_k}^{*\top}]^\top$ we obtain:

$$\begin{aligned} r^* &= T_K (\Sigma_c + K_{Sch})^{-1} \Gamma_c \, r_\ell^* \\ &= T_K (\Sigma_c + K_{Sch})^{-1} (\Gamma_{c_u} r_{\ell_u}^* + \Gamma_{c_k} r_{\ell_k}^*) \\ &= T_K (\Sigma_c + K_{Sch})^{-1} (\Gamma_{c_k} - \Gamma_{c_u} K_{\ell_{uu}}^{-1} K_{\ell_{uk}}) r_{\ell_k}^*, \end{aligned} \tag{IV.47}$$

which completes the proof.

□

The expression (IV.44) allows to compute the low-order model's equilibrium configuration to attain exactly with the desired equilibrium configuration of the full-order model. The result is analogously extended for the reduced-order model (IV.5).

Proposition IV.6. *Consider* (IV.5) *of order* n_r *such that* $n > n_r \geq m$, *and the matrices of Corollary IV.1. If* $\eta_c = r_r^* = T_p^\top T_K r_{n_k}^*$, *then:*

$$r_{n_k}^* = T_c^{-1} r_k^*, \tag{IV.48}$$

where $T_c \in \mathbb{R}^{m \times m}$ *is an invertible matrix defined as:*

$$T_c = (\Sigma_c + K_{Sch})^{-1} \Gamma_c \, (T_{p_k}^\top - T_{p_u}^\top K_{uu}^{-1} K_{uk}), \tag{IV.49}$$

where $T_{p_u} \in \mathbb{R}^{(n-m) \times n_r}$ *and* $T_{p_k} \in \mathbb{R}^{m \times n_r}$ *correspond to the partitions:*

$$T_p = \begin{bmatrix} T_{p_u} \\ T_{p_k} \end{bmatrix}. \tag{IV.50}$$

Proof. Analogously to the proof of Proposition IV.5 and noticing that $r_n^* \in \mathbb{R}^n$ is the full-order projection of r_r^* and it is different of r^*, from (IV.47) and using the partition $r_n^* = [r_{n_u}^{*\top} \;\; r_{n_k}^{*\top}]^\top$ we obtain:

$$\begin{aligned} r^* &= T_K \left(\Sigma_c + K_{Sch}\right)^{-1} \Gamma_c \, T_p^\top \, r_n^* \\ &= T_K \left(\Sigma_c + K_{Sch}\right)^{-1} \Gamma_c \left(T_{p_u}^\top r_{n_u}^* + T_{p_k}^\top r_{n_k}^*\right) \\ &= T_K \left(\Sigma_c + K_{Sch}\right)^{-1} \Gamma_c \left(T_{p_k}^\top - T_{p_u}^\top K_{uu}^{-1} K_{uk}\right) r_{n_k}^*, \end{aligned} \tag{IV.51}$$

where if $n_r \geq m$, T_c in (IV.49) is invertible.

□

IV.3.2.c Optimal criteria for arbitrary shapes

Until now, the desired configuration of the full-order model has been assumed to be an actual equilibrium configuration of the closed-loop system. However, when considering a controller design using Proposition IV.2, Proposition IV.3 or Corollary IV.1, if an arbitrary desired configuration is selected which is not an equilibrium of (IV.1), it is still possible to select η_c as an equilibrium configuration of the low/reduced order model which corresponds to the closest equilibrium configuration of (IV.1), since the closed-loop equilibrium is characterized by (IV.25). A possible criterion for choosing the closest equilibrium configuration is by minimizing the error between a desired shape $r_d \in \mathbb{R}^n$ and the achievable equilibrium shapes r^* that can be reached. The error is defined as: $\mathtt{e} = \|r_d - r^*\|_2^2$. The optimal choice of u_ℓ^* (analogously for u_r^*) that leads to the shape with minimum static error is:

$$u_\ell^{\text{opt}} = \min_{u_\ell^*} \|r_d - K^{-1} B \, T_u \, u_\ell^*\|_2^2 = (K^{-1} B \, T_u)^\dagger r_d, \tag{IV.52}$$

since r^* is written as in (IV.3). Similarly, the optimal choice of $r_{\ell_k}^*$ (analogously for $r_{n_k}^*$) is given by:

$$r_{\ell_k}^{\text{opt}} = \min_{r_{\ell_k}^*} \|r_d - T_K T_c \, r_{\ell_k}^*\|_2^2 = (T_K T_c)^\dagger r_d, \tag{IV.53}$$

since r^* is written as in (IV.47), or analogously as in (IV.51).

IV.4 Examples

In this section, we illustrate the application of the proposed control approach through two examples. The first example involves a Timoshenko beam with distributed inputs applied as patches along its length, aiming to reach a desired equilibrium configuration. The finite-dimensional model is developed using the mixed FEM based on the mLLM method. The second example considers a Mindlin plate controlled via pointwise inputs to achieve an optimal shape, which is the best approximation of an arbitrary desired shape that is not an equilibrium configuration. For this case, the finite-dimensional model is constructed using the standard FEM with the Penalty method.

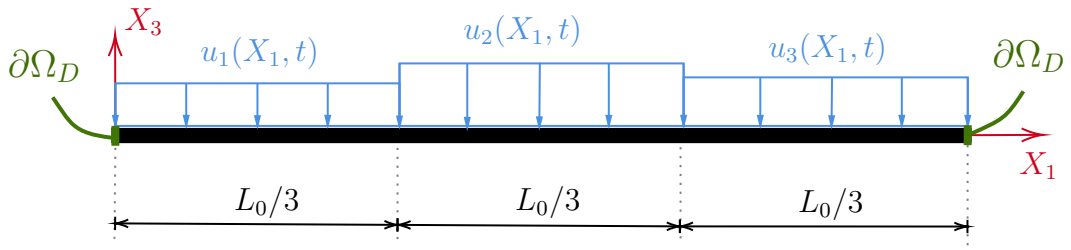

Figure IV.3 – Scheme of Timoshenko beam with distributed inputs.

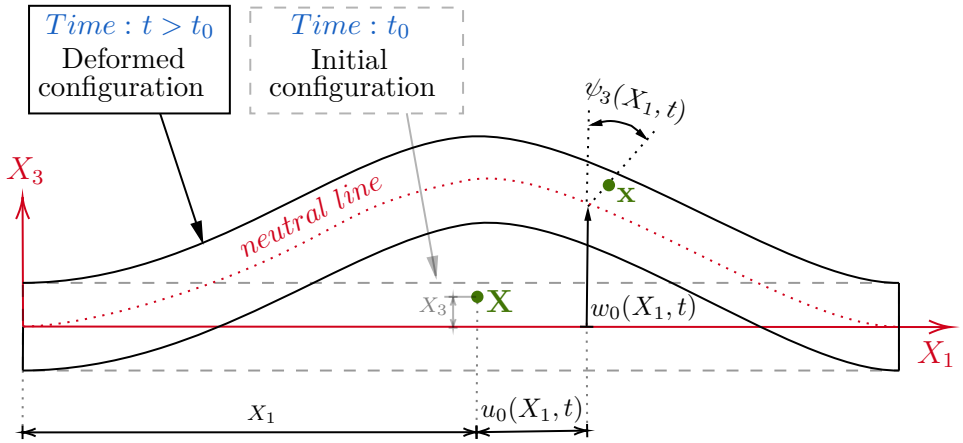

Figure IV.4 – Scheme of configurations of Timoshenko beam.

IV.4.1 One-dimensional planar beam

This section focuses on the control of a planar Timoshenko beam subject to distributed inputs, as illustrated in Figs. IV.3 and IV.4. The beam is modeled by a generalized displacement field $r(\mathtt{X},t) = [u_0(\mathtt{X},t)\ \psi_3(\mathtt{X},t)\ w_0(\mathtt{X},t)]^\top \in \mathbb{R}^3$, where $u_0(\mathtt{X},t)$ and $w_0(\mathtt{X},t)$ represent the axial and vertical displacements of points on the neutral line, respectively, and $\psi_3(\mathtt{X},t)$ is the cross section rotation. Here, $\mathtt{X} = X_1 \in \Omega = (0, L_0) \subset \mathbb{R}$ denotes the spatial domain, with L_0 representing the beam length in the reference configuration. Homogeneous Dirichlet boundary conditions are imposed at $\mathtt{S} = \{0, L_0\} \in \partial\Omega_D$, such that $v_D(\mathtt{S},t) = 0$. The key variables of the PHS are given by:

$$\mathcal{F}_{\mathtt{x}} = \begin{bmatrix} \partial_1 & 0 & 0 \\ 0 & \partial_1 & 0 \\ 0 & -1 & \partial_1 \end{bmatrix}, \quad \mathcal{M} = \rho_0 \begin{bmatrix} A_0 & 0 & 0 \\ 0 & \bar{I}_0 & 0 \\ 0 & 0 & A_0 \end{bmatrix}, \quad \mathcal{K}_\epsilon = \begin{bmatrix} EA_0 & 0 & 0 \\ 0 & E\bar{I}_0 & 0 \\ 0 & 0 & \kappa G A_0 \end{bmatrix}, \quad B_d = \begin{bmatrix} 0 \\ 0 \\ -1 \end{bmatrix},$$

where A_0 is the cross section area, $\bar{I}_0$ is the second moment of inertia of the cross section, ρ_0 is the density of the material, E is Young's modulus, $G = \frac{E}{2(1+\nu)}$ is the shear modulus, ν is Poisson's ratio, and κ is a correction factor. The distributed

input, $u_d(X_1, t) \in \mathbb{R}$, represents forces per unit of length and is defined as:

$$u_d(X_1, t) = \sum_{i=1}^{3} \Pi_i(X_1) q_i(t),$$

where $\Pi_i(X_1)$ is a spatial function defined by:

$$\Pi_i(X_1) = \begin{cases} 1; & \frac{(i-1)L_0}{3} < X_1 < \frac{i\,L_0}{3} \\ 0; & \text{othercase} \end{cases},$$

and $q_i(t)$ is the control input magnitude. The numerical values used are listed in Table III.2. For this example, the shape control problem aims to achieve the equilibrium configuration by applying the steady-state input:

$$\begin{bmatrix} q_1^* \\ q_2^* \\ q_3^* \end{bmatrix} = \begin{bmatrix} 1500 \\ -1000 \\ 750 \end{bmatrix} [N/m]. \tag{IV.54}$$

To apply the control approach, we first define the dimensions of the full-order model and reduced-order models used for the controller design. The full-order and low-order discretized models are constructed using the mixed FEM based on the mLLM method, as discussed in Chapter III, using second-order elements, a link factor $\beta = 50\,[-]$, and $n_e = 30$ finite elements for the full-order model and $n_e = 3$ finite elements for the low-order model. Shape functions are selected as canonical. Then, dimension of the state vector of the discretized models is given by $x \in \mathbb{R}^{2n}$, where $n = 2n_e + 1$. The distributed input is modeled using $N^e_{u_d}(X_1) = [\Pi_1(X_1)\ \Pi_2(X_1)\ \Pi_3(X_1)] \in \mathbb{R}^{1\times 3}$, such that $\hat{u}_d(t) = [q_1(t)\ q_2(t)\ q_3(t)]^\top \in \mathbb{R}^3$ is the control input of the finite-dimensional models. The reduced-order model is obtained through modal truncation, retaining the first $n_r = 6$ eigenfrequencies. Then, the dimension of the state vector of the reduced-order model is given by $x_r \in \mathbb{R}^{2n_r}$. Moreover, Rayleigh damping is considered for the full-order model, with parameters $a_M = 1 \cdot 10^{-3}$ and $a_K = 5 \cdot 10^{-6}$, resulting in the dissipation matrix $\hat{R} = \text{diag}\{\hat{D}_{LLM}, 0\}$, where $\hat{D}_{LLM} = a_M \hat{M} + a_K \hat{K}_{LLM}$.

To modify the dynamic response of the beam, the control parameter α must be selected such that $\alpha > \alpha_{min}$ to ensure asymptotic stability. For the models considered, the computed values of α_{min} are:

$$\begin{aligned}
\alpha_{min} &= 0.999\ [-], \quad \text{using a low-order model with } n_e = 3 \text{ elements,} \\
\alpha_{min} &= 0.849\ [-], \quad \text{using a reducer-order model with } n_r = 6,\ j = 6, \\
\alpha_{min} &= 0.849\ [-], \quad \text{using a reducer-order model with } n_r = 6,\ j = 5, \\
\alpha_{min} &= 0.659\ [-], \quad \text{using a reducer-order model with } n_r = 6,\ j = 4, \\
\alpha_{min} &= 0.126\ [-], \quad \text{using a reducer-order model with } n_r = 6,\ j = 3, \\
\alpha_{min} &= 0.000\ [-], \quad \text{using a reducer-order model with } n_r = 6,\ j = 2, \\
\alpha_{min} &= 0.000\ [-], \quad \text{using a reducer-order model with } n_r = 6,\ j = 1,
\end{aligned}$$

Notice that varying the degree of freedom j introduced in Corollary IV.1 affects the value of α_{min}, thereby providing more control over the permissible range of α values. For the following simulated results, we test the cases: $\alpha = 1.2$ using a

low-order model with $n_e = 3$ elements; $\alpha = 0.9$ using a reducer-order model with $n_r = 6$, $j = 6$; and $\alpha = 0.15$ using a reducer-order model with $n_r = 6$, $j = 3$. To introduce additional damping, the matrix D_c is set to $D_c = 20I_m$.

The results are illustrated in the Figs. IV.5 - IV.8. From the right parts of Figs. IV.5, IV.6, IV.7 (the control inputs), and from Fig. IV.8, it can be observed that all cases achieve the desired equilibrium configuration, irrespective of the selected value for α, as all inputs converge to the steady-state values specified in (IV.54). Figure IV.5, which employs a low-order model with $n_e = 3$ and $\alpha = 1.2$, shows rapid stabilization with minimal oscillations. However, the control inputs are notably large, indicating that the controller requires a significant initial effort to ensure fast convergence to the steady state. In contrast, Figs. IV.6 and IV.7,

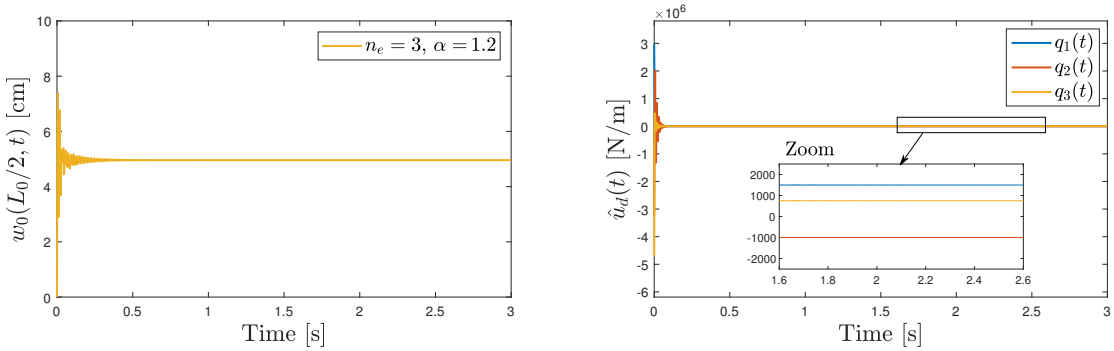

Figure IV.5 – Controller based on low-order model $n_e = 3$, $\alpha = 1.2$.

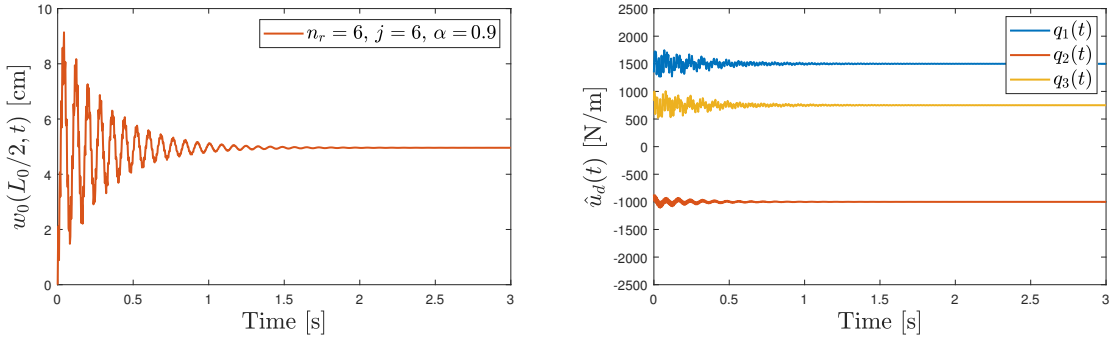

Figure IV.6 – Controller based on reduced-order model $n_r = 6$, $j = 6$, $\alpha = 0.9$.

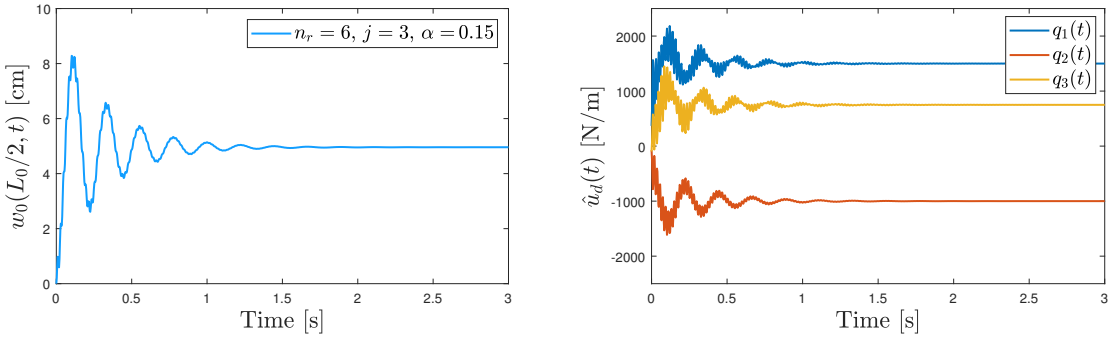

Figure IV.7 – Controller based on reduced-order model $n_r = 6$, $j = 3$, $\alpha = 0.15$.

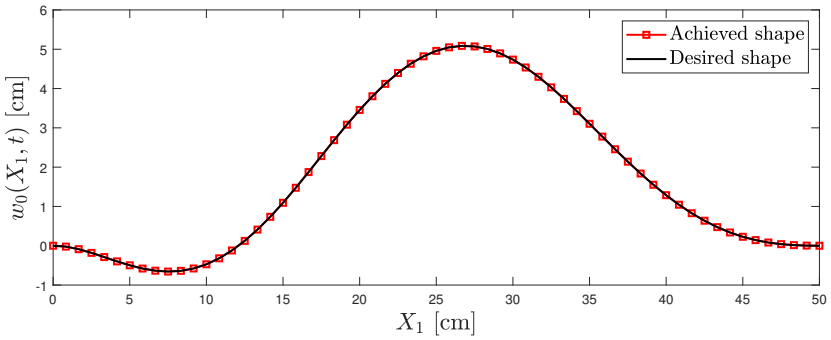

Figure IV.8 – Timoshenko beam: Desired shape and equilibrium shape.

based on reduced-order models with $n_r = 6$, exhibit more oscillatory behavior that decays more gradually. Nonetheless, the magnitudes of the control inputs in these cases are significantly smaller than in Fig. IV.5. As anticipated, the choice of α directly influences the frequency of oscillations, with smaller values of α (as seen in Fig. IV.7) resulting in more persistent yet lower-frequency oscillations. Overall, while the low-order model in Fig. IV.5 achieves quicker stabilization, it does so at the expense of much larger control efforts, whereas the reduced-order models in Figs. IV.6 and IV.7 require smaller control forces but exhibit more prolonged oscillatory dynamics.

IV.4.2 Two-dimensional plate

In this section we consider a Mindlin plate with pointwise inputs as shown in Fig. IV.9. We denote by $w_0(\mathtt{X},t) \in \mathbb{R}$ the vertical displacement, $\psi(\mathtt{X},t) = [\psi_1(\mathtt{X},t) \quad \psi_2(\mathtt{X},t)]^\top \in \mathbb{R}^2$ the rotation angles by the cross section, $\gamma(\mathtt{X},t) = \mathrm{grad}(w_0) - \psi \in \mathbb{R}^2$ the shear strain vector, $\mathbb{K}(\mathtt{X},t) = \mathrm{Grad}(\psi) \in \mathbb{R}^{2\times 2}$ the curvature tensor, and $\mathbb{M}(\mathtt{X},t) = \mathcal{D}(\mathbb{K}) \in \mathbb{R}^{2\times 2}$ as the internal bending moment

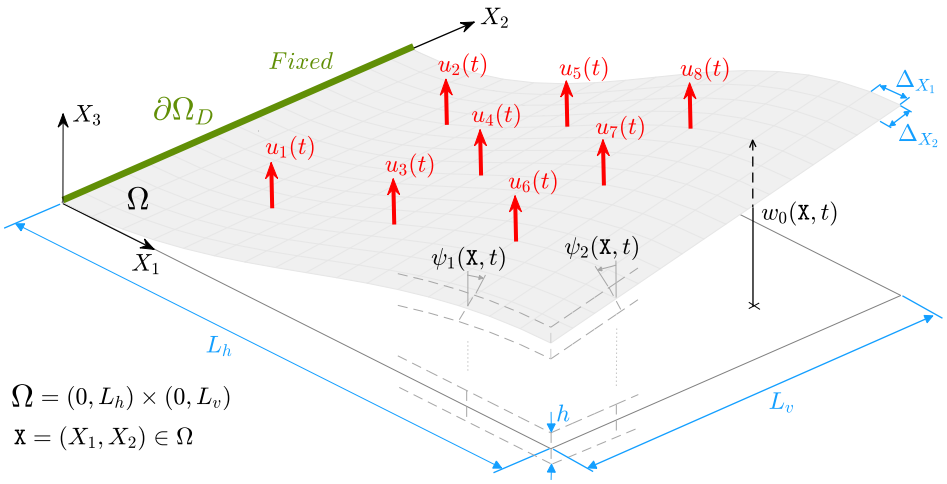

Figure IV.9 – Mindlin plate with pointwise inputs.

$u_i(t)$	$u_1(t)$	$u_2(t)$	$u_3(t)$	$u_4(t)$	$u_5(t)$	$u_6(t)$	$u_7(t)$	$u_8(t)$	$[N]$
$\mathtt{X}_i = \begin{pmatrix} X_1 \\ X_2 \end{pmatrix}_i$	$\begin{pmatrix} 3 \\ 2 \end{pmatrix}_1$	$\begin{pmatrix} 3 \\ 6 \end{pmatrix}_2$	$\begin{pmatrix} 6 \\ 2 \end{pmatrix}_3$	$\begin{pmatrix} 6 \\ 4 \end{pmatrix}_4$	$\begin{pmatrix} 6 \\ 6 \end{pmatrix}_5$	$\begin{pmatrix} 9 \\ 2 \end{pmatrix}_6$	$\begin{pmatrix} 9 \\ 4 \end{pmatrix}_7$	$\begin{pmatrix} 9 \\ 6 \end{pmatrix}_8$	$[cm]$

Table IV.1 – Coordinates where inputs are applied.

tensor, with grad $= \nabla(\cdot)$ the gradient operator applied to scalar fields, Grad $= \frac{1}{2}(\nabla(\cdot) + \nabla(\cdot)^\top)$ the symmetric part of the gradient operator applied to vector fields, and $\mathcal{D}(\cdot) = \frac{Eh^3}{12(1-\nu^2)}[(1-\nu)(\cdot) + \nu \mathrm{tr}(\cdot) I_{2\times 2}]$ the fourth-order internal bending moment constitutive tensor for isotropic plates, with $I_{2\times 2} \in \mathbb{R}^{2\times 2}$ an identity matrix, E Young's modulus, ν Poisson's ratio and h the thickness of the plate. Denoting div and Div as divergence operators $\nabla\cdot(\cdot)$ applied to vector and second-order tensor fields, respectively, the infinite-dimensional PHS representation of the Mindlin plate [Brugnoli 2019a] is given by:

$$\underbrace{\begin{bmatrix} \dot{p}_\psi \\ \dot{p}_w \\ \dot{\epsilon}_\psi \\ \dot{\epsilon}_w \\ \dot{\psi} \\ \dot{w}_0 \end{bmatrix}}_{\dot{x}(\mathtt{X},t)} = \underbrace{\begin{bmatrix} 0 & 0 & \mathrm{Div} & I_{2\times 2} & -I_{2\times 2} & 0 \\ 0 & 0 & 0 & \mathrm{div} & 0 & -1 \\ \mathrm{Grad} & 0 & 0 & 0 & 0 & 0 \\ -I_{2\times 2} & \mathrm{grad} & 0 & 0 & 0 & 0 \\ I_{2\times 2} & 0 & 0 & 0 & 0 & 0 \\ 0 & 1 & 0 & 0 & 0 & 0 \end{bmatrix}}_{\mathcal{J}=-\mathcal{J}^*} \underbrace{\begin{bmatrix} e_{p_\psi} \\ e_{p_w} \\ e_{\epsilon_\psi} \\ e_{\epsilon_w} \\ 0 \\ 0 \end{bmatrix}}_{\delta_x H} + \underbrace{\begin{bmatrix} 0 \\ 1 \\ 0 \\ 0 \\ 0 \\ 0 \end{bmatrix}}_{\mathcal{G}} u_d(\mathtt{X},t) \tag{IV.55}$$

$$\begin{aligned} y_d &= \mathcal{G}^* \delta_x H, \\ u_\partial &= \mathcal{B}_\partial(\delta_x H) = (\tau_\psi^N,\ \tau_w^N,\ v_\psi^D,\ v_w^D), \\ y_\partial &= \mathcal{C}_\partial(\delta_x H) = (v_\psi^N,\ v_w^N,\ \tau_\psi^D,\ \tau_w^D), \\ H(x) &= \frac{1}{2}\int_\Omega \left(\frac{p_w^2}{\rho_0 h} + \frac{12}{\rho_0 h^3} p_\psi \cdot p_\psi + \mathcal{D}(\epsilon_\psi) : \epsilon_\psi + \kappa G h\, \epsilon_w \cdot \epsilon_w \right) d\mathtt{X}, \end{aligned} \tag{IV.56}$$

where $\delta_x H$ is the variational derivative of $H(x)$ respect to $x(\mathtt{X},t)$, $\mathcal{J}$ is a formal skew-adjoint differential operator, $(\mathcal{G}, \mathcal{G}^*)$ are respectively the input map operator and its formal adjoint, and $(\mathcal{B}_\partial, \mathcal{C}_\partial)$ are the boundary operators chosen such that $u_\partial = 0$ corresponds to clamped boundary on the left-hand side and free boundary elsewhere. The physical properties of the material are the density ρ_0, Young's modulus E, shearing modulus G, Poisson's ratio ν, and the correction factor $\kappa = 5/6$. The energy and co-energy variables of (IV.55) are given by:

$$\begin{aligned} \dot{p}_\psi &= \frac{\partial p_\psi}{\partial t} = \frac{\rho_0 h^3}{12}\frac{\partial^2 \psi}{\partial t^2}, & e_{p_\psi} &= \frac{\delta H}{\delta p_\psi} = \frac{12}{\rho_0 h^3} p_\psi = \frac{\partial \psi}{\partial t}, \\ \dot{p}_w &= \frac{\partial p_w}{\partial t} = \rho_0 h \frac{\partial^2 w_0}{\partial t^2}, & e_{p_w} &= \frac{\delta H}{\delta p_w} = \frac{1}{\rho_0 h} p_w = \frac{\partial w_0}{\partial t}, \\ \dot{\epsilon}_\psi &= \frac{\partial \epsilon_\psi}{\partial t} = \frac{\partial}{\partial t}(\mathbb{K}), & e_{\epsilon_\psi} &= \frac{\delta H}{\delta \epsilon_\psi} = \mathcal{D}(\epsilon_\psi) = \mathbb{M}, \\ \dot{\epsilon}_w &= \frac{\partial \epsilon_w}{\partial t} = \frac{\partial}{\partial t}(\gamma), & e_{\epsilon_w} &= \frac{\delta H}{\delta \epsilon_w} = \kappa G h\, \epsilon_w = \kappa G h\, \gamma. \end{aligned}$$

The boundary is partitioned as $\partial\Omega = \partial\Omega_N \cup \partial\Omega_D$ with $\mathtt{S} \in \partial\Omega$, where $\partial\Omega_N$ is the Neumann boundary portion where generalized tractions $\tau_\psi^N(\mathtt{S},t)$ and $\tau_w^N(\mathtt{S},t)$ are imposed, and $\partial\Omega_D$ is the Dirichlet boundary portion where generalized velocities $v_\psi^D(\mathtt{S},t)$ and $v_w^D(\mathtt{S},t)$ are imposed. Thus, the boundary ports $u_\partial(\mathtt{S},t)$ and $y_\partial(\mathtt{S},t)$ are defined with respect to:

$$\begin{aligned} \tau_\psi^N = e_{\epsilon_\psi}\hat{n}, \quad \tau_w^N = e_{\epsilon_w}\cdot\hat{n}, \quad v_\psi^N = e_{p_\psi}, \quad v_w^N = e_{p_w} \qquad \text{on } \partial\Omega_N, \\ \tau_\psi^D = e_{\epsilon_\psi}\hat{n}, \quad \tau_w^D = e_{\epsilon_w}\cdot\hat{n}, \quad v_\psi^D = e_{p_\psi}, \quad v_w^D = e_{p_w} \qquad \text{on } \partial\Omega_D, \end{aligned}$$

with $\hat{n}(\mathtt{S}) = [\hat{n}_1(\mathtt{S}) \;\; \hat{n}_2(\mathtt{S})]^\top$ the outward unit normal vector to the boundary $\partial\Omega$. The geometrical and physical parameters of the plate are $L_h = 12\,[cm]$ and $L_v = 8\,[cm]$ the horizontal and vertical lengths, respectively, $h = 1\,[mm]$, $\rho_0 = 2970\,[kg/m^3]$, $E = 45\,[GPa]$, $G = 17.3\,[GPa]$, and $\nu = 0.3\,[-]$. The inputs within the domain are of the form $u_d(\mathtt{X},t) = \sum_{i=1}^m \delta(\mathtt{X}-\mathtt{X}_i)\,u_i(t)$ with $\delta(\mathtt{X}-\mathtt{X}_i) = \begin{cases} 1; & \mathtt{X}=\mathtt{X}_i \\ 0; & \mathtt{X}\neq\mathtt{X}_i \end{cases}$, where $\mathtt{X}_i\,[cm]$ are the coordinates where inputs $u_i(t)\,[N]$ are applied. The numerical values are gathered in Table IV.1.

Remark IV.3. *The PHS model of the Mindlin plate in (IV.55) can be derived by applying Methodology 1 presented in Chapter II, where the displacement field $\boldsymbol{u}(\boldsymbol{X},t) \in \mathbb{R}^3$ and the constitutive matrix $C_L \in \mathbb{R}^{5\times5}$ are given by:*

$$\boldsymbol{u}(\boldsymbol{X},t) = \underbrace{\begin{bmatrix} -X_3 & 0 & 0 \\ 0 & -X_3 & 0 \\ 0 & 0 & 1 \end{bmatrix}}_{\bar{M}_1(\mathtt{X}^c)} \underbrace{\begin{bmatrix} \psi_1(\mathtt{X},t) \\ \psi_2(\mathtt{X},t) \\ w_0(\mathtt{X},t) \end{bmatrix}}_{r(\mathtt{X},t)}, \quad C_L = \begin{bmatrix} \frac{E}{(1-\nu^2)} & \frac{E\nu}{(1-\nu^2)} & 0 & 0 & 0 \\ \frac{E\nu}{(1-\nu^2)} & \frac{E}{(1-\nu^2)} & 0 & 0 & 0 \\ 0 & 0 & \frac{E(1-\nu)}{2(1-\nu^2)} & 0 & 0 \\ 0 & 0 & 0 & \kappa G & 0 \\ 0 & 0 & 0 & 0 & \kappa G \end{bmatrix},$$

with $G = \frac{E}{2(1+\nu)}$. Following this methodology, the PHS representation of the Mindlin plate is fully characterized by the following matrices and operators:

$$\mathcal{M} = \begin{bmatrix} \rho_0\frac{h^3}{12} & 0 & 0 \\ 0 & \rho_0\frac{h^3}{12} & 0 \\ 0 & 0 & \rho_0 h \end{bmatrix}, \qquad \mathcal{K}_\epsilon = \begin{bmatrix} \bar{D} & \nu\bar{D} & 0 & 0 & 0 \\ \nu\bar{D} & \bar{D} & 0 & 0 & 0 \\ 0 & 0 & \bar{D}\frac{(1-\nu)}{2} & 0 & 0 \\ 0 & 0 & 0 & \kappa G h & 0 \\ 0 & 0 & 0 & 0 & \kappa G h \end{bmatrix},$$

$$\mathcal{F}_\mathtt{x} = \begin{bmatrix} \partial_1 & 0 & 0 \\ 0 & \partial_2 & 0 \\ \partial_2 & \partial_1 & 0 \\ -1 & 0 & \partial_1 \\ 0 & -1 & \partial_2 \end{bmatrix}, \qquad -\mathcal{F}_\mathtt{x}^* = \begin{bmatrix} \partial_1 & 0 & \partial_2 & 1 & 0 \\ 0 & \partial_2 & \partial_1 & 0 & 1 \\ 0 & 0 & 0 & \partial_1 & \partial_2 \end{bmatrix},$$

$$F_\partial = \begin{bmatrix} \hat{n}_1 & 0 & \hat{n}_2 & 0 & 0 \\ 0 & \hat{n}_2 & \hat{n}_1 & 0 & 0 \\ 0 & 0 & 0 & \hat{n}_1 & \hat{n}_2 \end{bmatrix}, \qquad B_d = \begin{bmatrix} 0 \\ 0 \\ 1 \end{bmatrix},$$

where $\bar{D} = \frac{Eh^3}{12(1-\nu^2)}$ is the bending stiffness of a plate. Note that this representation maintains the same structure as the PHS model presented in [Macchelli 2005].

Choice of model orders

In this example, the discretized models are obtained using the standard FEM with Penalty method, as discussed in Chapter III. First-order quadrilateral elements with canonical shape functions are employed. For the simulations, the numerical value of the penalty factor is set to $\beta_\infty = 1 \cdot 10^9\,[-]$, and reduced integration is used to mitigate the shear locking effect. To determine the dimensions of the models, consider that the mesh used to obtain the higher-order model is such that $\Delta_{X_1} = L_h/N_n$, $\Delta_{X_2} = L_v/N_n$, where Δ_{X_1} and Δ_{X_2} are the dimensions of each finite element, N_n^2 is the total number of finite elements in the mesh, and $n = 3(N_n+1)^2$ is the order of the high-order model. Given the location and the number of inputs ($m = 8$), the minimum number of finite elements N_ℓ^2 to obtain the low-order model with inputs applied directly at the nodes (thus achieving the input map B as in Assumption IV.1) is $N_\ell = 4$, and admissible meshes are expanded by multiples of four of N_ℓ.

A sensitivity analysis is performed using (IV.36) and (IV.41) to obtain α_{min}, and the results are shown graphically in Fig. IV.10. It can be observed from the figure that when N_n is sufficiently high, α_{min} converges. Considering as control objective to impose a value of $\alpha = 0.25$, from Fig. IV.10 it is seen that for $N_\ell = 8$, $n_r = 8$ with $j = \{1, 2, 3\}$, and $N_n \geq 20$, the values of α_{min} have converged and are less than 0.25.

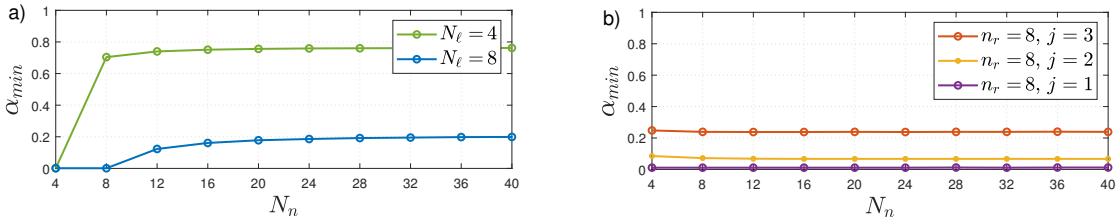

Figure IV.10 – Sensitivity analysis of the order of models.

Dynamic shape control of the Mindlin plate

To illustrate the control approach in this example, we use $N_n = 20$, $N_\ell = 8$, $n_r = 8$ with $j = \{2, 3\}$. The desired shape is arbitrarily chosen as:

$$f_w(\mathtt{X}) = (\cos(31.5X_1) - 1)(8(X_2 - 0.025)^2 - 4(X_1 - 0.06)^2).$$

Additionally, the matrix D_c of the controller is chosen as $D_c = 0.5\, I_m$, and the matrices (Σ_c, Γ_c) are calculated with parameters $\alpha = 0.25$ and $\alpha = 4$. One can remark that $f_w(\mathtt{X})$ is not an equilibrium configuration of the plate, and it is solely related to $w_0(\mathtt{X}, t)$. The desired rotation angles are also degrees of freedom for the controller design and are therefore free to choose. In this example, we consider the rotation angles to be consistent with the desired equilibrium configuration of a system with as many actuators as nodes in the mesh. Then, $r_d \in \mathbb{R}^n$ is

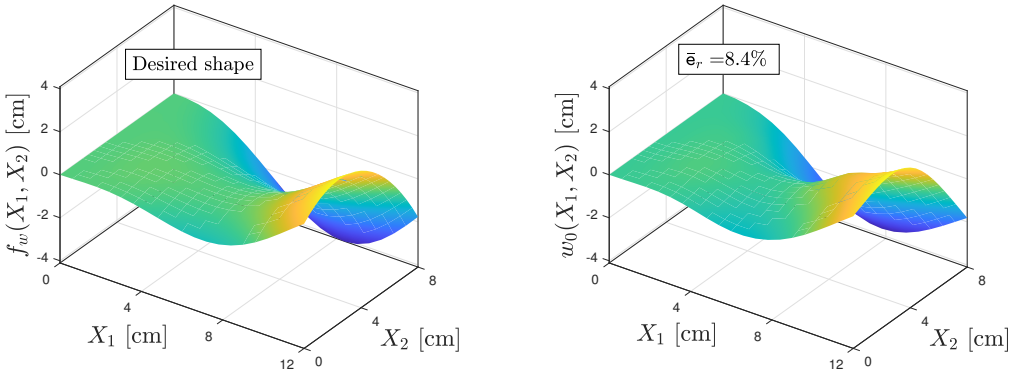

(a) Desired shape (b) Achieved optimal shape

Figure IV.11 – Desired shape and achieved shape.

calculated from (IV.38) by $r_d = T_K r_k$, where now r_k represents the coordinates associated with the vertical displacement of all nodes in the mesh obtained by projecting $f_w(\mathtt{X})$ onto those points, and T_K is calculated with respect to a partition of K consistent with r_k. So, from (IV.25) the steady-state equilibrium shape is computed in advance and also the static error. Graphically this is shown in Fig. IV.11. It is worth mentioning that all controllers designed from the different low/reduced order models and parametrizations of K_c achieve the same stationary shape with relative error $\bar{\mathtt{e}}_r = \frac{\|r_d - r^*\|_2^2}{\|r_d\|_2^2} \times 100 = 8.4\%$.

Remark IV.4. *The steady-state error $\bar{\mathtt{e}}_r$ is minimal considering a specific input map. Exploring the optimal number of inputs and their placement (as in [Agrawal 1994] or [Morris 2015]) to obtain lower steady-state errors is beyond the scope of this work and constitutes interesting future research.*

Figures IV.12 to IV.14 show the dynamic response of the plate for the different values of α, specifically it is shown the vertical displacement at the coordinate $w_0(X_1 = L_h, X_2 = 0, t)$. From the upper part of Figs. IV.12 and IV.13 we can see that $w_0(L_h, 0, t)$ contains less high-frequency content as j increases. This is expected since when $j = 2$, α only modifies the first two components of K_r which are related to the first two natural frequencies, leaving the rest of the higher natural frequencies unscaled. On the other hand, from the upper part of Fig. IV.14 a smoother transient response is observed, but from the bottom part the response has more frequency content for $\alpha = 4$. This is also expected since α multiplies the entire stiffness matrix K_ℓ, therefore the scaling factor is mapped to a higher frequency range in the higher order model. Moreover, from the previous figures it is seen that different values of α can affect significantly the transient response. Finally, in the case of model ℓ, the displacements are smoother at the expense of the actuator, while in the case of model n_r varying j there is more control regarding the smoothness of the displacements responses and inputs.

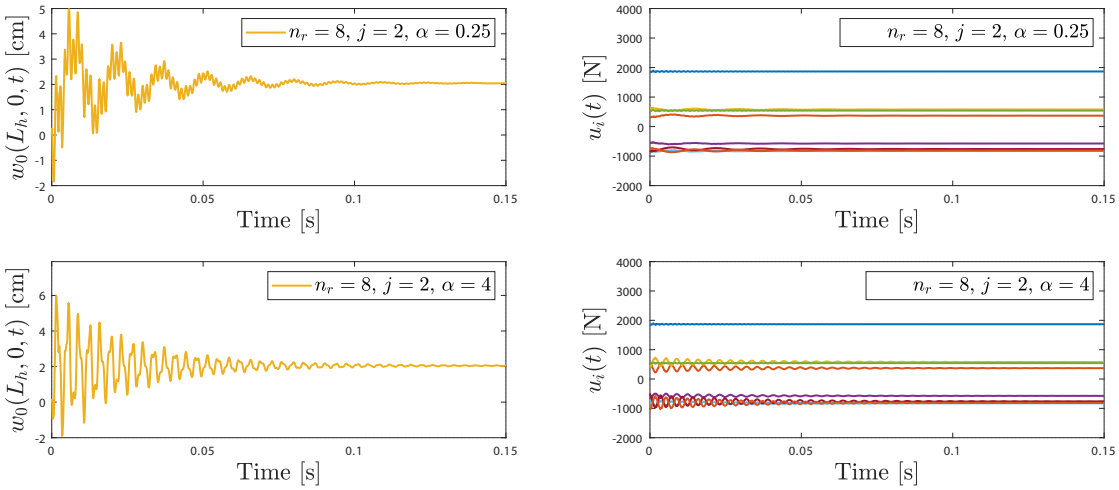

Figure IV.12 – Controller based on reduced-order model $n_r = 8$, $j = 2$.

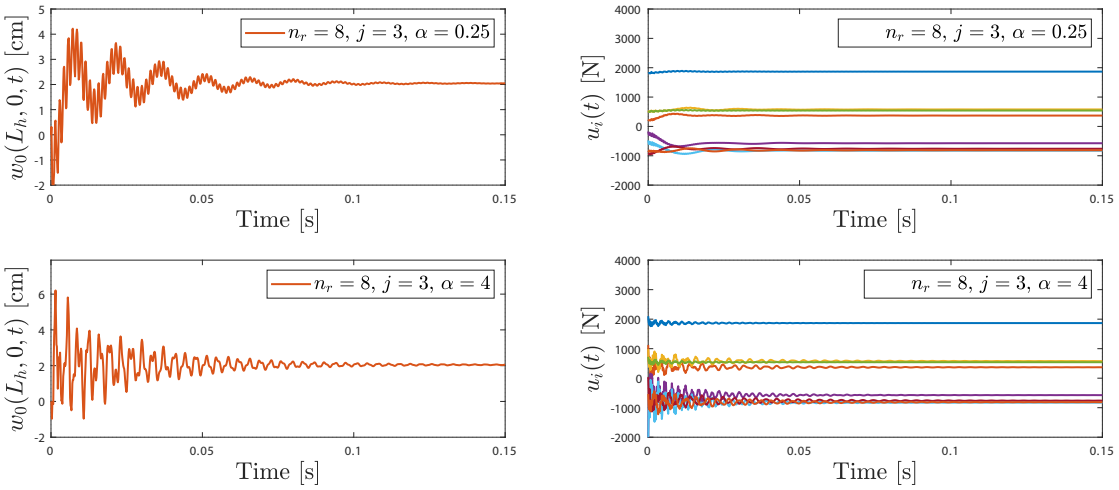

Figure IV.13 – Controller based on reduced-order model $n_r = 8$, $j = 3$.

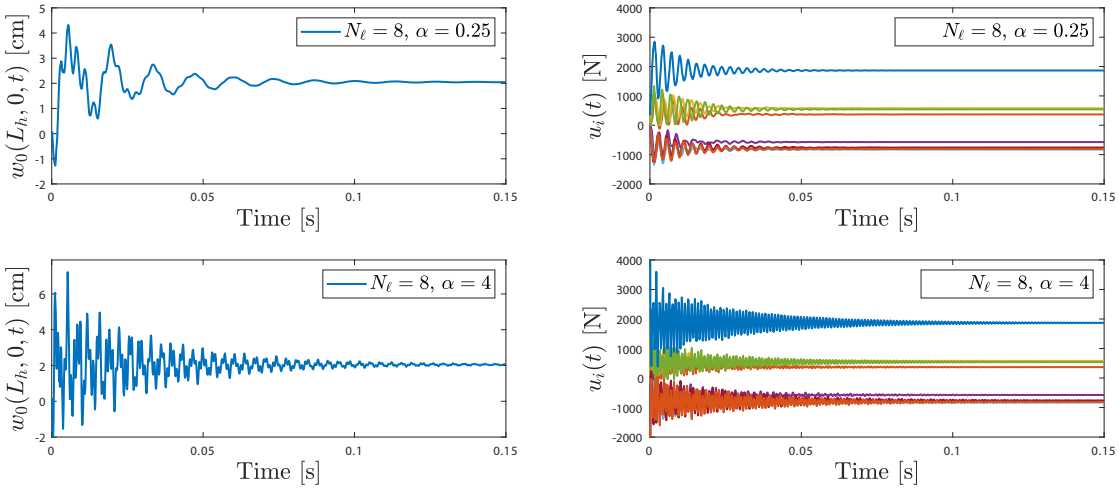

Figure IV.14 – Controller based on low-order model $N_\ell = 8$.

IV.5 Conclusion

The control design based on low/reduced order models of a class of linear PHS was presented. Using PBC techniques, Casimir functions were found linking the states of the full-order plant and those of the controller, where the equilibrium points and asymptotic stability conditions were parametrized by the controller parameters. Casimir functions are preserved for lower-order versions of the system with the same structure and also for reduced-order models arising from structure-preserving model reduction by modal truncation. In addition, optimal criteria were established to achieve the closest equilibrium configuration with respect to a desired one that can be arbitrary. The results were illustrated through simulations of discretized models of a Timoshenko beam with distributed actuation and a Mindlin plate with pointwise inputs. In these examples, it was observed that the systems converge exactly and optimally to the desired imposed shapes, respectively, regardless of the low/reduced order model employed for controller design. Moreover, by using the proposed parametrizations for the controller matrices, the transient response and the dynamics of the inputs can be influenced using physical notions, such as modifying the damping or the closed-loop stiffness, without affecting the stationary equilibrium shape.

A key advantage of controller design based on low-order models, particularly for systems with pointwise inputs, is the clear physical interpretation of the controller's states as displacements at the input locations. This facilitates the straightforward implementation of the control law through direct sensing of displacements or velocities, the latter being the power-conjugated output of the PHS plant, thereby simplifying analysis and interpretation. In contrast, reduced-order models lack this physical clarity, necessitating alternative implementation strategies, such as observers, which can introduce additional complexity. Nevertheless, reduced-order models typically offer more flexibility in selecting the control parameter α, as they tend to yield a lower α_{min}. This expands the range of applicable α values and enhances the controller's ability to impose slower oscillation speeds in the closed-loop system. Ultimately, the choice between low-order and reduced-order models involves a trade-off: low-order models prioritize simplicity for real-time implementation with clear physical interpretations, while reduced-order models provide enhanced performance and flexibility, albeit at the cost of increased complexity and the need for supplementary strategies for effective real-time application.

Future perspectives include performing a stability analysis of the proposed finite-dimensional PHS controller when interconnected with the infinite-dimensional PHS, following the strategy outlined in [Liu 2024]. Additionally, further research will focus on determining the optimal number and location of inputs, observer-based control, assessing robustness to model uncertainties, addressing trajectory tracking problems for time-varying shapes, and extending the results by employing PHS with a more general structure, including nonlinear systems.

Chapter V
Conclusions and perspectives

V.1 Conclusions

This thesis focused on the modeling, discretization, and control of flexible mechanical systems within the PHS framework. The work contributed to three main areas: (1) generalized methodologies for PHS modeling, (2) structure-preserving discretization techniques, and (3) control design based on low-order models.

The first contribution of the thesis involved the development of generalized methodologies for modeling both linear and nonlinear mechanical systems. These systematic and flexible methodologies, grounded in the generalized extended Hamilton's principle, have demonstrated broad applicability across various multidimensional flexible mechanical systems, enabling the derivation of explicit PHS and implicit PH-DAE representations. Furthermore, these methodologies incorporate systems with large deformations, hyperelastic materials, and constraints, representing an advancement beyond the current state of the art.

The second contribution focused on the discretization of PHS. Structure-preserving discretization techniques were developed using mixed Finite Element Methods (FEM), with both two-field and multi-field approaches. These methods were designed to preserve the PHS structure of the original system, and were applied to both linear and nonlinear PHS and PH-DAE systems. Through numerical validation, the proposed techniques were shown to accurately capture the dynamic behavior of the underlying continuous systems. The techniques were tested using both 1D and 2D examples, demonstrating their capability in preserving the system's physical structure during discretization.

The third contribution involved the design of controllers for linear PHS based on reduced or low-order models. A finite-dimensional controller was developed using passivity-based control techniques, ensuring asymptotic stability and optimal convergence to the desired system configurations. The design establishes a framework that uses Casimir functions to connect the controller and system states in an invariant manner, allowing for effective adjustments to the system's behavior while preserving its fundamental characteristics. The control design was applied to mechanical systems such as Timoshenko beams and Mindlin plates, showing that the proposed method ensures convergence to optimal shapes, regardless of the order of the model used for controller design.

Overall, the thesis provided a structured and versatile framework for modeling, discretization, and control of flexible mechanical systems, highlighting the utility of the port-Hamiltonian approach in these areas. The proposed methodologies, discretization techniques, and control design can be extended and adapted to a broad range of systems, offering a foundation for future research and applications.

V.2 Perspectives

Future work on the modeling framework established in this thesis can be enhanced by addressing more complex phenomena such as viscoelasticity, electroelasticity, and fluid-structure interactions. These developments will enable the modeling of advanced systems, particularly Dielectric Elastomer Actuators (DEAs) and Hydraulically Amplified Self-Healing Electrostatic (HASEL) actuators. Preliminary findings on the modeling and control of a HASEL actuator, using discretized models of beams for the mechanical component, can be found in our conferences papers:

- Cristobal Ponce, Nelson Cisneros, Yongxin Wu, Kanty Rabenorosoa, Yann Le Gorrec, Hector Ramirez. «Port-Hamiltonian modeling of large-scale curling HASEL actuators». *IFAC-PapersOnLine, 58(21), 238-243, (2024).* (Published)
- Nelson Cisneros, Cristobal Ponce, Yongxin Wu, Alessandro Macchelli, Yann Le Gorrec, Hector Ramirez (2025). «Position and anti-drift control of large-scale curling HASEL actuators». *IFAC NOLCOS (2025).* (Submitted)

In the realm of discretization, nonlinear systems present significant challenges. The need to integrate and assemble matrices and vectors at each time step results in highly time-consuming simulations. Additionally, the structure of the matrix varies with each time step, complicating its application in controller design. Therefore, there is a critical need to develop strategies for obtaining explicit global matrices, for instance, as proposed in [Pedersen 2006; Gülümser 2014]. Such approaches could enhance simulation efficiency and facilitate control design.

Perspectives in control design include demonstrating the stability of the infinite-dimensional PHS interconnected with the finite-dimensional PHS controllers (as discussed in [Liu 2024]), determining the optimal placement of inputs, ensuring effective trajectory tracking for time-varying shapes, and extending the control techniques to nonlinear systems. The control methodologies developed for linear systems still require experimental validation. To do so, an experimental setup has been built at FEMTO-ST, consisting of a carbon fiber beam with HASEL actuators functioning as distributed patches. Figs. V.1 and V.2 illustrate the experimental setup and preliminary open-loop results.

Regarding extensions to nonlinear systems, research by [Kinon 2023] has proposed a model for a nonlinear string that uses the deformation gradient tensor and the first Piola-Kirchhoff stress tensor as energy and co-energy variables. This results in a nonlinear PHS representation with a constant interconnection operator, where all geometric and material nonlinearities are embedded in the Hamiltonian. Exploring methods to achieve similar representations for other flexible systems could facilitate energy-shaping control, since the structural matrices would be constant and well defined at the discretized level. This consistency should facilitate the resolution of the matching equations and the identification of Casimir functions, thereby extending the proposed control methodologies. Additionally, it can lead to faster simulation times due to the reduced numerical complexity of the models.

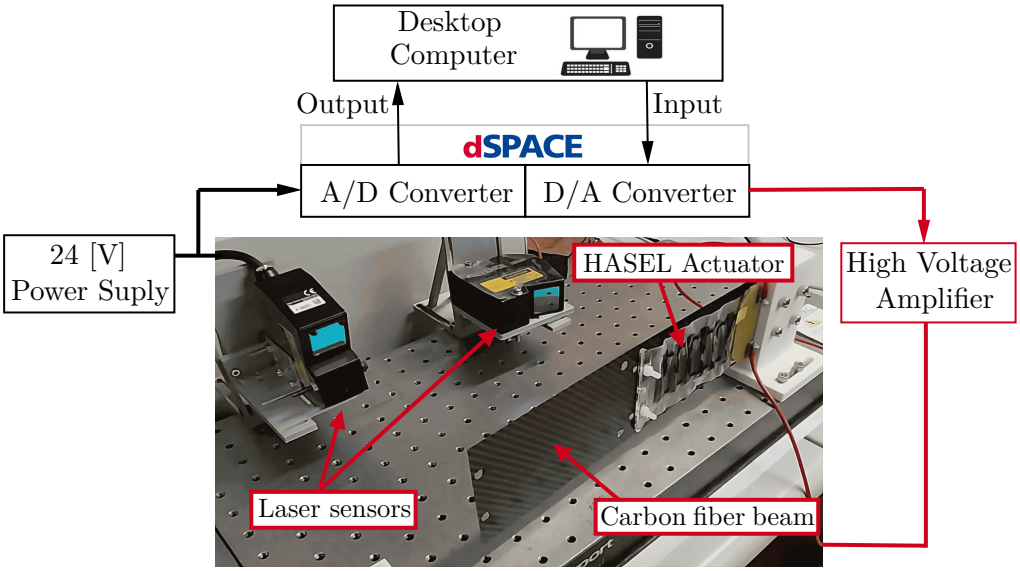

Figure V.1 – Experimental setup: HASEL actuated beam.

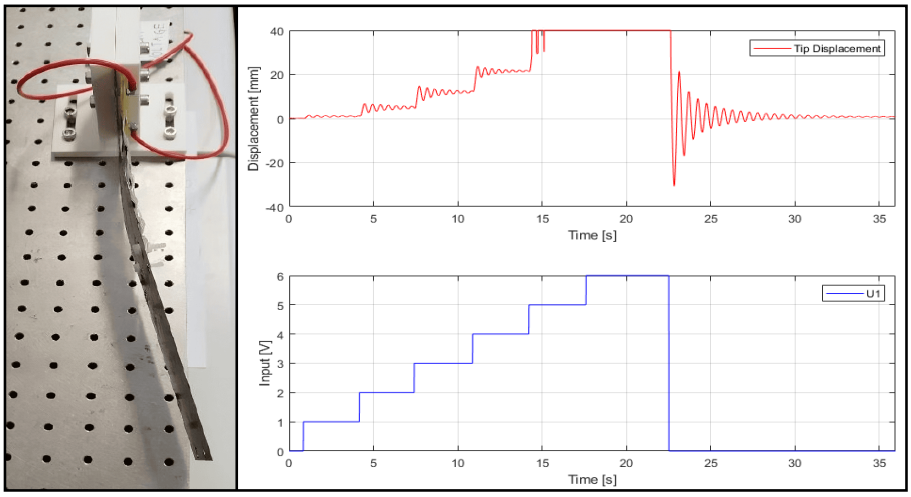

Figure V.2 – Experimental setup: Open-loop response.

Appendix A
Overview of continuum mechanics

Introduction

Continuum mechanics studies the behavior of materials treated as continuous masses rather than discrete particles. It encompasses the study of kinematics, focusing on motion and deformation without regard to the forces involved, as well as conservation laws governing mass, linear and angular momentum, and energy in material bodies. This appendix presents essential concepts for understanding deformation theory, including the deformation gradient, strain measures, and stress tensors such as the Cauchy stress tensor and the first and second Piola-Kirchhoff stress tensors. These concepts are critical for formulating both simple linear and complex nonlinear elastic models. For a comprehensive review of these topics, refer to [Tadmor 2012; Reddy 2007].

A.1 Kinematics

This section begins by presenting both reference and spatial configurations, which are crucial for understanding how material points are positioned and move over time. It then delves into the definitions of the deformation gradient and its polar decomposition, along with strain tensors used to measure deformation. Additionally, kinematic rates, which measure the rate of change of these quantities, are discussed. The section concludes with the analysis of the effects of superposing rigid body motions, which is called objectivity.

A.1.1 Fundamentals of deformation

In finite deformation analysis, different descriptions are used to characterize continuum quantities. When a quantity is expressed in terms of its position before deformation, it is referred to as a material or Lagrangian description (described in the reference configuration, also called the initial configuration). Conversely, when a quantity is expressed in terms of its position during deformation, it is known as a spatial or Eulerian description (described in the current configuration, also called the deformed configuration). From Fig. A.1, let $\{X_1, X_2, X_3\}$ and $\{x_1, x_2, x_3\}$ denote two Cartesian bases at times $t = t_0$ and $t > t_0$, respectively. The body is considered as a collection of material particles labeled by coordinates $\mathbf{X}$, where the volume of the body and its boundary are denoted as $\mathcal{B}_0$ and $\partial\mathcal{B}_0$ in the reference configuration, and as $\mathcal{B}$ and $\partial\mathcal{B}$ in the current configuration, respectively. Therefore, $\mathbf{X} = [X_1\ X_2\ X_3]^\top \in \mathcal{B}_0$ represents the material position vector of an arbitrary point in the initial configuration at $t = t_0$. Similarly, $\mathbf{x} = [x_1\ x_2\ x_3]^\top \in \mathcal{B}$ represents the spatial position vector of an arbitrary point in the current configuration at $t > t_0$. The motion of a material point can be mathematically described as:

$$\mathbf{x} = \varphi(\mathbf{X}, t), \tag{A.1}$$

$$\mathbf{X} = \varphi^{-1}(\mathbf{x}, t), \tag{A.2}$$

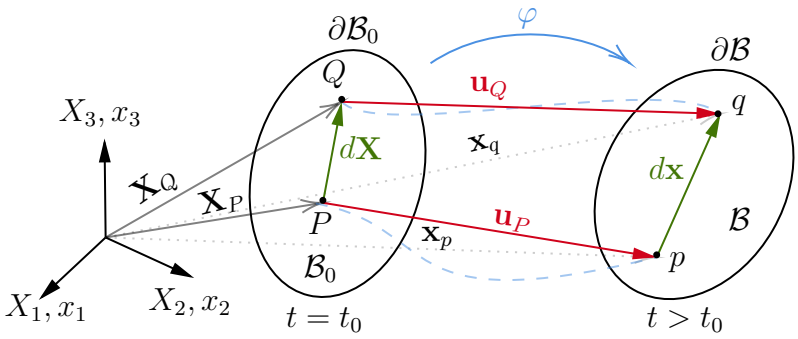

Figure A.1 – Material and spatial description of motion.

where $\varphi : \mathcal{B}_0 \to \mathcal{B}$ is the motion mapping, $\mathbf{x}$ is the current (spatial) position of a material point that occupies the position $\mathbf{X}$ in the initial configuration. Additionally, from Fig. A.1 we can define the displacement field $\mathbf{u}(\mathbf{X}, t) \in \mathbb{R}^3$ as:

$$\mathbf{u}(\mathbf{X}, t) = \varphi(\mathbf{X}, t) - \mathbf{X}, \tag{A.3}$$

which assigns to each material point $\mathbf{X} \in \mathcal{B}_0$ of the body a displacement vector that specifies its current position at time $t > t_0$ in the deformed configuration regarding its position in the initial configuration at time $t = t_0$.

Remark A.1. *In the material description, for instance, $\rho(\boldsymbol{X}, t) \in \mathbb{R}$ represents the density at time t at the position where a particle $\boldsymbol{X}$ was located in the initial configuration. In contrast, $\rho(\boldsymbol{x}, t) \in \mathbb{R}$ denotes the density at time t at the spatial position $\boldsymbol{x}$, regardless of which particle currently occupies that place. Regardless of the chosen description, the governing equations of motion are consistently formulated in the current configuration and thus primarily use the spatial description.*

A.1.2 Deformation gradient

The motion mapping φ allows us to relate positions between the initial and current configurations, but it does not provide information about changes in the immediate vicinity of a point after deformation. To fully describe deformation, we need to characterize how deformation affects the surrounding area of a point. The deformation gradient $\underline{\mathbf{F}} \in \mathbb{R}^{3\times3}$ enables us to relate the spatial positions of neighboring points before and after deformation. From Fig. A.1,

$$\begin{aligned} d\mathbf{x} &= \mathbf{x}_q - \mathbf{x}_p \\ &= \varphi(\mathbf{X}_P + d\mathbf{X}, t) - \varphi(\mathbf{X}_P, t) \\ &= \varphi(\mathbf{X}_P, t) + \frac{\partial \varphi}{\partial \mathbf{X}}\Big|_{\mathbf{X}\text{ fixed}} d\mathbf{X} \underbrace{+ \cdots}_{\text{h.o.t.}} - \varphi(\mathbf{X}_P, t) \\ &= \frac{\partial \varphi}{\partial \mathbf{X}}\, d\mathbf{X}. \end{aligned}$$

From the above, we define the deformation gradient tensor $\underline{\mathbf{F}} \in \mathbb{R}^{3\times3}$ as:

$$\underline{\mathbf{F}} = \frac{\partial \varphi}{\partial \mathbf{X}} = \nabla_0 \varphi = \begin{bmatrix} \frac{\partial x_1}{\partial X_1} & \frac{\partial x_1}{\partial X_2} & \frac{\partial x_1}{\partial X_3} \\ \frac{\partial x_2}{\partial X_1} & \frac{\partial x_2}{\partial X_2} & \frac{\partial x_2}{\partial X_3} \\ \frac{\partial x_3}{\partial X_1} & \frac{\partial x_3}{\partial X_2} & \frac{\partial x_3}{\partial X_3} \end{bmatrix}, \tag{A.4}$$

where ∇_0 represents the gradient operator w.r.t. material coordinates. With the previous definition we can express the relations:

$$d\mathbf{x} = \phi_\star \left[d\mathbf{X} \right] = \underline{\mathbf{F}}\, d\mathbf{X}, \tag{A.5}$$

$$d\mathbf{X} = \phi_\star^{-1} \left[d\mathbf{x} \right] = \underline{\mathbf{F}}^{-1}\, d\mathbf{x}, \tag{A.6}$$

where $\phi_\star \left[\cdot \right]$ and $\phi_\star^{-1} \left[\cdot \right]$ denote push forward and pull back operations applied to vectors, respectively. The tensor $\underline{\mathbf{F}}$ can be decomposed as:

$$\underline{\mathbf{F}} = \underline{\mathbf{R}}\underline{\mathbf{U}}, \quad \text{(right polar decomposition)} \tag{A.7}$$

where $\underline{\mathbf{R}} \in \mathbb{R}^{3\times3}$ is the orthogonal rotation tensor representing rotation and $\underline{\mathbf{U}} \in \mathbb{R}^{3\times3}$ is the symmetric tensor called material right stretch tensor. Alternatively,

$$\underline{\mathbf{F}} = \underline{\mathbf{V}}\underline{\mathbf{R}}, \quad \text{(left polar decomposition)} \tag{A.8}$$

where $\underline{\mathbf{R}} \in \mathbb{R}^{3\times3}$ is the orthogonal rotation tensor and $\underline{\mathbf{V}} \in \mathbb{R}^{3\times3}$ is the symmetric tensor called spatial left stretch tensor. Physically, the action of the deformation gradient is composed by stretching without rotation plus rotation without stretching (in the right polar decomposition, see Fig. A.2a), and conversely for the left polar decomposition (Fig. A.2b). We can observe that the lengths remains unchanged during rotation, for instance in the right polar decomposition we have: $d\mathbf{x} = \underline{\mathbf{F}} d\mathbf{X} = \underline{\mathbf{R}}\underline{\mathbf{U}} d\mathbf{X} = \underline{\mathbf{R}} d\mathbf{y}$, then

$$d\mathbf{x} \cdot d\mathbf{x} = \underline{\mathbf{R}} d\mathbf{y} \cdot \underline{\mathbf{R}} d\mathbf{y} = d\mathbf{y} \cdot \underline{\mathbf{R}}^\top \underline{\mathbf{R}} d\mathbf{y} = d\mathbf{y} \cdot d\mathbf{y}.$$

The result is the same for the left polar decomposition.

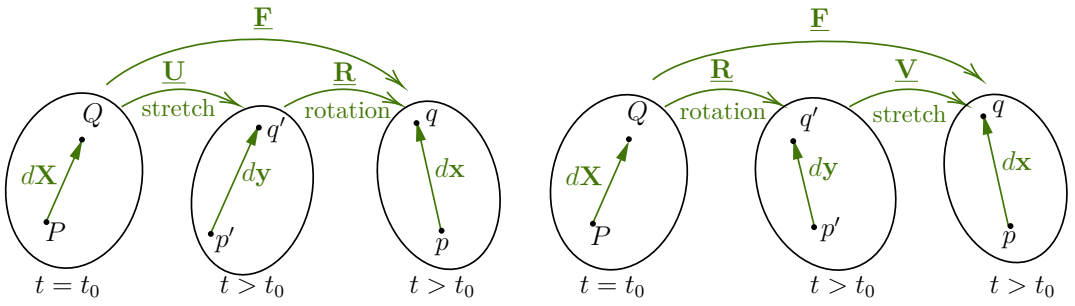

(a) Right polar decomposition (b) Left polar decomposition

Figure A.2 – Polar decomposition of the deformation gradient.

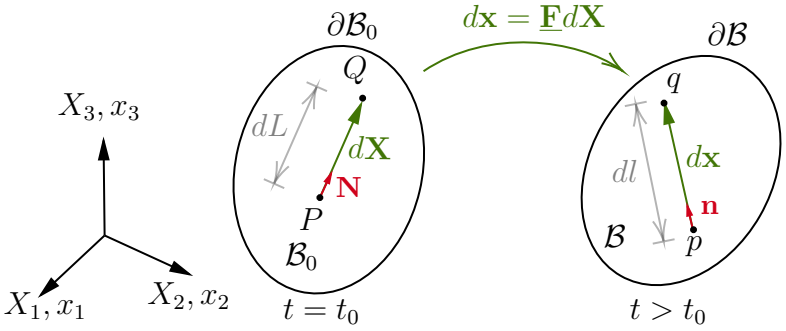

Figure A.3 – Change of length between internal points.

Now, consider the material vector $d\mathbf{X} = dL\,\mathbf{N}$ of length dL in the direction of $\mathbf{N}$, with $\mathbf{N}$ an eigenvector of $\underline{\mathbf{U}}$, as illustrated in Fig. A.3. Since $d\mathbf{x} = \underline{\mathbf{F}}d\mathbf{X} = dl\mathbf{n}$, and $\underline{\mathbf{F}} = \underline{\mathbf{R}}\underline{\mathbf{U}}$, we obtain $d\mathbf{x} = \underline{\mathbf{R}}\underline{\mathbf{U}}d\mathbf{X} = dL\underline{\mathbf{R}}\underline{\mathbf{U}}\mathbf{N}$, where replacing $\underline{\mathbf{U}}\mathbf{N} = \lambda_U\mathbf{N}$ with λ_U an eigenvalue of $\underline{\mathbf{U}}$ and $\underline{\mathbf{R}}\mathbf{N} = \mathbf{n}$ in the previous expression we get $d\mathbf{x} = dL\lambda_U\underline{\mathbf{R}}\mathbf{N} = dL\lambda_U\mathbf{n} = dl\mathbf{n}$. From the last expression we obtain:

$$\lambda_U = \frac{dl}{dL}, \tag{A.9}$$

which corresponds to the definition of stretch. Thus, the eigenvalues of $\underline{\mathbf{U}}$ represent the stretch ratios in the principal directions of deformation.

A.1.3 Strain measures

Consider two infinitesimal material vectors $d\mathbf{X}_1$, $d\mathbf{X}_2$ and their spatial vectors $d\mathbf{x}_1$, $d\mathbf{x}_2$. As we discussed previously, the scalar product between the last two involve stretching, i.e. change of the lengths of the vectors, as well as change in the angle between them, and is given by:

$$d\mathbf{x}_1 \cdot d\mathbf{x}_2 = \underline{\mathbf{F}}d\mathbf{X}_1 \cdot \underline{\mathbf{F}}d\mathbf{X}_2 = d\mathbf{X}_1 \cdot \underline{\mathbf{F}}^\top\underline{\mathbf{F}}d\mathbf{X}_2 = d\mathbf{X}_1 \cdot \underline{\mathbf{C}}d\mathbf{X}_2,$$

where $\underline{\mathbf{C}} \in \mathbb{R}^{3\times3}$ is defined as:

$$\underline{\mathbf{C}} = \underline{\mathbf{F}}^\top\underline{\mathbf{F}}, \tag{A.10}$$

and is called right Green-Cauchy tensor, which is a symmetric material tensor. Alternatively,

$$d\mathbf{X}_1\cdot d\mathbf{X}_2 = \underline{\mathbf{F}}^{-1}d\mathbf{x}_1\cdot\underline{\mathbf{F}}^{-1}d\mathbf{x}_2 = d\mathbf{x}_1\cdot\underline{\mathbf{F}}^{-\top}\underline{\mathbf{F}}^{-1}d\mathbf{x}_2 = d\mathbf{x}_1\cdot(\underline{\mathbf{F}}\underline{\mathbf{F}}^\top)^{-1}d\mathbf{x}_2 = d\mathbf{x}_1\cdot\underline{\mathbf{b}}^{-1}d\mathbf{x}_2,$$

where $\underline{\mathbf{b}} \in \mathbb{R}^{3\times3}$ is defined as:

$$\underline{\mathbf{b}} = \underline{\mathbf{F}}\underline{\mathbf{F}}^\top, \tag{A.11}$$

and is called left Green-Cauchy tensor, which is a symmetric spatial tensor.

Remark A.2. *Note that using the polar decomposition we easily find that* $\underline{\boldsymbol{C}} = \underline{\boldsymbol{U}}^\top\underline{\boldsymbol{U}}$ *and* $\underline{\boldsymbol{b}} = \underline{\boldsymbol{V}}\underline{\boldsymbol{V}}^\top$*. Therefore, it can be shown that the eigenvalues of* $\underline{\boldsymbol{C}}$ *are the square of the principal stretches.*

Now, consider the half of the difference between the scalar product of spatial and material vectors as:

$$\frac{1}{2}(d\mathbf{x}_1\cdot d\mathbf{x}_2-d\mathbf{X}_1\cdot d\mathbf{X}_2)=\frac{1}{2}(d\mathbf{X}_1\cdot\underline{\mathbf{C}}d\mathbf{X}_2-d\mathbf{X}_1\cdot d\mathbf{X}_2)=d\mathbf{X}_1\cdot\frac{1}{2}(\underline{\mathbf{C}}-\underline{\mathbf{I}})d\mathbf{X}_2 = d\mathbf{X}_1\cdot\underline{\mathbf{E}}d\mathbf{X}_2,$$

where $\underline{\mathbf{I}} \in \mathbb{R}^{3\times3}$ is the second order identity tensor and $\underline{\mathbf{E}} \in \mathbb{R}^{3\times3}$ is defined as:

$$\underline{\mathbf{E}} = \frac{1}{2}(\underline{\mathbf{C}} - \underline{\mathbf{I}}), \tag{A.12}$$

and is called Green-Lagrange strain tensor, which is a symmetric material tensor. Alternatively,

$$\frac{1}{2}(d\mathbf{x}_1\cdot d\mathbf{x}_2-d\mathbf{X}_1\cdot d\mathbf{X}_2) = \frac{1}{2}(d\mathbf{x}_1\cdot d\mathbf{x}_2-d\mathbf{x}_1\cdot\underline{\mathbf{b}}^{-1}d\mathbf{x}_2) = d\mathbf{x}_1\cdot\frac{1}{2}(\underline{\mathbf{I}}-\underline{\mathbf{b}}^{-1})d\mathbf{x}_2 = d\mathbf{x}_1\cdot\underline{\mathbf{e}}d\mathbf{x}_2,$$

where $\underline{\mathbf{e}} \in \mathbb{R}^{3\times3}$ is defined as:

$$\underline{\mathbf{e}} = \frac{1}{2}(\underline{\mathbf{I}} - \underline{\mathbf{b}}^{-1}), \tag{A.13}$$

and is called Euler-Almansi strain tensor, which is a symmetric spatial tensor. With the above, the change in the square of the length can be written as:

$$\frac{1}{2}(dl^2 - dL^2) = \frac{1}{2}(d\mathbf{x}\cdot d\mathbf{x} - d\mathbf{X}\cdot d\mathbf{X}) = d\mathbf{x}\cdot\underline{\mathbf{e}}\,d\mathbf{x} = d\mathbf{X}\cdot\underline{\mathbf{E}}\,d\mathbf{X}$$

where $d\mathbf{x}\cdot\underline{\mathbf{e}}\,d\mathbf{x} = d\mathbf{X}\cdot\underline{\mathbf{E}}\,d\mathbf{X} = \underline{\mathbf{F}}^{-1}d\mathbf{x}\cdot\underline{\mathbf{E}}\underline{\mathbf{F}}^{-1}d\mathbf{x} = d\mathbf{x}\cdot(\underline{\mathbf{F}}^{-\top}\underline{\mathbf{E}}\underline{\mathbf{F}}^{-1})d\mathbf{x}$. Therefore, with the previous equation we can express the relations:

$$\underline{\mathbf{e}} = \phi_\star\left[\underline{\mathbf{E}}\right] = \underline{\mathbf{F}}^{-\top}\underline{\mathbf{E}}\underline{\mathbf{F}}^{-1}, \tag{A.14}$$

$$\underline{\mathbf{E}} = \phi_\star^{-1}\left[\underline{\mathbf{e}}\right] = \underline{\mathbf{F}}^{\top}\underline{\mathbf{e}}\underline{\mathbf{F}}, \tag{A.15}$$

where $\phi_\star[\cdot]$ and $\phi_\star^{-1}[\cdot]$ denote push forward and pull back operations applied to second order tensors, respectively.

The deformation gradient $\underline{\mathbf{F}}$ and the Green-Lagrange strain tensor $\underline{\mathbf{E}}$ can be expressed in terms of the displacement field $\mathbf{u} = [u_1\ u_2\ u_3]^\top$ as:

$$\underline{\mathbf{F}} = \nabla_0\mathbf{u} + \underline{\mathbf{I}}, \tag{A.16}$$

$$\underline{\mathbf{E}} = \frac{1}{2}\left(\nabla_0\mathbf{u} + (\nabla_0\mathbf{u})^\top + (\nabla_0\mathbf{u})^\top\nabla_0\mathbf{u}\right), \tag{A.17}$$

where for a material Cartesian basis $\{X_1, X_2, X_3\}$ the components of the Green-Lagrange strain tensor $\underline{\mathbf{E}}$ are obtained from:

$$E_{ij} = \frac{1}{2}\left(\frac{\partial u_i}{\partial X_j} + \frac{\partial u_j}{\partial X_i} + \sum_{k=1}^{3}\frac{\partial u_k}{\partial X_i}\frac{\partial u_k}{\partial X_j}\right). \tag{A.18}$$

In the framework of linearized kinematics, the deformation is assumed to be sufficiently small ($\|\nabla_0\mathbf{u}\| \ll 1$) such that the changes in shape and size can be approximated linearly. In addition, due to the small deformations, the spatial

configuration is considered almost identical to the reference configuration, which implies $\mathbf{x} \approx \mathbf{X}$ and $\underline{\mathbf{F}} \approx \underline{\mathbf{I}}$. To derive a linear strain measure, first consider the directional derivative of $\underline{\mathbf{F}}$ in the direction of the displacement field $\mathbf{u}$ as:

$$\begin{aligned} D\underline{\mathbf{F}}[\mathbf{u}] &= \lim_{\eta\to 0} \frac{d}{d\eta}\left(\frac{\partial}{\partial \mathbf{X}}(\varphi + \eta\mathbf{u})\right) \\ &= \lim_{\eta\to 0} \frac{d}{d\eta}\left(\frac{\partial \varphi}{\partial \mathbf{X}} + \eta\frac{\partial \mathbf{u}}{\partial \mathbf{X}}\right) \\ &= \frac{\partial \mathbf{u}}{\partial \mathbf{X}} = \nabla_0 \mathbf{u} \\ &= \frac{\partial \mathbf{u}}{\partial \mathbf{x}}\frac{\partial \mathbf{x}}{\partial \mathbf{X}} = (\nabla \mathbf{u})\underline{\mathbf{F}}. \end{aligned} \tag{A.19}$$

Now, the directional derivative of the Green-Lagrange strain tensor is given by:

$$\begin{aligned} D\underline{\mathbf{E}}[\mathbf{u}] &= \frac{1}{2} D\left(\underline{\mathbf{F}}^\top \underline{\mathbf{F}} - \underline{\mathbf{I}}\right)[\mathbf{u}] \\ &= \frac{1}{2} D\left(\underline{\mathbf{F}}^\top \underline{\mathbf{F}}\right)[\mathbf{u}] \\ &= \frac{1}{2}\left(\underline{\mathbf{F}}^\top D\underline{\mathbf{F}}[\mathbf{u}] + D\underline{\mathbf{F}}[\mathbf{u}]^\top \underline{\mathbf{F}}\right) \\ &= \frac{1}{2}\left(\underline{\mathbf{F}}^\top (\nabla \mathbf{u})\underline{\mathbf{F}} + \underline{\mathbf{F}}^\top (\nabla \mathbf{u})^\top \underline{\mathbf{F}}\right) \\ &= \underline{\mathbf{F}}^\top \frac{1}{2}\left(\nabla \mathbf{u} + (\nabla \mathbf{u})^\top\right)\underline{\mathbf{F}} \\ &= \underline{\mathbf{F}}^\top \underline{\boldsymbol{\mathfrak{e}}}\, \underline{\mathbf{F}}, \end{aligned} \tag{A.20}$$

where $\underline{\boldsymbol{\mathfrak{e}}} \in \mathbb{R}^{3\times 3}$ is defined as:

$$\underline{\boldsymbol{\mathfrak{e}}} = \frac{1}{2}\left(\nabla \mathbf{u} + (\nabla \mathbf{u})^\top\right) = \frac{1}{2}\left(\nabla_0 \mathbf{u} + (\nabla_0 \mathbf{u})^\top\right), \tag{A.21}$$

and is called Infinitesimal strain tensor, which is a symmetric tensor. So, when Cartesian bases $\{X_1, X_2, X_3\}$ or $\{x_1, x_2, x_3\}$ are used, the components of the Infinitesimal strain tensor $\underline{\boldsymbol{\mathfrak{e}}}$ are obtained from:

$$\mathfrak{e}_{ij} = \frac{1}{2}\left(\frac{\partial u_i}{\partial X_j} + \frac{\partial u_j}{\partial X_i}\right) = \frac{1}{2}\left(\frac{\partial u_i}{\partial x_j} + \frac{\partial u_j}{\partial x_i}\right). \tag{A.22}$$

Remark A.3. *The von Kármán strains are a strain measure frequently used in the analysis of moderately large deformations. They are obtained from the Green-Lagrange strain tensor by neglecting the nonlinear stretching terms. As a result, they represent a middle ground between the linearized Infinitesimal strain tensor* $\underline{\boldsymbol{\mathfrak{e}}}$ *and the fully nonlinear Green-Lagrange strain tensor* $\underline{\boldsymbol{E}}$.

A.1.4 Volume and surface elements

Consider three material vectors along the X_1, X_2, X_3 directions as $d\mathbf{X}_1 = dX_1\hat{\mathbf{E}}_1$, $d\mathbf{X}_2 = dX_2\hat{\mathbf{E}}_2$ and $d\mathbf{X}_3 = dX_3\hat{\mathbf{E}}_3$, where $\hat{\mathbf{E}}_1$, $\hat{\mathbf{E}}_2$, $\hat{\mathbf{E}}_3$ are the unitary vectors of the Cartesian basis in the reference configuration. Additionally, consider their spatial

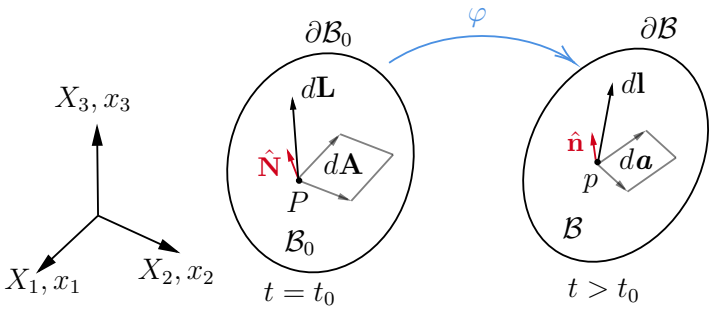

Figure A.4 – Surface elements.

vectors as $d\mathbf{x}_1 = \underline{\mathbf{F}} d\mathbf{X}_1 = \frac{\partial\varphi}{\partial\mathbf{X}} dX_1 \hat{\mathbf{E}}_1 = \frac{\partial\varphi}{\partial X_1} dX_1$, $d\mathbf{x}_2 = \frac{\partial\varphi}{\partial X_2} dX_2$ and $d\mathbf{x}_3 = \frac{\partial\varphi}{\partial X_3} dX_3$. The volume in the reference configuration is given by:

$$dV_0 = d\mathbf{X}_1 \cdot (d\mathbf{X}_2 \times d\mathbf{X}_3) = dX_1 dX_2 dX_3, \tag{A.23}$$

and the volume in the current configuration is:

$$dV = d\mathbf{x}_1 \cdot (d\mathbf{x}_2 \times d\mathbf{x}_3) = \underbrace{\frac{\partial\varphi}{\partial X_1} \cdot \left(\frac{\partial\varphi}{\partial X_2} \times \frac{\partial\varphi}{\partial X_3} \right)}_{\det(\underline{\mathbf{F}}) = J_\varepsilon} (dX_1 dX_2 dX_3) = J_\varepsilon dV_0. \tag{A.24}$$

Remark A.4. *When $J_\varepsilon = \det(\underline{\boldsymbol{F}}) = 1$, the volume is preserved during deformation, which is known as isochoric or incompressible deformation. This condition is often included as constraint in polymer models to accurately represent incompressibility, which is crucial to predict realistic behavior. Since $\underline{\boldsymbol{C}} = \underline{\boldsymbol{F}}^\top \underline{\boldsymbol{F}}$ it follows that $\det(\underline{\boldsymbol{C}}) = J_\varepsilon^2$. Therefore, imposing $\det(\underline{\boldsymbol{C}}) = 1$ as constraint is also a common choice to enforce incompressible deformation.*

Now, consider the surface elements in the reference and current configurations as $d\mathbf{A} = dA\hat{\mathbf{N}}$ and $d\boldsymbol{a} = da\hat{\mathbf{n}}$, respectively, where $\hat{\mathbf{N}}$ and $\hat{\mathbf{n}}$ are the outward-pointing unit normal vectors to the surfaces $\partial\mathcal{B}_0$ and $\partial\mathcal{B}$ in the reference and current configurations, respectively (see Fig. A.4). To compute the infinitesimal volume let consider an arbitrary material vector $d\mathbf{L}$ and its spatial counterpart $d\mathbf{l} = \underline{\mathbf{F}} d\mathbf{L}$. So, the volumes are given by $dV_0 = d\mathbf{L} \cdot d\mathbf{A}$ and $dV = d\mathbf{l} \cdot d\boldsymbol{a}$, then:

$$\begin{aligned} dV &= J_\varepsilon dV_0 \\ d\mathbf{l} \cdot d\boldsymbol{a} &= J_\varepsilon d\mathbf{L} \cdot d\mathbf{A} \\ \underline{\mathbf{F}} d\mathbf{L} \cdot d\boldsymbol{a} &= J_\varepsilon d\mathbf{L} \cdot d\mathbf{A} \\ d\mathbf{L} \cdot \underline{\mathbf{F}}^\top d\boldsymbol{a} &= d\mathbf{L} \cdot J_\varepsilon d\mathbf{A}, \end{aligned}$$

where we get the following expression:

$$d\boldsymbol{a} = J_\varepsilon \underline{\mathbf{F}}^{-\top} d\mathbf{A}, \tag{A.25}$$

which is called Nanson's formula.

A.1.5 Kinematic rates

In this section we introduce time derivative of kinematic quantities. Considering that the motion of the body is described by $\mathbf{x} = \varphi(\mathbf{X}, t)$, the velocity of a material particle $\mathbf{X}$ is defined as:

$$\mathbf{v}(\mathbf{X}, t) = \frac{\partial \varphi}{\partial t}\Big|_{\mathbf{X} \text{ fixed}} = \frac{\partial \mathbf{x}(\mathbf{X}, t)}{\partial t} = \frac{D\mathbf{x}(\mathbf{X}, t)}{Dt} = \dot{\mathbf{u}}(\mathbf{X}, t), \tag{A.26}$$

where $\mathbf{v}(\mathbf{X}, t) \in \mathbb{R}^3$ is the velocity vector. Similarly, for the acceleration vector $\mathbf{a}(\mathbf{X}, t) \in \mathbb{R}^3$ we have:

$$\mathbf{a}(\mathbf{X}, t) = \frac{\partial^2 \varphi}{\partial t^2}\Big|_{\mathbf{X} \text{ fixed}} = \frac{\partial \mathbf{v}(\mathbf{X}, t)}{\partial t} = \frac{D\mathbf{v}(\mathbf{X}, t)}{Dt} = \ddot{\mathbf{u}}(\mathbf{X}, t). \tag{A.27}$$

The velocity and acceleration vectors $\mathbf{v}(\mathbf{X}, t)$ and $\mathbf{a}(\mathbf{X}, t)$, respectively, are spatial vectors, even though they are expressed in terms of material coordinates of the particle $\mathbf{X}$. They represent the current velocity and acceleration (in the deformed configuration) of the particle that occupies the position $\mathbf{X}$ in the reference configuration. Using a slight abuse of notation and by means of $\mathbf{X} = \varphi^{-1}(\mathbf{x}, t)$, they can be expressed as $\mathbf{v}(\mathbf{x}, t)$ and $\mathbf{a}(\mathbf{x}, t)$, respectively.

The notation $\frac{D}{Dt}$ denotes the material time derivative, and it represents the time derivative when the material coordinates are fixed. For quantities expressed in terms of material coordinates, the time derivative $\frac{d}{dt}$ is equivalent to the material time derivative $\frac{D}{Dt}$, which is also equivalent to the partial time derivative $\frac{\partial}{\partial t}$. On the other hand, for spatial quantities, generically represented by the spatial field $g(\mathbf{x}, t)$, the material time derivative is given by:

$$\begin{aligned} \frac{Dg}{Dt} = \frac{dg}{dt} = \dot{g}(\mathbf{x}, t) &= \underbrace{\frac{\partial g(\mathbf{x}, t)}{\partial t}\Big|_{\mathbf{x} \text{ fixed}}}_{\text{local rate of change}} + \underbrace{\frac{\partial g(\mathbf{x}, t)}{\partial \mathbf{x}} \frac{\partial \mathbf{x}}{\partial t}\Big|_{\mathbf{x} \text{ fixed}}}_{\text{convective term}} \\ &= \frac{\partial g(\mathbf{x}, t)}{\partial t}\Big|_{\mathbf{x} \text{ fixed}} + (\nabla g(\mathbf{x}, t))\mathbf{v}(\mathbf{x}, t), \end{aligned} \tag{A.28}$$

where the local rate of change represents how the quantity $g(\mathbf{x}, t)$ changes at a fixed point $\mathbf{x}$ in space over time, while the convective term represents the rate of change on $g(\mathbf{x}, t)$ due to the changes of the configuration.

Remark A.5. *The notation $\boldsymbol{a}(\boldsymbol{x}, t)$ refers to $\boldsymbol{a}(\boldsymbol{x}, t) = \frac{\partial \boldsymbol{v}(\boldsymbol{x}, t)}{\partial t} + (\nabla \boldsymbol{v}(\boldsymbol{x}, t))\boldsymbol{v}(\boldsymbol{x}, t)$, while $\boldsymbol{a}(\boldsymbol{X}, t) = \ddot{\boldsymbol{u}}(\boldsymbol{X}, t)$. The distinction between $\boldsymbol{a}(\boldsymbol{x}, t)$ and $\boldsymbol{a}(\boldsymbol{X}, t)$ is important when establishing the equations of motion (balance of linear momentum) in the current and reference configurations, respectively.*

The material time derivative of the deformation gradient is given by:

$$\dot{\underline{\mathbf{F}}} = \frac{\partial}{\partial t}\left(\frac{\partial \varphi}{\partial \mathbf{X}}\right) = \frac{\partial}{\partial \mathbf{X}}\left(\frac{\partial \varphi}{\partial t}\right) = \nabla_0 \mathbf{v}. \tag{A.29}$$

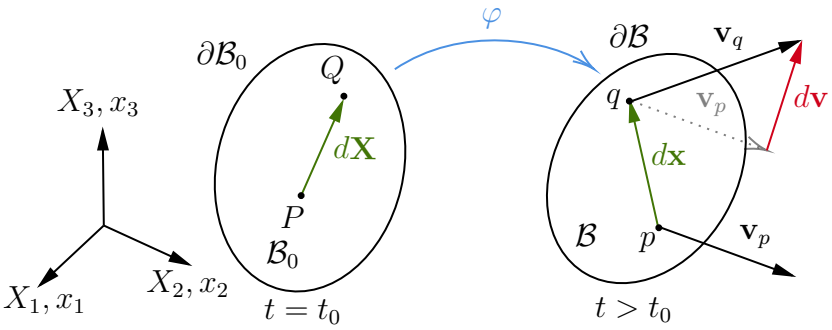

Figure A.5 – Velocity gradient tensor.

The velocity gradient tensor $\underline{\boldsymbol{\ell}} \in \mathbb{R}^{3\times3}$ is defined as the gradient of the velocity vector $\mathbf{v}(\mathbf{x}, t)$ w.r.t. the spatial coordinates $\mathbf{x}$, that is:

$$\underline{\boldsymbol{\ell}} = \frac{\partial \mathbf{v}}{\partial \mathbf{x}} = \nabla \mathbf{v}. \tag{A.30}$$

It is an spatial tensor and represents the relative velocity between points in the current configuration. From Fig. A.5, the relative velocity of a particle currently at point q w.r.t. a particle currently at point p is given by $d\mathbf{v} = \underline{\boldsymbol{\ell}}\, d\mathbf{x}$. The tensor $\underline{\boldsymbol{\ell}}$ can be used to express the material time derivative of $\underline{\mathbf{F}}$ as:

$$\dot{\underline{\mathbf{F}}} = \nabla_0 \mathbf{v} = \frac{\partial \mathbf{v}}{\partial \mathbf{X}} = \frac{\partial \mathbf{v}}{\partial \mathbf{x}} \frac{\partial \mathbf{x}}{\partial \mathbf{X}} = \underline{\boldsymbol{\ell}}\, \underline{\mathbf{F}}, \tag{A.31}$$

which implies $\underline{\boldsymbol{\ell}} = \dot{\underline{\mathbf{F}}} \underline{\mathbf{F}}^{-1}$. The velocity gradient tensor can be decomposed as $\underline{\boldsymbol{\ell}} = \underline{\mathbf{d}} + \underline{\mathbf{w}}$, where $\underline{\mathbf{w}} = -\underline{\mathbf{w}}^\top \in \mathbb{R}^{3\times3}$ is the skew-symmetric part of $\underline{\boldsymbol{\ell}}$ and is called spin tensor, and $\underline{\mathbf{d}} = \underline{\mathbf{d}}^\top \in \mathbb{R}^{3\times3}$ is the symmetric part of $\underline{\boldsymbol{\ell}}$ and is called rate of deformation tensor (or rate of strain tensor). The spin tensor represents the rate of rotation or angular velocity of material elements, while the rate of deformation tensor represents the local rate of stretching of the material without considering rotational motion. The material time derivative of the Green-Lagrange strain tensor $\underline{\mathbf{E}}$ is given by:

$$\begin{aligned}
\dot{\underline{\mathbf{E}}} &= \frac{1}{2}\left(\dot{\underline{\mathbf{F}}}^\top \underline{\mathbf{F}} + \underline{\mathbf{F}}^\top \dot{\underline{\mathbf{F}}}\right) \\
&= \frac{1}{2}\left[(\nabla \mathbf{v} \underline{\mathbf{F}})^\top \underline{\mathbf{F}} + \underline{\mathbf{F}}^\top (\nabla \mathbf{v} \underline{\mathbf{F}})\right] \\
&= \underline{\mathbf{F}}^\top \frac{1}{2}\left[(\nabla \mathbf{v})^\top + \nabla \mathbf{v}\right] \underline{\mathbf{F}} \\
&= \underline{\mathbf{F}}^\top \underline{\mathbf{d}}\, \underline{\mathbf{F}} = \phi_\star^{-1}\left[\underline{\mathbf{d}}\right].
\end{aligned} \tag{A.32}$$

Therefore, from the last expression we also get that $\underline{\mathbf{d}} = \phi_\star\left[\dot{\underline{\mathbf{E}}}\right] = \underline{\mathbf{F}}^{-\top} \dot{\underline{\mathbf{E}}} \underline{\mathbf{F}}^{-1}$.

Remark A.6. *The rate of deformation tensor $\underline{\boldsymbol{d}}$ is not the material time derivative of the Euler-Almansi strain tensor $\underline{\boldsymbol{e}}$. Since $\underline{\boldsymbol{E}} = \phi_\star^{-1}[\underline{\boldsymbol{e}}]$, the relation between $\underline{\boldsymbol{d}}$ and $\underline{\boldsymbol{e}}$ is given by:*

$$\underline{\boldsymbol{d}} = \phi_\star\left[\frac{d}{dt}\left(\phi_\star^{-1}[\underline{\boldsymbol{e}}]\right)\right] = \mathbb{L}_\phi[\underline{\boldsymbol{e}}], \tag{A.33}$$

where $\mathbb{L}_\phi[\cdot]$ denotes the Lie-derivative of the spatial quantity $(\cdot)$.

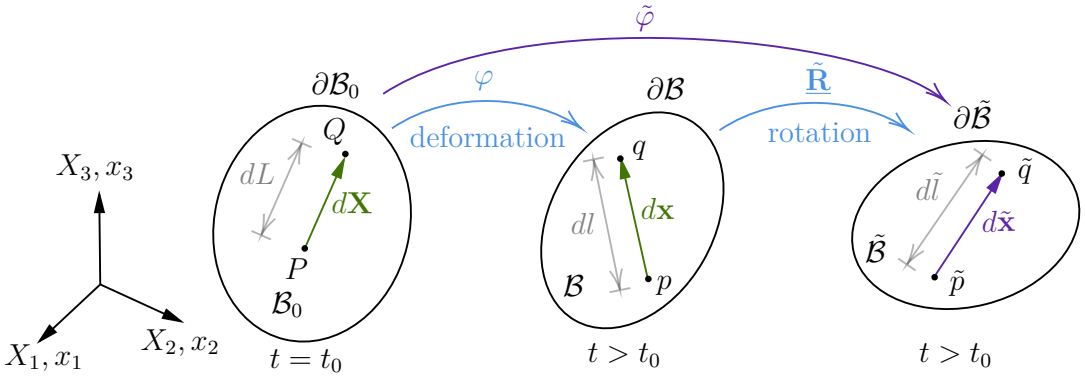

Figure A.6 – Superposed rigid body motion.

The rate of change of a volume element $\frac{d}{dt}(dV) = \dot{J}_\varepsilon dV_0$, is characterized by the material time derivative of J_ε, which is given by:

$$\dot{J}_\varepsilon = \frac{d(\det(\underline{\mathbf{F}}))}{dt} = \frac{\partial}{\partial \underline{\mathbf{F}}}(\det(\underline{\mathbf{F}})) : \dot{\underline{\mathbf{F}}} = \det(\underline{\mathbf{F}})\underline{\mathbf{F}}^{-\top} : \dot{\underline{\mathbf{F}}} = J_\varepsilon\, \underline{\mathbf{F}}^{-\top} : \underline{\boldsymbol{\ell}}\, \underline{\mathbf{F}},$$

where using the identity $A : (BC) = (CA^\top) : B$ we get:

$$\dot{J}_\varepsilon = J_\varepsilon\, \underline{\mathbf{F}}\underline{\mathbf{F}}^{-1} : \underline{\boldsymbol{\ell}} = J_\varepsilon\, \underline{\mathbf{I}} : \nabla \mathbf{v} = J_\varepsilon \operatorname{div}(\mathbf{v}) = J_\varepsilon \operatorname{tr}(\underline{\boldsymbol{\ell}}) = J_\varepsilon \operatorname{tr}(\underline{\mathbf{d}}). \tag{A.34}$$

Recalling from (A.25) that $d\boldsymbol{a} = J_\varepsilon\, \underline{\mathbf{F}}^{-\top} d\mathbf{A}$, the rate of change of a surface element is given by:

$$\begin{aligned}
\frac{d}{dt}(d\boldsymbol{a}) &= \frac{d}{dt}\left(J_\varepsilon\, \underline{\mathbf{F}}^{-\top}\right) d\mathbf{A} \\
&= \left(\dot{J}_\varepsilon\, \underline{\mathbf{F}}^{-\top} + J_\varepsilon\, \dot{\underline{\mathbf{F}}}^{-\top}\right) d\mathbf{A} \\
&= \left(J_\varepsilon \operatorname{div}(\mathbf{v})\underline{\mathbf{F}}^{-\top} - J_\varepsilon\, \underline{\boldsymbol{\ell}}^\top\, \underline{\mathbf{F}}^{-\top}\right) d\mathbf{A} \\
&= \left(\operatorname{div}(\mathbf{v}) - \underline{\boldsymbol{\ell}}^\top\right) J_\varepsilon\, \underline{\mathbf{F}}^{-\top} d\mathbf{A} \\
&= \left(\operatorname{div}(\mathbf{v}) - \underline{\boldsymbol{\ell}}^\top\right) d\boldsymbol{a}.
\end{aligned} \tag{A.35}$$

A.1.6 Objectivity of kinematic variables

Objective quantities, or frame-indifferent quantities, are those that remain invariant under a rigid body motion, meaning their intrinsic nature does not change even though their form may alter. The study of objectivity is important in continuum mechanics, particularly in the description of motion and in deriving constitutive laws, because it ensures that rigid body motions do not generate internal stresses, which is a fundamental requirement for physically meaningful models.

Consider a material vector $d\mathbf{X}$ in the reference configuration that deforms to the spatial vector $d\mathbf{x}$ in the current configuration as $d\mathbf{x} = \underline{\mathbf{F}} d\mathbf{X}$. Then, let the body undergo rigid body rotation so the spatial vector $d\mathbf{x}$ is rotated to the spatial vector

$d\tilde{\mathbf{x}}$, as illustrated in Fig. A.6. The expression for $d\tilde{\mathbf{x}}$ is given by:

$$d\tilde{\mathbf{x}} = \underline{\tilde{\mathbf{R}}}\, d\mathbf{x} = \underline{\tilde{\mathbf{R}}}\,\underline{\mathbf{F}} d\mathbf{X} = \underline{\tilde{\mathbf{F}}} d\mathbf{X} = \frac{\partial \tilde{\varphi}}{\partial \mathbf{X}} d\mathbf{X}, \tag{A.36}$$

where $\underline{\tilde{\mathbf{R}}} \in \mathbb{R}^{3\times 3}$ is an orthogonal rotation tensor which describe the superposed rigid body rotation, and $\tilde{\varphi}$ is the rotated motion mapping. Note that the length of $d\mathbf{x}$ remain unchanged: $d\tilde{\mathbf{x}} \cdot d\tilde{\mathbf{x}} = (\underline{\tilde{\mathbf{R}}}\, d\mathbf{x}) \cdot (\underline{\tilde{\mathbf{R}}}\, d\mathbf{x}) = d\mathbf{x} \cdot \underline{\tilde{\mathbf{R}}}^{\top} \underline{\tilde{\mathbf{R}}} d\mathbf{x} = d\mathbf{x} \cdot d\mathbf{x}$, so in this sense $d\mathbf{x}$ is objective under rigid body rotation.
Generalizing the previous result, we say that any vector $\mathbf{c} \in \mathbb{R}^3$ which transforms as:

$$\tilde{\mathbf{c}} = \underline{\tilde{\mathbf{R}}}\, \mathbf{c} \tag{A.37}$$

when undergoing rigid body rotation is called an objective vector. Note that the velocity vector $\mathbf{v}$ is not an objective quantity since it transform as:

$$\tilde{\mathbf{v}} = \frac{\partial \tilde{\varphi}}{\partial t} = \frac{\partial}{\partial t}(\underline{\tilde{\mathbf{R}}}\varphi) = \underline{\tilde{\mathbf{R}}} \frac{\partial \varphi}{\partial t} + \dot{\underline{\tilde{\mathbf{R}}}}\varphi = \underline{\tilde{\mathbf{R}}}\, \mathbf{v} + \dot{\underline{\tilde{\mathbf{R}}}}\, \mathbf{x}. \tag{A.38}$$

The above is expected since $\mathbf{v}$ is inherently a frame-dependent quantity because it measures the rate of change of position w.r.t. time in a given frame of reference.

Remark A.7. *Notice that* $\underline{\tilde{\boldsymbol{R}}}^{\top} \underline{\tilde{\boldsymbol{R}}} = \underline{\boldsymbol{I}}$*, which implies* $\frac{d}{dt}(\underline{\tilde{\boldsymbol{R}}}^{\top} \underline{\tilde{\boldsymbol{R}}}) = \dot{\underline{\tilde{\boldsymbol{R}}}}^{\top} \underline{\tilde{\boldsymbol{R}}} + \underline{\tilde{\boldsymbol{R}}}^{\top} \dot{\underline{\tilde{\boldsymbol{R}}}} = 0$*. Therefore,* $\dot{\underline{\tilde{\boldsymbol{R}}}}^{\top} \underline{\tilde{\boldsymbol{R}}} = -\underline{\tilde{\boldsymbol{R}}}^{\top} \dot{\underline{\tilde{\boldsymbol{R}}}}$ *is a skew-symmetric tensor.*

Consider the material tensors $\underline{\mathbf{C}}$, $\dot{\underline{\mathbf{C}}}$, $\underline{\mathbf{E}}$, and $\dot{\underline{\mathbf{E}}}$. The right Green-Cauchy tensor $\underline{\mathbf{C}} = \underline{\mathbf{F}}^{\top}\underline{\mathbf{F}}$ transforms as follows:

$$\underline{\tilde{\mathbf{C}}} = \underline{\tilde{\mathbf{F}}}^{\top} \underline{\tilde{\mathbf{F}}} = (\underline{\tilde{\mathbf{R}}}\,\underline{\mathbf{F}})^{\top} (\underline{\tilde{\mathbf{R}}}\,\underline{\mathbf{F}}) = \underline{\mathbf{F}}^{\top} \underline{\tilde{\mathbf{R}}}^{\top} \underline{\tilde{\mathbf{R}}}\underline{\mathbf{F}} = \underline{\mathbf{F}}^{\top}\underline{\mathbf{F}} = \underline{\mathbf{C}}. \tag{A.39}$$

The material time derivative of $\underline{\mathbf{C}}$ is given by $\dot{\underline{\mathbf{C}}} = \dot{\underline{\mathbf{F}}}^{\top}\underline{\mathbf{F}} + \underline{\mathbf{F}}^{\top}\dot{\underline{\mathbf{F}}}$, then:

$$\begin{aligned}
\dot{\underline{\tilde{\mathbf{C}}}} = \;& \dot{\underline{\tilde{\mathbf{F}}}}^{\top} \underline{\tilde{\mathbf{F}}} + \underline{\tilde{\mathbf{F}}}^{\top} \dot{\underline{\tilde{\mathbf{F}}}} \\
=\;& (\dot{\underline{\tilde{\mathbf{R}}}}\underline{\mathbf{F}} + \underline{\tilde{\mathbf{R}}}\dot{\underline{\mathbf{F}}})^{\top} \underline{\tilde{\mathbf{R}}}\underline{\mathbf{F}} + (\underline{\tilde{\mathbf{R}}}\underline{\mathbf{F}})^{\top} (\dot{\underline{\tilde{\mathbf{R}}}}\underline{\mathbf{F}} + \underline{\tilde{\mathbf{R}}}\dot{\underline{\mathbf{F}}}) \\
=\;& (\underline{\mathbf{F}}^{\top}\dot{\underline{\tilde{\mathbf{R}}}}^{\top} + \dot{\underline{\mathbf{F}}}^{\top}\underline{\tilde{\mathbf{R}}}^{\top})\underline{\tilde{\mathbf{R}}}\underline{\mathbf{F}} + (\underline{\mathbf{F}}^{\top}\underline{\tilde{\mathbf{R}}}^{\top})(\dot{\underline{\tilde{\mathbf{R}}}}\underline{\mathbf{F}} + \underline{\tilde{\mathbf{R}}}\dot{\underline{\mathbf{F}}}) \\
=\;& \underline{\mathbf{F}}^{\top}\dot{\underline{\tilde{\mathbf{R}}}}^{\top}\underline{\tilde{\mathbf{R}}}\underline{\mathbf{F}} + \dot{\underline{\mathbf{F}}}^{\top}\underline{\tilde{\mathbf{R}}}^{\top}\underline{\tilde{\mathbf{R}}}\underline{\mathbf{F}} + \underline{\mathbf{F}}^{\top}\underline{\tilde{\mathbf{R}}}^{\top}\dot{\underline{\tilde{\mathbf{R}}}}\underline{\mathbf{F}} + \underline{\mathbf{F}}^{\top}\underline{\tilde{\mathbf{R}}}^{\top}\underline{\tilde{\mathbf{R}}}\dot{\underline{\mathbf{F}}} \\
=\;& -\underline{\mathbf{F}}^{\top}\underline{\tilde{\mathbf{R}}}^{\top}\dot{\underline{\tilde{\mathbf{R}}}}\underline{\mathbf{F}} + \dot{\underline{\mathbf{F}}}^{\top}\underline{\mathbf{F}} + \underline{\mathbf{F}}^{\top}\underline{\tilde{\mathbf{R}}}^{\top}\dot{\underline{\tilde{\mathbf{R}}}}\underline{\mathbf{F}} + \underline{\mathbf{F}}^{\top}\dot{\underline{\mathbf{F}}} \\
=\;& \dot{\underline{\mathbf{F}}}^{\top}\underline{\mathbf{F}} + \underline{\mathbf{F}}^{\top}\dot{\underline{\mathbf{F}}} \\
=\;& \dot{\underline{\mathbf{C}}}.
\end{aligned}$$

Since the Green-Lagrange strain tensor is given by $\underline{\mathbf{E}} = \frac{1}{2}(\underline{\mathbf{C}} - \underline{\mathbf{I}})$, we directly obtain that $\underline{\tilde{\mathbf{E}}} = \underline{\mathbf{E}}$ and $\dot{\underline{\tilde{\mathbf{E}}}} = \dot{\underline{\mathbf{E}}}$. Therefore, $\underline{\mathbf{C}}$, $\dot{\underline{\mathbf{C}}}$, $\underline{\mathbf{E}}$, and $\dot{\underline{\mathbf{E}}}$ are objective tensors.

Now, consider the spatial tensors $\underline{\mathbf{b}}$, $\underline{\mathbf{e}}$, $\underline{\boldsymbol{\ell}}$ and $\underline{\mathbf{d}}$. The left Green-Cauchy tensor $\underline{\mathbf{b}} = \underline{\mathbf{F}}\underline{\mathbf{F}}^{\top}$ transforms as:

$$\underline{\tilde{\mathbf{b}}} = \underline{\tilde{\mathbf{F}}}\underline{\tilde{\mathbf{F}}}^{\top} = \underline{\tilde{\mathbf{R}}}\,\underline{\mathbf{F}}(\underline{\tilde{\mathbf{R}}}\,\underline{\mathbf{F}})^{\top} = \underline{\tilde{\mathbf{R}}}\underline{\mathbf{F}}\underline{\mathbf{F}}^{\top}\underline{\tilde{\mathbf{R}}} = \underline{\tilde{\mathbf{R}}}\underline{\mathbf{b}}\underline{\tilde{\mathbf{R}}}^{\top}. \tag{A.40}$$

Similarly, for the Euler-Almansi strain tensor we get $\tilde{\underline{\mathbf{e}}} = \underline{\tilde{\mathbf{R}}\mathbf{e}\tilde{\mathbf{R}}}^{\top}$. Note that although $\tilde{\underline{\mathbf{e}}} \neq \underline{\mathbf{e}}$, the intrinsic nature of both tensors remains unchanged. To see this, consider the following. We already shown that $d\tilde{\mathbf{x}} \cdot d\tilde{\mathbf{x}} = d\mathbf{x} \cdot d\mathbf{x}$, which according with Fig. A.6 implies $d\tilde{l} = dl$. Then:

$$\begin{aligned}\frac{1}{2}(d\tilde{l}^2 - dL^2) = \frac{1}{2}(dl^2 - dL^2) = \;& d\tilde{\mathbf{x}} \cdot \tilde{\underline{\mathbf{e}}}\, d\tilde{\mathbf{x}} \\ =\;& (\tilde{\underline{\mathbf{R}}} d\mathbf{x}) \cdot (\underline{\tilde{\mathbf{R}}\mathbf{e}\tilde{\mathbf{R}}}^{\top})\tilde{\underline{\mathbf{R}}} d\mathbf{x} \\ =\;& d\mathbf{x} \cdot \tilde{\underline{\mathbf{R}}}^{\top}\underline{\tilde{\mathbf{R}}\mathbf{e}\tilde{\mathbf{R}}}^{\top}\tilde{\underline{\mathbf{R}}} d\mathbf{x} \\ =\;& d\mathbf{x} \cdot \underline{\mathbf{e}}\, d\mathbf{x}.\end{aligned}$$

Thus, $\tilde{\underline{\mathbf{e}}}$ is an objective tensor since its physical meaning remains unchanged. Generalizing the previous result, any second order tensor $\underline{\mathbf{s}} \in \mathbb{R}^{3\times 3}$ that transforms as:

$$\tilde{\underline{\mathbf{s}}} = \underline{\tilde{\mathbf{R}}\mathbf{s}\tilde{\mathbf{R}}}^{\top} \tag{A.41}$$

when undergoing rigid body rotation is called an objective tensor. So, the left Green-Cauchy tensor $\underline{\mathbf{b}}$ is an objective tensor. The velocity gradient tensor $\underline{\boldsymbol{\ell}} = \underline{\dot{\mathbf{F}}\mathbf{F}}^{-1}$ transforms as follows:

$$\tilde{\underline{\boldsymbol{\ell}}} = \underline{\dot{\tilde{\mathbf{F}}}\tilde{\mathbf{F}}}^{-1} = (\underline{\dot{\tilde{\mathbf{R}}}\mathbf{F}} + \underline{\tilde{\mathbf{R}}\dot{\mathbf{F}}})\underline{\mathbf{F}}^{-1}\underline{\tilde{\mathbf{R}}}^{\top} = \underline{\dot{\tilde{\mathbf{R}}}\mathbf{F}\mathbf{F}}^{-1}\underline{\tilde{\mathbf{R}}}^{\top} + \underline{\tilde{\mathbf{R}}\dot{\mathbf{F}}\mathbf{F}}^{-1}\underline{\tilde{\mathbf{R}}}^{\top} = \underline{\dot{\tilde{\mathbf{R}}}\tilde{\mathbf{R}}}^{\top} + \underline{\tilde{\mathbf{R}}\boldsymbol{\ell}\tilde{\mathbf{R}}}^{\top}. \tag{A.42}$$

Thus, $\underline{\boldsymbol{\ell}}$ is not an objective tensor, which is expected since $\underline{\boldsymbol{\ell}}$ measure the relative velocity between points, considering both, the rotational effects by means of its skew-symmetric part (the spin tensor $\underline{\mathbf{w}}$), and the local rate of stretching by means of its symmetric part (the rate of deformation tensor $\underline{\mathbf{d}}$). Noticing that $\tilde{\underline{\boldsymbol{\ell}}} = \underline{\dot{\tilde{\mathbf{R}}}\tilde{\mathbf{R}}}^{\top} + \underline{\tilde{\mathbf{R}}\boldsymbol{\ell}\tilde{\mathbf{R}}}^{\top} = \tilde{\underline{\mathbf{d}}} + \tilde{\underline{\mathbf{w}}}$, where $\underline{\dot{\tilde{\mathbf{R}}}\tilde{\mathbf{R}}}^{\top}$ is skew-symmetric, it follows that $\tilde{\underline{\mathbf{d}}} = \underline{\tilde{\mathbf{R}}\mathbf{d}\tilde{\mathbf{R}}}^{\top}$, thus $\underline{\mathbf{d}}$ is an objective tensor.

A.2 Conservation and balance laws

In mechanics, fundamental laws govern the behavior of physical systems. These laws include conservation of mass, balance of linear and angular momentum, conservation of energy, and the second law of thermodynamics. These laws ensure mass and momentum are preserved, energy is conserved, and thermodynamic processes are consistent with entropy production. The second law is particularly significant in constitutive modeling, ensuring that material behavior, such as energy dissipation in viscoelastic or plastic materials, is thermodynamically consistent. For hyperelastic materials, the strain energy density function (a form of elastic potential energy) must respect these principles, allowing elastic deformations without energy dissipation.

A.2.1 Reynolds transport theorem

Before presenting the conservation and balance laws in solid mechanics, it is essential to establish the Reynolds transport theorem. This theorem provides a mathematical framework for relating the rates of change of physical quantities within a control volume to their corresponding rates in the material or spatial domain, facilitating the analysis of dynamic behavior in solid continua.

Consider an integral I of the spatial field $g(\mathbf{x}, t)$ over the body $\mathcal{B}$. The material time derivative is given by:

$$\dot{I} = \frac{D}{Dt} \int_{\mathcal{B}} g(\mathbf{x}, t)\, dV, \tag{A.43}$$

where D/Dt can not be placed inside the integral because dV depends on time. Using $dV = J_\epsilon dV_0$ and $\mathbf{x} = \varphi(\mathbf{X}, t)$, with $\bar{g}(\mathbf{X}, t) = g(\varphi(\mathbf{X}, t), t)$ we have:

$$\begin{aligned}
\dot{I} =& \frac{D}{Dt} \int_{\mathcal{B}_0} \bar{g}(\mathbf{X}, t)\, J_\epsilon\, dV_0 \\
=& \int_{\mathcal{B}_0} \left(\dot{\bar{g}}(\mathbf{X}, t) J_\epsilon + \bar{g}(\mathbf{X}, t) \dot{J}_\epsilon \right) dV_0 \\
=& \int_{\mathcal{B}_0} \left(\dot{\bar{g}}(\mathbf{X}, t) J_\epsilon + \bar{g}(\mathbf{X}, t) \mathrm{div}(\mathbf{v}) \right) J_\epsilon\, dV_0.
\end{aligned}$$

Returning to spatial coordinates, we obtain:

$$\dot{I} = \int_{\mathcal{B}} \left(\dot{g}(\mathbf{x}, t) + g(\mathbf{x}, t) \mathrm{div}(\mathbf{v}) \right) dV. \tag{A.44}$$

Using $\dot{g}(\mathbf{x}, t) = \frac{\partial g(\mathbf{x}, t)}{\partial t}\Big|_{\mathbf{x} \text{ fixed}} + (\nabla g(\mathbf{x}, t))\mathbf{v}(\mathbf{x}, t)$ and substituting into (A.44) we get:

$$\dot{I} = \int_{\mathcal{B}} \left(\frac{\partial g}{\partial t} + \mathrm{div}(g\mathbf{v}) \right) dV = \int_{\mathcal{B}} \frac{\partial g}{\partial t} dV + \int_{\partial \mathcal{B}} (g\mathbf{v} \cdot \hat{\mathbf{n}}) da, \tag{A.45}$$

where the first term represents the rate of production of g inside the body, and the second term represents the net transport of g across its boundary. The Reynolds transport theorem is represented by the equation (A.45), where it expresses the rate of change of the integral of a quantity $g(\mathbf{x}, t)$ over a moving or deforming control volume $\mathcal{B}$, accounting for both the local change inside the volume and the flux across the boundary $\partial\mathcal{B}$.

A.2.2 Conservation on mass

Conservation of mass ensures that mass is neither created nor destroyed in a system. Let us denote the mass in the reference and spatial configurations as $\mathfrak{M}(\mathcal{B}_0)$ and $\mathfrak{m}(\mathcal{B})$, respectively. The total mass in the reference and spatial configurations are given by:

$$\mathfrak{M}(\mathcal{B}_0) = \int_{\mathcal{B}_0} \rho_0(\mathbf{X}, t)\, dV_0, \quad \mathfrak{m}(\mathcal{B}) = \int_{\mathcal{B}} \rho(\mathbf{x}, t)\, dV,$$

respectively. Since $dV = J_\epsilon \, dV_0$ we get:

$$\mathfrak{M}(\mathcal{B}_0) - \mathfrak{m}(\mathcal{B}) = \int_{\mathcal{B}_0} (\rho_0(\mathbf{X}, t) - J_\epsilon \, \rho(\mathbf{x}, t)) \, dV_0 = 0,$$

then:

$$\rho_0(\mathbf{X}, t) = J_\epsilon \, \rho(\mathbf{x}, t), \tag{A.46}$$

which represents the material form of conservation of mass. Alternatively, taking the material time derivative of $\mathfrak{m}(\mathcal{B})$ and assuming that the mass remains conserved from one instant to the next, we obtain:

$$\frac{D\mathfrak{m}(\mathcal{B})}{Dt} = \frac{D}{Dt} \int_{\mathcal{B}} \rho(\mathbf{x}, t) \, dV = 0,$$

so applying the Reynolds transport theorem we get:

$$\dot{\mathfrak{m}}(\mathcal{B}) = \int_{\mathcal{B}} [\dot{\rho}(\mathbf{x}, t) + \rho(\mathbf{x}, t) \mathrm{div}(\mathbf{v}(\mathbf{x}, t))] \, dV = 0,$$

then:

$$\dot{\rho}(\mathbf{x}, t) + \rho(\mathbf{x}, t) \mathrm{div}(\mathbf{v}(\mathbf{x}, t)) = 0, \tag{A.47}$$

which represents the spatial form of conservation of mass. Notice that using $\dot{\rho}(\mathbf{x}, t) = \frac{\partial \rho(\mathbf{x}, t)}{\partial t}\Big|_{\mathbf{x} \text{ fixed}} + (\nabla \rho(\mathbf{x}, t))\mathbf{v}(\mathbf{x}, t)$ and substituting into (A.47) and after some computations we get:

$$\frac{\partial \rho(\mathbf{x}, t)}{\partial t}\Big|_{\mathbf{x} \text{ fixed}} + \mathrm{div}(\rho(\mathbf{x}, t)\mathbf{v}(\mathbf{x}, t)) = 0, \tag{A.48}$$

which represents the continuity equation commonly used in fluid mechanics.

The conservation of mass can be used to obtain a useful corollary of the Reynolds transport theorem, called Reynolds transport theorem for extensive quantities. [1]

Corollary A.1. *Let be $g(\boldsymbol{x}, t) = \rho(\boldsymbol{x}, t)\phi(\boldsymbol{x}, t)$ an extensive quantity ($g(\boldsymbol{x}, t)$ per unit of mass) with $\phi(\boldsymbol{x}, t)$ a density field, then:*

$$\frac{Dg(\boldsymbol{x}, t)}{Dt} = \int_{\mathcal{B}} \rho(\boldsymbol{x}, t)\dot{\phi}(\boldsymbol{x}, t) \, dV. \tag{A.49}$$

Proof. From the Reynolds transport theorem we have:

$$\begin{aligned}
\frac{Dg(\mathbf{x}, t)}{Dt} &= \int_{\mathcal{B}} \Big(\rho(\mathbf{x}, t)\dot{\phi}(\mathbf{x}, t) + \dot{\rho}(\mathbf{x}, t)\phi(\mathbf{x}, t) + \rho(\mathbf{x}, t)\phi(\mathbf{x}, t)\mathrm{div}(\mathbf{v})\Big) \\
&= \int_{\mathcal{B}} \{ \, \rho(\mathbf{x}, t)\dot{\phi}(\mathbf{x}, t) + \phi(\mathbf{x}, t) \underbrace{[\dot{\rho}(\mathbf{x}, t) + \rho(\mathbf{x}, t)\mathrm{div}(\mathbf{v}(\mathbf{x}, t))]}_{=0} \, \} \, dV \\
&= \int_{\mathcal{B}} \rho(\mathbf{x}, t)\dot{\phi}(\mathbf{x}, t) \, dV.
\end{aligned}$$

□

1. Extensive quantities are properties that are defined per unit of mass.

A.2.3 Cauchy stress tensor and internal tractions

Before presenting the balance of linear momentum, which relates internal loads to external loads, we must introduce one of the most important quantities in continuum mechanics: the Cauchy stress tensor $\underline{\boldsymbol{\sigma}}_C \in \mathbb{R}^{3\times3}$. In continuum mechanics, the Cauchy stress tensor describes the internal forces acting within a deformed material. It is a second-order tensor and relates the internal tractions $\mathbf{t} \in \mathbb{R}^3$ (internal forces) on a given plane to the external forces acting on the body, measuring force in the current configuration per unit of current area.

If we denote by $d\mathbf{f}(\mathbf{n})$ the force on a small area $da\mathbf{n}$ located at position $\mathbf{x}$, where $\mathbf{n}$ is the unit normal vector to an arbitrary internal surface in the current configuration, the traction vector $\mathbf{t}$ can be defined as:

$$\mathbf{t}(\mathbf{n}) = \lim_{\Delta a \to 0} \frac{\Delta \mathbf{f}(\mathbf{n})}{\Delta a}. \tag{A.50}$$

According to Cauchy's formula (see [Reddy 2007, Chapter 4.2.2] for the details), the internal tractions $\mathbf{t}$ acting on a current internal surface can be defined using the Cauchy stress tensor as:

$$\mathbf{t}(\mathbf{n}) = \underline{\boldsymbol{\sigma}}_C \cdot \mathbf{n}. \tag{A.51}$$

This expression indicates that the internal traction vector is determined by the Cauchy stress tensor acting on the plane defined by the normal vector $\mathbf{n}$ and measures force per unit surface referred to the current configuration.

A.2.4 Balance of linear momentum

Consider a continuum system and a small infinitesimal volume element dV of mass $d\mathfrak{m}$, as illustrated in Fig. A.7. The linear momentum $d\mathbf{L}$ within this volume is given by:

$$d\mathbf{L} = \dot{\mathbf{x}} d\mathfrak{m},$$

where $\dot{\mathbf{x}} = \mathbf{v}(\mathbf{x}, t)$ represents the velocity vector. The total linear momentum $\mathfrak{L}(\mathcal{B})$ of the body is obtained by integration over the volume $\mathcal{B}$:

$$\mathfrak{L}(\mathcal{B}) = \int_{\mathcal{B}} d\mathbf{L} = \int_{\mathcal{B}} \rho(\mathbf{x}, t)\mathbf{v}(\mathbf{x}, t)\, dV. \tag{A.52}$$

Taking the material time derivative of the total linear momentum gives:

$$\frac{D\mathfrak{L}(\mathcal{B})}{Dt} = \frac{D}{Dt}\int_{\mathcal{B}} \rho(\mathbf{x}, t)\mathbf{v}(\mathbf{x}, t)\, dV = \int_{\mathcal{B}} \rho(\mathbf{x}, t)\mathbf{a}(\mathbf{x}, t)\, dV = \mathbf{F}_{ext}(\mathcal{B}), \tag{A.53}$$

where $\mathbf{a}(\mathbf{x}, t)$ is the acceleration vector, and $\mathbf{F}_{ext}(\mathcal{B})$ represents the sum of all external forces applied to the body $\mathcal{B}$. The external forces can be classified into:

- Body forces: Forces acting over the entire volume, such as gravity, electromagnetic forces, and inertial forces (centrifugal and coriolis effects).
- Surface forces: Forces acting on the boundary of the body, like pressure and contact forces.

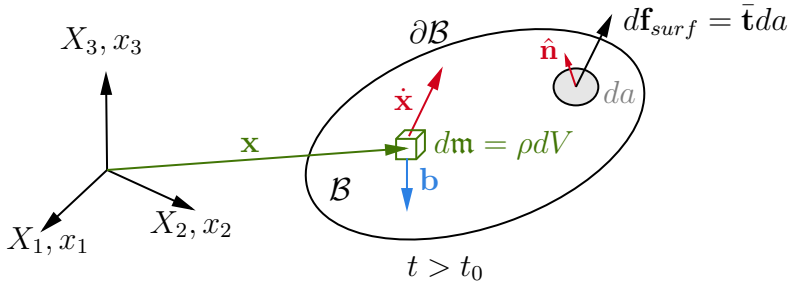

Figure A.7 – Kinetics and balance of linear momentum.

The total body force density field $\mathbf{b}(\mathbf{x}, t) \in \mathbb{R}^3$ (per unit of volume) is expressed as:

$$\text{Total body force} = \int_{\mathcal{B}} \mathbf{b}(\mathbf{x}, t)\, dV, \tag{A.54}$$

and the surface forces are defined by the traction field $\bar{\mathbf{t}}(\mathbf{x}, t)$:

$$\int_{\partial\mathcal{B}} d\mathbf{f}_{surf} = \int_{\partial\mathcal{B}} \bar{\mathbf{t}}(\mathbf{x}, t)\, da. \tag{A.55}$$

The total external force $\mathbf{F}_{ext}(\mathcal{B})$ is the sum of body force and surface forces. It is then given by:

$$\mathbf{F}_{ext}(\mathcal{B}) = \int_{\mathcal{B}} \mathbf{b}(\mathbf{x}, t)\, dV + \int_{\partial\mathcal{B}} \bar{\mathbf{t}}(\mathbf{x}, t)\, da. \tag{A.56}$$

Substituting the expression for the external forces in (A.53) yields:

$$\int_{\mathcal{B}} \rho(\mathbf{x}, t)\mathbf{a}(\mathbf{x}, t)\, dV = \int_{\mathcal{B}} \mathbf{b}(\mathbf{x}, t)\, dV + \int_{\partial\mathcal{B}} \bar{\mathbf{t}}(\mathbf{x}, t)\, da, \tag{A.57}$$

where replacing $\bar{\mathbf{t}} = \underline{\boldsymbol{\sigma}}_C \cdot \hat{\mathbf{n}}$ with $\hat{\mathbf{n}}$ the unit normal vector to an external surface element in $\partial\mathcal{B}$, we obtain:

$$\int_{\mathcal{B}} \rho(\mathbf{x}, t)\mathbf{a}(\mathbf{x}, t)\, dV - \int_{\mathcal{B}} \mathbf{b}(\mathbf{x}, t)\, dV - \int_{\partial\mathcal{B}} \underline{\boldsymbol{\sigma}}_C \cdot \hat{\mathbf{n}} da = 0$$
$$\int_{\mathcal{B}} (\rho(\mathbf{x}, t)\mathbf{a}(\mathbf{x}, t) - \mathbf{b}(\mathbf{x}, t) - \operatorname{div}(\underline{\boldsymbol{\sigma}}_C))\, dV = 0.$$

Thus, the strong form of the balance of linear momentum in the spatial configuration is given by:

$$\rho(\mathbf{x}, t)\mathbf{a}(\mathbf{x}, t) = \operatorname{div}(\underline{\boldsymbol{\sigma}}_C) + \mathbf{b}(\mathbf{x}, t), \quad \text{for all } \mathbf{x} \in \mathcal{B}. \tag{A.58}$$

Remark A.8. *The conservation of angular momentum is a fundamental principle in continuum mechanics that states the total angular momentum of a system must remain constant if no external torques are acting on it. For a continuum, this principle leads to the requirement that the Cauchy stress tensor must be symmetric, i.e.,* $\underline{\boldsymbol{\sigma}}_C = \underline{\boldsymbol{\sigma}}_C^\top$ *[Reddy 2007, Chapter 5.3.3].*

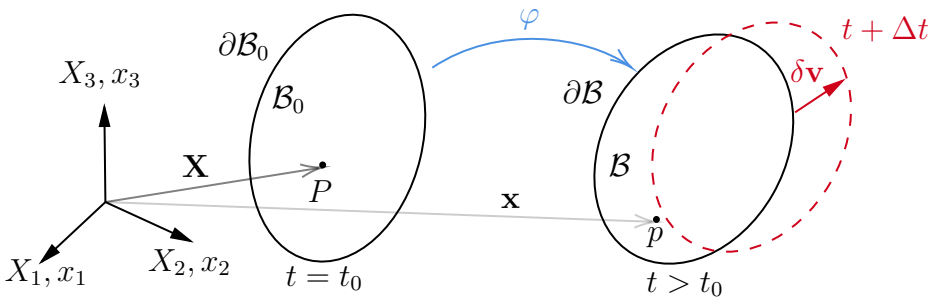

Figure A.8 – Virtual motion.

A.2.5 Virtual power principle

In continuum mechanics, the principles of virtual work and virtual power provide a foundation for deriving the weak form of the governing equations. The strong form, which describes the equations of motion at every point in the domain $\mathcal{B}$, can be challenging to satisfy due to the infinite number of points involved. To overcome this challenge, the weak form is formulated, which allows for solutions to be approximated in an average sense, focusing on finite discrete points rather than the entire domain.

Consider a virtual velocity $\delta\mathbf{v}(\mathbf{x}, t)$ from the current configuration of the body, as illustrated in Fig. A.8. To improve clarity, the spatial and temporal dependencies will often be omitted. The virtual power $\delta P \in \mathbb{R}$ generated by internal forces during a virtual motion is is expressed as:

$$\delta P = \int_{\mathcal{B}} (-\rho\ddot{\mathbf{x}} + \mathbf{b} + \operatorname{div}(\underline{\boldsymbol{\sigma}}_C)) \cdot \delta\mathbf{v}\, dV = \int_{\mathcal{B}} [(-\rho\ddot{\mathbf{x}} + \mathbf{b}) \cdot \delta\mathbf{v} + \operatorname{div}(\underline{\boldsymbol{\sigma}}_C) \cdot \delta\mathbf{v}]\, dV = 0.$$

Using the identity $\operatorname{div}(\underline{\boldsymbol{\sigma}}_C^{\top}\mathbf{v}) = \underline{\boldsymbol{\sigma}}_C : \nabla\mathbf{v} + \mathbf{v} \cdot \operatorname{div}(\underline{\boldsymbol{\sigma}}_C)$, we can rewrite the term $\operatorname{div}(\underline{\boldsymbol{\sigma}}_C) \cdot \delta\mathbf{v}$ as $\operatorname{div}(\underline{\boldsymbol{\sigma}}_C) \cdot \delta\mathbf{v} = \operatorname{div}(\underline{\boldsymbol{\sigma}}_C\delta\mathbf{v}) - \underline{\boldsymbol{\sigma}}_C : \nabla\delta\mathbf{v}$. Substituting this into the previous expression for δP yields:

$$\delta P = \int_{\mathcal{B}} (-\rho\ddot{\mathbf{x}} + \mathbf{b}) \cdot \delta\mathbf{v}\, dV + \int_{\mathcal{B}} \operatorname{div}(\underline{\boldsymbol{\sigma}}_C\delta\mathbf{v}) dV - \int_{\mathcal{B}} \underline{\boldsymbol{\sigma}}_C : \nabla\delta\mathbf{v}\, dV = 0.$$

Applying the Gauss divergence theorem to the second integral term and noting that $\nabla\delta\mathbf{v} = \delta\nabla\mathbf{v} = \delta\underline{\boldsymbol{\ell}}$, we obtain:

$$\delta P = \int_{\mathcal{B}} (-\rho\ddot{\mathbf{x}} + \mathbf{b}) \cdot \delta\mathbf{v}\, dV + \int_{\partial\mathcal{B}} \underline{\boldsymbol{\sigma}}_C \cdot \hat{\mathbf{n}} \cdot \delta\mathbf{v}\, da - \int_{\mathcal{B}} \underline{\boldsymbol{\sigma}}_C : \delta\underline{\boldsymbol{\ell}}\, dV = 0.$$

Substituting $\underline{\boldsymbol{\sigma}}_C \cdot \hat{\mathbf{n}} = \bar{\mathbf{t}}$, where $\bar{\mathbf{t}}$ is the applied traction vector, and recognizing that $\underline{\boldsymbol{\sigma}}_C : \delta\underline{\boldsymbol{\ell}} = \underline{\boldsymbol{\sigma}}_C : \delta\underline{\mathbf{d}}$ (with $\underline{\mathbf{d}}$ the rate of deformation tensor), the virtual power equation becomes:

$$\delta P = \int_{\mathcal{B}} (-\rho\ddot{\mathbf{x}} \cdot \delta\mathbf{v} + \mathbf{b} \cdot \delta\mathbf{v} - \underline{\boldsymbol{\sigma}}_C : \delta\underline{\mathbf{d}})\, dV + \int_{\partial\mathcal{B}} \bar{\mathbf{t}} \cdot \delta\mathbf{v}\, da = 0, \tag{A.59}$$

which represents the spatial form of the virtual power principle. From (A.59), the internal virtual power δP_{int} is defined as:

$$\delta P_{int} = \int_{\mathcal{B}} \underline{\boldsymbol{\sigma}}_C : \delta \underline{\mathbf{d}} \, dV. \tag{A.60}$$

Thus, it can be observed that the Cauchy stress tensor $\underline{\boldsymbol{\sigma}}_C$ and the rate of deformation tensor $\underline{\mathbf{d}}$ are power-conjugated with respect to the current volume $\mathcal{B}$.

If the expression for the internal virtual power δP_{int} in (A.60) is expressed in the reference configuration, then alternative power conjugate pairs of stresses and strain rates emerge. Recall that $dV = J_\epsilon \, dV_0$. So, substituting this in (A.60) yields:

$$\delta P_{int} = \int_{\mathcal{B}} \underline{\boldsymbol{\sigma}}_C : \delta \underline{\mathbf{d}} \, dV = \int_{\mathcal{B}_0} J_\epsilon \underline{\boldsymbol{\sigma}}_C : \delta \underline{\mathbf{d}} \, dV_0 = \int_{\mathcal{B}_0} \underline{\tau}_K : \delta \underline{\mathbf{d}} \, dV_0, \tag{A.61}$$

where $\underline{\tau}_K = J_\epsilon \, \underline{\boldsymbol{\sigma}}_C$ is defined as the Kirchhoff stress tensor. Thus, $\underline{\tau}_K$ and $\underline{\mathbf{d}}$ are power-conjugated with respect to the reference volume $\mathcal{B}_0$. The expression for δP_{int} in (A.61) is inconsistent due to $\underline{\tau}_K$ and $\underline{\mathbf{d}}$ are spatial tensors integrated over the reference configuration. To alleviate this inconsistency:

$$\begin{aligned}
\delta P_{int} &= \int_{\mathcal{B}_0} J_\epsilon \underline{\boldsymbol{\sigma}}_C : \delta \underline{\mathbf{d}} \, dV_0 \\
&= \int_{\mathcal{B}_0} J_\epsilon \, \underline{\boldsymbol{\sigma}}_C : \delta \underline{\boldsymbol{\ell}} \, dV_0 \\
&= \int_{\mathcal{B}_0} J_\epsilon \, \underline{\boldsymbol{\sigma}}_C : \left(\delta \dot{\underline{\mathbf{F}}} \underline{\mathbf{F}}^{-1} \right) dV_0.
\end{aligned}$$

Using the identity $\underline{\mathbf{A}} : \underline{\mathbf{B}} = \mathrm{tr}(\underline{\mathbf{A}}\underline{\mathbf{B}}^\top) = \mathrm{tr}(\underline{\mathbf{A}}^\top \underline{\mathbf{B}})$, where $\underline{\mathbf{A}} = J_\epsilon \, \underline{\boldsymbol{\sigma}}_C$ and $\underline{\mathbf{B}} = \delta \dot{\underline{\mathbf{F}}} \underline{\mathbf{F}}^{-1}$, we obtain:

$$\begin{aligned}
\delta P_{int} &= \int_{\mathcal{B}_0} J_\epsilon \, \underline{\boldsymbol{\sigma}}_C : \left(\delta \dot{\underline{\mathbf{F}}} \underline{\mathbf{F}}^{-1} \right) dV_0 \\
&= \int_{\mathcal{B}_0} \mathrm{tr} \left(J_\epsilon \, \underline{\boldsymbol{\sigma}}_C \left(\delta \dot{\underline{\mathbf{F}}} \underline{\mathbf{F}}^{-1} \right)^\top \right) dV_0 \\
&= \int_{\mathcal{B}_0} \mathrm{tr} \left(J_\epsilon \, \underline{\boldsymbol{\sigma}}_C \underline{\mathbf{F}}^{-\top} \delta \dot{\underline{\mathbf{F}}}^\top \right) dV_0 \\
&= \int_{\mathcal{B}_0} J_\epsilon \, \underline{\boldsymbol{\sigma}}_C \underline{\mathbf{F}}^{-\top} : \delta \dot{\underline{\mathbf{F}}} \, dV_0 \\
&= \int_{\mathcal{B}_0} \underline{\mathbf{P}} : \delta \dot{\underline{\mathbf{F}}} \, dV_0,
\end{aligned} \tag{A.62}$$

where $\underline{\mathbf{P}} = J_\epsilon \, \underline{\boldsymbol{\sigma}}_C \underline{\mathbf{F}}^{-\top}$ is defined as the first Piola-Kirchhoff stress tensor. Thus, from (A.62) it can be observed that the first Piola-Kirchhoff stress tensor $\underline{\mathbf{P}}$ and the rate of deformation gradient tensor $\dot{\underline{\mathbf{F}}}$ are power-conjugated with respect to the reference volume $\mathcal{B}_0$.

The tensors $\underline{\mathbf{F}}$ and $\underline{\mathbf{P}}$ are both non-symmetric two-point tensors, as they relate the reference and spatial configurations. In particular, the first Piola-Kirchhoff stress tensor $\underline{\mathbf{P}}$ is merely a mathematical representation of the Cauchy stress tensor, introduced for convenience. This means that $\underline{\mathbf{P}}$ is not a new physical quantity, but rather an alternative measure of stress that relates forces in the current configuration to a unit area in the current surface, often referred to as engineering stress or nominal stress tensors.

The expression for δP_{int} in (A.62) can be modified to express it in terms of fully Lagrangian quantities (referred to the reference configuration). Recalling that $\delta\underline{\mathbf{d}} = \phi_\star\left[\delta\underline{\dot{\mathbf{E}}}\right] = \underline{\mathbf{F}}^{-\top}\delta\underline{\dot{\mathbf{E}}}\underline{\mathbf{F}}^{-1}$ and $dV = J_\epsilon\, dV_0$, we obtain:

$$\begin{aligned}
\delta P_{int} &= \int_{\mathcal{B}} \underline{\boldsymbol{\sigma}}_C : \delta\underline{\mathbf{d}}\, dV \\
&= \int_{\mathcal{B}_0} J_\epsilon\, \underline{\boldsymbol{\sigma}}_C : \left(\underline{\mathbf{F}}^{-\top}\delta\underline{\dot{\mathbf{E}}}\underline{\mathbf{F}}^{-1}\right) dV_0 \\
&= \int_{\mathcal{B}_0} \mathrm{tr}\left(J_\epsilon\, \underline{\boldsymbol{\sigma}}_C \left(\underline{\mathbf{F}}^{-\top}\delta\underline{\dot{\mathbf{E}}}\underline{\mathbf{F}}^{-1}\right)^\top\right) dV_0 \\
&= \int_{\mathcal{B}_0} \mathrm{tr}\left(J_\epsilon\, \underline{\boldsymbol{\sigma}}_C\underline{\mathbf{F}}^{-\top}\delta\underline{\dot{\mathbf{E}}}^\top\underline{\mathbf{F}}^{-1}\right) dV_0 \\
&= \int_{\mathcal{B}_0} \mathrm{tr}\left(J_\epsilon\, \underline{\mathbf{F}}^{-1}\underline{\boldsymbol{\sigma}}_C\underline{\mathbf{F}}^{-\top}\delta\underline{\dot{\mathbf{E}}}\right) dV_0 \\
&= \int_{\mathcal{B}_0} J_\epsilon\, \underline{\mathbf{F}}^{-1}\underline{\boldsymbol{\sigma}}_C\underline{\mathbf{F}}^{-\top} : \delta\underline{\dot{\mathbf{E}}}\, dV_0 \\
&= \int_{\mathcal{B}_0} \underline{\mathbf{S}} : \delta\underline{\dot{\mathbf{E}}}\, dV_0,
\end{aligned} \tag{A.63}$$

where $\underline{\mathbf{S}} = \underline{\mathbf{F}}^{-1}J_\epsilon\,\underline{\boldsymbol{\sigma}}_C\underline{\mathbf{F}}^{-\top} = \underline{\mathbf{F}}^{-1}\underline{\mathbf{P}}$ is the symmetric second Piola-Kirchhoff stress tensor, and it is power-conjugated to the rate of Green-Lagrange strain tensor $\underline{\dot{\mathbf{E}}}$ with respect to the reference volume $\mathcal{B}_0$. The second Piola-Kirchhoff stress tensor $\underline{\mathbf{S}}$ measures force in the initial configuration per unit of initial area.

Remark A.9. *Notice that the balance of linear and angular momentum, which constitute the equations of motion of the body, can be expressed equivalently as:*

$$\begin{aligned}
&\textit{Current configuration}: \quad \rho(\boldsymbol{x},t)\boldsymbol{a}(\boldsymbol{x},t) = \mathit{div}(\underline{\boldsymbol{\sigma}}_C) + \boldsymbol{b}(\boldsymbol{x},t) \\
&\qquad\qquad\qquad\qquad\qquad\qquad \underline{\boldsymbol{\sigma}}_C = \underline{\boldsymbol{\sigma}}_C^\top
\end{aligned} \tag{A.64}$$

$$\begin{aligned}
&\textit{Reference configuration}: \quad \rho_0(\boldsymbol{X})\ddot{\boldsymbol{u}}(\boldsymbol{X},t) = \mathit{DIV}(\underline{\boldsymbol{P}}) + \boldsymbol{b}_0(\boldsymbol{X},t) \\
&\qquad\qquad\qquad\qquad\qquad\qquad \underline{\boldsymbol{P}\boldsymbol{F}}^\top = \underline{\boldsymbol{F}\boldsymbol{P}}^\top
\end{aligned} \tag{A.65}$$

$$\begin{aligned}
&\textit{Reference configuration}: \quad \rho_0(\boldsymbol{X})\ddot{\boldsymbol{u}}(\boldsymbol{X},t) = \mathit{DIV}(\underline{\boldsymbol{F}\boldsymbol{S}}) + \boldsymbol{b}_0(\boldsymbol{X},t) \\
&\qquad\qquad\qquad\qquad\qquad\qquad \underline{\boldsymbol{S}} = \underline{\boldsymbol{S}}^\top
\end{aligned} \tag{A.66}$$

where $\boldsymbol{b}(\boldsymbol{x},t)$ and $\boldsymbol{b}_0(\boldsymbol{X},t)$ are the body forces acting on the body referred to as the current and reference configurations, respectively, and $\mathit{div}(\cdot)$ and $\mathit{DIV}(\cdot)$ are the divergence operators with respect to spatial and material coordinates, respectively.

Appendix B

Displacement fields for typical elasticity models

B.1 Displacement fields

This appendix presents the displacement fields derived from the kinematic assumptions of various elasticity-based models, including general elasticity problems in 1D, 2D, and 3D, as well as vibrating strings. It also covers models for beams and plates based on Kirchhoff theory, first-order shear deformation theory, and third-order shear deformation theory, including Rayleigh beams, Euler-Bernoulli beams, Timoshenko beams, Reddy beams, Kirchhoff-Rayleigh plates, Kirchhoff-Love plates, Mindlin plates, and Reddy plates. These displacement fields serve as the starting point for deriving models and can lead to different formulations depending on the deformation theory applied and the specific constitutive model used.

B.1.1 General elasticity in 1D

Consider a three-dimensional elastic body that can be treated as a one-dimensional one, as the one illustrated in Fig. B.1, where its volume in the reference configuration is given by $\mathcal{B}_0 = \Omega \times \Omega^c \subset \mathbb{R}^3$, where $\Omega = (0, L_0) \subset \mathbb{R}$ is the one-dimensional spatial domain and $\Omega^c = A_0 \subset \mathbb{R}^2$ is the complementary domain denoting the cross section area. The displacement field for the general elasticity problem in 1D is given by:

$$\mathbf{u}(\mathbf{X}, t) = \underbrace{\begin{bmatrix} 1 \\ 0 \\ 0 \end{bmatrix}}_{\bar{M}_1(\mathtt{X}^c)} \underbrace{\big[u_1(\mathtt{X}, t)\big]}_{r(\mathtt{X},t)}, \tag{B.1}$$

where $\mathtt{X} = \{X_1\}$ is the coordinate of an arbitrary point in Ω, and $u_1(\mathtt{X}, t)$ is the displacement in the direction of the axis X_1.

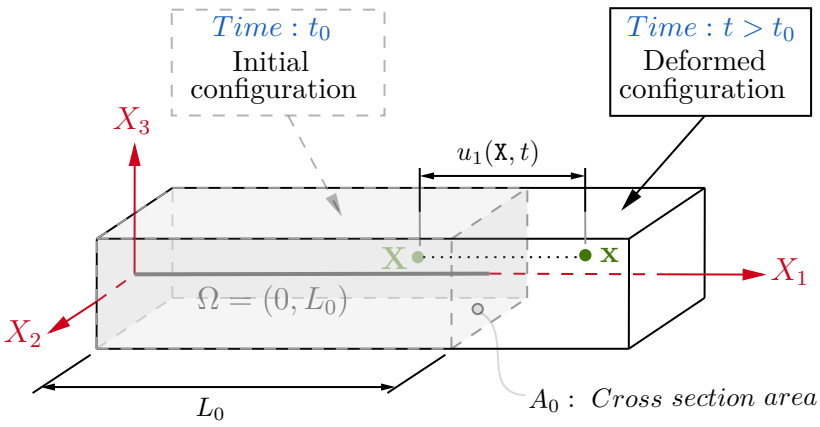

Figure B.1 – Kinematic variable of the general elasticity in 1D.

B.1.2 General elasticity in 2D

Consider a three-dimensional elastic body that can be treated as a two-dimensional one, as the one illustrated in Fig. B.2, where its volume in the reference configuration is given by $\mathcal{B}_0 = \Omega \times \Omega^c \subset \mathbb{R}^3$, where $\Omega \subset \mathbb{R}^2$ is the two-dimensional spatial domain and $\Omega^c = \left(-\frac{h}{2}, \frac{h}{2}\right) \subset \mathbb{R}$ is the complementary domain denoting the thickness h. The displacement field for the general elasticity problem in 2D is given by:

$$\mathbf{u}(\mathbf{X}, t) = \underbrace{\begin{bmatrix} 1 & 0 \\ 0 & 1 \\ 0 & 0 \end{bmatrix}}_{\bar{M}_1(\mathtt{X}^c)} \underbrace{\begin{bmatrix} u_1(\mathtt{X}, t) \\ u_2(\mathtt{X}, t) \end{bmatrix}}_{r(\mathtt{X},t)}, \tag{B.2}$$

where $\mathtt{X} = \{X_1, X_2\}$ are the coordinates of an arbitrary point in Ω, and $u_1(\mathtt{X}, t)$ and $u_2(\mathtt{X}, t)$ are the displacements in the direction of the axes X_1 and X_2, respectively.

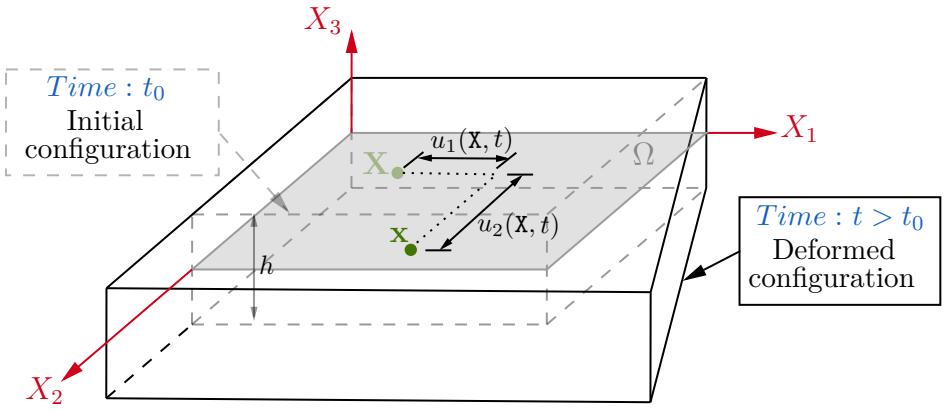

Figure B.2 – Kinematic variables of the general elasticity in 2D.

B.1.3 General elasticity in 3D

Consider a three-dimensional elastic body, as the one illustrated in Fig. B.3, where its volume in the reference configuration is denoted by $\mathcal{B}_0 = \Omega \subset \mathbb{R}^3$. The displacement field for the general elasticity problem in 3D is given by:

$$\mathbf{u}(\mathbf{X}, t) = \underbrace{\begin{bmatrix} 1 & 0 & 0 \\ 0 & 1 & 0 \\ 0 & 0 & 1 \end{bmatrix}}_{\bar{M}_1(\mathtt{X}^c)} \underbrace{\begin{bmatrix} u_1(\mathtt{X}, t) \\ u_2(\mathtt{X}, t) \\ u_3(\mathtt{X}, t) \end{bmatrix}}_{r(\mathtt{X},t)}, \tag{B.3}$$

where $\mathtt{X} = \{X_1, X_2, X_3\}$ are the coordinates of an arbitrary point in Ω, and $u_1(\mathtt{X}, t)$, $u_2(\mathtt{X}, t)$ and $u_3(\mathtt{X}, t)$ are the displacements in the direction of the axes X_1, X_2 and X_3, respectively.

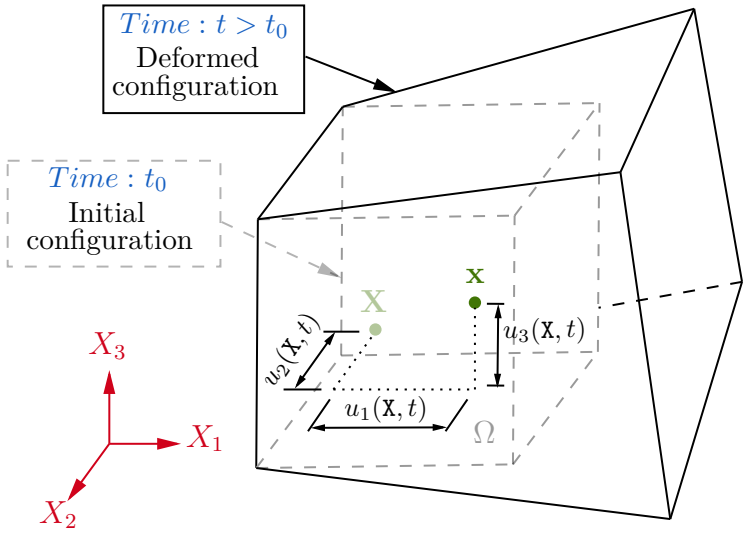

Figure B.3 – Kinematic variables of the general elasticity in 3D.

B.1.4 Planar string

Consider a three-dimensional elastic body that can be treated as a one-dimensional one, as the one illustrated in Fig. B.4, where its volume in the reference configuration is given by $\mathcal{B}_0 = \Omega \times \Omega^c \subset \mathbb{R}^3$, where $\Omega = (0, L_0) \subset \mathbb{R}$ is the one-dimensional spatial domain and $\Omega^c = A_0 \subset \mathbb{R}^2$ is the complementary domain denoting the cross section area. The displacement field for the planar string is given by:

$$\mathbf{u}(\mathbf{X}, t) = \underbrace{\begin{bmatrix} 0 \\ 0 \\ 1 \end{bmatrix}}_{\bar{M}_1(\mathtt{X}^c)} \underbrace{\big[w_0(\mathtt{X}, t)\big]}_{r(\mathtt{X},t)}, \tag{B.4}$$

where $\mathtt{X} = \{X_1\}$ is the coordinate of an arbitrary point in Ω, and $w_0(\mathtt{X}, t)$ is the vertical displacement of points along the axis X_1.

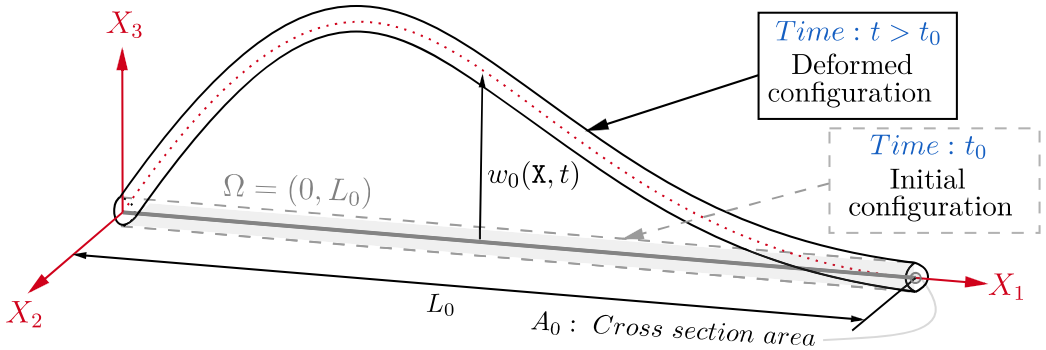

Figure B.4 – Kinematic variable of the planar string.

B.1.5 Spatial string

Consider a three-dimensional elastic body that can be treated as a one-dimensional one, as the one illustrated in Fig. B.4, where its volume in the reference configuration is given by $\mathcal{B}_0 = \Omega \times \Omega^c \subset \mathbb{R}^3$, where $\Omega = (0, L_0) \subset \mathbb{R}$ is the one-dimensional spatial domain and $\Omega^c = A_0 \subset \mathbb{R}^2$ is the complementary domain denoting the cross section area. The displacement field for the spatial string is given by:

$$\mathbf{u}(\mathbf{X}, t) = \underbrace{\begin{bmatrix} 1 & 0 & 0 \\ 0 & 1 & 0 \\ 0 & 0 & 1 \end{bmatrix}}_{\bar{M}_1(\mathtt{X}^c)} \underbrace{\begin{bmatrix} u_0(\mathtt{X}, t) \\ v_0(\mathtt{X}, t) \\ w_0(\mathtt{X}, t) \end{bmatrix}}_{r(\mathtt{X},t)}, \tag{B.5}$$

where $\mathtt{X} = \{X_1\}$ is the coordinate of an arbitrary point in Ω, and $u_0(\mathtt{X}, t)$, $v_0(\mathtt{X}, t)$ and $w_0(\mathtt{X}, t)$ are the axial, horizontal and vertical displacements of points along the axis X_1.

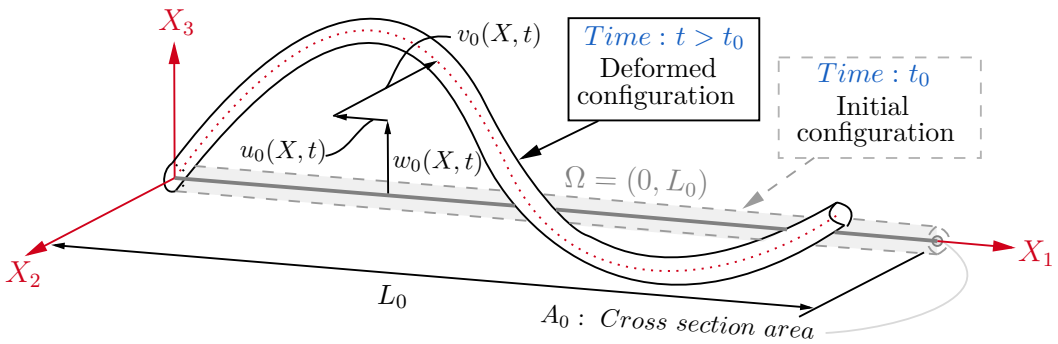

Figure B.5 – Kinematic variable of the spatial string.

B.1.6 Planar Timoshenko beam

Consider a three-dimensional elastic body that can be treated as a one-dimensional one, as the one illustrated in Fig. B.6, where its volume in the reference configuration is given by $\mathcal{B}_0 = \Omega \times \Omega^c \subset \mathbb{R}^3$, where $\Omega = (0, L_0) \subset \mathbb{R}$ is the one-dimensional spatial domain and $\Omega^c = A_0 \subset \mathbb{R}^2$ is the complementary domain denoting the cross section area. The planar Timoshenko beam model is based on the kinematic assumption of first-order shear deformation theory [Reddy 2006, Chapter 10.1], which states that plane sections normal to the neutral line before deformation remain plane but are not necessarily normal to the neutral axis after deformation. The displacement field of the planar Timoshenko beam is then expressed as:

$$\mathbf{u}(\mathbf{X}, t) = \underbrace{\begin{bmatrix} -X_3 & 1 & 0 \\ 0 & 0 & 0 \\ 0 & 0 & 1 \end{bmatrix}}_{\bar{M}_1(\mathtt{X}^c)} \underbrace{\begin{bmatrix} \psi_3(\mathtt{X}, t) \\ u_0(\mathtt{X}, t) \\ w_0(\mathtt{X}, t) \end{bmatrix}}_{r(\mathtt{X},t)}, \tag{B.6}$$

where $\mathtt{X} = \{X_1\} \in \Omega$, $u_0(\mathtt{X}, t)$ and $w_0(\mathtt{X}, t)$ are the axial and vertical displacements, respectively, and $\psi_3(\mathtt{X}, t)$ is the angle of rotation of the cross section. Often, the displacement field in (B.6) is simplified by neglecting $u_0(\mathtt{X}, t)$ from $r(\mathtt{X}, t)$, particularly in cases where the primary interest is in predicting the vertical displacement $w_0(\mathtt{X}, t)$. Therefore, the simplified displacement field of the planar Timoshenko beam is expressed as:

$$\mathbf{u}(\mathbf{X}, t) = \underbrace{\begin{bmatrix} -X_3 & 0 \\ 0 & 0 \\ 0 & 1 \end{bmatrix}}_{\bar{M}_1(\mathtt{X}^c)} \underbrace{\begin{bmatrix} \psi_3(\mathtt{X}, t) \\ w_0(\mathtt{X}, t) \end{bmatrix}}_{r(\mathtt{X},t)}. \tag{B.7}$$

The displacement field in (B.6) and the simplified one in (B.7) are used to derive the PHS models proposed in [Voss 2014] and [Macchelli 2004a], respectively.

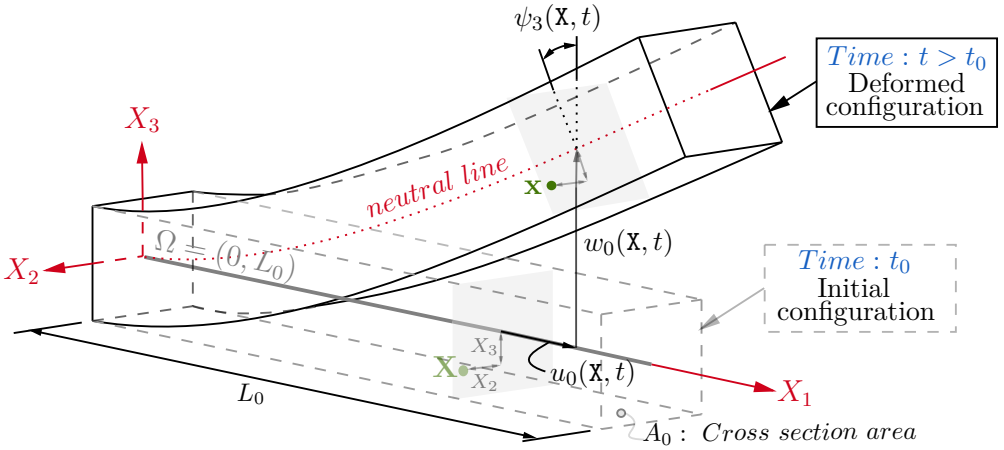

Figure B.6 – Kinematic variables of the planar Timoshenko beam.

B.1.7 Spatial Timoshenko beam

Consider a three-dimensional elastic body that can be treated as a one-dimensional one, as the one illustrated in Fig. B.7, where its volume in the reference configuration is given by $\mathcal{B}_0 = \Omega \times \Omega^c \subset \mathbb{R}^3$, where $\Omega = (0, L_0) \subset \mathbb{R}$ is the one-dimensional spatial domain and $\Omega^c = A_0 \subset \mathbb{R}^2$ is the complementary domain denoting the cross section area. The spatial Timoshenko beam model, like the planar version, is based on the first-order shear deformation theory. However, unlike the planar case where deformation is restricted to the plane, the spatial Timoshenko beam deforms in the three-dimensional space. The displacement field of the spatial Timoshenko beam is then expressed as:

$$\mathbf{u}(\mathbf{X}, t) = \underbrace{\begin{bmatrix} -X_2 & -X_3 & 1 & 0 & 0 \\ 0 & 0 & 0 & 1 & 0 \\ 0 & 0 & 0 & 0 & 1 \end{bmatrix}}_{\bar{M}_1(\mathtt{X}^c)} \underbrace{\begin{bmatrix} \psi_2(\mathtt{X}, t) \\ \psi_3(\mathtt{X}, t) \\ u_0(\mathtt{X}, t) \\ v_0(\mathtt{X}, t) \\ w_0(\mathtt{X}, t) \end{bmatrix}}_{r(\mathtt{X},t)}, \tag{B.8}$$

where $\mathtt{X} = \{X_1\} \in \Omega$, $u_0(\mathtt{X}, t)$, $v_0(\mathtt{X}, t)$ and $w_0(\mathtt{X}, t)$ are the axial, horizontal and vertical displacements, respectively, and $\psi_2(\mathtt{X}, t)$ and $\psi_3(\mathtt{X}, t)$ are the angles of rotation of the cross section.

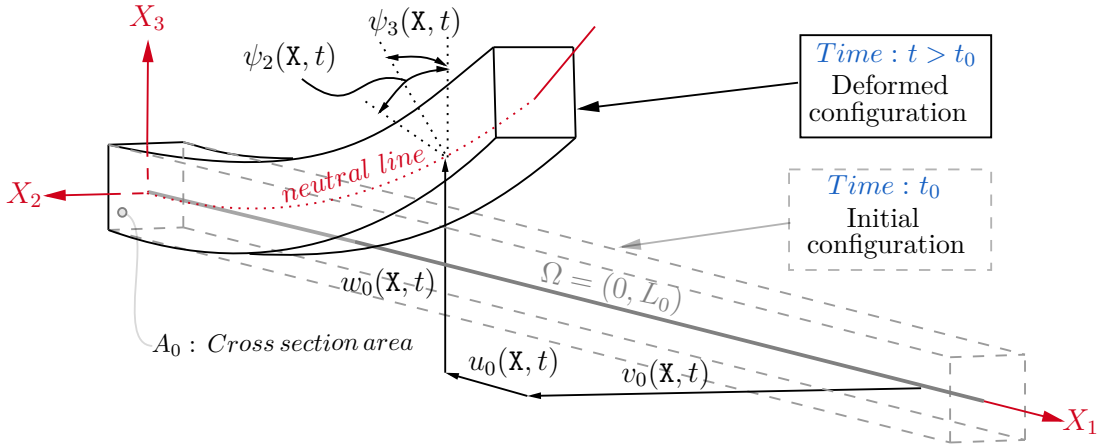

Figure B.7 – Kinematic variables of the spatial Timoshenko beam.

B.1.8 Mindlin plate

Consider a three-dimensional elastic body that can be treated as a two-dimensional one, as illustrated in Fig. B.8, where its volume in the reference configuration is given by $\mathcal{B}_0 = \Omega \times \Omega^c \subset \mathbb{R}^3$, where $\Omega \subset \mathbb{R}^2$ is the two-dimensional spatial domain and $\Omega^c = \left(-\frac{h}{2}, \frac{h}{2}\right) \subset \mathbb{R}$ is the complementary domain denoting the thickness h. The Mindlin plate model can be seen as the two-dimensional extension of the Timoshenko beam model, so it is also based on the first-order shear deformation theory. The displacement field of the Mindlin plate is expressed as:

$$\mathbf{u}(\mathbf{X}, t) = \underbrace{\begin{bmatrix} 0 & -X_3 & 1 & 0 & 0 \\ -X_3 & 0 & 0 & 1 & 0 \\ 0 & 0 & 0 & 0 & 1 \end{bmatrix}}_{\bar{M}_1(\mathtt{X}^c)} \underbrace{\begin{bmatrix} \psi_2(\mathtt{X}, t) \\ \psi_3(\mathtt{X}, t) \\ u_0(\mathtt{X}, t) \\ v_0(\mathtt{X}, t) \\ w_0(\mathtt{X}, t) \end{bmatrix}}_{r(\mathtt{X}, t)}, \tag{B.9}$$

where $\mathtt{X} = \{X_1, X_2\} \in \Omega$, $u_0(\mathtt{X}, t)$, $v_0(\mathtt{X}, t)$ and $w_0(\mathtt{X}, t)$ are the axial, horizontal and vertical displacements, respectively, and $\psi_2(\mathtt{X}, t)$ and $\psi_3(\mathtt{X}, t)$ are the angles of rotation of the cross section. When the interest is primarily in predicting the vertical displacement $w_0(\mathtt{X}, t)$, it is common to simplify $\mathbf{u}(\mathbf{X}, t)$ in (B.9) to derive simpler models. In such cases, it is sufficient to retain $w_0(\mathtt{X}, t)$ along with the rotation angles $\psi_2(\mathtt{X}, t)$ and $\psi_3(\mathtt{X}, t)$. Thus, the simplified displacement field of the Mindlin plate is expressed as:

$$\mathbf{u}(\mathbf{X}, t) = \underbrace{\begin{bmatrix} 0 & -X_3 & 0 \\ -X_3 & 0 & 0 \\ 0 & 0 & 1 \end{bmatrix}}_{\bar{M}_1(\mathtt{X}^c)} \underbrace{\begin{bmatrix} \psi_2(\mathtt{X}, t) \\ \psi_3(\mathtt{X}, t) \\ w_0(\mathtt{X}, t) \end{bmatrix}}_{r(\mathtt{X}, t)}. \tag{B.10}$$

The displacement field $\mathbf{u}(\mathbf{X}, t)$ in (B.10) is the basis for deriving the PHS models proposed in [Macchelli 2005; Brugnoli 2019a].

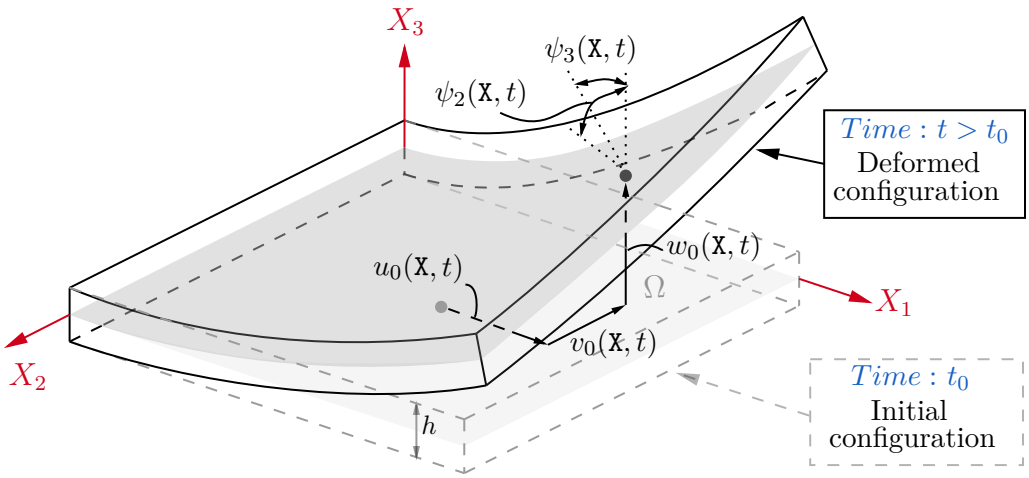

Figure B.8 – Kinematic variables of the Mindlin plate.

B.1.9 Planar Rayleigh and Euler-Bernoulli beams

Consider a three-dimensional elastic body that can be treated as a one-dimensional one, as the one illustrated in Fig. B.11, where its volume in the reference configuration is given by $\mathcal{B}_0 = \Omega \times \Omega^c \subset \mathbb{R}^3$, where $\Omega = (0, L_0) \subset \mathbb{R}$ is the one-dimensional spatial domain and $\Omega^c = A_0 \subset \mathbb{R}^2$ is the complementary domain denoting the cross section area. The Rayleigh beam model is based on the Kirchhoff theory, which states that plane sections normal to the neutral line before deformation remain plane and normal to the neutral line after deformation. The Euler-Bernoulli beam is derived using the same theory, but in its formulation, the effect of rotary inertia is neglected when computing the kinetic energy. The displacement fields for both Rayleigh and Euler-Bernoulli beams are then expressed as:

$$\mathbf{u}(\mathbf{X}, t) = \underbrace{\begin{bmatrix} -X_3 & 1 & 0 \\ 0 & 0 & 0 \\ 0 & 0 & 1 \end{bmatrix}}_{\bar{M}_1(\mathtt{X}^c)} \underbrace{\begin{bmatrix} \partial_1 w_0(\mathtt{X}, t) \\ u_0(\mathtt{X}, t) \\ w_0(\mathtt{X}, t) \end{bmatrix}}_{r(\mathtt{X}, t)}, \tag{B.11}$$

where $\mathtt{X} = \{X_1\} \in \Omega$, and $u_0(\mathtt{X}, t)$ and $w_0(\mathtt{X}, t)$ are the axial and vertical displacements, respectively. Often, the displacement field in (B.11) is simplified by neglecting $u_0(\mathtt{X}, t)$ from $r(\mathtt{X}, t)$, particularly in cases where the primary interest is in predicting the vertical displacement $w_0(\mathtt{X}, t)$. Therefore, the simplified displacement field is expressed as:

$$\mathbf{u}(\mathbf{X}, t) = \underbrace{\begin{bmatrix} -X_3 & 0 \\ 0 & 0 \\ 0 & 1 \end{bmatrix}}_{\bar{M}_1(\mathtt{X}^c)} \underbrace{\begin{bmatrix} \partial_1 w_0(\mathtt{X}, t) \\ w_0(\mathtt{X}, t) \end{bmatrix}}_{r(\mathtt{X}, t)}. \tag{B.12}$$

The displacement field in (B.11) is used in [Voss 2008; Brugnoli 2021] to derive nonlinear Euler-Bernoulli beam models, while the simplified displacement field in (B.12) is employed in [Cardoso-Ribeiro 2016] to derive a linear piezo-actuated Euler-Bernoulli beam model, all formulated as PHS representations.

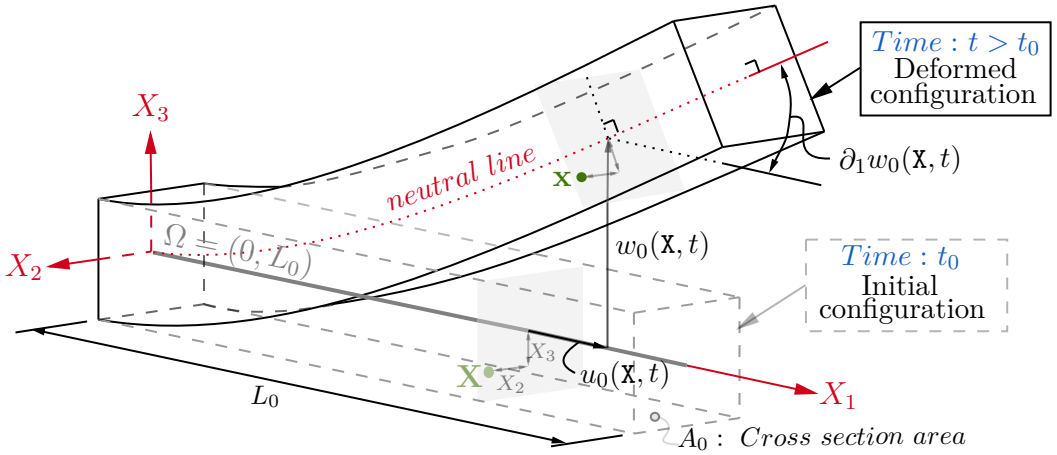

Figure B.9 – Kinematic variables of the planar Rayleigh beam and Euler-Bernoulli beam.

B.1.10 Kirchhoff-Rayleigh and Kirchhoff-Love plates

Consider a three-dimensional elastic body that can be treated as a two-dimensional one, as the one illustrated in Fig. B.10, where its volume in the reference configuration is given by $\mathcal{B}_0 = \Omega \times \Omega^c \subset \mathbb{R}^3$, where $\Omega \subset \mathbb{R}^2$ is the two-dimensional spatial domain and $\Omega^c = \left(-\frac{h}{2}, \frac{h}{2}\right) \subset \mathbb{R}$ is the complementary domain denoting the thickness h. The Kirchhoff-Rayleigh and the Kirchhoff-Love plates can be considered as the two-dimensional extension of the Rayleigh beam and Euler-Bernoulli beam, respectively, where in the Kirchhoff-Love plate is neglected the effect of the rotary inertia when computing the kinetic energy. Therefore, they are also based on the same kinematic assumption, i.e., Kirchhoff theory. The displacement field of the Kirchhoff-Rayleigh and the Kirchhoff-Love plates is then expressed as:

$$\mathbf{u}(\mathbf{X}, t) = \underbrace{\begin{bmatrix} -X_3 & 0 & 1 & 0 & 0 \\ 0 & -X_3 & 0 & 1 & 0 \\ 0 & 0 & 0 & 0 & 1 \end{bmatrix}}_{\bar{M}_1(\mathtt{X}^c)} \underbrace{\begin{bmatrix} \partial_1 w_0(\mathtt{X}, t) \\ \partial_2 w_0(\mathtt{X}, t) \\ u_0(\mathtt{X}, t) \\ v_0(\mathtt{X}, t) \\ w_0(\mathtt{X}, t) \end{bmatrix}}_{r(\mathtt{X}, t)}, \tag{B.13}$$

where $\mathtt{X} = \{X_1, X_2\} \in \Omega$, $u_0(\mathtt{X}, t)$, $v_0(\mathtt{X}, t)$ and $w_0(\mathtt{X}, t)$ are the axial, horizontal and vertical displacements, respectively. When the interest is primarily in predicting the vertical displacement $w_0(\mathtt{X}, t)$, it is common to simplify $\mathbf{u}(\mathbf{X}, t)$ in (B.13) to

derive simpler models. In such cases, it is sufficient to retain $w_0(\mathtt{X},t)$ along with $\partial_1 w_0(\mathtt{X},t)$ and $\partial_2 w_0(\mathtt{X},t)$. Thus, the simplified displacement field is expressed as:

$$\mathbf{u}(\mathbf{X},t) = \underbrace{\begin{bmatrix} -X_3 & 0 & 0 \\ 0 & -X_3 & 0 \\ 0 & 0 & 1 \end{bmatrix}}_{\bar{M}_1(\mathtt{X}^c)} \underbrace{\begin{bmatrix} \partial_1 w_0(\mathtt{X},t) \\ \partial_2 w_0(\mathtt{X},t) \\ w_0(\mathtt{X},t) \end{bmatrix}}_{r(\mathtt{X},t)}. \tag{B.14}$$

The displacement field $\mathbf{u}(\mathbf{X},t)$ in (B.14) is the basis for deriving the linear and nonlinear PHS models proposed in [Brugnoli 2019b] and [Brugnoli 2022a], respectively.

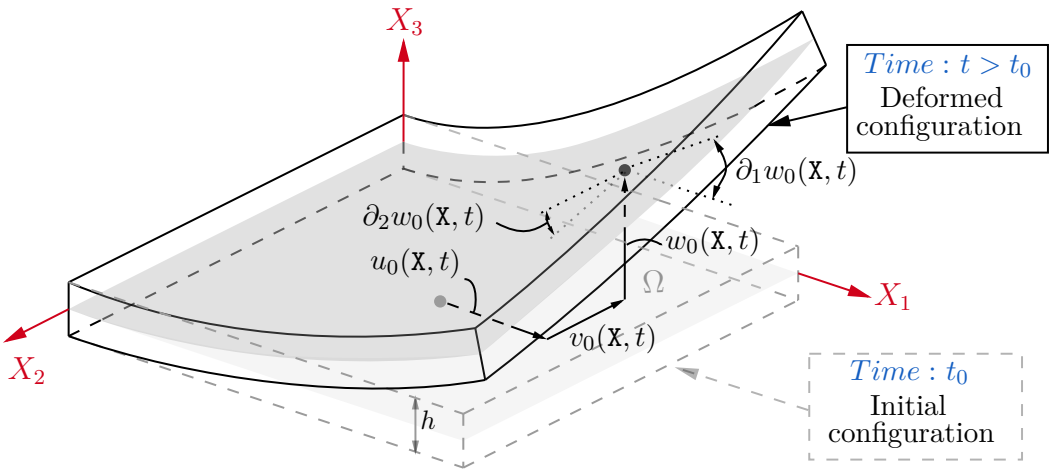

Figure B.10 – Kinematic variables of the Kirchhoff-Rayleigh and Kirchhoff-Love plates.

B.1.11 Planar Reddy beam

Consider a three-dimensional elastic body that can be treated as a one-dimensional one, as the one illustrated in Fig. B.11, where its volume in the reference configuration is given by $\mathcal{B}_0 = \Omega \times \Omega^c \subset \mathbb{R}^3$, where $\Omega = (0, L_0) \subset \mathbb{R}$ is the one-dimensional spatial domain and $\Omega^c = A_0 \subset \mathbb{R}^2$ is the complementary domain denoting the cross section area. The planar Reddy beam model is based on the third-order shear deformation theory, which accounts for a cubic variation of transverse shear strains through the beam's thickness h [Reddy 1984; Reddy 2006, Chapter 11]. This kinematic assumption provides a more accurate representation of shear deformation, eliminating the need for shear correction factors, and enables the model to capture higher-order effects compared to first-order theories used in Timoshenko beam and Mindlin plate models. The displacement field of the Reddy beam is then expressed as:

$$\mathbf{u}(\mathbf{X},t) = \underbrace{\begin{bmatrix} -(X_3 - \alpha X_3^3) & -\alpha X_3^3 & 1 & 0 \\ 0 & 0 & 0 & 0 \\ 0 & 0 & 0 & 1 \end{bmatrix}}_{\bar{M}_1(\mathtt{X}^c)} \underbrace{\begin{bmatrix} \psi_3(\mathtt{X},t) \\ \partial_1 w_0(\mathtt{X},t) \\ u_0(\mathtt{X},t) \\ w_0(\mathtt{X},t) \end{bmatrix}}_{r(\mathtt{X},t)}, \tag{B.15}$$

where $\mathtt{X} = \{X_1\} \in \Omega$, $\alpha = \frac{4}{3h^2}$ is a constant, and $u_0(\mathtt{X}, t)$ and $w_0(\mathtt{X}, t)$ are the axial and vertical displacements, respectively. The variable $\psi_3(\mathtt{X}, t)$ represents the angle of rotation of a plane cross section before deformation. It is defined as the angle between the vertical axis and the tangent to the curved cross section evaluated at the neutral axis (in the deformed configuration). It can be observed that if the cubic terms are neglected, there is no need to include $\partial_1 w_0(\mathtt{X}, t)$ in $r(\mathtt{X}, t)$, and the displacement field $\mathbf{u}(\mathbf{X}, t)$ in (B.15) leads to that of the planar Timoshenko beam.

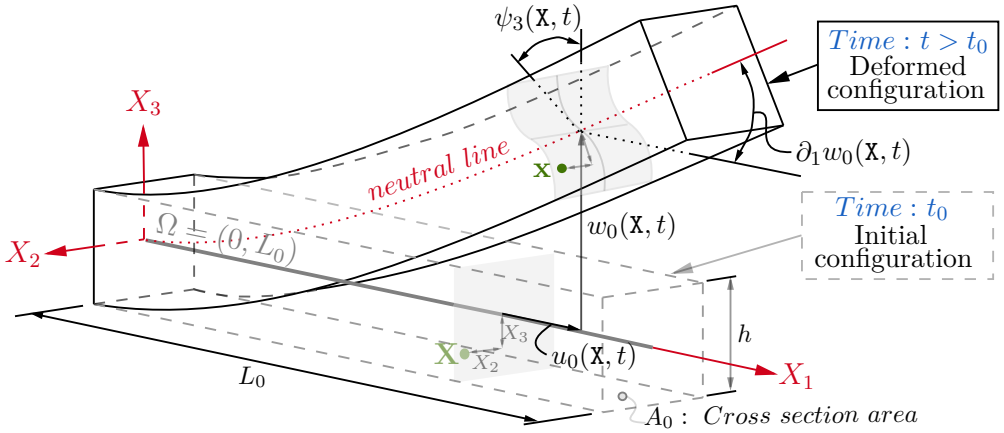

Figure B.11 – Kinematic variables of the planar Reddy beam.

B.1.12 Reddy plate

Consider a three-dimensional elastic body that can be treated as a two-dimensional one, as the one illustrated in Fig. B.12, where its volume in the reference configuration is given by $\mathcal{B}_0 = \Omega \times \Omega^c \subset \mathbb{R}^3$, where $\Omega \subset \mathbb{R}^2$ is the two-dimensional spatial domain and $\Omega^c = \left(-\frac{h}{2}, \frac{h}{2}\right) \subset \mathbb{R}$ is the complementary domain denoting the thickness h. The Reddy plate can be seen as the two-dimensional extension of the Reddy beam, so it is also based on the same kinematic assumption, i.e., third-order shear deformation theory. The displacement field of the Reddy plate is then expressed as:

$$\mathbf{u}(\mathbf{X}, t) = \underbrace{\begin{bmatrix} 0 & -(X_3 - \alpha X_3^3) & -\alpha X_3^3 & 0 & 1 & 0 & 0 \\ -(X_3 - \alpha X_3^3) & 0 & 0 & -\alpha X_3^3 & 0 & 1 & 0 \\ 0 & 0 & 0 & 0 & 0 & 0 & 1 \end{bmatrix}}_{\bar{M}_1(\mathtt{X}^c)} \underbrace{\begin{bmatrix} \psi_2(\mathtt{X}, t) \\ \psi_3(\mathtt{X}, t) \\ \partial_1 w_0(\mathtt{X}, t) \\ \partial_2 w_0(\mathtt{X}, t) \\ u_0(\mathtt{X}, t) \\ v_0(\mathtt{X}, t) \\ w_0(\mathtt{X}, t) \end{bmatrix}}_{r(\mathtt{X}, t)}, \tag{B.16}$$

where $\mathtt{X} = \{X_1, X_2\} \in \Omega$, $\alpha = \frac{4}{3h^2}$ is a constant, and $u_0(\mathtt{X}, t)$, $v_0(\mathtt{X}, t)$ and $w_0(\mathtt{X}, t)$ are the axial, horizontal and vertical displacements, respectively. The variables $\psi_2(\mathtt{X}, t)$ and $\psi_3(\mathtt{X}, t)$ represent the angles of rotation of a plane cross section before

deformation. They are defined as the angles between the vertical axis and the tangents to the curved cross section evaluated at the neutral axis (in the deformed configuration). It can be observed that if the cubic terms are neglected, there is no need to include $\partial_1 w_0(\mathtt{X},t)$ and $\partial_2 w_0(\mathtt{X},t)$ in $r(\mathtt{X},t)$, so the displacement field $\mathbf{u}(\mathbf{X},t)$ in (B.16) leads to that of the Mindlin plate in (B.9). When the interest is primarily in predicting the vertical displacement $w_0(\mathtt{X},t)$, it is common to simplify $\mathbf{u}(\mathbf{X},t)$ in (B.16) to derive simpler models. In such cases, it is sufficient to retain $w_0(\mathtt{X},t)$, $\psi_2(\mathtt{X},t)$, $\psi_3(\mathtt{X},t)$ along with $\partial_1 w_0(\mathtt{X},t)$ and $\partial_2 w_0(\mathtt{X},t)$. Thus, the simplified displacement field of the Reddy plate is expressed as:

$$\mathbf{u}(\mathbf{X},t)=\underbrace{\begin{bmatrix} 0 & -(X_3-\alpha X_3^3) & -\alpha X_3^3 & 0 & 0\\ -(X_3-\alpha X_3^3) & 0 & 0 & -\alpha X_3^3 & 0\\ 0 & 0 & 0 & 0 & 1\end{bmatrix}}_{\bar{M}_1(\mathtt{X}^c)}\underbrace{\begin{bmatrix}\psi_2(\mathtt{X},t)\\ \psi_3(\mathtt{X},t)\\ \partial_1 w_0(\mathtt{X},t)\\ \partial_2 w_0(\mathtt{X},t)\\ w_0(\mathtt{X},t)\end{bmatrix}}_{r(\mathtt{X},t)}. \tag{B.17}$$

The displacement field $\mathbf{u}(\mathbf{X},t)$ in (B.17) is the basis for deriving the linear PHS model proposed in our paper in [Ponce 2024].

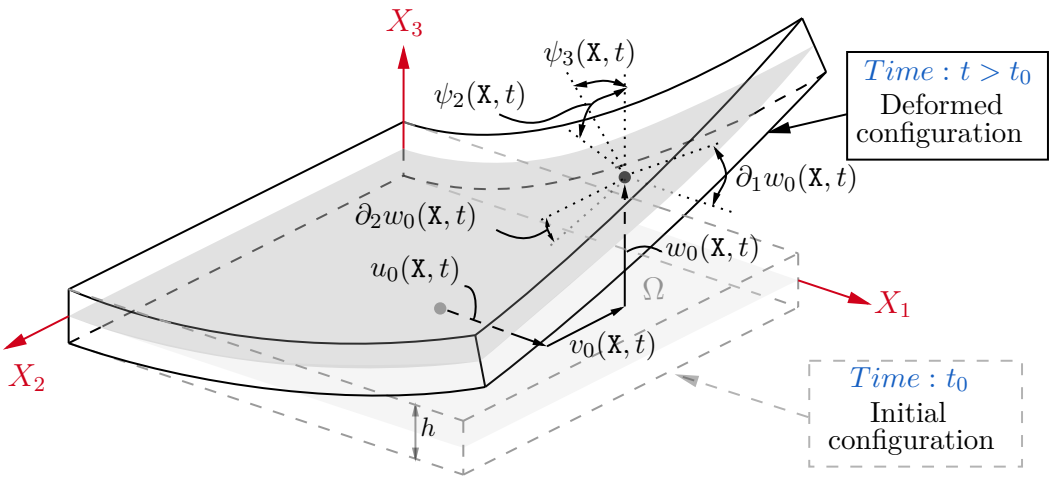

Figure B.12 – Kinematic variables of the Reddy plate.

Remarks

While this appendix focuses on selected displacement fields relevant to the discussed models, numerous other displacement fields addressing various elasticity problems exist in the literature. These include models for torsion in circular and prismatic bars, elastic waves in 2D, and beams and plates based on higher-order shear deformation theories, among others. Additionally, the linear PHS models derived from many of the displacement fields presented in this appendix are detailed in our arXiv paper in [Ponce 2023, Appendix D]. In that paper, the modeling Methodology 1 proposed in Chapter II page 53 is followed, and the corresponding constitutive matrices under Hooke's law are presented.

Appendix C

User-friendly MATLAB code for linear FEM

Infinite-dimensional models

In addition to the theoretical results developed in this thesis, an user-friendly MATLAB code has been created to facilitate the finite element discretization of linear PHS. This appendix provides an overview of the code, including guidance on its usage and configuration. The code is oriented to discretize linear PHS of the form:

$$\underbrace{\begin{bmatrix}\dot{p}(\mathtt{X},t)\\ \dot{\epsilon}(\mathtt{X},t)\\ \dot{r}(\mathtt{X},t)\end{bmatrix}}_{\dot{x}} = \underbrace{\begin{bmatrix}0 & -\mathcal{F}_{\mathtt{x}}{}^* & -1\\ \mathcal{F}_{\mathtt{x}} & 0 & 0\\ 1 & 0 & 0\end{bmatrix}}_{\mathcal{J}=-\mathcal{J}^*}\underbrace{\begin{bmatrix}e_p(\mathtt{X},t)\\ e_\epsilon(\mathtt{X},t)\\ -b(\mathtt{X})\end{bmatrix}}_{\delta_x H(x)},$$

$$H(x) = \int_\Omega \left(\frac{1}{2}\,p(\mathtt{X},t)^\top \mathcal{M}(\mathtt{X})^{-1} p(\mathtt{X},t) + \frac{1}{2}\,\epsilon(\mathtt{X},t)^\top \mathcal{K}_\epsilon(\mathtt{X})\epsilon(\mathtt{X},t) - r(\mathtt{X},t)^\top b(\mathtt{X})\right) d\mathtt{X},$$

where $\Omega \subset \mathbb{R}^\ell$ with $\ell = \{1,2\}$ is the spatial domain, $p(\mathtt{X},t) \in \mathbb{R}^n$ is the generalized momentum, $\epsilon(\mathtt{X},t) \in \mathbb{R}^m$ is the generalized strain, $r(\mathtt{X},t) \in \mathbb{R}^n$ is the generalized displacement, $e_p(\mathtt{X},t) = \mathcal{M}(\mathtt{X})^{-1}p(\mathtt{X},t) = \dot{r}(\mathtt{X},t) \in \mathbb{R}^n$ is the generalized velocity with $\mathcal{M}(\mathtt{X}) = \mathcal{M}(\mathtt{X})^\top > 0 \in \mathbb{R}^{n\times n}$ the mass density matrix, $e_\epsilon(\mathtt{X},t) = \mathcal{K}_\epsilon(\mathtt{X})\epsilon(\mathtt{X},t) \in \mathbb{R}^m$ is the generalized stress with $\mathcal{K}_\epsilon(\mathtt{X}) = \mathcal{K}_\epsilon(\mathtt{X})^\top > 0 \in \mathbb{R}^{m\times m}$ the stiffness density matrix, $b(\mathtt{X}) \in \mathbb{R}^n$ is the generalized body load, and $\mathcal{F}_{\mathtt{x}}$ is a first-order linear differential operator with $\mathcal{F}_{\mathtt{x}}{}^*$ its formal adjoint. Considering $\mathtt{X} = \{X_1, \ldots, X_\ell\}$, these operators are defined as:

$$\begin{aligned}\mathcal{F}_{\mathtt{x}}\, e_p(\mathtt{X},t) &= F_0\, e_p(\mathtt{X},t) + \textstyle\sum_{k=1}^{\ell} F_k\, \partial_k e_p(\mathtt{X},t),\\ \mathcal{F}_{\mathtt{x}}{}^* e_\epsilon(\mathtt{X},t) &= F_0^\top e_\epsilon(\mathtt{X},t) - \textstyle\sum_{k=1}^{\ell} F_k^\top \partial_k e_\epsilon(\mathtt{X},t),\end{aligned}$$

with $\partial_k = \partial/\partial X_k$ and F_0, $F_k \in \mathbb{R}^{m\times n}$ constant matrices.

Assuming a mixed boundary problem with $\partial\Omega = \partial\Omega_D \cup \partial\Omega_N$, where $\partial\Omega_D$ and $\partial\Omega_N$ are the boundary portions where Dirichlet and Neumann boundary conditions are imposed, respectively, the boundary inputs $u_\partial(\mathtt{S},t) \in \mathbb{R}^{2n}$ and boundary outputs $y_\partial(\mathtt{S},t) \in \mathbb{R}^{2n}$ are given by:

$$u_\partial(\mathtt{S},t) = \begin{bmatrix}\tau_N(\mathtt{S},t)^\top & v_D(\mathtt{S},t)^\top\end{bmatrix}^\top, \quad y_\partial(\mathtt{S},t) = \begin{bmatrix}v_N(\mathtt{S},t)^\top & \tau_D(\mathtt{S},t)^\top\end{bmatrix}^\top,$$

with $v_D(\mathtt{S},t)$ and $\tau_N(\mathtt{S},t)$ the prescribed velocities and tractions, and $\tau_D(\mathtt{S},t)$ and $v_N(\mathtt{S},t)$ their power-conjugated reactions, defined as:

$$\begin{aligned}\tau_N(\mathtt{S},t) &= F_\partial(\mathtt{S})e_\epsilon(\mathtt{S},t), \quad v_N(\mathtt{S},t) = e_p(\mathtt{S},t) \quad (\text{on } \partial\Omega_N),\\ \tau_D(\mathtt{S},t) &= F_\partial(\mathtt{S})e_\epsilon(\mathtt{S},t), \quad v_D(\mathtt{S},t) = e_p(\mathtt{S},t) \quad (\text{on } \partial\Omega_D),\end{aligned}$$

where $F_\partial(\mathtt{S}) = \sum_{k=1}^{\ell} F_k^\top \hat{n}_k(\mathtt{S}) \in \mathbb{R}^{n\times m}$ is a boundary valued matrix induced by $\mathcal{F}_{\mathtt{x}}$, and $\hat{n}_k(\mathtt{S})$ is the k-component of the outward unit normal vector to the boundary $\partial\Omega$ projected on the axis X_k. For more details see Chapter II.3.1.

Finite-dimensional models

The MATLAB code performs the FEM discretization using various schemes, including both standard and mixed approaches. The implemented schemes are:

- Standard FEM: using Lagrange Multipliers (LM) or the Penalty Method (PM) to enforce Dirichlet boundary conditions.
- Mixed FEM: using the Hellinger-Reissner (HR), Generalized Hamiltons's Principle (GHP) or modified Linked Lagrange Multiplier (mLLM) methods.

A brief description of each of these finite-dimensional models is presented below. Details are discussed in Chapter III.

a) *Standard FEM using Lagrange Multipliers (LM)*: The finite-dimensional model has the structure of a PH-DAE given by:

$$\underbrace{\begin{bmatrix} I_{N_\Omega} & 0 & 0 \\ 0 & I_{N_\Omega} & 0 \\ 0 & 0 & 0 \end{bmatrix}}_{\hat{E}} \underbrace{\begin{bmatrix} \dot{\hat{p}}(t) \\ \dot{\hat{r}}(t) \\ \dot{\hat{\lambda}}(t) \end{bmatrix}}_{\dot{\hat{z}}(t)} = \underbrace{\begin{bmatrix} 0 & -I_{N_\Omega} & -\hat{B}_\lambda^\top \\ I_{N_\Omega} & 0 & 0 \\ \hat{B}_\lambda & 0 & 0 \end{bmatrix}}_{\hat{J}=-\hat{J}^\top} \underbrace{\begin{bmatrix} \hat{e}_p(t) \\ \hat{e}_r(t) \\ \hat{\lambda}(t) \end{bmatrix}}_{\hat{Z}(\hat{z})} + \underbrace{\begin{bmatrix} \hat{B}_{\tau_N} & 0 \\ 0 & 0 \\ 0 & -\hat{B}_{LM} \end{bmatrix}}_{\hat{G}} \underbrace{\begin{bmatrix} \hat{\tau}_N(t) \\ \hat{v}_D(t) \end{bmatrix}}_{\hat{u}_\partial(t)}$$

$$\hat{y}_\partial(t) = \hat{G}^\top \hat{Z}(\hat{z})$$

$$\hat{H}_{LM}(\hat{z}) = \frac{1}{2}\,\hat{p}(t)^\top \hat{M}^{-1} \hat{p}(t) + \frac{1}{2}\,\hat{r}(t)^\top \hat{K}_r\,\hat{r}(t) - \hat{r}(t)^\top \hat{b},$$

where $\hat{e}_p(t) = \hat{M}^{-1}\hat{p}(t)$, $\hat{e}_r(t) = \hat{K}_r\,\hat{r}(t) - \hat{b}$, and I_{N_Ω} is an identity matrix. The involved matrices and vectors are given by:

$$\begin{aligned}
\hat{M} &= \sum_{e=1}^{n_e} (L_r^e)^\top \int_{\Omega^e} N_r^e(\mathtt{X})^\top \mathcal{M}(\mathtt{X}) N_r^e(\mathtt{X})\, d\mathtt{X}\, L_r^e, \\
\hat{K}_r &= \sum_{e=1}^{n_e} (L_r^e)^\top \int_{\Omega^e} (\mathcal{F}_{\mathtt{x}} N_r^e(\mathtt{X}))^\top \mathcal{K}_\epsilon(\mathtt{X}) (\mathcal{F}_{\mathtt{x}} N_r^e(\mathtt{X}))\, d\mathtt{X}\, L_r^e, \\
\hat{b} &= \sum_{e=1}^{n_e} (L_r^e)^\top \int_{\Omega^e} N_r^e(\mathtt{X})^\top b(\mathtt{X})\, d\mathtt{X}, \\
\hat{B}_{\tau_N} &= \sum_{e=1}^{n_e} (L_r^e)^\top \int_{\partial\Omega_N^e} N_r^e(\mathtt{S})^\top N_{\tau_N}^e(\mathtt{S})\, d\mathtt{S}\, L_{\tau_N}^e, \\
\hat{B}_\lambda &= \sum_{e=1}^{n_e} (L_\lambda^e)^\top \int_{\partial\Omega_D^e} N_\lambda^e(\mathtt{S})^\top N_r^e(\mathtt{S})\, d\mathtt{S}\, L_r^e, \\
\hat{B}_{LM} &= \sum_{e=1}^{n_e} (L_\lambda^e)^\top \int_{\partial\Omega_D^e} N_\lambda^e(\mathtt{S})^\top N_{r_D}^e(\mathtt{S})\, d\mathtt{S}\, L_{r_D}^e,
\end{aligned}$$

where $N_\square^e(\mathtt{X})$ is the local shape function in the element e, $L_\square^e$ is the location (assembly) matrix, and n_e is the total number of finite elements.

b) *Standard FEM using Penalty Method (PM)*: The finite-dimensional model has the structure of a PHS given by:

$$\underbrace{\begin{bmatrix}\dot{\hat{p}}(t)\\ \dot{\hat{r}}(t)\end{bmatrix}}_{\dot{\hat{z}}(t)} = \underbrace{\begin{bmatrix}0 & -I_{N_\Omega}\\ I_{N_\Omega} & 0\end{bmatrix}}_{\hat{J}=-\hat{J}^\top}\underbrace{\begin{bmatrix}\hat{e}_p(t)\\ \hat{e}_r(t)\end{bmatrix}}_{\nabla_{\hat{z}}\hat{H}_{PM}(\hat{z})} + \underbrace{\begin{bmatrix}\hat{B}_{\tau_N} & \hat{B}_{PM}\\ 0 & 0\end{bmatrix}}_{\hat{G}}\underbrace{\begin{bmatrix}\hat{\tau}_N(t)\\ \hat{r}_D(t)\end{bmatrix}}_{\hat{u}_\partial(t)}$$
$$\hat{y}(t) = \hat{G}^\top \nabla_{\hat{z}}\hat{H}_{PM}(\hat{z})$$
$$\hat{H}_{PM}(\hat{z}) = \frac{1}{2}\,\hat{p}(t)^\top \hat{M}^{-1}\hat{p}(t) + \frac{1}{2}\,\hat{r}(t)^\top \hat{K}_{PM}\,\hat{r}(t) - \hat{r}(t)^\top \hat{b},$$

where $\hat{e}_p(t) = \hat{M}^{-1}\hat{p}(t)$, $\hat{e}_r(t) = \hat{K}_{PM}\,\hat{r}(t) - \hat{b}$, and $\hat{K}_{PM} = \hat{K}_r + \hat{K}_\infty$. The other involved matrices are given by:

$$\hat{K}_\infty = \beta_\infty \sum_{e=1}^{n_e} (L_r^e)^\top \int_{\partial\Omega_D^e} N_r^e(\mathtt{S})^\top N_r^e(\mathtt{S})\, d\mathtt{S}\, L_r^e,$$
$$\hat{B}_{PM} = \beta_\infty \sum_{e=1}^{n_e} (L_r^e)^\top \int_{\partial\Omega_D^e} N_r^e(\mathtt{S})^\top N_{r_D}^e(\mathtt{S})\, d\mathtt{S}\, L_{r_D}^e,$$

where $\beta_\infty \to \infty$ is the penalty factor, and $\hat{r}_D(t)$ is the imposed position on $\partial\Omega_D$, which satisfies $\hat{v}_D(t) = \dot{\hat{r}}_D(t)$.

c) *Mixed FEM using the Hellinger-Reissner method (HR)*: The finite-dimensional model has the structure of a PHS given by:

$$\underbrace{\begin{bmatrix}\dot{\hat{p}}(t)\\ \dot{\hat{\epsilon}}(t)\\ \dot{\hat{r}}(t)\end{bmatrix}}_{\dot{\hat{x}}(t)} = \underbrace{\begin{bmatrix}0 & -\hat{F}^\top & -I_{N_\Omega}\\ \hat{F} & 0 & 0\\ I_{N_\Omega} & 0 & 0\end{bmatrix}}_{\hat{J}=-\hat{J}^\top}\underbrace{\begin{bmatrix}\hat{e}_p(t)\\ \hat{e}_\epsilon(t)\\ -\hat{b}\end{bmatrix}}_{\nabla_{\hat{x}}\hat{H}_{HR}(\hat{x})} + \underbrace{\begin{bmatrix}\hat{B}_{\tau_N} & 0\\ 0 & \hat{B}_{v_D}\\ 0 & 0\end{bmatrix}}_{\hat{G}}\underbrace{\begin{bmatrix}\hat{\tau}_N(t)\\ \hat{v}_D(t)\end{bmatrix}}_{\hat{u}_\partial(t)}$$
$$\hat{y}_\partial(t) = \hat{G}^\top \nabla_{\hat{x}}\hat{H}_{HR}(\hat{x})$$
$$\hat{H}_{HR}(\hat{x}) = \frac{1}{2}\,\hat{p}(t)^\top \hat{M}^{-1}\hat{p}(t) + \frac{1}{2}\,\hat{\epsilon}(t)^\top \hat{C}_\epsilon^{-1}\,\hat{\epsilon}(t) - \hat{r}(t)^\top \hat{b},$$

where $\hat{e}_p(t) = \hat{M}^{-1}\hat{p}(t)$ and $\hat{e}_\epsilon(t) = \hat{C}_\epsilon^{-1}\,\hat{\epsilon}(t)$. The other matrices are given by:

$$\hat{C}_\epsilon = \sum_{e=1}^{n_e} (L_e^e)^\top \int_{\Omega^e} N_e^e(\mathtt{X})^\top \mathcal{C}_\epsilon(\mathtt{X}) N_e^e(\mathtt{X})\, d\mathtt{X}\, L_e^e,$$
$$\hat{F}^\top = \sum_{e=1}^{n_e} (L_r^e)^\top \left(\int_{\Omega^e} (\mathcal{F}_{\mathtt{x}} N_r^e(\mathtt{X}))^\top N_e^e(\mathtt{X})\, d\mathtt{X} - \int_{\partial\Omega_D^e} N_r^e(\mathtt{S})^\top F_\partial(\mathtt{S}) N_e^e(\mathtt{S})\, d\mathtt{S} \right) L_e^e,$$
$$\hat{B}_{v_D} = \sum_{e=1}^{n_e} (L_e^e)^\top \int_{\partial\Omega_D^e} N_e^e(\mathtt{S})^\top F_\partial(\mathtt{S})^\top N_{r_D}^e(\mathtt{S})\, d\mathtt{S}\, L_{r_D}^e,$$

where $\mathcal{C}_\epsilon(\mathtt{X}) = \mathcal{K}_\epsilon(\mathtt{X})^{-1}$ is the compliance density matrix.

d) *Mixed FEM using the Generalized Hamilton's Principle method (GHP)*: The finite-dimensional model has the structure of a PHS given by:

$$\underbrace{\begin{bmatrix}\dot{\hat{p}}(t)\\ \dot{\hat{\epsilon}}(t)\\ \dot{\hat{r}}(t)\end{bmatrix}}_{\dot{\hat{x}}(t)} = \underbrace{\begin{bmatrix}0 & -\hat{F}_x^\top & -I_{N_\Omega}\\ \hat{F}_x & 0 & 0\\ I_{N_\Omega} & 0 & 0\end{bmatrix}}_{\hat{J}=-\hat{J}^\top}\underbrace{\begin{bmatrix}\hat{e}_p(t)\\ \hat{e}_\epsilon(t)\\ -\hat{b}\end{bmatrix}}_{\nabla_{\hat{x}}\hat{H}_{GHP}(\hat{x})} + \underbrace{\begin{bmatrix}\hat{B}_{\tau_N} & 0\\ 0 & \hat{B}_v\\ 0 & 0\end{bmatrix}}_{\hat{G}}\underbrace{\begin{bmatrix}\hat{\tau}_N(t)\\ \hat{v}_D(t)\end{bmatrix}}_{\hat{u}_\partial(t)}$$
$$\hat{y}_\partial(t) = \hat{G}^\top \nabla_{\hat{x}}\hat{H}_{GHP}(\hat{x})$$

$$\hat{H}_{GHP}(\hat{x}) = \frac{1}{2}\,\hat{p}(t)^\top \hat{M}^{-1}\hat{p}(t) + \frac{1}{2}\,\hat{\epsilon}(t)^\top \hat{K}_\epsilon\,\hat{\epsilon}(t) - \hat{r}(t)^\top \hat{b},$$

where $\hat{e}_p(t) = \hat{M}^{-1}\hat{p}(t)$ and $\hat{e}_\epsilon(t) = \hat{K}_\epsilon\,\hat{\epsilon}(t)$. In addition, $\hat{F}_x = \hat{M}_\epsilon^{-1}\hat{F}$ and $\hat{B}_v = \hat{M}_\epsilon^{-1}\hat{B}_{v_D}$, and the other matrices are given by:

$$\hat{M}_\epsilon = \sum_{e=1}^{n_e}(L_e^e)^\top \int_{\Omega^e} N_e^e(\mathtt{X})^\top N_\epsilon^e(\mathtt{X})\,d\mathtt{X}\,L_\epsilon^e,$$
$$\hat{K}_\epsilon = \sum_{e=1}^{n_e}(L_\epsilon^e)^\top \int_{\Omega^e} N_\epsilon^e(\mathtt{X})^\top \mathcal{K}_\epsilon(\mathtt{X})\,N_\epsilon^e(\mathtt{X})\,d\mathtt{X}\,L_\epsilon^e.$$

e) *Mixed FEM using the modified Linked Lagrange Multiplier method (mLLM)*: The finite-dimensional model has the structure of a PHS given by:

$$\underbrace{\begin{bmatrix}\dot{\hat{p}}(t)\\ \dot{\hat{\epsilon}}_D(t)\\ \dot{\hat{r}}(t)\end{bmatrix}}_{\dot{\hat{x}}(t)} = \underbrace{\begin{bmatrix}0 & -\hat{F}_D^\top & -I_{N_\Omega}\\ \hat{F}_D & 0 & 0\\ I_{N_\Omega} & 0 & 0\end{bmatrix}}_{\hat{J}=-\hat{J}^\top}\underbrace{\begin{bmatrix}\hat{e}_p(t)\\ \hat{e}_{\epsilon_D}(t)\\ \hat{e}_r(t)\end{bmatrix}}_{\nabla_{\hat{x}}\hat{H}_{LLM}(\hat{x})} + \underbrace{\begin{bmatrix}\hat{B}_{\tau_N} & 0\\ 0 & \hat{B}_D\\ 0 & 0\end{bmatrix}}_{\hat{G}}\underbrace{\begin{bmatrix}\hat{\tau}_N(t)\\ \hat{v}_D(t)\end{bmatrix}}_{\hat{u}_\partial(t)}$$
$$\hat{y}_\partial(t) = \hat{G}^\top \nabla_{\hat{x}}\hat{H}_{LLM}(\hat{x})$$

$$\hat{H}_{LLM}(\hat{x}) = \frac{1}{2}\,\hat{p}(t)^\top \hat{M}^{-1}\hat{p}(t) + \frac{1}{2}\,\hat{r}(t)^\top \hat{K}_r\,\hat{r}(t) - \hat{r}(t)^\top \hat{b} + \Delta\hat{U}_{\Omega_D}(\hat{r},\hat{\epsilon}_D),$$
$$\Delta\hat{U}_{\Omega_D}(\hat{r},\hat{\epsilon}_D) = \frac{1}{2}\hat{\epsilon}_D(t)^\top \hat{C}_{\epsilon_D}^{-1}\,\hat{\epsilon}_D(t) - \frac{1}{2}\,\hat{r}(t)^\top \hat{K}_D\,\hat{r}(t),$$

where $\hat{e}_p(t) = \hat{M}^{-1}\hat{p}(t)$, $\hat{e}_{\epsilon_D}(t) = \hat{C}_{\epsilon_D}^{-1}\hat{\epsilon}_D(t)$, and $\hat{e}_r(t) = (\hat{K}_r - \hat{K}_D)\,\hat{r}(t) - \hat{b}$. The other involved matrices are given by:

$$\hat{C}_{\epsilon_D} = \sum_{e=1}^{n_e}(L_D^e)^\top \frac{1}{\beta}\int_{\Omega_D^e} N_e^e(\mathtt{X})^\top \mathcal{C}_\epsilon(\mathtt{X}) N_e^e(\mathtt{X})\,d\mathtt{X}\,L_D^e,$$
$$\hat{K}_D = \sum_{e=1}^{n_e}(L_r^e)^\top \frac{1}{\beta}\int_{\Omega_D^e} (\mathcal{F}_{\mathtt{x}} N_r^e(\mathtt{X}))^\top \mathcal{K}_\epsilon(\mathtt{X})(\mathcal{F}_{\mathtt{x}} N_r^e(\mathtt{X}))\,d\mathtt{X}\,L_r^e,$$
$$\hat{F}_D^\top = \sum_{e=1}^{n_e}(L_r^e)^\top \left(\frac{1}{\beta}\int_{\Omega_D^e}(\mathcal{F}_{\mathtt{x}} N_r^e(\mathtt{X}))^\top N_e^e(\mathtt{X})\,d\mathtt{X} - \int_{\partial\Omega_D^e} N_r^e(\mathtt{S})^\top F_\partial(\mathtt{S}) N_e^e(\mathtt{S})\,d\mathtt{S}\right) L_D^e,$$
$$\hat{B}_D = \sum_{e=1}^{n_e}(L_D^e)^\top \int_{\partial\Omega_D^e} N_e^e(\mathtt{S})^\top F_\partial(\mathtt{S})^\top N_{r_D}^e(\mathtt{S})\,d\mathtt{S}\,L_{r_D}^e,$$

where $\beta > 1$ is the link factor, and Ω_D^e represents any element within the Dirichlet domain (see the details in III.3.1, Fig. III.3).

C.1 One-dimensional models

The code features a `Main_script.m` where users define the infinite-dimensional linear PHS model to be discretized and specify the desired properties of the approximate model. Additionally, it includes a set of MATLAB functions designed to perform each required subroutine. The MATLAB functions developed for the FEM discretization of 1D systems are:

- `gMesh1D.m`: Generates the 1D mesh.
- `int_1D.m`: Performs integration in 1D.
- `bint_1D.m`: Performs boundary integration in 1D.
- `elementProp1D.m`: Assigns properties to each element.
- `shapefunctions1D.m`: Creates the shape functions.
- `FEM_PHS_1D.m`: Return the discretized models.

For simplicity, this section focuses on explaining how to configure the `Main_script` using as example the Timoshenko beam model. If you have any questions regarding other examples or with the MATLAB functions, please do not hesitate to contact me (emails: cristobal.ponces@usm.cl or cristobal.ponce@femto-st.fr).

Example: linear Timoshenko beam model

The linear Timoshenko beam model is defined on $\Omega = (0, L)$, and:

$$r = \begin{bmatrix} \psi_3 \\ w_0 \end{bmatrix}, \quad \mathcal{F}_{\mathtt{X}} = \begin{bmatrix} \partial_1 & 0 \\ -1 & \partial_1 \end{bmatrix}, \quad \mathcal{M} = \begin{bmatrix} \rho I_0 & 0 \\ 0 & \rho A_0 \end{bmatrix}, \quad \mathcal{K}_\epsilon = \begin{bmatrix} EI_0 & 0 \\ 0 & \kappa G A_0 \end{bmatrix}, \quad b = \begin{bmatrix} 0 \\ -\rho g A_0 \end{bmatrix},$$

where $w_0(\mathtt{X}, t)$ and $\psi_3(\mathtt{X}, t)$ are the vertical displacement and the rotation angle of the cross section, respectively.

Part I of the `Main_script.m`: Definition of physical parameters.

```
% Physical parameters
rho   = 7800;          % Density of the material
E     = 2.1e11;        % Young's Modulus
v     = 0.3;           % Poisson Ratio
G     = E/(2*(1+v));   % Shear modulus
g     = 9.806;         % Acceleration of gravity
kappa = 5/6;           % Correction factor
L     = 30/100;        % Length of the beam
b     = 3/100;         % Width of the beam
h     = 1/1000;        % Thickness of the beam
A0    = b*h;           % Cross section area
I0    = b*(h^3)/12;    % Second moment of inertia
```

The second part of the `Main_script` consists in defining the PDE and the portions where Dirichlet and Neumann boundary conditions are applied.

Part II of the `Main_script.m`: Definition of the PDE.

```
% Infinite-dimensional model (Timoshenko beam)
prop.dom = [0 L];
prop.M = @(x) [rho*I0 0;0 rho*A0];
prop.K = @(x) [E*I0 0;0 kappa*G*A0];
prop.b = @(x) [0;-rho*g*A0];
prop.F0 = [0 0;-1 0];
prop.F1 = [1 0;0 1];

% Boundary conditions
prop.Dirichlet = prop.dom(1);
prop.Neumann   = prop.dom(2);
prop.Didx = [0 1];
prop.Nidx = [0 1];
```

Description:

- `prop.dom`: Specifies the spatial domain $\Omega = (0, L)$.
- `prop.M`, `prop.K`, `prop.b`: Specify $\mathcal{M}(\mathtt{X})$, $\mathcal{K}_\epsilon(\mathtt{X})$ and $b(\mathtt{X})$, respectively. In general, they can be explicitly dependent on the spatial coordinate $\mathtt{X} =$ `@(x)`.
- `prop.F0`, `prop.F1`: They are the matrices F_0 and F_1 associated with the differential operator $\mathcal{F}_{\mathtt{x}}(\cdot) = F_0(\cdot) + F_1\partial_1(\cdot)$.
- `prop.Dirichlet`, `prop.Neumann`: Specify the Dirichlet and Neumann boundary portions $\partial\Omega_D$ and $\partial\Omega_N$, respectively. They can be defined as:
  - `prop.Dirichlet = prop.dom(1);` if $\mathtt{S} = \{0\} \in \partial\Omega_D$.
  - `prop.Dirichlet = prop.dom(2);` if $\mathtt{S} = \{L\} \in \partial\Omega_D$.
  - `prop.Dirichlet = prop.dom;` if $\mathtt{S} = \{0, L\} \in \partial\Omega_D$.
  - `prop.Dirichlet = [];` if $\mathtt{S} = \{\emptyset\} \in \partial\Omega_D$.

  Analogously for `prop.Neumann`.
- `prop.Didx`, `prop.Nidx`: Selectors used to specify which components of the velocity or traction, respectively, are applied as control inputs. For example:
  - `prop.Didx = [0 1];` indicates that the second component of $v_D(\mathtt{S}, t) = [\dot{\psi}_3(\mathtt{S}, t)^\top \ \dot{w}_0(\mathtt{S}, t)^\top]^\top$ will serve as a control input.
  - `prop.Nidx = [1 0];` indicates that the first component of the traction $\tau_N(\mathtt{S}, t) = [\tau_N^\psi(\mathtt{S}, t)^\top \ \tau_N^w(\mathtt{S}, t)^\top]^\top$ will serve as a control input. In this case, $\tau_N^\psi(\mathtt{S}, t)$ represents applied bending moment.

  It is important to highlight that these selectors are only to define the control inputs for simulations. If `prop.Dirichlet = prop.dom(1)` and `prop.Didx = [0 0]`, means that the Dirichlet boundary conditions will be imposed as

homogeneous in $\mathtt{S} = 0$. If `prop.Dirichlet = prop.dom(1)` and `prop.Didx = [0 1]`, means that we can impose inhomogeneous Dirichlet boundary conditions. In this scenario, we can impose $\dot{w}_0(\mathtt{S}, t) \neq 0$ in $\mathtt{S} = 0$.

The last part of the `Main_script` consists in generating the Mesh and choose the desired FEM method.

Part III of the `Main_script.m`: Mesh and FEM discretization.

```
% Generate mesh
TAG = 'C-C';  % 'C-D' or 'C-C'

FEM_order = 2;  %  Order of finite elements
Nelements = 20; %  Number of finite elements
meshFEM = gMesh1D(prop,Nelements,FEM_order); meshFEM.TAG = TAG;

% Generate finite-dimensional model
prop.beta = 50;        % Link factor for mLLM method
prop.beta_inf = 1e9;   % Penalty factor for penalty method

% FEM methods: 'LM', 'PM', 'HR', 'mLLM', 'GHP'
[model] = FEM_PHS_1D(prop,meshFEM,'GHP');
```

Description:

- `TAG`: For mixed FEM, it is common to use piecewise linear continuous shape functions to interpolate displacements and piecewise constant discontinuous shape functions to interpolate strains and stresses. The term:
  - `TAG = 'C-D';` refers to the use continuous shape functions for displacements and discontinuous shape functions for strains and stresses.
  - `TAG = 'C-C';` indicates that all shape functions are piecewise continuous of order `FEM_order`.
- `FEM_order`: Specifies to the degree of the shape functions used for interpolation. For example, `FEM_order = 1;` corresponds to linear shape functions, and `FEM_order = 2;` corresponds to quadratic shape functions.
- `Nelements`: The total number of finite elements used to generate the mesh, with uniformly spaced nodes.
- `meshFEM`: An object that contains the mesh information. The main variables that can be extracted are:
  - `meshFEM.coor:` A matrix containing the spatial coordinates of all nodes in the mesh.
  - `meshFEM.conec:` A matrix that defines the topology of the mesh, where the k-th row specifies the nodes connected to form the element k.

- `model`: An object that contains the model information. The main variables that can be extracted are the matrices of the finite-dimensional model, which vary depending on the FEM method chosen to discretize the PDE. For instance, using the `'GHP'` method, the following matrices and vectors can be extracted:
  - `model.M`: The discretized mass matrix $\hat{M}$.
  - `model.Ke`: The discretized stiffnes matrix $\hat{K}_\epsilon$.
  - `model.Fx`: The discretized differential operator $\hat{F}_x$.
  - `model.b`: The discretized body load $\hat{b}$.
  - `model.B_tN`: The input map $\hat{B}_{\tau_N}$.
  - `model.Bv`: The input map $\hat{B}_v$.

Comments

With the discretized models available, they can be applied to analyze eigenmodes to study the natural frequencies and mode shapes of the system, perform time simulations to evaluate its dynamic response under various inputs, and design control strategies to achieve desired performance objectives.

C.2 Two-dimensional models

Similarly to the code for 1D models, the code for 2D models includes a `Main_script` where users define the infinite-dimensional linear PHS model to be discretized and specify the desired properties of the approximate model. Additionally, it includes a set of MATLAB functions designed to perform each required subroutine. The MATLAB functions developed for the FEM discretization of 2D systems are:

- `saveDomain.m`: Creates the 2D domain.
- `gMesh2D.m`: Generates the 2D mesh using triangular elements.
- `int_triang.m`: Performs 2D integration over triangles.
- `bint_triang.m`: Performs boundary integration in 2D over triangles.
- `elementPropTriang.m`: Assigns properties to each triangular element.
- `shapefunctionsTriang.m`: Creates the shape functions.
- `FEM_PHS_2D.m`: Return the discretized models.

For simplicity, this section focuses on explaining how to configure the `Main_script` using as example the Mindlin plate model.

Example: Mindlin plate model

The linear Mindlin plate model is defined on $\Omega \subset \mathbb{R}^2$, and:

$$r = \begin{bmatrix} \psi_1 \\ \psi_2 \\ w_0 \end{bmatrix}, \qquad \mathcal{M} = \begin{bmatrix} \rho_0 \frac{h^3}{12} & 0 & 0 \\ 0 & \rho_0 \frac{h^3}{12} & 0 \\ 0 & 0 & \rho_0 h \end{bmatrix}, \qquad b = \begin{bmatrix} 0 \\ 0 \\ -\rho_0 g h \end{bmatrix},$$

$$\mathcal{F}_{\mathtt{x}} = \begin{bmatrix} \partial_1 & 0 & 0 \\ 0 & \partial_2 & 0 \\ \partial_2 & \partial_1 & 0 \\ -1 & 0 & \partial_1 \\ 0 & -1 & \partial_2 \end{bmatrix}, \quad \mathcal{K}_\epsilon = \begin{bmatrix} \bar{D} & \nu\bar{D} & 0 & 0 & 0 \\ \nu\bar{D} & \bar{D} & 0 & 0 & 0 \\ 0 & 0 & \bar{D}\frac{(1-\nu)}{2} & 0 & 0 \\ 0 & 0 & 0 & \kappa G h & 0 \\ 0 & 0 & 0 & 0 & \kappa G h \end{bmatrix},$$

where $w_0(\mathtt{X}, t)$, $\psi_1(\mathtt{X}, t)$ and $\psi_2(\mathtt{X}, t)$ are the vertical displacement and the rotation angles of the cross section, respectively. In addition, $\bar{D} = \frac{Eh^3}{12(1-\nu^2)}$ is the bending stiffness of a plate.

Part I of the `Main_script.m`: Definition of physical parameters.

```
% Physical parameters
h   = 1/1000;          % Thickness
rho = 7730;            % Density of the material
I2  = (h^3)/12;        % Second moment of inertia of the thickness
k   = 5/6;             % Correction factor
g   = 9.806;           % Acceleration of gravity
E   = 2.05e11;         % Young's modulus
v   = 0.3;             % Poisson's ratio
G   = E/(2*(1+v));     % Shear modulus
D   = (I2*E)/(1-v^2); % Bending stiffness of the plate
Cs  = k*[G 0;0 G];     % Constitutive matrix for shearing stress
Cb  = (D/I2)*[1 v 0;   % Constitutive matrix for plane stress
              v 1 0;
            0 0 (1-v)/2];
```

The second part of the `Main_script` involves generating the spatial domain and the mesh. To create the spatial domain, the `saveDomain.m` script must be executed. Upon starting, the MATLAB PDE Modeler app will open.

- Step 1: Draw the spatial domain in the PDE Modeler app. The usage of this tool is not explained here. For documentation refer to [Langemyr 1996].
- Step 2: Generate the boundary of the drawn domain by pressing $\partial\Omega$.
- Step 3: Export the geometry. `Boundary` → `Export Decomposed Geometry`.

Once the geometry is exported, the `saveDomain.m` script will prompt for a file name to save the domain object. In this example, the domain object is saved as `DomainPlate.mat`. See Figures C.1 and C.2 for guidance.

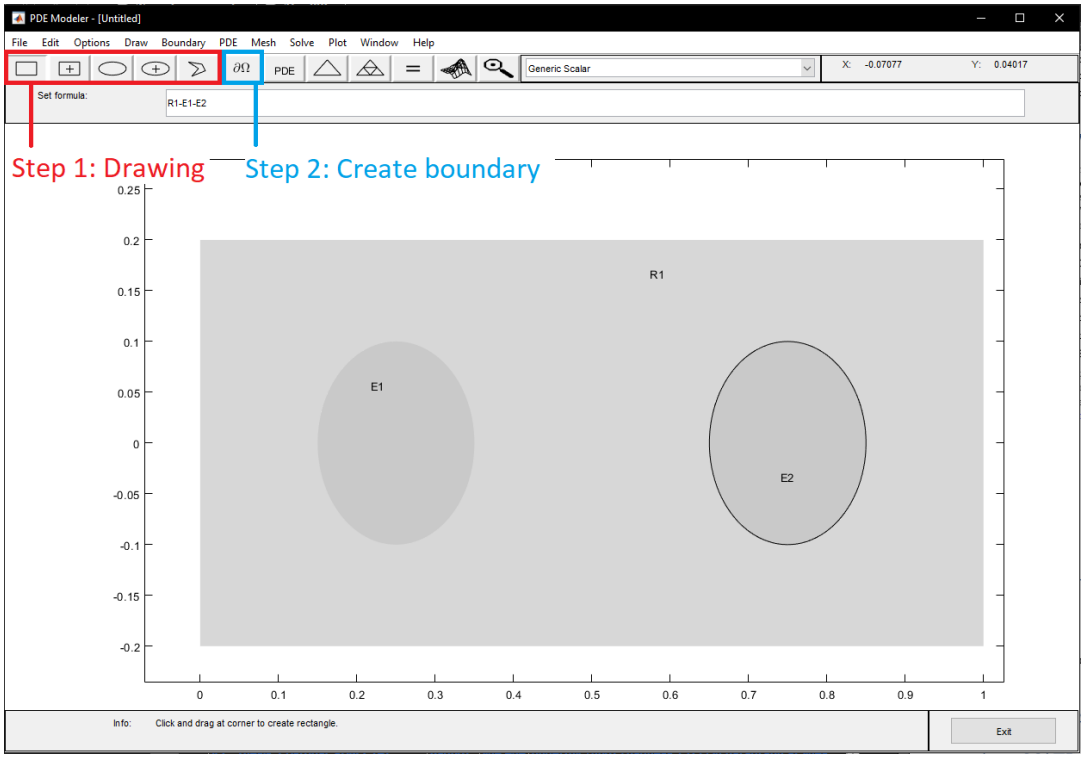

Figure C.1 – First and second steps in creating the domain.

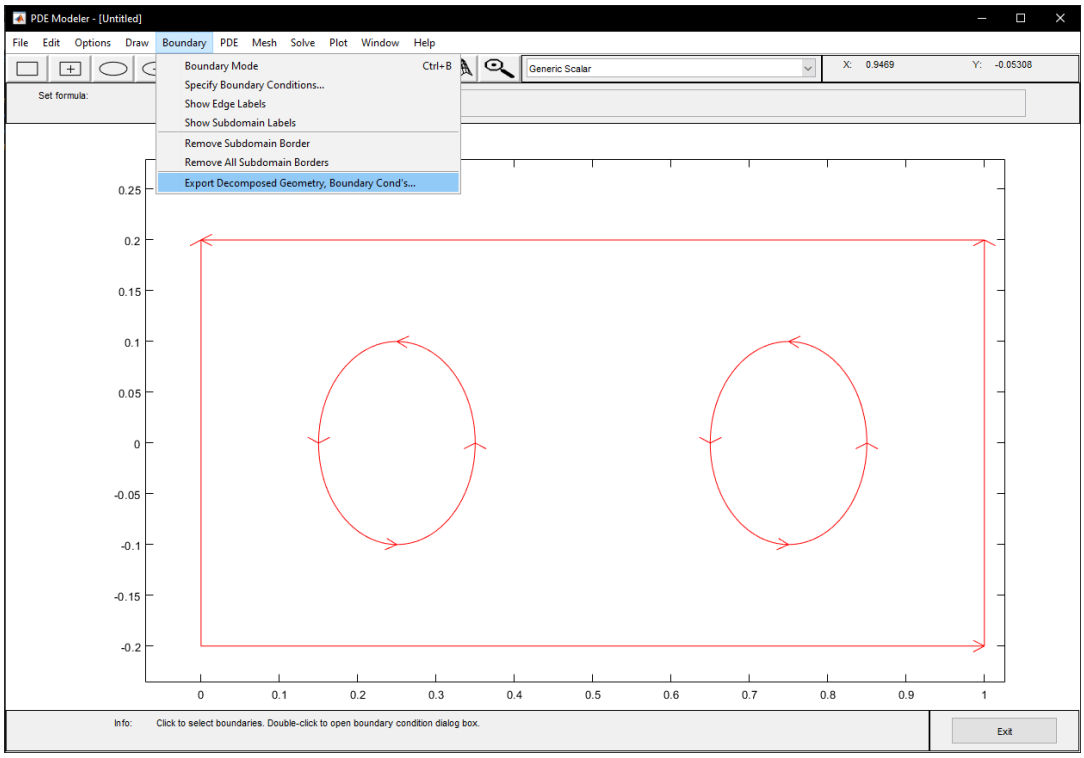

Figure C.2 – Third step in creating the domain.

Part II of the `Main_script.m`: Generation of the domain and Mesh.

```
% Generate mesh
DomainObj = load('DomainPlate.mat');
order = 2;       % Mesh order  (1 or 2)
Hmax = 0.1;      % Maximum mesh edge length
Hmin = 0.1;      % Minimum mesh edge length
tag_Nodes = 'off'; tag_Edges = 'on'; tag_Elements = 'off';

meshFEM = gMesh2D(DomainObj.g,order,Hmax,Hmin,...
                  tag_Nodes,tag_Edges,tag_Elements);
```

Description:

- `order`: Specifies the degree of the shape functions used for interpolation. Valid options are `order = 1;` for linear functions or `order = 2;` for quadratic functions.
- `Hmax`, `Hmin`: Parameters for mesh tuning, representing the maximum and minimum edge lengths in the mesh, respectively. To generate the mesh automatically, set both as `Hmax = [];` and `Hmin = [];`.
- `tag_Nodes`, `tag_Edges`, `tag_Elements`: Switches to display or hide the global numbering of nodes, edges, and elements in the figure. This is useful for specifying the Dirichlet and Neumann boundary portions.
- `meshFEM`: An object containing the mesh information. The main variables that can be extracted include:
  - `meshFEM.coor`: A matrix containing the spatial coordinates of all nodes in the mesh.
  - `meshFEM.conec`: A matrix defining the mesh topology, where the k-th row specifies the nodes connected to form the element k.
  - `meshFEM.Bconec`: A matrix containing the topology of the boundaries, where the j-th row specifies the nodes connected to form the boundary edge E_j.
  - `meshFEM.coor1`, `meshFEM.conec1`: Matrices containing the spatial coordinates and topology for first-order triangular elements. When `order = 1`, these matrices are identical to `meshFEM.coor` and `meshFEM.conec`. These matrices are particularly useful for plotting results when using second-order meshes, as many MATLAB functions only support first-order topology.
  - `meshFEM.p`, `meshFEM.e`, `meshFEM.t`: Matrices that describe the mesh topology and are often required for plotting results.

Once this part of the code is executed, a figure displaying the domain along with the numbering of nodes, edges, and elements is generated. See Figure C.3 for the results obtained in this example.

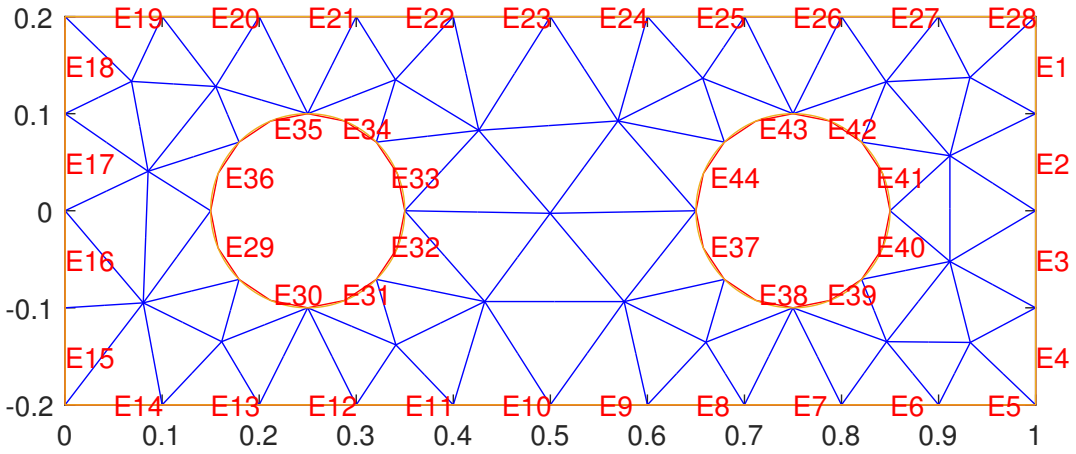

Figure C.3 – Spatial domain, mesh and global numbering.

The third part of the `Main_script` consists in defining the PDE and the portions where Dirichlet and Neumann boundary conditions are applied.

Part III of the `Main_script.m`: Definition of the PDE.

```
% Infinite-dimensional model (Mindlin plate)
prop.M  = @(x,y) rho*diag([I2,I2,h]);
prop.K  = @(x,y) blkdiag(I2*Cb,h*Cs);
prop.b  = @(x,y) [0;0;-rho*g*h];
prop.F0 = [zeros(3,2) zeros(3,1);-eye(2) zeros(2,1)];
prop.F1 = [1 0 0;0 0 0;0 1 0;0 0 1;0 0 0];
prop.F2 = [0 0 0;0 1 0;1 0 0;0 0 0;0 0 1];

% Boundary conditions
prop.Dirichlet_Edges = (15:18)';
prop.Din  = prop.Dirichlet_Edges;
prop.Didx = [0 0 1];
prop.Nin  = [9 24]';
prop.Nidx = [0 0 1];
```

Description:

- `prop.M`, `prop.K`, `prop.b`: Specify $\mathcal{M}(\mathtt{X})$, $\mathcal{K}_\epsilon(\mathtt{X})$ and $b(\mathtt{X})$, respectively. In general, they can be dependent on the spatial coordinates $\mathtt{X} =$ `@(x,y)`.
- `prop.F0`, `prop.F1`, `prop.F2`: They are the matrices F_0, F_1 and F_2 associated with the differential operator $\mathcal{F}_{\mathtt{x}}(\cdot) = F_0(\cdot) + F_1\partial_1(\cdot) + F_2\partial_2(\cdot)$.
- `prop.Dirichlet_Edges`: Specifies the boundary edges that belong to the Dirichlet boundary portion $\partial\Omega_D$. Boundary edges not selected are automatically assigned to the Neumann boundary portion $\partial\Omega_N$.

- `prop.Didx`, `prop.Nidx`: Selectors used to specify which components of the velocity or traction, respectively, are applied as control inputs. For example:
  - `prop.Didx = [0 0 1];` indicates that the third component of $v_D(\mathtt{S},t) = [\dot{\psi}_1(\mathtt{S},t)^\top \ \dot{\psi}_2(\mathtt{S},t)^\top \ \dot{w}_0(\mathtt{S},t)^\top]^\top$ will serve as control input.
  - `prop.Nidx = [0 0 1];` indicates that the third component of the traction $\tau_N(\mathtt{S},t) = [\tau_N^{\psi_1}(\mathtt{S},t)^\top \ \tau_N^{\psi_2}(\mathtt{S},t)^\top \ \tau_N^{w}(\mathtt{S},t)^\top]^\top$ will serve as control input. In this case, $\tau_N^w(\mathtt{S},t)$ represents applied vertical force.

  As in the 1D case, it is important to highlight that these selectors are only to define the control inputs for simulations.
- `prop.Din`, `prop.Nin`: Selectors used to specify in which boundary edges the velocity or traction, respectively, are applied as control inputs. For example:
  - `prop.Din = prop.Dirichlet_Edges;` together with `prop.Didx = [0 0 1];` means that in all boundary edges on $\partial\Omega_D$ will be imposed a nonzero $\dot{w}_0(\mathtt{S},t)$ as control input.
  - `prop.Nidx = [9 24]';` together with `prop.Nidx = [0 0 1];` means that in the boundary edges E9 and E24 (which belong to $\partial\Omega_N$) will be imposed a nonzero $\tau_N^w(\mathtt{S},t)$ as control input.

The last part of the `Main_script` consists of choosing the desired FEM method and obtaining the model.

Part IV of the `Main_script.m`: FEM discretization.

```
% Generate finite-dimensional model
prop.beta = 50;        % Link factor for mLLM method
prop.beta_inf = 1e9;   % Penalty factor for penalty method

% FEM methods: 'LM', 'PM', 'HR', 'mLLM', 'GHP'
[model] = FEM_PHS_2D(prop,meshFEM,'LM');
```

Description:

- `model`: An object that contains the model information. The main variables that can be extracted are the matrices of the finite-dimensional model, which vary depending on the FEM method chosen to discretize the PDE. For instance, using the `'LM'` method, the following matrices and vectors can be extracted:
  - `model.M`: The discretized mass matrix $\hat{M}$.
  - `model.Kr`: The discretized stiffnes matrix $\hat{K}_r$.
  - `model.b`: The discretized body load $\hat{b}$.
  - `model.B_lam`: The matrix $\hat{B}_\lambda$.
  - `model.B_tN`: The input map $\hat{B}_{\tau_N}$.
  - `model.B_LM`: The input map $\hat{B}_{LM}$.

As in the 1D case, with the discretized models available, they can be applied to analyze eigenmodes to study the natural frequencies and mode shapes of the system, perform time simulations to evaluate its dynamic response under various inputs, and design control strategies to achieve desired performance objectives. For illustrative purposes, the first eight modal shapes of the plate are shown in Figure C.4.

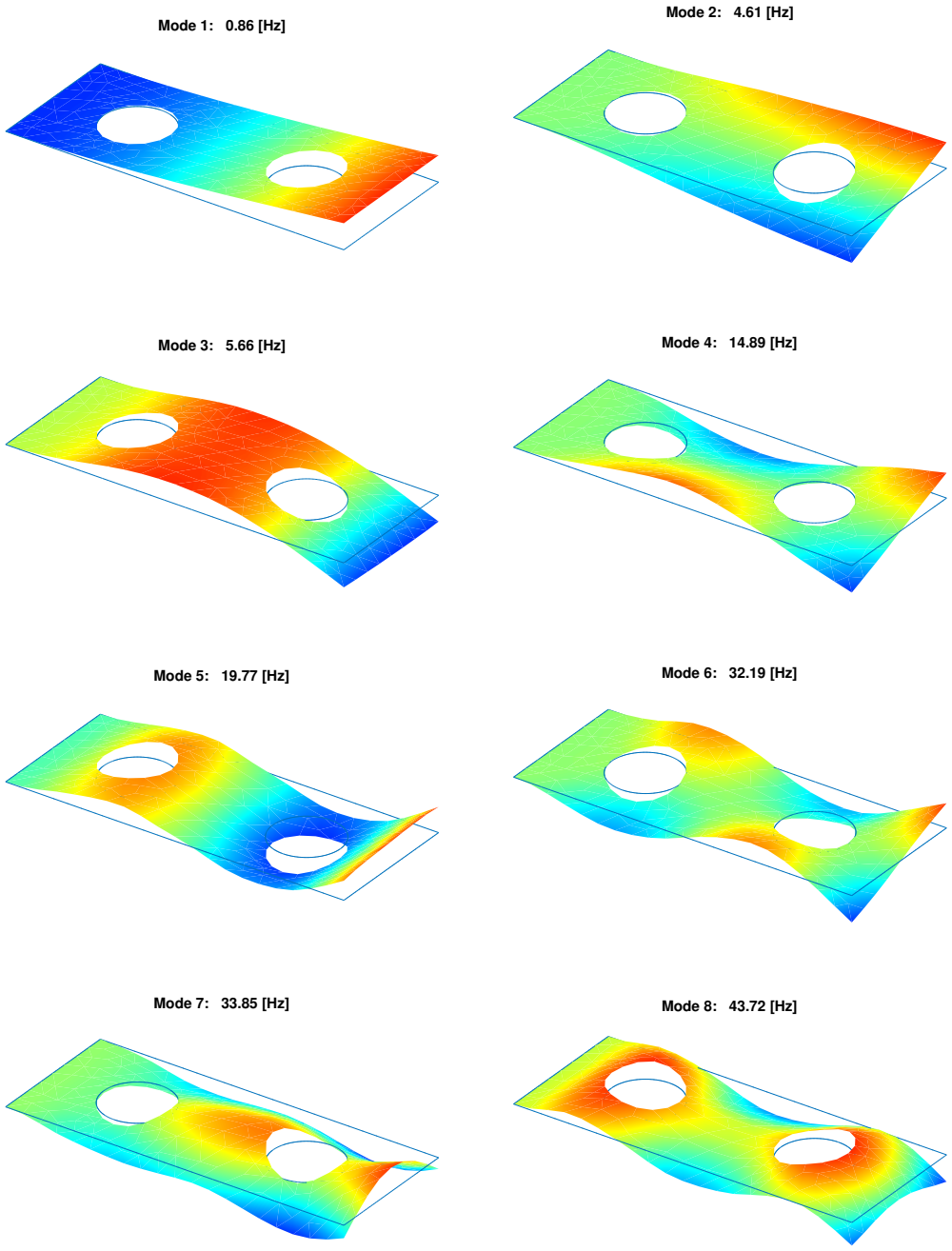

Figure C.4 – Modal shapes of the plate.

C.3 MATLAB Code

The developed code is freely available for use and can be downloaded from the following link: Click here to download the MATLAB code.

For any inquiries or if the link becomes unavailable, please do not hesitate to contact me at emails: cristobal.ponces@usm.cl or cristobal.ponce@femto-st.fr. Additionally, I kindly request that you appropriately reference my work, including the thesis and related papers, in any publications or applications of the code.

Bibliography

[Agrawal 1997] Brij Agrawal, Mostafa Elshafei. « Shape control of composite material plates using piezoelectric actuators ». 3241 (1997), pp. 300–311.

[Agrawal 1999] Brij Agrawal, Kirk Treanor. « Shape control of a beam using piezoelectric actuators ». *Smart Materials and Structures* 8.6 (1999), p. 729.

[Agrawal 1994] Sunil Agrawal, Daqun Tong, Kamsali Nagaraja. « Modeling and shape control of piezoelectric actuator embedded elastic plates ». *Journal of Intelligent Material Systems and Structures* 5.4 (1994), pp. 514–521.

[Arnol'd 2013] Vladimir Arnol'd. *Mathematical methods of classical mechanics*. Vol. 60. Springer Science & Business Media, 2013.

[Azarniya 2023] Omid Azarniya, Gholamhossein Rahimi, Ali Forooghi. « Large deformation analysis of a hyperplastic beam using experimental/FEM/meshless collocation method ». *Waves in Random and Complex Media* (2023), pp. 1–20.

[Babuška 1973a] Ivo Babuška. « The finite element method with Lagrangian multipliers ». *Numerische Mathematik* 20.3 (1973), pp. 179–192.

[Babuška 1973b] Ivo Babuška. « The finite element method with penalty ». *Mathematics of computation* 27.122 (1973), pp. 221–228.

[Baiges 2012] Joan Baiges, Ramon Codina, Florian Henke, Shadan Shahmiri, Wolfgang Wall. « A symmetric method for weakly imposing Dirichlet boundary conditions in embedded finite element meshes ». *International Journal for Numerical Methods in Engineering* 90.5 (2012), pp. 636–658.

[Beattie 2018] Christopher Beattie, Volker Mehrmann, Hongguo Xu, Hans Zwart. « Linear port-Hamiltonian descriptor systems ». *Mathematics of Control, Signals, and Systems* 30 (2018), pp. 1–27.

[Beda 2007] Tibi Beda. « Modeling hyperelastic behavior of rubber: A novel invariant-based and a review of constitutive models ». *Journal of Polymer Science Part B: Polymer Physics* 45.13 (2007), pp. 1713–1732.

[Bedford 1985] Anthony Bedford. *Hamilton's principle in continuum mechanics*. Vol. 139. Springer, 1985.

[Belytschko 2014] Ted Belytschko, Wing Kam Liu, Brian Moran, Khalil Elkhodary. *Nonlinear finite elements for continua and structures*. John wiley & sons, 2014.

[Bochev 2006] Pavel Bochev, James Hyman. « Principles of mimetic discretizations of differential operators ». *Compatible spatial discretizations* (2006), pp. 89–119.

[Boyd 2004] Stephen Boyd, Lieven Vandenberghe. *Convex optimization*. Cambridge university press, 2004.

[Brugnoli 2020] Andrea Brugnoli. « A port-Hamiltonian formulation of flexible structures. Modelling and structure-preserving finite element discretization ». PhD thesis. Toulouse, ISAE, 2020.

[Brugnoli 2019a] Andrea Brugnoli, Daniel Alazard, Valérie Pommier-Budinger, Denis Matignon. « Port-Hamiltonian formulation and symplectic discretization of plate models Part I: Mindlin model for thick plates ». *Applied Mathematical Modelling* 75 (2019), pp. 940–960.

[Brugnoli 2019b] Andrea Brugnoli, Daniel Alazard, Valérie Pommier-Budinger, Denis Matignon. « Port-Hamiltonian formulation and symplectic discretization of plate models Part II: Kirchhoff model for thin plates ». *Applied Mathematical Modelling* 75 (2019), pp. 961–981.

[Brugnoli 2020a] Andrea Brugnoli, Flávio Cardoso-Ribeiro, Ghislain Haine, Paul Kotyczka. « Partitioned finite element method for structured discretization with mixed boundary conditions ». *IFAC-PapersOnLine* 53.2 (2020), pp. 7557–7562.

[Brugnoli 2020b] Andrea Brugnoli, Ghislain Haine, Anass Serhani, Xavier Vasseur. « Numerical approximation of port-Hamiltonian systems for hyperbolic or parabolic PDEs with boundary control ». *arXiv preprint arXiv:2007.08326* (2020).

[Brugnoli 2022a] Andrea Brugnoli, Denis Matignon. « A port-Hamiltonian formulation for the full von-Kármán plate model ». *10th European Nonlinear Dynamics Conference (ENOC), Jul 2022, Lyon, France*. 2022.

[Brugnoli 2024] Andrea Brugnoli, Volker Mehrmann. « On the discrete equivalence of Lagrangian, Hamiltonian and mixed finite element formulations for linear wave phenomena ». *arXiv preprint arXiv:2401.09348* (2024).

[Brugnoli 2021] Andrea Brugnoli, Ramy Rashad, Federico Califano, Stefano Stramigioli, Denis Matignon. « Mixed finite elements for port-Hamiltonian models of von Kármán beams ». *IFAC-papersonline* 54.19 (2021), pp. 186–191.

[Brugnoli 2022b] Andrea Brugnoli, Ramy Rashad, Stefano Stramigioli. « Dual field structure-preserving discretization of port-Hamiltonian systems using finite element exterior calculus ». *Journal of computational physics* 471 (2022), p. 111601.

[Cardoso-Ribeiro 2018] Flávio Cardoso-Ribeiro, Denis Matignon, Laurent Lefevre. « A structure-preserving partitioned finite element method for the 2D wave equation ». *IFAC-PapersOnLine* 51.3 (2018), pp. 119–124.

[Cardoso-Ribeiro 2016] Flávio Cardoso-Ribeiro, Denis Matignon, Valérie Pommier-Budinger. « Piezoelectric beam with distributed control ports: a power-preserving discretization using weak formulation. » *IFAC-PapersOnLine* 49.8 (2016), pp. 290–297.

[Chagnon 2015] Grégory Chagnon, Marie Rebouah, Denis Favier. « Hyperelastic energy densities for soft biological tissues: a review ». *Journal of Elasticity* 120 (2015), pp. 129–160.

[Chandrashekhara 1997] K Chandrashekhara, Sharad Varadarajan. « Adaptive shape control of composite beams with piezoelectric actuators ». *Journal of Intelligent Material Systems and Structures* 8.2 (1997), pp. 112–124.

[Chaturantabut 2016] Saifon Chaturantabut, Chris Beattie, Serkan Gugercin. « Structure-preserving model reduction for nonlinear port-Hamiltonian systems ». *SIAM Journal on Scientific Computing* 38.5 (2016), B837–B865.

[Childs 2021] Jake Childs, Caleb Rucker. « Leveraging geometry to enable high-strength continuum robots ». *Frontiers in Robotics and AI* 8 (2021), p. 629871.

[Clemente-Gallardo 2002] Jesus Clemente-Gallardo, Ricardo Lopezlena, Jacquelien Scherpen. « Geometric discretization of fluid dynamics ». *Proceedings of the 41st IEEE Conference on Decision and Control*. 4 (2002), pp. 4185–4190.

[Clough 2003] Ray Clough, Joseph Penzien. *Dynamics of structures. Berkeley*. 2003.

[Codina 2015] Ramon Codina, Joan Baiges. « Weak imposition of essential boundary conditions in the finite element approximation of elliptic problems with non-matching meshes ». *International Journal for Numerical Methods in Engineering* 104.7 (2015), pp. 624–654.

[Cook 2007] Robert Cook, David Malkus, Michael Plesha, Robert Witt. *Concepts and applications of finite element analysis*. 2007.

[Donthireddy 1996] Prabhakar Donthireddy, K Chandrashekhara. « Modeling and shape control of composite beams with embedded piezoelectric actuators ». *Composite structures* 35.2 (1996), pp. 237–244.

[Duindam 2009] Vincent Duindam, Alessandro Macchelli, Stefano Stramigioli, Herman Bruyninckx. *Modeling and control of complex physical systems: the port-Hamiltonian approach*. Springer Science & Business Media, 2009.

[Dupont 2022] Pierre Dupont, Nabil Simaan, Howie Choset, Caleb Rucker. « Continuum robots for medical interventions ». *Proceedings of the IEEE* 110.7 (2022), pp. 847–870.

[Eberard 2007] Damien Eberard, Bernhard Maschke, Arjan van der Schaft. « On the interconnection structures of discretized port-Hamiltonian systems ». *Proceedings in Applied Mathematics and Mechanics* 7.1 (2007), pp. 3030005–3030006.

[Ghosh 1995] Kingshook Ghosh, Romesh Batra. « Shape control of plates using piezoceramic elements ». *aIaa Journal* 33.7 (1995), pp. 1354–1357.

[Goldstein 2002] Herbert Goldstein, Charles Poole, John Safko. *Classical mechanics*. American Association of Physics Teachers, 2002.

[Golo 2002] Goran Golo, Viswanath Talasila, Arjan van der Schaft. « Approximation of the Telegrapher's equations ». *Proceedings of the 41st IEEE Conference on Decision and Control.* 4 (2002), pp. 4587–4592.

[Golo 2004] Goran Golo, Viswanath Talasila, Arjan van der Schaft, Bernhard Maschke. « Hamiltonian discretization of boundary control systems ». *Automatica* 40.5 (2004), pp. 757–771.

[Gugercin 2012] Serkan Gugercin, Rostyslav Polyuga, Christopher Beattie, Arjan van der Schaft. « Structure-preserving tangential interpolation for model reduction of port-Hamiltonian systems ». *Automatica* 48.9 (2012), pp. 1963–1974.

[Gülümser 2014] Emir Gülümser, Uğur Güdükbay, Sinan Filiz. « Fast stiffness matrix calculation for nonlinear finite element method ». *Journal of Applied Mathematics* 2014.1 (2014), p. 932314.

[Haftka 1985] Raphael Haftka, Howard Adelman. « An analytical investigation of shape control of large space structures by applied temperatures ». *AIAA journal* 23.3 (1985), pp. 450–457.

[Hamroun 2010] Boussad Hamroun, Alexandru Dimofte, Laurent Lefèvre, Eduardo Mendes. « Control by interconnection and energy-shaping methods of port-Hamiltonian models. Application to the shallow water equations ». *European Journal of Control* 16.5 (2010), pp. 545–563.

[Hartmann 2010] Carsten Hartmann, Valentina-Mira Vulcanov, Christof Schütte. « Balanced truncation of linear second-order systems: a Hamiltonian approach ». *Multiscale Modeling & Simulation* 8.4 (2010), pp. 1348–1367.

[Hassani 2013] Sadri Hassani. *Mathematical physics: A modern introduction to its foundations*. Springer Science & Business Media, 2013.

[Henderson 1981] Harold Henderson, Shayle Searle. « On deriving the inverse of a sum of matrices ». *Siam Review* 23.1 (1981), pp. 53–60.

[Ionescu 2013] Tudor Ionescu, Alessandro Astolfi. « Families of moment matching based, structure preserving approximations for linear port-Hamiltonian systems ». *Automatica* 49.8 (2013), pp. 2424–2434.

[Kawano 2018] Yu Kawano, Jacquelien Scherpen. « Structure preserving truncation of nonlinear port-Hamiltonian systems ». *IEEE Transactions on Automatic Control* 63.12 (2018), pp. 4286–4293.

[Khaniki 2022] Hossein Khaniki, Mergen Ghayesh, Rey Chin, Marco Amabili. « A review on the nonlinear dynamics of hyperelastic structures ». *Nonlinear Dynamics* 110.2 (2022), pp. 963–994.

[Kinon 2023] Philipp Kinon, Tobias Thoma, Peter Betsch, Paul Kotyczka. « Port-Hamiltonian formulation and structure-preserving discretization of hyperelastic strings ». *ECCOMAS Thematic Conference on Multibody Dynamics* (Aug. 2023).

[Kotyczka 2016] Paul Kotyczka. « Finite volume structure-preserving discretization of 1D distributed parameter port-Hamiltonian systems ». *IFAC-PapersOnLine* 49.8 (2016), pp. 298–303.

[Kwon 2018] Young Kwon, Hyochoong Bang. *The finite element method using MATLAB*. CRC press, 2018.

[Lanczos 2012] Cornelius Lanczos. *The variational principles of mechanics*. Courier Corporation, 2012.

[Landau 2013] Lev Landau, Evgenii Lifshitz. *Course of theoretical physics*. Elsevier, 2013.

[Langemyr 1996] Lars Langemyr. *Partial Differential Equation Toolbox: For Use with MATLAB; User's Guide*. MathWorks, 1996.

[Larson 2010] Mats Larson, Fredrik Bengzon. *The finite element method: theory, implementation, and practice*. Springer, 2010.

[Le Gorrec 2004] Yann Le Gorrec, Hans Zwart, Bernhard Maschke. « A semigroup approach to port-Hamiltonian systems associated with linear skew-symmetric operator ». *16th international symposium on mathematical theory of networks and systems (MTNS)* (2004).

[Le Gorrec 2005] Yann Le Gorrec, Hans Zwart, Bernhard Maschke. « Dirac structures and boundary control systems associated with skew-symmetric differential operators ». *SIAM journal on control and optimization* 44.5 (2005), pp. 1864–1892.

[León 2011] Manuel de León, Paulo Rodrigues. *Methods of differential geometry in analytical mechanics*. Elsevier, 2011.

[Li 2013] Tiefeng Li, Christoph Keplinger, Richard Baumgartner, Siegfried Bauer, Wei Yang, Zhigang Suo. « Giant voltage-induced deformation in dielectric elastomers near the verge of snap-through instability ». *Journal of the Mechanics and Physics of Solids* 61.2 (2013), pp. 611–628.

[Liu 2018] Chong Liu, Boyong Mao, Gangting Huang, Qichen Wu, Shilin Xie, Minglong Xu. « Optimization of shape control of a cantilever beam using dielectric elastomer actuators ». *AIP Advances* 8.5 (2018), p. 055015.

[Liu 2024] Ning Liu, Yongxin Wu, Yann Le Gorrec, Laurent Lefèvre, Hector Ramirez. « Reduced order in domain control of distributed parameter port-Hamiltonian systems via energy shaping ». *Automatica* 161 (2024), p. 111500.

[Lopezlena 2004] Ricardo Lopezlena, Jacquelien Scherpen. « Lumped approximation of transmission line with an alternative geometric discretization ». *IFAC Proceedings Volumes* 37.21 (2004), pp. 381–386.

[Lu 2019] Kaizhou Lu, Charles Augarde, William Coombs, Zhendong Hu. « Weak impositions of Dirichlet boundary conditions in solid mechanics: a critique of current approaches and extension to partially prescribed boundaries ». *Computer Methods in Applied Mechanics and Engineering* 348 (2019), pp. 632–659.

[Luo 2006] Quantian Luo, Liyong Tong. « High precision shape control of plates using orthotropic piezoelectric actuators ». *Finite elements in analysis and design* 42.11 (2006), pp. 1009–1020.

[Macchelli 2004a] Alessandro Macchelli, Claudio Melchiorri. « Modeling and control of the Timoshenko beam. The distributed port-Hamiltonian approach ». *SIAM journal on control and optimization* 43.2 (2004), pp. 743–767.

[Macchelli 2005] Alessandro Macchelli, Claudio Melchiorri, Luca Bassi. « Port-based modelling and control of the Mindlin plate ». *Proceedings of the 44th IEEE Conference on Decision and Control* (2005), pp. 5989–5994.

[Macchelli 2004b] Alessandro Macchelli, Arjan van der Schaft, Claudio Melchiorri. « Port-Hamiltonian formulation of infinite-dimensional systems I. Modeling ». *43rd IEEE Conference on Decision and Control (CDC)* 4 (2004), pp. 3762–3767.

[Malzer 2019] Tobias Malzer, Hubert Rams, Markus Schöberl. « Energy-based in-domain control of a piezo-actuated Euler-Bernoulli beam ». *IFAC-PapersOnLine* 52.2 (2019), pp. 144–149.

[Malzer 2020] Tobias Malzer, Hubert Rams, Markus Schöberl. « On structural invariants in the energy-based in-domain control of infinite-dimensional port-Hamiltonian systems ». *Systems & Control Letters* 145 (2020), p. 104778.

[Maschke 1992] Bernhard Maschke, Arjan van der Schaft. « Port-controlled Hamiltonian systems: modelling origins and systemtheoretic properties ». *IFAC: Nonlinear Control Systems Design* (1992), pp. 359–365.

[Maschke 2023] Bernhard Maschke, Arjan van der Schaft. « Linear boundary port-Hamiltonian systems with implicitly defined energy ». *arXiv preprint arXiv:2305.13772* (2023).

[Mattioni 2021] Andrea Mattioni. « Modelling and stability analysis of flexible robots: a distributed parameter port-Hamiltonian approach ». PhD thesis. Université Bourgogne Franche-Comté, 2021.

[Mehrmann 2019] Volker Mehrmann, Riccardo Morandin. « Structure-preserving discretization for port-Hamiltonian descriptor systems ». *IEEE 58th Conference on Decision and Control (CDC)* (2019), pp. 6863–6868.

[Mehrmann 2023] Volker Mehrmann, Arjan van der Schaft. « Differential-algebraic systems with dissipative Hamiltonian structure ». *Mathematics of Control, Signals, and Systems* 35.3 (2023), pp. 541–584.

[Melly 2021] Stephen Melly, Liwu Liu, Yanju Liu, Jinsong Leng. « A review on material models for isotropic hyperelasticity ». *International Journal of Mechanical System Dynamics* 1.1 (2021), pp. 71–88.

[Morris 2015] Kirsten Morris, Michael Demetriou, Steven Yang. « Using H2-control performance metrics for the optimal actuator location of distributed parameter systems ». *IEEE Transactions on Automatic Control* 60.2 (2015), pp. 450–462.

[Moulla 2012] Redha Moulla, Laurent Lefevre, Bernhard Maschke. « Pseudo-spectral methods for the spatial symplectic reduction of open systems of conservation laws ». *Journal of computational Physics* 231.4 (2012), pp. 1272–1292.

[Mourllion 2013] Benjamin Mourllion, Abderazik Birouche. « Modal truncation for linear Hamiltonian systems: a physical energy approach ». *Dynamical Systems* 28.2 (2013), pp. 187–202.

[Nishida 2004] Gou Nishida, Masaki Yamakita. « A higher order Stokes-Dirac structure for distributed-parameter port-Hamiltonian systems ». *Proceedings of the 2004 American Control Conference* 6 (2004), pp. 5004–5009.

[Nishida 2005] Gou Nishida, Masaki Yamakita. « Formal distributed port-Hamiltonian representation of field equations ». *Proceedings of the 44th IEEE Conference on Decision and Control* (2005), pp. 6009–6015.

[Nishida 2006] Gou Nishida, Masaki Yamakita, Zhi-wei Luo. « Field port-Lagrangian representation of conservation laws for variational symmetries ». *Proceedings of the 45th IEEE Conference on Decision and Control* (2006), pp. 5875–5881.

[Ortega 2002] Romeo Ortega, Arjan van der Schaft, Bernhard Maschke, Gerardo Escobar. « Interconnection and damping assignment passivity-based control of port-controlled Hamiltonian systems ». *Automatica* 38.4 (2002), pp. 585–596.

[Ozturk 2022] Caglar Ozturk, Luca Rosalia, Ellen Roche. « A multi-domain simulation study of a pulsatile-flow pump device for heart failure with preserved ejection fraction ». *Frontiers in Physiology* 13 (2022), p. 815787.

[Pedersen 2006] Pauli Pedersen. « Analytical stiffness matrices for tetrahedral elements ». *Computer methods in applied mechanics and engineering* 196.1-3 (2006), pp. 261–278.

[Plotnikova 2020] Svetlana Plotnikova, Gennady Kulikov. « Shape control of composite plates with distributed piezoelectric actuators in a three-dimensional formulation ». *Mechanics of Composite Materials* 56.5 (2020), pp. 557–572.

[Polyuga 2010a] Rostyslav Polyuga, Arjan van der Schaft. « Model reduction of port-Hamiltonian systems as structured systems ». *Proceedings of the 19th International Symposium on Mathematical Theory of Networks and Systems-MTNS* 5.9 (2010).

[Polyuga 2010b] Rostyslav Polyuga, Arjan van der Schaft. « Structure preserving model reduction of port-Hamiltonian systems by moment matching at infinity ». *Automatica* 46.4 (2010), pp. 665–672.

[Ponce 2023] Cristobal Ponce, Yongxin Wu, Yann Le Gorrec, Hector Ramirez. « Port-Hamiltonian modeling of multidimensional flexible mechanical structures defined by linear elastic relations ». *arXiv preprint arXiv:2311.03796* (2023).

[Ponce 2024] Cristobal Ponce, Yongxin Wu, Yann Le Gorrec, Hector Ramirez. « A systematic methodology for port-Hamiltonian modeling of multidimensional flexible linear mechanical systems ». *Applied Mathematical Modelling* (2024).

[Rashad 2020] Ramy Rashad, Federico Califano, Arjan van der Schaft, Stefano Stramigioli. « Twenty years of distributed port-Hamiltonian systems: a literature review ». *IMA Journal of Mathematical Control and Information* 37.4 (2020), pp. 1400–1422.

[Reddy 1984] Junuthula Reddy. « A Simple Higher-Order Theory for Laminated Composite Plates ». *Journal of Applied Mechanics* 51.4 (1984), pp. 745–752.

[Reddy 2005] Junuthula Reddy. *An introduction to the finite element method*. Vol. 3. McGraw Hill New York, 2005.

[Reddy 2006] Junuthula Reddy. *Theory and analysis of elastic plates and shells*. CRC press, 2006.

[Reddy 2007] Junuthula Reddy. *An introduction to continuum mechanics*. Cambridge university press, 2007.

[Reddy 2014] Junuthula Reddy. *An Introduction to Nonlinear Finite Element Analysis Second Edition: with applications to heat transfer, fluid mechanics, and solid mechanics*. OUP Oxford, 2014.

[Reddy 2017] Junuthula Reddy. *Energy principles and variational methods in applied mechanics*. John Wiley & Sons, 2017.

[Roze 2024] David Roze, Thomas Hélie, Emmanuelle Rouhaud. « Time-space formulation of a conservative string subject to finite transformations ». *IFAC-PapersOnLine* 58.6 (2024), pp. 232–237.

[Scherpen 1993] Jacqueline Scherpen. « Balancing for nonlinear systems ». *Systems & Control Letters* 21.2 (1993), pp. 143–153.

[Schöberl 2013] Markus Schöberl, Andreas Siuka. « Analysis and comparison of port-Hamiltonian formulations for field theories-demonstrated by means of the Mindlin plate ». *2013 European Control Conference (ECC)* (2013), pp. 548–553.

[Schöberl 2014] Markus Schöberl, Andreas Siuka. « Jet bundle formulation of infinite dimensional port-Hamiltonian systems using differential operators ». *Automatica* 50.2 (2014), pp. 607–613.

[Schulze 2023] Philipp Schulze. « Structure-preserving model reduction for port-Hamiltonian systems based on separable nonlinear approximation ansatzes ». *Frontiers in Applied Mathematics and Statistics* 9 (2023), p. 1160250.

[Serhani 2018] Anass Serhani, Denis Matignon, Ghislain Haine. « Structure-preserving finite volume method for 2D linear and non-linear port-Hamiltonian systems ». *IFAC-PapersOnLine* 51.3 (2018), pp. 131–136.

[Seslija 2012] Marko Seslija, Arjan van der Schaft, Jacquelien Scherpen. « Discrete exterior geometry approach to structure-preserving discretization of distributed-parameter port-Hamiltonian systems ». *Journal of Geometry and Physics* 62.6 (2012), pp. 1509–1531.

[Seslija 2011] Marko Seslija, Jacquelien Scherpen, Arjan van der Schaft. « A discrete exterior approach to structure-preserving discretization of distributed-parameter port-Hamiltonian systems ». *2011 50th IEEE Conference on Decision and Control and European Control Conference* (2011), pp. 7003–7008.

[Seslija 2014] Marko Seslija, Jacquelien Scherpen, Arjan van der Schaft. « Explicit simplicial discretization of distributed-parameter port-Hamiltonian systems ». *Automatica* 50.2 (2014), pp. 369–377.

[Shintake 2018] Jun Shintake, Vito Cacucciolo, Dario Floreano, Herbert Shea. « Soft robotic grippers ». *Advanced materials* 30.29 (2018), p. 1707035.

[Stolarski 1987] Henryk Stolarski, Ted Belytschko. « Limitation principles for mixed finite elements based on the Hu-Washizu variational formulation ». *Computer Methods in Applied Mechanics and Engineering* 60.2 (1987), pp. 195–216.

[Suri 1996] Manil Suri. « Analytical and computational assessment of locking in the hp finite element method ». *Computer methods in applied mechanics and engineering* 133.3-4 (1996), pp. 347–371.

[Tadmor 2012] Ellad Tadmor, Ronald Miller, Ryan Elliott. *Continuum mechanics and thermodynamics: from fundamental concepts to governing equations*. Cambridge University Press, 2012.

[Talasila 2002] Viswanath Talasila, Goran Golo, Arjan van der Schaft. « The wave equation as a port-Hamiltonian system and a finite dimensional approximation ». *Proceedings of 15th international symposium mathematical theory of networks and systems (MTNS), South Bend* (2002).

[Thoma 2022a] Tobias Thoma, Paul Kotyczka. « Explicit port-Hamiltonian FEM models for geometrically nonlinear mechanical systems ». *arXiv preprint arXiv:2202.02097* (2022).

[Thoma 2022b] Tobias Thoma, Paul Kotyczka. « Explicit port-Hamiltonian FEM-models for linear mechanical systems with non-uniform boundary conditions ». *IFAC-PapersOnLine* 55.20 (2022), pp. 499–504.

[Thoma 2024] Tobias Thoma, Paul Kotyczka, Herbert Egger. « On the velocity-stress formulation for geometrically nonlinear elastodynamics and its structure-preserving discretization ». *arXiv preprint arXiv:2202.02097* (2024).

[Trenchant 2018] Vincent Trenchant, Hector Ramirez, Yann Le Gorrec, Paul Kotyczka. « Finite differences on staggered grids preserving the port-Hamiltonian structure with application to an acoustic duct ». *Journal of Computational Physics* 373 (2018), pp. 673–697.

[Trenchant 2017] Vincent Trenchant, Trang Vu, Hector Ramirez, Laurent Lefèvre, Yann Le Gorrec. « On the use of structural invariants for the distributed control of infinite dimensional port-Hamitonian systems ». *IEEE 56th Annual Conference on Decision and Control (CDC)* (2017), pp. 47–52.

[Trivedi 2015] Megha V Trivedi, Ravi N Banavar, Paul Kotyczka. « Port-Hamiltonian Modelling for Buckling Control of a Vertical Flexible Beam with Actuation at the Bottom ». *IFAC-PapersOnLine* 48.13 (2015), pp. 31–38.

[van der Schaft 2011] Arjan van der Schaft. « On the relation between port-Hamiltonian and gradient systems ». *IFAC Proceedings Volumes* 44.1 (2011), pp. 3321–3326.

[van der Schaft 2013] Arjan van der Schaft. « Port-Hamiltonian differential-algebraic systems ». *Surveys in Differential-Algebraic Equations I* (2013), pp. 173–226.

[van der Schaft 2017] Arjan van der Schaft. *L2-Gain and Passivity Techniques in Nonlinear Control*. Springer, 2017. DOI: 10.1007/978-3-319-49992-5.

[van der Schaft 2002] Arjan van der Schaft, Bernhard Maschke. « Hamiltonian formulation of distributed parameter systems with boundary energy flow ». *Journal of Geometry and physics* 42.1-2 (2002), pp. 166–194.

[van der Schaft 2018] Arjan van der Schaft, Bernhard Maschke. « Generalized port-Hamiltonian DAE systems ». *Systems & Control Letters* 121 (2018), pp. 31–37.

[van der Schaft 2020] Arjan van der Schaft, Bernhard Maschke. « Dirac and Lagrange algebraic constraints in nonlinear port-Hamiltonian systems ». *Vietnam Journal of Mathematics* 48.4 (2020), pp. 929–939.

[van der Schaft 2023] Arjan van der Schaft, Volker Mehrmann. « Linear port-Hamiltonian DAE systems revisited ». *Systems & Control Letters* 177 (2023), p. 105564.

[Varadarajan 1998] Sharad Varadarajan, K Chandrashekhara, Sanjeev Agarwal. « Adaptive shape control of laminated composite plates using piezoelectric materials ». *AIAA journal* 36.9 (1998), pp. 1694–1698.

[Viebahn 2018] Nils Viebahn, Karl Steeger, Jörg Schröder. « A simple and efficient Hellinger-Reissner type mixed finite element for nearly incompressible elasticity ». *Computer Methods in Applied Mechanics and Engineering* 340 (2018), pp. 278–295.

[Voß 2011] Thomas Voß, Jacquelien Scherpen. « Stabilization and shape control of a 1D piezoelectric Timoshenko beam ». *Automatica* 47.12 (2011), pp. 2780–2785.

[Voss 2014] Thomas Voss, Jacquelien Scherpen. « Port-Hamiltonian modeling of a nonlinear Timoshenko beam with piezo actuation ». *SIAM Journal on Control and Optimization* 52.1 (2014), pp. 493–519.

[Voss 2008] Thomas Voss, Jacquelien Scherpen, Patrick Onck. « Modeling for control of an inflatable space reflector, the nonlinear 1-D case ». *47th IEEE Conference on Decision and Control* (2008), pp. 1777–1782.

[Warsewa 2021] Alexander Warsewa, Michael Böhm, Oliver Sawodny, Cristina Tarín. « A port-Hamiltonian approach to modeling the structural dynamics of complex systems ». *Applied Mathematical Modelling* 89 (2021), pp. 1528–1546.

[Wolf 2010] Thomas Wolf, Boris Lohmann, Rudy Eid, Paul Kotyczka. « Passivity and structure preserving order reduction of linear port-Hamiltonian systems using Krylov subspaces ». *European Journal of Control* 16.4 (2010), pp. 401–406.

[Wu 2014] Yongxin Wu, Boussad Hamroun, Yann Le Gorrec, Bernhard Maschke. « Port-hamiltonian system in descriptor form for balanced reduction: Application to a nanotweezer ». *IFAC Proceedings Volumes* 47.3 (2014), pp. 11404–11409.

[Wu 2015] Yongxin Wu, Boussad Hamroun, Yann Le Gorrec, Bernhard Maschke. « Power preserving model reduction of 2D vibro-acoustic system: a port-Hamiltonian approach ». *IFAC-PapersOnLine* 48.13 (2015), pp. 206–211.

[Xu 2019] Kangli Xu, Yaolin Jiang. « Structure-preserving interval-limited balanced truncation reduced models for port-Hamiltonian systems ». *IET Control Theory & Applications* 14.3 (2019), pp. 405–414.

[Yang 2006] Seung-Man Yang, Jin-Ho Roh, Jae-Hung Han, In Lee. « Experimental studies on active shape control of composite structures using SMA actuators ». *Journal of intelligent material systems and structures* 17.8-9 (2006), pp. 767–777.

[Yang 2000] Shengyuan Yang, Bryan Ngoi. « Shape control of beams by piezoelectric actuators ». *AIAA journal* 38.12 (2000), pp. 2292–2298.

[Yeh 2022] Yu Yeh, Nelson Cisneros, Yongxin Wu, Kanty Rabenorosoa, Yann Le Gorrec. « Modeling and Position Control of the HASEL Actuator via Port-Hamiltonian Approach ». *IEEE Robotics and Automation Letters* 7.3 (2022), pp. 7100–7107.

[Yi-Yuan 1964] Yu Yi-Yuan. « Generalized Hamilton's principles and variational equation of motion in nonlinear elasticity theory with application to plate theory ». *JASA* 36.1 (1964), p. 111.

[Yoder 2023] Zachary Yoder, Daniela Macari, Gavriel Kleinwaks, Ingemar Schmidt, Eric Acome, Christoph Keplinger. « A soft, fast and versatile electrohydraulic gripper with capacitive object size detection ». *Advanced Functional Materials* 33.3 (2023), p. 2209080.

[Yunhua 1998] Luo Yunhua. « Explanation and elimination of shear locking and membrane locking with field consistence approach ». *Computer Methods in Applied Mechanics and Engineering* 162.1-4 (1998), pp. 249–269.

[Zhou 2019] Fanghao Zhou, Mingqi Zhang, Xunuo Cao, Zhen Zhang, Xiangping Chen, Youhua Xiao, Yiming Liang, Tuck-Whye Wong, Tiefeng Li, Zhongbin Xu. « Fabrication and modeling of dielectric elastomer soft actuator with 3D printed thermoplastic frame ». *Sensors and Actuators A: Physical* 292 (2019), pp. 112–120.

[Zhou 1996] Kemin Zhou, John Doyle, Keith Glover. « Robust and optimal control ». *Prentice hall New Jersey* (1996).

[Zhou 2021] Weijun Zhou, Yongxin Wu, Haiqiang Hu, Yanjun Li, Yu Wang. « Port-Hamiltonian modeling and IDA-PBC control of an IPMC-actuated flexible beam ». *Actuators* 10.9 (2021), p. 236.

[Zienkiewicz 2005] Olek Zienkiewicz, Robert Taylor, Jian Zhu. *The finite element method: its basis and fundamentals*. Elsevier, 2005.

SPIM

Titre : Modélisation port-Hamiltonienne, discrétisation et contrôle de forme de systèmes mécaniques flexibles multidimensionnels

Mots clefs: Systèmes port-Hamiltoniens, Modélisation, Discrétisation FEM, Contrôle de forme, Hyperélasticité

Résumé : Cette thèse traite de la modélisation, de la discrétisation et du contrôle de forme des systèmes mécaniques flexibles dans le cadre des systèmes Port-Hamiltoniens (PHS). Les contributions sont triples. Tout d'abord, nous proposons des méthodologies généralisées pour la modélisation des systèmes mécaniques multidimensionnels, linéaires et non linéaires, en utilisant le principe de Hamilton généralisé et étendu, fournissant des représentations explicites et implicites des PHS. Ensuite, nous développons des techniques de discrétisation préservant la structure à travers des méthodes d'éléments finis mixtes (FEM), incluant des approches à deux, trois et quatre champs adaptées aux systèmes PHS et PH-DAE linéaires et non linéaires. Enfin, nous introduisons un contrôleur en dimension finie basé sur des approximations d'ordre faible de systèmes PHS linéaires discrétisés à grande échelle. Ce contrôleur garantit la convergence vers les formes optimales, offrant la meilleure approximation des configurations désirées, tout en assurant la stabilité asymptotique du système discrétisé à grande échelle.

Title : Port-Hamiltonian modeling, discretization and shape control of multidimensional flexible mechanical systems

Keywords : Port-Hamiltonian systems, Modeling, FEM discretization, Shape control, Hyperelasticity

Abstract : This thesis addresses the modeling, discretization, and shape control of flexible mechanical systems within the Port-Hamiltonian Systems (PHS) framework. The contributions are threefold. First, we propose generalized methodologies for modeling both linear and nonlinear multidimensional mechanical systems using the generalized extended Hamilton's principle, providing explicit and implicit PHS representations. Second, we develop structure-preserving discretization techniques via mixed Finite Element Methods (FEM), including two, three, and four-field approaches tailored to linear and nonlinear PHS and PH-DAE systems. Finally, we introduce a finite-dimensional controller based on low-order approximations of large-scale discretized linear PHS. This controller ensures convergence to the optimal shapes, offering the best approximation to the desired configurations, while guaranteeing asymptotic stability of the large-scale discretized system.

UBFC UNIVERSITÉ BOURGOGNE FRANCHE-COMTÉ

Université Bourgogne Franche-Comté
32, avenue de l'Observatoire
25000 Besançon